

School of Earth and Planetary Sciences

**Realistic and Theoretical 3D Modelling of the Sedimentation,
Burial, Thermal and Tectonic History of the Gippsland Rift
Basin**

Xuemei Yang

0000-0002-4137-7037

**This thesis is presented for the Degree of
Doctor of Philosophy
of
Curtin University**

January 2022

Declaration

To the best of my knowledge and belief this thesis contains no material previously published by any other person except where due acknowledgement has been made.

This thesis contains no material which has been accepted for the award of any other degree or diploma in any university.

Signature: Xuemei Yang

Date: 28/Jan/2022

Abstract

Reconstruction of the history of sedimentary basins is important for better understanding basin evolution, land surface processes, climate change, environmental science and their geological applications in, for example, the water resources, minerals and petroleum industries. Two ways to investigate this are palaeo-landscape reconstruction and 3D burial and thermal history analysis. Reconstruction of the palaeo-landscape is a complicated process controlled and affected by multiple variables, including tectonics, palaeo-environment, sea-level change, rainfall, sediment erosion, transportation, deposition etc. 3D burial history analysis furnishes a picture of organic and petrological changes, which record the palaeo-thermal and pressure changes and are a window into the Pressure-Temperature-time history of the basin.

The project investigated the sedimentary, burial, thermal and tectonic history of the Gippsland rift basin, a relatively simple, rapidly buried, young basin developed in a divergent-margin tectonic setting. Firstly extensive geological datasets were used to build a full 3D realistic structural and stratigraphic model populated with different lithological and physical properties using the *Petrel* (Schlumberger) software. This was based on extensive 2D and 3D seismic data, over 200 onshore and offshore wells with logs, analytical and biostratigraphic data and interpreted gravity data. The data-driven realistic 3D model of the basin was then used to constrain the forward deterministic models made in the Basin and Landscape Dynamics software (*Badlands*, ARC Basin GENESIS Hub) and *PetroMod* (Schlumberger) software.

An efficient Experimental Design approach was used to guide the scenario set-up for the numerical simulation in *Badlands*, process the numerical simulation results of the palaeo-landscapes, and generate the multivariate equations that define and identify the critical controlling variables. The approach was used to test and identify the main uncertainties and their possible ranges, based on actual field data, while at the same time ensuring that the full multi-dimensional space for those variables was covered to enable computation of multivariate equations using the minimum number of scenario runs. The experimental design matrix generated 22 scenarios for palaeo-landscape simulation of the Gippsland Basin in *Badlands* by fitting 12 identified variables and evaluating for possible interactions with each other. The *Badlands* models were calibrated to the corresponding

3D realistic model. The most significant controlling variables are non-marine *Erodibility*, *Rainfall*, the *Exponent m* for (*rainfall x Area*) and *Maximum % Marine Deposition*. *Sea Level*, *Critical Slope*, *slope exponent n* while the Initial Topographic Map are important secondary variables. The *Exponent m* for (*rainfall x Area*) and *Slope exponent n* both have significant interactions with the *non-marine Erodibility*.

The palaeo-landscape reconstruction helps generating a best fit model to the geological history of the Gippsland Basin, and the modelling results offer several insights. The initial paleo-topography at ca. 137 Ma defined an extensive highland area. The Early Cretaceous paleo-environment was intracratonic, with fluvial sediment transport from East to West, and at some stage turned into a shallow inland sea. The mid-Cretaceous uplift caused the emergence of the entire basin, substantial regional erosion and changed the basin architecture. Subsidence associated with the Tasman Sea rifting formed the Central Deep and flipped the fluvial paleo-drainage system towards the east. By the Oligocene, the Latrobe Group sediments filled the basin progressively as a result of transgression by rising sea level which flooded most areas. The models simulate the progradation of the carbonate shelf sediments and sub-marine channels over the basin subsequent to the Latrobe Group formed.

The 3D burial history of the Gippsland Basin was modelled using *PetroMod* constrained by the realistic 3D structural, stratigraphic model built in *Petrel*. Critical depth maps and fault framework were extracted from the realistic model and used to constrain the depth and age simulation in the burial history model. The *Petrel* property model also generated vitrinite reflectance (Ro) maps, total organic carbon (TOC) and hydrogen index (HI) maps, and facies maps corresponding to the depth maps. These property maps conditioned the 3D burial history model by empirical sedimentary and thermal data. The 3D burial history reconstruction identified seven erosion events with significant variations in erosion across the basin. Analysis of the heat flow model and the fit with the thermal history of the Gippsland Basin suggest the presence of two rift events which have different main areas of influence. In addition, the 3D burial history model highlights the sites of three potential mature source rocks intervals within the Latrobe Group spanning the Late Cretaceous to the early Palaeocene.

Acknowledgements

I want to express my sincere gratitude to my supervisor Prof. Greg Smith, for the treasured support of my PhD study. His patience, motivation, meticulousness, immense knowledge and plentiful industry experience have encouraged me in my academic research. I am also very grateful to my supervisor Prof. Chris Elders, who has been supporting my PhD studies both academically and administratively. His extensive knowledge, continued advice and constructive feedbacks have been invaluable to the completion of this study. Without their support, I could not have completed this research project.

Many other people have provided tremendous support and advice towards the project. In particular, Assoc. Prof. Ritu Gupta was generous with her time and knowledge, and introduced me to statistical analysis and guided me to apply it to this research. As well, Dr Guy Holdgate was extremely generous with sharing his knowledge and provided valuable data. Thanks also to Dr Tristan Salles from Sydney University and Dr Xuesong Ding from the University of California, Los Angeles, for software development, generous support and assistance with *Badlands* software. Dr Sabin Zahirovic, from Sydney University, provided professional technical support and kind help with *GPlates* software. The research also benefitted from discussions with Dr Martin Norvick, Dr Vladimir Puzyrev, Dr Alan Partridge, Assoc. Prof. Kevin Hill and Dr Sara Morón on different aspects of this research.

Great thanks to Geoscience Australia for the provision of seismic data and Geological Survey staff in Geoscience Victoria for coal bore, petroleum well data and the 3D model packages.

Schlumberger kindly provides the *Petrel* and *PetroMod* software to the School of Earth & Planetary Sciences, Curtin University. BHP Petroleum kindly provided some of the well data in *Petrel* format, and ExxonMobil Australia provided some of the samples and data used in the original analytical studies.

Thanks also to the Australian government for the financial support provided to me by the Research Training Program (RTP) stipend scholarship.

Finally, I sincerely thank my family for their continued love, tolerance and support.



Attribution Statement

Statement of contribution



This research presented in this thesis was designed, analysed, interpreted, modelled and manuscripts prepared by Xuemei Yang. Contributions of supervisors and co-authors are mentioned below.

Co-Supervisor Professor Greg Smith assisted in the entire project development and design and assisted with planning and reviewing all chapters of the thesis. Primary Supervisor Professor Chris Elders also assisted by reviewing of all chapters of the thesis. Data sources and usage are described in detail in Chapter 3.


Chapter 4 Structural, stratigraphic, tectonic modelling:

	Conception and Design	Acquisition of Data and Method	Data Conditioning and Manipulation	Analysis and Statistical Method	Interpretation and Discussion
Greg Smith	√			√	√
I acknowledge that these represent my contribution to the above research output.					
Signature:					
Chris Elders		√			
I acknowledge that these represent my contribution to the above research output.					
Signature:					


Chapter 5 Palaeo-landscape modelling in Badlands guided by Experimental Design:

	Conception and Design	Acquisition of Data and Method	Data Conditioning and Manipulation	Analysis and Statistical Method	Interpretation and Discussion
Greg Smith	√		√	√	√
I acknowledge that these represent my contribution to the above research output.					
Signature:					
Ritu Gupta	√			√	√
I acknowledge that these represent my contribution to the above research output.					
Signature:					



Chapter 6 Palaeo-landscape and Best Fit model to Geological history:

	Conception and Design	Acquisition of Data and Method	Data Conditioning and Manipulation	Analysis and Statistical Method	Interpretation and Discussion
Greg Smith					√
I acknowledge that these represent my contribution to the above research output.					
Signature:					

Chapter 7 Property Modelling:

	Conception and Design	Acquisition of Data and Method	Data Conditioning and Manipulation	Analysis and Statistical Method	Interpretation and Discussion
Greg Smith	√		√	√	√
I acknowledge that these represent my contribution to the above research output.					
Signature: 					

Chapter 8 Burial and Thermal history:

	Conception and Design	Acquisition of Data and Method	Data Conditioning and Manipulation	Analysis and Statistical Method	Interpretation and Discussion
Greg Smith	√				√
I acknowledge that these represent my contribution to the above research output.					
Signature: 					
Chris Elders					√
I acknowledge that these represent my contribution to the above research output.					
Signature: 					

Contents

Declaration	i
Abstract	ii
Acknowledgements	iv
Attribution Statement	v
Contents	vii
List of Figures	xi
List of Tables	xxiii
Chapter 1. Introduction	1
1.1 Existing Models in the Gippsland Basin	3
1.2 Previous Landscape Evolution and Basin-Fill Studies	4
1.3 Research Aims.....	5
Chapter 2. Regional Geology	7
2.1 Tectonic Background.....	7
2.2 Stratigraphy	10
Chapter 3. Method: Data, Software & Workflow	17
3.1 Source of data	17
3.2 Technical Software	19
3.3 Overall Workflow.....	20
Chapter 4. Tectonic, Structural and Stratigraphic Models	26
4.1 Tectonic Reconstruction in <i>GPlates</i> Software.....	26
4.1.1 Plate Tectonic Reconstruction	26
4.1.2 Crustal Thickness and Crustal Stretching Factor.....	29
4.2 Structural and Stratigraphic Analysis in <i>Petrel</i> Software.....	30

4.2.1	Well Correlations.....	31
4.2.2	Seismic Interpretation.....	33
4.2.3	Velocity Model & Depth Conversion.....	37
4.3	Structural and Stratigraphic Models	40
4.3.1	Entire Gippsland Basin model.....	41
4.3.2	Latrobe Valley model	49
Chapter 5. Landscape evolution modelling in <i>Badlands</i> guided by Experimental Design.....		52
5.1	<i>Badlands</i> settings.....	54
5.1.1	Simulation Input Data & Equations.....	54
5.1.2	<i>Badlands</i> Simulation Workflow	62
5.2	Sensitivity test and Experimental Design.....	64
5.2.1	Uncertainty Framing.....	64
5.2.2	Reference Case Sensitivity Analysis	65
5.2.3	Experimental Design Analysis (EDA).....	71
5.3	Analysis result and Discussion.....	76
5.3.1	Statistical Analysis Results.....	76
5.3.2	Discussion of Controlling Variables.....	86
Chapter 6. Palaeo-landscape and Best Fit model to Geological history		95
6.1	New Model	95
6.1.1	Early Cretaceous.....	95
6.1.2	Mid-Cretaceous (Cenomanian-Santonian) Emperor Subgroup.....	99
6.1.3	Late Cretaceous (Santonian to Early Campanian) Golden Beach Subgroup.....	107
6.1.4	Middle Campanian to Palaeocene Spreading	109
6.1.5	Eocene Transition Phase.....	111
6.1.6	Oligocene to Recent Post Rift.....	115

6.2	Summary Conclusions from the <i>Badlands</i> Simulation Models.....	119
6.2.1	Tectono-Sedimentary Evolution.....	119
6.2.2	Potential Reservoirs and Source Rocks in the Cretaceous:	120
Chapter 7. Realistic Property Modelling		122
7.1	Latrobe Valley	122
7.1.1	Facies model.....	126
7.1.2	Moisture model.....	129
7.1.3	Carbon model	134
7.2	Entire Gippsland Basin.....	136
7.2.1	Facies model.....	137
7.2.2	Thermal model (Temperature).....	140
7.2.3	Vitrinite reflectance model (Ro).....	144
7.2.4	Pressure model.....	150
7.3	Realistic model input data for Thermal Modelling.....	152
7.3.1	Simple 3D grid.....	152
7.3.2	Facies model.....	153
7.3.3	Total Organic Content (TOC).....	156
7.3.4	Hydrogen Index (HI)	160
Chapter 8. 3D Burial History Model.....		166
8.1	Workflow.....	166
8.2	Geological input settings	167
8.2.1	Erosion events.....	171
8.2.2	Reconstruction of the basin geometry	174
8.2.3	Boundary Conditions: Paleo Water Depth, Interface temperature & Heat flow	175
8.2.4	Lithology/Facies	179

8.2.5	Source-rock properties and kinetics.....	180
8.3	Quality control & thermal calibration.....	182
8.4	<i>PetroMod</i> Modelling Results.....	185
8.4.1	Burial Model.....	186
8.4.2	Temperature Model	188
8.4.3	Reflectance Maturation Model	191
8.4.4	Pressure Model	196
8.4.5	Validating Temperature, Ro and Pressure values in <i>PetroMod</i> using the <i>Petrel</i> Model	200
8.5	Discussion.....	206
8.5.1	Potential Source Rocks.....	206
8.5.2	Tectonic evolution	221
Chapter 9 Discussion		226
9.1	Tectono-Stratigraphic Model.....	226
9.2	Regional Gippsland and Latrobe Valley Models.....	227
9.3	Controls on Basin Sedimentary Evolution	229
9.4	Palaeo-landscape evolution	231
9.5	3D Burial, Pressure and Thermal models	235
9.6	Insights and Suggestions	237
9.6.1	Theoretical modelling guided by empirical data	237
9.6.2	Petroleum Systems	238
9.6.3	Geothermal Energy.....	239
9.6.4	Basin Architecture	240
Chapter 10 Conclusions.....		242
References		243

List of Figures

Figure 1-1 Location and topography-bathymetry of the Gippsland Basin	3
Figure 2-1 Stratigraphy with Spore-Pollen zonations and tectonic phases for Gippsland Basin (Modified from Partridge, 1999; Tosolini et al., 1999; Constantine, 2001; Bernecker & Partridge, 2001; Norvick, 2005; Holdgate et al., 2015). Two syn-rift phases and the Cainozoic compression phase are shown in the right hand column (note timing of rift onset is younger to the east in the Gippsland Basin than further west in the Otway Basin).....	9
Figure 2-2 Cretaceous Strzelecki Group Chronostratigraphy (Constantine, 2001; Holdgate et al., 2015).	12
Figure 2-3 East-west cross-section commencing at the eastern end of the Baragwanath Anticline (Boundary Creek-2) trending west into the Latrobe Valley, northwest over the Glengarry basement block to the Moe basin in the west (Megascolides-1) (Holdgate et al., 2015).	13
Figure 3-1 The study area showing the seismic coverage. Merged 3D seismic survey shows in aqua lines with inline and crossline numbers; other colourful lines are different 2D seismic surveys. The white line is the coastline.....	19
Figure 3-2 Workflow adopted by this research.	21
Figure 3-3 Examples from Petrel structural, stratigraphic model (seismic interpretation, zone property, and surface from structural model).	22
Figure 3-4 The summary process workflow for the Petrel to the PetroMod modelling.	25
Figure 4-1 The velocity domain points coverage at 0Ma (shown as orange dots).	27
Figure 4-2 Key time reconstructions from the GPLates modelling from Early to Late Cretaceous (based on the GPLates model data of Müller et al., 2019). Arrows indicate the tectonic plate velocity fields and the colours relate to the age. Colour dots show the stretching factors coloured as per the legend.	28
Figure 4-3 Key time reconstructions from the GPLates modelling from Palaeocene to Early Eocene (based on the GPLates model data of Müller et al., 2019). Arrows indicate the tectonic plate velocity fields and the colours relate to the age. Colour dots show the stretching factors coloured as per the legend.	28
Figure 4-4 Key time reconstructions from the GPLates modelling from Middle Eocene to Recent (based on the GPLates model data of Müller et al., 2019). Colour dots show the stretching factors coloured as per the legend.	29

Figure 4-5 Crustal thickness of Australian Plate, Gippsland area and surroundings, shown by the global density points. a. crustal thickness at 140 Ma; b. crustal thickness at 99 Ma (Captured from GPlates model, Müller et al., 2019).	30
Figure 4-6 Well panel from Bignose-1 from the eastern part of the offshore basin and Barracouta-1 in the west of the offshore basin showing the substantial facies and log changes in the subcropping units at the Top Latrobe. From left to right: GR, Lithofacies detailed log, Lithofacies blocked layer model property, Palynology zone, DT, NPHI & RHOB, Temperature blocked layer model and data (black dots), Vitrinite reflectance blocked layer model and measured core Ro data (black dots), TOC blocked layer model and RockEval data (black dots), Pressure blocked layer model and Wireline Formation Test Pressure (black dots).	33
Figure 4-7 Merged 3D seismic survey (at Z = -2556) and 2D seismic survey 'gdpi 10' shown in purple lines. The green line shows the coastline.	35
Figure 4-8 Seismic interpretation at Inline-4141 showing interpreted horizons. The Base Cobia pick is not shown as it is close to the Top Latrobe on this section. The red dashed line indicates the probable top Basement.	35
Figure 4-9 Seismic interpretation throughout the 3D volume and the 2D survey on the South Platform, the Bass Canyon and part of the North Platform. Left: top Lakes Entrance Formation; Right: top Latrobe Group.	36
Figure 4-10 a: base Cobia Subgroup map, generated from depth seismic interpretation. b: top Golden Beach Subgroup map, generated from TWT seismic interpretation. The faults are in blue, coastline in black....	36
Figure 4-11 2D map of the GeoVic Gippsland velocity 3D cube survey.	37
Figure 4-12 Interval velocity map for each layer: a. Seafloor; b. top Latrobe; c. top Strzelecki; d. top Basement. The two-way time is used for the visual vertical position.	38
Figure 4-13 Merged Depth maps of major stratigraphic surfaces of the Gippsland Basin. The coastline is shown in blue.	39
Figure 4-14 Interpreted faults, which have been selected and utilised in the structural modelling via the pillar grid method are shown at the merged Top Traralgon Seam - Top Latrobe Group Surface.	40
Figure 4-15 Structural model examples: Strzelecki active faults and top Strzelecki group surface are shown in a 3D window view (a); west-east cross-section through the centre of the basin (b).	42
Figure 4-16 Isopachs for each of the nine stratigraphic zones used in the 3D structural and stratigraphic model.	48
Figure 4-17 NNE-SSW trending section shows the structural style and growth fault that accommodate Emperor Subgroup thickness changes (Power, 2003).	49

Figure 4-18 Latrobe Valley structural model, using the land surface as an example. Wells in yellow, towns in black, locally structures in black. The location of Figure 4-19 is shown as black dash-line.....	51
Figure 4-19 A west-east geological cross-section between Yallourn syncline and Holey Hill anticline (Z Scale: 1:10) shows the geo-unit layers determined by the Latrobe Valley 3D structural model. The section location is shown in Figure 4-18.	51
Figure 5-1 A schematic landscape evolution model shows the main variables and modules simulated in Badlands.	55
Figure 5-2 Flow diagram of the simulation process in Badlands modelling (modified from Salles et al., 2018). SPL = stream power law.	56
Figure 5-3 a: The diagram shows the depression-filling parameter and the maximum fill parameter <fillmax>; b: The parameters of alluvial plain forced deposits; c: Explanation of the marine depositional parameters. (modified from Salles et al., 2019)	61
Figure 5-4 a. Annual median wave height and power in 2003; b. measured wave heights at Kingfish B platform in 2003 (Sustainable Energy Authority , 2004).	62
Figure 5-5 Badlands simulation modelling and analysis workflow.	64
Figure 5-6 Cretaceous Strzelecki Group Chronostratigraphy (Constantine, 2001; Holdgate et al., 2015).	67
Figure 5-7 Simulation results where the input initial topographic map only has mountains to the north and east. The black line shows the present coastline.	67
Figure 5-8 Initial topographic map required to start the simulations of the Gippsland Basin, showing mountains over the entire region, in order to provide sufficient sediment supply to balance the basin fill.	68
Figure 5-9 Simulation results where the input initial topographic map has highlands all around the Strzelecki basin. Two different scenarios are shown in Figures a and b. The black line shows the present coastline.	68
Figure 5-10 Histograms at the present day elevation at (0Ma) for different scenarios. Chart a shows the result of a scenario with thicker uplift isopachs, while chart b shows the result of a scenario with thinner uplift isopachs. Other settings and inputs of these two scenarios are kept the same.	70
Figure 5-11 (a) Maps at 32Ma for two scenarios one run with a low erosion rate and (b) one run with a high erosion rate	71
Figure 5-12 An East-West section comparing the top Basement depth horizons from the Badlands simulations with the realistic structural model showing the range of simulation fits (line of section is shown on Figure 5-13).	75
Figure 5-13 The difference map between the realistic model depth horizon and the equivalent Badlands landscape surface for the Reference Case at top Latrobe Group time. The map covers the area of good	

data control, the white line is the present day coastline and the red dashed line is the location line for the Cross-section shown in Figure 5-12.	76
Figure 5-14 Plot of the absolute Group Means versus the Group Standard Deviations calculated from the difference maps for top Basement horizon to the Topography horizon for all 22 scenarios.	78
Figure 5-15 Mean of the difference Map at selected horizons or time periods for each scenario. The series correspond to each of the scenarios and the green dotted line is the Reference Case.	78
Figure 5-16 Response for Mean Sum absolute Differences of Scenario Maps from Realistic Model over top Basement to top Latrobe horizons (a) Cumulative Frequency Probability plot of response equation fit to the 22 scenarios. (b) Tornado chart showing co-efficients in response equation for each variable ranked according to t-significance value (smallest values are the most significant).	79
Figure 5-17 Comparison of a preliminary Tornado chart (top) with the Tornado chart for the Reference Case (bottom).	80
Figure 5-18 Absolute mean of cumulative erosion versus time for 23 scenarios (extracted at 17 Ma time steps).	82
Figure 5-19 Cumulative Deposition versus time for 23 scenarios (extracted at 17 Ma time steps).	82
Figure 5-20 Accumulative probability curve of the deposition rate during 102-68Ma and 67-0Ma ranges. The reference case is marked as different colour.	83
Figure 5-21 Tornado charts showing co-efficients in response equations for each variable ranked according to t-significance value (smallest values are the most significant). Note the second order effect of Sea Level Curve is highly significant whereas the first order linear effect is of low significance.	85
Figure 5-22 Fluvial system of two different scenarios: (a) scenario 1, low rainfall; (b) scenario 3, high rainfall.	89
Figure 5-23 Four extreme scenarios selected by their resulting mountain height at 0Ma to show the effects of m, erodibility, rainfall and onshore sediment flux: (a) high initial topography with high erosion in scenario 3 (a) and scenario 20 (b); versus low initial topography with low erosion in scenario 6 (c) and scenario 18 (d).	91
Figure 6-1 Cretaceous Strzelecki Group Chronostratigraphy (modified from Constantine, 2001; Holdgate et al., 2015).	96
Figure 6-2 Aptian to Albian: a. Gippsland Basin begins to form with intracratonic non-marine deposition and drainage to the West; b. the rivers stabilise in the Gippsland Basin while lacustrine to shallow marine sedimentation develops in Bass Strait. The brown line shows the zero contour. The black line is present coastline.	97
Figure 6-3 a. A flood plain begins in the western edge of the basin by the end of Albian. B. Fluvio-deltaic sediments build into a very shallow inland sea in the Cenomanian. The brown line shows the zero	

contour, the yellow locations mark the sites of marine fossils (see also Figure 6-4). The black line is present coastline.	98
Figure 6-4 Early Cretaceous tetrapod sites, and associated biota (modified Dettmann & Douglas, 1988 and Kear 2006). Red circles highlight the plesiosaur remains locations: Inverloch, Cape Paterson, and Cape Otway.	98
Figure 6-5 Box-plots for the Mid Cretaceous uplift map (mean 477m, median 354m, P75 910m, P25 70m, minimum 0m, maximum 1027m) and for the Late Cretaceous uplift map (mean 349m, median 260m, P75 522m, P25 253m, minimum 0m, maximum 926m)	101
Figure 6-6 a. The inland sea closed by the Early Cenomanian, and the east-west fluvial system became dominate again in the entire Gippsland Basin; b. Multiple small lakes begin to occur in Central Deep area; the highlands arise in the north, due to the uplift. The brown line shows the zero contour. The black line is present coastline.	101
Figure 6-7 In Turonian time, lacustrine-fluvial dominated palaeo-environment appeared again in the Gippsland Basin. The result of the Mid Cretaceous uplift is the drainage direction starts to change. The brown line shows the zero contour. The black line is present coastline.....	103
Figure 6-8 Cross-sections through Reference Case simulation with vertical exaggeration $Z = 1:4$. Composite section SW-NE Bream-2 to Marlin-1, then NW-SE Flounder-1 to Blackback-1. Upper cross-section coloured by 1Ma layers (white zone highlights 94 - 89 Ma). Middle section coloured by thickness to indicate sediment deposition per time step. Lower cross-section is coloured by palaeo-elevation to demonstrate the relative water depth and facies in each tectonic phase.....	106
Figure 6-9 Badlands simulated palaeo-landscape result of the best fit model, extract at 94, 93, 90 and 89Ma.	107
Figure 6-10 Palaeo-landscape at 86Ma and 85Ma. a. Pre-breakup time, most of the Gippsland Basin is terrestrial, an inland lake appears first, the sedimentary transport direction changes from west to east. b. Tasman Sea opening, a restricted shallow marine environment develops in offshore Gippsland Basin. The brown line shows the zero contour. The black line is present coastline.....	108
Figure 6-11 The simulations around 83~79 Ma show deposition of fluvio-deltaic sediments in the Central Deep passing into restricted shallow marine sediments (Anemone Formation). The brown line shows the zero contour. The black line is present coastline.....	108
Figure 6-12 Badlands model simulations in the Middle Campanian (T.lilliei).....	109
Figure 6-13 Badlands model simulations in the Maastrichtian. Initial regression produced a widespread flat floodplain with an open marine strandline in place by at least 74Ma (a), followed by marine transgressions towards the West around 72Ma (b); continuing through 69Ma where Blackback and Madfish lie on the coastal plain with less than 30m elevation (c); to 65Ma where Blackback, Madfish and	

Whaleshark are inundated by shallow marine sediments (d). The pink, brown, orange and blue lines represent contours at 50m, 0, -50m, -100m. The black line is present coastline.....	110
Figure 6-14 The 54, 51 and 45 Ma topographic simulations fit well with Johnstone et al. (2001) tectonostratigraphic development study of Eocene age. The brown, orange and blue lines represent contours at 0, -50m, -100m separately. The black line is present coastline.	114
Figure 6-15 Badlands simulation at 37 and 35Ma, showing the marine incursion extent. The brown, orange and blue lines represent contours at 0, -50m, -100m separately. The black line is present coastline.	114
Figure 6-16 Palaeo-topography near top Latrobe Group at 33 Ma. a. at 33Ma, the fluvial-deltaic sediments were transgressed into the Seaspray Depression; b. at 31Ma, a shoreline regression is modelled. The brown, orange and blue lines represent contours at 0, -50m, -100m separately. The black line is present coastline.....	116
Figure 6-17 Palaeo-landscapes at 26Ma and 5Ma when the main regression occurred.	116
Figure 6-18 Present Day simulated topography and bathymetry after 137 Myers of simulation. The brown, orange, blue and yellow lines represent contours at 0, -50m, -100m and -3500m separately. The black line is present coastline.....	117
Figure 6-19 NE-SW cross-section through Marlin-1 and Bream-2. a. cross-section through Badlands model, coloured by sediments thickness per 1Ma time steps, at 1:4 ratio; b. two-way time 3D seismic data at 1:5 ratio.....	118
Figure 6-20 Depth maps from Badlands best fit model compared with Petrel structural model.....	118
Figure 7-1 Latrobe Valley structural model, 2D land surface as an example (top). Wells in yellow, towns in black. Faults in black. 3D View at top Morwell 2 Seam, faults in white (bottom).	123
Figure 7-2 Three cross-sections through the Latrobe Valley 3D structural model. AA': E-W section from Yallourn syncline to Holey Hill anticline (Z Scale: 1:10); BB': N-S then E-W section from Morwell monocline (Yallourn Power-1) south to Traralgon syncline (H1333 bore), then east over Loy Yang Dome to Holey Hill Anticline (Z Scale: 1:9); CC': W-E section from Yallourn Open Cut to Rosedale (Z Scale: 1:10). See Figure 4-18 for the location of section lines.....	125
Figure 7-3 The extent of Yallourn Seam in the Latrobe Valley, background surface is top Strzelecki Group	126
Figure 7-4 The extent of Morwell 1A and 1B Seams in the Latrobe Valley, background surface is top Strzelecki Group.....	127
Figure 7-5 The extent of Morwell 2 and Traralgon Seams in the Latrobe Valley, background surface is top Strzelecki Group.....	128

Figure 7-6 N-S then E-W section from the Morwell monocline (Yallourn Power-1) south into Traralgon syncline (H1333 bore), then east over the Loy Yang Dome to Holey Hill Anticline, showing the facies model in the Latrobe Valley 3D model. See Figure 4-18 for the location of the section line.....	129
Figure 7-7 Latrobe Valley Moisture model map view. The red dash line shows the location of Figure 7-8.	130
Figure 7-8 Top: Moisture property on an East-west geological cross-section from Yallourn Fault to Baragwanath anticline. The moisture of interseam beds is set as undefined. Bottom: the corresponding stratigraphy in the Latrobe Valley 3D structural model. Cross-section location marked in Figure 7-7...	132
Figure 7-9 Histogram of Moisture values in the Latrobe Valle.....	133
Figure 7-10 A cross-section shows the moisture content change across the fault (Top) and the same section dated on top M2A seam to show approximate reconstruction. See the location in Figure 7-7.....	134
Figure 7-11 Maps of Carbon % for each coal seam from the Latrobe Valley Carbon model. The inset graph is the Carbon histogram for the same seam showing the gross mean value.	136
Figure 7-12 West-east geological cross-section between Yallourn Fault and Baragwanath anticline showing the coal carbon as determined from the Latrobe Valley 3D carbon property model. For the location of the cross-section, see Figure 7-7.	136
Figure 7-13 Wells with a Lithofacies log used to build the facies model. Background surface is top Traralgon Formation – top Latrobe group, dark blue line is coastline. Blue lines are the location of sections in Figure 7-14.....	138
Figure 7-14 Two cross-sections of the facies model (see Figure 7-13 for location). a: southwest-northeast geological cross-section through South Platform (Groper), South Terrace, Central Deep (Veilfin, Cod), North terrace (Sunfish) to North Platform (Baleen); b: southwest-southeast cross-section from Churchill north (Hazelwood) trending northeast into the Latrobe Valley, northwest over the Rosedale area, through the Lake Wellington Depression and Central Deep (Barracouta, Veilfin) to the southeast (Mackerel). .	139
Figure 7-15 a: Traralgon formation Eocene total coal seam extent from full Gippsland Basin facies model; b: Palaeocene- early Eocene total coal seam extent.	140
Figure 7-16 Wells with Temperature logs used to build the Temperature model. Background surface is top Traralgon Formation – top Latrobe group, dark blue line is coastline. Blue lines are the location of sections given in Figure 7-17.	141
Figure 7-17 Two cross-sections of the Temperature property model. a: SSW-NNE geological cross-section through South Platform, South Terrace, Central Deep (Bream, Cod), North terrace to North Platform; b: west-east cross-section from the Latrobe Valley (Loy Yang), through the Seaspray Depression (Burong) to the Central Deep (Swordfish, Pilotfish) in the east. See Figure 7-16 for the location of section lines.	142

Figure 7-18 a: Thermal Gradient map, calculated from topography-bathymetry to top Strzelecki group; b: Thickness map, calculated from topography-bathymetry to top Strzelecki group. The area without data control has been removed.....	144
Figure 7-19 Wells with vitrinite reflectance data used to build the vitrinite reflectance model. Background surface is top Traralgon Formation – top Latrobe group, dark blue line is coastline. Light blue lines are the cross-section locations in Figure 7-20.....	145
Figure 7-20 Two cross-sections show the Vitrinite reflectance (Ro) property model variation with depth. a: SSW-NNE geological cross-section through South Platform, South Terrace (Moray), Central Deep (Bonita, Mackerel), North Terrace (Kipper, Admiral) to North Platform; b: west-east cross-section from the Latrobe Valley, through Seaspray Depression (North Seaspray) to the Central Deep (Veilfin, Drummer) in the east. See Figure 7-19 for the location of section lines.....	146
Figure 7-21 Shark-1 vitrinite reflectance values from core samples. Blue dashed line shows the Ro trend.	147
Figure 7-22 Two cross-sections showing Reflectance Gradient with Depth Ro/Z property model. a: SSW-NNE geological cross-section through South Platform, South Terrace (Moray), Central Deep (Bonita, Mackerel), North terrace (Kipper, Admiral) to North Platform; b: west-east cross-section from the Latrobe Valley, through Seaspray Depression (North Seaspray) to the Central Deep (Veilfin, Drummer) in the east. See Figure 7-19 for the location of section lines.....	148
Figure 7-23 Vitrinite reflectance value extracted at top Halibut subgroup, central deep, north and south terraces showing that Ro is not related to the age of the sample (ie. Time).....	149
Figure 7-24 Burial plots of well Bream-5 and Omeo-1, extracted from 3D burial and thermal model (See Chapter 8).....	149
Figure 7-25 Vitrinite reflectance vs Depth chart: a. Whiting-2 (Bostwick, 1986); b. Bream field (Lindsay & Djakic, 1985). The red symbol highlights the outliers of Ro, which are produced by the intrusion.....	150
Figure 7-26 Wells with pressure log, which have been used to build the pressure model. Background surface is top Traralgon Formation – top Latrobe group, dark blue line is coastline. Light blue lines are the location of Figure 7-27.....	151
Figure 7-27 Two cross-sections showing the Pressure property model. a: SSW-NNE geological cross-section through South Platform, South Terrace(Pike), Central Deep (Kingfish, Marlin), North Terrace(Baleen) to North Platform; b: west-east cross-section from the Latrobe Valley (Hazelwood), through the Seaspray Depression (Wombat) to the Central Deep (Luderick, Gudgeon) in the east. See Figure 7-26 Figure 7-16 for the location of section lines.	152
Figure 7-28. The refined lithofacies property model for the entire Gippsland Basin.....	154

Figure 7-29 A cross-section reveals the facies property through the basin from WNW-ESE direction and crosses Strzelecki Mountains, Latrobe Valley, near shore, broad offshore and Bass Canyon. Location shows in Figure 7-28.	155
Figure 7-30 A cross-section reveals the facies property through the basin from SW-NE direction and crosses South Platform, South Terrace, Central Deep, North Terrace and North Platform. Location shows in Figure 7-28.	155
Figure 7-31 A cross-section showing the TOC value, same section as Figure 7-29. Location shows in Figure 7-28.	157
Figure 7-32 Hydrocarbon Potential plots of S2 versus Total Organic Carbon from RockEval analyses for the main stratigraphic zones. Note, the very different amounts of organic matter in the coals relative to the shales requires use of different scales for the three main stratigraphic sub-groups	160
Figure 7-33 A cross-section shows the HI value, exact location as Figure 7-29. Location shows in Figure 7-28.	161
Figure 7-34 Plot of HI versus OI values for samples from the main geo-zones in the Gippsland Basin.	163
Figure 7-35 Histogram of HI for each lithofacies in the main geo-zones. The green, yellow, and red dashed lines represent the HI value of 50, 250 and 600 mgHC/gTOC.	165
Figure 8-1 The summary process workflow for the Petrel to the PetroMod modelling.	167
Figure 8-2 The locations of 1D and 2D burial-thermal models and related wells. The wells used to build the 1D models are coloured in orange, and the lines used to build the 2D model are coloured in purple.	168
Figure 8-3 Uninterpreted (top) and Interpreted (bottom) southwest-northeast seismic profile in the Gippsland Basin showing the structure with formations and faults. See the location in Figure 8-2. The top Basement surface is modified from the OZSEEBASE Interpreted Gravity map.	169
Figure 8-4 The temperature calibrations from the 1D models indicate that modelled temperature trends are much lower than the measured data.	170
Figure 8-5 The temperature calibrations from 2D models indicate that modelled temperature trends start to provide better matches to the measured data.	170
Figure 8-6 The 2D model results: the calculated heat flow trend at Bream-5 (top); the vitrinite reflectance calibrations at Bream-5, Angelfish-1 and Veilfin-1 (bottom).	171
Figure 8-7 Composite diagram illustrating stratal erosion amount using vitrinite reflectance data in Petrel.	173
Figure 8-8 a: The total erosion amount of seven erosion events; b: Erosion map simulating the Otway Unconformity at ca. 99Ma. See Appendix 13 for the erosion maps at the other unconformities.	173
Figure 8-9 The simulated best fit palaeo-landscape of the Gippsland Basin, at 33, 32 and 31Ma.	174

Figure 8-10 A seismic cross-section indicates the canyon systems formed at different ages: mid Miocene canyon (1) and Early Oligocene canyon (2). The mid Miocene surface is coloured in blue and top Latrobe surface is coloured in red.....	174
Figure 8-11 (a) Mid-Miocene and Early Oligocene structural maps coloured with the corresponding erosion amount. The green dashed-line highlights the mid-Miocene canyon system. (b) the Early Oligocene canyon system is marked with a red dash line.	174
Figure 8-12 The 3D model illustrating the present-day geometry with faults in black, orange arrow points to the north, vertical scale in metres and horizontal scale in km.	175
Figure 8-13 Calculated heat flow maps for the entire Gippsland Basin.	179
Figure 8-14 Clipped 3D facies model in PetroMod, exported from Petrel facies property model (see Chapter 7).....	179
Figure 8-15 The maturity and kerogen type plot of source rock in different subgroups: Cobia & Halibut, Golden Beach, and Emperor Subgroups.	181
Figure 8-16 Total organic carbon (TOC) (top) and hydrogen index(HI) (bottom) for the source rock units assigned in the PetroMod 3D model.	182
Figure 8-17 Map showing locations for wells used as examples of model fits in Figure 8-18. Red lines show locations of Figure 8-23, Figure 8-38.....	183
Figure 8-18 Comparison of modelled temperature and vitrinite reflectance trends (lines) and measured data (crosses). The trends are extracted at corresponding wells from the 3D burial-thermal model. The selected wells are highlighted in red in Figure 8-17, while the wells shown in black are given in Appendix 14..	185
Figure 8-19 Pressure depth calibration between the 3D PetroMod model and measured well data; example wells are Bream-5, Angelfish-1 and Archer-1.	185
Figure 8-20 Burial history plots extracted from the 3D model at inshore area (Barracouta-1), Central Deep (Veilfin-1), shelf edge (Mackerel-1) and Terrace (Omeo-1).....	188
Figure 8-21 3D present-day temperature model clipped across the maximum temperature area.	189
Figure 8-22 Burial-thermal history plots extracted from the 3D model at Angelfish-1, Veilfin-1 and Mackerel-1 showing the modelled temperature overlay. The circled numbers mark the regional unconformities: Otway, North Longtom, Seahorse and Marlin unconformities.	190
Figure 8-23 Cross-sections are showing the modelled thermomaturity at present-day. Locations are shown in Figure 8-17.	192
Figure 8-24 Burial-thermal history extracted from the 3D model at well Mackerel-1, Marlin-1, Barracouta-1 and Perch-1 (from top to bottom), overlay with Ro. The circled numbers marked the regional unconformities: Otway, North Longtom, Seahorse and Marlin unconformities.	196

Figure 8-25 3D present-day pressure models: hydrostatic pressure (top) and lithostatic pressure (bottom), with the southern part of the 3D volume clipped to show an axial section through the maximum pressure area.	198
Figure 8-26 Simulated 3D overpressure model, shown on depth slices at -4600m, -4000m and 3600m.	199
Figure 8-27 Pressure plot extracted from the 3D burial model for Kipper-2 showing the match to the measured pressure data. The overpressure is associated with volcanic intervals.	200
Figure 8-28 E-W and NNE-SSW sections comparing the Petrel temperature model (a top) and the PetroMod temperature model (b bottom).	201
Figure 8-29 NNE-SSW sections through Archer-1, Selene-1 and Blackback-1 comparing the Petrel model (a) and the PetroMod model (b) at the shelf edge of the Central Deep. c: The temperature calibration extracted from the PetroMod theoretical 3D model at well Archer-1. The marked horizons are the same as in Figure 8-28.	201
Figure 8-30 The comparison of modelled Ro results between Petrel realistic model (a & c) and PetroMod theoretical model (b & d). The results are extracted from the same cross-section locations, shows in Figure 8-17.	203
Figure 8-31 Maps showing difference between Ro in Petrel and PetroMod models at Top Traralgon Seam- Top Latrobe, Base Palaeocene, Top Emperor Subgroup.	203
Figure 8-32 The maturation phase comparison between the 3D realistic Petrel model (a & b) and the PetroMod forward model.	204
Figure 8-33 Temperature calibration plot extracted at well Archer-1. Blue dash line is the initial model using a 2.4 km erosion amount; the red is the modelled curve using a 5 km erosion amount.	205
Figure 8-34 Left: the temperature calibration plot extracted at well Archer-1. Right: the vitrinite reflectance calibration plot extract at Shark-1. The blue dash-line is the initial model using continental granite crust, while the pink line is the modelled curve using continental average crust. Crosses denote the measured data.	205
Figure 8-35 The pressure model compares the Petrel property model (a, b) and the PetroMod burial-thermal model (c, d) using SSW-NNE and west-east cross-sections.	206
Figure 8-36 Palaeo-landscape of the Gippsland Basin at 93 Ma, 84 Ma and 65 Ma (Appendix 7).	207
Figure 8-37 Clipped 3D model in PetroMod, the Latrobe Group, coloured by TR and the Seaspray and Strzelecki Groups are coloured by the age of deposition.	209
Figure 8-38 Cross-sections demonstrate the modelled organic transformation (TR) at present-day. Locations are shown in Figure 8-17.	211

Figure 8-39 The Organic Transformation ratio (TR, %) plots extracted at Angelfish-1, Veilfin-1, Barracouta-1 and Luderick-1.	214
Figure 8-40 Organic transformation ratio (TR) maps of Golden Beach Subgroup and lower Halibut Subgroup source rocks at 30 Ma, 15 Ma and 0 Ma.	220
Figure 8-41 The calculated heat flow trends extracted at Pike-1, Snapper-1 and Tuna-1, the dashed lines mark the approximated end time for each of the two syn-rifts.....	223
Figure 8-42 Maps of Crust and Mantle stretching factors for the two rift phases.....	224
Figure 8-43 Reconstruction model from GPlates showing the three-arm rifting style of the first rift event (a) and the second rift event (b). The red lines indicate the two successful rift arms, and the orange line shows the failed rif arm.	224
Figure 8-44 a: Top Basement structural map; b: Top Strzelecki Group structural map. The red line marks the southern boundary of the depocenter which shifts to the north from the Otway rift to the Tasman rift. .	225
• Figure 1 Structural modelling (pillar gridding), boundary, faults and trends are shown in a 2D window view.	272
• Figure 2 Settings for Horizon in 'Make horizon' process, entire Gippsland model.....	272
• Figure 3 Zone division of each zone, entire Gippsland model.....	272

List of Tables

Table 4-1 Palynology data from multiple offshore and onshore wells indicating the regional unconformity between the Strzelecki Group and Latrobe Group	32
Table 4-2 Seismic horizons with the corresponding well tops and approximate age.....	36
Table 4-3 Horizons and Zones used in the Basinwide Petrel model	38
Table 4-4 Input settings for Horizon in 'Make horizon' process, Latrobe Valley model.....	51
Table 5-1 The input isopachs of major geo-units with the corresponding approximate time period, biostratigraphy and boundary surfaces (NB surfaces are in part diachronous).....	58
Table 5-2 Typical values of Erodibility k, m, n and m/n from previous published studies.....	59
Table 5-3 Uncertainty framework showing the main identified uncertainties and ranges. * Ref Case isopachs are from the 3D realistic model, the High Case isopachs are thicker to account for potential errors including from the velocity model.	65
Table 5-4 Design size sensitivity, total number of scenarios depends on number of factors and number of settings for each factor.	72
Table 5-5 The input variables, their tested levels and their interactions used as input to GSAT.	73
Table 5-6 Experimental design for Gippsland Basin scenarios.....	73
Table 5-7 The significance of each Variable and the main Interactions between different map levels: top Basement to top Strzelecki Group (Basement-Strzelecki); top Strzelecki Group to Base Palaeocene (Strzelecki -KT); Base Palaeocene to top Latrobe Group (KT-Latrobe); entire Latrobe Group and entire Seaspray Group.	81
Table 5-8 Response equations for Deposition Rate between 102-68Ma and 67-0Ma including: co-efficients for each variable, equivalent absolute values, t-value (probability variable is not significant; ns = not significant).....	84
Table 5-9 Comparison of settings for Scenarios 4 and 10.....	86
Table 5-10 The significance results from the ANOVA for top Basement to top Latrobe level. The analysed response is the sum of the absolute means for each of the difference maps. The significance levels indicate the probability that the variable is not significant (low values are most significant).....	88
Table 5-11 Scenarios separated into two groups based on discharge level.....	89
Table 5-12 Extreme scenarios showing how erosion rate is controlled mainly by exponent m (for Rainfall*Area) and Erodibility.....	90

Table 6-1 Scenario outcomes according to time at which palaeocurrent flips from westward to eastward in the Gippsland Basin. The best fit models are highlighted in yellow, early flip models in blue, and poorly fitting models are shown in red.	103
Table 7-1 Mean Vitrinite Reflectance (Ro) values calculated in different areas for stratigraphic zones.	147
Table 7-2 The Rock-Eval interpretation of the Emperor Subgroup Shale sample	162
Table 8-1 Physical parameters of the sedimentary rocks used in the 3D model (PetroMod default parameters).	180
Table 8-2 Kinetic data of source rock units	181

Chapter 1. Introduction

Palaeo-landscape studies and burial and thermal history analysis are useful ways to investigate the geological history of a sedimentary basin. Palaeo-landscape studies are important to better understand land surface processes, climate change, environmental science and their geological applications. They can guide exploration to locate potential organic-rich rocks, mineral occurrences, aquifers or reservoirs, seals and traps. Burial and thermal history analysis simulates organic and petrological changes, recording the palaeo-temperature, pressure, basin maturation and fluid migration. Understanding temperature and pressure changes with depth and facies through time from basin initiation to the present has many practical applications for exploration, development and production, including maturation of source rock, migration of charge, reservoir preservation, drilling hazards and aquifer support during production.

In the past 20-30 years, numerous software platforms have been written to simulate basin-fill processes with varying degrees of constraint to real field data that allow researchers to build and test models in a more efficient way, for example: *Badlands* (Salles & Hardiman, 2016); *DionisosFlow* (Granjeon et al., 2018); *SedSim* (Griffiths et al., 2001) and *PetroMod* (Schlumberger). However, these simulation programs mainly rely on deterministic physical equations mostly developed from a theoretical basis (e.g., fluid flow, gravity). Few studies use these simulation programs with a rigorous Experimental Design (ED) to statistically test a range for each variable (Smith et al., 2004; Montgomery, 2017). Furthermore, reconstruction of the palaeo-landscape or burial and thermal history of a basin requires a good understanding and simulation of the basin evolution, which is a complicated process controlled and affected by multiple variables, including tectonics, paleo-environment, rates of erosion, rainfall, sea-level change, sediment type, etc. It is essential to understand the relationship between these variables and the basin evolution process and the interactions between the variables, which often have a more pronounced effect than the individual variables on their own. Hence, a realistic 3D structural and stratigraphic model populated with different lithological and physical properties can provide an ideal starting point for both palaeo-landscape reconstruction and burial and thermal history analysis constrained by empirical data.

Given a large number of possible variables and the difficulty of measuring interactions, this makes estimation of the importance of each variable challenging. Complex numerical simulation and advanced statistical analysis methods are required to solve this problem. Modern numerical simulation software allows many scenarios to be rapidly built but it is not obvious which are valid or good fits to field data. This needs to be coupled with properly designed experiments and statistical analysis to guide the scenario set-up, process the numerical simulation results of the palaeo-landscapes, and generate the multi-variate equations that define and identify the important controlling variables.

This approach has been applied here to the Gippsland Basin, one of the leading petroleum, coal and agricultural basins in Australia, containing giant oil and gas fields, enormous reserves of brown coal, and substantial water and agricultural resources Figure 1-1. It is a young multi-phase rift basin developed on a divergent margin located in South-Eastern Australia and consists of a large volume of sediment from Early Cretaceous to Recent. Petroleum, coal and water exploration and development in Gippsland have provided abundant geological data which makes it ideal for such a study, including: 3D and 2D seismic and gravity data; plus downhole log, analytical and biostratigraphic data, sourced from the onshore coal and water bores and the onshore and offshore petroleum wells.

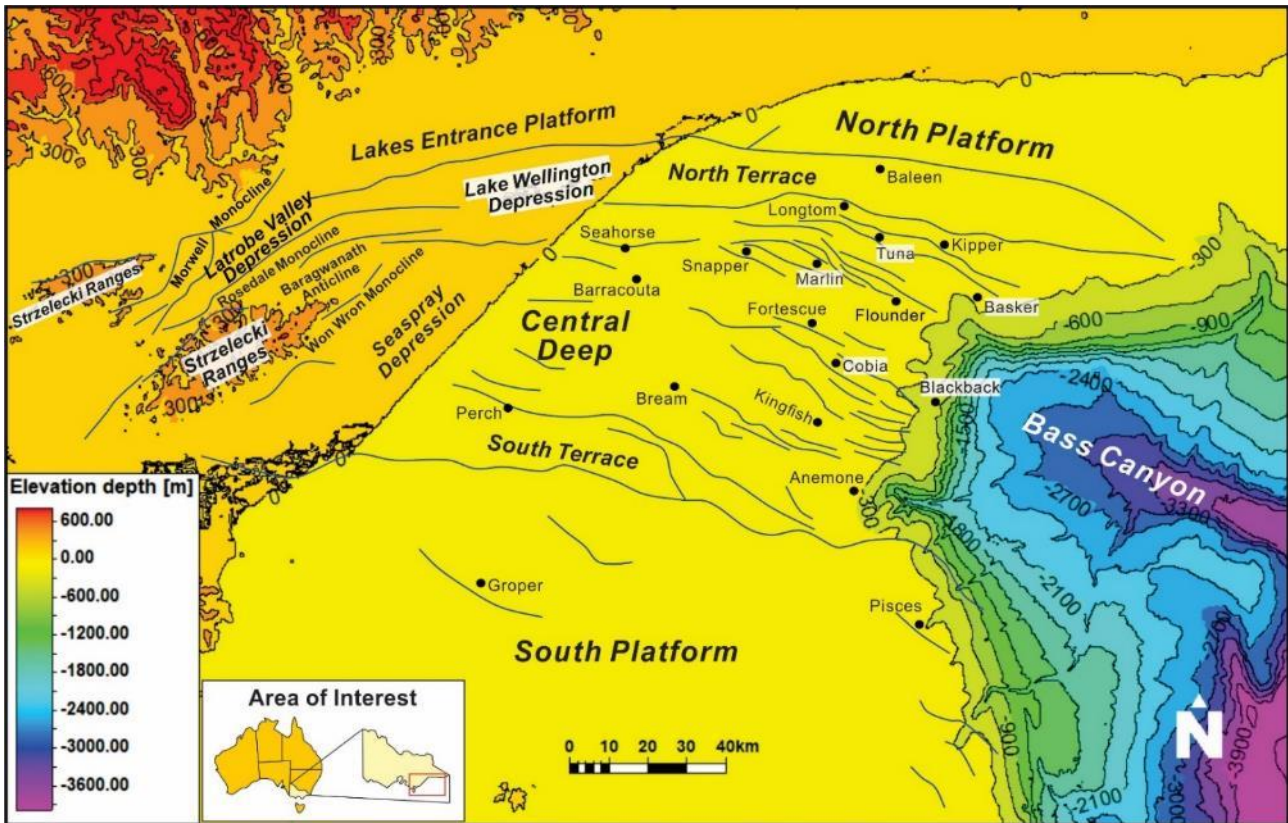


Figure 1-1 Location and topography-bathymetry of the Gippsland Basin

1.1 Existing Models in the Gippsland Basin

There are many tectonic, stratigraphic or palaeo-environmental conceptual models that have been proposed for the Gippsland Basin since the 1980s. Some researchers focus on the Palaeocene, Eocene and Miocene periods and proposed palaeo-geographic interpretations and palaeo-facies models for this part of the basin history (Blake, 1986; Rahmanian et al., 1990; Gallagher et al., 2001; Johnstone et al., 2001 and Root et al., 2004). Some are interested more in the Cretaceous sedimentation and corresponding depositional environments (Tosolini et al., 1999; Constantine, 2001; Bernecker and Partridge, 2001; Riordan et al., 2004; Holdgate, 2005 and Aghaei et al., 2017). There are a few studies that reconstruct the geo-history from the Late Cretaceous to the Cenozoic (Smith, 1982; Bodard et al., 1986; Liu et al., 1994; Norvick, 2005). The regional tectonics and basin-scale structural evolution have been studied by Gleadow and Duddy (1981), Duddy and Green (1992), Willcox et al. (1992, 2001), Bryan et al. (1997), Norvick and Smith (2001), Norvick et al. (2001), Power (2003), Czarnota et al. (2014), Aghaei et al. (2015), Mahon and Wallace (2020), using various methods including fission-track, mineral chemistry analysis, seismic interpretations

and well log correlation. Smith (1982), Cull and Beardsmore (1992), and Harrison et al. (2012) estimated present-day heat flow data and proposed geothermal gradients in parts of the basin.

Some of the models focused on a large area which includes multiple oil/gas fields, while some models were generated over a single field. These models are relatively localised and mainly emphasise various stages of the tectonostratigraphic development of the basin. Some tectonic studies at the plate/craton scale provide good regional tectonic reconstructions, but it is hard for these models to capture the detailed features within the basin at such a coarse resolution.

Researchers began to analyse and build burial thermal models for the Gippsland Basin since the early 1980s (Smith & Cook, 1984; Hegarty et al., 1985; Alexander et al., 1991; Featherstone et al., 1991; Moore et al., 1992; Harrison et al., 2012; Röth et al., 2021). However, most burial thermal models are 1D only and the 3D model of Röth et al. (2021) used only one simplified rift phase confined to the offshore area and consequently doesn't fit the measured thermal data.

1.2 Previous Landscape Evolution and Basin-Fill Studies

The controls on landscape evolution and basin-fill have been debated for a long time in both the geologic and physical geography disciplines. There are many controversial and unresolved issues, different approaches and objectives that have impeded progress. Many earth scientists have collected field data for landscape evolution and basin-fill studies (Howard & Kerby, 1983; Seidl et al., 1992; Young & McDougall, 1993; Seidl et al., 1994; Hallet et al., 1996; Stock & Montgomery, 1999; Debnath et al., 2007; Perron et al., 2009; Hobbey et al., 2011; Ferrier et al., 2013; Murphy et al., 2016; Shobe et al., 2017). Mostly they have measured different variables that are specific to the studied region, and either derived best-fit equations for that dataset or have used existing general equations with previously derived constants to help fit their models. In these cases, the results are not generally applicable because each proposed model equation fits well with the specific dataset, but it is either hard to use the data in a different basin or with different model equations. This also reduces the ability to identify the dominant variables that control landscape development, and their use in the more difficult task of modelling landscape evolution through deep time over many millions of years, and for an entire basin. Brewer et al. (2020) compared the different methods to estimate sediment fluxes in ancient sediment routing systems and found that

different models were sensitive to different parameters, and this generates significant inherent uncertainty. In addition, most landscape researchers are primarily interested in modelling present-day landscape evolution and detailed stream behaviour (Perron et al., 2009; Salles et al., 2011; Shobe et al., 2017). Geologists are mostly interested in longer-term deep time basin-wide development.

1.3 Research Aims

The aim of the project is to develop an overall model for the sedimentary, burial, thermal and tectonic history of the Gippsland Basin, by using actual realistic 3D models of the basin made in *Petrel* (Schlumberger) software, to constrain theoretical deterministic 3D models made in *Badlands* and *PetroMod*. The *Badlands* simulations aim to model both the landscape evolution and its evolution over deep time for an entire basin. The *PetroMod* modelling aims to assess the relationships between Temperature-Pressure-time by tracking the changes with sedimentary and burial history, and measuring effects on temperature, vitrinite reflectance, pressure, and organic matter transformation ratio in the Gippsland Basin. An experimental design was used to test and identify the critical controlling variables and their possible ranges for the *Badlands* simulation, and to produce the associated statistical equations.

In summary this involved:

- *Petrel* software: build realistic 3D structural, stratigraphic and property models for both the Latrobe Valley and the entire Gippsland Basin, using empirical data (seismic, well logs, palynology, Petrophysical logs, downhole pressures, etc). Preparation of input data for the theoretical modelling, such as isopach maps, erosion maps, lithological or facies models and Petrophysical property models etc.
- Experimental Design Analysis: generate uncertainty matrix for *Badlands* simulations to minimise the essential scenario runs; identify and evaluate the main controlling variables for basin development.

- *Badlands* software: generate 3D forward Palaeo-landscape models based on empirical data and experimental design matrix, reconstruct the entire tectono-stratigraphic evolution history of the basin.
- *PetroMod* software: build 3D burial and thermal models of the entire basin constrained by input data from the realistic model to reconstruct the burial and thermal history; evaluate the potential source rock intervals and assess the basin tectonic history by fitting the burial history and heat flow.
- Synthesize the above models to better understand the overall geological history of the Gippsland Basin. Secondly, to identify those elements of the above that can be related to rift and post-rift phases and potentially used to better understand and assess existing general rift basin models.

Chapter 2. Regional Geology

2.1 Tectonic Background

The Gippsland Basin is located in south-eastern Australia and covers approximately 46,000 Km², of which the offshore area occupies about two-thirds of the Basin (Gippsland Basin, 2021) (Figure 1-1). It was initiated during the latest Jurassic/Early Cretaceous as part of the lithospheric extension between Australia and Antarctica (Smith, 1982; Duddy and Green, 1992; Willcox et al., 1992, 2001; Norvick and Smith, 2001; Norvick et al., 2001; Aghaei et al., 2015 and Gippsland Basin, 2021). The approximately east-west rifting between Australia and Antarctica started with the development of half grabens further west in the Bight and Otway Basins during the latest Jurassic, with the rifting moving eastwards with time into the Gippsland and Bass Basins.

The main structural elements of the Gippsland Basin are shown in Figure 1-1. The offshore area is dominated by the Central Deep which is bounded by the Lake Wellington and Rosedale Fault systems on the north and by the Foster and Darriman Fault systems along the southern margin (Bernecker and Partridge, 2001; Aghaei et al., 2015). The onshore area comprises the Strzelecki Ranges which outcrop within and are overlapped by the younger sediments that occur in several structural depressions. The Basin as a whole is flanked by highlands that have been subject to substantial uplift, thereby providing significant sediment supply (Czarnota et al., 2014).

The oldest syn-rift sediments in the adjacent Otway Basin are the latest Tithonian Casterton Beds at the base of the Otway Group (*R. watharoonensis* spore pollen zone). In the Gippsland Basin the oldest units are volcanics found only in the Duck Bay-1 well interpreted to be latest Tithonian (*R. watharoonensis* spore pollen zone; Constantine, 2001). The volcanics sit unconformably on Permian basement, are correlatives of the Casterton Beds in the Otway Basin, and are unconformably overlain by the Strzelecki Group sediments.

Several basin-wide depositional sequences (Figure 2-1) record the tectonic evolution of the Gippsland Basin from the latest Jurassic to Recent (Bernecker and Partridge, 2001; Gippsland Basin, 2021). The Basin experienced two main rift events which are related to continental breakup of south-eastern Australia (Smith, 1982; Norvick and Smith, 2001). The first rift phase occurred in the latest Jurassic to Early Cretaceous controlled by the NNE-SSW separation of Australia and

Antarctica. The Strzelecki Group records this phase but is deeply buried except onshore, and most wells do not reach this section except on the basin margins (e.g., Northern and Southern Terraces, the Seaspray Depression, Lakes Entrance Platform and Latrobe Valley Depression). According to Tosolini et al. (1999) and Holdgate et al. (2015) the oldest Cretaceous Strzelecki Group sediment in the Gippsland Basin is the Tyers Conglomerate which has a maximum age of Berriasian (Figure 2-2). This rift phase was terminated by an uplift phase in the middle Cretaceous.

The second rift phase started in the early Late Cretaceous associated with the formation of the Tasman Sea (Smith, 1982; Cull and Beardsmore, 1992; Bernecker and Partridge, 2001). The Gippsland Basin entered a post-rift subsidence stage towards the end of the Late Cretaceous (Hegarty et al., 1985; Cull and Beardsmore, 1992; Johnstone et al., 2001). Subsidence during the syn-rift phase was rapid and mainly mechanically controlled, whereas during the post-rift phase it was slower and mainly thermally controlled. In the late Eocene, the Gippsland Basin was affected by rapid sea-level incursions and began to experience compression (Smith, 1982; Bernecker and Partridge, 2001; Johnstone et al., 2001; Power et al., 2001; Müller et al., 2019; Mahon and Wallace, 2020 and Gippsland Basin, 2021). The compressional phase occurred from the latest Eocene (ca. 34Ma) to at least the Mid Miocene (ca. 10Ma), probably continuing to the present day (Mahon and Wallace, 2020). It formed large NE-SW trending anticlines comprising the major hydrocarbon traps in the basin (Brown, 1986; Bernecker and Partridge, 2001; Johnstone et al., 2001; Power et al., 2001). During the Oligocene, marine transgression occurred over the basin and a sequence of calcareous mudstone and marl, comprising the Lakes Entrance Formation, was deposited over the regional Latrobe unconformity (Bernecker and Partridge, 2001; Johnstone et al., 2001; Gippsland Basin, 2021). This was followed by the deposition of the Gippsland Limestone from the Late Miocene to present-day, which comprises very thick marine sediments (over 2 km) associated with giant submarine canyons in the Central Deep.

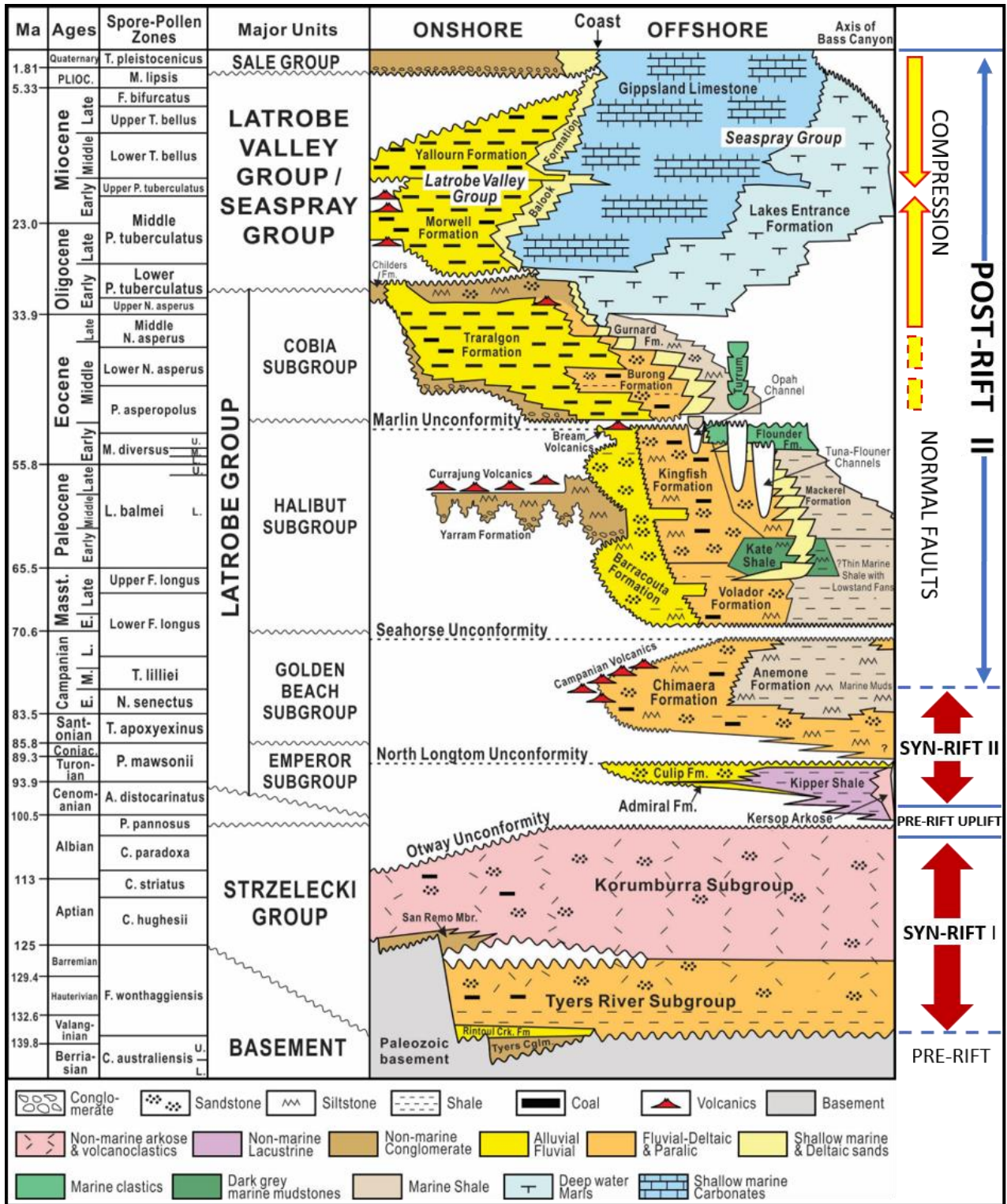


Figure 2-1 Stratigraphy with Spore-Pollen zonations and tectonic phases for Gippsland Basin (Modified from Partridge, 1999; Tosolini et al., 1999; Constantine, 2001; Bernecker & Partridge, 2001; Norvick, 2005; Holdgate et al., 2015). Two syn-rift phases and the Cainozoic compression phase are shown in the right hand column (note timing of rift onset is younger to the east in the Gippsland Basin than further west in the Otway Basin).

2.2 Stratigraphy

The total thickness of sediments in the offshore Gippsland Basin is over 10,000 m (Willcox et al. 1992; Norvick et al., 2001). The basin-fill within the Gippsland Basin can be subdivided into three main chronostratigraphic groups, corresponding to the episodes of tectonic evolution (Figure 2-1):

- The Strzelecki Group (Early Cretaceous) sediments were deposited in a rift valley prior to continental breakup and seafloor spreading (Figure 2-2). Its stratigraphy is best known from onshore outcrops being deeply buried offshore where it is only rarely penetrated on the platform areas. The Strzelecki Group has been subdivided into two Subgroups though it is entirely non-marine making it difficult to differentiate (Figure 2-2). The Tyers River Subgroup (Tosolini et al., 1999) or the Boola Boola Subgroup (Constantine, 2001) is the oldest and is conformably or in-places unconformably overlain by the Wonthaggi or Korumburra Subgroup (Constantine, 2001; Bernecker and Partridge, 2001). The Strzelecki Group is taken to span the Early Cretaceous *F. wonthaggiensis* to *P. pannosus* spore-pollen zone (Berriasian to Albian) as described in the Latrobe Valley region by Holdgate et al. (2015), although the oldest samples in most of the basin are thought to be Hauterivian (A. Partridge, pers. comm.). The basin was at high latitudes and the palaeo-climate was periglacial with cold, wet permafrost conditions, analogous to present day climates that occur in northern Canada westward through Alaska to northern Siberia (Constantine, 2001).

The Tyers River Subgroup (Tosolini et al., 1999) is developed principally in the Tyers district in the northwest where it is up to 600 m thick and is the equivalent of the Boola Boola Subgroup (Constantine, 2001). The Tyers River Subgroup probably can be assigned to the *F. wonthaggiensis* Zone (Hauterivian to Barremian) (Tyers Conglomerate), and sedimentation appears to have been restricted to small half grabens.

The basal unit onshore is the Tyers Conglomerate, which represents the initial terrestrial deposits laid down during early rifting, and it comprises fining up sequences of lower conglomeratic fan units containing basement derived metasediments (Tosolini et al., 1999; Constantine, 2001). The overlying Rintoul Creek Formation contains a lower part dominated by siltstone with minor sandstones and thin coals (Locmany Member) becoming mainly sandstones in the upper part (Exalt Member). The Rintoul Creek Formation passes westwards

into the Rhyll Arkose.

A sedimentary facies study by Tosolini et al. (1999) indicated that the Tyers River Subgroup and the Rhyll Arkose represented three main facies associations: gravelly channels; sandy channel/crevasse splays; and flood plain assemblages deposited in alluvial valleys. These entirely non-marine systems shifted from high-energy, braided river and alluvial-fan environments during deposition of the Tyers Conglomerate, through more sluggish floodplain environments during deposition of the Locmany Member, returning to active sandy, braided fluvial systems during deposition of the Exalt Member.

The overlying Wonthaggi Subgroup spans the *P. notensis* to *P. pannosus* spore-pollen zones (Barremian to Albian) and comprises coarse metasediments and grey-green brown volcanoclastic sandstones deposited mostly in fluvial and alluvial environments dominated by muddy braided channels, overbank mudstones and widespread lacustrine sediments over a more extensive rift area (Tosolini et al., 1999; Constantine, 2001; Holdgate, 2005; Norvick, 2005). A number of stacked thin discontinuous coals occur mostly towards the base and form several sub-economic coal fields in the Wonthaggi region (Edwards et al., 1944). The lacustrine sediments in places are characterised by varves, anoxia and a variety of fossils including fish groups, clam shrimps (conchostracans or spinicaudatans), horseshoe crabs, amphibians, xiphosurans and ichthyosaurs suggesting inland seas and lakes (Tuite, 2016). The Wonthaggi Formation mainly comprises volcanogenic sediment and the derivation has been debated for many decades in the literature. Edwards and Baker (1943) concluded that the coarse clastics in the Tyers River and Wonthaggi sub-groups were derived locally and Gleadow and Duddy (1981) concluded the volcanoclastics were mainly sourced from intra-rift volcanics. A more recent alternative view is that the volcanoclastics were derived from a contemporaneous volcanic source further to the east and outside of the Gippsland basin, including a volcanic arc (Veevers et al., 1982; Bryan et al., 1997) or from the main Tasman Sea rift volcanics including the Whitsunday Volcanic Province (Bryan et al., 1997; Constantine, 2001).

The Strzelecki Group was progressively uplifted and truncated over the Glengarry and Tyers basement ridges, as indicated by the broad palynological dates, which show that successively

older units subcrop beneath the base-Cenozoic unconformity (Holdgate et al., 2015). The vitrinite reflectance cross-section in Holdgate et al. (2015) suggests that the total Strzelecki Group thickness along the southern Latrobe Valley could exceed 4km (Figure 2-3). Similar Aptian-Barremian aged *P. notensis* and *F. wonthaggiensis* beds occur over an approximately 2km thickness of Strzelecki Group in the Megascollides-2 well with the well reaching volcanic basement at 1946m (Grosser 2005). The original Strzelecki thickness is uncertain, with previous estimates about 6 km onshore (Dudley, 1959) to 9 km offshore (Willcox et al., 1992). In Gippsland Basin offshore wells, the vitrinite reflectance at 2 km depth ranges from 0.32% to 0.65%. In contrast, the onshore well Hazelwood-1 shows a high vitrinite reflectance (over 6.0%) at a relatively shallow depth (~2000m) (Figure 2-3), which indicates the onshore Strzelecki Group has experienced significant uplift and erosion (Constantine, 2001; Holdgate et al., 2015).

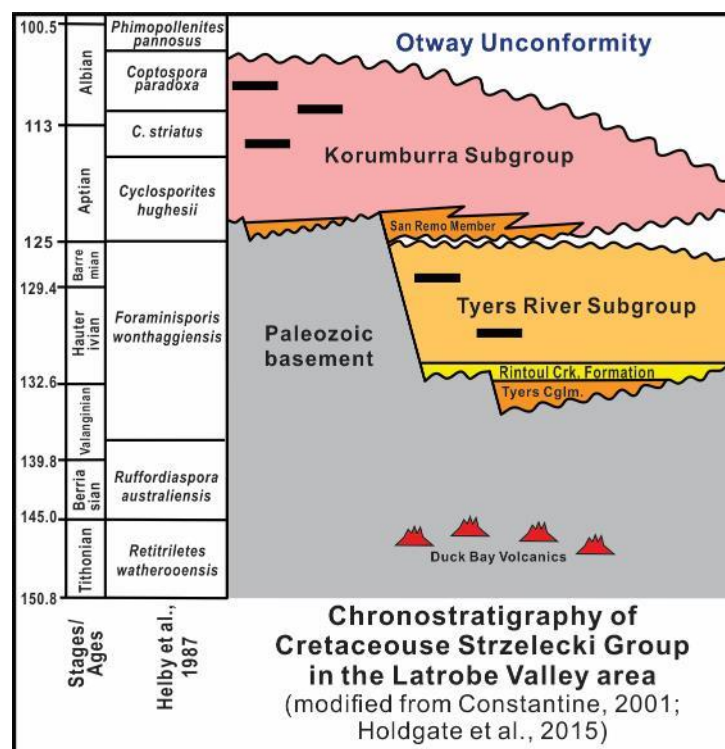


Figure 2-2 Cretaceous Strzelecki Group Chronostratigraphy (Constantine, 2001; Holdgate et al., 2015).

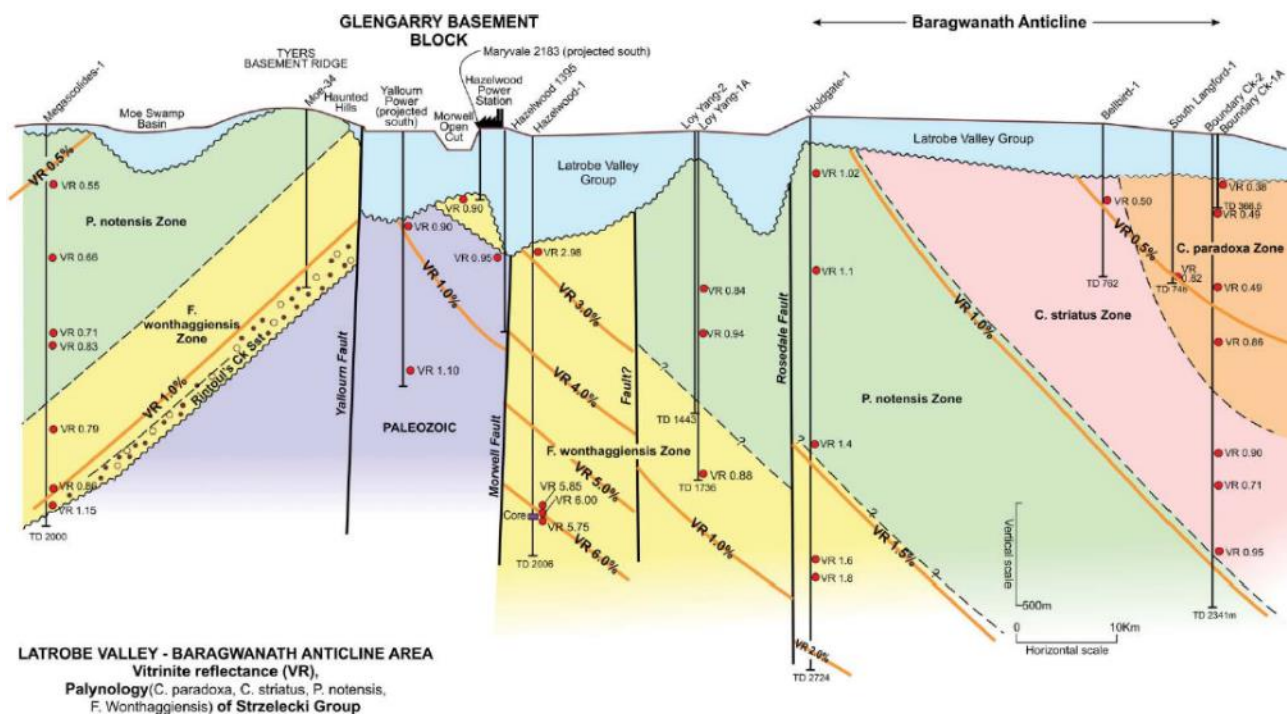


Figure 2-3 East-west cross-section commencing at the eastern end of the Baragwanath Anticline (Boundary Creek-2) trending west into the Latrobe Valley, northwest over the Glengarry basement block to the Moe basin in the west (Megascolides-1) (Holdgate et al., 2015).

- The Latrobe Group (Late Cretaceous to Eocene) records the sediments deposited in the second rift and the transition from the initial seafloor spreading phase to the post-rift phase. It unconformably overlies the Strzelecki Group and comprises lower siliciclastics and mudstone sequences mainly confined to the Central Deep, passing upwards into sand-rich siliciclastics and coals that spread out laterally over most of the offshore parts of the basin. In the Palaeocene the upper Latrobe Group passes onshore into the Latrobe Valley Group coal measures that accumulate until the Late Miocene. Bernecker and Partridge (2001) recognised four main unconformities within the Latrobe Group: the Longtom, Seahorse, Marlin and Latrobe unconformities, which separate the Latrobe Group into four subgroups (Bernecker & Partridge, 2001): Emperor Subgroup (Cenomanian-Coniacian); Golden Beach Subgroup (Coniacian-Campanian); Halibut Subgroup (Masstrichtian-Early Eocene); and Cobia Subgroup (Eocene-Oligocene) (Figure 2-1).
 The Emperor Subgroup sediments (Bernecker and Partridge, 2001) are mainly non-marine to lacustrine clastics that are notably less volcanoclastic than the Strzelecki Group. They were deposited in a much smaller intracratonic rift drainage basin confined to the Central Deep and have only been drilled around the margins where it is up to 1km thick though thicker sections

occur in the centre at depths of over 5km. Alluvial fan and fluvial conglomerates and sandstones occur at the base and around the margins of the basin (the Kersop Arkose in the south and the Admiral Formation in the north) with fluvial sandstones and shallow lacustrine mudstones increasing up section. The overlying Kipper Shale is widespread and comprises a thick shallow to deep-water sequence of lacustrine sediments inter-fingered with the coarser clastics around the margins. This passes upwards into the Curlip Formation of fluvial sandstones with interbedded mudstones and some very thin coals indicating the development of coastal environments fringing the inland seas.

The Emperor Subgroup is terminated by the Longtom unconformity in the Coniacian which is enigmatic in its origin, with Bernecker and Partridge (2001) noting there seems no tectonic basis for this and suggesting it might record the onset of spreading in the south Tasman, though this is well before the earliest known age of oceanic crust.

The Golden Beach Subgroup (Bernecker and Partridge, 2001) is also mostly restricted to the Central Deep but locally spills out over the platform areas. It is characterised by quartz clastics derived from the Palaeozoic basement and granitic terranes which marks a significant change from the earlier volcanoclastic sediment sources. The sedimentary facies comprise coarse alluvial to low-sinuosity fluvial clastics at the base and to the west becoming high-sinuosity fluvial to coastal plain shales and some coals further east (Bodard et al., 1986) that are referable to the Chimaera Formation. The first shallow marine clastic sediments were deposited further to the east with initiation of spreading in the south Tasman Sea (Anemone Formation). A series of basaltic volcanics of Campanian age occur in the upper part of the Golden Beach Formation.

The Golden Beach Subgroup is interpreted to terminate at the Seahorse unconformity in the late Campanian by Bernecker and Partridge (2001) though they note that there is no regional unconformity around 80Ma as interpreted by Lowry and Longley (1991). Sections are missing in the *T. lilliei* and *F. longus* zones, with the Campanian volcanics lying in the *T. lilliei* Zone with Golden Beach sediments above and below in places, and this period marks the transition to the post-rift or drift phase (Smith, 1982).

The Halibut Subgroup comprises a thick succession of fluvial, deltaic and marine sediments

that show marked facies change from west to east and are mainly aggradational with time: the Yarram Formation (alluvial and fluvial incised valley fill), Barracouta Formation (alluvial and upper coastal plain fluvial sediments including thin coals), the Volador and Kingfish Formations (lower coastal plain with common thin inertinitic coals), the transgressive marine Kate Shale deposited near base Paleogene, and the Mackerel Formation (barrier and near-shore marine sandstones with intercalated marine shales deposited well to the east). The Halibut Subgroup is separated from the Cobia Subgroup by a disconformity/unconformity in many offshore wells (the Marlin unconformity), which resulted from the cessation of extensional faulting and the onset of basinwide transgression that accompanied the end of ocean floor spreading in the Tasman Sea and the initiation of regional compression. It is characterized by non-deposition or erosion of upper *M. diversus* and or *P. asperopolus* aged strata in the late Early Eocene associated with several episodes of falling sea level (Bernecker and Partridge, 2001; Johnson et al., 2001). Anticlines began to form and a series of canyon systems resulted known as the Tuna-Flounder, Marlin, and Opah channels (Brown, 1986; Johnstone et al., 2001; Norvick et al., 2001; Gippsland Basin, 2021). The Tuna-Flounder channel was filled later by transgressive sediments (Flounder formation), while the Marlin channel is partly filled by the Turrum Formation (Brown, 1986; Root et al., 2004). The precise controls for these events and the relative contribution of hinterland uplift, sediment supply and sea level change are considered speculative (Norvick, 2005).

The overlying Cobia Subgroup (Middle Eocene to Early Oligocene) is thinner and comprises several retrogradational cycles of progradation and transgression that overall backstep to the west. Shallow to open marine sedimentary deposition in the east (Gurnard Formation, Turrum Formation) passes into the Burong Formation, comprising a well developed barrier system with marginal marine back barrier lagoons and lakes. The non-marine to marginal marine Traralgon Formation developed to the west and extends well into the onshore parts of the basin comprising lower and upper coastal plain sediments including thick and continuous coal seams (Holdgate et al., 2000). The end of Cobia Subgroup deposition is marked by the drowning of the offshore basin by the early Oligocene whereby the barrier systems had back stepped over 100km to the west into the present onshore part of the basin.

- The Seaspray Group, Latrobe Valley Group, and Sale Group were deposited from the late Eocene-early Oligocene to Recent following the major transgression and represent the changed lateral facies distribution over the basin.

The marine Seaspray Group now dominated the basin and comprises up to 2500 m of marine cool water carbonates and fine-grained clastics, initially deposited as shallow marine transgressive units, passing upwards into thick carbonate and fine clastic sediments. This succession comprises a complex series of progrades that cut and fill back across the basin into deep water as thermal subsidence and margin flexure continued in the post-rift phase (Willcox et al. 1992; Bernecker and Partridge, 2001; Moore and Wong 2001; O'Halloran and Johnstone, 2001; Power et al., 2001; Mitchell et al., 2007). The Seaspray Group is separated onshore into a number of formations and members (Holdgate and Gallagher, 2003), while traditionally the offshore section has been separated into: the Gippsland Limestone comprising proximal shelf carbonates consisting of calcarenites with interbedded marls; and the Lakes Entrance Formation consisting of more distal shelf marls, claystone and interbedded siltstones. More recently it has been subdivided based on petrology and seismic (Bernecker et al., 1997; Holdgate et al., 2000) to comprise basal pelagic marls and fine-grained turbidites (Albacore Subgroup); overlain by channel fill carbonates of bioclastic marls or wackestones with abundant carbonate, becoming coarser and more quartz-rich bioclastic packstones inshore (Albacore Subgroup); and shelf slope carbonates comprising highly fossiliferous carbonate packstones and wackestones or marls with interbedded siliclastic units (Hapuku Subgroup). East of the Seaspray Group a long lived aggradational barrier system developed some 150km along strike (Balook Formation) behind which and to the west thick non-marine coal-bearing sequences accumulated in the Latrobe Valley and Alberton depression from the Oligocene to Miocene (Holdgate and Clarke, 2000). Very thick coal seams developed with thin interseam sandstones and mudstones (Morwell and Yallourn formations).

A Late Miocene to Recent non-marine to marginal marine sequence unconformably overlies the Latrobe Valley and Seaspray Groups (Sale Group) that is mostly undifferentiated further to the east and offshore where it becomes marine and part of the shelf succession (Holdgate and Gallagher, 2003).

Chapter 3. Method: Data, Software & Workflow

3.1 Source of data

The project involved multiple types of open-source data, including 2D and 3D seismic data, coal bore datasets, onshore and offshore wells with log data, biostratigraphic data and interpreted gravity data, etc.

- 2D and 3D seismic data are sourced from GeoScience Australia (<http://www.ga.gov.au/>) and GeoScience Victoria (<http://earthresources.vic.gov.au/>). The 3D seismic data is a merged dataset, which includes many different surveys covering the main part of the offshore area, merged by 3D-Geo Pty. Ltd. The 2D seismic surveys cover the entire offshore Gippsland Basin, especially the south platform area, which is without 3D seismic data control and outside of the merged 3D dataset. The 2D seismic data overlaps the 3D merged dataset thereby helping interpretation of the area between different 3D surveys and some Central Deep areas, where the 3D seismic is blurred and discontinuous in the lower Latrobe Group. Figure 3-1 shows the study area and the seismic coverage.
- The coal bore dataset was downloaded from GeoScience Victoria (<http://earthresources.vic.gov.au/>). The project utilised data from two coal bore datasets, the Latrobe Valley coal model basic package finished in 2003 and from the Latrobe Valley coal model completed in 2011. Overall, these two coal bore datasets provide over 9000 bores with stratigraphic data, lithology, proximates and ultimates including ash and moisture and other detailed analyses. Over most of the western Latrobe Valley these bores were drilled at 400m spacing with the spacing decreasing in some coal mine areas and increasing east of Gormandale. The coal seam moisture and ash analyses were done at 3m vertical intervals, the ash constituents on 6m composites, proximates and ultimates on 12m composites.
- The onshore and offshore petroleum well information included over 900 wells downloaded from Geoscience Australia (www.ga.gov.au), National Offshore Petroleum Information Management System (NOPIMS) (<http://www.ga.gov.au/nopims>) and Geological Survey of Victoria (<http://earthresources.vic.gov.au/>) and of these some 345 were mainly used in this study. The

data that were downloaded included basic information (e.g., well location, total depth, deviation data, velocity checkshots, bottom hole temperature), interpreted data (e.g., stratigraphic formation tops and lithology data from sidewall core or cuttings) and well completion reports. The digital onshore well log data was provided by the Geological Survey of Victoria, Earth Resources department, while the digital offshore well log data was provided by BHP Billiton augmented by data downloaded from NOPIMS. These wells are typically at a spacing of several km but mostly on the highs, more closely spaced over the petroleum fields and more widely spaced over the deep synclines.

- The core analytical and biostratigraphic data was downloaded from Geoscience Australia (www.ga.gov.au).
- Petroleum well pressure data (DST, FITP, WFT) was provided by CSIRO from their PressurePHG database (<http://www.pressureplot.com/>) for some 616 wells. This dataset also includes temperature, porosity and permeability data.
- The source rock dataset was downloaded from Geological Survey of Victoria (<http://earthresources.vic.gov.au/>) and includes vitrinite reflectance and RockEval data. Professor Greg Smith provided some vitrinite reflectance data while some coal analytical data, such as moisture, was provided by Dr Guy Holdgate.
- Other petroleum well data including porosity, permeability, density and heat flow data were downloaded from Geological Survey of Victoria (<http://earthresources.vic.gov.au/>).
- Interpreted gravity data included the top Basement map, total sediment thickness map and crustal thickness map provided by OZSEEBASE, Frogtech Geoscience.
- The Australian bathymetry and topography grids were downloaded from Geoscience Australia (www.ga.gov.au).
- The High-quality Australian monthly rainfall climate dataset was downloaded from <ftp://ftp.bom.gov.au/anon/home/ncc/www/change/HQmonthlyR>.
- Some interpreted maps were downloaded as packages from Geological Survey of Victoria to guide the preliminary interpretation (<http://earthresources.vic.gov.au/>).

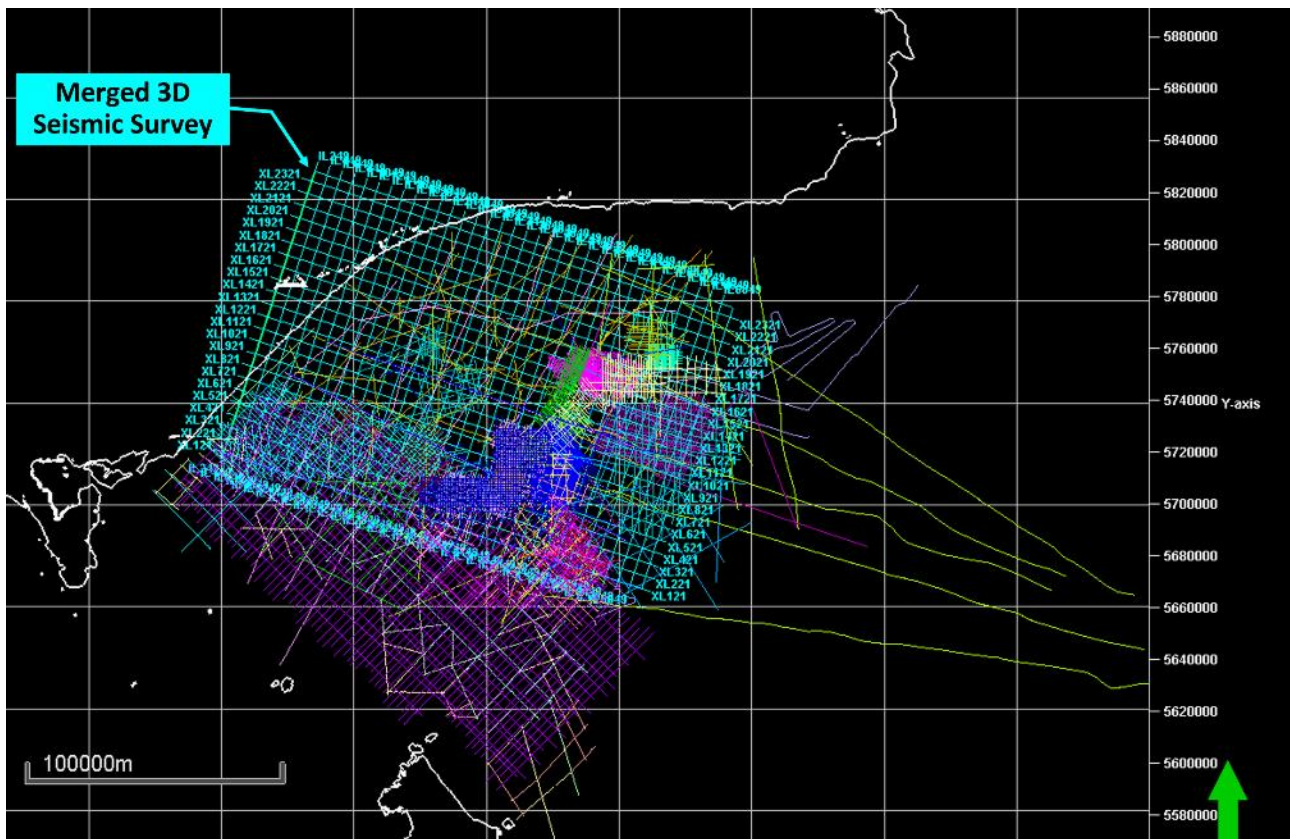


Figure 3-1 The study area showing the seismic coverage. Merged 3D seismic survey shows in aqua lines with inline and crossline numbers; other colourful lines are different 2D seismic surveys. The white line is the coastline.

3.2 Technical Software

- The Schlumberger *Petrel* Software is used to analyse the subsurface data (e.g., seismic, well log, coal bores, rock/fluid physical properties) and then to interpret the basin architecture and build the geological model for the basin. *ArcGIS* was used to visualise and process the interpreted gravity data and convert it to the same coordinate system with the proper format.
- *Badlands*, a Basin and Landscape evolution modelling program (*Badlands*, 2019) was used to conduct forward stratigraphic modelling. It is an open-source Python-based code developed by the software team at Sydney University led by Dr Tristan Salles, as part of the Sydney University, Melbourne University and Curtin University collaboration in the ARC Basin GENESIS Hub (ARC Council Grant IH130200012). The *Badlands* simulations are carried out using Python scripts and processed in the Docker container environment developed by Docker Inc.

- The *Badlands* simulation results are visualised the *ParaView* software, numerical values were extracted using *HDFView* software, and imported back to *Petrel*, to compare with the actual geological model surfaces.
- The Experimental Design analysis is done using a General Scenario Analysis Tool (*GSAT*) which is an R wrapper program developed at Curtin University. *GSAT* produces and optimises experimental design to minimise the number of essential scenarios. It ensures the entire multi-dimensional space is statistically populated and all critical effects and interactions are tested (Collinson et al., 2008). *GSAT* also allows statistical analysis of the response results.
- *GPlates*, a plate tectonics program, is used to manipulate reconstructions of geological and paleogeographic features through geological time (Müller et al., 2019). It is developed by the EarthByte Group at the University of Sydney and the Division of Geological and Planetary Sciences (GPS) at California Institute of Technology (CalTech). This study uses the *GPlates* software to reconstruct the geological evolution, understand the syn-rift and post-rift timing of the Gippsland Basin, and assess the palaeo-crust thickness and the stretching factor β .
- *PetroMod* (Schlumberger software) is used to build a series of 1D, 2D and 3D burial history models of the onshore and offshore Gippsland Basin to recreate the basin burial-thermal history from the Early Cretaceous to the Present.

3.3 Overall Workflow

Details of the method used for each of the modelling steps are given in the relevant chapters. A summary of the overall workflow is shown in Figure 3-2 and described briefly below.

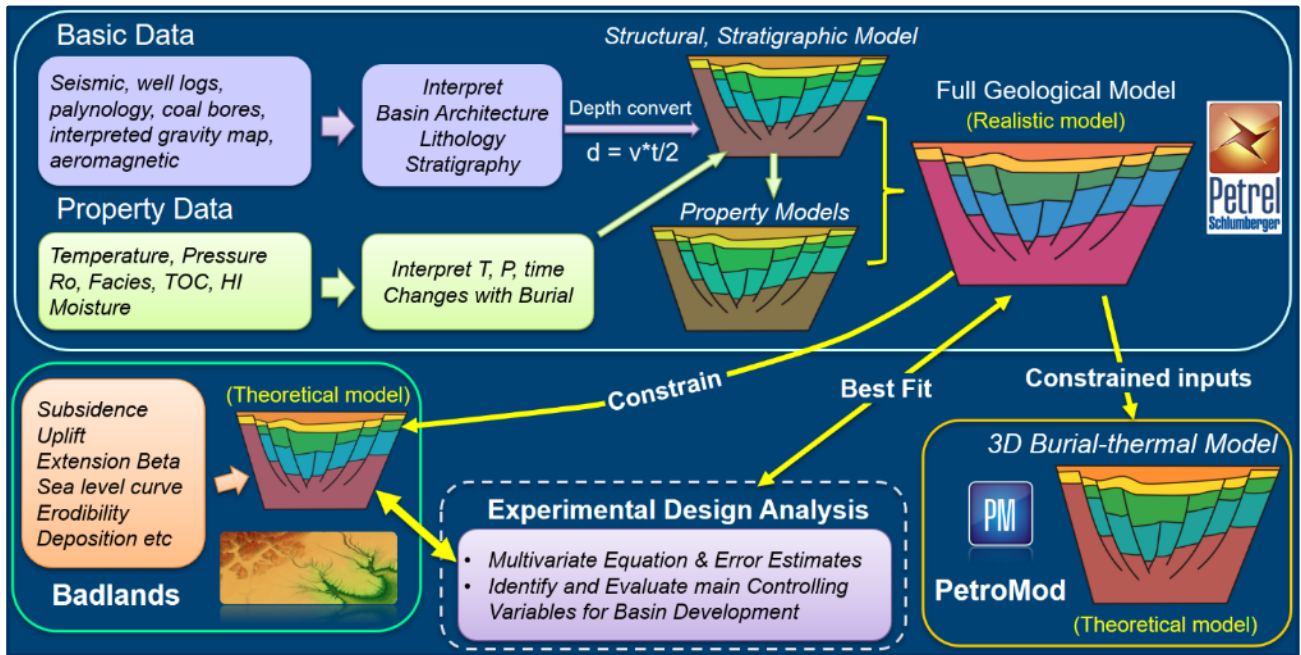


Figure 3-2 Workflow adopted by this research.

The project comprises five major steps:

1. Build the realistic 3D structural, stratigraphic model and property models in *Petrel* Software:

The realistic model built using the *Petrel* software utilised 3D and 2D seismic data, onshore and offshore wells, biostratigraphic data and interpreted gravity data. The seismic data (in two-way time, TWT) is used to define the basin architecture by interpreting the key horizons, including seafloor, top Latrobe Group, base Tertiary, top Golden Beach Subgroup and top Strzelecki Group, and the main faults in the basin (Figure 3-3). The biostratigraphic data, well logs and well formation analytical data are used to interpret the stratigraphy and lithology across the basin. The results provide the age information for burial history reconstruction in *PetroMod* and the facies and lithological information for the property modelling in *Petrel*. Over 200 petroleum well checkshot datasets and formation data are used to tie the key horizons to the wells and build the velocity model in *Petrel* (described in Chapter 4). This allows depth conversion of the seismic data, maps and faults from TWT to Depth. These data in depth and the interpreted gravity map (top Basement) were utilised to build a realistic 3D structural depth model and generate the depth maps that constrain the theoretical modelling in *Badlands*.

The 3D structural model is built using the Pillar Gridding method in *Petrel* (detailed in Chapter 4). The key wireline log data of over 200 petroleum wells, including Gamma Ray

(GR), Bulk Density, Neutron Porosity, Sonic (DT) and Resistivity, were used to define the main lithologies, such as clean sandstone, siltstone, shale, coal and basalt. Property models were built for a number of physical variables, including facies, porosity, pressure, temperature, vitrinite reflectance (R_o) and total organic carbon (TOC) (see Chapter 7). The property models of pressure, temperature and vitrinite reflectance (R_o) were used to study the relationships between pressure and temperature change with depth and build the 3D burial history in the *PetroMod* software.

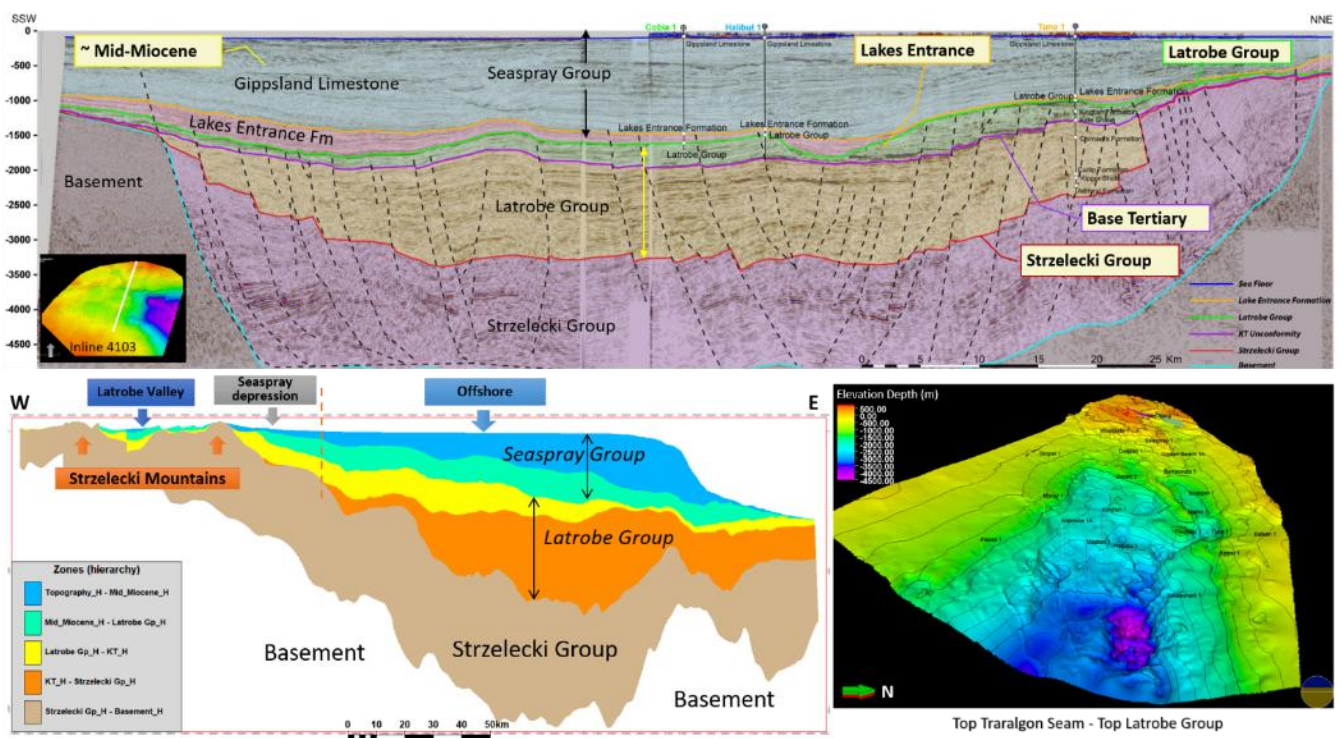


Figure 3-3 Examples from Petrel structural, stratigraphic model (seismic interpretation, zone property, and surface from structural model).

2. Use realistic model thickness maps and other properties to constrain the theoretical forward 3D model in *Badlands* and *PetroMod* software:

The 3D structural, stratigraphic depth model provides key depth maps for certain horizon ages that were used to generate isopach maps (thickness maps) to constrain the tectonic subsidence simulation of the theoretical modelling in *Badlands*. These isopach maps were used to guide the subsidence processes related to rifting and thermal sag and the regional uplift. Six surface maps were used to generate the isopach maps: merged topography-bathymetry, top Lakes Entrance Formation, top Latrobe Group, base Tertiary, top Strzelecki

and top Basement. These maps were chosen as key intervals to guide the tectonic displacement of the Gippsland Basin: Early Cretaceous rifting and the subsequent regional uplift, the Tasman Sea rift and the associated minor uplift and subsidence in Mid-Late Cretaceous, and Cainozoic thermal subsidence with minor overprinted compression. These maps also correspond to significant regional unconformities at key times, which helps guide the *Badlands* forward modelling. Note however, the thickness maps are used as displacement maps to guide the *Badlands* software to create the accommodation space. The sediment erosion and deposition processes in *Badlands* are controlled by many other variables so that once initiated a forward simulation can deviate significantly (see Chapter 5 for details). Hence, the simulations need to be evaluated for fit to the realistic model (e.g., depth map matching is one of the evaluation indicators used here).

3. Set up scenario modelling guided by experimental design:

An Experimental Design (ED) is followed to guide the *Badlands* forward simulations and manage the large number of variables identified in the Uncertainty Framing (see Chapter 5 for details). An ED is required because the simulation of the entire history of a rift basin needs to utilise about nine different simulation modules, including: the tectonic module, rainfall, sediment erosion/deposition, sediment transport, submarine-canyon, carbonate and wave modules. Multiple parameters must be specified within each module to control the simulation processes (see Chapter 5 for details and Figure 5.1). Hence, the complexity of the basin evolution history reconstruction in *Badlands* requires many different modules to work together and this may result in a large number of significant uncertain variables. This requires a structured approach to manage the uncertainties and analyse the possible scenarios. The Curtin University GSAT is used to define the ED and minimise the number of essential scenarios, while ensuring the entire multi-dimensional space is statistically populated and all critical effects and interactions are tested (Collinson et al., 2008).

4. Experimental Design Analysis

The *Badlands* forward simulations provide 3D landscape maps at 1Myr time steps thereby capturing the sediment accumulation with time which can be compared to the stratigraphy

in the 3D *Petrel* model and analysed for a variety of outputs (see Chapter 5 for details). *Badlands* simulation results, such as the palaeo-landscape maps for each million year and cross-sections of the stratigraphic architecture, were first visualised in *ParaView*. Palaeo-landscape surfaces at key time horizons were selected to compare with the realistic model horizons and other published sedimentary models. The simulation outputs such as the depth maps were converted from hdf5 to ASCII using python scripts and imported back into *Petrel* to compare with the realistic model surfaces. Response estimation was done in *Petrel* by setting up a workflow to calculate various statistics, including statistics to measure the difference between the simulation depth maps and the corresponding realistic depth map (e.g., Mean difference and Standard Deviation) and rates of deposition for various tectonic phases that were also done in excel. The responses for the Experimental Design runs were analysed in *GSAT* to estimate the best-fit polynomial function, the co-efficients for each input variable and their significance obtained from an Analysis of Variance (ANOVA), which can also be displayed in Tornado charts.

5. Build 3D burial history model

The burial and thermal history of the Gippsland Basin is modelled using *PetroMod* in conjunction with *Petrel*. Details are given in Chapter 8 and the summary workflow is shown in Figure 3-4. Ten 1D burial-thermal models were first built across the basin, at selected wells in the Seaspray Depression, Lakes Entrance Platform, Northern Terrace, Central Deep, Southern Terrace, and Southern Platform to provide a good understanding of the burial-thermal differences across the entire onshore and offshore Gippsland Basin. The interpreted seismic data and gravity map were used to select these wells. Six 2D burial-thermal models were built on regional cross-sections to simulate the heat flow trends utilising the advanced simulation option in *PetroMod*. The 1D and 2D modelling results were then used to guide the construction of a full 3D burial-thermal model from the onshore to offshore areas in *PetroMod* which has not been undertaken previously.

All of the main aspects in the 3D *PetroMod* model are constrained by the realistic *Petrel* model. Key depth maps and the fault framework were extracted from the realistic model and used to constrain the depth and age simulations of the burial history model in

PetroMod. Depth maps and fault interpretations from the full *Petrel* 3D structural model were converted into a simple 3D grid to constrain the 3D *PetroMod* grid. The age assignment and the layer processes are guided by the structural-stratigraphic model and tied to the well tops. Reconstruction of the depositional history is thereby controlled by the *Petrel* stratigraphic and facies models including the age assignment, layering and lithofacies definition. The *Petrel* 3D geological model also included property models for total organic carbon (TOC) and hydrogen index (HI), which are required inputs for *PetroMod* (details for the property models are given in Chapter 7). These property maps were imported to *PetroMod* to ensure measured sedimentary property data constrain the 3D burial history model at critical geological times. Measured temperature and vitrinite reflectance (Ro) data were used for comparison with the modelled temperature and Ro values estimated by *PetroMod*. For more details, see Chapter 8.

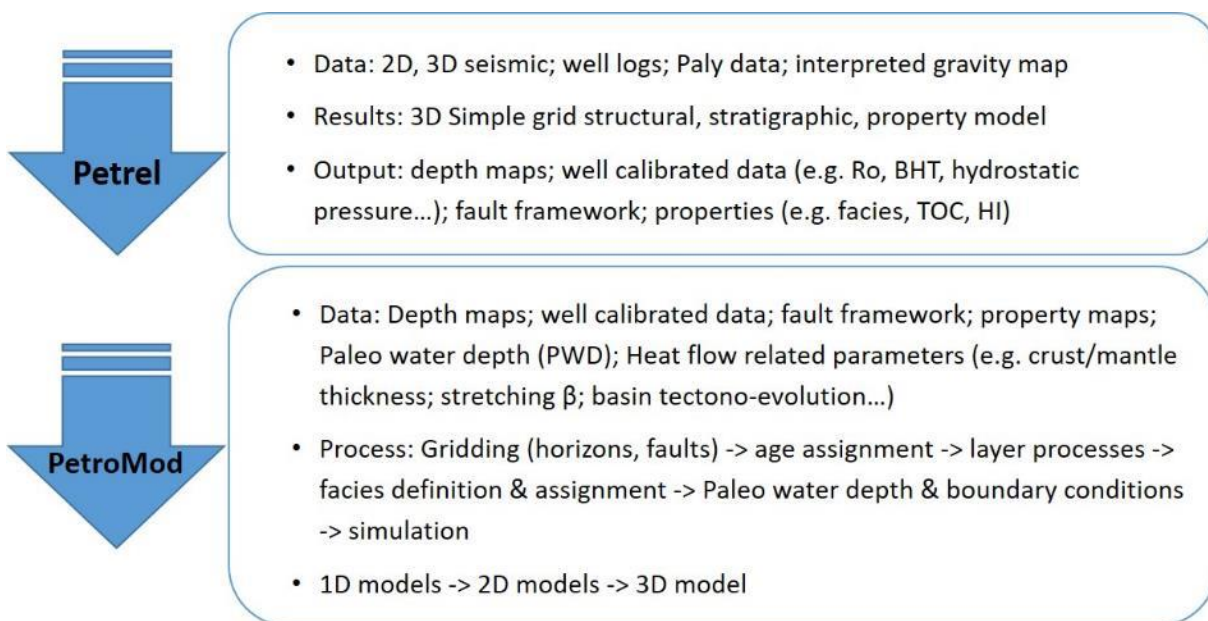


Figure 3-4 The summary process workflow for the *Petrel* to the *PetroMod* modelling.

The detailed methodology of each part is discussed in the individual corresponding chapter.

Chapter 4. Tectonic, Structural and Stratigraphic Models

4.1 Tectonic Reconstruction in *GPlates* Software

A good understanding of tectonic history is required to model the structure, stratigraphy, burial and thermal histories of the Gippsland Basin which are the aims of this research. The modelling also requires several types of input data from the tectonic models, including crustal thickness, the stretching factor β and the rate of plate movement. Much has been written about the tectono-stratigraphic history of the Gippsland Basin based on various geological aspects or datasets but the fundamental tectonic plate movements has rarely been used as a starting point to constrain the analysis. Hence, this study started by going back to the basic plate tectonics movements and data rather than assuming previous work was correct.

The *GPlates* software is probably the best and most widely used software designed for interactive modelling and visualisation of plate tectonics and has been used in this study (Müller et al. 2018).

4.1.1 Plate Tectonic Reconstruction

The Müller et al. (2019) global absolute plate motions model is used here in *GPlates* to visualise and capture the plate tectonic reconstruction in and around the Gippsland Basin. The reconstruction interval has been set from 140 Ma to 0 Ma anchored on the Australia Plate (ID 801). The velocity domain points were generated to show the calculated velocity value and direction, constrained by latitude and longitude extents (latitude range: -34° ~ -45° ; longitude range: 140° ~ 165°) (Figure 4-1). The reconstructions model the separation on the southern Australia-Antarctica margin and the separation of the south-eastern margin and Zealandia forming the Tasman Sea.

The plate tectonic reconstruction provides timing control for the major tectonic phases that the Gippsland Basin experienced, which are later used to guide the theoretical modelling processes (ie. the Palaeo-landscape simulation in *Badlands* in Chapter 5, 6; Burial-thermal modelling in *PetroMod* in Chapter 8). The *GPlates* models also estimate the crustal thickness, stretching factor β and velocity vectors for the separations that are used as inputs for the Burial and Thermal modelling (Chapter 8). The full animation of the tectonic reconstruction model of the Gippsland

Basin and surroundings is given in Appendix 6 and snapshots at key times are shown in Figure 4-2 and Figure 4-3.

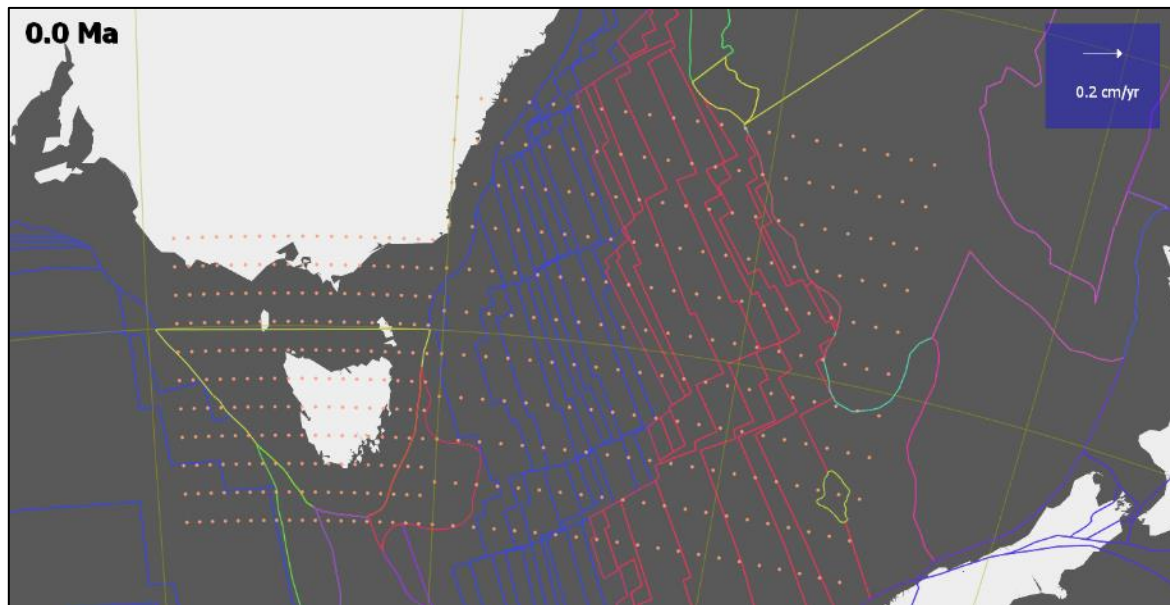


Figure 4-1 The velocity domain points coverage at 0Ma (shown as orange dots).

The reconstructions demonstrate that two main phases of separation can be recognised on the margins of the Gippsland Basin, one involving the Australia-Antarctic separation and the other involving the Australia-Zealandia separation of the Tasman Sea opening. However, in both tectonic events the Gippsland Basin remained as a failed rift basin, the first taken to be associated with the east-west Great Australian Bight – Otway – Strzelecki rift in the Early Cretaceous, the second as a failed arm orthogonal to the main Tasman rift between Australia and Zealandia in the Late Cretaceous (Smith, 1982; Duddy and Green, 1992; Willcox et al., 1992, 2001; Brown et al., 2003; Norvick, 2005).

The reconstructions shown here, based on the Müller et al. (2019) model data, demonstrates the following key events:

1. the first Strzelecki rift extension starts forming at 136 Ma and ends at 100 Ma, mainly in a NE-SW to NNE-SSW direction, consistent with separation of Australia and Antarctica (Figure 4-2)
2. the second Tasman extension phase is from 98.5 Ma to 79 Ma, with a west-east stretching direction, associated with subsequent separation of SE Australia and Zealandia and the opening of the Tasman Sea (Figure 4-2).

3. Tasman Sea spreading started between 83-79 Ma and ended in the Early Eocene, around 52 Ma – 51.5 Ma (Figure 4-3) and Gaina et al. (1998).
4. The end of Tasman spreading marks the start of Gippsland post rift thermal subsidence phase with flexural collapse.
5. Gippsland compression started in the Eocene at about 45 Ma, resulting from continued NNW spreading south and east of the South Tasman Rise, initiation of the Australian-Pacific plate boundary along the Tonga-Kermadoc subduction zone, and within Zealandia along the proto-Alpine strike-slip fault and development of the associated subduction of the Australian-Pacific plate to the south-west (Figure 4-3 and Figure 4-4) (Bache et al., 2014; Sutherland et al., 2017; Sutherland et al., 2020).

The results of the tectonic modelling provide a firm basis to proceed with the subsequent modelling of the structure, stratigraphy, burial and thermal history.

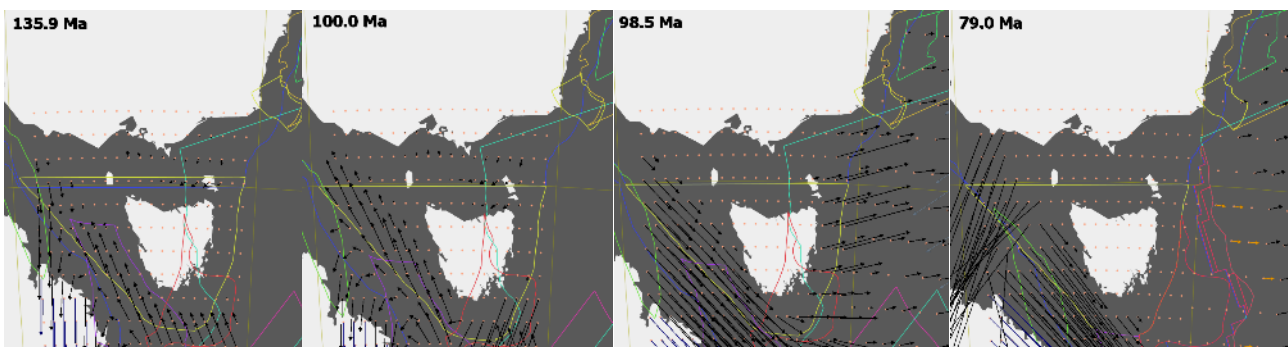


Figure 4-2 Key time reconstructions from the GPlates modelling from Early to Late Cretaceous (based on the GPlates model data of Müller et al., 2019). Arrows indicate the tectonic plate velocity fields and the colours relate to the age. Colour dots show the stretching factors coloured as per the legend.

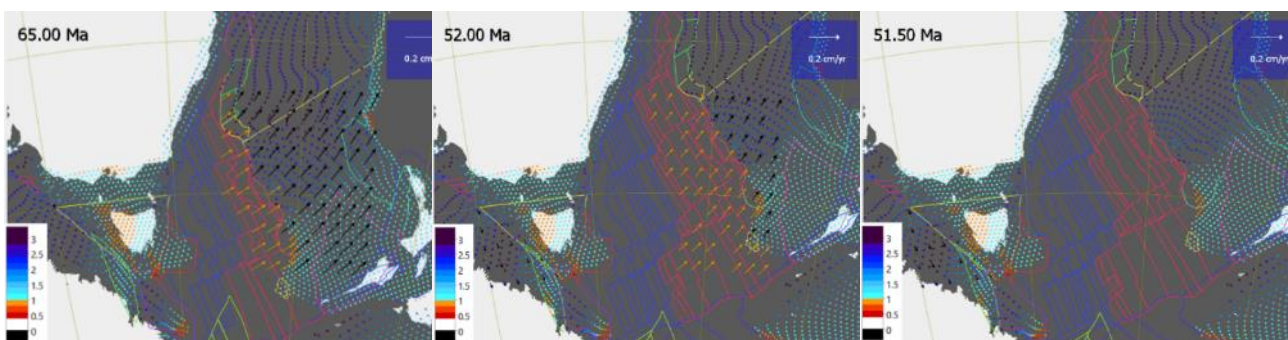


Figure 4-3 Key time reconstructions from the GPlates modelling from Palaeocene to Early Eocene (based on the GPlates model data of Müller et al., 2019). Arrows indicate the tectonic plate velocity fields and the colours relate to the age. Colour dots show the stretching factors coloured as per the legend.

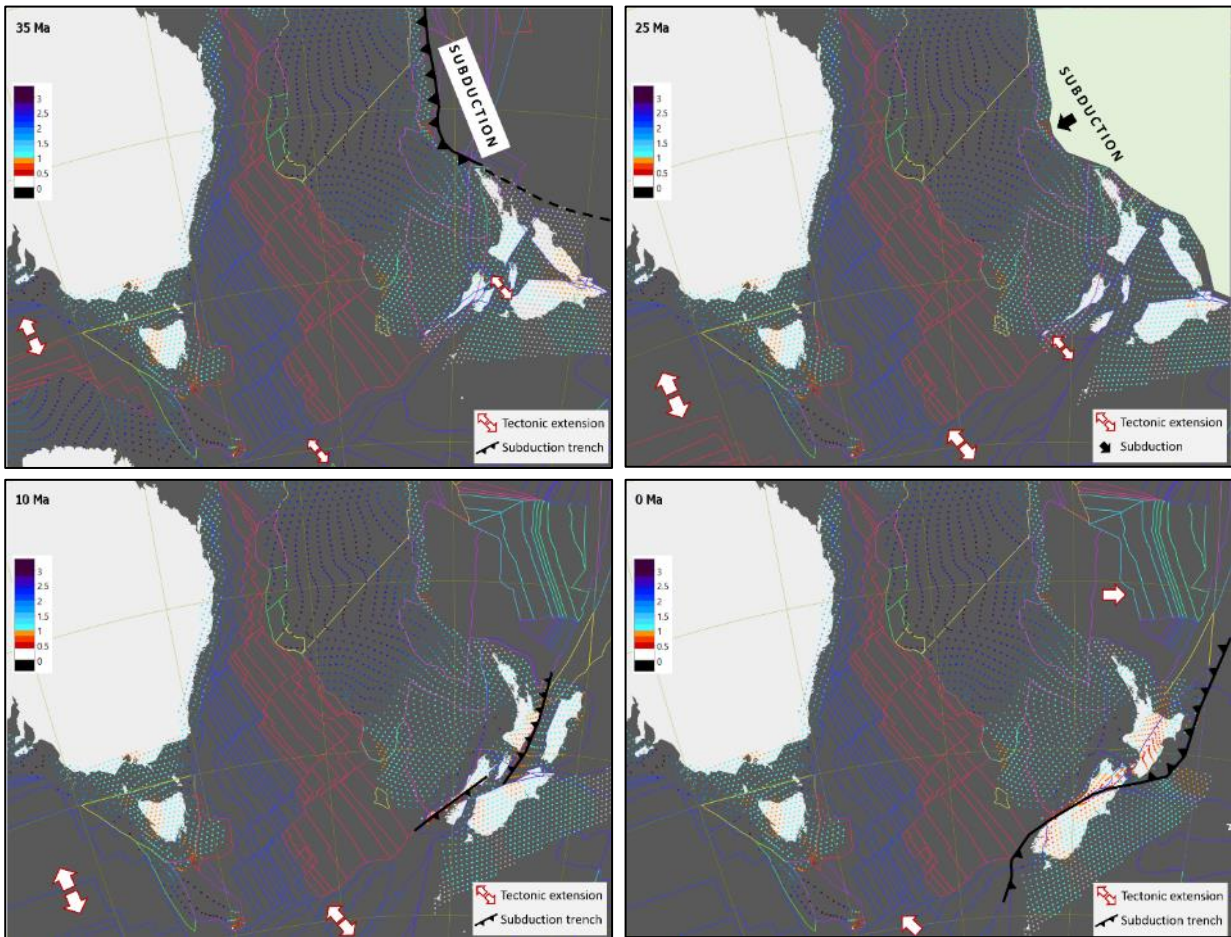


Figure 4-4 Key time reconstructions from the GPlates modelling from Middle Eocene to Recent (based on the GPlates model data of Müller et al., 2019). Colour dots show the stretching factors coloured as per the legend.

4.1.2 Crustal Thickness and Crustal Stretching Factor

Scalar crustal stretching factors and the stress field in the study area are indicated on the GPlates reconstructions by the coloured dots (Figure 4-1). A stretching factor above one means the area is experiencing extensional deformation, shown as light blue to dark purple colour dots (Figure 4-3), while a factor below one means the compression, shown as orange to red colour dots. The stretching factor in the Gippsland Basin mainly varies between 1.2-1.7 (Müller et al., 2019). The maximum value (~2.7) occurred at the outer eastern edge of the basin, which is related to Tasman Sea spreading (Figure 4-3). The crustal stretching factor assumed an initial crust thickness of 35 km at 140 Ma before the first rift (Figure 4-5a). The crustal thickness of the Gippsland area is about 30 km before the second rift event at 99 Ma (Figure 4-5b).

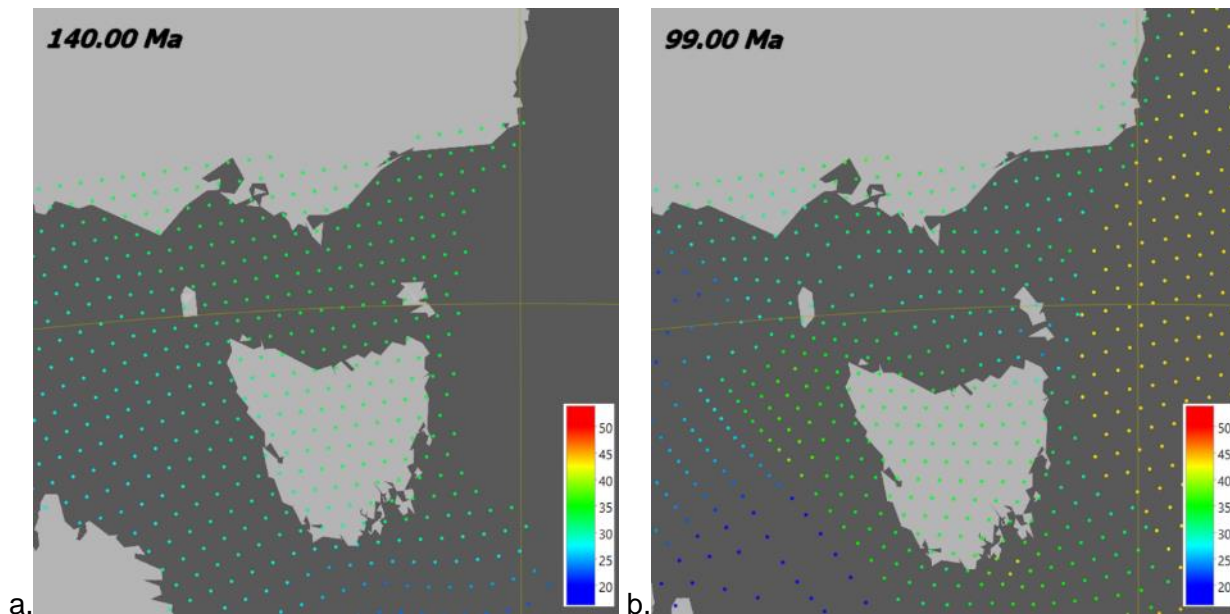


Figure 4-5 Crustal thickness of Australian Plate, Gippsland area and surroundings, shown by the global density points. a. crustal thickness at 140 Ma; b. crustal thickness at 99 Ma (Captured from GPlates model, Müller et al., 2019).

4.2 Structural and Stratigraphic Analysis in *Petrel* Software

A good basin-wide 3D structural and stratigraphic model of the Gippsland Basin is made in *Petrel*, which has not been done previously, and will provide:

- a much better understanding of the geology over the onshore and offshore regions
- the ability to constrain and validate the forward simulation of the sedimentary history
- the ability to constrain and validate the burial and thermal model in *PetroMod*.

The Gippsland Basin has been extensively studied, explored and developed for its coal, water and petroleum resources on a continuous basis for almost a hundred years. Consequently there is a large amount of geoscience data available for detailed basin analysis. Chapter 3 details the sources and types of data used in this study.

The data sets imported into *Petrel* to build the 3D realistic model include:

- 2D & 3D seismic surveys and interpreted gravity maps used to interpret the faults and horizons and thereby build the gross structural and horizon model.
- Location, downhole survey and checkshot data for the wells and coal bores used to locate the well data and tie to the seismic interpretations.

- Downhole well logs for the petroleum and stratigraphic bores. Most have gamma-ray (GR), sonic (DT), Neutron (NPHI) and Density (RHOB) logs but many other logs were loaded where available.
- Lithology logs for the coal bores. These are mostly drillers logs some augmented with downhole electric logs.
- Biostratigraphic data includes palynological spore pollen and dinoflagellate zones, microplankton and planktonic foraminifera zones (Partridge, 2006). These were used to estimate horizon and strata ages to build the stratigraphic model and burial history models.
- Property data includes formation temperature (mainly bottom hole and some downhole temperature data), formation pressure, vitrinite reflectance (Ro), total organic matter (TOC), hydrogen index (HI), moisture, ash and various other properties where available. The property data is used to build the property models within the structural and stratigraphic 3D model. Together, the full geological model provides the realistic constraints for the theoretical models (see Chapter 4, Chapter 5 and Chapter 8).

4.2.1 Well Correlations

The well correlation aimed to produce a set of consistent well top picks from well to well rather than redefine an optimum set of well top picks. This is a practical approach for a regional basin-wide modelling of the entire Early Cretaceous to Holocene stratigraphy, especially given the very large number of wells and the extreme lateral facies changes in the basin. Well tops were imported from the various government databases but the long history of the basin means that formation names and hence well tops have changed through time, and the criteria for picking formation tops also varies from one field to another. Hence, these well tops were used to provide a first pass well correlation and the main well top picks required a quality check in all the main wells for consistency.

Picking the well tops was assisted by generating consistent lithofacies logs from the most common well logs using appropriate log cut-offs and the calculator functions in *Petrel* (e.g., GR, Sonic, NPHI-RHOB) as given in Appendix 1. Then the biostratigraphic data was used in conjunction with the seismic and well logs to pick the main regional unconformities which form good reference

marker horizons (e.g., the top Latrobe, Marlin, Seahorse, North Longtom and Otway unconformities). These unconformities or correlatives in most cases have corresponding palynological zones or missing zones, are mostly visible on seismic, and are important boundaries between groups or subgroups required for modelling the geological history. For example, both onshore and offshore biostratigraphic data clearly indicate the significant missing palyno-zones between the early Cretaceous and Eocene (Table 4-1), which represents the regional Otway unconformity that marks the boundary between the Strzelecki and Latrobe groups. Long-term palyno-zone gaps such as this may involve multiple regional unconformable events.

The logs, palynology and seismic data were used to follow the well tops, as much as practicable, for the main picks used in previous studies as provided by the most recent or relevant Well Completion Reports (WCR) to create the well correlations used in this study (Figure 4-6). For example, the well top of the top Latrobe Group is commonly picked at the top coarse clastic layer in the Latrobe group or just above the top to include some of the canyon fill (e.g., Flounder Formation) to account for facies change and either can be overlain directly by clean carbonates with low GR signatures.

Table 4-1 Palynology data from multiple offshore and onshore wells indicating the regional unconformity between the Strzelecki Group and Latrobe Group

Age(Ma)	Spore Pollen zones	Depth (m)											
		Baleen 1	Flathead 1	Gannet 1	Kyarra 1A	Leatherjacket 1	Patricia 1	Salt Lake 1	Sperm Whale 1	Tarra 1	Wahoo 1	Wellington Park 1	Whale 1
33.89-38.4	<i>middle N. asperus</i>	658-698 (swc)		676.66	1013-1148 (swc)		705 (swc)			2177.5-2232.5 (swc)			445 (swc)
38.4-45	<i>lower N. asperus</i>	Paly zone missing	455.68-462.08 (swc)	697.99	1148.5-1166 (swc)	750.7-754 (swc)	720-739.5 (core)			2237-2257 (swc)	458.11 (swc)		462 (swc)
45-50.5	<i>P. asperopolus</i>		472.14-472.44 (swc)			755.6 (swc)	743.5 (core)						463.5 (swc)
50.5-53.2	<i>upper M. diversus</i>						757.4-759.8 (swc)						
53.2-54.3	<i>middle M. diversus</i>						775.9-809.9 (swc)						
54.3-55.8	<i>lower M. diversus</i>									2274-2305.5 (swc)			
55.8-57	<i>upper L. balmei</i>					1215 (swc)			1192.99 (swc)		2362.1 (swc)	480.06-487.68 (swc)	
57-65.5	<i>lower L. balmei</i>								1293.57-1524 (swc)	846-851 (swc)	2446 (swc)		1133.55-1135.38 (swc)
65.5-67	<i>upper F. longus</i>										2474-2579 (swc)	562.05-576.07 (swc)	
67-75.5	<i>lower F. longus</i>												
75.5-80.6	<i>T. lillieii</i>												
80.6-83.4	<i>N. senectus</i>												
83.4-85.8	<i>T. apoxyxinus</i>												
85.8-93.5	<i>P. mawsonii</i>					838.8-849 (swc)							
93.5-99.6	<i>A. distocarinatus</i>												
99.6-103.5	<i>P. pannosus</i>						821-880 (swc)						
103.5-110.4	<i>C. paradoxa</i>	709-1014.1 (swc)											
110.4-115.5	<i>C. striatus</i>		481.58-1064.97 (swc)	719.33						2599-2879.9 (swc)	592.23-735.48 (swc)	1163.73-1322.83 (swc)	475-806 (swc)
115.5-125	<i>C. hughesii</i>			725.42-1450.85	1257 (swc)	910.7 (swc)		1574.29-1602.94 (swc)					

This is complicated by the overlying carbonate log signatures and the top Latrobe being a composite regional unconformity, with the subcropping facies of the uppermost unit varying in age

and lithofacies above and below the unconformity, commonly from more marine in the eastern part of the basin to fluvial-deltaic, non-marine lacustrine and alluvial further west in the onshore areas. Figure 4-6 for instance, shows how in Bignose-1 the Lakes Entrance carbonates above the unconformity have a much lower GR value than the Flounder Formation which consists of fine-grained glauconitic marine clastics. These in-turn have higher GR values than the coarse clean sands of the older Kingfish Formation of the Latrobe Group which here are barrier or shoreface sands in a marginal marine section. Whereas in Barracouta-1 further inshore to the east the upper part of the Latrobe Group is much younger and comprises a thin barrier sand section overlying a lower coastal plain section with well-developed coals. The complete well section of Barracouta-1 and Bignose-1 is given in Appendix 2.

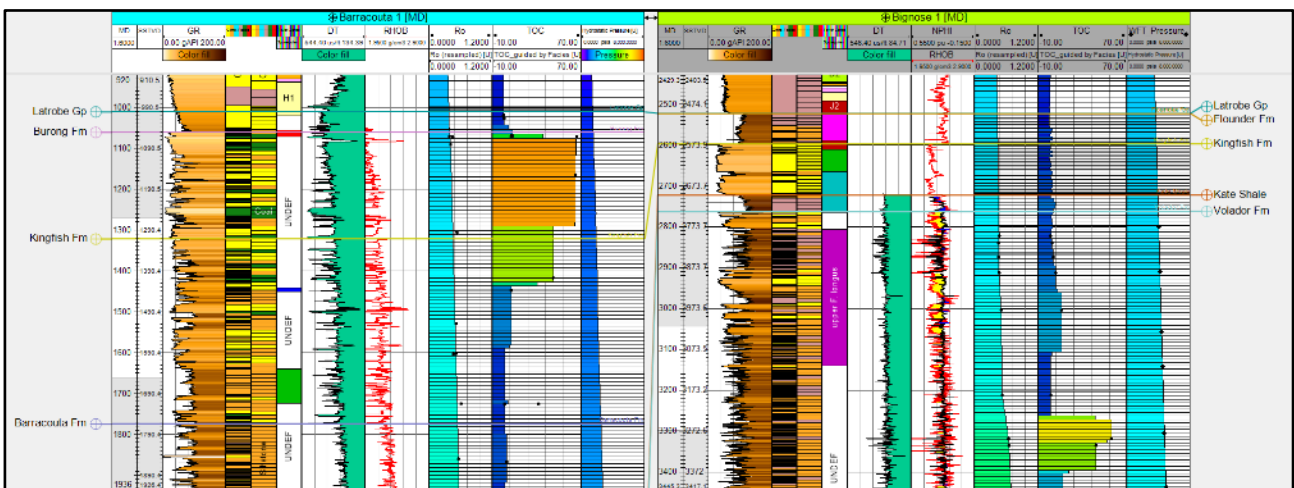


Figure 4-6 Well panel from Bignose-1 from the eastern part of the offshore basin and Barracouta-1 in the west of the offshore basin showing the substantial facies and log changes in the subcropping units at the Top Latrobe. From left to right: GR, Lithofacies detailed log, Lithofacies blocked layer model property, Palynology zone, DT, NPHI & RHOB, Temperature blocked layer model and data (black dots), Vitrinite reflectance blocked layer model and measured core Ro data (black dots), TOC blocked layer model and RockEval data (black dots), Pressure blocked layer model and Wireline Formation Test Pressure (black dots).

4.2.2 Seismic Interpretation

The seismic interpretation is based on interpretation of the merged 3D survey and the 2D lines to provide coverage of most of the basin. The 3D and 2D seismic surveys are in two-way-time (TWT) and these were used for the main interpretation. In addition, the TWT 3D seismic survey has been converted to a 3D seismic survey in depth using a new average velocity model to assist the modelling (see 4.2.3). The merged 3D survey covers the major offshore part of the Gippsland Basin, including part of the North Platform, Northern Terrace, Central Deep and Southern Terrace.

Interpretation of the South Platform used the 'gdpi 10' 2D survey (Figure 4-7). In addition to the Seafloor surface seven horizons were interpreted: Mid Miocene, top Lakes Entrance Formation, top Latrobe Group, base Cobia Subgroup, Kate Shale/near Base Tertiary, top Golden Beach Subgroup and top Strzelecki Group Figure 4-8. Some interpreted maps are available at the Victoria Geological Survey GeoVic website. Hence, some of the horizons were imported from this source to guide the final interpretation. The Horizons generated are described below:

- The Seafloor map was imported from the Australian bathymetry and topography grids downloaded from Geoscience Australia.
- The Mid Miocene was imported from the Regional 3D geological framework model, Victorian gas program (Powell et al., 2020) and GeoVic 3D model packages (in turn based on the 2005 3D Geo Pty Ltd interpretation) and in-part re-interpreted and corrected based on the revised well correlations and some regional lines provided by Dr Guy Holdgate. This is a very complex surface resulting from the shelf canyoning and is mainly required to help guide the burial modelling around the mid-Miocene level.
- The top Lakes Entrance Formation/near top Oligocene) and the top Latrobe Group (Figure 4-9) were interpreted throughout the 2D survey on the South Platform. In the area covered by the 3D seismic survey these horizons were re-interpreted where necessary and tied to the revised well tops from horizons imported from the GeoVic 3D model seismic horizons .
- The base Cobia Subgroup and top Golden Beach Subgroup are interpreted throughout the 3D seismic volume, and the resulting maps are shown in Figure 4-10.
- The Kate Shale/near Base Paleogene and the top Strzelecki Group, were re-interpreted and tied to the revised well tops from horizons imported from the GeoVic 3D model seismic horizons.

The Horizons were tied to the corresponding well tops in twt and depth via the checkshot surveys. They are assigned approximate ages for the burial modelling based on the biostratigraphic data, noting that most of the formations and well tops are diachronous (Table 4-2).

The fault interpretation included manual picking of over 170 main faults and over 690 fault patches were generated by ant-tracking to help to guide the interpretation (e.g., Figure 4-8).

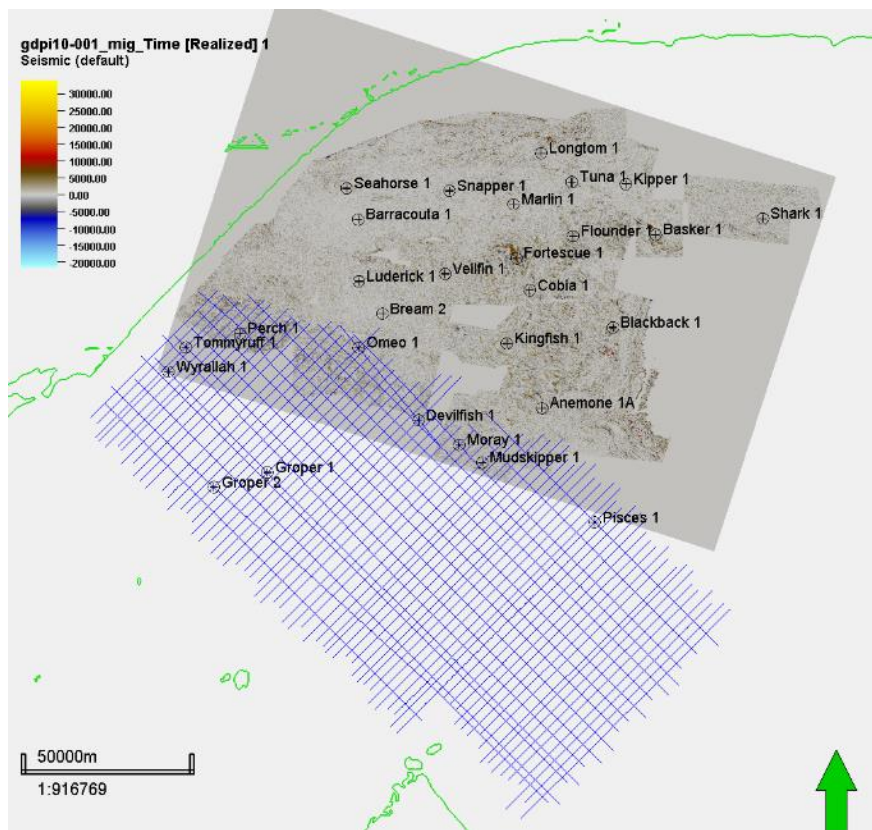


Figure 4-7 Merged 3D seismic survey (at Z = -2556) and 2D seismic survey 'gdpi 10' shown in purple lines. The green line shows the coastline.

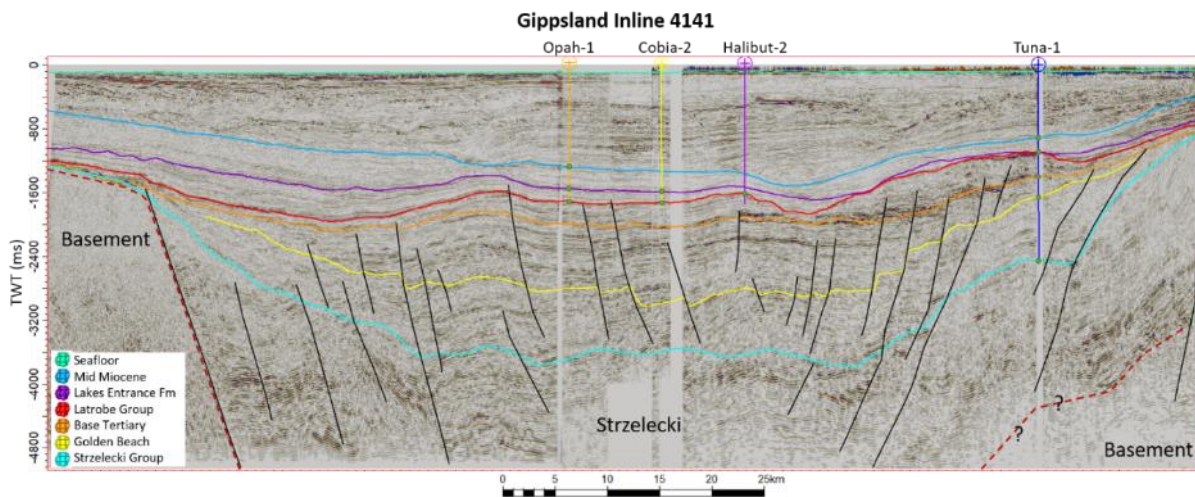


Figure 4-8 Seismic interpretation at Inline-4141 showing interpreted horizons. The Base Cobia pick is not shown as it is close to the Top Latrobe on this section. The red dashed line indicates the probable top Basement.

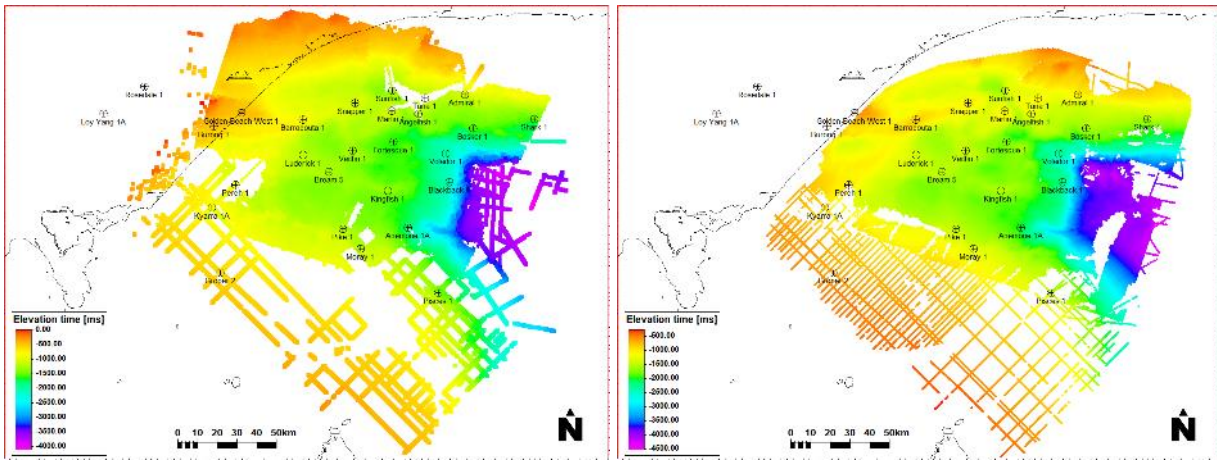


Figure 4-9 Seismic interpretation throughout the 3D volume and the 2D survey on the South Platform, the Bass Canyon and part of the North Platform. Left: top Lakes Entrance Formation; Right: top Latrobe Group.

Table 4-2 Seismic horizons with the corresponding well tops and approximate age

Seismic Horizons	Well Tops offshore	Approximate Age
Topography-Bathymetry	Land Surface or Seafloor	0 Ma
Mid Miocene	Lower T. bellus/ D1, D2, E1, E2 (Talyor 1961)	11.6-16.2 Ma
Top Lakes Entrance	Lakes Entrance Formation	~23 Ma
Top Latrobe Group	Latrobe Group	~32 Ma
Base Cobia Subgroup	Barracouta/Kingfish/Flounder Formation	~48 Ma
Base Paleogene	Kate Shale	~65 Ma
Top Golden Beach Subgroup	Anemone Formation/Chimaera Formation	~75 Ma
Top Strzelecki Group	Strzelecki Group	~93.9-100 Ma

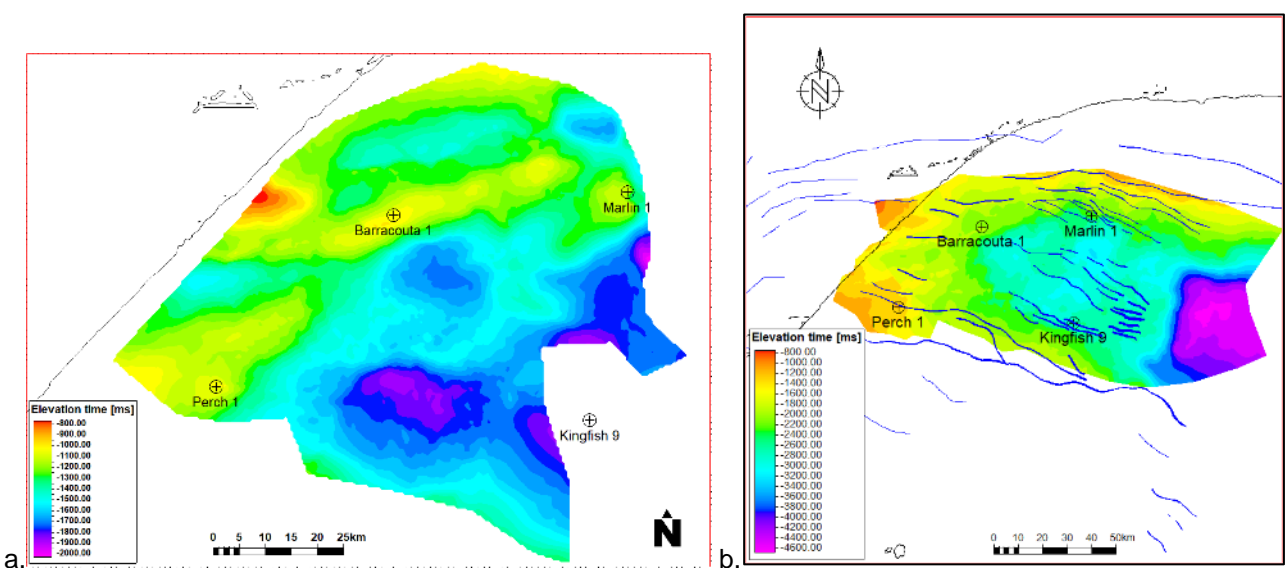


Figure 4-10 a: base Cobia Subgroup map, generated from depth seismic interpretation. b: top Golden Beach Subgroup map, generated from TWT seismic interpretation. The faults are in blue, coastline in black.

4.2.3 Velocity Model & Depth Conversion

The velocity model released by GeoScience Victoria in 2013 (McLean & Blackburn, 2013) partially covers the Gippsland Basin offshore area, but does not fully cover the study area (Figure 4-11).

Hence, the GeoVic velocity model was used as a reference and a new interval velocity model was built to cover the entire study area.

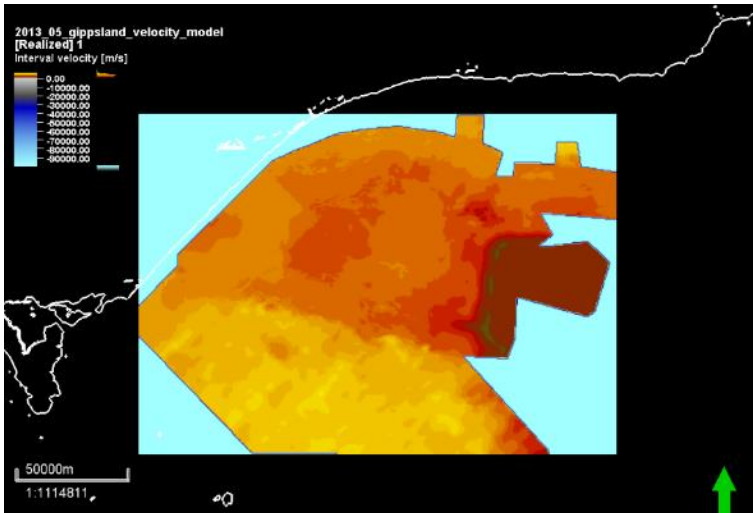


Figure 4-11 2D map of the GeoVic Gippsland velocity 3D cube survey.

The new velocity model was built using the 'Advanced velocity model' process in *Petrel*, for which the settings and method details are given in Appendix 3. The velocity model converts from two-way time (TWT) to Depth (Z), using the equation $V = V_0 + K * Z$ (k values derived from the well time-depth relationship). The velocity modelling utilises four surfaces: Seafloor, top Latrobe Group, top Strzelecki and top Basement. The Seafloor depth map was calculated from the seafloor time map using an average seawater velocity of 1515 m/s. The basement depth map is calculated and re-gridded from the OZSEEBASE interpreted gravity map to assist with Strzelecki modelling which adds an extra Horizon to the overall modelling. Figure 4-12 shows the interval velocity maps for each layer in the new velocity model. The velocity model well tie report is given in Appendix 4.

The new velocity model was used to depth convert the TWT 3D seismic survey and the interpreted seismic TWT maps. The converted depth maps were then merged with the corresponding onshore depth maps of equivalent age which were imported and gridded from Geoscience Victoria VGP20 packages (Powell et al., 2020) (Table 4-3). The merged depth maps (Figure 4-13) were quality checked and prepared as input horizons for the structural modelling. The velocity model was also

used to depth convert 74 of the main faults that were selected for use in the basin-wide 3D *Petrel* structural model (Figure 4-14).

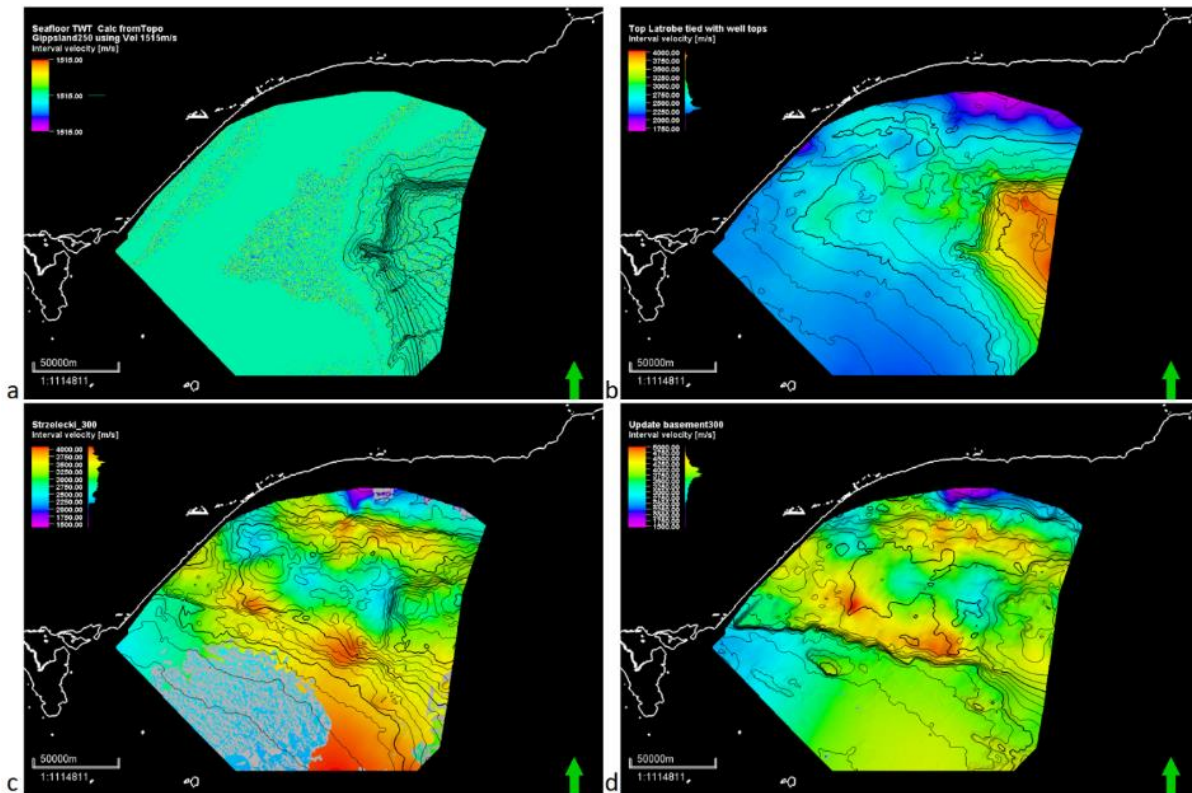


Figure 4-12 Interval velocity map for each layer: a. Seafloor; b. top Latrobe; c. top Strzelecki; d. top Basement. The two-way time is used for the visual vertical position.

Table 4-3 Horizons and Zones used in the Basinwide *Petrel* model

ONSHORE	OFFSHORE	ZONES
Topography	Bathymetry	
		Post Mid Miocene
Top Yallourn Seam	Mid Miocene	
		Early-Mid Miocene
Top Morwell 1B Seam	Top Lakes Entrance Formation	
		Oligocene-Early Miocene
Top Traralgon Seam	Top Latrobe Group	
		Cobia Subgroup
	Base Cobia Subgroup	
		Upper Halibut Subgroup
	Base Paleogene/Kate Shale	
		Lower Halibut Subgroup
	Top Golden Beach Subgroup	
		Golden Beach Subgroup
	Top Emperor Subgroup	
		Emperor Subgroup
Top Strzelecki Group	Top Strzelecki Group	
		Strzelecki Group
Basement	Basement	

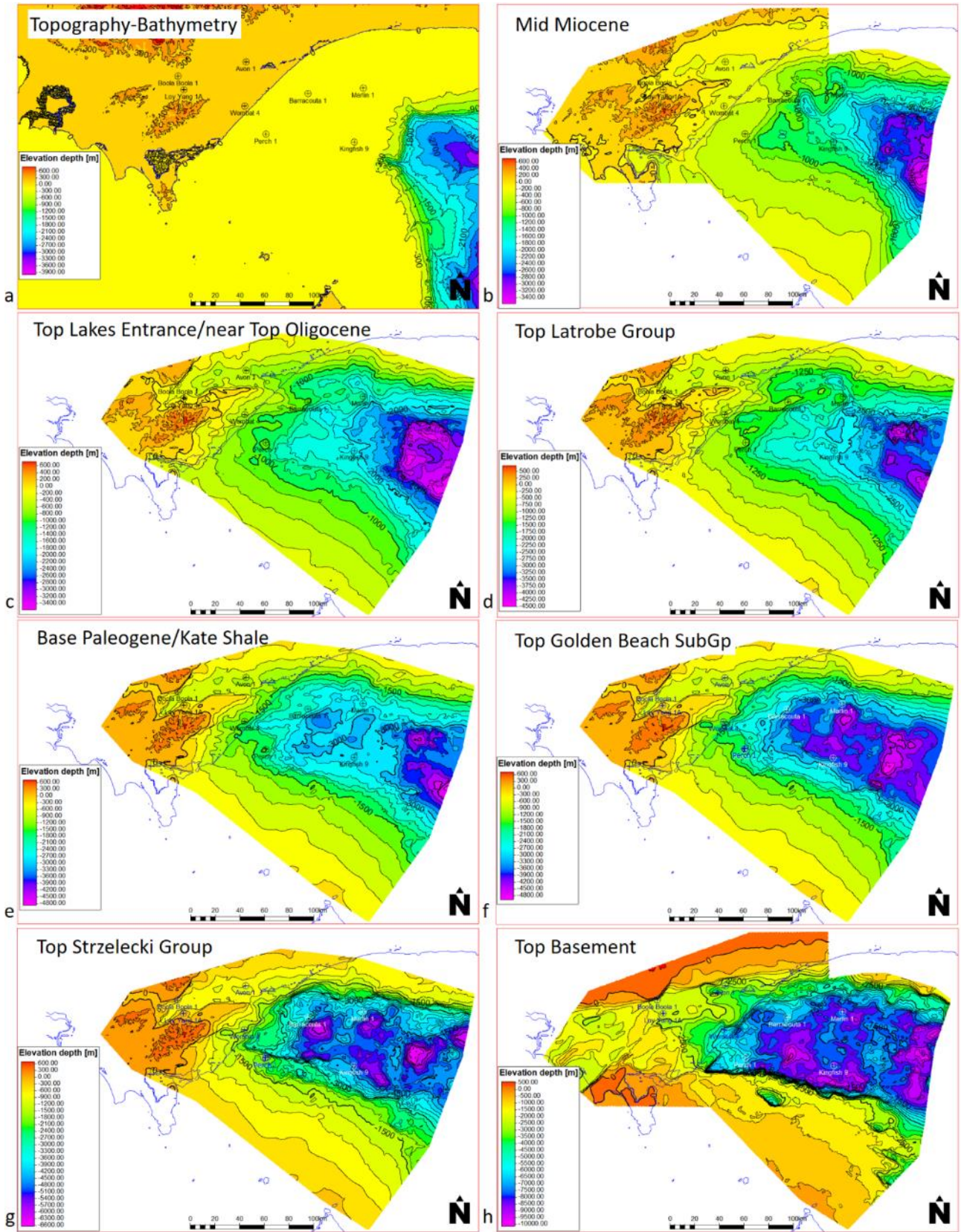


Figure 4-13 Merged Depth maps of major stratigraphic surfaces of the Gippsland Basin. The coastline is shown in blue.

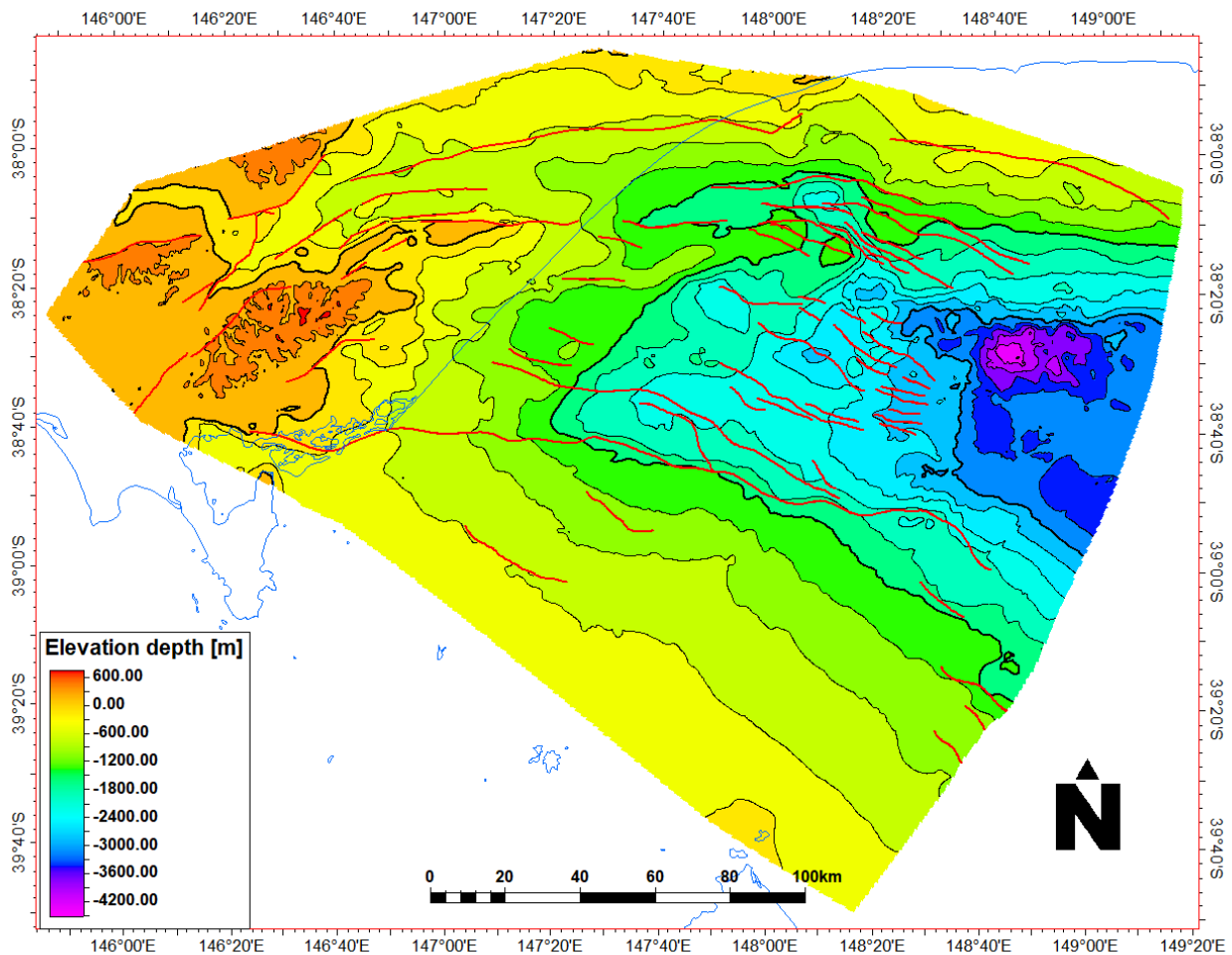


Figure 4-14 Interpreted faults, which have been selected and utilised in the structural modelling via the pillar grid method are shown at the merged Top Traralgon Seam - Top Latrobe Group Surface.

4.3 Structural and Stratigraphic Models

There are several methods available in *Petrel* to build a structural-stratigraphic model. The Structural Framework method was tried but the complexity and scale of the faulting with long inverted normal faults that change throw along strike meant the results were not satisfactory. The best results and the most efficient method was to use the Corner Point gridding method which involved:

- Fault Modelling of each fault and editing of the pillars
- Pillar Gridding of the faults with trends
- Make Horizon modelling with editing of fault throws on horizons to produce Horizon lines.

This method ensured a good integrated 3D structural and stratigraphic model. The input horizons and faults were already in depth so there was no need to depth convert the 3D grid.

The Stratigraphy was then refined using:

- Make Zones for the main sequences or Subgroups between the seismic horizons
- Layering to insert the number of Layers in each zone so that their thickness was adequate for practical modelling of the Properties.

Details of the above methods are given in Appendix 5.

Separate structural and stratigraphic models were built for the entire Gippsland Basin and a more detailed model for the Latrobe Valley.

4.3.1 Entire Gippsland Basin model

The 3D structural model of the entire Gippsland Basin contains nine horizons, nine stratigraphic zones, and 540 layers with a grid resolution of 500x500 metres. The horizons used were the merged depth maps (Figure 4-13) and major faults. The resulting stratigraphic zones consist of the post Mid-Miocene zone, the Mid-Miocene zone, the Lakes Entrance Formation, the Cobia Subgroup, the Upper Halibut Subgroup, Lower Halibut Group, Golden Beach Subgroup, Emperor Subgroup and Strzelecki Group (Table 4-3). The Seaspray and Strzelecki Groups have coarser layer thickness, while the Latrobe Group uses a finer layer structure, with an average thickness of about 10m for each layer to capture more precisely the lithological and petrophysical detail.

Figure 4-15a shows an example of the basin-wide structural model at the top Strzelecki Group level with the Strzelecki fault planes. The east-west cross-section through the 3D model demonstrates the major geological units that are captured in the model across the Latrobe Valley, Seaspray Depression, offshore area and below the Bass canyon (Figure 4-15b). The structural model suggests the onshore part contains many reverse faults associated with the Strzelecki Group that cut the younger sediments and Basement including some large faults that bound the onshore basin. Faults developed offshore consist of many extensional faults and some large reverse faults with associated folds. The offshore boundary faults have large displacement and indicate that extensional movement waned by the late Eocene (near top Latrobe Group). The

reverse faults and associated folds were still active during the Oligocene, and are related to the compression from the Eocene to Holocene.

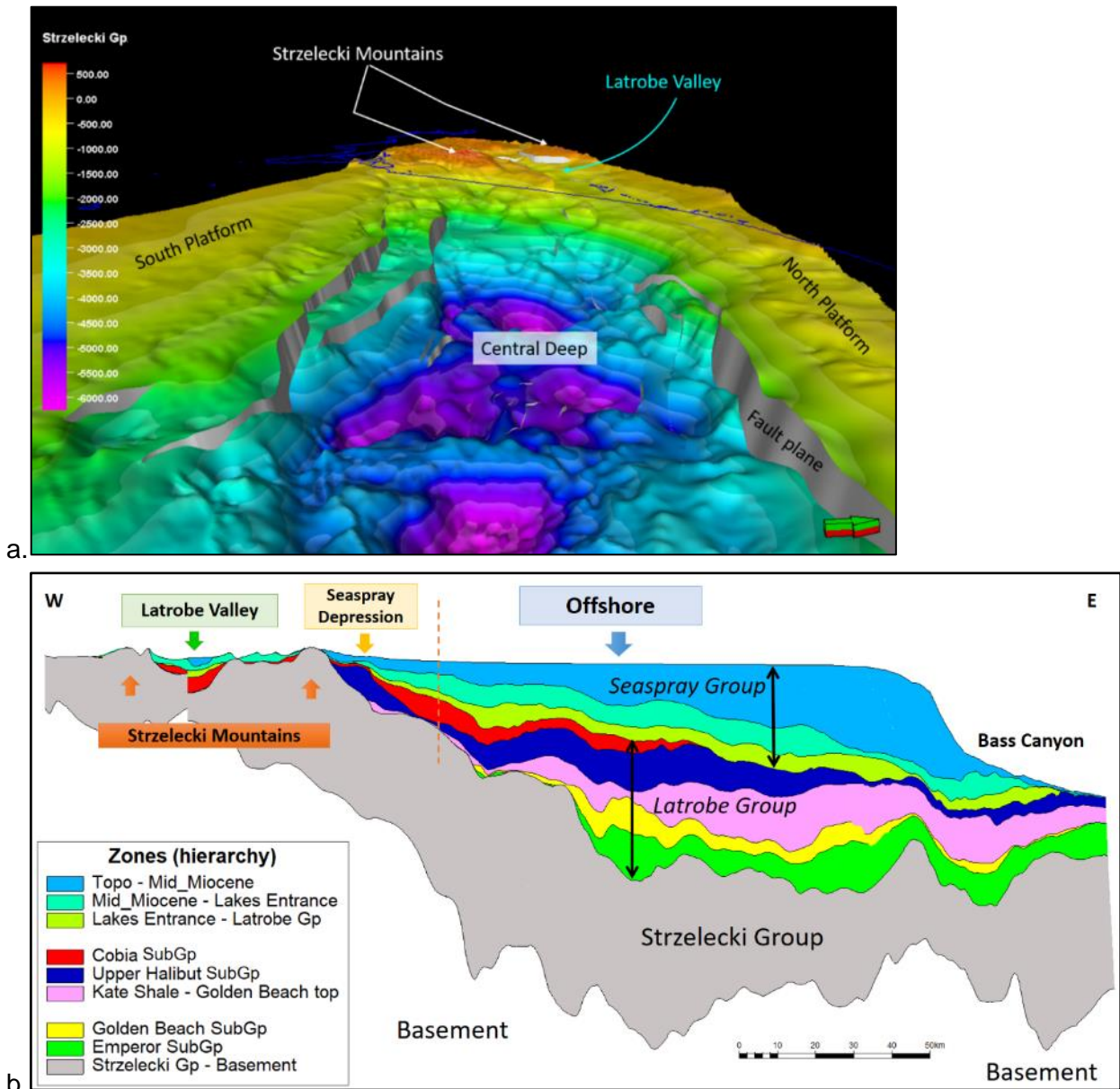


Figure 4-15 Structural model examples: Strzelecki active faults and top Strzelecki group surface are shown in a 3D window view (a); west-east cross-section through the centre of the basin (b).

The isopachs for each stratigraphic zone used in the 3D structural and stratigraphic model are shown in Figure 4-16. The modelled zones approximate to very large scale sequences developed across the basin and their isopachs are useful indicators of sedimentation, erosion and burial. These modelled zones are briefly described below (details of the stratigraphy have been given in Chapter 3 and the sedimentary evolution are given in Chapters 5 and 6):

4.3.1.1 *Sale, Seaspray and Latrobe Valley Group*

- **Post Mid-Miocene zone** is the youngest depositional modelled zone and covers most of the basin (Figure 4-16a). In the western onshore areas this zone is thin and mainly consists of uppermost alluvial-fluvial sediments (Post Yallourn Formation and Sale Group), with slightly thicker fluvial-deltaic to coastal sediments below and further east (Tambo River Formation), but thickening rapidly offshore into the Central Deep, comprising shallow marine carbonates to deep water marls (Seaspray Group, Hapuku Subgroup). The preserved thickness of the post Mid-Miocene zone is between 100 to 400 metres in the onshore area and over the North and South Platforms. Offshore the thickness varies rapidly from about 500 metres inshore to a maximum thickness of about 2300 metres in the north and central areas of the Central Deep, near the head of the present Bass Canyon (for which no clear explanation currently exists for its origin; Norvick, 2005). Some large-scale submarine canyons developed during this period and cut into the Mid-Miocene sediments and their locations tend to lie above the older canyons. There have been numerous episodes of cut and fill by these canyons suggesting the current Bass Canyon has also migrated away from the location of the underlying canyons. Much thinner sediments are deposited in the Bass Canyon area with the suggestion that turbidites may exist downslope.
- **Early-Mid Miocene sediments** in the western onshore areas consist of alluvial and floodplain sediments with very thick coal seams (Yallourn and Morwell 1A coal seams) becoming lower coastal sediments further east where the coal seams thin and are split by mudstones and sandstones behind a barrier system (Balook Formation). Offshore the sediments comprise shallow marine sandstones and carbonates (Gippsland Limestone) to deep water marls (Albacore Subgroup). The Early-Mid Miocene sediments are about 100 metres thick in the Latrobe Valley increasing to about 500 metres inshore with a maximum thickness of about 1200 metres in the south-west near the Pisces Sub-basin. The main depocentre is the Central Deep thinning towards the platforms and onshore and overlapping the Strzelecki Ranges. Post Mid-Miocene canyon development mainly orientated NNW has reduced the isopachs by erosion and non-deposition in some areas (Figure 4-16b)

- **Early Oligocene to Mid Miocene Zone** consists of alluvial and floodplain sediments with very thick coal seams (Morwell 1B and Morwell 2 seams), becoming lower coastal sediments further east where the coal seams thin and are split by mudstones and sandstones behind the barrier system (Balook Formation). Offshore the sediments comprise shallow marine sandstones and carbonates (Lakes Entrance Formation) to deep water marls (Angler Subgroup). This zone is about 100-200 metres thick in the Latrobe Valley to the west, increasing to about 500m inshore with a maximum thickness is about 1140 metres to the east near Volador-1. Most sediments are preserved within the Central Deep and Latrobe Valley Depression but are missing from erosion or non-deposition above the anticlines such as Barracouta, Snapper, Marlin and some onshore anticlines. The Turrum channel system in particular removed a large volume of the Lakes Entrance Formation (Figure 4-16c).

4.3.1.2 *Latrobe Group and Equivalents*

- **Cobia Subgroup** comprises several formations that occur in the upper part of the Latrobe Group (mainly Burong Formation) and its equivalents onshore (Traralgon Formation) and is approximately Middle Eocene to Early Oligocene in age. It is bounded by the Latrobe Unconformity at the top and equivalents onshore and the Marlin Unconformity at the base and contains some significant hydrocarbon reservoirs. Deposition of alluvial and fluvial sediments with thick coal seams was initiated for the first time in the Latrobe Valley to the west during this time (Traralgon Formation). The main Cobia Subgroup deposition comprises fluvial-deltaic to coastal sediments (Traralgon/Burong formations) and is best developed in the eastern part of the onshore Seaspray Depression and western part of the Central Deep, after the barrier systems were pushed westwards by the Early Oligocene transgressions (Figure 4-16d). It thins towards the east being absent in the Kingfish field, or where it has been entirely eroded by submarine channels (e.g., Marlin), and comprises shallow marine and condensed shales (Gurnard, Turrum formations). The average thickness of the Cobia Subgroup is only about 130 metres, with the maximum thickness about 750 metres in the nearshore area close to Golden Beach-1.
- **Upper Halibut Subgroup** contains several of the major hydrocarbon reservoirs within the Latrobe Group and is mainly Palaeocene to Middle Eocene, lying between the Marlin

unconformity and the Base Paleogene marker and equivalents. It is poorly developed onshore where it mainly consists of thin non-marine conglomerate and sandstone (Yarram Formation) with the Currajung Volcanics. The Upper Halibut is mainly confined to the western part of the offshore basin, thinning towards the east where it has been partially eroded by submarine channels (e.g., Tuna-Flounder channels), with thin units in the Pisces sub-basin (Figure 4-16e). It comprises fluvial-upper delta plain sediments with thin coals (Barracouta Formation), fluvial-lower delta or lower coastal plain sediments with thicker coal seams (Kingfish Formation), and nearshore marine sands and shallow marine shales (Mackerel Formation). The average thickness is about 170 metres and the maximum thickness is about 1600 metres in the Central Deep along the Barracouta- Snapper anticlinal trend. Only sporadic thin sediments of this zone have been preserved on the North and South Platforms whereas deep marine fans downslope from the Tuna-Flounder canyons are possible.

- **Lower Halibut Subgroup** spans the late Campanian and Palaeocene and is more widespread being preserved over all the Central Deep, on the North Terrace and in the Pisces sub-basin to the south-east (Figure 4-16f). It has a similar facies distribution, consisting of alluvial and fluvial-upper delta sediments with minor thin coals (Barracouta Formation), fluvial-lower delta to coastal plain sediments with thin coal seams (Volador Formation), overlain by a widespread dark grey shale associated with a marine incursion (Kate Shale) and shallow marine sandstones and shales on the eastern margins (Mackerel Formation facies equivalents). The average thickness is about 160 metres, and the maximum thickness is about 1590 metres near the Kingfish and Fortescue fields.
- **Golden Beach Subgroup** forms the lower Latrobe Group from the Santonian to the end Campanian. It is confined to the Central Deep with thin occurrences mainly on the North Terrace. The facies distribution is poorly known mainly from wells drilled near the edge of central deep and a similar number located on the North Terrace. It mainly includes fluvial-deltaic sediments deposited over most of the Central Deep area (Chimaera Formation) developed behind a proto-barrier system with marine shales to the east (Anemone Formation). Campanian volcanics are known from several wells and on seismic. The seismic data also shows that the Golden Beach Subgroup is limited by and controlled by the basin boundary

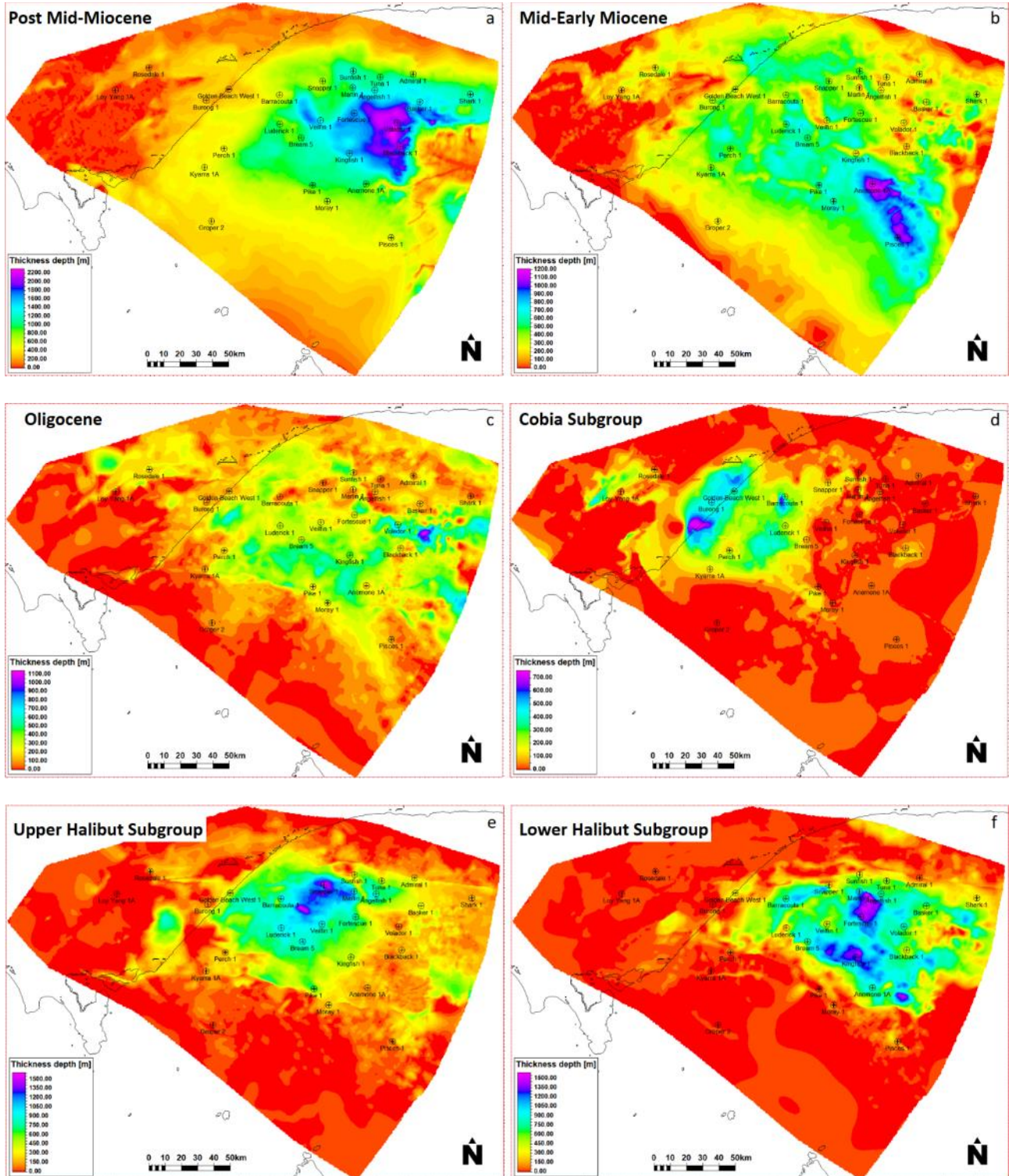
faults with the sediment thickness varying from tens of metres on the margins up to more than 1180 metres (Figure 4-16g). The seismic data and thickness trends show that the major NW-SE faults are syndepositional extensional faults with rotation in places and asymmetric thickening in the hanging walls on both the southern and northern margins. Consequently, the thickest sections are deposited in the south-western and north-eastern parts of the Central Deep with thinner interpreted sections in the middle and elsewhere.

- **Emperor Subgroup** is the oldest depositional zone mapped in the Latrobe Group (Cenomanian-Coniacian) that has been mapped between the North Longtom Unconformity at the top and the Otway Unconformity at the base. The Emperor Subgroup is known from a number of wells mainly drilled on the North Platform-Terrace with a small number on the South Platform-Terrace. It consists of alluvial and fluvial sediments mainly deposited around the southern basin margins (Kersop Arkose) and the northern basin margin (Curlip and Admiral formations). Non-marine lacustrine shales with thin interbedded sands (Kipper Shale) are interpreted to cover most of the basin centre. The Emperor Subgroup has been preserved mainly in the Central Deep, the North Terrace and Pisces Sub-basin, with average thickness about 170 metres and up to a maximum thickness of about 2000 metres in several locations (Figure 4-16h). Fault control is not as clear in this zone and confident seismic interpretation is more difficult at the greater depths. Nevertheless, it appears both the WSW and NE orientated faults were active and have produced thickening in a series of smaller half grabens (Power, 2003) (Figure 4-17).

4.3.1.3 *The Strzelecki Group*

This is the oldest depositional unit of the Gippsland Basin, formed during the Early Cretaceous with a complex stratigraphy dominated by non-marine and lacustrine intracratonic quartz clastic and volcano-clastic sediments (refer Chapter 3). Two main boundary faults and some South Platform extensional faults create the main mapped structures for the Strzelecki Group. Onshore sediments are thinner than offshore sediments. Most sediments are preserved onshore where they outcrop with uplift and erosion causing significantly loss of section. Thicker sections are preserved in the Central Deep and on the North Platform and Terrace. In the south the Strzelecki Group only occurs on the South Terrace and is not preserved over the South Platform except in an undrilled

asymmetric sub-basin between Groper-2 and Pike-1. The Strzelecki Group basin fill is asymmetric with the thickest sections occurring along and in the hanging wall of the main extensional faults on the southern margin. Typically the thickness for this zone is over 2000 metres and the maximum estimated thickness is up to 6650 metres towards the southern boundary fault.



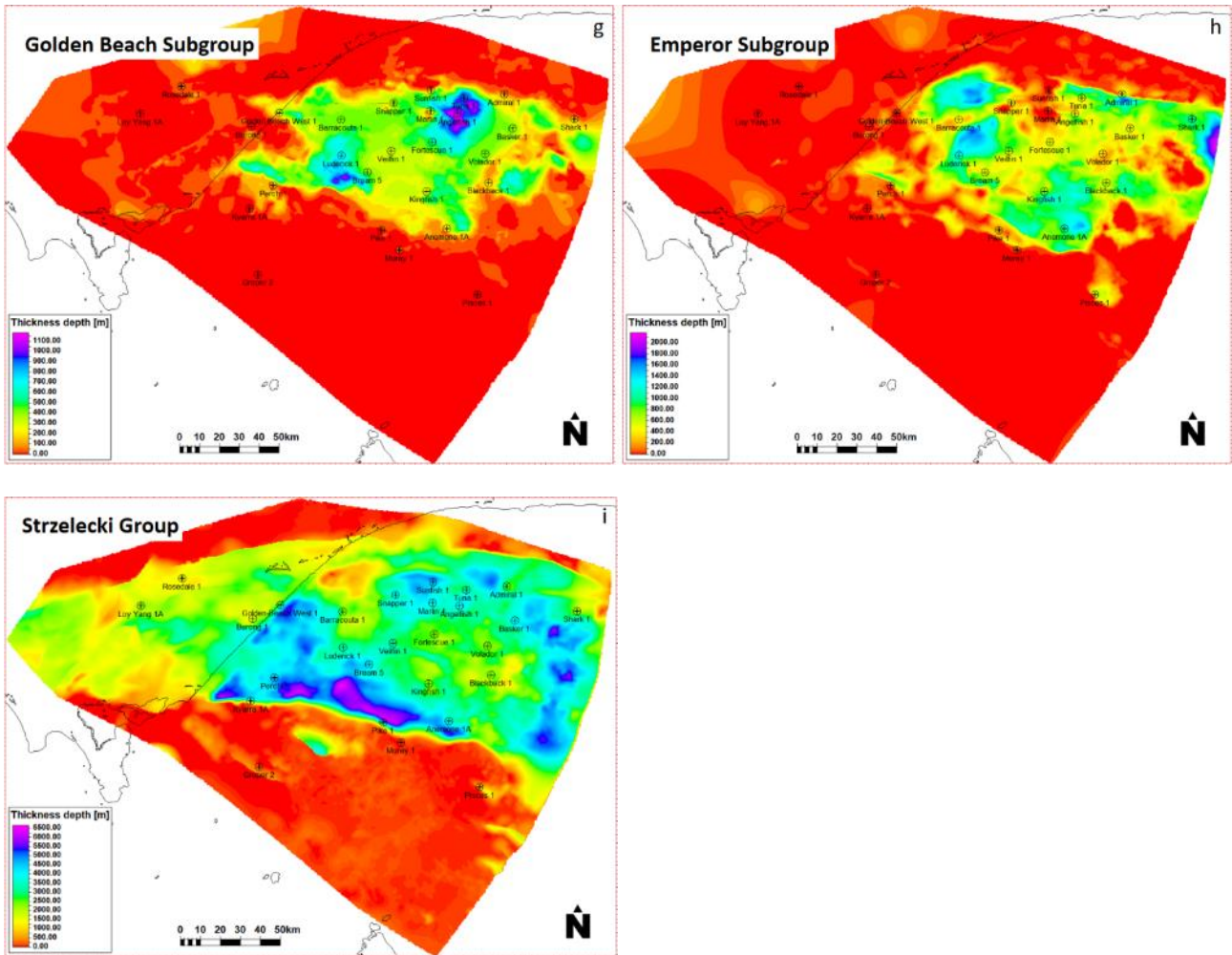


Figure 4-16 Isopachs for each of the nine stratigraphic zones used in the 3D structural and stratigraphic model.

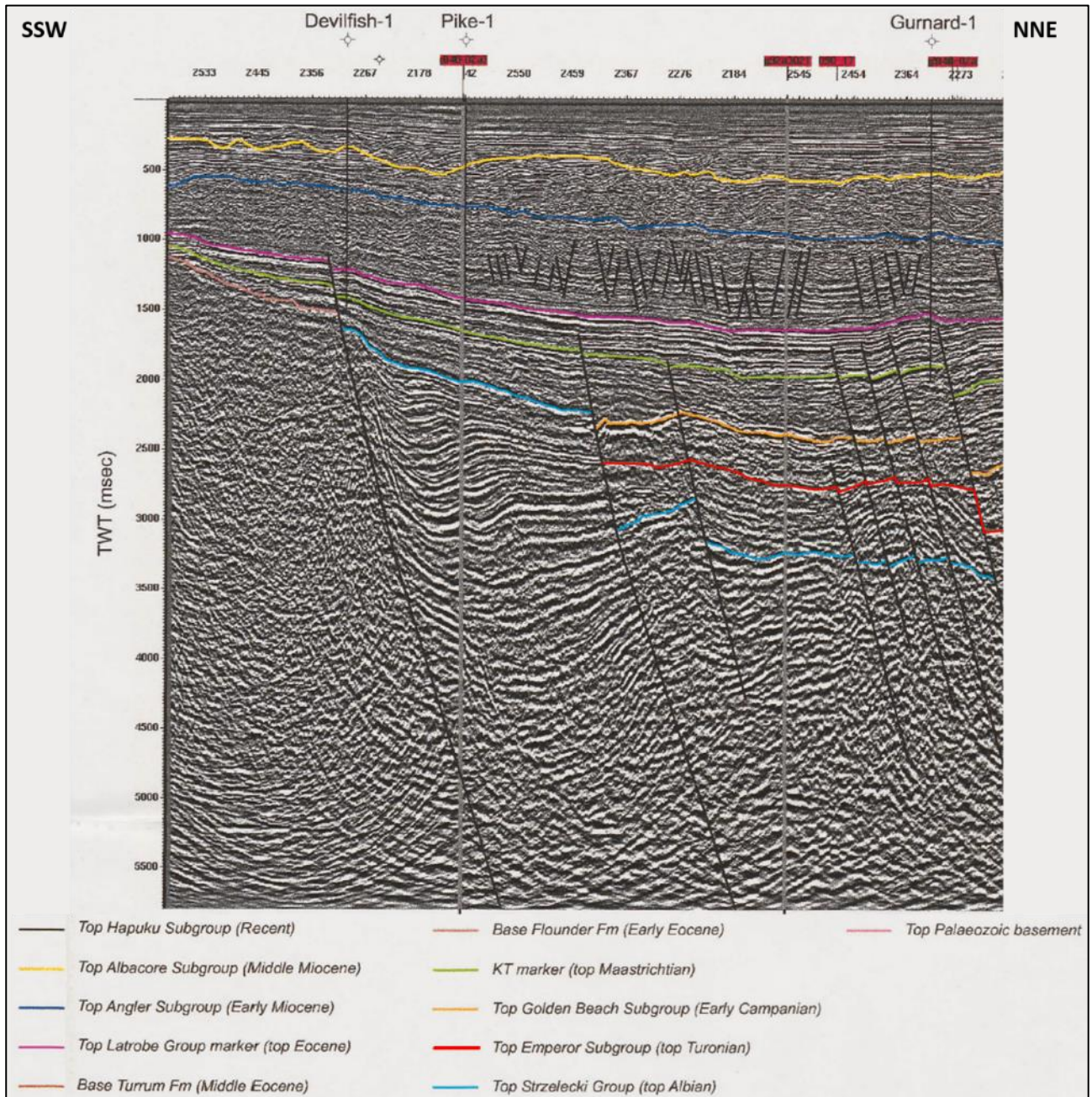


Figure 4-17 NNE-SSW trending section shows the structural style and growth fault that accommodate Emperor Subgroup thickness changes (Power, 2003).

4.3.2 Latrobe Valley model

The Latrobe Valley in the onshore Gippsland Basin is one of the world's major coal bearing basins, containing several brown coal seams deposited in the Eocene, Oligocene and Miocene. The coal seams are individually up to 100 metres thick and are vertically stacked so in places, such as the Morwell open cut, total coal thicknesses are up to several hundred metres (Holdgate, 1985; 2005). In contrast, there are no known significant occurrences of Late Cretaceous sediments and the preserved sediment sections of Paleocene to Early Eocene age in the Latrobe Valley are thin,

which is very different to the offshore Gippsland Basin, where the equivalent section is over 10km thick.

The Latrobe Valley records a detailed record of sedimentation and burial synchronous with the change from extensional to compressional structuring and low rank coal is very sensitive to physical stress. An extensive bore, log and analytical dataset exists with some, poor quality, seismic data. Hence, a finer scaled 3D model was built for the Latrobe Valley to capture the detailed coal seam structure, stratigraphy and property changes to see if any relationships could be determined. Comparable 3D models were built in 2003 and 2011 containing stratigraphic and block models. However, they are mainly reliable in the open cuts whereas the well tops and correlations outside of the mine areas were found to be inconsistent and not suitable for regional modelling. In addition, they mainly focused on stratigraphic modelling and didn't include coal property models, such as moisture, carbon models. In addition, their Strzelecki and Basement surfaces were derived from points, including top Carrajung Volcanics, Strzelecki Formation and Palaeozoic outcrops. These points were triangulated, and triangulated surfaces were applied during modelling, which was not accurate and not suitable for regional modelling.

The Latrobe Valley structural model is cropped from the entire Gippsland Basin structural model to cover just the Latrobe Valley region. Hence, the structural (pillar grids) remains the same.

However, it consists of more input horizons for which the detailed settings are shown in Table 4-4. Overall, the Latrobe Valley model contains ten faults, eight horizons, 22 zones, and 136 layers with a grid size of 500x500 metres. The structural model as shown in Figure 4-18 shows that the Latrobe Valley is an elongated, asymmetric, east-pitching syncline, with a series of mappable en echelon local structures, known as the Yallourn Syncline, Morwell Monocline, Traralgon Syncline, Loy Yang Dome, Rosedale Monocline and Baragwanath Anticline.

Sediment layers within the valley are relatively flat and sub-parallel and a vertical scale at 1:10 is used in Figure 4-19 to demonstrate the structural folds. In general, the thick, continuous coal seams have been kept at low ranks in the valley by the shallow burial depth (Figure 4-19). In contrast, the coal seams in synclines are buried much deeper below a thicker overburden and this has increased the physical rank significantly.

Table 4-4 Input settings for Horizon in 'Make horizon' process, Latrobe Valley model.

Horizon name	Tied Well tops	Input maps
Topography	-	Topographic map
Yallourn Formation	Yallourn Formation	Top Yallourn Formation
Morwell 1A Seam	Morwell 1A Seam Roof	Top Morwell 1A Seam
Morwell 1B Seam	Morwell 1B Seam Roof	Top Morwell 1B Seam
Morwell 2 Seam	Morwell 2 Seam Roof	Top Morwell 2 Seam
Traralgon Formation	Traralgon 1 Seam Roof	Top Traralgon 1 Seam
Strzelecki Group	Strzelecki Group	Top Strzelecki Group
Basement	-	Top Basement

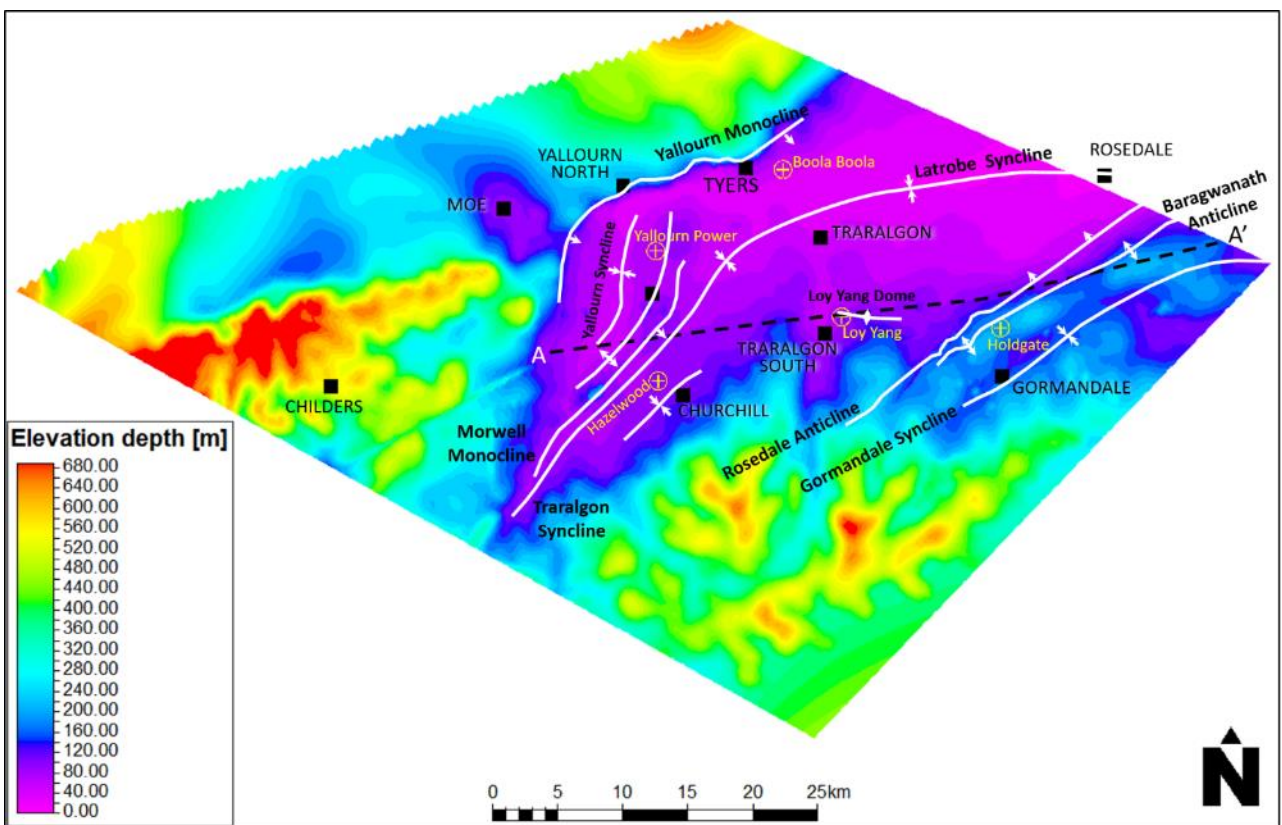


Figure 4-18 Latrobe Valley structural model, using the land surface as an example. Wells in yellow, towns in black, locally structures in black. The location of Figure 4-19 is shown as black dash-line.

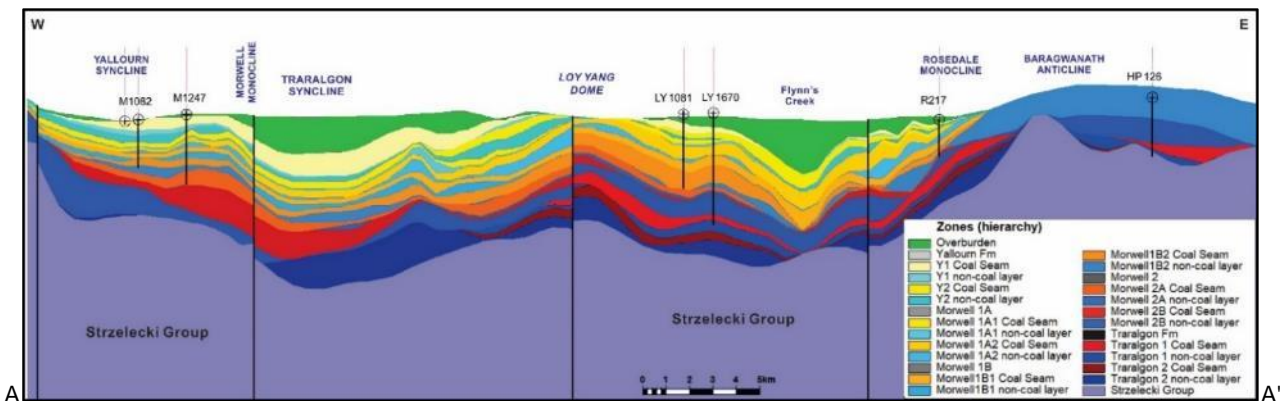


Figure 4-19 A west-east geological cross-section between Yallourn syncline and Holey Hill anticline (Z Scale: 1:10) shows the geo-unit layers determined by the Latrobe Valley 3D structural model. The section location is shown in Figure 4-18.

Chapter 5. Landscape evolution modelling in *Badlands* guided by

Experimental Design

Palaeo-landscape studies are important for better understanding land surface processes, climate change and environmental science and their geological applications, for example, in the petroleum industry. They can guide exploration to locate potential source rocks and reservoirs and also aid 3D reservoir and seal modelling for development studies. However, reconstruction of the palaeo-landscape requires a good understanding and simulation of the basin evolution history which is a complicated process controlled and affected by multiple variables, including tectonics, paleo-environment, sea-level change, sediment type, rainfall, etc. It is essential to understand the relationship between those variables and the basin evolution process, and also the interactions between the variables which often have a more pronounced effect than the individual variables on their own. Given the large number of possible variables and the difficulty of measuring interactions this makes estimation of the importance of each variable challenging. Complex numerical simulation and advanced statistical analysis methods are required to solve this problem. The numerical simulation software allows many scenarios to be rapidly built within a reasonable time. This needs to be coupled with properly designed experiments and statistical analysis to guide the scenario set-up, process the numerical simulation results of the palaeo-landscapes, and generate the multi-variate equations that define and identify the important controlling variables.

A full suite of 3D theoretical forward scenario models of the onshore and offshore Gippsland Basin has been used to recreate the basin history from the Early Cretaceous to Holocene with the Basin and Landscape Dynamics software - *Badlands*, 2019 (Salles and Hardiman, 2016; Salles et al., 2018). The models are calibrated to the corresponding full 3D realistic structural, stratigraphic and property models of the basin that have been built in *Petrel* (Schlumberger software). This constrains the sedimentary, stratigraphic, burial, and thermal histories to the subsidence rates and basin-fill for each geological sequence by using their isopachs as input to the *Badlands* modelling.

The *Badlands* forward modelling allows rapid recreation of various sedimentary and structural scenarios of the palaeo-environments that occur with subsidence and extension, over the time span covering the geological history of the Gippsland Basin. The geological history can be

replicated across a range of scenarios to produce a variety of outcomes by varying the input controls, and the relative importance of these input controls can be investigated, using appropriate experimental designs and statistical analysis of the results. The *Badlands* software incorporates a suite of modules, each comprising a set of model equations that require relevant input variables (Figure 5-1) to simulate changes in tectonics (ie. input maps for subsidence and uplift amounts), erosion and sediment supply (slope topography, erodibility, rainfall), sediment transportation and deposition (sediment residency, dispersal and overall flux), climate and sea-level change. This allows the recreation of the sediment distribution throughout the basin through time and thereby builds up the palaeo-facies and burial history.

The controls on landscape evolution and basin-fill have been debated for a long time in both the geologic and physical geography disciplines. There are many controversial and unresolved issues, different approaches and objectives that have impeded progress. Many earth scientists have collected field data for landscape evolution and basin-fill studies (Howard & Kerby, 1983; Seidl & Dietrich, 1992; Young & McDougall, 1993; Seidl et al., 1994; Hallet et al., 1996; Stock & Montgomery, 1999; Debnath et al., 2007; Perron et al., 2009; Hobbiey et al., 2011; Ferrier et al., 2013; Murphy et al., 2016; Shobe et al., 2017). Mostly they have measured different variables that are specific to the studied region, and either derived best-fit equations for that dataset or they have used existing general equations with previously derived constants to help fit their models. In these cases, the results are not generally applicable because each proposed model equation fits well with the specific dataset but it is either hard to use the data in a different basin or with different model equations. This also confuses the ability to identify the dominant variables that control landscape development and their use in the more difficult task of modelling landscape evolution through deep time over many millions of years and for an entire basin. Brewer et al. (2020) compared the different methods to estimate sediment fluxes in ancient sediment routing systems and found that different models were sensitive to different parameters, and this generates significant inherent uncertainty.

In the past 20-30 years, numerous software platforms have been written to simulate basin-fill processes with varying degrees of constraint to real field data that allow researchers to build and test models in a more efficient way (e.g., *Badlands*, *DionisosFlow*, *SedSim* (Granjeon et al., 2018;

Griffiths et al., 2001; Salles & Hardiman, 2016)). However, these simulation programs mainly rely on deterministic physical equations mostly developed from a theoretical basis (e.g., fluid flow, gravity). Few studies use these simulation programs with a rigorous Experimental Design (ED) to statistically test a range for each variable. In addition, most landscape researchers are primarily interested in modelling present-day landscape evolution and detailed stream behaviour (Perron et al., 2009; Salles et al., 2011; Shobe et al., 2017). Geologists are mostly interested in longer-term deep time basin-wide development, which is the aim of this study.

The large number of input variables that control basin development means there is no unique model that will correctly answer how the geological history of the Gippsland Basin (or any basin) was produced over time, instead there are a multitude of possible scenarios. Each scenario might also be dominated by some controlling factors, whereas other scenarios might be dominated by a different set of controlling factors. Hence, identification of the most likely geological history and the most consistently important controlling variables requires a rigorously structured approach to manage the uncertainties and statistically analyse the possible scenarios, rather than using a 'black box' in which expected mid-values and combinations of variables are chosen using 'educated guesses'. Instead, an efficient Experimental Design approach was used in this study to test and identify the main uncertainties and their possible ranges,

based on actual field data, while at the same time ensuring that the full multi-dimensional space for those variables is covered by the minimum number of scenario runs. The experimental design guided the makeup of the simulation runs that were required to reconstruct possible scenarios for the basin evolution, estimate the most likely geological history, and identify the most important controlling variables at each phase of the basin history.

5.1 *Badlands* settings

5.1.1 Simulation Input Data & Equations

The *Badlands* software has many different modules to simulate and reconstruct different dynamic landscape evolution processes, such as the fluvial system, hillslope processes, wave-induced longshore drift, tectonic processes and carbonate production, etc. (Figure 5-1). Each module has multiple variables calculated with sets of parameters used to guide the module. In this study, the

reconstruction of the entire tectonic history of a rift basin requires many modules working together, which leads to a large number of variables and parameters with some of the main ones shown in Figure 5-2.

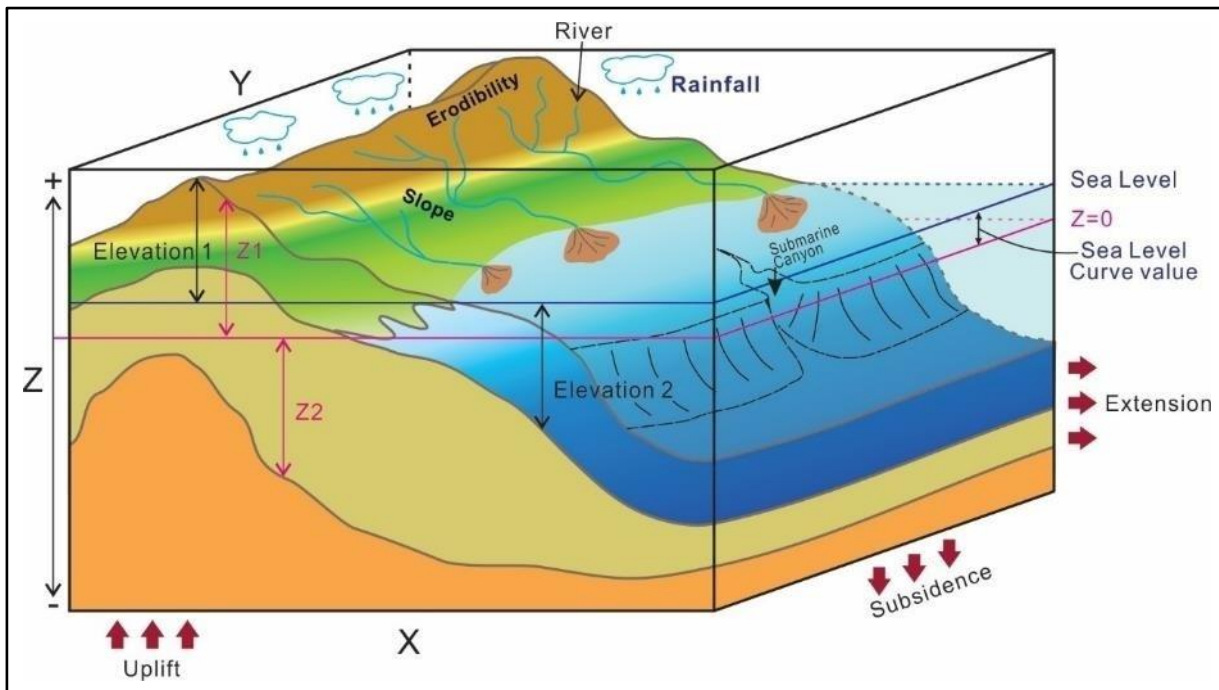


Figure 5-1 A schematic landscape evolution model shows the main variables and modules simulated in Badlands.

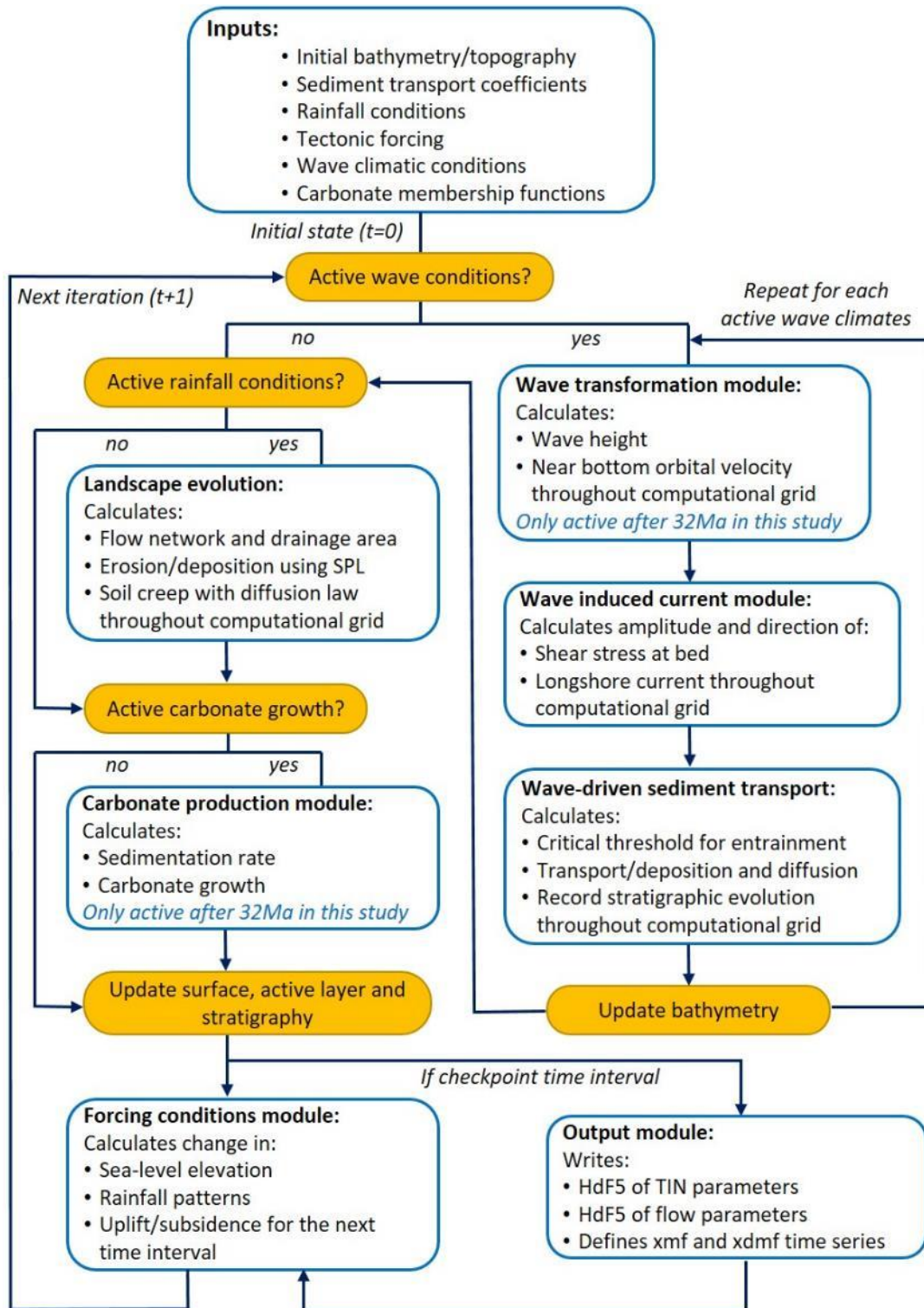


Figure 5-2 Flow diagram of the simulation process in Badlands modelling (modified from Salles et al., 2018). SPL = stream power law.

The main *Badlands* modules used in this study and their input variables are outlined below. A more complete description is given in the *Badlands* user manuals

(<https://Badlands.readthedocs.io/en/latest/xml.html>) and in Salles and Hardiman (2016), Salles et al., 2018. The results found for each of these variables are discussed in detail within later sections especially 5.3.

Initial Topography and Grid structure: the initial topographic map defines the initial surface area over which the landscape processes are computed for the grid. This surface will be the oldest landscape of the study area from which *Badlands* will compute the 3D forward model.

Stratal Time Steps: the start, end times and step interval (in years) define the period that will be computed for each simulation. This study simulates the entire history of the Gippsland Basin from the Early Cretaceous (137 Ma) to present-day (0 Ma) with a step interval or stratal resolution of one million years (giving 137 stratal time steps). Smaller studies focussed on particular areas, processes or time intervals could use much closer time steps.

Structural Grid: this determines the lateral resolution of the record and together with the 1Ma time steps controls the definition of stratigraphic architecture over time. The grid resolution was set at 1000 m to keep the total cell number for the entire 3D model manageable given the large simulation area (500x366 km), a total sediment thickness over 10 km and a long time scale (137 million years). This gave a total model cell size of 183,866 nodes.

Sea-level History: the sea-level position for the given time step is normalized to a present day zero datum from the Haq sea-level curve (1987), which is appropriate for the Gippsland-Otway basins since it is based in part on the relative sea-level curves derived from these basins.

Tectonic Structure: this variable simulates the displacement related to tectonic events (i.e. subsidence related to extension, thermal subsidence and uplift). The amount of subsidence is input using isopachs to constrain the displacement. Here the isopachs were generated from the 3D realistic model, which helps to constrain the numerical model to the empirical data from the Gippsland Basin (See Chapter 4). The isopachs obtained from the 3D *Petrel* model and input to *Badlands* are given in Table 5-1. The 3D structural-stratigraphic model represents the preserved sediments during evolution of the basin so will tend to estimate the minimum amount of subsidence. Hence, the isopachs of major geological units are only used as a guide for the *relative* amount of subsidence that occurred during the formation of the main geological units.

The *Badlands* forward models are 3D simulations that cover the time span of the rift events caused by extensional stretching in the basin. In practice, this is modelled by including the interpreted

faults and fault throws in the 3D structural model, so that the extension is simulated by the changes in thickness across the faults when modelled as increments of 1 Ma time steps.

The uplift maps were generated using estimates based on previous studies (Moore et al., 1986; Duddy & Green, 1992; Corcoran & Doré, 2005; Czarnota et al., 2014; Green et al., 2018; Aghaei et al., 2020). However, there is no satisfactory map that can be used directly, hence some sensitivity tests were run to estimate the most likely uplift maps (see Section 5.2.1 below). All the isopach and uplift maps have age control, which allows simulation and separate testing of multiple tectonic events within the one simulation model.

Table 5-1 The input isopachs of major geo-units with the corresponding approximate time period, biostratigraphy and boundary surfaces (NB surfaces are in part diachronous).

Geo-Zone	Time (Ma)	Biostratigraphic Zones at top of Surface	Top & Base surfaces
			Topography - Bathymetry
Neogene	0-23		
		Middle <i>P. tuberculatus</i> /N4	Top Lakes Entrance Formation – Top Morwell 1B
Oligocene-Early Miocene	23-32		
		Upper <i>N. asperus</i>	Top Latrobe Group – Top Traralgon Formation
Upper Latrobe Group	32-65		
		Upper <i>F. longus</i>	Kate Shale - Base Paleogene
Lower Latrobe Group	65-92		
		<i>P. pannosus</i>	Top Strzelecki Group
Strzelecki Group	92-137		
		Lower <i>C. australiensis</i> APK1.2/Stage 3b/Stage 2	Top Basement

Precipitation Areal Trends: the main climate response for the model is defined by the precipitation trend maps through time, which influence the fluvial related sediment erosion and transport. The precipitation value can be kept constant for a time step or can be calculated from the change in topography with time, and both scenarios were tested in this study.

Sediment Supply by Surface Erosion: The supply of sediment in the modelling is calculated from hillslope erosion and fluvial incision based on the detachment-limited stream power law. This assumes all loose sediment can be transported, that is, a pure detachment or pure erosive model

(Hobley et al., 2011; Murphy et al., 2016). This equation states that the erosion rate ϵ depends on the *precipitation* (P), *drainage area* (A), and *slope* (S):

Equation 5-1 Erosion Rate

$$\epsilon = k(PA)^m S^n \quad (5-1)$$

where k is a constant coefficient which describes the Erodibility of the channel bed, with m and n as positive exponents (Salles et al., 2018).

In previous studies, the values of m and n were estimated by fitting the measured data with the model equation, hence the input values of m and n have varied between studies and some studies have used other analogous equations (Howard & Kerby, 1983; Seidl et al., 1994; Stock & Montgomery, 1999; Perron et al., 2009; Braun et al., 2014; Chen et al., 2014; Murphy et al., 2016). Some researchers have used a ratio of m/n rather than use individual values (Tucker & Slingerland, 1994; Whipple & Tucker, 1999; Salles & Hardiman, 2016) (Table 5-2). The analysis is also complicated by the combination of *Precipitation* and *Area* within the one exponent m which convolves these two variables together and makes the resolution of their true effects more difficult to identify.

Table 5-2 Typical values of Erodibility k , m , n and m/n from previous published studies.

Study area	Erodibility (k)	m	n	m/n	References
Hawaii	2.67E-7 ~ 6.37E-7	0.43 ~ 0.51	0.67 ~ 1.17	0.43 ~ 0.64	Murphy et al., 2016
Australia	4.4E-7 ~ 4.3E-6	0.1 ~ 0.5	0.5 ~ 1.0	0.2 ~ 1.0	Stock & Montgomery, 1999
Virginia & Utah	-	0.439 ~ 0.442	0.63 ~ 0.68	0.64 ~ 0.7	Howard & Kerby, 1983
Siuslaw, Umpqua, Aslea	-	-	-	1.0	Seidl & Dietrich, 1992
Kauai	1.53E-8 ~ 1.45E-7	0.5 ~ 0.59	0.33 ~ 1.0	0.5 ~ 1.78	Ferrier et al., 2013
United States	-	0.31 ~ 0.42	0.74 ~ 0.84	0.5 ~ 1.0	Perron et al., 2009

Sediment Transport and Deposition: Basin evolution modelling requires that the sediments moving downslope are deposited and this occurs in the simulations within three different situations: depressed areas of relative negative relief; on an alluvial plain where the slope approaches base level, and in offshore marine seas. These parameters together are in effect modelling the deposition to accord with the concept of accommodation space.

Firstly, deposition occurs in depressions and is controlled by a depression-filling algorithm using the maximum fill parameter to control amount of fill (*fillmax*, Figure 5-3a). This constrains formation of a potential water body during one time step by the maximum elevation of the surrounding grid nodes (Planchon and Darboux, 2002).

Secondly, on alluvial plains the non-marine or aerial deposition is identified and forced by two parameters: the critical slope and maximum amount of deposition (Figure 5-3b). These two parameters are tested first to ensure there is no non-tectonic caused slope reversal during the simulation process. The critical value of slope is used to determine whether transportation or deposition takes place at any particular cell once the new slope has been calculated at a time step. The maximum amount of deposition (as a percentage) limits the amount of sediment deposited at each node per time step for the given slope. If the S_x is smaller than the critical slope S_o , deposition at grid node x is calculated based on the equation:

$$D_x = V * b \quad (5-2)$$

where D_x is the amount of sediment which deposits at grid node x , V is the sediment volume that has been transported by rivers to that node, b is the percentage of the maximum deposition retained at node x , with the remaining sediment moving to the next cell (Salles et al., 2018).

The sediment transport or flux along and down slope of the non-marine or marine sediments is mainly controlled by gravity. This is modelled here by the linear diffusion law which is used to simulate sediment relocation downslope from one cell to the next, commonly referred to as soil creep (Tucker and Hancock, 2010; Salles and Duclaux, 2015):

$$\frac{\partial z}{\partial t} = k_{hl} \nabla^2 z \quad (5-3)$$

where k_{hl} is the (hillslope) diffusion coefficient of sediment flux; this has a different value for aerial deposition (*caerial*), movement of inshore marine sediment (*cmarine*) and to promote deep marine sediment gravity dispersion from river mouths (*criver*) (Salles et al., 2018).

Thirdly, in marine or inland sea environments the subaerial sediment is first transported from the shoreline using the same linear diffusion law for sediment. However, this sediment is then dispersed across the shelf further into deep marine environments using an additional equation given below:

$$D_x = \frac{V * diffprop}{diffnb} \quad (5-4)$$

where D_x is the amount of sediment deposited at grid node x ; V is the sediment transported by river to the shoreline; $diffprop$ is the diffusion proportion, that is, the percent maximum thickness that can be deposited on a given grid node based on the surrounding node elevations; and $diffnb$ is the diffusion number used to divide the initial sediment volume into several equal units to control the dispersion distance (Figure 5-3c, Salles et al., 2018). Note that the variable Max % Marine Deposition ($diffprop$) is relevant for deposition in any water body below base level which can include marine environments, lakes, lagoons or inland seas and is the local accommodation space.

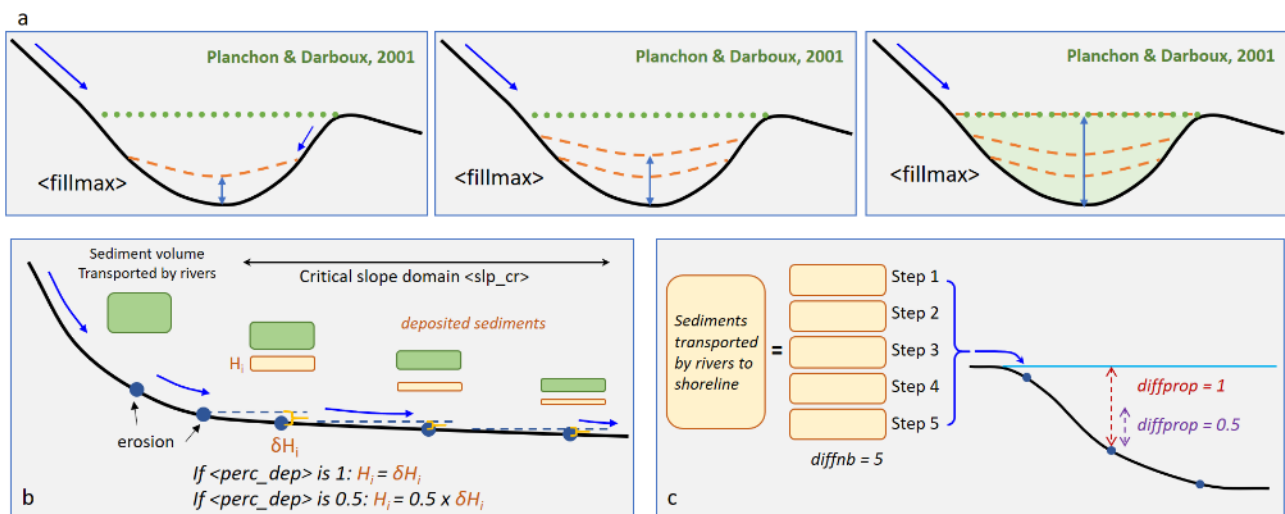


Figure 5-3 a: The diagram shows the depression-filling parameter and the maximum fill parameter $\langle fillmax \rangle$; b: The parameters of alluvial plain forced deposits; c: Explanation of the marine depositional parameters. (modified from Salles et al., 2019)

Carbonate Deposition: this module allows modelling of the cold carbonate shelf platform that developed from the Eocene to the present day. The required input includes a cold carbonate deposit rate versus depth over the relevant time period. The cold carbonate deposit rates were based on data provided in Bernecker et al. (1997). This module could not be run together with the other modules described above which meant that the simulations were run from 137 Ma to 32 Ma using the other modules and then restarted from 32 Ma to 0 Ma using the carbonate module. This has no effect on the results since the equation calculations start again at each time step anyway.

Wave module: the wave module is required for the carbonate module. It simulates the marine coastal wave conditions and then calculates the wave-induced sediment erosion and transportation. The module requires definition of the wave base, typical wave height, mean wave direction, erosion thickness and timing. The current Gippsland ocean conditions were assumed to

be similar to those occurring in the past, which is reasonable since open ocean conditions were established after opening of the Tasman Sea and the circum-Antarctic current between about 36-30 Ma (Figure 5-4). Hence, the wave base was set as 20 metres; the typical wave height at 2 metres, and a mean wave direction from the south-east with the wave module active from 32 Ma.

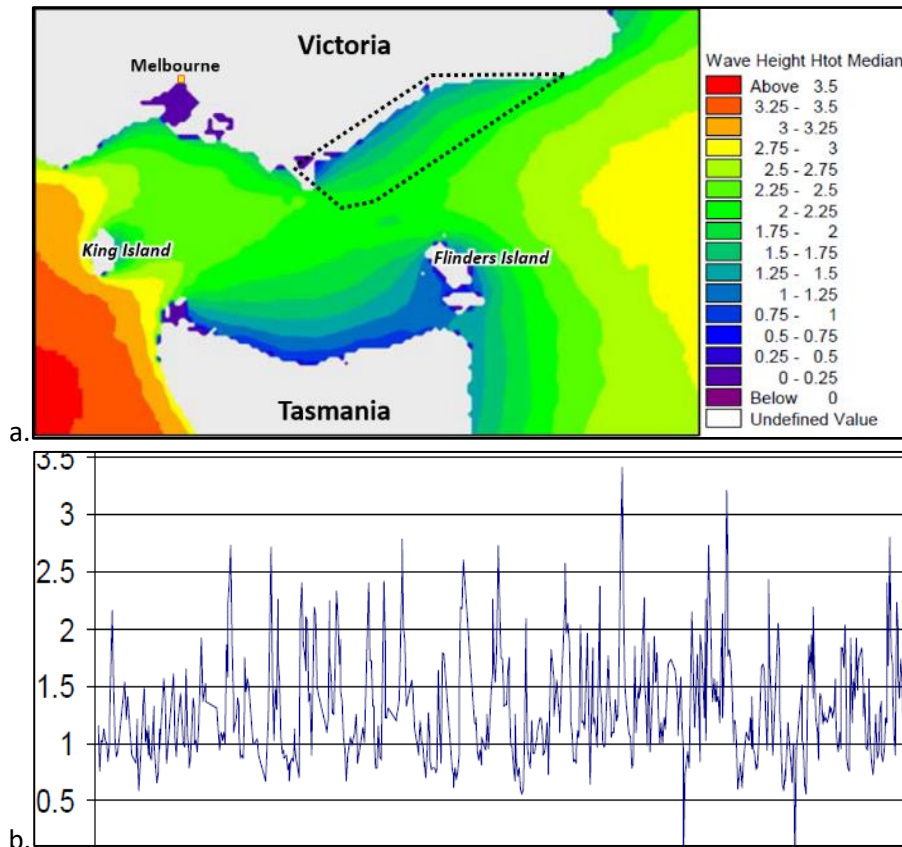


Figure 5-4 a. Annual median wave height and power in 2003; b. measured wave heights at Kingfish B platform in 2003 (Sustainable Energy Authority, 2004).

The simulations were run via a series of python scripts that provide the input variable data and call up the software modules that include the relevant equations. The complete python script is given in Appendix 8. Each simulation was run for 1Ma to provide 137 time steps in total.

5.1.2 Badlands Simulation Workflow

The full workflow for the simulation modelling and analysis is summarised below and in Figure 5-5. There are seven main steps in the process (Figure 5-5) which are summarised below and discussed further in the following sections:

1. Build the Realistic Empirical Model: interpret the seismic and well data and build a 3D structural depth model of the basin in *Petrel* to generate the tectonic input maps (burial isopach and uplift maps) as described in the previous Chapter 4.

2. *Badlands* Module Testing and Uncertainty Framing: write the Python scripts and run model test flows in *Badlands* to determine how to couple the different modules required to reconstruct the Gippsland Basin history. Secondly, define the overall Uncertainty Framework to capture the most likely critical variables to be tested in *Badlands* that are potentially the main uncertainties required to model the geological history of the Gippsland Basin. Tabulate these variables with possible ranges for each based on real field data available in the literature (Table 5-3).
3. Reference Case Model and Sensitivity Analysis: An initial Reference Case is then made from the mid range values to customise the numerical modelling in *Badlands* for the Gippsland Basin. Then run sensitivity tests for the variables required by *Badlands*, using the available field data, to determine realistic low to high ranges for each variable in the Gippsland Basin with the aid of an initial tornado analysis.
4. Experimental Design: use the *GSAT* to determine the experimental design matrix for the number and appropriate levels of each variable based on the uncertainty framework, Reference Case and sensitivity results.
5. Numerical Modelling: run the specified scenario simulations in *Badlands* using Python scripts as defined by the experimental design matrix given in Table 5-6.
6. Calculate Scenario Response: import the *Badlands* simulations back into *Petrel* to calculate their relative fit to the Realistic model. Determine relative fit responses of each simulated scenario in *Petrel* using maps and summary statistics.
7. Statistical Analysis of the Response: undertake statistical analysis of variance (ANOVA) for those responses in *GSAT* to ascertain the probability of each scenario and the significance of each variable modelled in *Badlands*.

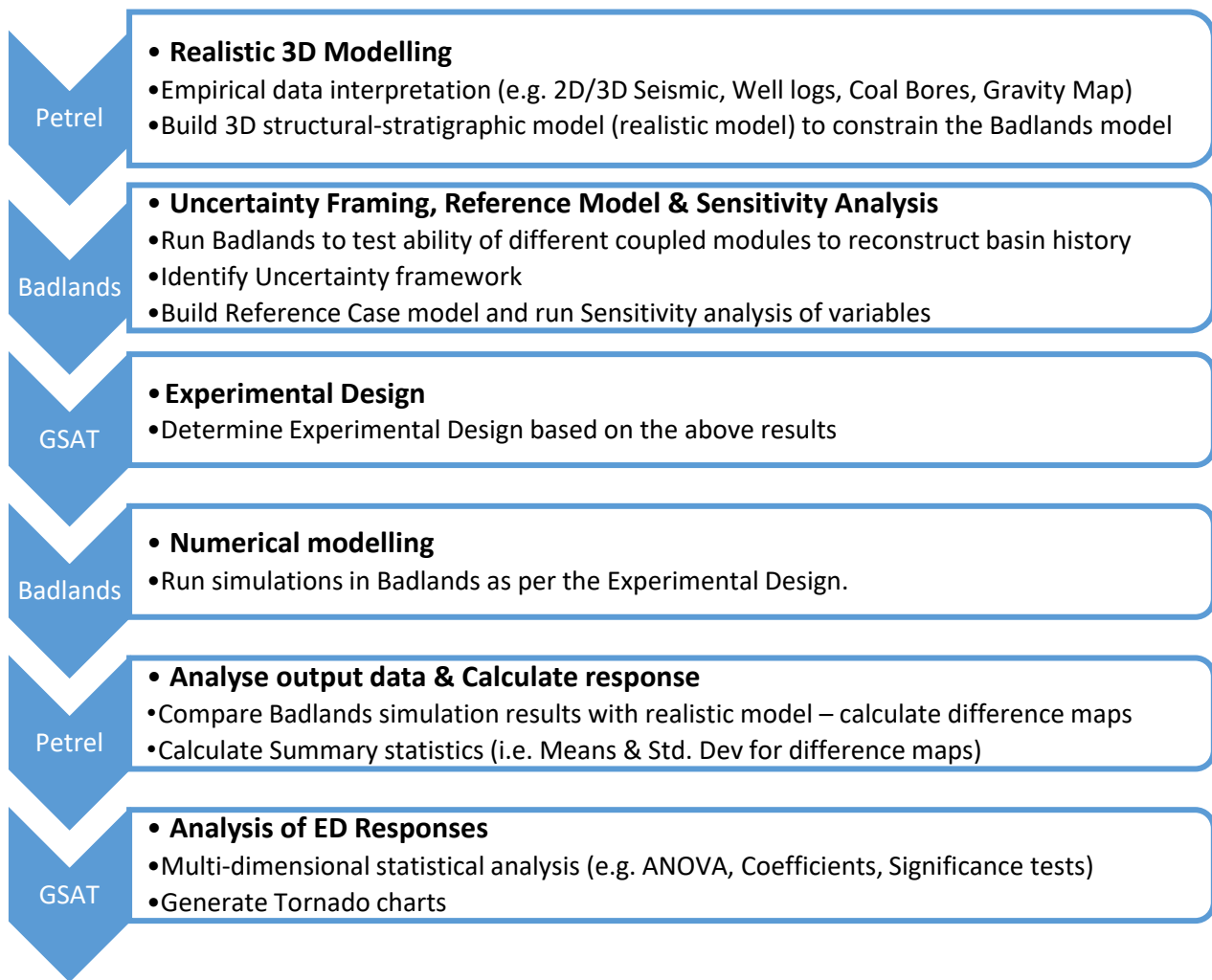


Figure 5-5 Badlands simulation modelling and analysis workflow.

5.2 Sensitivity test and Experimental Design

5.2.1 Uncertainty Framing

The Gippsland Basin has a wealth of empirical data and geological background information and using all of the data to reconstruct its entire evolutionary history requires comprehensive and complex modelling. This is especially the case building basin models with 3D forward modelling software such as *Badlands* rather than a back-stripping model, because the only controllable data are the input variables, and no corrections can be made once the simulation starts. *Badlands* provides a large number of potential variables that can be incorporated in the simulation modelling and this means there are a very large number of possible scenarios.

A logical statistical approach is essential to direct the number of input variables, their ranges, and the scenarios that are run. This requires a rigorous procedure that follows a Design of Experiment

(DOE) process including defining an Uncertainty Framework and construction of a Reference Case scenario that is used to run Sensitivity Cases. The *Badlands* test runs, the Realistic Model, the available Landscape field data and the literature on the Gippsland Basin formed the basis of the ‘expert knowledge’ used as input to formulate the initial Uncertainty Framework. Some 13 variables or uncertainties were selected as the main variables used as input for the *Badlands* simulations, including: the initial topography, sea level, tectonics, climate (*rainfall* and *m*), *slope* and *n*, erosion (*erodibility*), sediment transportation and deposition (various parameters). These variables and their possible ranges formed the basis of the Uncertainty Framework for an Experimental Design as given in Table 5-3 (discussed in more detail in the following sections).

Table 5-3 Uncertainty framework showing the main identified uncertainties and ranges. * Ref Case isopachs are from the 3D realistic model, the High Case isopachs are thicker to account for potential errors including from the velocity model.

Modules	Variables	Low	Reference	High
Topography	Initial Map Topography	Low elevation	Low elevation	High elevation
Sea level	Sea Level Curve	0.5	1	1.5
Tectonic	Subsidence Isopach Maps	Ref Case* Isopach Maps	Ref Case* Isopach Maps	Thicker* Isopach maps
Climate	Rainfall	0.2 m/yr	∝ elevation	3 m/yr
	Rainfall & Area Exponent <i>m</i>	0.40	0.50	0.55
Slope	Slope Exponent <i>n</i>	1.00	1.10	1.30
	Non Marine Deposition Minimum Slope	0.0005 m/m	0.001 m/m	0.01 m/m
Erosion	Non Marine Erodibility	1.00E-07	2.00E-07	9.00E-07
Sediment transportation & deposition	Aerial Sediment Flux	0.001 m ² /yr	0.001 m ² /yr	0.1 m ² /yr
	Marine-River Sediment Flux	0.2 m ² /yr	10 m ² /yr	1000 m ² /yr
	Marine-Gravity Sediment Flux	0.001 m ² /yr	0.005 m ² /yr	0.1 m ² /yr
	Number Time Steps To Distribute Marine Deposits	5	10	15
	Max % Marine Deposition	0.10	0.60	0.90

5.2.2 Reference Case Sensitivity Analysis

A Reference Case model was constructed in *Badlands* using constraints from the realistic 3D geological model, and approximate mid values for the required variables determined from the available field data. The Reference Case allows testing and better understanding of the modelling process and helps identify the potential critical variables and their possible ranges. This can reduce the number of variables and produce a more accurate uncertainty framework which has a direct impact on the size and quality of the experimental design. The Reference Case is useful though it

may not turn out to be the mid case of the entire possible scenarios and the analysis needs to avoid the Reference Case anchoring the mid-point of the response distribution. The Reference Case needs to be made using reasonable estimates that fit all the available evidence.

One of the main challenges in modelling extension, subsidence and sedimentation is to match the accommodation with the sediment supply to obtain a good balance. The Gippsland Basin has been studied and explored since the 1950s, and a large amount of information is available to guide building the Reference Case and constrain the possible ranges for some variables such as extension, subsidence, sedimentary facies and sea level change. However, there is little data available for many fundamental sedimentary variables such as erodibility, precipitation, stream grade, sediment flux and initial elevation. Typical values for these variables are known from many landscape studies (Howard & Kerby, 1983; Seidl & Dietrich, 1992; Young & McDongall, 1993; Hallet et al., 1996; Stock & Montgomery, 1999; Debnath et al., 2007; Hobley et al., 2011; Ferrier et al., 2013; Murphy et al., 2016 and Shobe et al., 2017). However, the field data show a wide range of values which appear dependent on the basin and the dominant sedimentary environments (Table 5-2). It is not clear which are most relevant to the Gippsland Basin, so these values were tested in initial sensitivity analyses and ranges that worked for the Gippsland Basin (from high to low) were adopted in the final scenario analysis.

5.2.2.1 *Initial topographic map*

The oldest Cretaceous Strzelecki Group sedimentary rocks in Gippsland Basin belong to the Tyers Conglomerate (Tosolini et al., 1999; Partridge, 1999; Constantine, 2001; Holdgate et al., 2015). This formation contains a palynoflora assigned to the *Foraminisporis wonthaggiensis* palynozone in Duck Bay 1, Wellington Park 1, Woodside 2 and Perch 1 (Figure 5-6). This age is also consistent with the *GPlates* modelling. Hence, the simulation was set to start from 137 Ma.

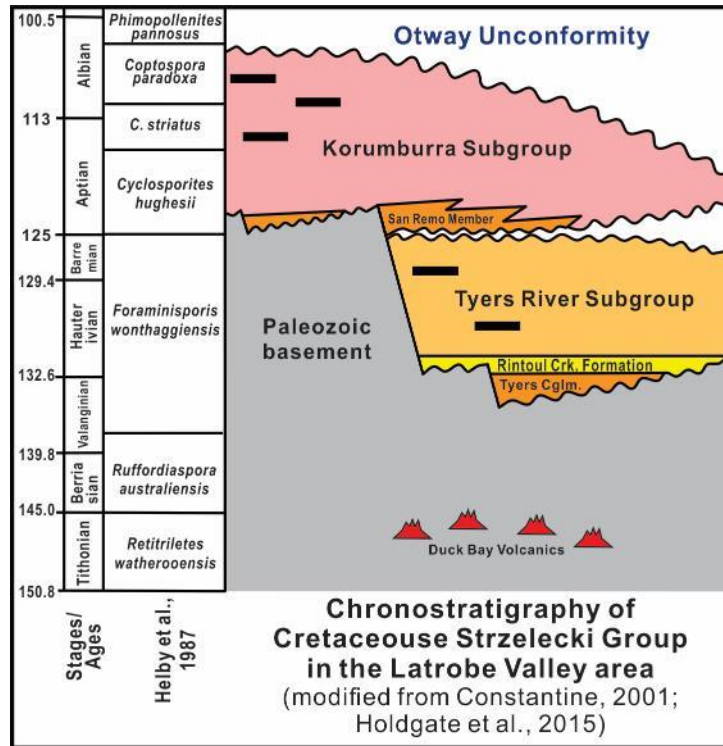


Figure 5-6 Cretaceous Strzelecki Group Chronostratigraphy (Constantine, 2001; Holdgate et al., 2015).

The initial topography, however, cannot be estimated from the current topography but has to be found by running a range of cases to match the required sediment budget in the Early Cretaceous. The first simulations were started using a topographic map with mountains in the north and west only, similar to the present-day topography, but this provides insufficient sediment supply into the basin and produces deep open marine palaeoenvironments across offshore Gippsland within a few million year time steps (Figure 5-7). This does not fit the onshore or offshore well data and the Gippsland Basin did not become open marine in the east earlier than about 80Ma with the start of the Tasman Sea spreading as noted in Chapter 4.

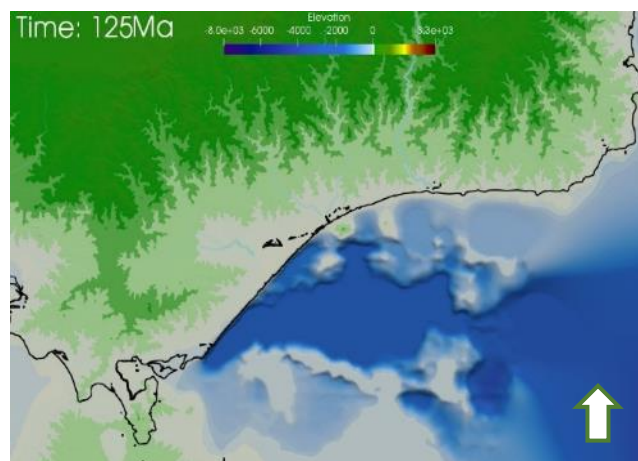


Figure 5-7 Simulation results where the input initial topographic map only has mountains to the north and east. The black line shows the present coastline.

A series of sensitivity runs demonstrated that only the models run with mountains to the north, south and east provide enough sediment input into the Gippsland Basin during the first syn-rift event to balance the sediment budget and fill the accommodation space (Figure 5-8). In this case east-west orientated rift basins, with associated inland drainage or small shallow lakes, are produced by about 124 Ma, varying with the precise scenario (Figure 5-9).

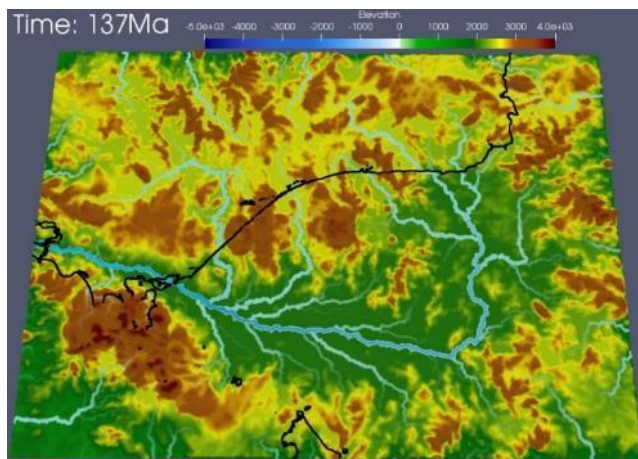


Figure 5-8 Initial topographic map required to start the simulations of the Gippsland Basin, showing mountains over the entire region, in order to provide sufficient sediment supply to balance the basin fill.

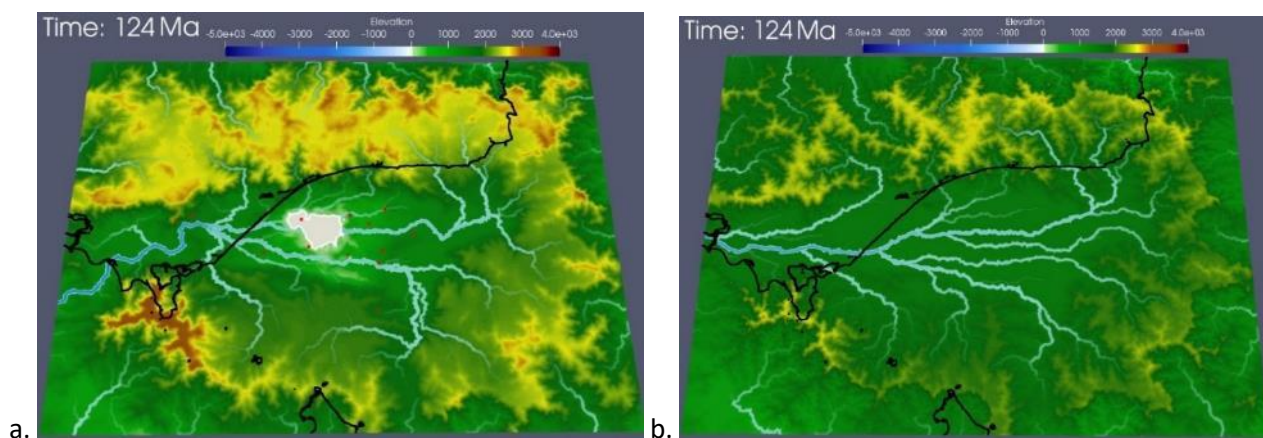


Figure 5-9 Simulation results where the input initial topographic map has highlands all around the Strzelecki basin. Two different scenarios are shown in Figures a and b. The black line shows the present coastline.

The models with highland areas to the north, east and south of the basin, are consistent with studies of the onshore Wonthaggi Coalfield by Edwards and Baker (1943), where detailed drill data shows that coarser sediments flank both the northern and southern margins of the east-west trough, with mostly mudstones and coals occurring more along the central axis. The lithic and in-places arkosic nature of some units in the Strzelecki Group indicates derivation from the Palaeozoic basement rocks in the adjacent highlands (Edwards and Baker, 1943) which is supported by these results. Others have suggested input from contemporaneous Jurassic to Early

Cretaceous volcanics that occur to the south in Tasmania and the north in western Victoria (Gleadow and Duddy, 1980) and again these results would support that possibility. Veevers (1982) also suggested derivation of the volcano-clastic component of the Strzelecki Group could be derived from an andesitic arc to the east and Bryan et al. (1997) suggested that these were rift volcanics from the main Tasman rift. The modelling indicates that high mountainous areas in the north, south and east are needed to provide sufficient sediment and or that sediments were being transported a long distance from outside the Gippsland Basin which is not likely. Hence, all three of the previous suggestions for sediment supply are valid and probable and any one on their own would not be sufficient.

5.2.2.2 *Tectonic simulation (displacement maps)*

As described earlier, *Badlands* software utilises displacement maps to simulate tectonic processes (i.e. extension, subsidence and uplift). The displacement maps used to guide the subsidence and extension were generated as isopach maps from the full 3D geological realistic model and cover the main geographic areas (Latrobe Valley, Strzelecki Mountains, Seaspray depression and offshore region) for all of the major geological units. However, it is more difficult to generate the regional uplift isopach maps as mentioned earlier. Previous studies have estimated the regional uplift by calculating exhumation based on apatite fission track and vitrinite reflectance data or by analysing river profiles (Moore et al., 1986; Duddy & Green, 1992; Corcoran & Doré, 2005; Czarnota et al., 2014; Green et al., 2018; Aghaei et al., 2020). Their studies demonstrate that large scale regional uplift occurred in Eastern Australia during the mid Cretaceous and subsequently during the Cenozoic. The onshore Strzelecki Group sediments show a missing section of at least 1-3 km and more in some areas mainly from mid-Cretaceous uplift (Appendix 10) (Smith, 1982; Holdgate et al., 2015; Aghaei et al., 2020).

Several sensitivity tests were run based on the published results to generate the preliminary uplift maps by constraining the amount of cumulative uplift and balancing it with the amount of sediment erosion. An example is given in Figure 5-10, which shows two scenarios that use different uplift isopachs as input while the other inputs are kept constant: (a) a higher uplift scenario produced using thicker uplift isopachs (with a median isopach thickness ~550 m); (b) a lower uplift scenario produced using thinner uplift isopachs (with a median isopach thickness ~350 m). The present day

topography produced by the higher uplift scenario simulation has a range of topographic heights over the modelled region that has a maximum mountain height of over 3200 m and is consistently higher than in the lower uplift scenario. The lower uplift scenario has a maximum mountain height of only about 2000 m and most elevations across the region are lower. Inspection of a range of scenarios indicates that, the medium land elevation at any particular time is typically about a quarter of the thickness of the missing section, because this is a dynamic process of erosion with uplift that continues over a long period of time. Hence, estimates of missing section should not be translated directly into estimates of uplifted mountain height.

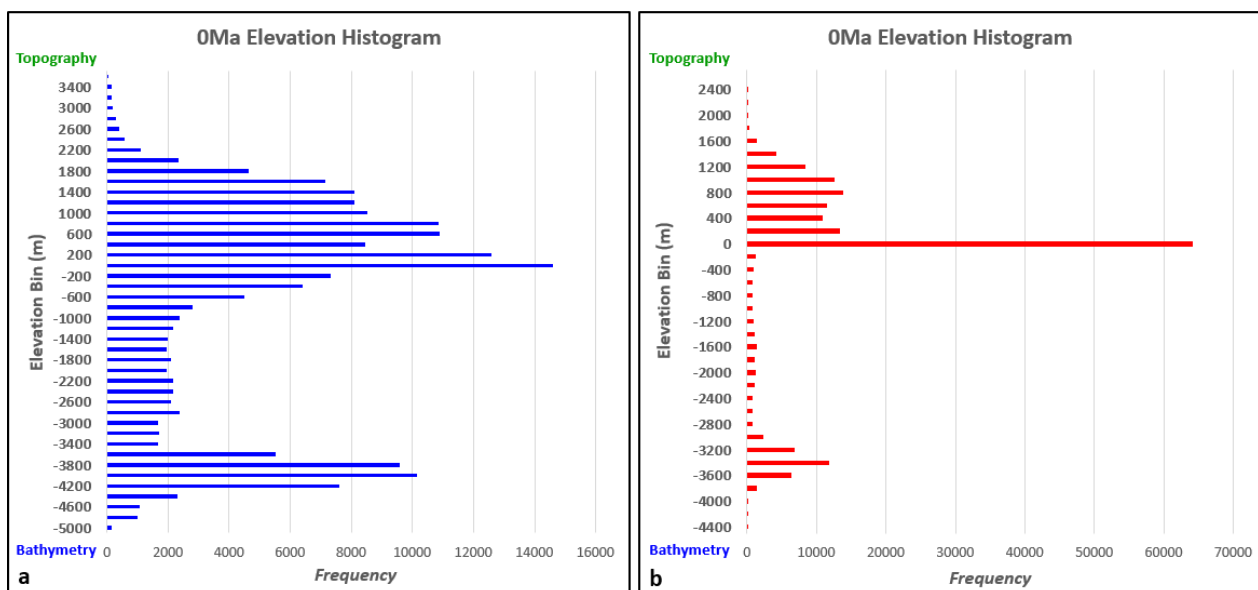


Figure 5-10 Histograms at the present day elevation at (0Ma) for different scenarios. Chart a shows the result of a scenario with thicker uplift isopachs, while chart b shows the result of a scenario with thinner uplift isopachs. Other settings and inputs of these two scenarios are kept the same.

5.2.2.3 Erosion rate:

Erosion rate (ϵ) is also an important variable in landscape modelling as discussed earlier. Equation 1 is commonly used.

$$\epsilon = k(PA)^m S^n \quad (5-5)$$

Many studies have tried to quantify the relationship between erosion rate and the relevant area, the slope, erodibility and precipitation. The value of the erodibility coefficient k and the exponents m and n has been found to change from basin to basin and it is reasonable to assume they also vary in a particular basin with time (Table 5-2). However, the measured field data may not be relevant to the Gippsland Basin, hence to use this equation, sensitivity tests were run for k , m and n to find the range of possible values that matched the data in the realistic 3D model of the Gippsland Basin.

Figure 5-11 shows two extreme examples of a high erosion rate versus a low erosion rate to show the effect on the resulting topography at 32 Ma.

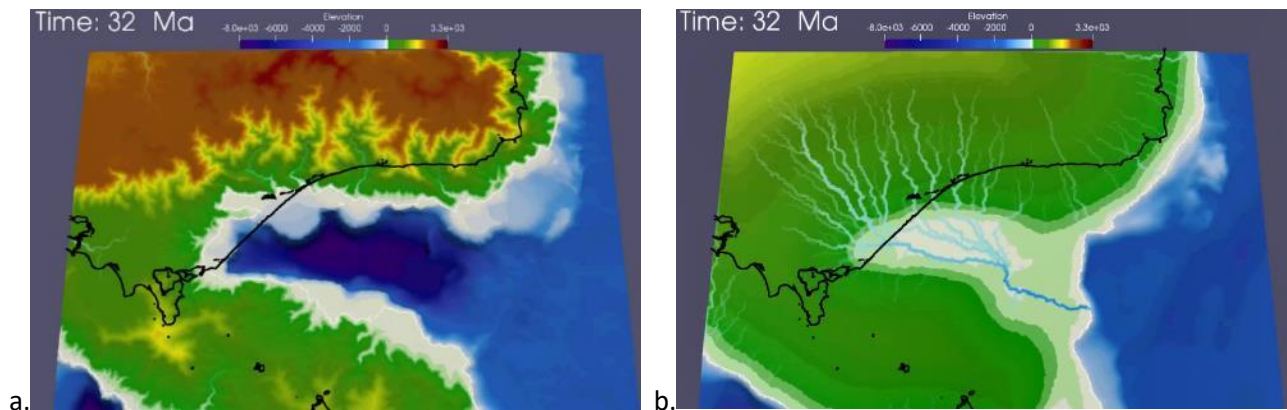


Figure 5-11 (a) Maps at 32Ma for two scenarios one run with a low erosion rate and (b) one run with a high erosion rate .

5.2.2.4 Other variables:

The control of climate on river incision has been studied and reported widely in the past by many earth scientists (Seidl & Dietrich, 1992; Ferrier et al., 2013 and Murphy et al., 2016). The main effect on erosion and sedimentation is usually related to the amount of precipitation. Hence, here the precipitation is controlled by elevation and the amount input to the modelling relies on the Australian monthly rainfall dataset for Gippsland to calibrate the relationship.

Similarly, the input data for diffusion of sediment flux and wave properties used here rely on present-day records (Flemings & Jordan, 1989; Water Technology report, 2004, Figure 5-4). The growth rate of the cold carbonate platforms that built during the late Cenozoic is based on Bernecker et al. (1997).

5.2.3 Experimental Design Analysis (EDA)

An experimental design (ED) has been used to guide the selection of the scenarios run through the *Badlands* simulations. Each simulation run in this study involves 13 variables or factors, which means there is a multitude of possible scenario combinations as given below:

$$\text{Number of possible factorial combinations } N = L^n$$

where n = the number of factors and L = the number of levels estimated for each factor.

From Table 5-4, L=3 and n=13, resulting in N=1,594,323. In general, if you have L factors, each to be tested at l_i settings, then the total number of possible combinations are

$$N = \prod_{i=1}^L l_i$$

Table 5-4 Design size sensitivity, total number of scenarios depends on number of factors and number of settings for each factor.

2 setting for each factor		3 setting for each factor	
Number of factors	Number of scenarios	Number of factors	Number of scenarios
2	4	2	9
3	8	3	27
4	16	4	81
5	32	5	243
6	64	6	729
7	128	7	2187
8	256	8	6561
9	512	9	19683
10	1024	10	59049

Given the large number of variables in this study an experimental design is required to determine an efficient set of scenarios. The Curtin University *GSAT* R wrapper (General Scenario Analysis Tool), which calls up R code (R Core Team, 2021) was used to create an optimum safe design that includes sufficient scenarios to estimate the main effects and the first order interactions between the variables. *GSAT* provides a logical scenario design to guide the composition of the *Badlands* numerical simulations and it allows multi-dimensional statistical analysis for the responses from those numerical simulation results.

The initial uncertainty framework proposed was too broad and had over 150,000 scenarios. Further screening of the uncertainty framework indicated running a Scenario analysis with 12 uncertainties at two levels and one uncertainty (sea level) set at three levels would be sufficient. Further sensitivity analysis suggested there were six main interactions (Table 5-5) indicating an economical design would be satisfactory (i.e. fractional factorial, estimating effect of all variables and interactions). The experimental design matrix generated by *GSAT* has 22 scenarios as given in Table 5-6 and requires less than 1% of all possible scenarios (12,288). The 22 scenarios for the experimental design were run in *Badlands* using a set of python scripts at time steps of 1 million year increments (Appendix 8).

Table 5-5 The input variables, their tested levels and their interactions used as input to GSAT.

Variables		Levels		
Initial Map		Low		High
Sea Level		Low	Mid	High
Tectonic Maps		Low		High
Non-Marine Erodibility		Low		High
Rainfall		Low		High
(Rainfall x Area) Exponent <i>m</i>		Low		High
Minimum Slope (Non Marine Deposition)		Low		High
Slope Exponent <i>n</i>		Low		High
Aerial Sediment Flux		Low		High
Marine-River Sediment Flux		Low		High
Marine-Gravity Sediment Flux		Low		High
Number Time Steps to Distribute Marine Deposits		Low		High
Max % Marine Deposition		Low		High
Interactions	<i>m</i> : Erodibility			
	Sea-level : Tectonic Maps			
	<i>n</i> : Erodibility			
	<i>m</i> : <i>n</i>			
	Number Time Steps to Distribute Marine Deposits : Max % Marine Deposition			
	Sea-level : Initial Map			

Table 5-6 Experimental design for Gippsland Basin scenarios.

Run#	Initial Map	SeaLevel	Tectonic Map	Erodibility	Rainfall	(Rainfall * Area) Exponent <i>m</i>	Critical Slope	Slope Exponent <i>n</i>	Aerial Sed. Flux	Marine-River Sed. Flux	Marine-Gravity Sed. Flux	No. Time Steps to Distribute Marine Deposits	Max % Marine Deposition
1	High	High	Low	Low	Low	High	Low	High	Low	High	High	Low	Low
2	Low	Low	High	High	High	Low	Low	Low	High	Low	Low	Low	Low
3	High	Mid	Low	High	High	High	Low	Low	High	Low	High	Low	Low
4	Low	Mid	High	High	Low	Low	High	High	Low	Low	High	Low	Low
5	Low	High	High	High	High	High	High	High	High	High	High	Low	Low
6	Low	Mid	Low	Low	High	Low	Low	Low	Low	High	Low	High	Low
7	High	High	High	Low	Low	Low	Low	High	High	High	High	High	Low
8	High	Low	Low	Low	High	High	High	High	High	Low	Low	High	Low
9	High	High	Low	Low	High	High	High	Low	Low	Low	High	High	Low
10	Low	High	Low	High	Low	Low	Low	Low	High	Low	High	High	Low
11	Low	Low	High	High	Low	High	High	Low	Low	High	Low	High	Low
12	Low	High	High	Low	Low	High	Low	Low	Low	Low	Low	Low	High
13	High	Low	High	Low	Low	Low	High	Low	High	Low	High	Low	High
14	Low	Mid	High	Low	High	High	High	High	High	High	High	Low	High
15	Low	Low	Low	High	High	High	Low	High	Low	Low	High	Low	High
16	High	Low	Low	High	Low	Low	High	Low	Low	High	Low	Low	High
17	High	High	Low	High	High	Low	High	High	High	High	Low	Low	High
18	Low	High	Low	Low	High	Low	High	High	Low	Low	Low	High	High
19	Low	Low	Low	Low	Low	High	High	Low	High	High	High	High	High
20	High	Mid	High	High	Low	High	Low	High	High	Low	Low	High	High
21	High	Low	High	High	High	Low	Low	High	Low	High	High	High	High
22	High	High	High	High	High	Low	High	Low	Low	Low	High	High	High

The *Badlands* simulations provided 137 maps that represent the response to the input variables at each time step for each of the 22 scenarios (3,014 maps) and consequently are difficult to compare visually, comprehend and assess. The present day maps are easier to compare against the current

topography in the realistic 3D model, but they don't necessarily provide the best fit scenario, because they may have been preceded by many simulations that were poor fits to earlier structural maps in the realistic 3D model. The *Badlands* simulations of the forward landscape maps build up a 3D sediment accumulation model comparable to the 3D realistic structural model in *Petrel*.

Hence, six of the most significant response depth maps were selected from each scenario, each representing key time episodes in the history of the Gippsland Basin, to assess the response of the simulations through time and their goodness of fit to the real data. These response maps were imported back into *Petrel* and compared with the equivalent age realistic model surfaces, to estimate their goodness of fit through time (Figure 5-12). The six selected maps are top Basement, top Strzelecki Group, base Palaeocene (KT), top Latrobe Group, top Lakes Entrance Formation and the Topography (Topo). These maps are equivalent to the key horizon maps which were used to build the realistic structural model and to initiate the simulations in the *Badlands* tectonic module. However, the various simulation modules recreate the erosional, depositional and burial history in an attempt to fill that accommodation space but will only succeed if their interaction produces a good match to the actual geological history, that is, they were not tied by the input maps.

The age of these horizons and their tectonic significance is generally agreed by previous workers, and their selection provides a good assessment of the geological evolution through time. The *Badlands* response maps imported into *Petrel* were used to calculate a map of the difference or deviation in metres from the equivalent realistic 3D model map for each and every node in the grid (14,190 nodes for each map). The mean sum differences map for each of the six horizons were inspected, and the results show that some are more or less good fits everywhere, whereas others are very poor fits in some parts of the basin (Figure 5-13). This can be measured by calculating the mean and standard deviation of all the nodes in each difference map to give an overall measure of the goodness of fit (the mean) and of the lateral variation (the standard deviation) respectively. The scenarios that are the best fits overall for all the maps can be estimated by calculating the group mean for each scenario, that is, the mean of the individual map means for each scenario.

The results of the above statistical analysis of the difference maps can be used to represent responses for each of the multi-dimensional scenarios and, by importing the responses back into

GSAT, are used to undertake the statistical analysis of the scenarios. This includes calculation of the multivariate response equation for all significant factor variables, and a statistical analysis of variance (ANOVA), to test the significance of each factor and all the interactions between factors (Table 5-7). The GSAT analysis highlights the critical variables and their importance by the coefficient weightings for each factor, which also provides a better understanding of how some equations in the *Badlands* software influence the scenario outcomes. In addition, the extreme range of key variables is highlighted by the Tornado charts that were generated in GSAT (Figure 5-17).

The results of the above analysis are discussed in the Section 5.3.1 below for the Statistical Analysis Results.

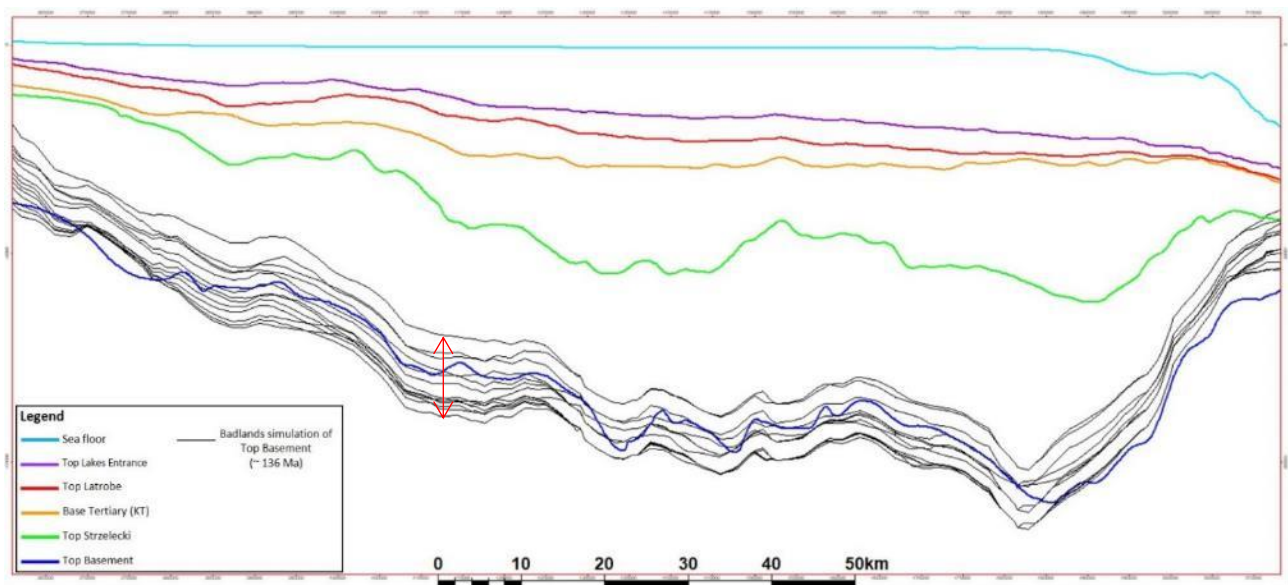


Figure 5-12 An East-West section comparing the top Basement depth horizons from the Badlands simulations with the realistic structural model showing the range of simulation fits (line of section is shown on Figure 5-13).

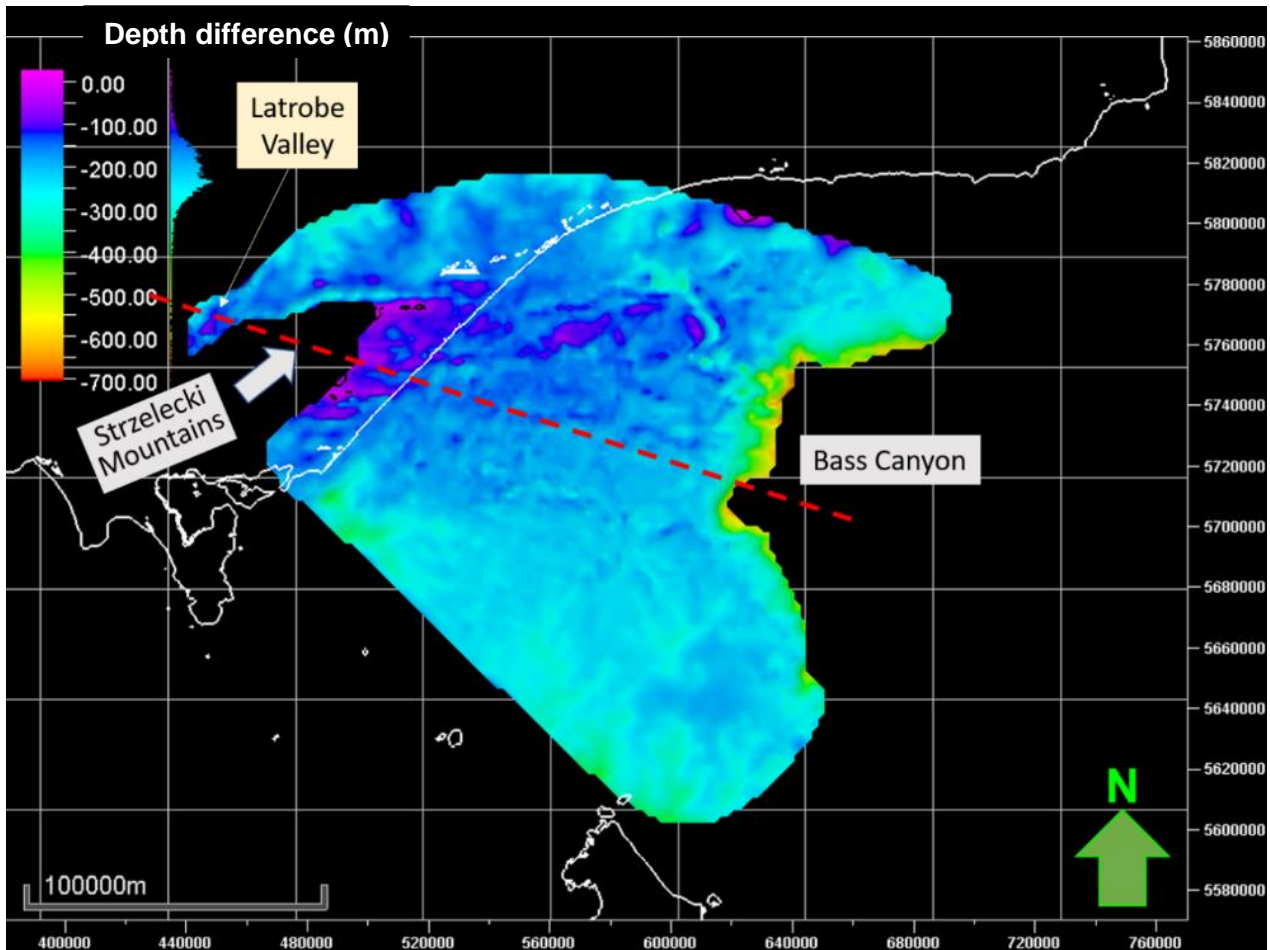


Figure 5-13 The difference map between the realistic model depth horizon and the equivalent Badlands landscape surface for the Reference Case at top Latrobe Group time. The map covers the area of good data control, the white line is the present day coastline and the red dashed line is the location line for the Cross-section shown in Figure 5-12.

5.3 Analysis result and Discussion

5.3.1 Statistical Analysis Results

The mean, standard deviation and summed means responses for the difference maps calculated for the six horizons in each of the 22 scenarios provide good measures to assess the basin-wide maps of the vertical and lateral variability. The mean differences for each horizon and the mean sum differences of all 22 scenarios were analysed in GSAT to do the statistical analysis (ANOVA).

The plot of the sum of the absolute means versus the sum of the standard deviation of the difference map, from top Basement level to topographic or bathymetric level is shown in Figure 5-14. It shows that most scenarios are reasonable fits to the data and highlights the cases with very poor fits (scenarios 7, 13, 18) and poor fits (scenarios 6, 4). The Reference Case for the top Latrobe Group difference map has a mean and standard deviation of -220 m and 77 m,

respectively (Figure 5-13). In contrast, the extreme case top Latrobe Group difference map of the mean and standard deviation (Scenario 7) is 881m and 3965m indicating both a poor fit and substantial lateral heterogeneity at the Top Latrobe Group (Figure 5-14).

The means of the difference maps at the main tectono-stratigraphic time steps for each scenario are plotted against age in Figure 5-15. Most scenarios show good convergence at the topographic-bathymetry level, whereas, four extreme scenarios 7, 13, 18, 6 finish with very poor matches. The dominant thick cold carbonate shelf deposition in the Seaspray Group (from top Latrobe to Topography) is built using the pelagic control rather than reef build-up and this may partly reduce any late stage divergence in many cases. Also, the carbonate shelf sedimentation is relatively homogeneous, so to limit the number of variables in the experimental design, some variables related to the carbonate module are not included in the design.

Hence, the sum of the absolute mean of the difference map, from top Basement level to top Latrobe level, is also used to assess the long term response to remove any different effects from the carbonate module. The cumulative probability frequency plot for the response of the sum of the absolute mean of the difference maps, from top Basement level to top Latrobe level, is shown in Figure 5-16(a).

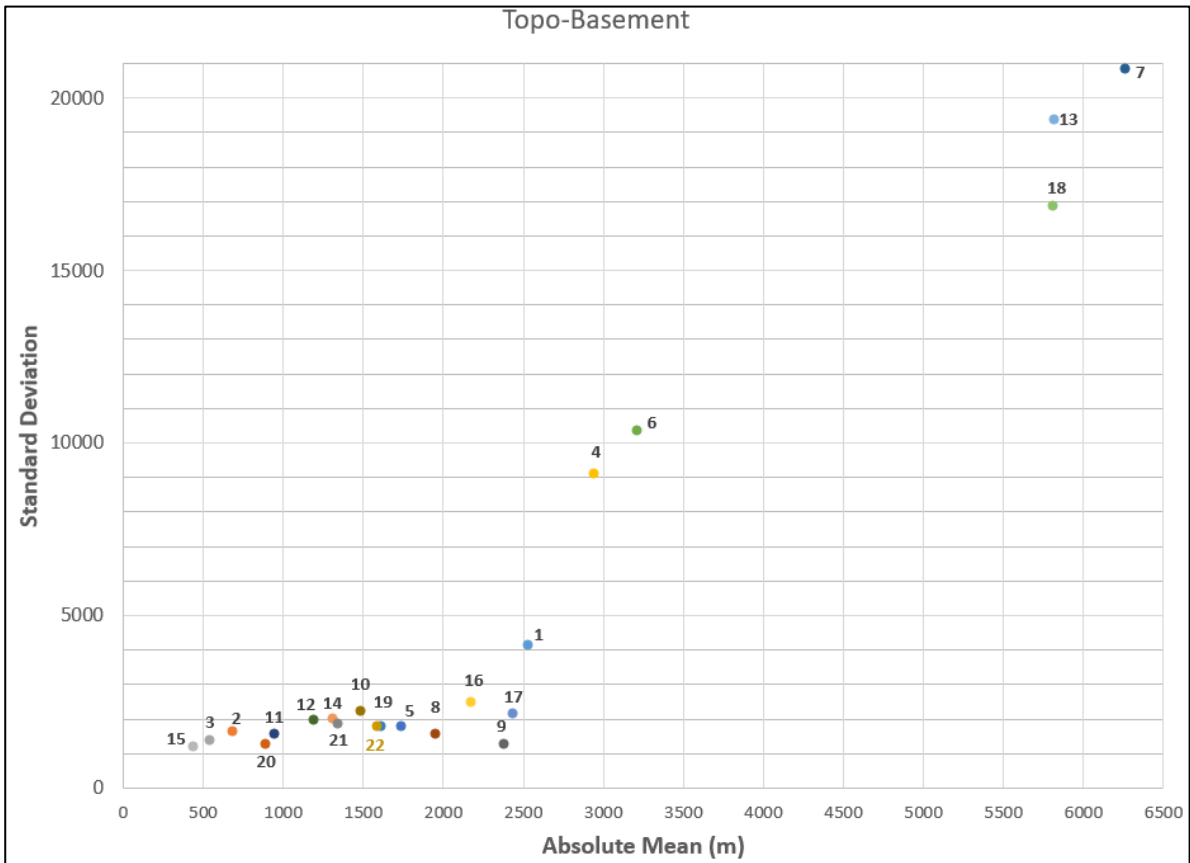


Figure 5-14 Plot of the absolute Group Means versus the Group Standard Deviations calculated from the difference maps for top Basement horizon to the Topography horizon for all 22 scenarios.

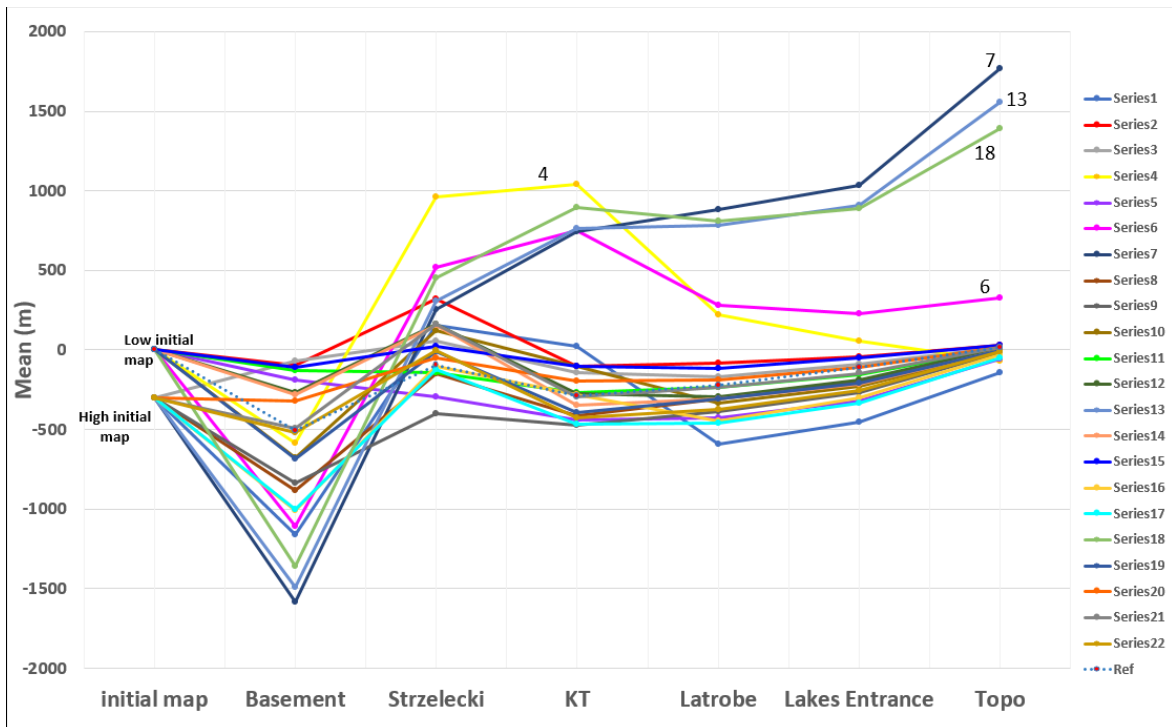


Figure 5-15 Mean of the difference Map at selected horizons or time periods for each scenario. The series correspond to each of the scenarios and the green dotted line is the Reference Case.

Figure 5-16(a) indicates that the experimental design matrix provides good coverage of the possible scenarios across the complex multi-dimensional space. Scenarios 8, 16, 19, 22 that lie between P40 - P60 are expected to be the best fits to the most likely response for the geological history from Basement to top Latrobe Group. The co-efficients for each variable in the response equation are shown in Figure 5-16 (b) which gives a good indication of the relative effects for each of the variables.

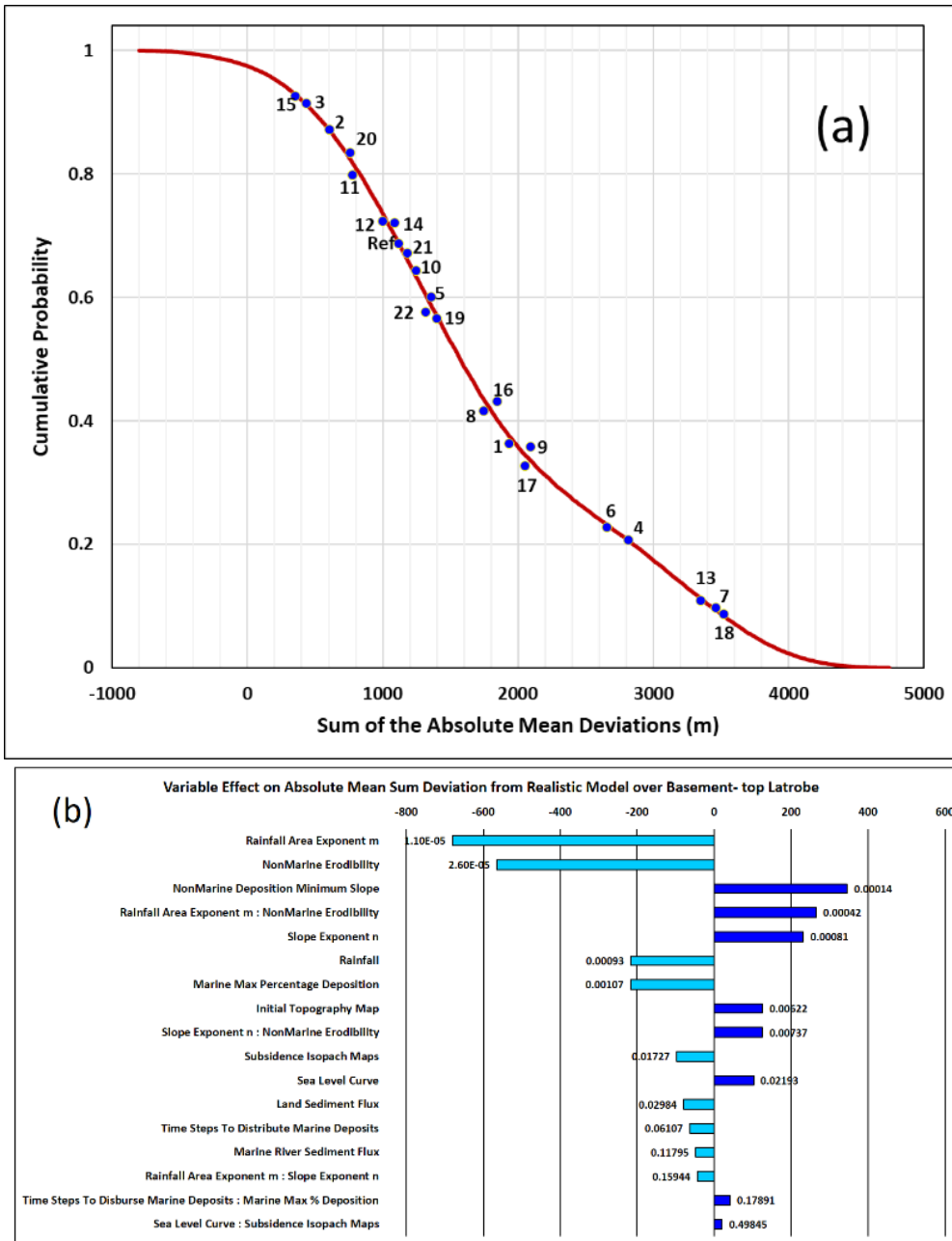


Figure 5-16 Response for Mean Sum absolute Differences of Scenario Maps from Realistic Model over top Basement to top Latrobe horizons (a) Cumulative Frequency Probability plot of response equation fit to the 22 scenarios. (b) Tornado chart showing co-efficients in response equation for each variable ranked according to t-significance value (smallest values are the most significant).

The statistical analyses help to better understand the effect of some variables modelled in the *Badlands* software. The tornado charts generated in *GSAT* help to highlight the modelled effects for key variables, especially anomalously extreme ranges so that the tested ranges can be adjusted to more realistic values or field data (Figure 5-17). For example, preliminary ranges used in early simulation runs produced a tornado chart that indicated two of the variables, *Erodibility* and the exponent m for ($Rainfall \times Area$) were much larger than other variables, potentially hiding the real significance and relationships between other variables. The ranges were adjusted for these variables in simulation of the subsequent Reference Case and the resulting tornado chart more evenly shows the influence of all the variables (Figure 5-17). *Erodibility* and exponent m are still the most significant variables, but other variables including the *Minimum Slope of non-marine deposition*, *maximum Marine Deposition%* and *Rainfall* are now also important. The results show how several iterations of the scenario analysis allows better focus on the critical variables and that some variables that are not significant can be removed from the experimental design or replaced by other candidate variables.

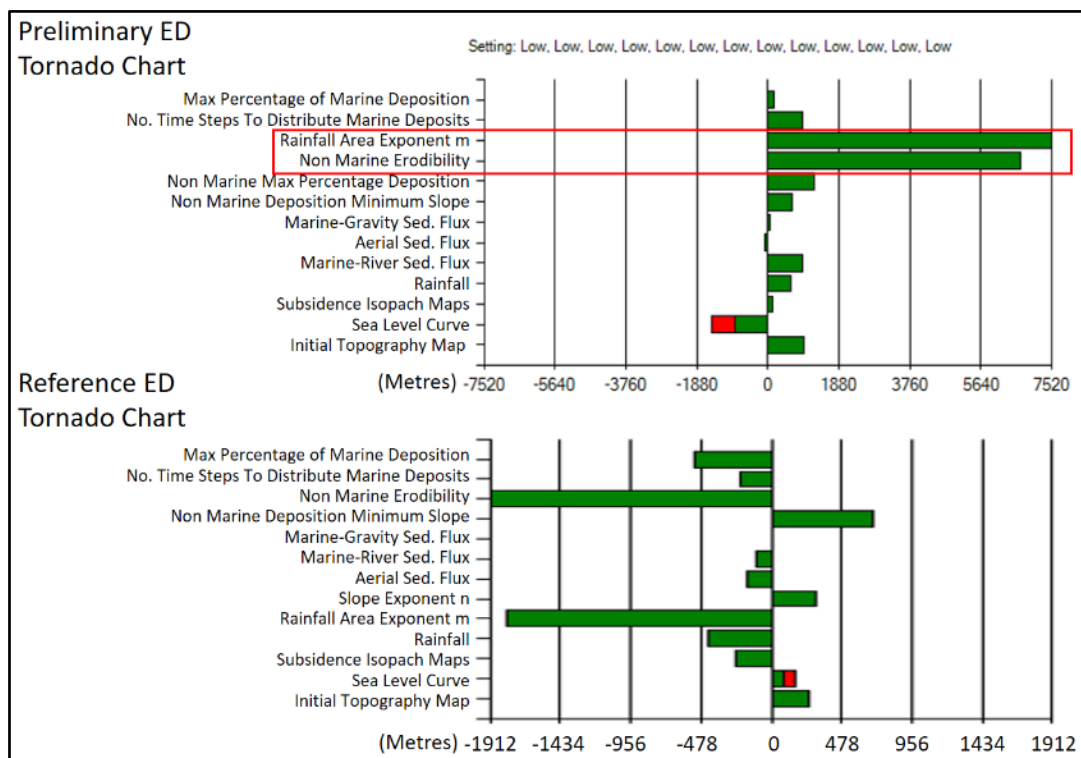


Figure 5-17 Comparison of a preliminary Tornado chart (top) with the Tornado chart for the Reference Case (bottom).

The statistical analysis of the fit of simulations for each isopach is given in Table 5-7 for: top Basement to top Strzelecki Group (Basement-Strzelecki); top Strzelecki Group to Base

Palaeocene (Strzelecki -KT); Base Palaeocene to top Latrobe Group (KT-Latrobe). The results for the global means for the entire Latrobe and Seaspray Groups are also listed in Table 5-7.

Table 5-7 The significance of each Variable and the main Interactions between different map levels: top Basement to top Strzelecki Group (Basement-Strzelecki); top Strzelecki Group to Base Palaeocene (Strzelecki -KT); Base Palaeocene to top Latrobe Group (KT-Latrobe); entire Latrobe Group and entire Seaspray Group.

VARIABLES		Basement - Strzelecki	Strzelecki - KT	KT - Latrobe	Latrobe Group	Seaspray Group
Initial Map		*				*
Sea Level		**			ns	*
Tectonic Maps		●	**		ns	●
Non-Marine Erodibility		***	***		**	*
Rainfall		**	*	*	*	*
(Rainfall * Area) Exponent m		***	**	●	***	*
Critical Slope		●			ns	*
Slope Exponent n		**		●	*	●
Aerial Sed. Flux			**	*		●
Marine-River Sed. Flux				ns	ns	ns
Marine-Gravity Sed. Flux			ns	●	●	
No. Time Steps to Distribute Marine Deposits			ns			
Max % Marine Deposition		*	***	*	●	
Interactions	m : Erodibility		●	**	*	
	Sea level : Tectonic Maps		ns	ns		
	n : Erodibility	**		ns		
	m : n	*		ns		
	No. Time Steps to Distribute Marine Deposits : Max % Marine Deposition	ns		●		
Sea level : Initial Map		ns				
Significance codes:		0 ' *** ' 0.001 ' ** ' 0.01 ' * ' 0.05 ' ● ' 0.1 ' ' 1				
		High Signif. <-----> Low Signif.				
		ns: variable effect is too tiny to be recorded				

The Gippsland Basin has undergone several phases of subsidence, uplift and sedimentation and none of these variables are constant with time. The simulation results can be used to investigate the changes in the amount of erosion and deposition with time as shown in Figure 5-18 and Figure 5-19. The patterns exhibited by the different scenarios show a range of simulated histories of erosion and deposition through time around the Reference Case (red dotted case in Figure 5-18 and Figure 5-19). Some scenarios share similar patterns as the Reference Case (scenarios 5, 9, 11, 20) while some show very different patterns (e.g., scenarios 3, 12, 15, 16, 17). However, many cases end up towards a much smaller range, compared to the large variation towards the beginning (119 - 85 Ma), and most cases demonstrate balanced fill and good fits through time, though they have followed very different geological histories.

The end member scenarios 2, 3, 15, 20 have very high amounts of erosion and or of deposition yet on average are good fits to the basin history with low average mean differences and standard deviations to the Reference Case (Figure 5-13, Figure 5-16). In contrast, the scenarios 7, 13, 18, 6

are all poor fits to the Reference Case. These cases generate under-filled basins that end up with deep depressions, which demonstrates the result when subsidence outstrips erosion and deposition resulting in a starved basin.

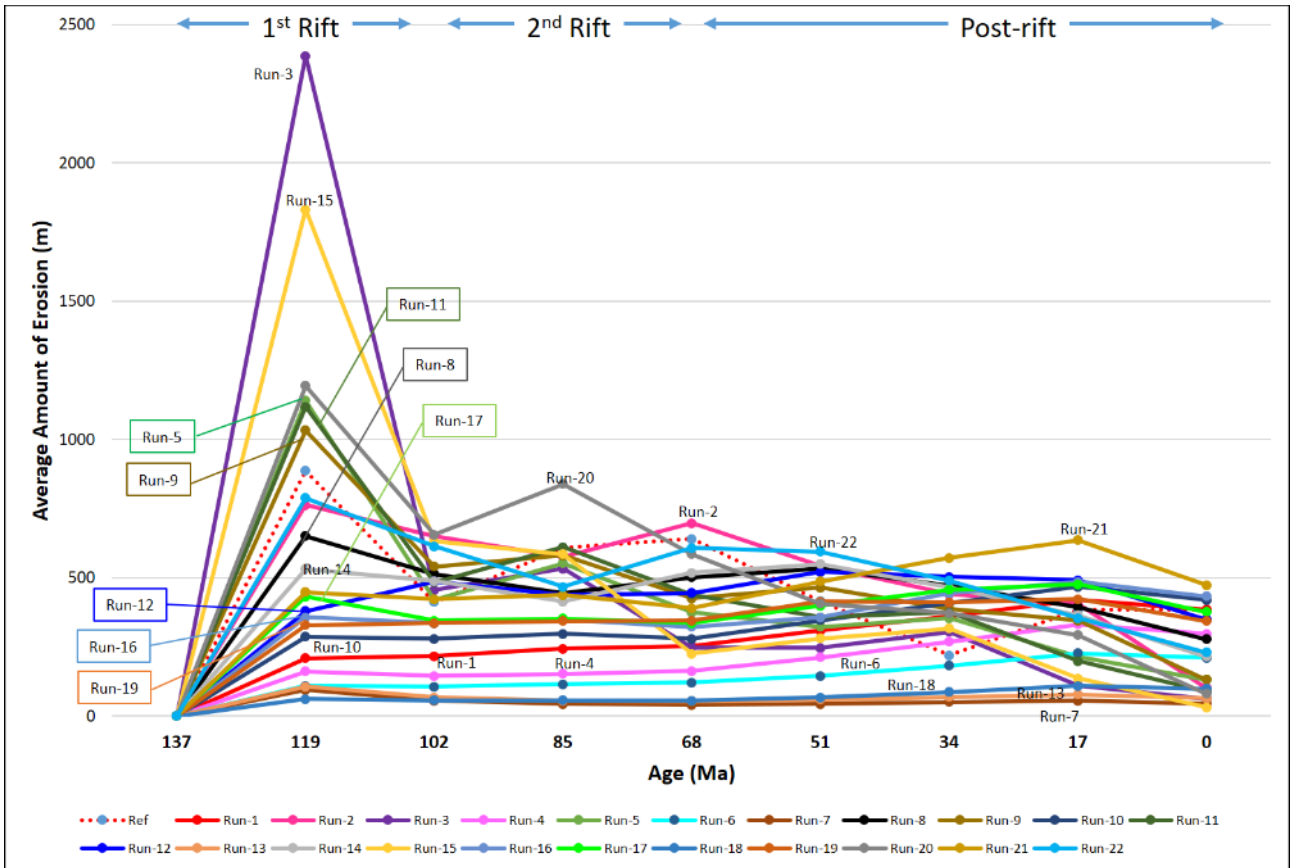


Figure 5-18 Absolute mean of cumulative erosion versus time for 23 scenarios (extracted at 17 Ma time steps).

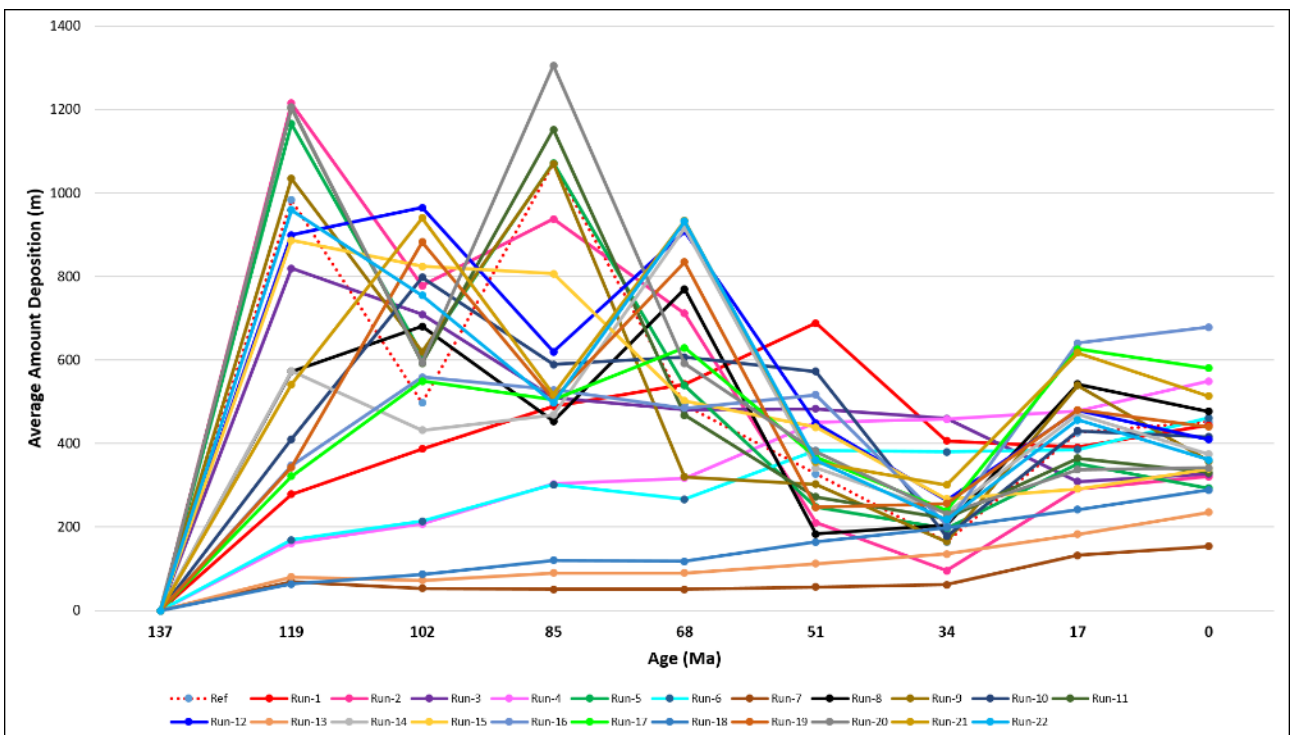


Figure 5-19 Cumulative Deposition versus time for 23 scenarios (extracted at 17 Ma time steps).

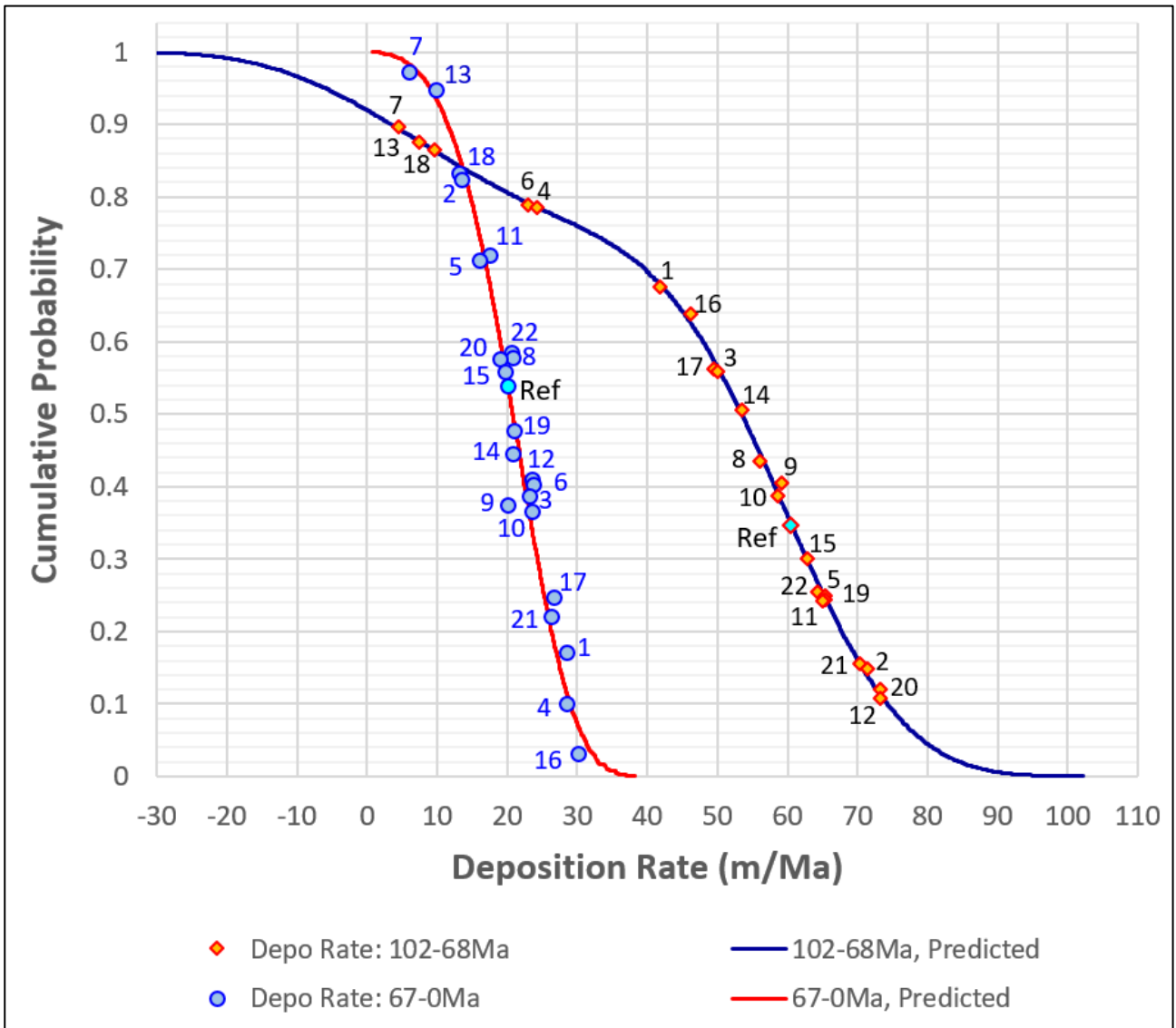


Figure 5-20 Accumulative probability curve of the deposition rate during 102-68Ma and 67-0Ma ranges. The reference case is marked as different colour.

Depositional rates can be extracted from the results for different phases, such as the second extensional phase (e.g., 102-68 Ma) and the sag phase (e.g., 67-0 Ma). The depositional rates for each of the scenarios over those two time periods and the best-fit equations to the scenarios are shown in Figure 5-20. The respective equation co-efficients are given in Table 5-8. The relative effects of each variable are shown in the tornado charts for the two periods in Figure 5-21 in which each variable is ordered by the t-values from most to least significant.

Table 5-8 Response equations for Deposition Rate between 102-68Ma and 67-0Ma including: co-efficients for each variable, equivalent absolute values, t-value (probability variable is not significant; ns = not significant).

	102-68Ma Deposition Rate			67-0Ma Deposition Rate		
	Estimate	Absolute Estimate	Pr(> t)	Estimate	Absolute Estimate	Pr(> t)
(Intercept)	40.5	40.5	0.017	24.4	24.4	3.70E-08
Initial Topography Map	-1.8	1.8	0.175	0.6	0.6	0.21509
Sea Level Curve	0.7	0.7	0.478	0.3	0.3	0.57018
Subsidence Isopach Maps	4.0	4.0	0.084	-2.5	2.5	0.00102
Rainfall	4.7	4.7	0.071	-0.7	0.7	0.15789
Rainfall Area Exponent <i>m</i>	15.9	15.9	0.022	1.0	1.0	0.06821
Slope Exponent <i>n</i>	-4.9	4.9	0.071	-0.1	0.1	0.89413
Land Sediment Flux	1.8	1.8	0.176	-2.2	2.2	0.00185
Marine River Sediment Flux	1.7	1.7	0.194	1.5	1.5	0.01536
Marine Gravity Sediment Flux	-3.2	3.2	0.107	ns	ns	ns
Non-Marine Deposition Minimum Slope	-5.0	5.0	0.067	ns	ns	ns
Non-Marine Erodibility	12.0	12.0	0.03	2.4	2.4	0.00148
No Time Steps To Distribute Marine Deposits	5.3	5.3	0.064	-0.6	0.6	0.26293
Marine Max Percentage Deposition	3.4	3.4	0.104	ns	ns	ns
Sea Level Curve²	8.8	8.8	0.091	-5.8	5.8	0.0012
Rainfall Area Exponent <i>m</i>:NonMarine Erodibility	-10.9	10.9	0.031	-3.6	3.6	0.00011
Sea Level Curve : Subsidence Isopach Maps	-0.4	0.4	0.61	ns	ns	ns
Initial Topography Map : Sea Level Curve	-0.7	0.7	0.435	-1.5	1.5	0.02409
Slope Exponent <i>n</i> : Non-Marine Erodibility	2.7	2.7	0.127	0.7	0.7	0.15251
Rainfall Area Exponent <i>m</i>:Slope Exponent <i>n</i>	2.3	2.3	0.153	ns	ns	ns
No Time Steps To Distribute Marine Deposits : Marine Max Percentage Deposition	0.8	0.8	0.405	ns	ns	ns

Notes: the +/- sign for each estimate is related to the variable level settings.

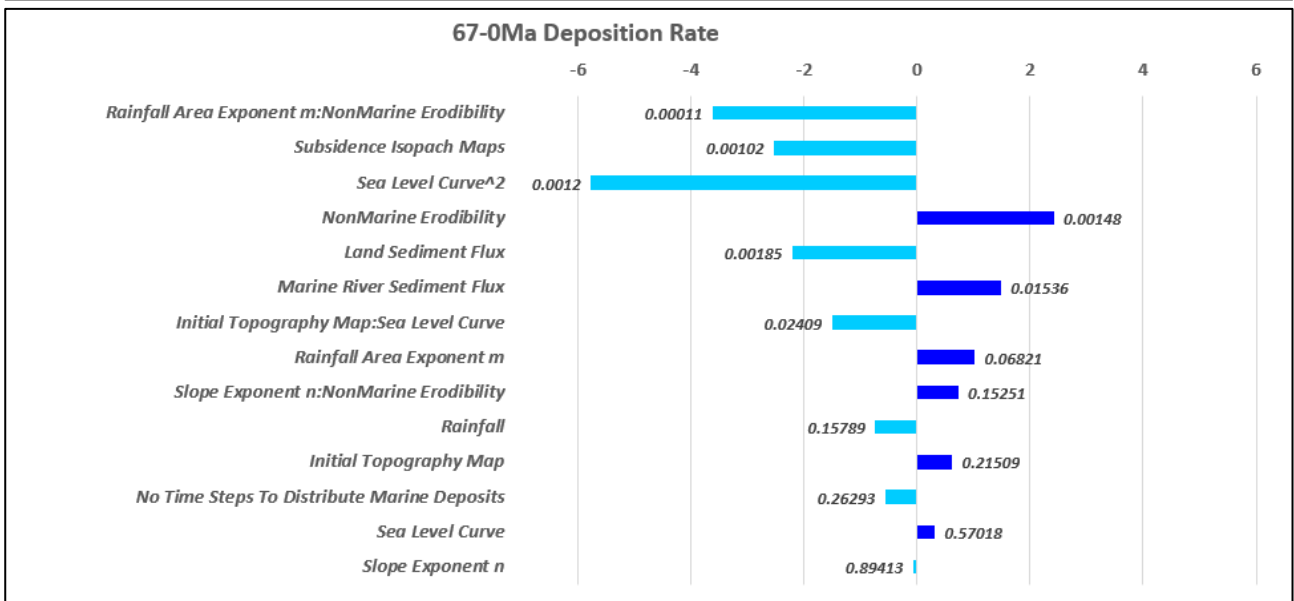
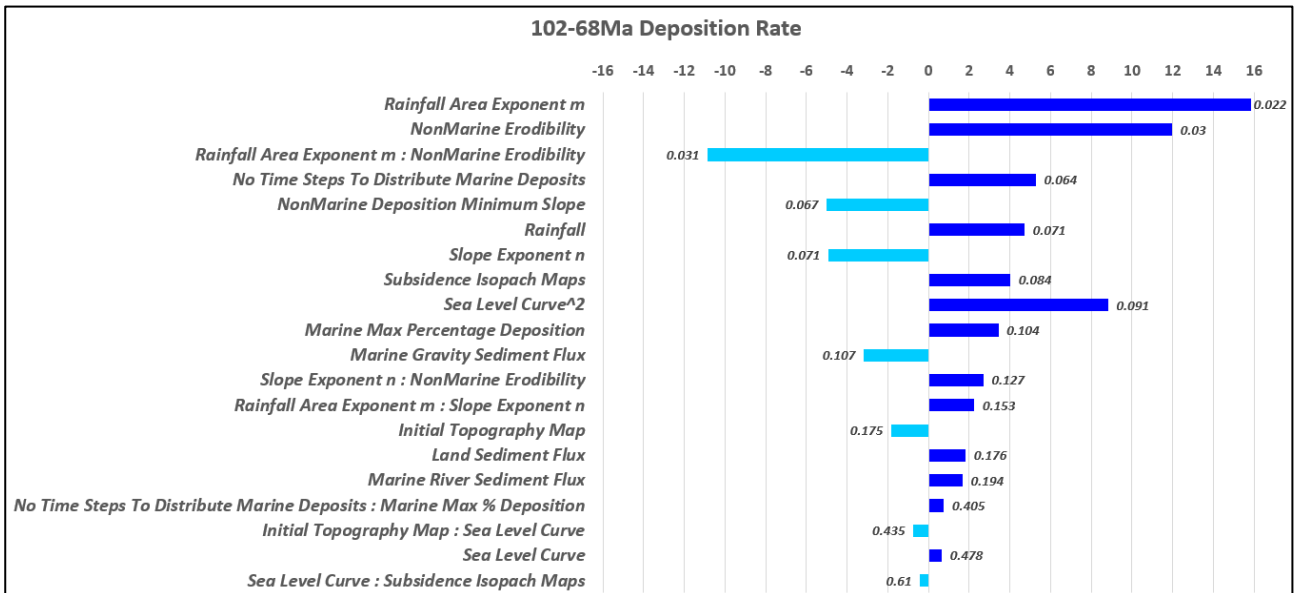


Figure 5-21 Tornado charts showing co-efficients in response equations for each variable ranked according to *t*-significance value (smallest values are the most significant). Note the second order effect of Sea Level Curve is highly significant whereas the first order linear effect is of low significance.

The relative size of the co-efficients give an indication of the corresponding effect for each variable and the equations demonstrate that the amount of erosion and deposition at any one time result from a complex interplay of all the variables including interactions. Hence, analysis or sensitivity runs of a single variable to investigate its effect can give very misleading results. The table of variable significances Table 5-8 and the tornado charts (Figure 5-21) show that *erodibility* is a critical variable, however, its effects can be countered by combinations and interactions with other variables that can significantly impact the basin filling process. For example, Scenario 4 has a high *erodibility* but is a poor fit to the reference model resulting from low *rainfall exponent m* and low deposition settings (Figure 5-16), whereas Scenario 10 is a good fit even though it has the same high *erodibility* and low *rainfall exponent m* settings as scenario 4 (Table 5-9). This is because

these settings are more in balance with its low initial highlands and tectonic maps, low critical slope and slope exponent n settings, which are more consistent with the resulting low amount of erosion.

Table 5-9 Comparison of settings for Scenarios 4 and 10

Run#	Initial Map	SeaLevel	Tectonic Map	Erodibility	Rainfall	(Rainfall * Area) Exponent m	Critical Slope	Slope Exponent n	Aerial Sed. Flux	Marine-River Sed. Flux	Marine-Gravity Sed. Flux	No. Time Steps to Distribute Marine Deposits	Max % Marine Deposition
4	Low	Mid	High	High	Low	Low	High	High	Low	Low	High	Low	Low
10	Low	High	Low	High	Low	Low	Low	Low	High	Low	High	High	Low

5.3.2 Discussion of Controlling Variables

The significant variables that control the development of the Gippsland Basin and how they interact can be determined from the simulated landscape results of the 22 scenarios, the response equations and the ANOVA results given above. Some variables are significant controls during some time periods but are not as significant at other times, so that there is an evolving landscape that changes its response to both internal (eg *slope* and *erodibility*) and external (eg climate, sea level and subsidence) influences, as indicated in Table 5-7. The absolute mean sum of the difference maps for the Basement to Latrobe Group provides an overall summary of the influence for each variable as given in Table 5-10 and Figure 5-16. The analysis of depositional rates provides similar results but clearly shows how the impact of these variables changes from the rift to the post-rift phases Table 5-8 and Figure 5-21.

Overall, the results given in these tables and figures indicate that, although a large number of variables and equations were included in the simulations, the most significant variables produced by the *Badlands* simulations are mostly related to the amount of erosion via the detachment-limited stream power law, where the erosion rate ϵ depends on the erodibility k , net precipitation P , drainage area A and slope S in the equation $\epsilon = k(PA)^m S^n$.

They include:

- (a) *Rainfall* and the (*Rainfall x Area*) exponent m ;
- (b) Non-marine *Erodibility* and the m :*Erodibility* interaction; and
- (c) Critical *Slope* and Slope exponent n .

These variables have high significance not only in each map level but also over the long term for the Latrobe Group and the entire modelled time period (Table 5-7 and Table 5-10). Moderate

controls are exerted by the initial topographic map and the amount of marine accommodation space as measured by the parameter *maximum % marine deposition*. *Sea level*, tectonic maps and *non-marine aerial sediment flux* have secondary impacts, mainly over specific time periods where they are most influential, becoming less important in the long term in the post-rift phase.

In contrast, the variables associated with dispersion of the marine sediment including from the rivers to marine shelf (*marine river sediment flux*), and to the deep marine (*marine gravity sediment flux*) do not have much effect over small or long term time periods in this study, though this may be due to the dominance in the Gippsland Basin of non-marine sedimentation until the last phase. It seems that while changes in subsidence, uplift and sea-level create the accommodation space and landscape slope, the resulting balance between erosion and deposition control whether a basin is filled or underfilled and is significantly related to climate (*precipitation*). These results are discussed in more detail below using the Reference Case which lies in the most likely cluster of scenarios for various measures (between ~P35-P60 percentiles).

The relative influence of the tested variables can be demonstrated using the calculated Mean summed differences between the Realistic Model surfaces and the *Badlands* Reference Case model for the entire Gippsland Basin over the full-time period (Table 5-10). The corresponding cumulative probability frequency plot of the mean sum differences for each scenario, from top Basement level to top Latrobe level, and the best-fit response equation are shown in Figure 5-16.

The resulting response equation as measured by the sum of the Absolute Means from Basement-Latrobe is given below, noting that the size of the coefficients indicate the corresponding effect (shown in Figure 5-16):

$$\begin{aligned} \text{Deviation of Reference Case from Realistic Model} = & 1768 + 126*\text{InitialMap} + 102*\text{Sealevel} - \\ & 98*\text{TectonicMap} - 216*\text{Rainfall} - 680*m + 232*n - 79*\text{AerialSed.Flux} - \\ & 48*\text{MarineRiverSed.Flux} + 346*\text{CriticalSlope} - 565*\text{Erodibility} - 63*\text{No.TimeSteps} - \\ & 217*\text{MarineMax\%Deposition} + 265*(m:\text{Erodibility}) + 21*(\text{sealevel}:\text{TectonicMap}) + \\ & 125*(n:\text{Erodibility}) - 44*(m:n) + 41*(\text{No.TimeSteps}:\text{Max\%MarineDeposition}) \end{aligned}$$

Table 5-10 The significance results from the ANOVA for top Basement to top Latrobe level. The analysed response is the sum of the absolute means for each of the difference maps. The significance levels indicate the probability that the variable is not significant (low values are most significant).

VARIABLES		Significance	Pr(> t)
Initial Map		**	0.006220
Sea Level		*	0.021930
Tectonic Maps		*	0.017270
Non-Marine Erodibility		***	0.000026
Rainfall		***	0.000930
(Rainfall * Area) Exponent <i>m</i>		***	0.000011
Critical Slope		***	0.000140
Slope Exponent <i>n</i>		***	0.000810
Aerial Sediment Flux		*	0.029840
Marine-River Sediment Flux			0.117950
Marine-Gravity Sediment Flux		ns	ns
Number Time Steps to Distribute Marine Deposits		•	0.061070
Max % Marine Deposition		**	0.001070
Interactions	<i>m</i> : Erodibility	***	0.000420
	Sea level : Tectonic Maps		0.498450
	<i>n</i> : Erodibility	**	0.007370
	<i>m</i> : <i>n</i>		0.159440
	No. Time Steps to Distribute Marine Deposits : Max % Marine Deposition		0.178910
	Sea level : Initial Map	ns	ns
Signif. codes: 0 '***', 0.001 '**', 0.01 '*', 0.05 '.', 0.1 ' ', 1			
High Signif. <-----> Low Signif.			
ns: the variable effect is too small to be recorded			

5.3.2.1 Rainfall

Rainfall (precipitation) is a significant variable overall especially during deposition of the Strzelecki Group which is dominantly non-marine. Rainfall is the main control on the fluvial discharge as expected: the scenarios that begin with low rainfall result in low stream discharge (e.g., 2.1E+10 m³/yr) and produce a smaller stream system with thinner streams, whereas the scenarios with high rainfall have high stream discharge (3.2E+11 m³/yr) and produce a much more developed, complex and widespread fluvial system, as shown by the landscape views in Figure 5-22. Hence, the scenarios can be separated into two groups based on discharge value (Table 5-11). The effect of *Rainfall* is enhanced by the exponent *m* for the combined variable (*Precipitation x Area*) in the stream power law equation and this combined effect is even more significant than the single variable *Rainfall* on its own. This shows that the size of the basin hinterland is important with larger

basins receiving high *rainfall* able to provide more sediment and the sediment supply more able to keep pace with the subsidence and fill for large rift basins, whereas it becomes less important in the post-rift phase dominated by the marine Seaspray Group.

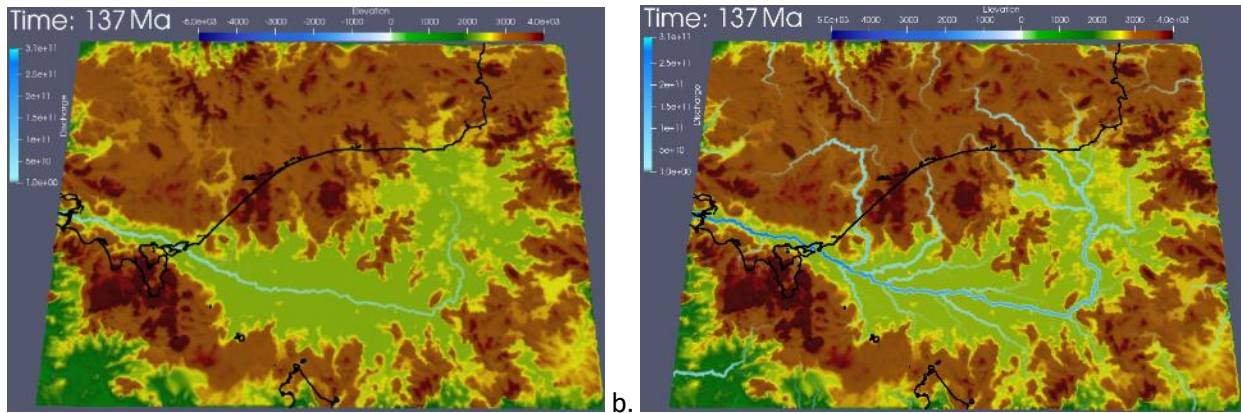


Figure 5-22 Fluvial system of two different scenarios: (a) scenario 1, low rainfall; (b) scenario 3, high rainfall.

Table 5-11 Scenarios separated into two groups based on discharge level.

Run#	discharge at 137Ma	discharge at OMa	Run#	Initial Map	SeaLevel	Tectonic Map	Erodibility	Rainfall	(Rainfall * Area) Exponent <i>m</i>	Critical Slope	Slope Exponent <i>n</i>	Aerial Sed. Flux	Marine-River Sed. Flux	Marine-Gravity Sed. Flux	No. Time Steps to Distribute Marine Deposits	Max % Marine Deposition
1	2.11E+10	1.71E+09	1	High	High	Low	Low	Low	High	Low	High	Low	High	High	Low	Low
16	2.11E+10	1.83E+09	16	High	Low	Low	High	Low	Low	High	Low	Low	High	Low	Low	High
10	2.11E+10	1.84E+09	10	Low	High	Low	High	Low	Low	Low	Low	High	Low	High	High	Low
4	2.11E+10	2.19E+09	4	Low	Mid	High	High	Low	Low	High	High	Low	Low	High	Low	Low
12	2.11E+10	2.46E+09	12	Low	High	High	Low	Low	High	Low	Low	Low	Low	Low	Low	High
13	2.11E+10	2.64E+09	13	High	Low	High	Low	Low	Low	Low	Low	High	Low	High	Low	High
7	2.11E+10	2.92E+09	7	High	High	High	Low	Low	Low	Low	High	High	High	High	High	Low
20	2.11E+10	3.69E+09	20	High	Mid	High	High	Low	High	Low	High	High	Low	Low	High	High
11	2.11E+10	3.80E+09	11	Low	Low	High	High	Low	High	Low	Low	Low	High	Low	High	Low
19	2.11E+10	1.87E+10	19	Low	Low	Low	Low	Low	High	High	Low	High	High	High	High	High
6	3.17E+11	2.62E+10	6	Low	Mid	Low	Low	High	Low	Low	Low	Low	High	Low	High	Low
21	3.17E+11	2.68E+10	21	High	Low	High	High	High	Low	Low	High	Low	High	High	High	High
18	3.17E+11	2.84E+10	18	Low	High	Low	Low	High	Low	High	High	Low	Low	Low	High	High
17	3.17E+11	2.94E+10	17	High	High	Low	High	High	Low	High	High	High	Low	Low	Low	High
2	3.17E+11	3.22E+10	2	Low	Low	High	High	High	Low	Low	Low	High	Low	Low	Low	Low
5	3.17E+11	3.41E+10	5	Low	High	High	High	High	High	High	High	High	High	High	Low	Low
8	3.17E+11	3.48E+10	8	High	Low	Low	Low	High	High	High	High	High	Low	Low	High	Low
15	3.17E+11	3.56E+10	15	Low	Low	Low	Low	High	High	Low	High	Low	Low	High	Low	High
14	3.17E+11	3.79E+10	14	Low	Mid	High	Low	High	High	High	High	High	High	High	Low	High
3	3.17E+11	4.20E+10	3	High	Mid	Low	High	High	High	Low	Low	High	Low	High	Low	Low
22	3.17E+11	6.60E+10	22	High	High	High	High	High	Low	High	Low	Low	Low	High	High	High
9	3.17E+11	7.56E+10	9	High	High	Low	Low	High	High	High	Low	Low	Low	High	High	Low

5.3.2.2 Erodibility

Erodibility is another highly significant variable, with a high *Erodibility* allowing rapid erosion, whereas a low *Erodibility* produces slower and smaller erosion (Figure 5-11 and Figure 5-23). This result may seem trivial and was suggested by the preliminary sensitivity analysis of the Reference Case (section Reference Case Sensitivity Analysis). However, the measured effects show that this is not so simple because *Erodibility* also significantly interacts with the *Rainfall x Area* exponent *m* and with the *Slope* exponent *n* to compound their effect on the rate of erosion.

The combined effect of high *Erodibility* and high *m* can be seen in Scenarios 3 and 20 (compounded by high rainfall in the case of scenario 3) where a high land erosion rate produces a

strong response in the present-day mountain height which dominates any other combination of factors (Table 5-12; Figure 5-23, top). These scenarios begin with a high initial topographic map, which is rapidly reduced to a flat-lying onshore area with a minimum mountain height and an over-filled marine basin by 0 Ma. In contrast, scenarios 6 and 18 begin with a low initial topographic map and have low tectonic uplift, but with the minimal erosion rate resulting from a low *Erodibility* and low *Rainfall x Area* exponent *m*, they retain a final high mountain relief and produce an underfilled deep graben over the marine basin at 0 Ma (Figure 5-23, bottom). Again this result is irrespective of any combination of other factors including keeping the tectonic uplift low. The experimental design results for these four scenarios given in the matrix below clearly show that *Erodibility*, *Rainfall x Area* and its exponent *m* are the dominant controlling variables that affect the mountain height caused by land erosion. Secondary effects are produced by the *Slope* and its exponent *n*. Note the *aerial sediment flux* only has a minor effect on the mountain height as indicated by its low significance in Table 5-10.

Table 5-12 Extreme scenarios showing how erosion rate is controlled mainly by exponent *m* (for *Rainfall*Area*) and *Erodibility*.

Run#	Mountain Height at 0 Ma	Run#	Initial Map	SeaLevel	Tectonic Map	Erodibility	Rainfall	(Rainfall * Area) Exponent <i>m</i>	Critical Slope	Slope Exponent <i>n</i>	Aerial Sed. Flux	Marine-River Sed. Flux	Marine-Gravity Sed. Flux	No. Time Steps to Distribute Marine Deposits	Max % Marine Deposition
3	100	3	High	Mid	Low	High	High	High	Low	Low	High	Low	High	Low	Low
20	500	20	High	Mid	High	High	Low	High	Low	High	High	Low	Low	High	High
6	6000	6	Low	Mid	Low	Low	High	Low	Low	Low	Low	High	Low	High	Low
18	7200	18	Low	High	Low	Low	High	Low	High	High	Low	Low	Low	High	High

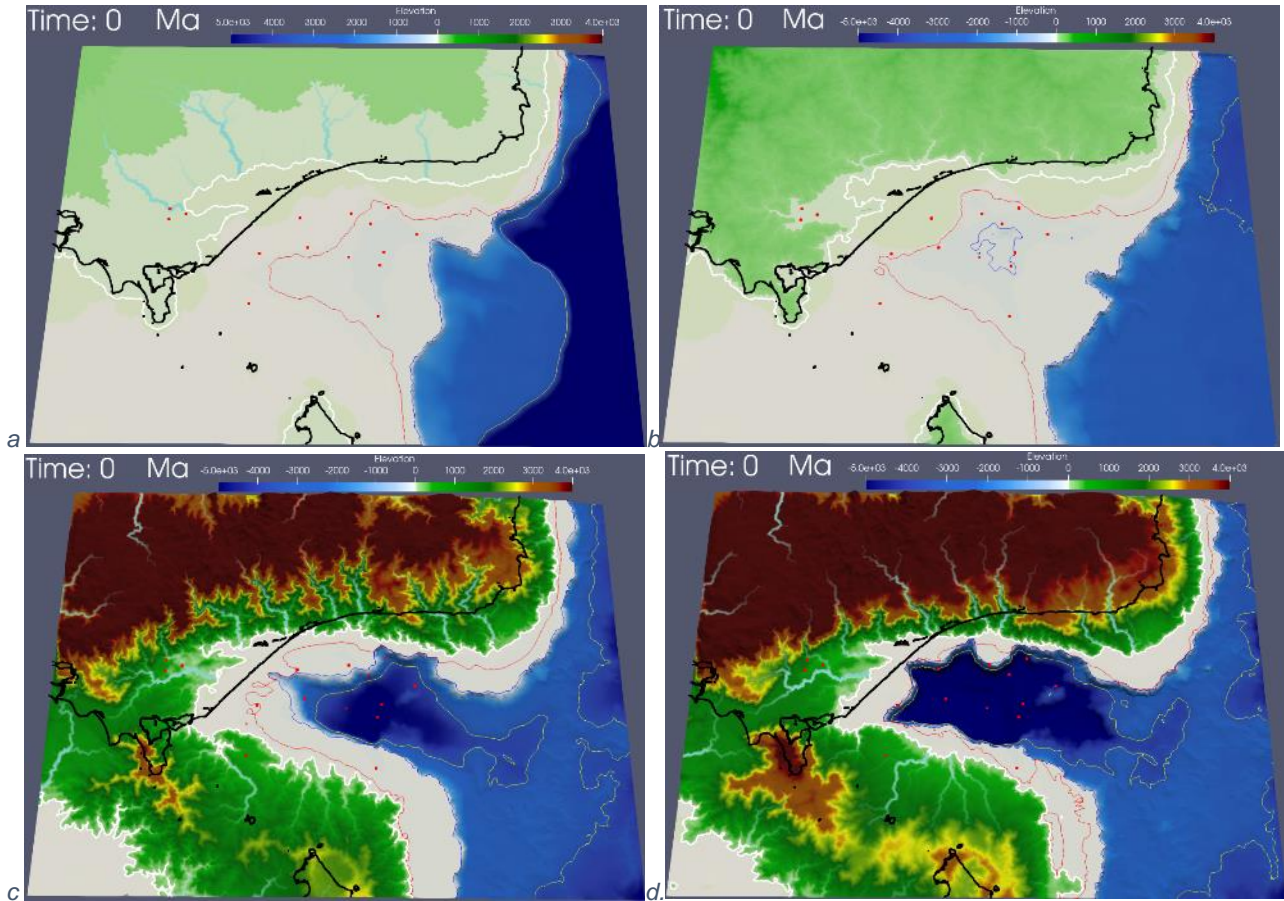


Figure 5-23 Four extreme scenarios selected by their resulting mountain height at 0Ma to show the effects of m , erodibility, rainfall and onshore sediment flux: (a) high initial topography with high erosion in scenario 3 (a) and scenario 20 (b); versus low initial topography with low erosion in scenario 6 (c) and scenario 18 (d).

5.3.2.3 Slope

Slope is another important variable that controls the sediment supply and distribution. The *Slope* exponent n has a major impact on erosion, with steeper slopes increasing erosion and supply of loose sediment. Similarly, the *critical slope* is important in controlling the downslope movement of sediment by affecting both erosion and deposition. The *slope* and its exponent n are the second-most critical factors which boost the erosion rate level (Table 5-12). This is shown by two end-member scenarios for critical slope and n : Scenario 3 which has low settings for *critical slope* and n ; versus Scenario 18 which has high settings for *critical slope* and n (Figure 5-23).

5.3.2.4 The Maximum % Marine Deposition

The *Maximum % Marine Deposition* that provides the amount of accommodation space at any given time interval in a marine or sea depression is also a critical variable. This controls the sediment deposition in open marine areas and any large water system, such as inland seas, lakes, lagoons. The corresponding *Maximum % Deposition* in the non-marine environments such as on alluvial plains was tested over a range and was not found to be significant so was kept constant at

95%. However, the *maximum % marine deposition* variable demonstrates moderate influence in the Early Cretaceous (Strzelecki Group) and high significance in the Late Cretaceous (lower Latrobe Group) (Table 5-7). In particular, it affects the amount of sediment fill and accommodation space. It can create a starved or over-filled basin depending on the amount of tectonic subsidence, which is especially relevant during the two rapidly subsiding rift events if they subside below base level.

The tectonic maps guide the subsidence and uplift processes and are significant during deposition of the Strzelecki Group (first syn-rift phase) and of the lower Latrobe Group (second syn-rift phase) (Table 5-7). This is consistent with the occurrence of high subsidence rates during the syn-rift phases, where the subsidence overshadows the other variables, whereas subsequently its effect diminishes into the post-rift phases. Notably, the tectonic maps show greater significance during the second syn-rift phase in the Late Cretaceous (top Strzelecki-KT), which suggests the uninterrupted subsidence during the second rift phase had a greater effect on the Latrobe Group deposition than the first rift phase had on the Strzelecki Group.

The initial topographic map had a large impact during deposition of the Strzelecki Group (first syn-rift phase) though this declines for the subsequent phases once a good balance of sediment supply and subsidence was obtained in the sensitivity analysis of the reference case (Table 5-7). This shows the initial topographic map mainly has a short term impact on initiation of the simulations and is not maintained over the entire history of the Gippsland Basin. Many simulations end up with good fits to the current topographic map which is why the topographic maps for each time-step in the final Seaspray phase are also significant factors as shown in Table 5-7.

The sea-level curve linear effect is not as significant as expected over most of the geological history of the Gippsland Basin, even though tested at substantially high and low levels. However, the second order term has a marked effect indicating rapid changes in *sea level* can outpace the other variables, whereas constant slow or fast changes are mostly accommodated by sediment supply and subsidence. Relative sea-level was found to be significant during the deposition of the Strzelecki and Seaspray groups, but not during deposition of the Latrobe Group (Table 5-7). This result seems unexpected, as the Gippsland Basin was non-marine during the early Cretaceous.

However, *Badlands* measures relative sea level versus the absolute depth value (z) to define the relative area of land to sea. Hence, sea-level helps to define the size of the drainage area which feeds back into the $(\text{Rainfall} \times \text{Area})^m$ part of Equation 5-1 for erosion rate, and these variables are highly significant as discussed earlier. Also, the landscape simulations indicate the formation of inland seas and lakes during deposition in the Early Cretaceous, which is confirmed by marine fossil occurrences. These indicate there may have been a link to the Otway basin which makes it easier to understand the control by sea level change. Another factor is the relative sea level curve changed markedly and frequently during the Early Cretaceous and again from the Oligocene to Recent, whereas it is much more stable from Late Cretaceous to Eocene (Appendix 9).

5.3.2.5 *Synthesis*

The gravity and seismic data show that the first rift created substantial deposition space in a very short time. Also the palynology data indicate that the palaeo-environment remained non-marine, which means a large amount of sediment was eroded, transported and filled the depositional space. The experimental design results support the above basin history during the formation of the Strzelecki group: with significant erosion occurring mainly controlled by the variables *non-marine erodibility*, *rainfall*, $(\text{Rainfall} \times \text{Area})^m$ and *slope exponent* n . The fluvial system is dominant during Strzelecki Group time when the palaeo-environment is surrounded by highlands with some shallow inland sea/lakes controlled mainly by the *sea level* and *max % marine deposition* which takes effect for any water depressions. The *sea level* and *marine max % deposition* have high significance.

In the second rift phase (modelled here from top Strzelecki level to Base Palaeocene), the dominate variables include the: tectonic maps, the erosion related variables such as *non-marine erodibility*, *rainfall*, $(\text{Rainfall} \times \text{Area})^m$, and *marine max % deposition*. Also, the basin uplift caused a west-east flip in the palaeo-slope whereby some of the highlands were replaced by a relatively flat broad land surface. This resulted in an increase in the effect of aerial sediment flux during this phase.

In the post rift phase, the basin's shape was more established, and the effect of many variables tends to be more even. The experimental design analysis results for the Seaspray Group indicates

moderated effects from most of the variables including: *initial topography*, *sea level*, *non-marine erodibility*, *rainfall*, $(\text{Rainfall} \times \text{Area})^m$ and the *critical slope*. The *tectonic subsidence* and *uplift*, Slope^n and *aerial sediment flux* only have small impacts on the model. There are several possible explanations. Most of the sedimentation and burial occurs within the Seaspray group which mainly consists of carbonate deposits that are controlled by the carbonate module, whereas the clastic sediment deposition only affects the onshore and near shore areas. The carbonate sediments in the Gippsland basin are mainly cold water carbonate platform deposits whereas the carbonate module mainly relies on water depth and the depositional space to simulate carbonate reef build-up. Given the above and since there are few variables in the carbonate module, it was decided not to include these in the Experimental Design, since they are not relevant to most of the basin history and would over-complicate the analysis.

Chapter 6. Palaeo-landscape and Best Fit model to Geological history

The known geological history of the Gippsland Basin was summarised in Chapter 2 for which the stratigraphy is shown in (Figure 2-1). The geological history of the Gippsland Basin can now be reviewed using the results from the *GPlates* together with the 3D Realistic (Chapter 4) and the *Badlands* modelling (Chapter 5). The theoretical *Badlands* model simulations that provide the best fits to the realistic 3D model have been identified using the experimental design statistical analysis. They indicate the most likely geological history and they also highlight the critical variables which control the landscape evolution in this rift basin that may be applicable to rift basins in general.

In particular, a review of the best fit simulations can be used to predict the location of potential Cretaceous reservoirs and source rock units in deep parts of the basin that are poorly understood because this section is penetrated by very few wells. The forward simulation models can also guide reconstruction of the maturation history of the lower Halibut, Golden Beach and Emperor Subgroups to assess the source rock kitchens. Current knowledge of potential deep reservoirs is scant yet they probably hold the key to future exploration given the top Latrobe Group sands have been intensively explored. Similarly, knowledge of the source rocks is limited mainly to the organic-rich, non-marine, coastal plain mudstones and coals in the upper parts of the Latrobe Group that are accepted as the main source rocks for the majority of oil and gas in the basin (Burns and Emmett, 1984; Burns et al., 1987; Moore et al., 1992). In contrast, any deeper and more lacustrine source rocks have been inferred (Bernecker and Partridge, 2001) with a lacustrine source contribution being indicated by the organic geochemistry (Tuite, Flannery & Williford, 2016).

6.1 New Model

See the *Badlands* animation of best fit case in Appendix 7.

6.1.1 Early Cretaceous

The Gippsland Basin was initiated probably in the late Berriasian around 137 Ma in the last stage of the east-west rifting between Australia and Antarctica, that is known to have started with the development of half grabens further west in the Bight and Otway Basins during the latest Jurassic,

with the rifting moving eastwards with time into the Gippsland and Bass Basins (Smith, 1982; Duddy and Green, 1992; Willcox et al., 1992, 2001; Norvick, 2005). This early rift phase is probably associated with heating and uplift of highlands throughout the basin which fits with the occurrence of the Tithonian volcanics and minor sediments found in Duck Bay-1 that herald the onset of rifting (Constantine, 2001). The *GPlates* models indicate that extension was recognizable from about 136Ma in the Valanginian and this fits with the minor Valanginian sediments in Duck-Bay-1 that unconformably overlie the volcanics. The *Badlands* simulations indicate that substantial subsidence did not occur until sometime later around 124Ma in the Hauterivian which is supported by the oldest common occurrence of sediments (A. Partridge, *pers. comm.*; Holdgate et al., 2015). This indicates early uplift and volcanism in the Tithonian-Berriasian, a time gap wherein the highlands are eroded with localised deposition in the Valanginian, and subsequent widespread deposition of sediments by the Hauterivian (Figure 6-1).

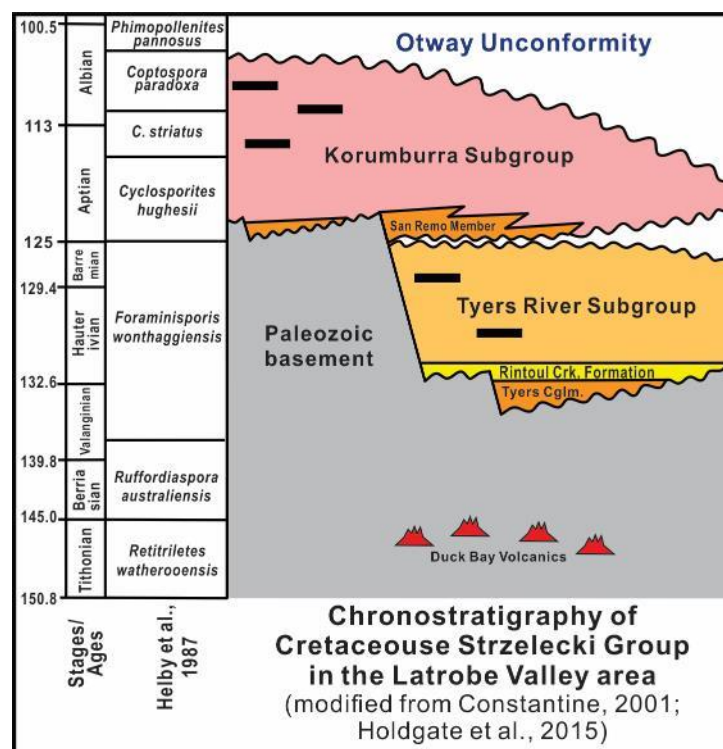


Figure 6-1 Cretaceous Strzelecki Group Chronostratigraphy (modified from Constantine, 2001; Holdgate et al., 2015)

The *Badlands* simulations started from 137Ma and run to 99Ma to model the Strzelecki Group extensional syn-rift consistent with the chronostratigraphy described above. The most likely simulations (ie the Reference Case and especially simulations 14, 19 and also 8, 10; Figure 5-20) show formation of the Gippsland Basin as an intracratonic basin, initially with non-marine

deposition in an narrow east to west drainage basin, developed between and surrounded by steep highlands to the north, east and west, that gradually erode producing a lower relief and wider basin (Figure 6-2, a & b). Substantial subsidence occurred from about 124-100 Ma (Figure 5-19 and Figure 5-20), accompanied by rapid deposition dominated by widespread flood plains and braid plains, with extension of the basin eastward over the current Strzelecki ranges and Latrobe Valley areas by the Albian.

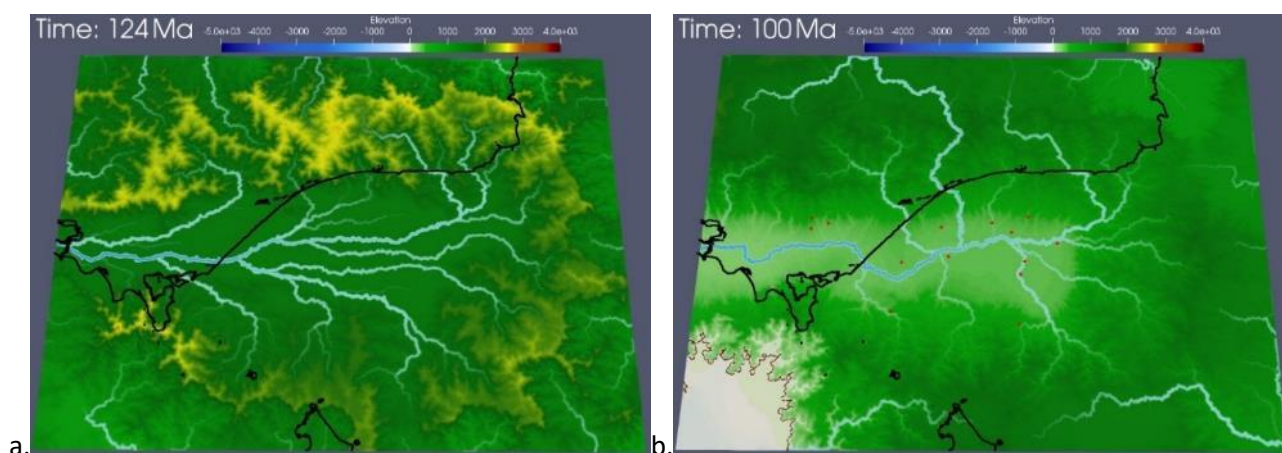


Figure 6-2 Aptian to Albian: a. Gippsland Basin begins to form with intracratonic non-marine deposition and drainage to the West; b. the rivers stabilise in the Gippsland Basin while lacustrine to shallow marine sedimentation develops in Bass Strait. The brown line shows the zero contour. The black line is present coastline.

As separation of Antarctica and Australia progressed, an inland sea appears at the western edge of the basin that was probably connected with the Otway Basin around 99Ma (Figure 6-3a). Fluvio-deltaic sediments build into this shallow inland sea during Albian-Cenomanian time and with continued rifting the sea expands from west to east into western Gippsland (Figure 6-3b).

The overall transport direction from east to west, with local swings in direction from WNW to WSW, is consistent with known palaeocurrent data from the Wonthaggi and Eumeralla formations (Constantine, 2001). The development of a shallow inland sea is also consistent with palaeontological evidence including the Koonwarra fish beds, plesiosaur fossils, dental and postcranial remains, found from Early Cretaceous inland freshwater lakes and estuaries within the Wonthaggi and Eumeralla formations, in both the Gippsland and Otway Basins (Kear, 2006) as shown in Figure 6-4. The Plesiosaurian specimens discovered to-date in Gippsland are relatively small, though adult Plesiosaurians vary in length from 1.5 metres to about 15 metres (Tarlo, 1959), requiring that parts of these inland seas, lakes and estuaries at times may have been extensive and reasonably deep. The corresponding fossil locations are marked on the *Badlands* simulations in Figure 6-3b.

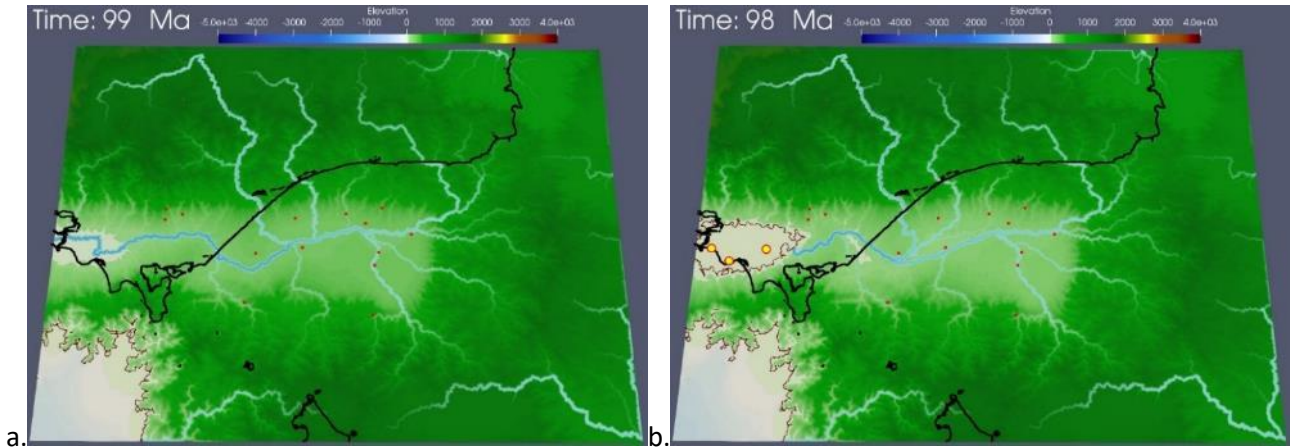


Figure 6-3 a. A flood plain begins in the western edge of the basin by the end of Albian. B. Fluvio-deltaic sediments build into a very shallow inland sea in the Cenomanian. The brown line shows the zero contour, the yellow locations mark the sites of marine fossils (see also Figure 6-4). The black line is present coastline.

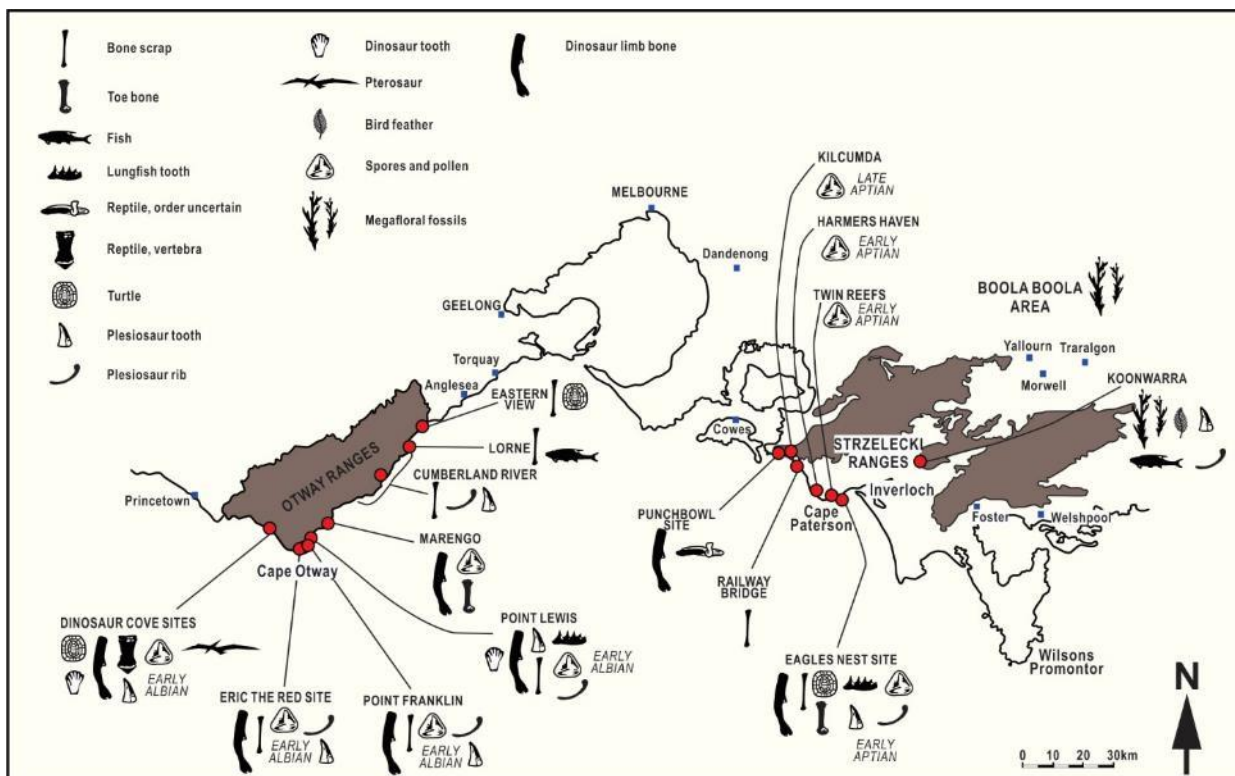


Figure 6-4 Early Cretaceous tetrapod sites, and associated biota (modified Dettmann & Douglas, 1988 and Kear 2006). Red circles highlight the plesiosaur remains locations: Inverloch, Cape Paterson, and Cape Otway.

6.1.1.1 Potential Strzelecki Group Reservoirs

Initially, the Strzelecki Group is dominated by coarse clastics eroded from Palaeozoic basement rocks and transported by the rivers from the northern and southern highlands, producing the sediments in the Tyers River Subgroups. These sediments are mainly coarse-grained quartz and feldspathic litharenites and can form good reservoirs. The simulations demonstrate that these sediments need to form from a long-term essentially continuous sediment supply and, although they are predominately at the base of the sequences, they also occur as marginal fans and braided

stream facies that may continue up through the section into the Korumburra Subgroup and the Wonthaggi Coal Measures.

Subsequently, the Strzelecki Group becomes dominated by volcano-clastics that were sourced from contemporaneous volcanics in the rift system (Gleadow and Duddy, 1980) but mostly derived and moved along the Gippsland rift from the east to the west from the main Tasman rift margins developed between Australia and Zealandia. The volcanic-clastics have undergone significant diagenesis and catagenesis due to their labile compositions and in general do not have good porosity or permeability. However, this study has shown that while the main source is to the east it is also augmented by sources from the northern and southern highland areas and locally could include good reservoirs.

6.1.1.2 Potential Strzelecki Group Source Rocks

The occurrence of widespread shallow marine lacustrine, marginal marine and coaly sediments in the Strzelecki raises the possibility that they could have source rock potential. Good quality source rocks are not well researched in the Strzelecki Group but have been recognised in some wells such as in the Locmany Member of the Tyers River Subgroup by Holdgate et al. (2015). Their RockEval and vitrinite reflectance data showed good TOC >5 %, S₂>10 and hydrogen indices >350, together indicating oil prone potential. The vitrinite reflectance data placed the source rocks in the oil window with R_o values between 0.8-0.9 %. Organic petrology to identify algal organic macerals has not been reported though algae should be common in shallow marginal marine environments.

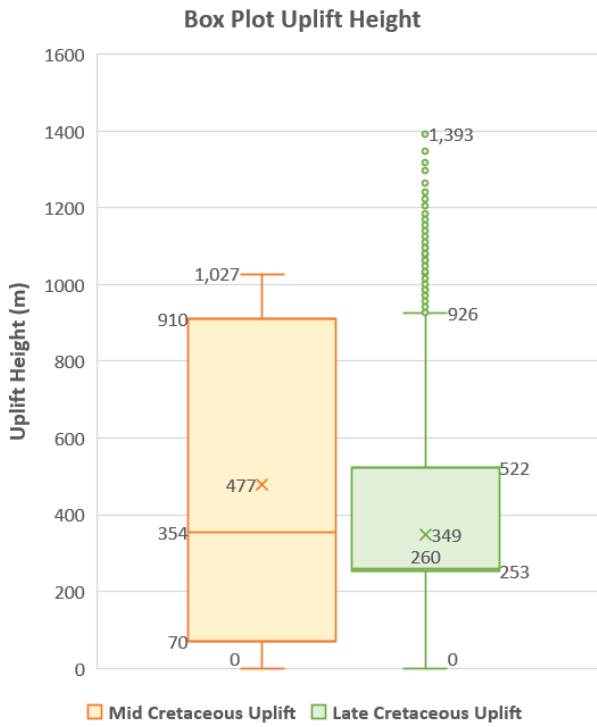
6.1.2 Mid-Cretaceous (Cenomanian-Santonian) Emperor Subgroup

Regional thermal uplift occurred in the western Gippsland and eastern Otway area from about 100-90 Ma (Duddy and Green, 1992) associated with basaltic intrusive (Older Volcanics). This major tectonic event in south-east Australia is associated with cessation of rifting at the eastern end of the Otway Basin, with the Strzelecki rift in Gippsland essentially aborted, prior to initiation of seafloor spreading between Australia and Antarctica. Rifting transferred into the eastern offshore part of the Gippsland Basin, which formed an arm off the newly initiated rift associated with breakup of Australia and Zealandia and Tasman Sea formation. This second Tasman Sea rift

event produced a short syn-rift phase characterised by extensional faulting, that was confined mostly to the offshore Gippsland Basin, which subsequently became a failed arm of the Tasman Sea rift (Smith, 1982).

The stratigraphic record in the Gippsland Basin records a significant unconformity between the Strzelecki and Latrobe Groups, with missing section of 1-3 km and more in some areas. This is a composite unconformity produced by uplift and erosion in the mid-Cretaceous, with further episodes in the early Campanian and continuing in places through the Cainozoic especially after the Eocene, as discussed below (Smith, 1982; O'Sullivan et al., 2000; Holdgate et al., 2015; Aghaei et al., 2017).

The Mid Cretaceous uplift was simulated by input of uplift maps for the 98-95 Ma time steps into *Badlands* that produced rapid re-emergence of the Strzelecki basin over the 100-90 Ma period. This uplift process affects multiple variables, such as the slope, drainage area and precipitation and these variables in turn impact the erosion process. A balance of sediment supply and the amount of Mid-Cretaceous uplift was found using sensitivity tests run in *Badlands* for uplift and deposition across the Gippsland Basin. In the Reference Case this required a Mid-Cretaceous uplift map, equally apportioned for each time step, that had a median uplift height of 354 m (mean of 477 m), with a maximum uplift height of 1027 m (Figure 6-5). Notably, the Strzelecki rift valley topography remained considerably below the original palaeo-topography because the continual erosion is able to remove large thicknesses of uplifted Strzelecki Group sediments in a dynamic process, without the Strzelecki Highlands needing to attain a great height at any time. The total uplift seen today is a function of the uplift over several episodes as indicated in Figure 6-5.



Element	Meaning
Top of upper whisker	Maximum value of the sample
Top of box	75th percentile of the sample
Line through the box	Median of the sample
Bottom of the box	25th percentile of the sample
Bottom of the lower whisker	Minimum of the sample
× markers	Mean of the sample

Figure 6-5 Box-plots for the Mid Cretaceous uplift map (mean 477m, median 354m, P75 910m, P25 70m, minimum 0m, maximum 1027m) and for the Late Cretaceous uplift map (mean 349m, median 260m, P75 522m, P25 253m, minimum 0m, maximum 926m)

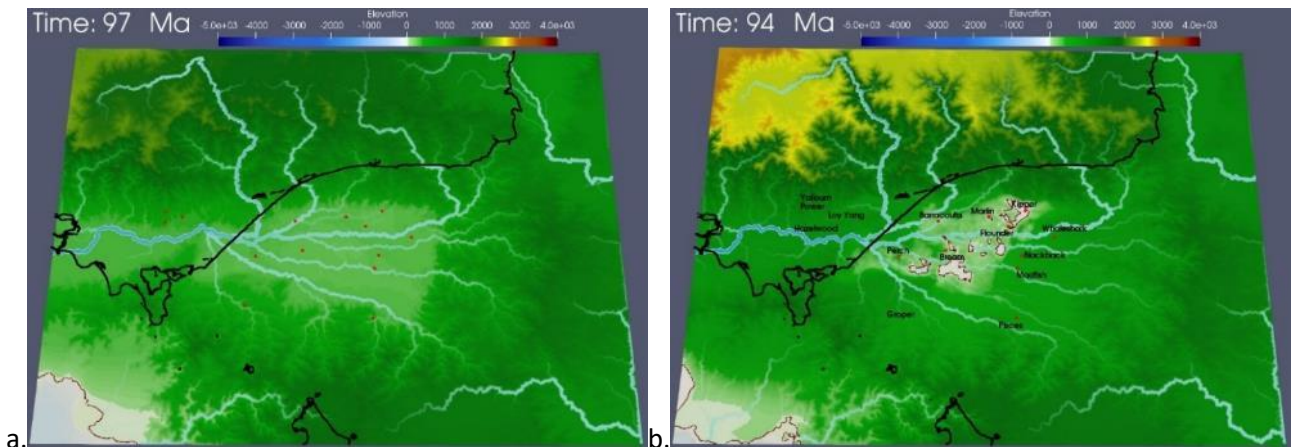


Figure 6-6 a. The inland sea closed by the Early Cenomanian, and the east-west fluvial system became dominant again in the entire Gippsland Basin; b. Multiple small lakes begin to occur in Central Deep area; the highlands arise in the north, due to the uplift. The brown line shows the zero contour. The black line is present coastline.

In the Early Cenomanian (97 Ma) the emerging landscape resulted in retreat of the inland sea, which was replaced by a large-scale east-west trending fluvial system again dominated by flood plain and braid plain deposition with widespread erosion of the uplands, and these landscapes persisted until the late Cenomanian (Figure 6-6a). Some small lakes started forming in Central Deep area which began to subside rapidly by the end of the Cenomanian around 94 Ma, while continued uplift of the highlands in the north which maintained the old east-west palaeo-drainage direction (Figure 6-6b).

In the Turonian the mild uplift to the north and west continued while substantial subsidence of the Central Deep region in offshore Gippsland accelerated with Tasman Sea rifting. Together this combination of hinterland uplift and rapid rift subsidence led to capture of the river systems in the east, which flipped the eastern fluvial drainage system from a westerly direction to an easterly direction presumably eroding most of the Cenomanian sediments. This explains the occurrence of a widespread unconformity between the Emperor and Golden Beach Subgroups which would not be expected mid-way within a rift phase (Figure 6-7a and Figure 2-1).

The *Badlands* simulations suggest thick fluvial and lacustrine palaeo-environments developed during the Turonian (94 Ma – 89 Ma) and this matches well with deposition of the Emperor Subgroup sediments (Bernecker and Partridge, 2001), notably the fluvial Admiral and Kersop formations and the lacustrine Kipper Shale, that accumulated in the Central Deep (Figure 2-1). The basin grade was finally reversed by the end of Turonian, resulting in transport of large amounts of clastic sediments from surrounding mountain areas via the fluvial systems, gradually filling up the inland lake systems, with the braid and flood plains moving out over the basin towards the east and south, continuing into the Coniacian. This is an unstable period where the simulations struggle to decide to which direction each river system should flow, given the uncertainty in the precise locations of the rift zones, and the separating highland branches to the east and south. Some simulations flip most of the stream palaeocurrent directions early from 97-94 Ma in the Cenomanian, whereas more likely simulations around the P50 flip most streams between 92-86 Ma in the Turonian, while others flip the streams later from 83-75 Ma, and poor fitting simulations do not flip all the streams until 74-73 Ma (Table 6-1). Similar time-variable sedimentary switching occurs in specific drainage sub-basins within the Red Sea rift systems (Rosendahl, 1987).

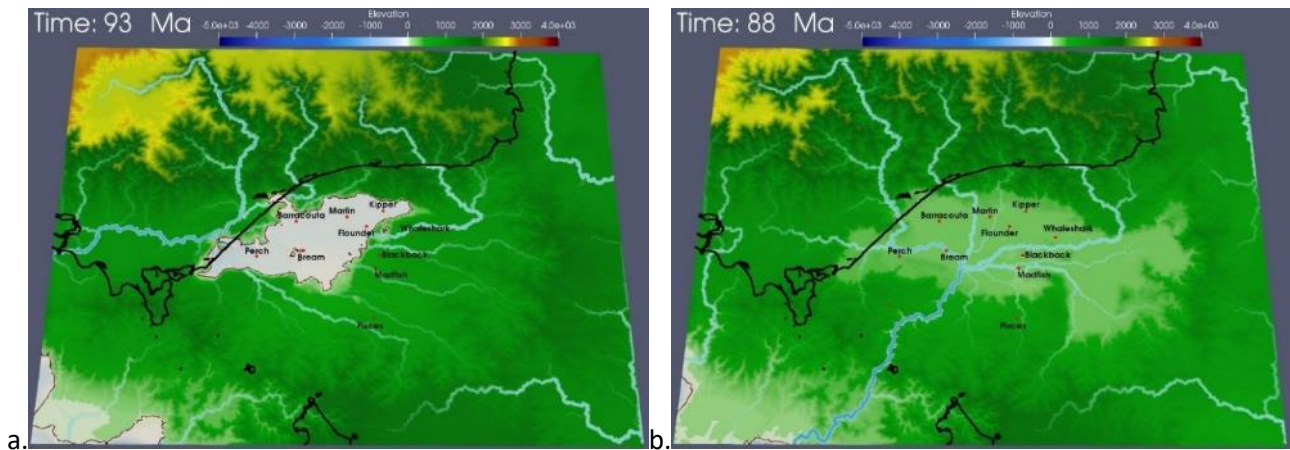


Figure 6-7 In Turonian time, lacustrine-fluvial dominated palaeo-environment appeared again in the Gippsland Basin. The result of the Mid Cretaceous uplift is the drainage direction starts to change. The brown line shows the zero contour. The black line is present coastline.

Table 6-1 Scenario outcomes according to time at which palaeocurrent flips from westward to eastward in the Gippsland Basin. The best fit models are highlighted in yellow, early flip models in blue, and poorly fitting models are shown in red.

RUN Number	Start time (Ma) for Palaeocurrent Flip
1, 6, 13	73
4, 7, 18	74
10	75
16	76
17	78
21	79
19	82
8	83
12, 14, 22	86
Ref	92
2	94
9, 20	95
5, 11	96
3, 15	97

6.1.2.1 Potential Emperor Subgroup Reservoirs

The Mid Cretaceous regional uplift combined with the palaeocurrent flip to easterly flowing systems opened the way for significant changes in sediment source and supply. More mature clastics poured into the basin transported from north, south-west and west with unroofing of both Palaeozoic and Strzelecki strata and granites in the south along the Flinders Island-Wilsons Promontory trend. The sediment supply of volcanic-clastics from the east shut-down with initiation of the Tasman Sea spreading and any intra-rift volcanics were overwhelmed by the amount of

more siliclastic sediment. This also partly explains the large amount of Strzelecki sediments eroded from the onshore and Latrobe Valley regions. Consequently, this change in palaeoslope marks the most significant change in the occurrence of good reservoir rocks which progressively become cleaner with time during the Later Cretaceous as the proportion of volcanic detritus diminishes.

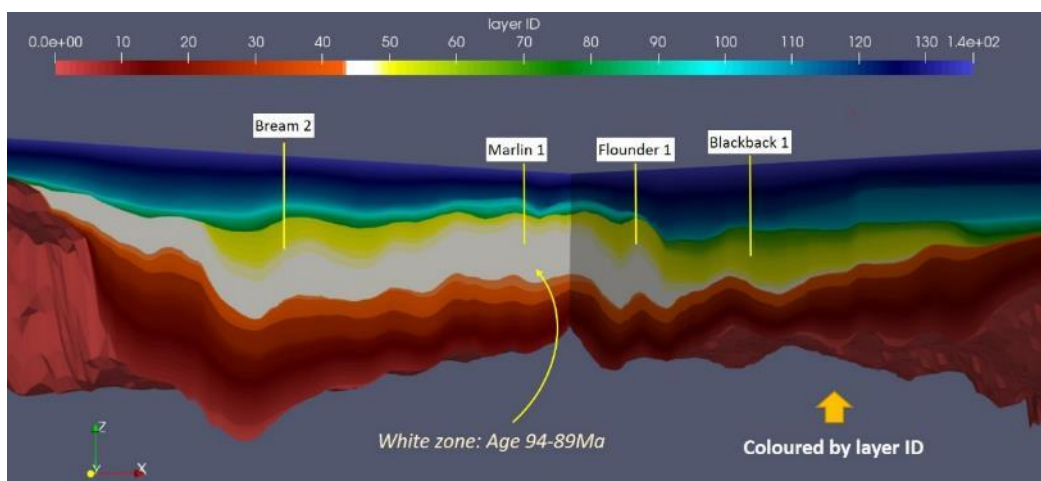
6.1.2.2 *Potential Emperor Subgroup Source Rocks*

The simulations show how around the Cenomanian-Turonian boundary and into the Coniacian (e.g., 97~86 Ma) a fluvio-lacustrine dominated paleo-environment developed in the offshore Central Deep area within the Emperor Subgroup (Figure 2-1), with initiation of many intra-cratonic lakes that at times probably coalesced into an extensive shallow inland seaway. This area of pervasive lacustrine to shallow inland seaway lies beneath all of the major petroleum fields, including the giant Kingfish, Halibut, Fortescue, Flounder, Bream, Barracouta, Marlin, Snapper, Kipper, Tuna and Perch (Figure 6-6 and Figure 6-7). The simulations indicate these pervasive lacustrine to shallow sea facies were reasonably persistent and stabilised over a period of about 4-7 million years, long enough to deposit thick non-marine organic rich black shales and sapropelic coals, as shown on cross-sections through the simulations (Figure 6-8). These mainly Turonian shales deposited in these restricted depositional and intra-rift tectonic settings are highly likely to have had poor circulation, possible density stratification, be hyper-saline in places with bottom anoxia and local euxinic conditions. These settings are ideal for accumulation and preservation of liptinites including alginite and bituminite and could be the additional missing source rock for Gippsland oils postulated by Murray et al. (2021). Remarkably, this period is coincident with the Cenomanian-Turonian Ocean Anoxic Event (OAE) seen elsewhere in many basins that is one of the world's largest global carbon cycle perturbations (Jarvis et al., 2011).

The rock-eval analysis, organic petrology and the palynology for the Emperor Subgroup suggest an organic rich non-marine to marine environment. In Shark-1 HI values are over 600 mgHC/gTOC in a probable stratified lacustrine environment. The organic petrology for the side-wall-core (swc) samples reports common *Botryococcus* spp. related telalginite in cannel coals, which indicates a largely fresh water or brackish lacustrine environment. They noted a low reflectance groundmass of bituminite or perhydrous detrovitrinite, which together with the algae should form an excellent

source rock. This is supported by the palynological studies that found bright yellow fluorescence from bitumen/oil drops from slightly deeper swc samples in glauconitic siltstones.

Hence, the *Badlands* palaeo-environment reconstructions for parts of the Emperor Subgroup match with the geochemical records and imply potential for good source rocks. The simulations indicate that the palaeo-environment involved recurring shifts between floodplain lakes, coastal swamps and marshes and shallow inland seas, as shown in Figure 6-9. These fluvial-deltaic-coastal coaly environments that develop at the edge of shallow inland seas, commonly include complex, low energy distributary channel systems with associated peats, feeding into anoxic interdistributary bays and lagoons behind extensive barrier sands, which are ideal for accumulation of very good source rocks. In contrast, the sediments deposited in the deeper water further from the shore were probably more aerobic in the central parts of the inland sea. These environments commonly have lower source rock potential, which matches with the low-medium rock-eval results in the thicker shale sections. The best potential source rocks are probably developed in the shales and associated channel coals in the marginal marine intervals.



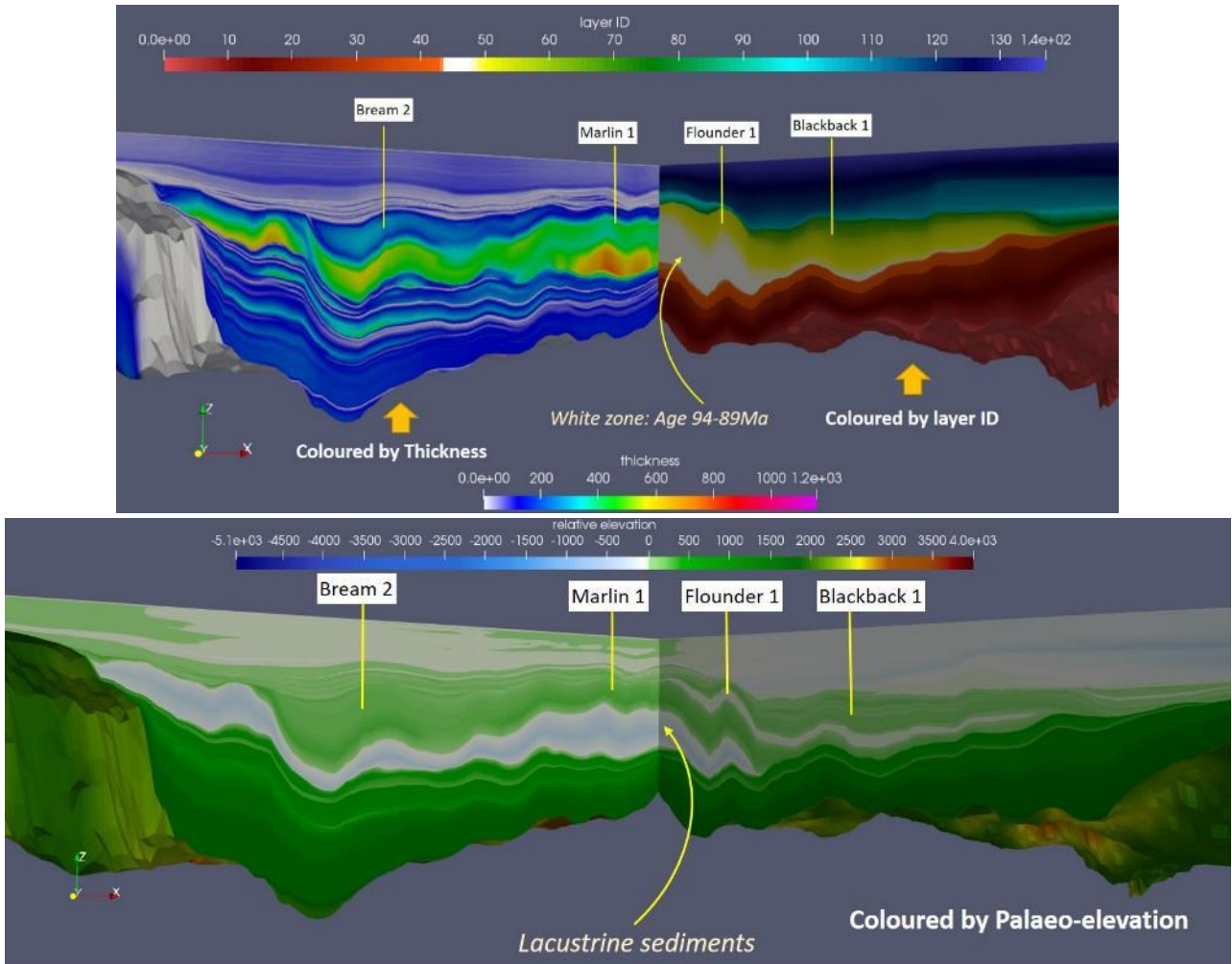


Figure 6-8 Cross-sections through Reference Case simulation with vertical exaggeration $Z = 1:4$. Composite section SW-NE Bream-2 to Marlin-1, then NW-SE Flounder-1 to Blackback-1. Upper cross-section coloured by 1Ma layers (white zone highlights 94 - 89 Ma). Middle section coloured by thickness to indicate sediment deposition per time step. Lower cross-section is coloured by palaeo-elevation to demonstrate the relative water depth and facies in each tectonic phase.

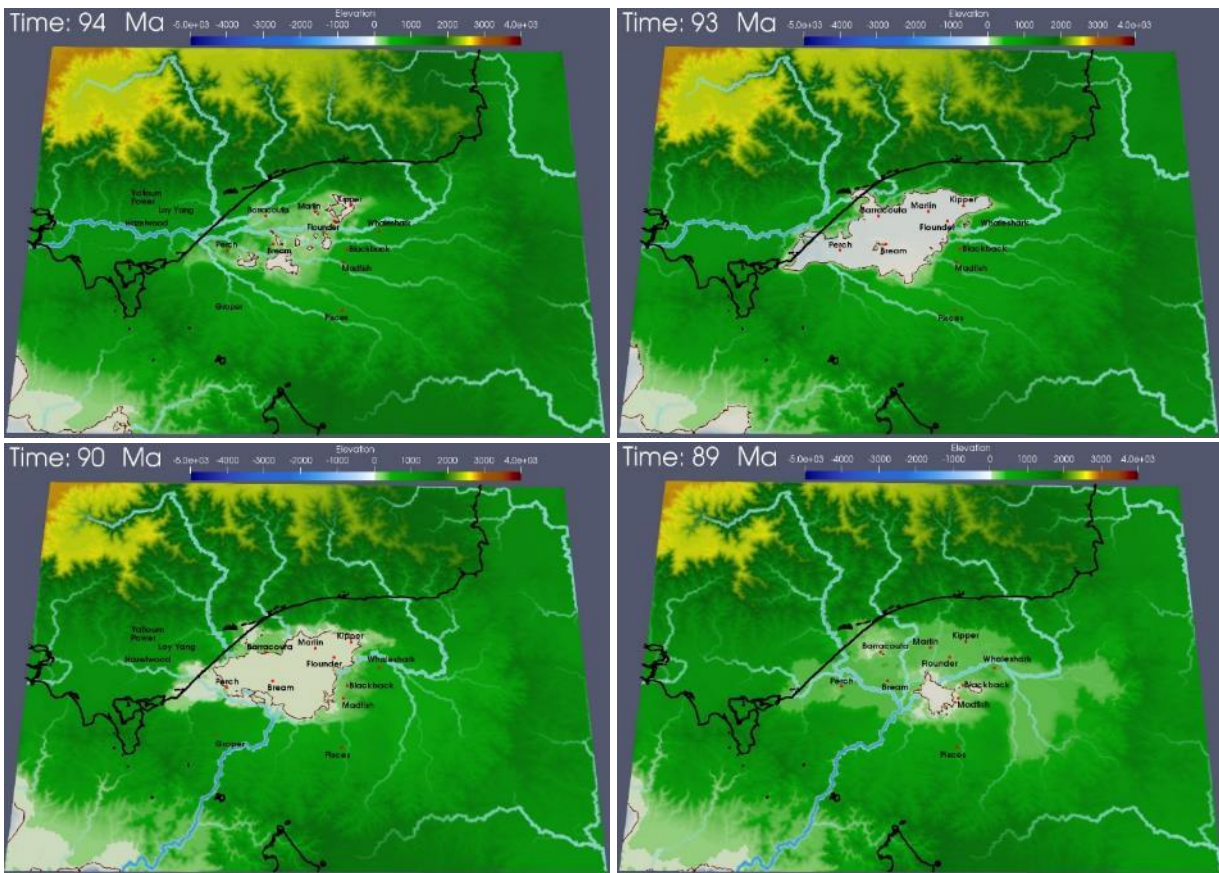


Figure 6-9 Badlands simulated palaeo-landscape result of the best fit model, extract at 94, 93, 90 and 89Ma.

6.1.3 Late Cretaceous (Santonian to Early Campanian) Golden Beach Subgroup

The Golden Beach Subgroup is recorded in the offshore Central Deep area from Santonian to Campanian (*T.apoxyexinus* – lower *T.lillie*). The corresponding simulations between about 86–79 Ma (Figure 6-10) show more subdued subsidence and a gradual eastwards progression over the Central Deep from deposition of fluvio-lacustrine sediments in the west to fluvio-deltaic sediments (Chimaera Formation) passing into restricted shallow marine sediments further east (Anemone Formation). This corresponds to the change between pre-breakup to more open sea conditions with initiation of break-up further to the south-east with flooding of the rifts. Palynological and core analysis from Madfish 1 and Anemone-1 confirm the Golden Beach Subgroup contains shallow marine shales and shoreline sandstones within the *N.senectus* and *T.lillie* biozones (Figure 2-1). This is consistent with localised ocean floor spreading starting in the south Tasman Sea about magnetic zone C34 by the early Santonian (Gaina et al., 1998; Norvick, 2005).

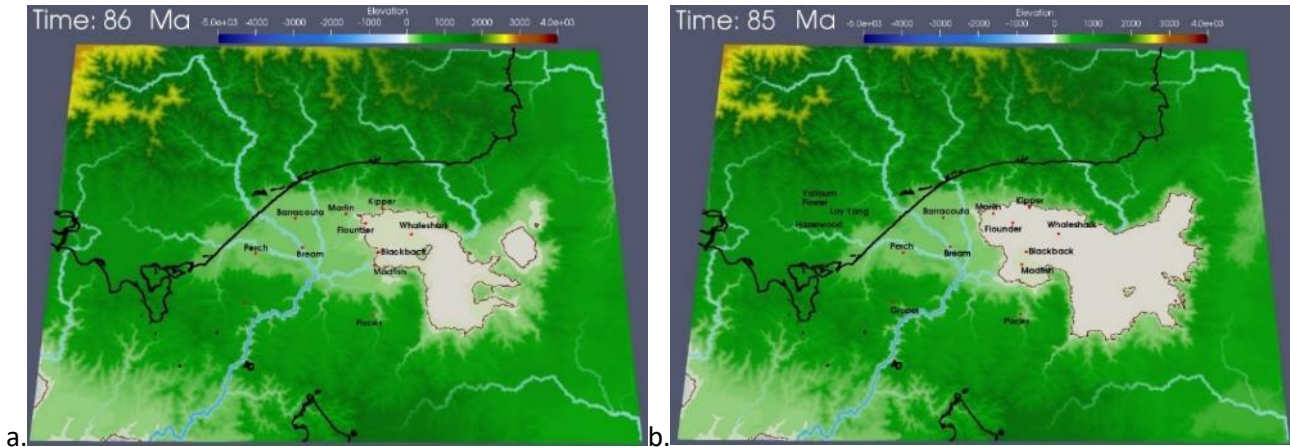


Figure 6-10 Palaeo-landscape at 86Ma and 85Ma. a. Pre-breakup time, most of the Gippsland Basin is terrestrial, an inland lake appears first, the sedimentary transport direction changes from west to east. b. Tasman Sea opening, a restricted shallow marine environment develops in offshore Gippsland Basin. The brown line shows the zero contour. The black line is present coastline.

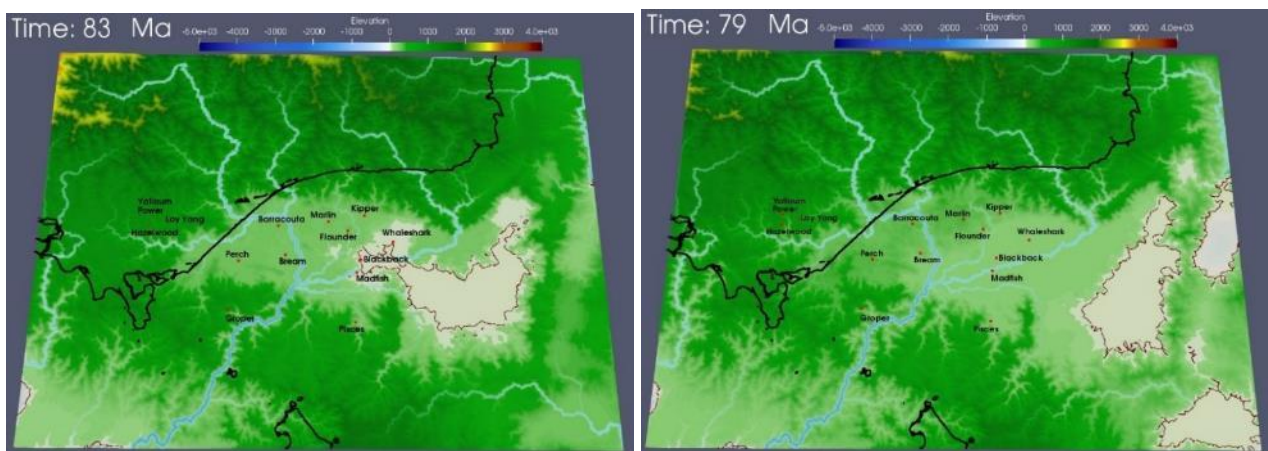


Figure 6-11 The simulations around 83–79 Ma show deposition of fluvio-deltaic sediments in the Central Deep passing into restricted shallow marine sediments (Anemone Formation). The brown line shows the zero contour. The black line is present coastline.

Initiation of active spreading in the southern part of the Tasman Sea around 85Ma started a second period of moderate isostatic uplift along the margins of south-eastern Australia, including on the Gippsland Basin margins, which continued through the Late Cretaceous and this fixed the palaeo-drainage direction from west to east. The most likely *Badlands* simulations were able to match the stratigraphic record of basin deposition via continued erosion from about 84-65 Ma removing most of the prior sedimentation throughout onshore Gippsland, including in the Latrobe Valley, and over the north and south platform offshore areas. The simulations indicated that the median height of this second period of uplift was 260 m (Figure 6-5) and this has the added effect of moderating the syn-rift subsidence during deposition of the Golden Beach Subgroup.

6.1.3.1 Potential Coniacian-Santonian Reservoir and Source Rocks

The deposition of fluvio – deltaic facies around the margins of the Central Deep in the Chimaera Formation includes coarse clastics that continued to be derived from the Palaeozoic and granitic

terraces around the basin margins and are known to include potential reservoir sandstones (Bernecker and Partridge, 2001). Clean marine sandstones also developed for the first time around the inland sea shorelines (e.g., at Anenome-1). The simulations indicate further development of low energy peatlands, lacustrine, lagoonal and newly developed restricted marine facies that provide good potential source rocks. The location of these various facies extended from the Marlin area, through the Blackback field and beyond to the eastern end of the present day Bass Canyon.

6.1.4 Middle Campanian to Palaeocene Spreading

Oceanic spreading had moved north in the Tasman Sea adjacent to Gippsland by around 80 Ma (Middle Campanian) and this is associated with development of minor unconformities in the Central Deep and extrusion of basalts (Kipper Volcanics). The extensional growth faulting diminished along with subsidence rates in this phase (Power et al., 2001). The *Badlands* simulations from 79–75 Ma show the initial marine sediments in the east were succeeded by a regressive phase, leading to deposition of a widespread flat floodplain, with fluvial and deltaic sediments over much of the basin (Figure 6-12).

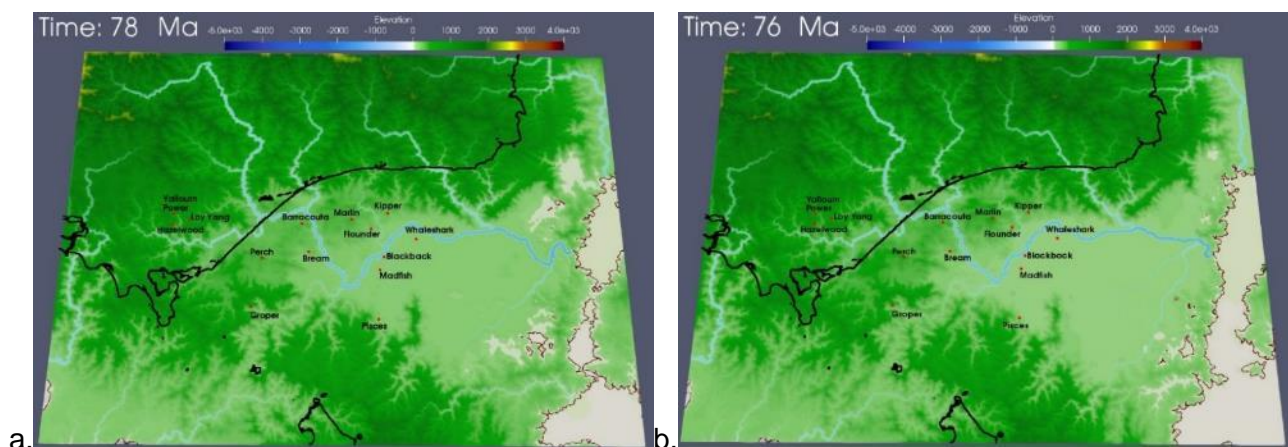


Figure 6-12 *Badlands* model simulations in the Middle Campanian (*T.lilliei*).

The marine sediments had been pushed further to the east where an open marine strandline was in place by at least 74 Ma. The overlying sediments between 74–65 Ma record aggradational coastal plain facies developed behind barrier systems but with episodic transgressive phases in the Maastrichtian. The general trends illustrated by the simulations match the depositional history as seen from wells in the east of the Central Deep. The oldest palynological data from the deepest part of the well section in Blackback 1, for example, is Lower *T.longus* (75.5 – 67 Ma). The section generally lacks coals and contains rare Maastrichtian dinoflagellates which together suggest at

least marginal marine conditions. The overlying section records coastal plain coals, shales and sandstone units that regressed from the west out to the east. This section in turn is overlain by transgressive marginal marine sediments containing glauconite and dinoflagellates including the diagnostic *Manumiella druggii* indicating a second marine incursion. In the more distal Whaleshark 1, a thick marine Maastrichtian (Upper *F. longus* ~65 Ma) section extends to the total depth of the well and is characterised by the absence of coal seams and the presence of dinoflagellates.

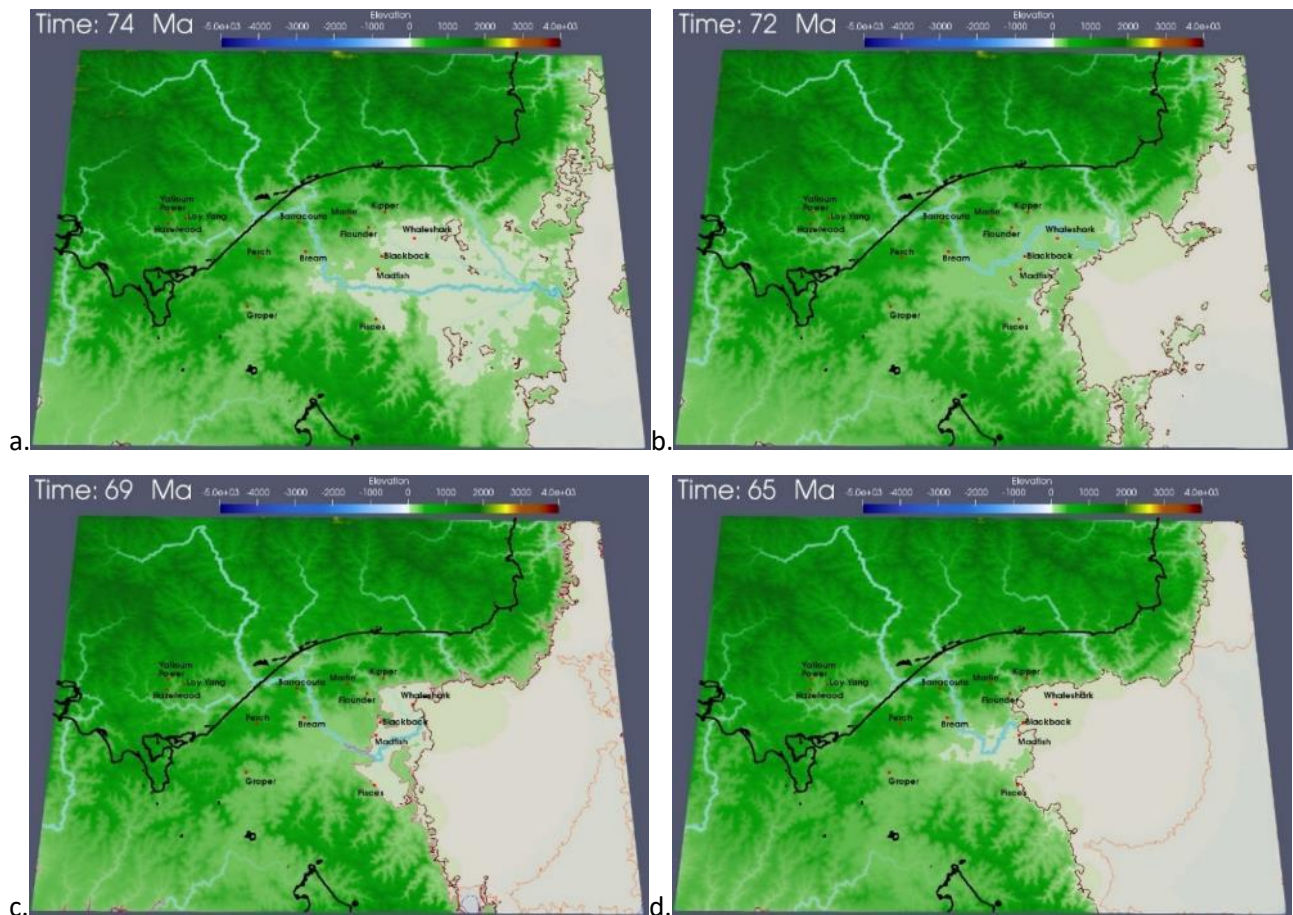


Figure 6-13 Badlands model simulations in the Maastrichtian. Initial regression produced a widespread flat floodplain with an open marine strandline in place by at least 74Ma (a), followed by marine transgressions towards the West around 72Ma (b); continuing through 69Ma where Blackback and Madfish lie on the coastal plain with less than 30m elevation (c); to 65Ma where Blackback, Madfish and Whaleshark are inundated by shallow marine sediments (d). The pink, brown, orange and blue lines represent contours at 50m, 0, -50m, -100m. The black line is present coastline.

In the Palaeocene (*L. balmei* palynozone) the basin saw continued marine incursions with at least three cycles. The initial cycle saw widespread deposition of the Kate Shale, after which the system stayed more stable with fluvio-lacustrine and deltaic – coastal barrier systems mostly aggrading with minor retrogradation. However, the fluvio-lacustrine facies extended much further west onshore over the Palaeozoic and Early Cretaceous basements (compare the current onshore and inshore areas at 65 Ma and 54 Ma) and the first submarine canyons began to cut into the developing shelf-slope during low stands. North-south spreading began at the South Tasman Rise

by the end of the Palaeocene starting to put Gippsland under compression as shown by the *GPlates* reconstructions (Smith, 1982; Brown et al., 2003).

6.1.5 Eocene Transition Phase

The Eocene is a major period of change in the Gippsland Basin resulting from several interrelated factors. Tasman Sea spreading ended in the Early Eocene (Gaina et al., 1998) around upper *M. diversus* to *P. asperopolus* time as shown by the *GPlates* reconstructions (Figure 4-3). Structurally this phase marks the start of the main phase of post drift thermal subsidence over the entire basin, the end of widespread normal growth faulting, and the transition to a compressional regime with NNW spreading at the South Tasman Rise and convergence of the Australian and Pacific plates through Zealandia (see Chapter 4). This resulted in the development of low relief broad anticlines over the older faults that were slowly inverted. Depositionally this phase marks the end of regional Latrobe Group progradation and the start of a major episode of retrogradation of the shoreface across the offshore Gippsland Basin. The retrogradation of the non-marine sediments initially led to starvation of the marine environments, with development of incised valleys and submarine channels into the Latrobe Group sediments during short lowstands, with widespread erosion and development of unconformity surfaces exacerbated by uplift and tilting from the folding (in part equivalent to the “Marlin Unconformity” of Bernecker and Partridge, 2001).

In contrast to the Palaeocene, the simulations in the Eocene after about 55 Ma show more frequent and shorter transgressive-regressive cycles as the overall retrogradation of the shorelines progresses. The transgression was discussed in Chapter 5 where it was shown this resulted from a change in the balance between:

- sediment supply, which slowed with decreased uplift, precipitation and consequently erosion
- slower subsidence with the cessation of spreading, and
- an overall high and rising sea level with long rises and short falls that accompanied this period of major climate change from warm-wet to cold-drier climates.

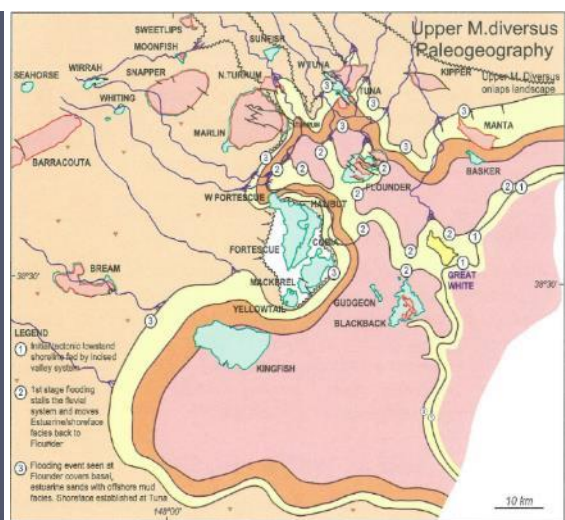
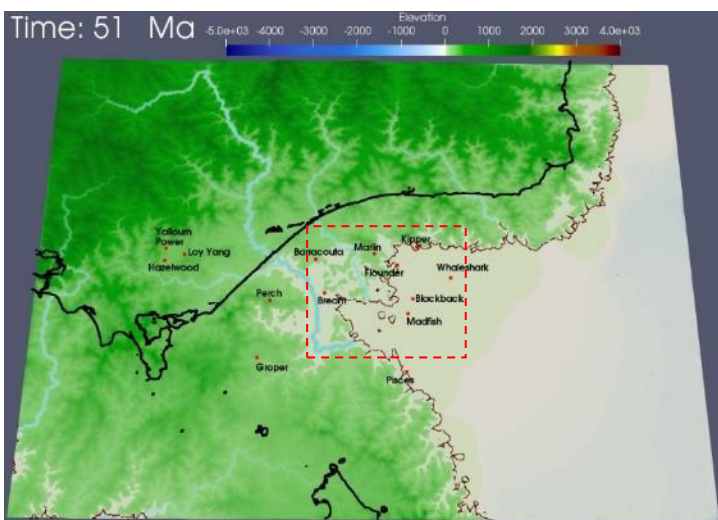
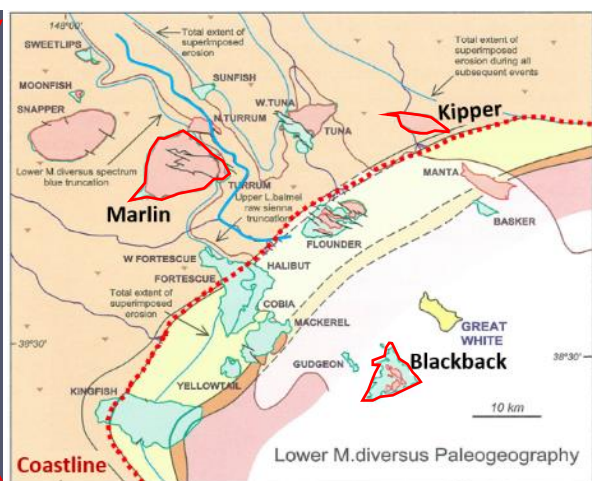
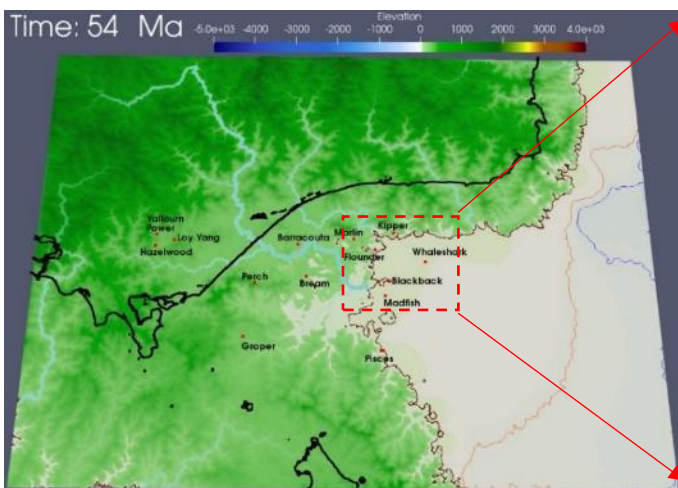
The simulations show how these effects resulted in the fluvio-deltaic sediments being pushed back by the transgressive marine sediments during the Eocene to early Oligocene, in a series of

retrogradational steps across the entire width of the offshore basin (compare simulation maps at 54Ma and 33Ma in Figure 6-14 and Figure 6-16). Onshore channel belt river systems formed valleys that were incised especially during low stands and these fed into the shelf. These valleys were drowned during subsequent transgressions, and develop into submarine canyon systems as the transgressions push back the non-marine facies more and more with time, and as a shelf-slope develops causing sediment starvation further east on the shelf and in deeper water. The combination of transgression with compression, the latter causing inversion of the faults and development of low relief anticlines, together resulted in development of a composite unconformity above sub-cropping Latrobe Group sediments.

Several authors have documented details of this phase in the development of the offshore Gippsland Basin including debate over whether the “channelling” was subaerial or submarine (e.g., Brown, 1986; Smith, 1988; Partridge, 1999; Johnstone et al., 2001; Holdgate and Gallagher, 2003; Norvick, 2005). The *Badlands* simulations provide the opportunity to show how this actually works. The results over the Eocene closely match the tectono-stratigraphic style and evolution outlined by Johnstone et al. (2001). At 1 Ma time steps they reproduce the main features of the regression-transgressions including the river channel belt and valley systems, the coastal shoreline barrier systems and the submarine canyon development that allow an understanding of how these changes evolved. However, a range of good-fit models should be inspected, and we should not expect them to be precise to 1Ma, or to have the resolution to reproduce all the detail at time scales less than 1 Ma, for example to 0.5 Ma (Figure 6-14).

Around 54Ma, the simulations produce large river systems that feed into an offshore area far to the east of the present coastline (Figure 6-14). The basin is dominated by fluvial floodplains and coastal-delta plain deposition, with several major river channel belt systems producing incised valleys during the Lower *M. diversus* time, notably the one between the Marlin and Tuna fields (Figure 6-14). The coastline is moderately straight NE-SW suggesting coastal wave-dominated barrier systems. This coastline migrates from east to west over the Kipper and Flounder fields during Upper *M. diversus* time, while similarly transgression occurred over Kingfish with the shoreface moving closer to the Bream field. The river channel belts appear structurally controlled by the inversions, especially of the Kingfish, Halibut-Mackerel and Marlin areas, and together with

the transgressions this results in an irregular embayed coastline, which closely matches the palaeo-facies maps of Johnstone et al. (2001) (Figure 6-14). The marine transgression drowns the coastal areas and erodes the channel valleys, which are back-filled by shallow marine and shelf sediments to initiate the Tuna-Flounder submarine canyon system, and deposit the shallow marine mudstones and glauconitic sandstones of the Flounder Formation and equivalents. This is analogous to the river valley cut and fill by transgressive systems that has occurred in recent times in Sydney Harbour (Birch & Lound, 2021) and Port Phillip Bay (Holdgate et al., 2001).



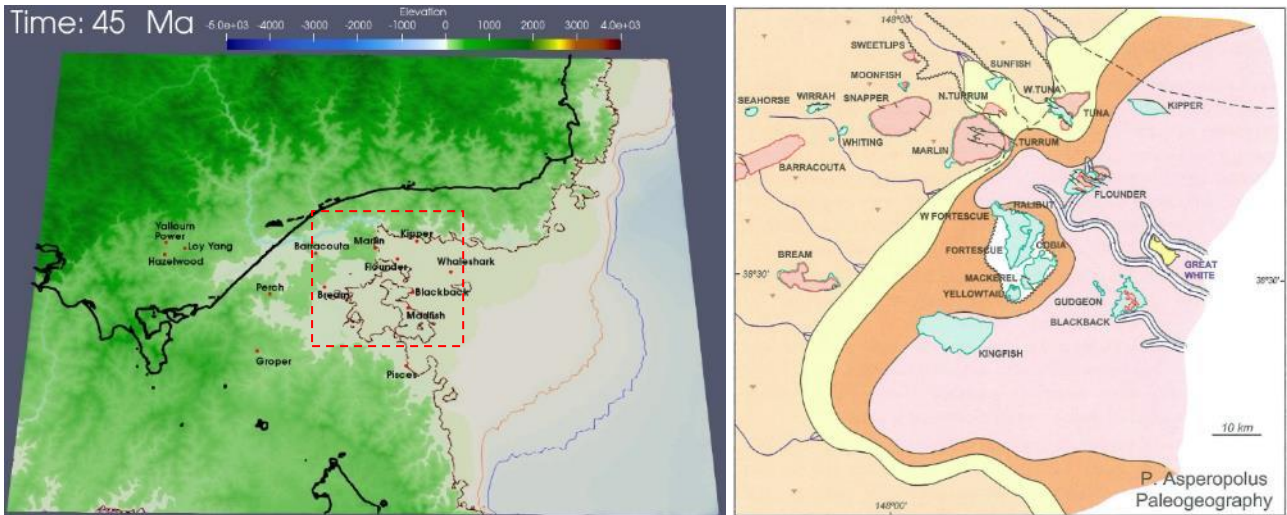


Figure 6-14 The 54, 51 and 45 Ma topographic simulations fit well with Johnstone et al. (2001) tectonostratigraphic development study of Eocene age. The brown, orange and blue lines represent contours at 0, -50m, -100m separately. The black line is present coastline.

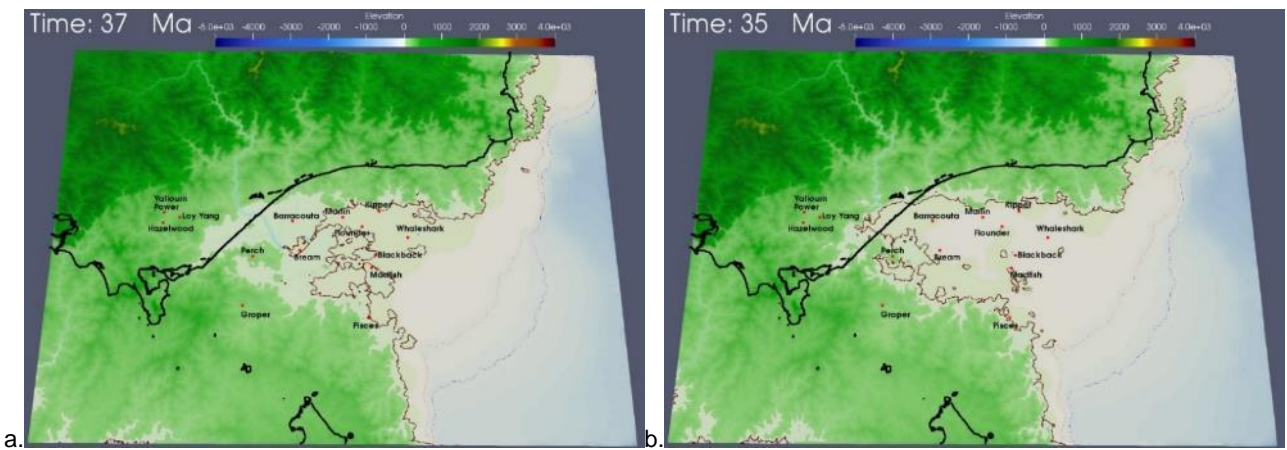


Figure 6-15 Badlands simulation at 37 and 35Ma, showing the marine incursion extent. The brown, orange and blue lines represent contours at 0, -50m, -100m separately. The black line is present coastline.

Several cycles occurred over *P. asperopolus* and *N. asperus* time (e.g., see 45 Ma simulation) each of about 3-5 Ma duration, comprising downward shifts depositing regressive fluvio-deltaic deposits, followed by marine transgressions depositing coastal-shallow marine sediments. These cycles shifted the coastline back and forth in the order of 20km or more. This resulted in the development of widespread Top Latrobe composite unconformities, with shallow marine glauconitic sediments deposited widely offshore (Gurnard Formation) and more focused cut of the incised valleys and transgressive fill of the canyons (e.g., the Marlin canyon system) by mudstones and glauconitic sandstones recorded as the Turrum Formation and equivalents (e.g., in Blackback 1) (refer Figure 2-2). The marginal marine incursions had transgressed far into the onshore area by the late Eocene occurring as interseam deposits within the Traralgon Formation (*N. asperus* time, see ~38Ma map, Figure 6-15 and Holdgate et al., 2021).

6.1.6 Oligocene to Recent Post Rift

The Eocene marine transgressions continued into the Oligocene and Miocene with coastal barrier systems moving into the Seaspray Depression and marginal marine coastal facies developed further inland (during *P. tuberculatus* time). East of the shorelines a thick cold-carbonate shelf developed further offshore, after the onset of southern ocean circulation that started around 36Ma in the late Eocene (Scher et al., 2015) and became fully open in the early Oligocene by 30 Ma (Bialas et al., 2019). A period of continuous marine sedimentation ensued driven by thermal subsidence with increasing margin collapse probably accentuated by flexural loading with build-up and loading of the shelf (see Chapter 8). Compression continued to produce reverse faulting and folding and apparent episodic uplift in different parts of the basin, with the Tasman Sea floor now rigid and rapid N-S spreading at the South Tasman Rise, and strike-slip starting within Zealandia along the proto-Alpine fault and development of the associated subduction of the Australian-Pacific plate to the south-west (Bache et al., 2014; Sutherland et al., 2020). Several cycles of marine incursion and regression occurred during the Oligocene to Recent that have been simulated as described below. Detailed descriptions of the stratigraphy have been documented in Partridge (1999), Holgate and Gallagher (2003) and Holdgate et al. (2021), while the structural history is given in Mahon and Wallace (2020).

The *Badlands* simulations have been able to capture the main features of this complicated geological history. However, as for the Eocene, modelling all the fine detail would require smaller time steps than 1Ma to capture all the rapid shoreline changes, submarine channelling and shelf progradation. The palaeo-topography of the near Top Latrobe simulation at about 33Ma indicates a shoreline that had transgressed into the Seaspray Depression with marginal marine sediments further inland and an offshore marine carbonate shelf to the east (Figure 6-16a). The simulations show rapid transgressive-regressive cycles about every 1-2 Ma as shown by comparison of the simulation maps at 33 and 31 Ma, which depending on the time scale used, is very close to the marginal marine incursions mapped onshore by Holdgate et al. (2021). The coastal plain is very flat and the *Badlands* simulations indicate small changes in any parameter (e.g., hinterland uplift, sediment supply, subsidence, sea level etc) causes large shoreline movements. This is similar to actual mapped incursions which show movement of the marginal marine facies and shorelines

over 20 km in less than 1-2 Ma. The barrier systems stabilised further to the west near the Sale area by the Miocene as shown by the simulation at 26 Ma (Figure 6-17).

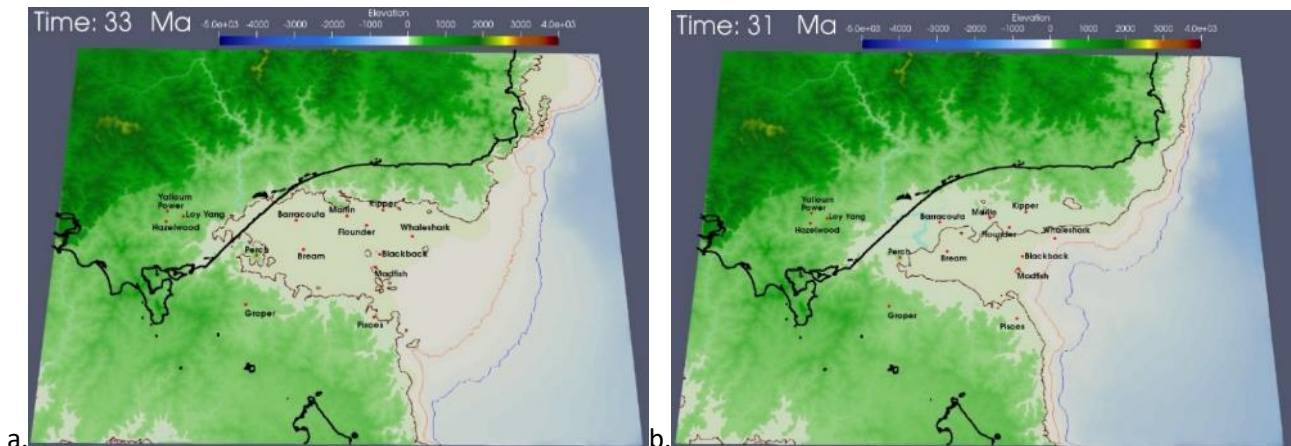


Figure 6-16 Palaeo-topography near top Latrobe Group at 33 Ma. a. at 33Ma, the fluvial-deltaic sediments were transgressed into the Seaspray Depression; b. at 31Ma, a shoreline regression is modelled. The brown, orange and blue lines represent contours at 0, -50m, -100m separately. The black line is present coastline.

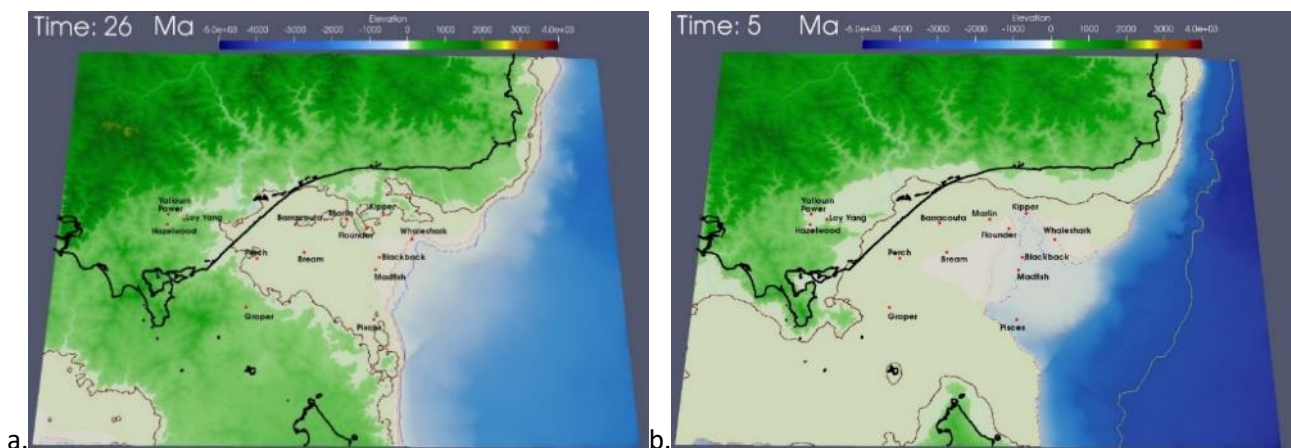


Figure 6-17 Palaeo-landscapes at 26Ma and 5Ma when the main regression occurred.

The phase of cold water carbonate deposition from the Oligocene onwards was simulated using the *Badlands* carbonate module to add a carbonate rain to the clastic dispersion from the land. This added complication improved the simulation fits of the Gippsland Limestone sedimentation to the realistic model and produced reasonably close matches in the Oligocene to Recent period. After 137 Ma of simulations the present-day coastline is a good fit to the 1 Ma simulation (Figure 6-18). However, the present day modelled transgression has moved too far west back into the Seaspray Depression, with a very shallow marginal marine incursion shown in the final step in the reference model - though perhaps it is just getting ahead of where it will end sometime in the next 500 thousand years? The submarine canyon module in *Badlands* has been used to produce a submarine canyon system, which models the detailed cut and backfill with rising sea level, though

their location is not precise in these coarse time steps (Figure 6-19). The simulations reproduce the Bass canyon though its current location is not simulated precisely in the reference simulation. Some of the other scenario models provide better final fits and more accurate simulation of these details could be obtained by finer time steps than 1 Ma.

A cross-section through the reference case scenario model is shown in Figure 6-20. The main six depth maps from *Badlands* are shown for one of the best fit models to compare with the actual *Petrel* structural model. The *Badlands* model is a good fit with the palaeo-environments, the amount of sediment deposition over the 137 Ma period, and the relief of various depositional elements including the canyon systems.

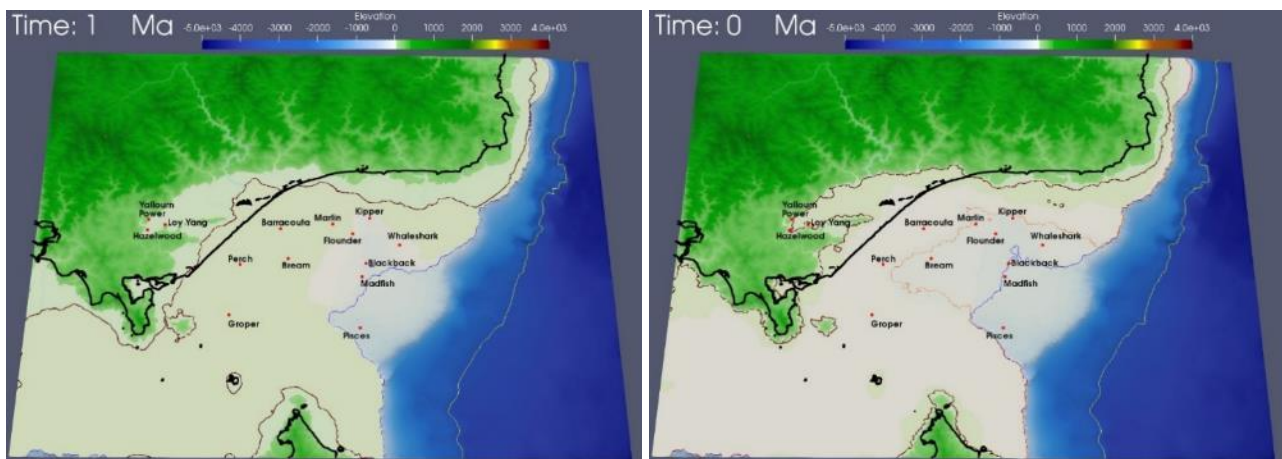


Figure 6-18 Present Day simulated topography and bathymetry after 137 Myers of simulation. The brown, orange, blue and yellow lines represent contours at 0, -50m, -100m and -3500m separately. The black line is present coastline.

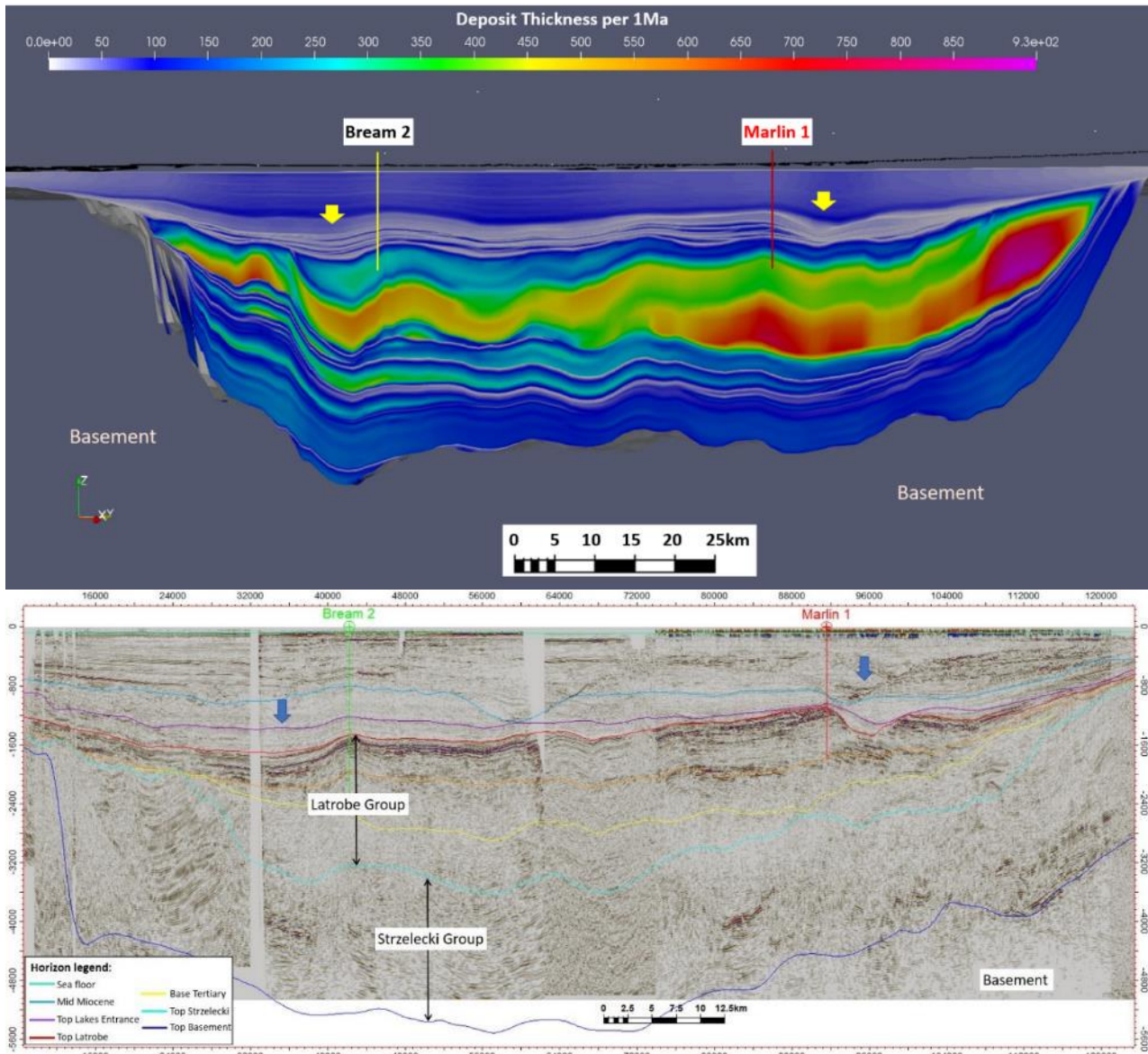


Figure 6-19 NE-SW cross-section through Marlin-1 and Bream-2. a. cross-section through Badlands model, coloured by sediments thickness per 1Ma time steps, at 1:4 ratio; b. two-way time 3D seismic data at 1:5 ratio.

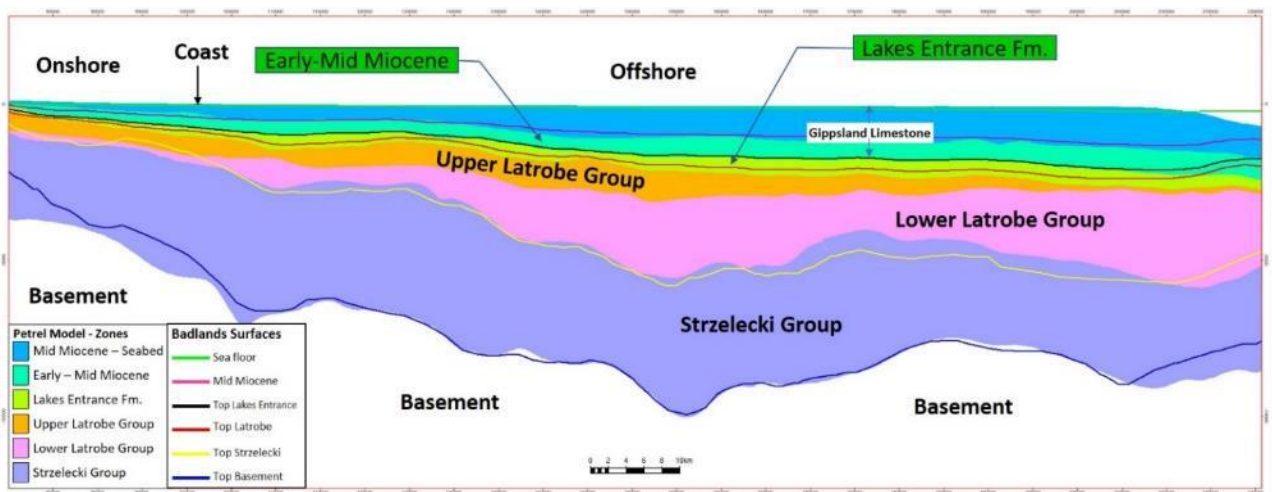


Figure 6-20 Depth maps from Badlands best fit model compared with Petrel structural model.

6.2 Summary Conclusions from the *Badlands* Simulation Models

The realistic 3D *Petrel* model and statistical experimental design constrained and guided the *Badlands* theoretical modelling process to reconstruct a better understanding of the rift and post-rift basin evolution for the Gippsland Basin. The *Badlands* simulations of the palaeo-landscape and geological history have been able to capture the main features of this complicated geological history for the first time and predict additional reservoirs and source rocks at depths below most wells. A summary is recapped below:

6.2.1 Tectono-Sedimentary Evolution

- Early Cretaceous: the Gippsland Basin formed as an intracratonic rift basin, initially with non-marine deposition in a narrow east to west drainage basin, developed between steep highlands that gradually erode producing a lower relief and wider basin. A system of shallow lakes developed into a shallow inland sea at the western edge of the basin that was probably connected with the Otway Basin. Fluvio-deltaic sediments build into this shallow inland sea during Albian-Cenomanian time with continued rifting, and the sea expands from west to east into western Gippsland.
- Mid-Cretaceous: The region was rejuvenated by widespread uplift and the simulations show that continuous erosion is able to remove large thicknesses of Strzelecki Group sediments as uplift occurs in a dynamic process without the Strzelecki highlands needing to attain a great height at any time. In the Turonian, hinterland uplift in the west with rapid rift subsidence towards the east accelerated by Tasman Sea rifting led to the capture of the river systems in the west, which flipped the fluvial drainage system in the east from a westerly direction to an easterly direction. A large amount of clastic sediments were transported via the fluvial systems, filling up the inland lake systems by the end of Turonian.
- Late Cretaceous: The simulations show more subdued subsidence and a gradual eastwards progression over the Central Deep, from deposition of fluvio-lacustrine sediments in the west, to fluvio-deltaic sediments that pass into restricted shallow marine sediments further east. The simulations from 79-75 Ma show the initial marine sediments in the east were succeeded by a regressive phase, leading to deposition of a widespread flat floodplain, with fluvial and deltaic sediments over much of the basin. The overlying

sediments between 74~65 Ma record aggradational coastal plain facies with episodic transgressive phases.

- Palaeocene to Eocene: In the Palaeocene, the basin saw continued marine incursions with at least three cycles. The simulations in the Eocene show more frequent and shorter transgressive-regressive cycles and resulted in the fluvio-deltaic sediments being pushed back by early Oligocene into the current onshore area.
- Oligocene to Recent: The phase of cold water carbonate deposition from the Oligocene onwards added a carbonate rain to the clastic dispersion from the land. The shelf subsided rapidly with episodic canyon cut and fill in part structurally controlled by anticlines that developed after the onset of regional compression. The present-day coastline is a good fit to the 1 Ma simulation.

6.2.2 Potential Reservoirs and Source Rocks in the Cretaceous:

- Early Cretaceous Strzelecki Group: the rivers from northern and southern highlands transported coarse Palaeozoic clastics that were eroded from the basement into both the Tyers River and Korumburra sub-groups to form good potential reservoirs. These are much better than the younger volcanic-clastic sediments brought mainly from the east and deposited in the Korumburra Subgroup that are typically discussed in the literature. Similarly, good potential source rocks occur associated with the extensive lakes and shallow seas.
- Mid-Cretaceous Emperor Reservoirs: More mature clastics poured into the basin from north, south-west and west with unroofing of both Palaeozoic and Strzelecki strata and from granites to the south along the Flinders Island-Wilsons Promontory trend. The sediment supply of volcanic-clastics from the east shut-down with initiation of the Tasman Sea spreading and any intra-rift volcanics were overwhelmed by the amount of siliclastic sediment.
- Mid-Cretaceous Emperor Source rocks: An area of pervasive lakes and shallow inland seas lie beneath the major petroleum fields, that persisted over a period of about 4-7 million years, in which thick organic rich black shales and sapropelic coals were deposited in marginal marine environments.

- Late Cretaceous Golden Beach Source and Reservoir Rocks: The simulations indicate further development of low energy peatlands, lacustrine, lagoonal and newly developed restricted marine facies that provide good potential source rocks. The location of these various facies extended from the Marlin area, through the Blackback field and beyond to the eastern end of the present day Bass Canyon.

Good reservoir sandstones continued to be deposited and generally become cleaner up section. This includes marginal marine barrier and beach sandstones associated with an open marine barrier system that was established for the first time.

Chapter 7. Realistic Property Modelling

The Property models are built in the 3D structural and stratigraphic *Petrel* model as detailed in Chapter 4. The property models interpolate various properties in each well, from logs or sample analyses, throughout the 3D grids provided by the structural and stratigraphic models. They can also be guided between wells using seismic data. The primary property model is the facies model which can be used to control the distribution of the other properties according to lithofacies. This ensures that the other properties are distributed according to depth, stratigraphy and lithofacies (eg appropriate porosities are allocated to sands and shales from separate sand and shale distributions and according to their depth and age).

The resulting property models provide a 3D model of the vertical and lateral variation of the lithofacies and other properties. This allows a good understanding of the basin from many points of view, such as palaeo-environment, sedimentation, biostratigraphy, paleo-water depth, porosity, permeability, temperature, pressure, and maturation. The property modelling for the entire basin focusses on basin-wide variation in facies, temperature, pressure and vitrinite reflectance. The finer scaled Latrobe Valley structural model was built to analyse the unique coal-related sedimentary and tectonic features in an area where a high data density is available.

7.1 Latrobe Valley

The Latrobe Valley model includes ten coal seams or splits, from youngest to oldest being: Yallourn 1, 2; Morwell 1A1, 1A2; Morwell 1B1, 1B2; Morwell 2A, 2B; and Traralgon 1, 2 seams. The very thick coal seams in the Yallourn and Morwell formations developed behind a barrier system (the Balook Formation) and are equivalent to the Seaspray Group sediments that mainly comprise a succession of shelfal limestones, marls and mudstones (Figure 2-1). The older Traralgon Formation was deposited behind a barrier system much further to the east in the offshore area, that back-stepped during the Eocene to early Oligocene, and so extends out beneath the Seaspray Group and is equivalent to the Burong Formation in the Latrobe Group offshore (Figure 2-1). Several inter-seam units of mudstones and sands occur between each of the seams including some marginal marine sandstone incursions with dinoflagellates and these assist in the dating and correlations (Holdgate et al., 2021).

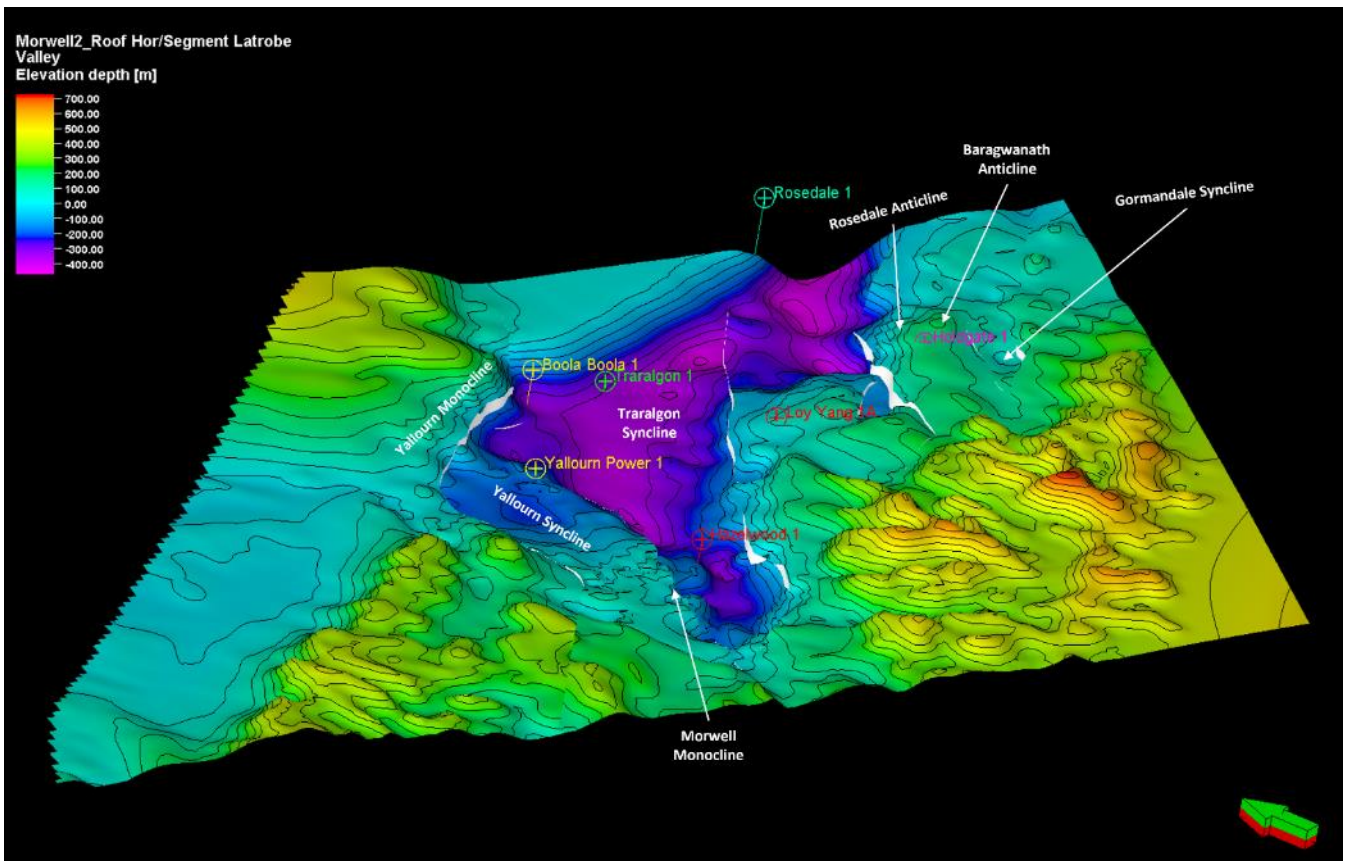
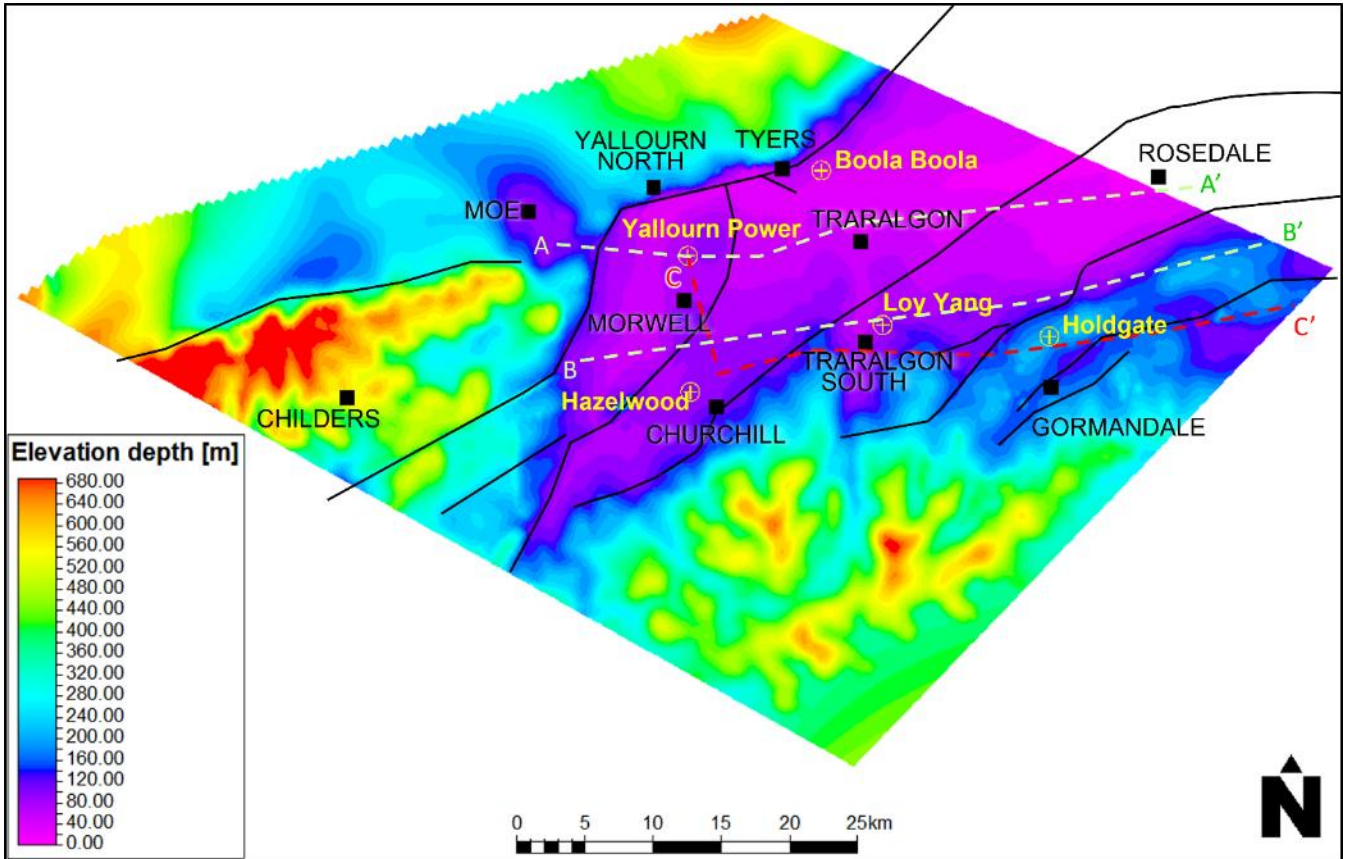
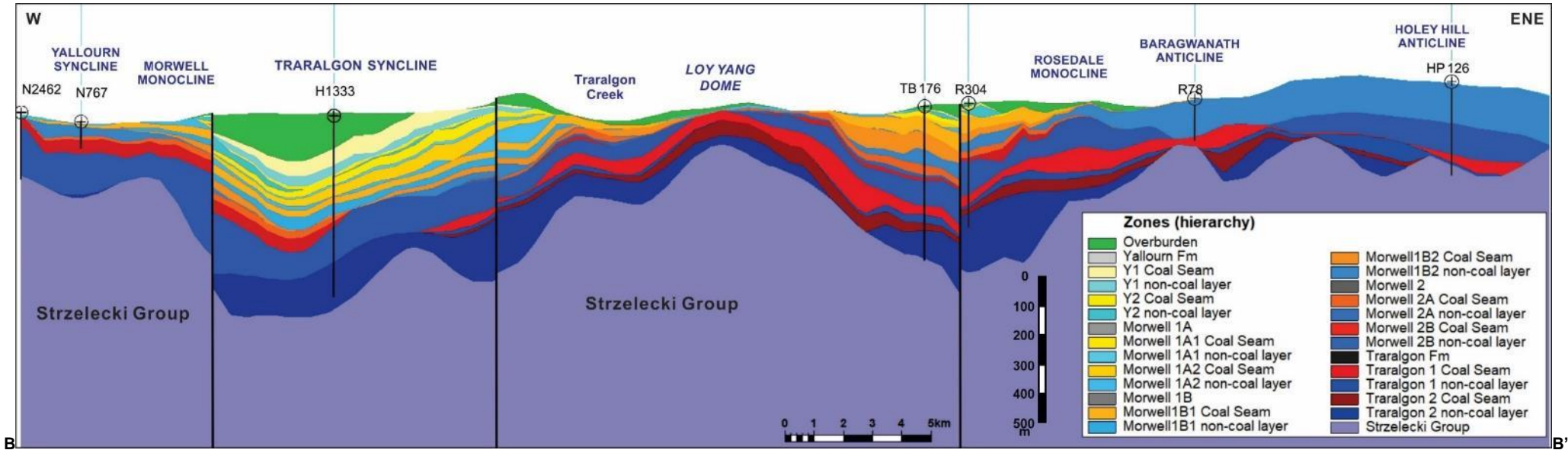
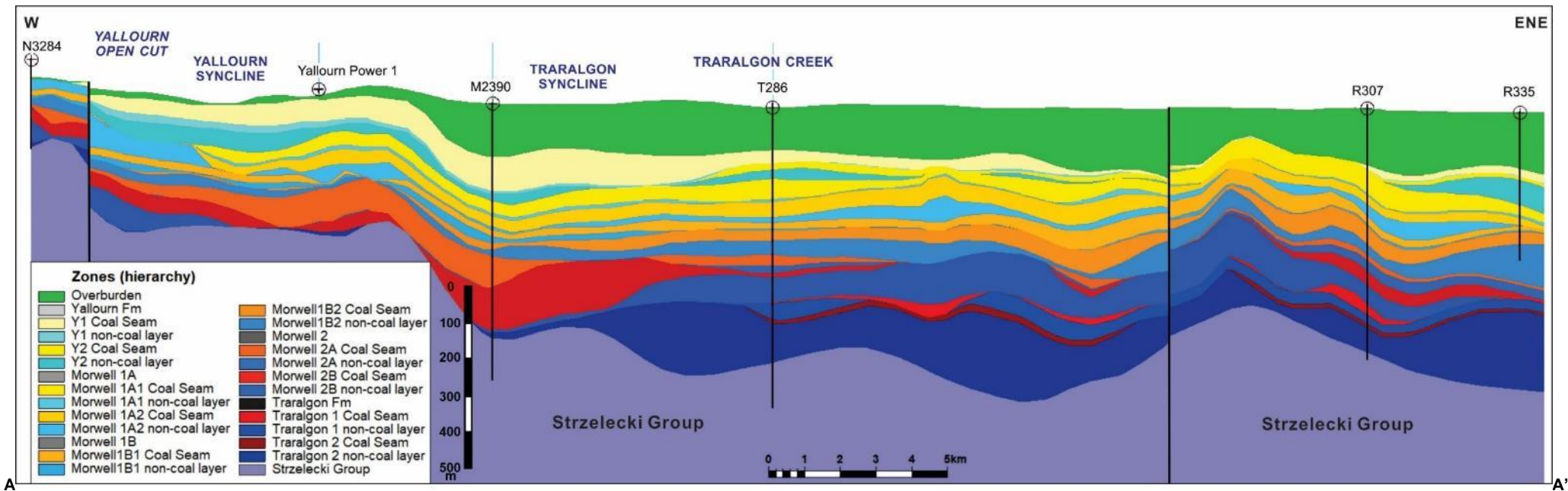


Figure 7-1 Latrobe Valley structural model, 2D land surface as an example (top). Wells in yellow, towns in black. Faults in black. 3D View at top Morwell 2 Seam, faults in white (bottom).



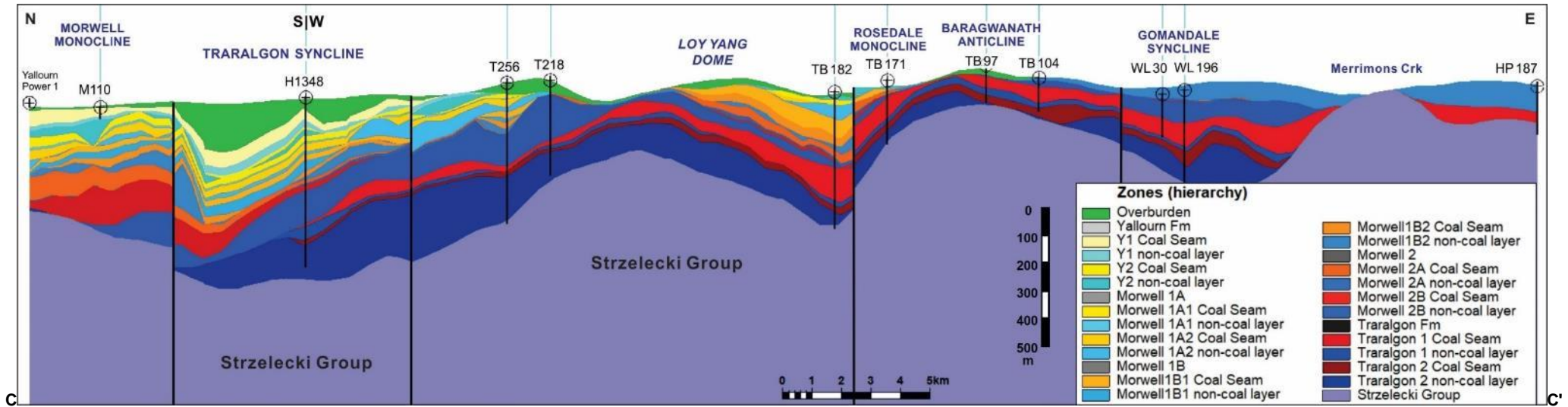


Figure 7-2 Three cross-sections through the Latrobe Valley 3D structural model. AA': E-W section from Yallourn syncline to Holey Hill anticline (Z Scale: 1:10); BB': N-S then E-W section from Morwell monocline (Yallourn Power-1) south to Traralgon syncline (H1333 bore), then east over Loy Yang Dome to Holey Hill Anticline (Z Scale: 1:9); CC': W-E section from Yallourn Open Cut to Rosedale (Z Scale: 1:10). See Figure 4-18 for the location of section lines.

7.1.1 Facies model

The facies model utilised lithological data from Geological Survey of Victoria Latrobe Valley Coal Model reports (2003, 2011) and aims to guide other property models through the coal seam stratigraphy and properties that are distinct to the interseam clastics (Figure 7-6). The areas where the coal seams are modelled are similar to previous studies (Holdgate, 1985; 2005): the Yallourn seams and Morwell 1A coal seams are limited within the valley and bounded by the Yallourn monocline at the northwest, the Churchill-Loy Yang open cut mine to the south and the Rosedale monocline to the east (Figure 7-3, Figure 7-4). The Morwell 1B and Morwell 2 seams are more widespread occurring across the Yallourn monocline towards Moe in the west with some thin coal layers in the Gormandale syncline; the Traralgon seams are limited to eastern parts of the valley, e.g., Loy Yang, Baragwanath anticlines, Gormandale syncline (Figure 7-4, Figure 7-5).

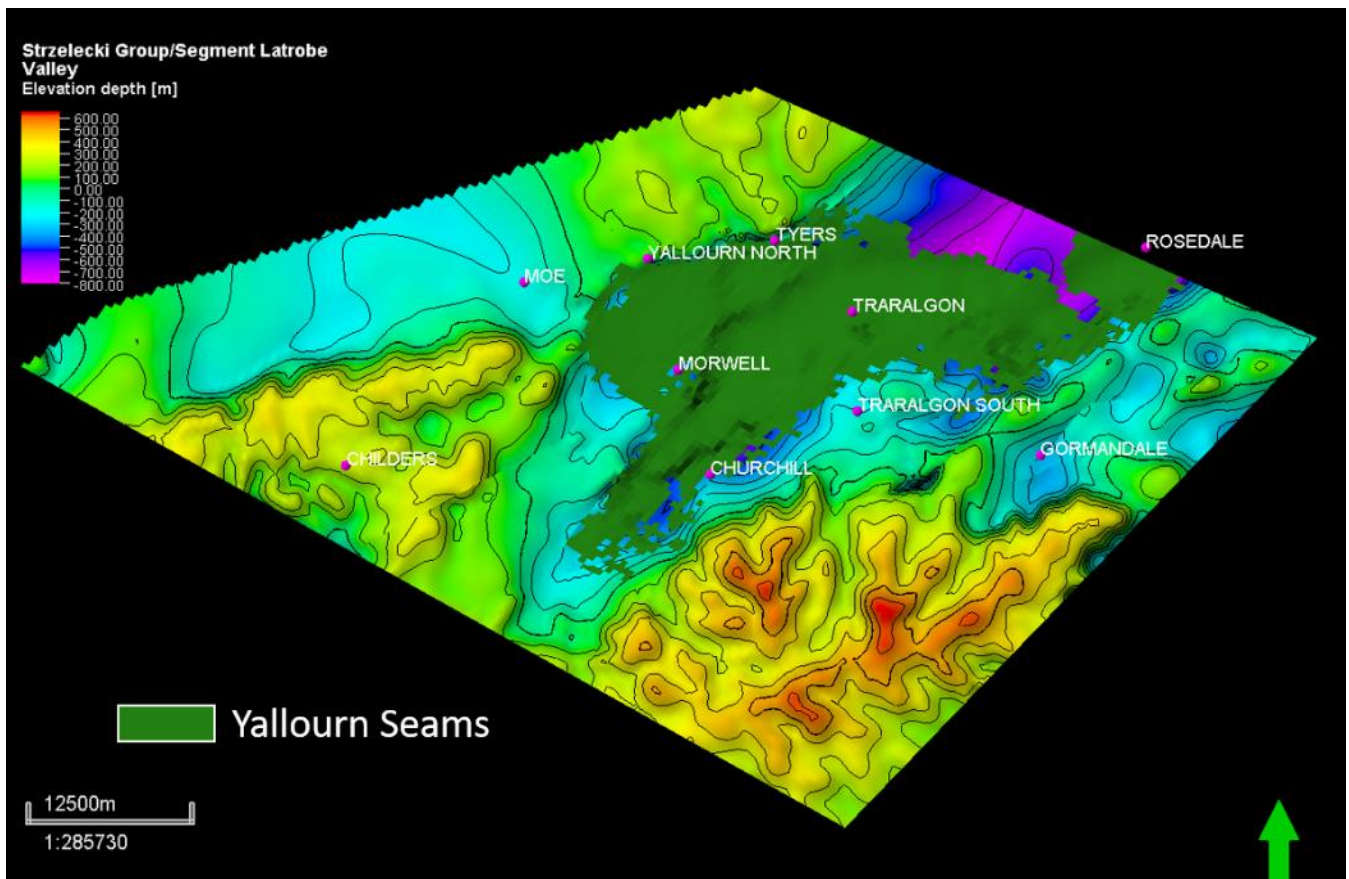


Figure 7-3 The extent of Yallourn Seam in the Latrobe Valley, background surface is top Strzelecki Group

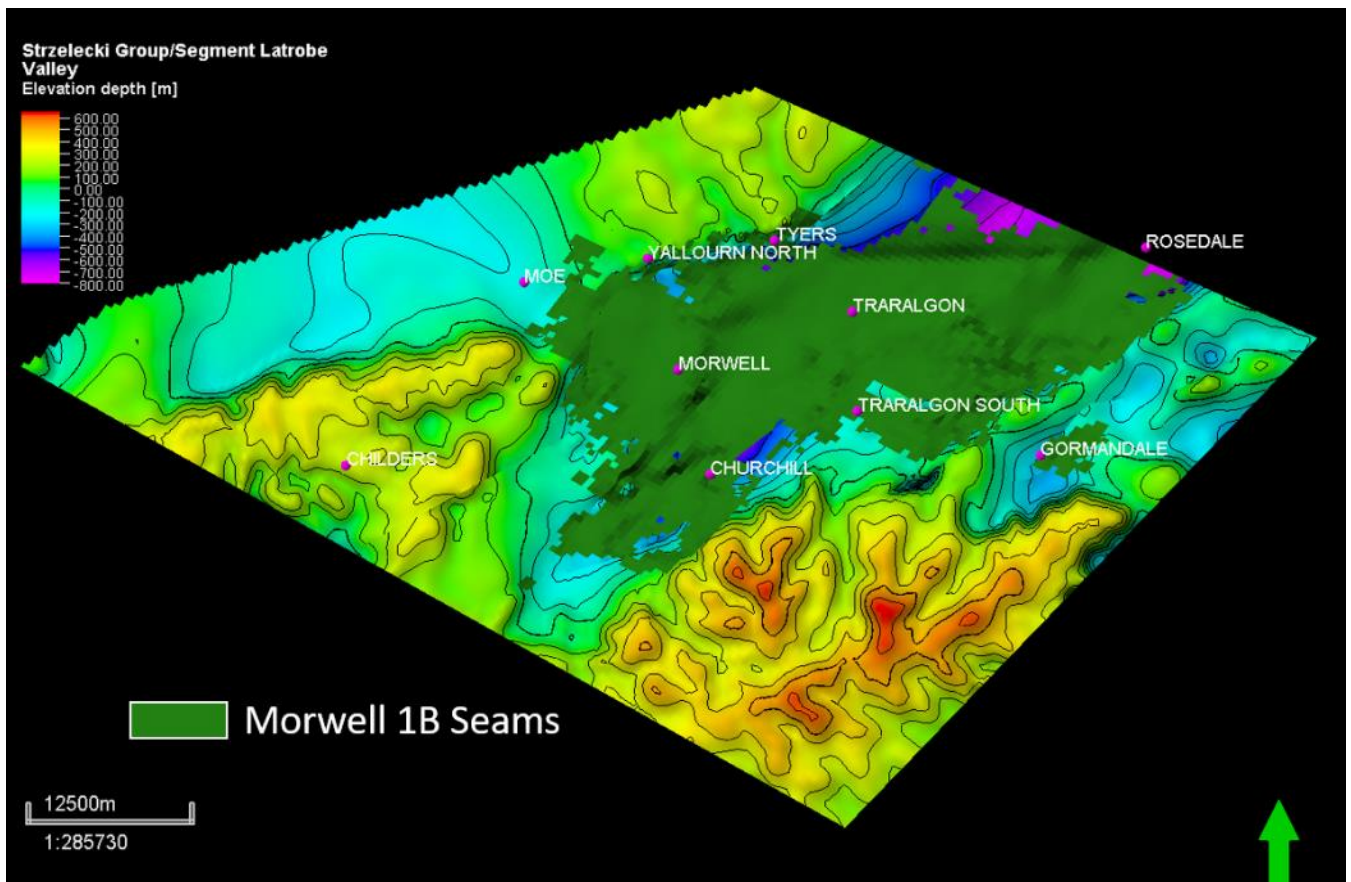
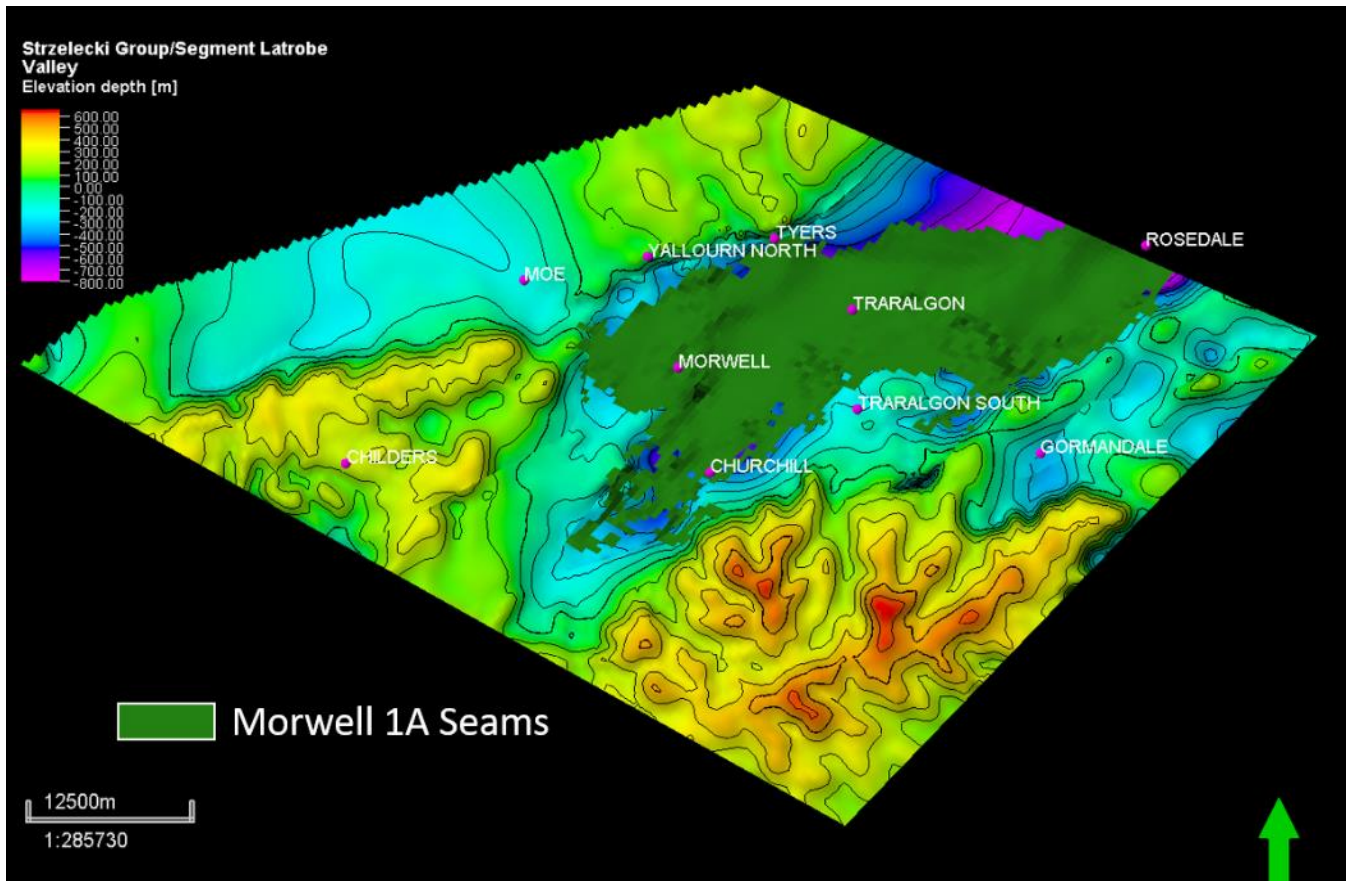


Figure 7-4 The extent of Morwell 1A and 1B Seams in the Latrobe Valley, background surface is top Strzelecki Group.

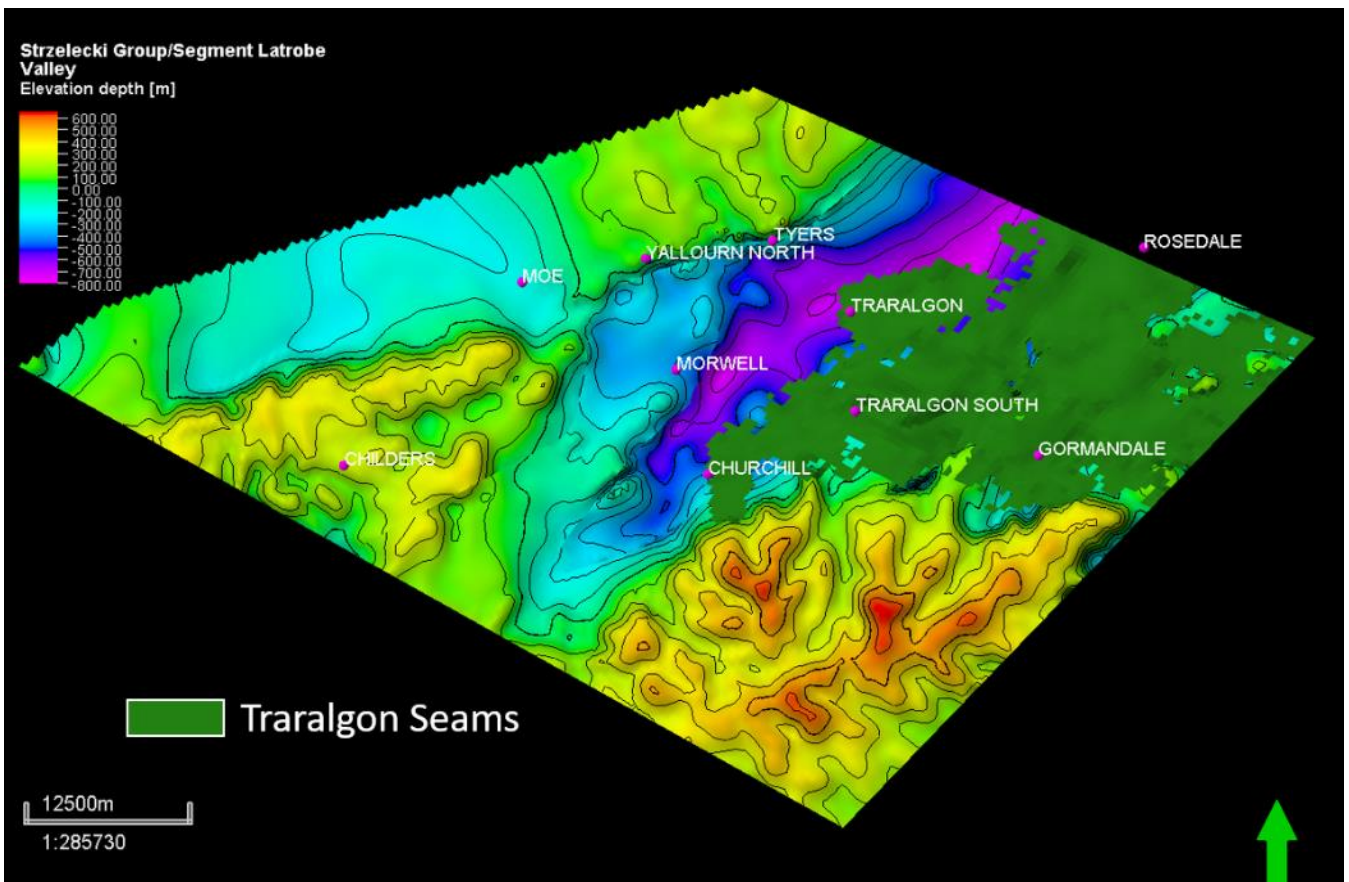
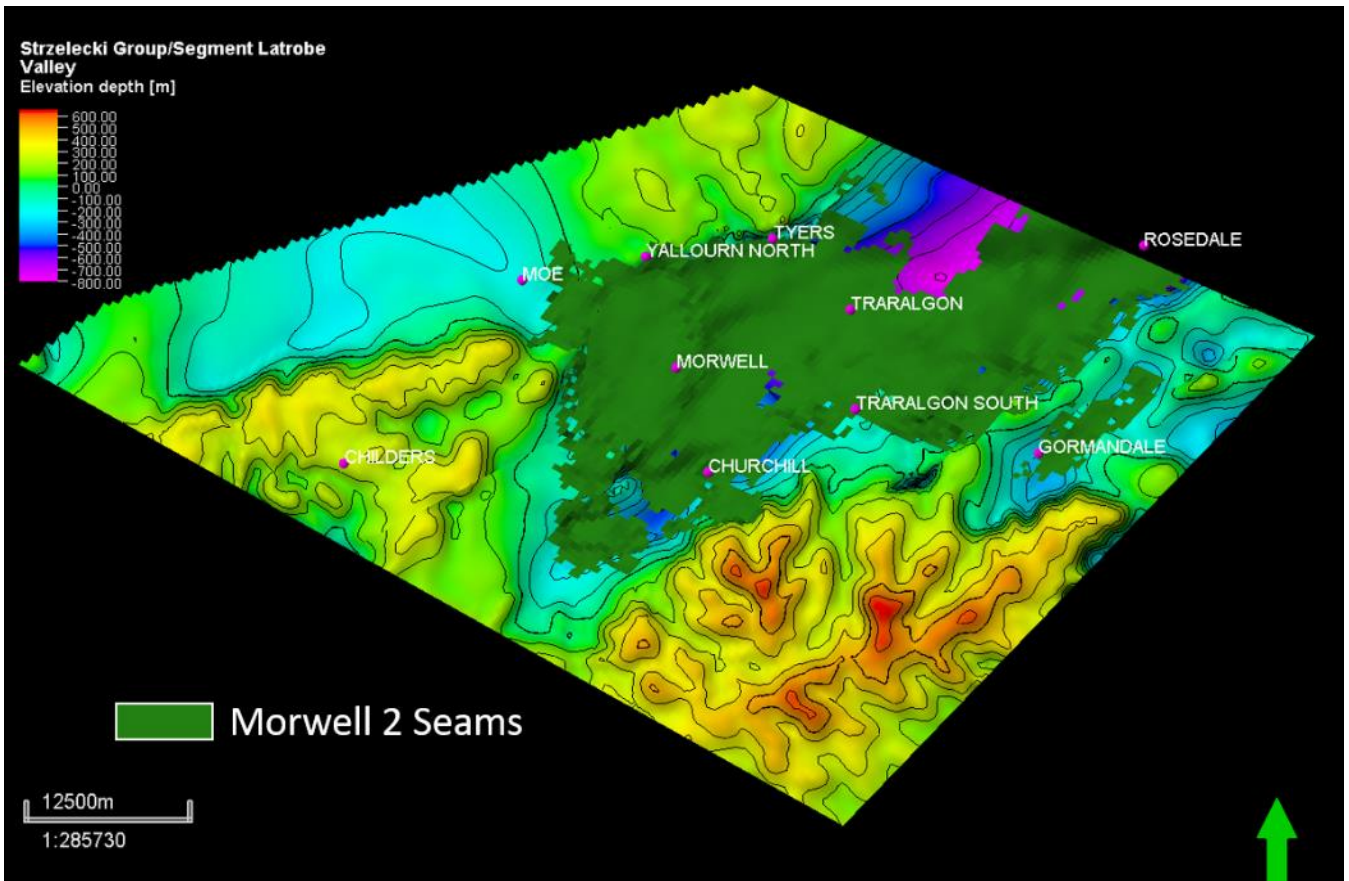


Figure 7-5 The extent of Morwell 2 and Traralgon Seams in the Latrobe Valley, background surface is top Strzelecki Group.

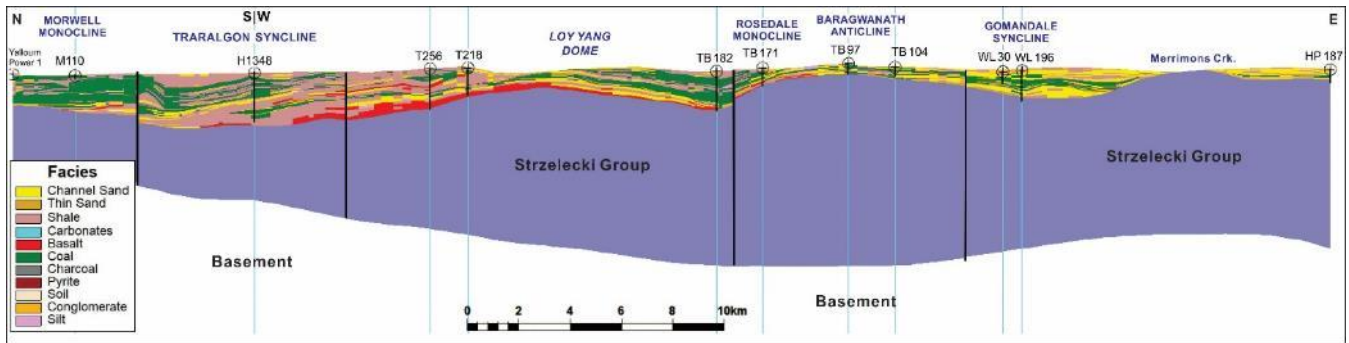


Figure 7-6 N-S then E-W section from the Morwell monocline (Yallourn Power-1) south into Traralgon syncline (H1333 bore), then east over the Loy Yang Dome to Hole Hill Anticline, showing the facies model in the Latrobe Valley 3D model. See Figure 4-18 for the location of the section line.

7.1.2 Moisture model

The brown coals of the Gippsland Basin are very low rank and have high moisture contents from about 70-30% (moisture content as measured is the water present in the coal as water molecules (H₂O) which are released when heated to 105-110 °C; Allardice, 1991). The high moisture contents are a major impediment to their commercial utilization. The variation in moisture content is caused by different factors, including petrographic variation with the depositional peat lithotype, effects caused by burial depth such as physical compaction and temperature related coalification, secondary effects from compression associated with folding, and chemical and thermal effects on water bonding (Edwards, 1945; Allardice, 1991; Holdgate, 2005). The importance of moisture content for its utilization mean that there is a lot of moisture data available. Hence, the moisture data is modelled here because it provides a useful means to study the structural and facies controls on burial compaction in these coal seams. Note that the routine borehole moisture analyses are measured on 3m composites which smoothes the lithotype variation so the resolution in these models is not sufficient for detailed lithotype analysis.

The moisture model for the Latrobe Valley is based on first removing any moisture values from the bore logs for the inter-seam beds, including very thin layers within the thick coal seams. The coal moisture log is filtered based on a sample having a minimum carbon % and maximum ash values of 10% using the well log calculator in *Petrel* as below:

- coal moisture = if(carbon >=60, moisture, U)
- coal moisture = if(ash <=10, moisture, U)

Note: carbon: carbon log; ash: ash log; moisture: moisture log; U: undefined value.

The moisture bore log data were then analysed in Data Analysis to derive a Variogram to guide the lateral grid interpolation (the variogram was anisotropic with a major range of 4544 metres and minor range of 3125 metres orientated at 20-degree azimuth (see Appendix 11). The data was also transformed to normal scores for each coal seam at each zone level. The property model interpolation uses simple kriging with facies control to guide the final modelling of the coals. The other facies are set as an undefined value using the 'Assign values' method since the moisture contents and controls of other lithologies are very different to the clean coal.

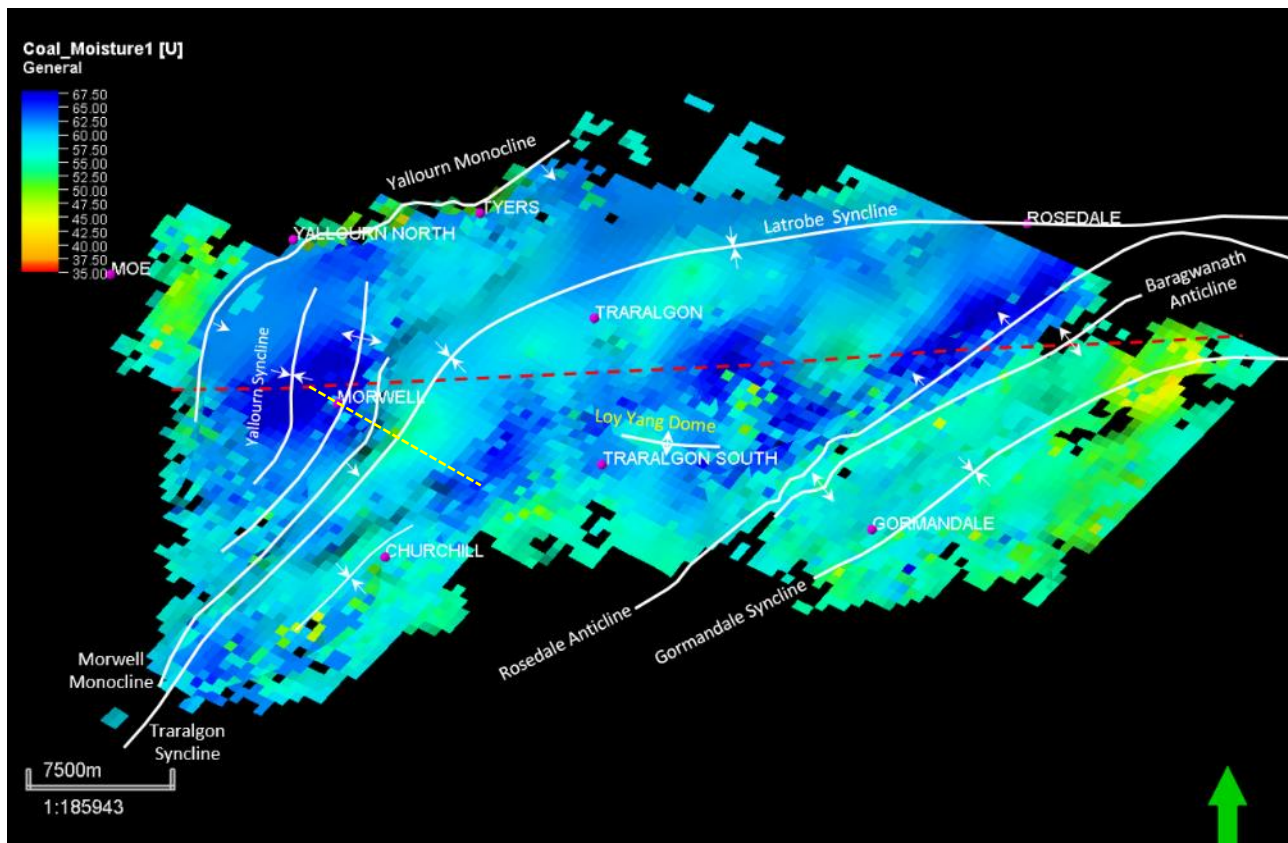


Figure 7-7 Latrobe Valley Moisture model map view. The red dash line shows the location of Figure 7-8.

The moisture model in the Latrobe Valley demonstrates the lateral and vertical variation in moisture (Figure 7-7 and Figure 7-8). The dominant trend in moisture variation is with depth due to burial. The moisture values decrease from over 65% near the surface to 55% or less at 500m depth or more as shown clearly on the cross-section in Figure 7-8. This effect is also shown on the histograms for each coal seam from youngest to oldest in Figure 7-9, in which the gross average for all the data shows a small decrease in moisture from the Yallourn seam (62%) to the Traralgon seam (54%), noting that these averages are also affected by marked changes in burial depth from one area in the valley to another within the one seam. This is shown clearly by the effects of overall structure, with high moisture values in the same seam occurring over the main shallow burial areas and lower moisture

values in the same seam occurring in the deeply buried synclines. The Yallourn Seam shows this clearly going from the Yallourn syncline over the Morwell monocline into the Traralgon syncline (Figure 7-7).

The Latrobe Valley coal seams have experienced regional compression trending mostly WNW-ESE (Tokarev et al., 1999). Consequently, a subtle secondary effect on moisture also occurs over folds that are associated with inverted normal faults that are now high angle reverse faults (Figure 7-8). The moisture variation within the same seam shows these tectonic effects, with the moisture value decreasing in the compression structures, such as in strongly folded areas and adjacent to the reverse faults (see arrows on Figure 7-8). Note how the moisture content can decrease over the crests of some of the deeper anticlines, being less than the moisture content in the same seam in the adjacent synclines away from the compression structures. The moisture content only shows minor variation across normal faults with some large faults clearly showing growth. Here the moisture difference between the down-throw side and the up-throw side is only about one percent or less when reconstructed (Figure 7-10).

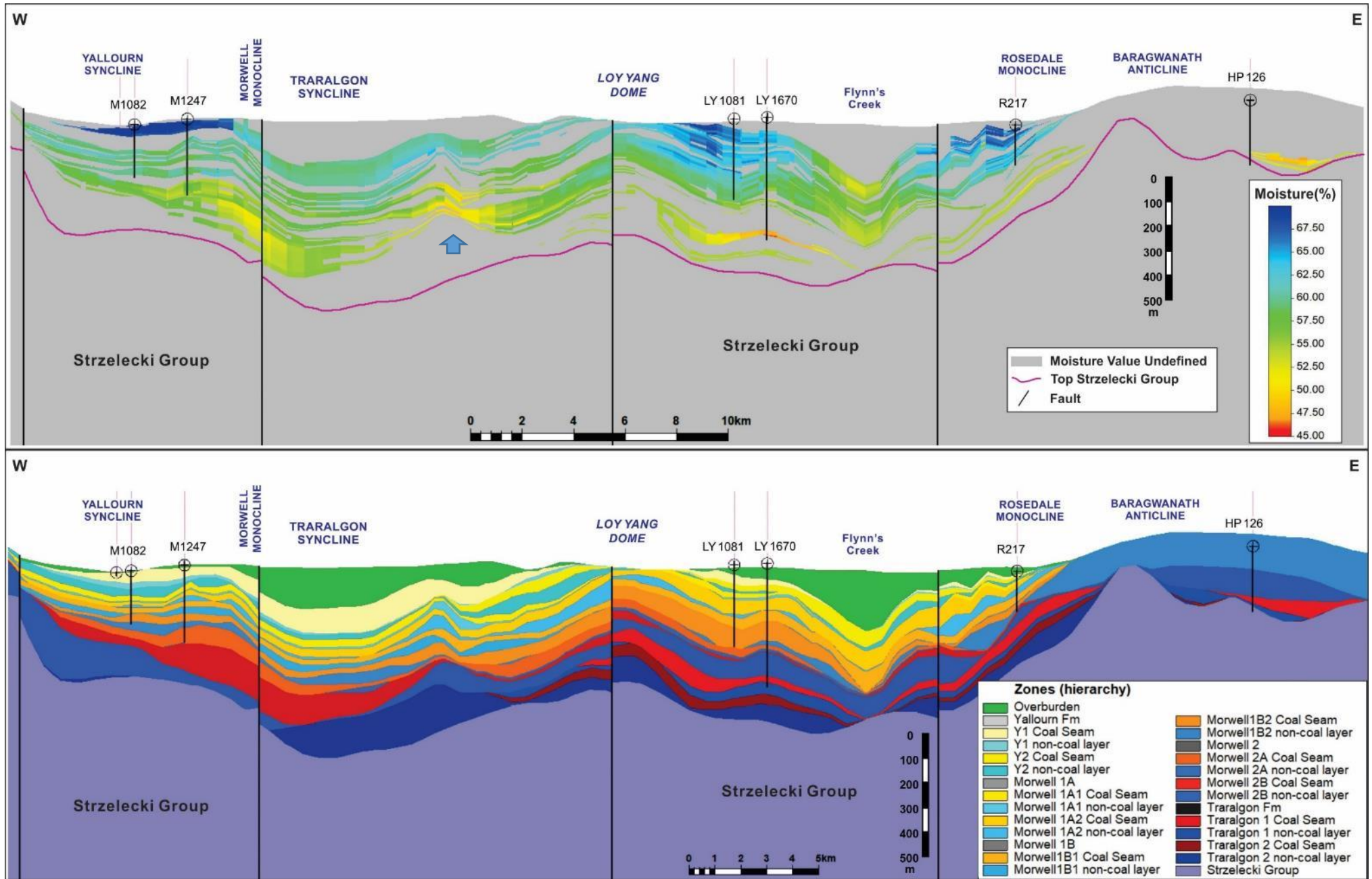


Figure 7-8 Top: Moisture property on an East-west geological cross-section from Yallourn Fault to Baragwanath anticline. The moisture of interseam beds is set as undefined. Bottom: the corresponding stratigraphy in the Latrobe Valley 3D structural model. Cross-section location marked in Figure 7-7.

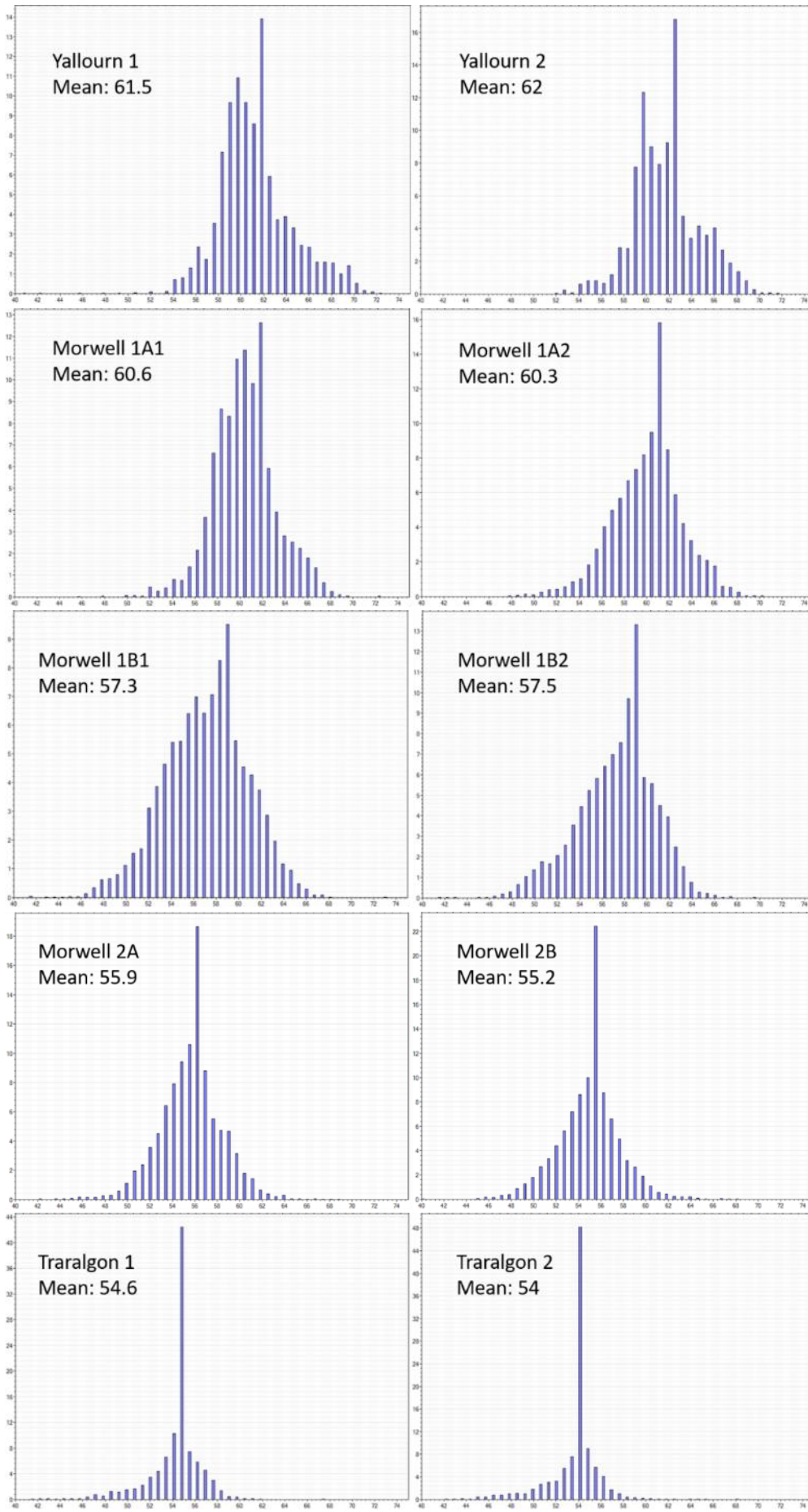


Figure 7-9 Histogram of Moisture values in the Latrobe Valle

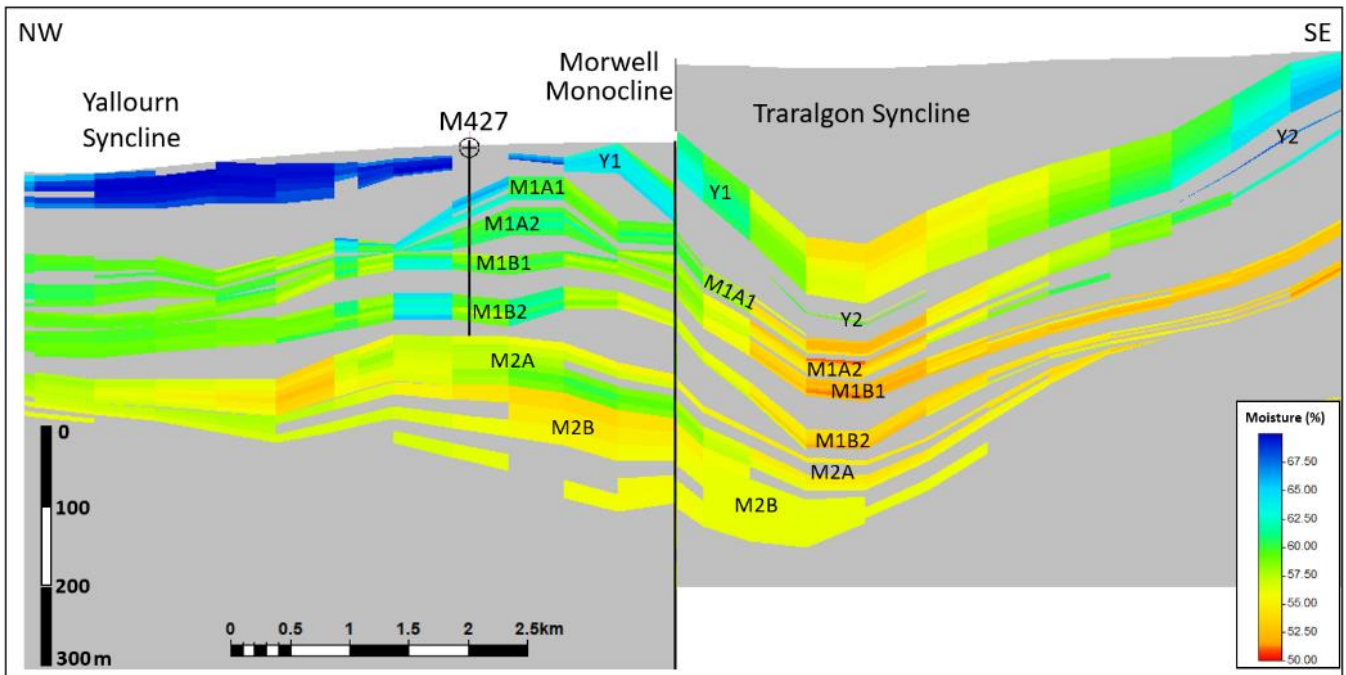
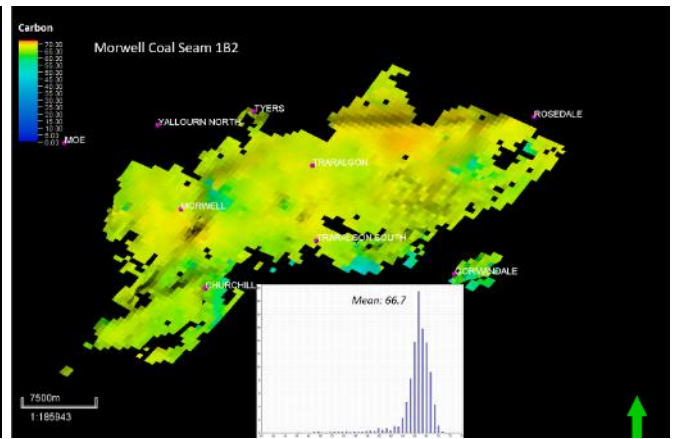
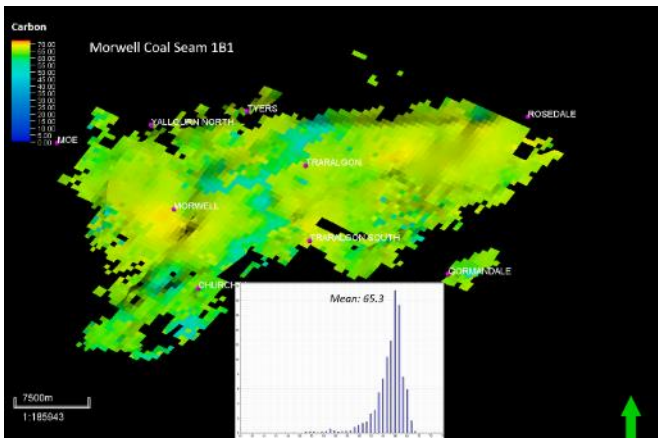
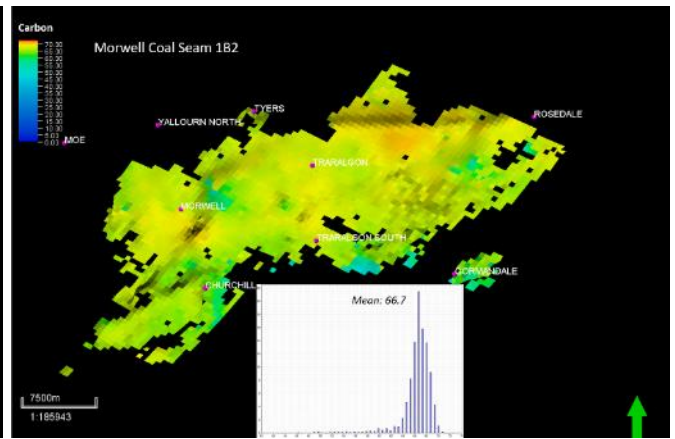
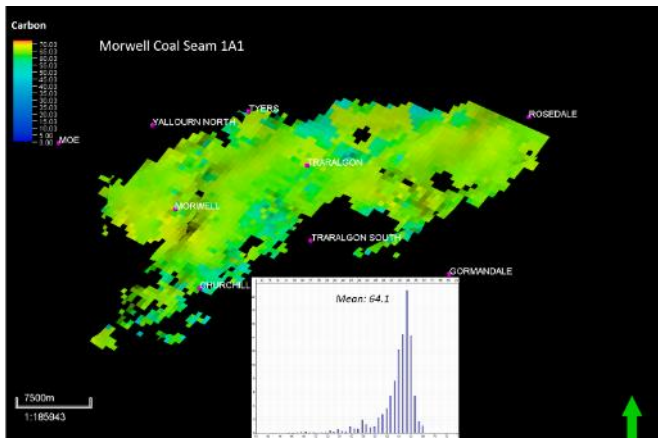
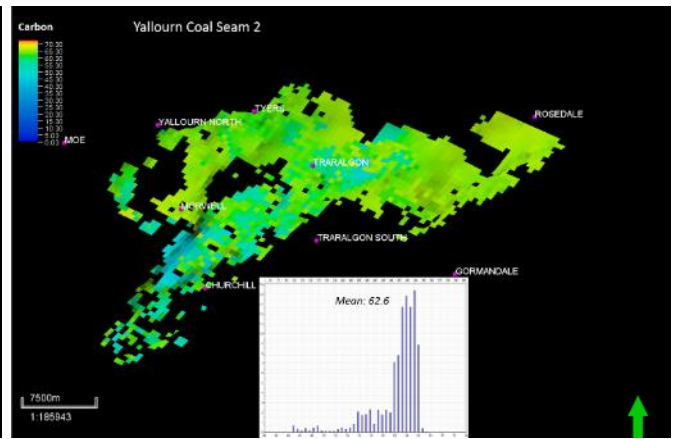
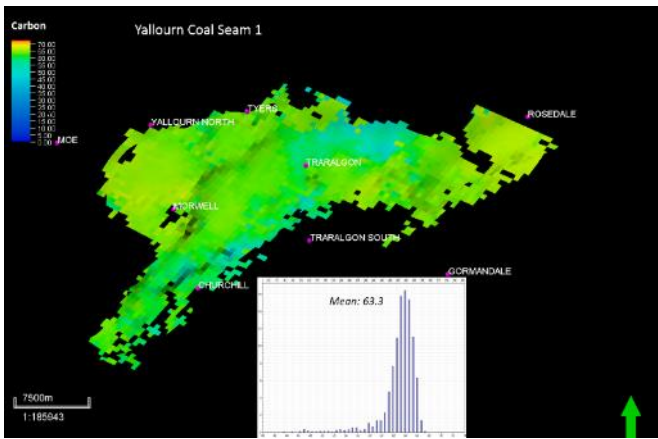


Figure 7-10 A cross-section shows the moisture content change across the fault (Top) and the same section datumed on top M2A seam to show approximate reconstruction. See the location in Figure 7-7.

7.1.3 Carbon model

The carbon content of coal is a chemical rank indicator, generally ranging from 65 to 72% (dry ash free basis) (George & Mackay, 1991). The carbon % borehole logs were modelled in *Petrel* using the Gaussian simulation method with facies control.

Histograms of the carbon content of routine borehole analyses for each coal seam indicate that most of the coal samples vary from 62 to 67% carbon, with a minor low carbon tail which represents higher ash coals. The carbon model (Figure 7-11) shows that the coal rank in Latrobe Valley is low, with only a slight increase of carbon content from shallow level coal seams (Yallourn seams) to the deep level coal seams (Traralgon seams), which is consistent with a minor increase of chemical rank as expected (Holdgate, 1985; 2005).



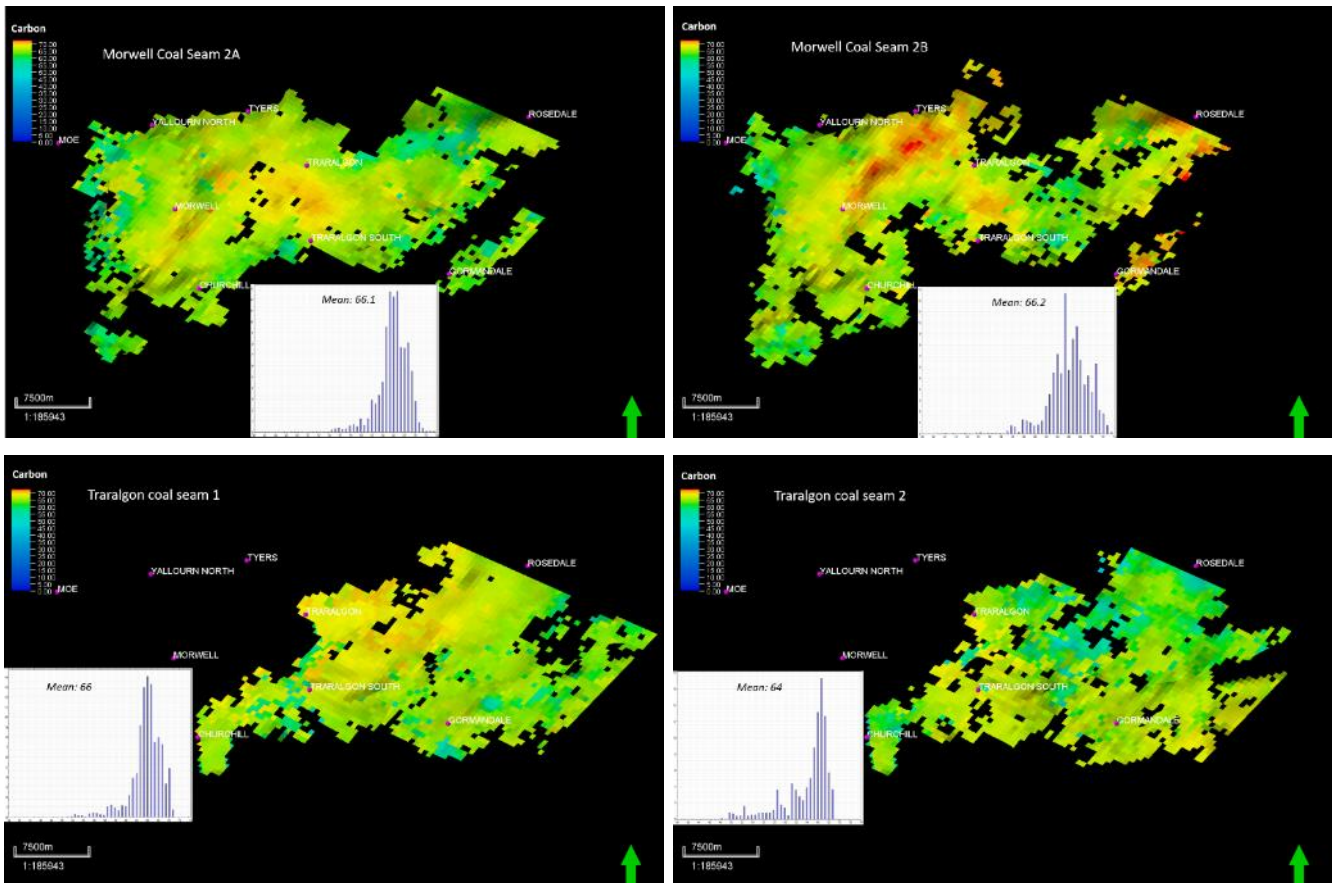


Figure 7-11 Maps of Carbon % for each coal seam from the Latrobe Valley Carbon model. The inset graph is the Carbon histogram for the same seam showing the gross mean value.

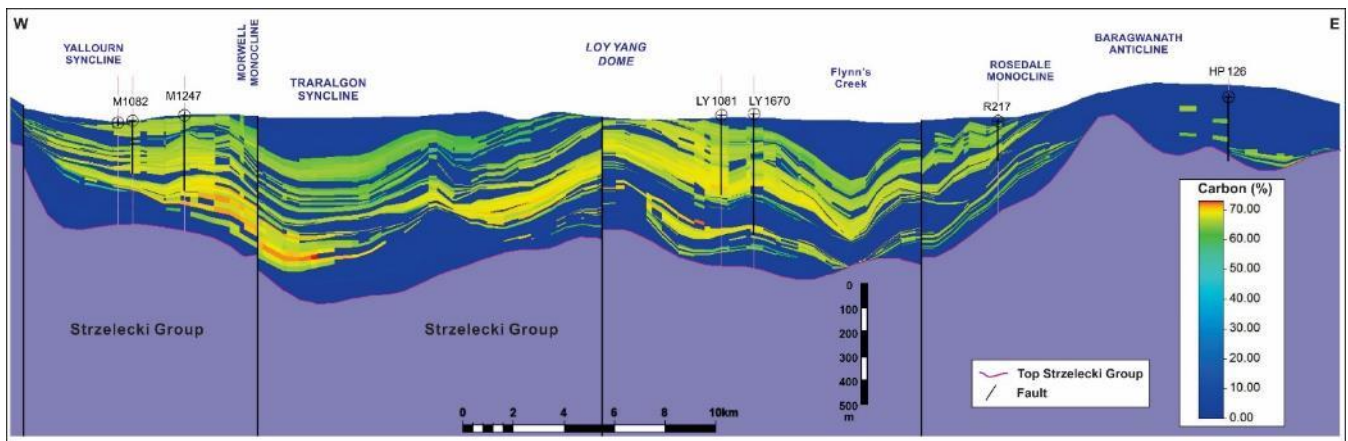


Figure 7-12 West-east geological cross-section between Yallourn Fault and Baragwanath anticline showing the coal carbon as determined from the Latrobe Valley 3D carbon property model. For the location of the cross-section, see Figure 7-7.

7.2 Entire Gippsland Basin

The entire Gippsland model aims to link and model the onshore and offshore parts of the Gippsland Basin. There are stratigraphic and structural differences between the onshore and offshore:

- Onshore sequences are much thinner compared to the offshore, and Late Cretaceous sediments are missing in most of the onshore area.
- In the Latrobe valley, the section is Eocene to Holocene.

- Onshore, all the younger sediments are deposited directly on the Early Cretaceous Strzelecki sediments, whereas offshore the stratigraphy is relatively continuous.
- The onshore Cainozoic sediments have only been buried to shallow depths, while offshore the sediments have experienced much deeper and mostly more rapid burial process.

The entire Gippsland has been a connected deposition system since the Eocene. For instance, the mid-late Eocene coal seams (Traralgon seams) are well developed and extend from the Latrobe Valley through the Lake Wellington depression into the offshore area (Holdgate and Sluiter, 2021). Hence, a model covering the entire basin provides an excellent opportunity to explore the commonality and diversity of the basin from offshore to onshore. Six properties have been analysed and modelled in the full basin model: Facies, Temperature, Vitrinite Reflectance (R_o), Hydrostatic Pressure, Total Organic Content (TOC) and Hydrogen Index (HI). The TOC and HI property models are made for *PetroMod* burial-thermal modelling, see Chapter 8.

7.2.1 Facies model

The facies property model is the primary property model, which is used to control and guide the subsequent property models. There are five steps to build the facies property model:

1. The lithofacies log is generated based on interpretation of the downhole well logs (*e.g.*, GR, Neutron, Density, Sonic) and quality checked against the lithology log from the Well Completion Report (Chapter 3).
2. Upscale the facies log: weighting the different facies types in each zone to ensure that the thin beds (*e.g.*, coal) were picked up using most of method. See weighting settings in Appendix 12.
3. Generate the probability trend maps to control the lateral distribution of the different lithologies (*e.g.*, coal, igneous, and carbonates).
4. Data Analysis: fit a vertical trend for each lithofacies and zone based on the vertical histogram.
5. Facies modelling: use Truncated Gaussian simulation and the vertical proportion curves from the Data analysis step.

A good coverage of wells has been used in the facies models over the entire Gippsland Basin including over the main oil and gas fields (Figure 7-13). Overall the modelling used 239 petroleum wells and 54 deep bores.

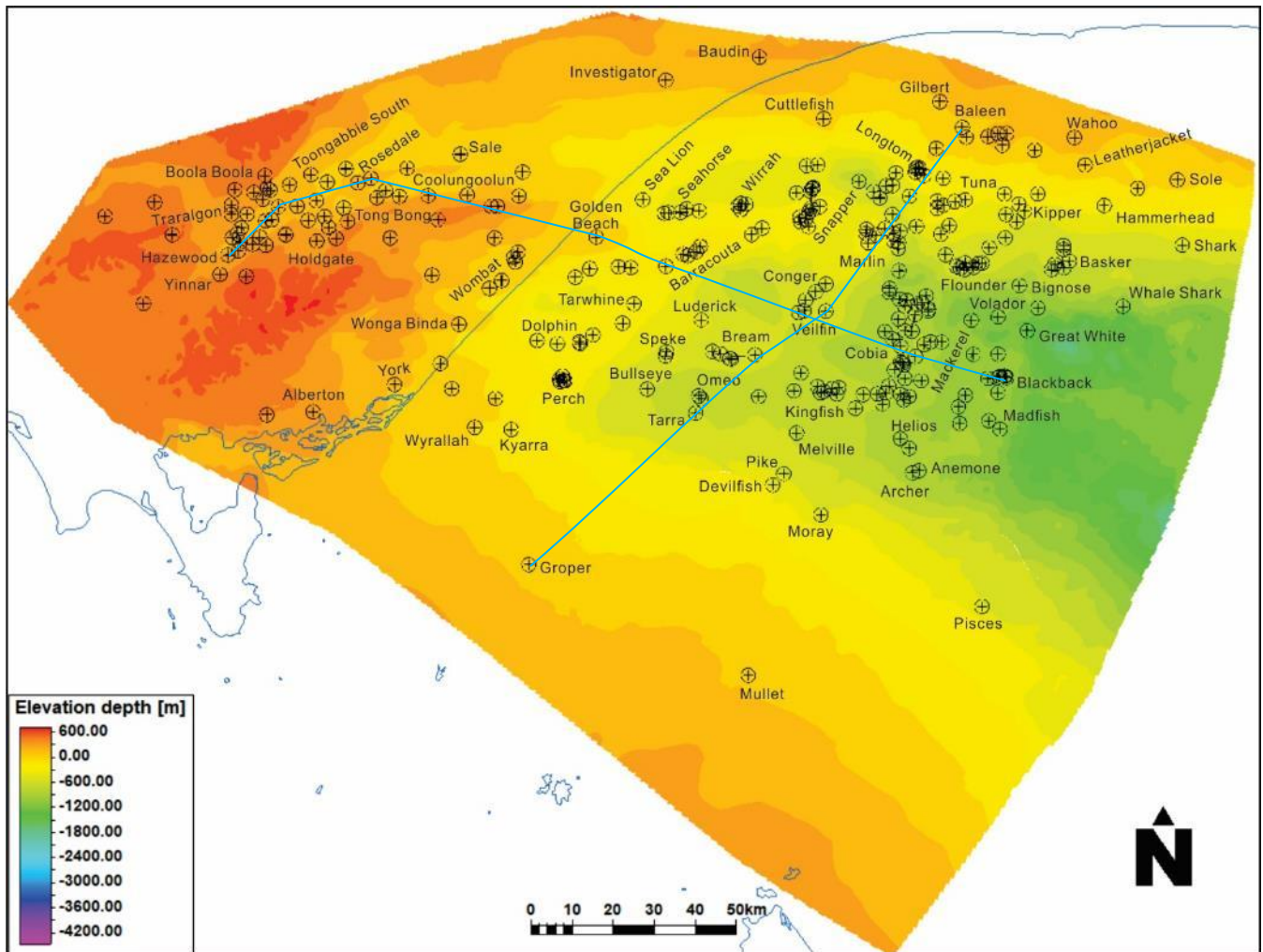


Figure 7-13 Wells with a Lithofacies log used to build the facies model. Background surface is top Traralgon Formation – top Latrobe group, dark blue line is coastline. Blue lines are the location of sections in Figure 7-14.

The 3D facies model of the entire Gippsland basin reproduces the facies variation laterally, from west to east (onshore-offshore) and north to south (from north platform-central deep-south platform), and vertically from the top Seaspray Group to base Latrobe Group. The thick coal seams and the thin interseam non-marine clastics are adequately captured in the onshore part of the basin (in both the detailed and full models) (refer Figure 7-2). The lithofacies in the offshore Seaspray Group is less detailed and more homogeneous but is a satisfactory mix of shallow marine carbonates at the top and marls and marine shales of Oligocene-mid Miocene age, which gradually increase towards the east (Figure 7-14). The Eocene Traralgon Seams are modelled in the Latrobe Valley and extend into the Central Deep region within the offshore Cobia Subgroup (Figure 7-15, a). The Cobia Subgroup lithofacies model captures the east-west facies changes for the interbedded sandstones, siltstones, shales and coals in the fluvial-deltaic and coastal environments with a high proportion of coals. The upper Halibut subgroup (*L. balmei* – *M. diversus*) contains fluvial and deltaic clastics (mainly sandstone and siltstone) with multiple coal inter-beds and thin but extensive total coal thickness in the north-

western part of the basin (Figure 7-15, b). In the lower Latrobe Group (ca. 93 – 65 Ma) coals are thinner and less common and overall sediments became shalier, though some areas contain more sandstones. The model captures igneous rocks that mainly occur along the North Terrace and into the Seahorse-Barracouta area further east and are mostly Late Cretaceous (especially Senonian).

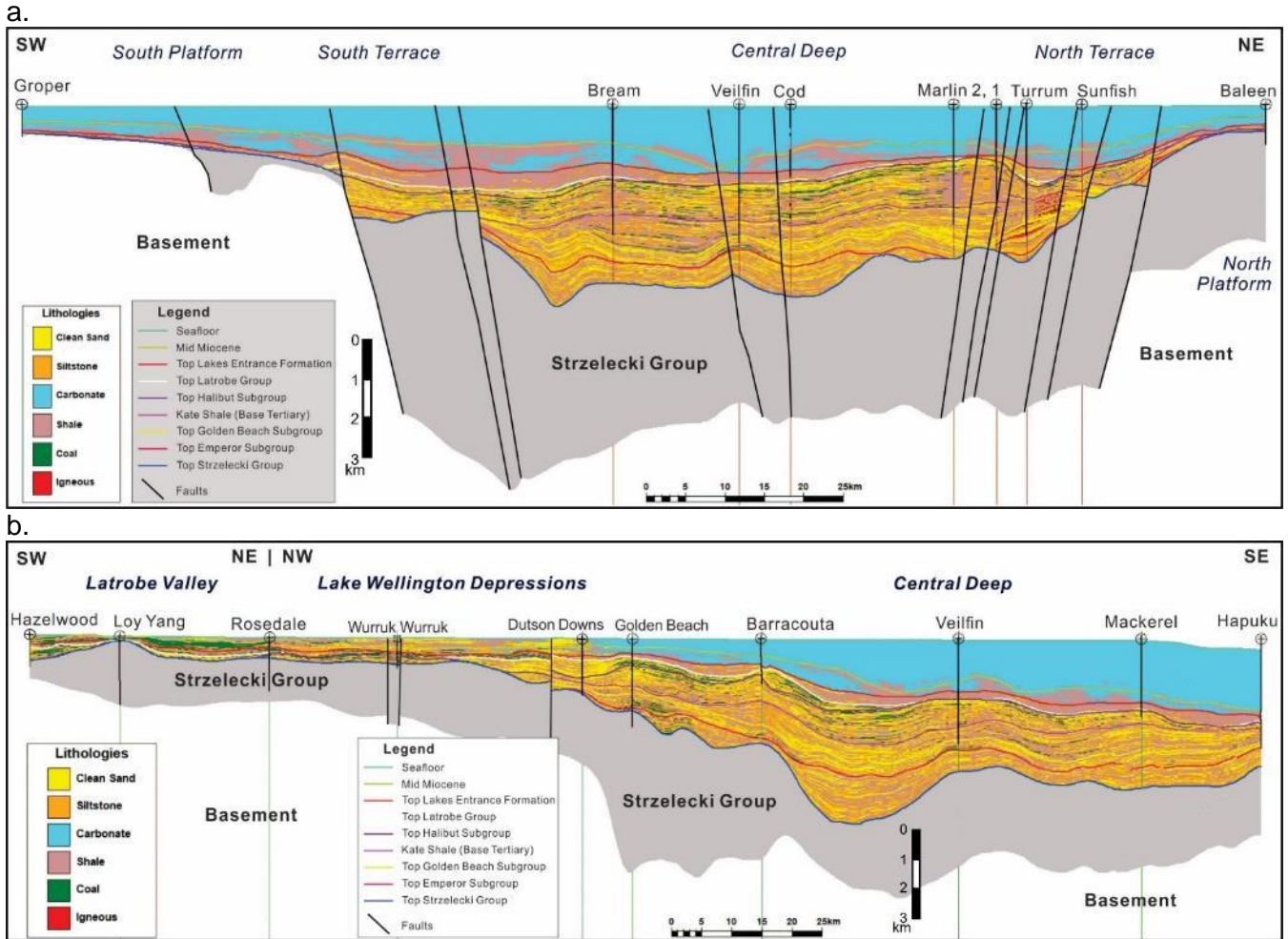


Figure 7-14 Two cross-sections of the facies model (see Figure 7-13 for location). a: southwest-northeast geological cross-section through South Platform (Groper), South Terrace, Central Deep (Veilfin, Cod), North terrace (Sunfish) to North Platform (Baleen); b: southwest-southeast cross-section from Churchill north (Hazelwood) trending northeast into the Latrobe Valley, northwest over the Rosedale area, through the Lake Wellington Depression and Central Deep (Barracouta, Veilfin) to the southeast (Mackerel).

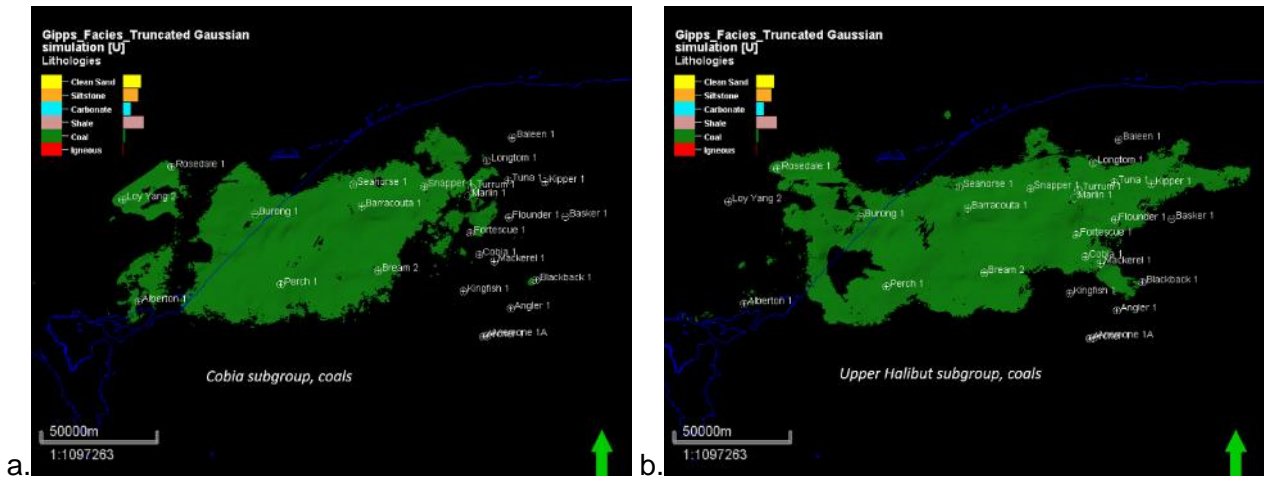


Figure 7-15 a: Traralgon formation Eocene total coal seam extent from full Gippsland Basin facies model; b: Palaeocene-early Eocene total coal seam extent.

7.2.2 Thermal model (Temperature)

The temperature property model utilised bottom hole temperature (BHT) data and other temperature data measured along with the pressure logs. The formation temperature vertical trend at each well should fit a relatively linear trend, and most wells only have a bottom hole temperature value, which is not enough to simulate the temperature from the top surface to the bottom of the model. Therefore, a constant surface temperature value (20 degC) is added to the temperature log in each well by assigning the surface temperature value at the topography-bathymetry surface. A new temperature log was then created by resampling every 0.5 metres in *Petrel*. The resampled temperature logs are analysed and modelled in the Property modelling using the Kriging method.

The spread of wells used in the temperature model indicate a good coverage of the entire basin and includes the main oil and gas fields in the Gippsland Basin (Figure 7-16). Overall the model used 263 petroleum wells and ten bores.

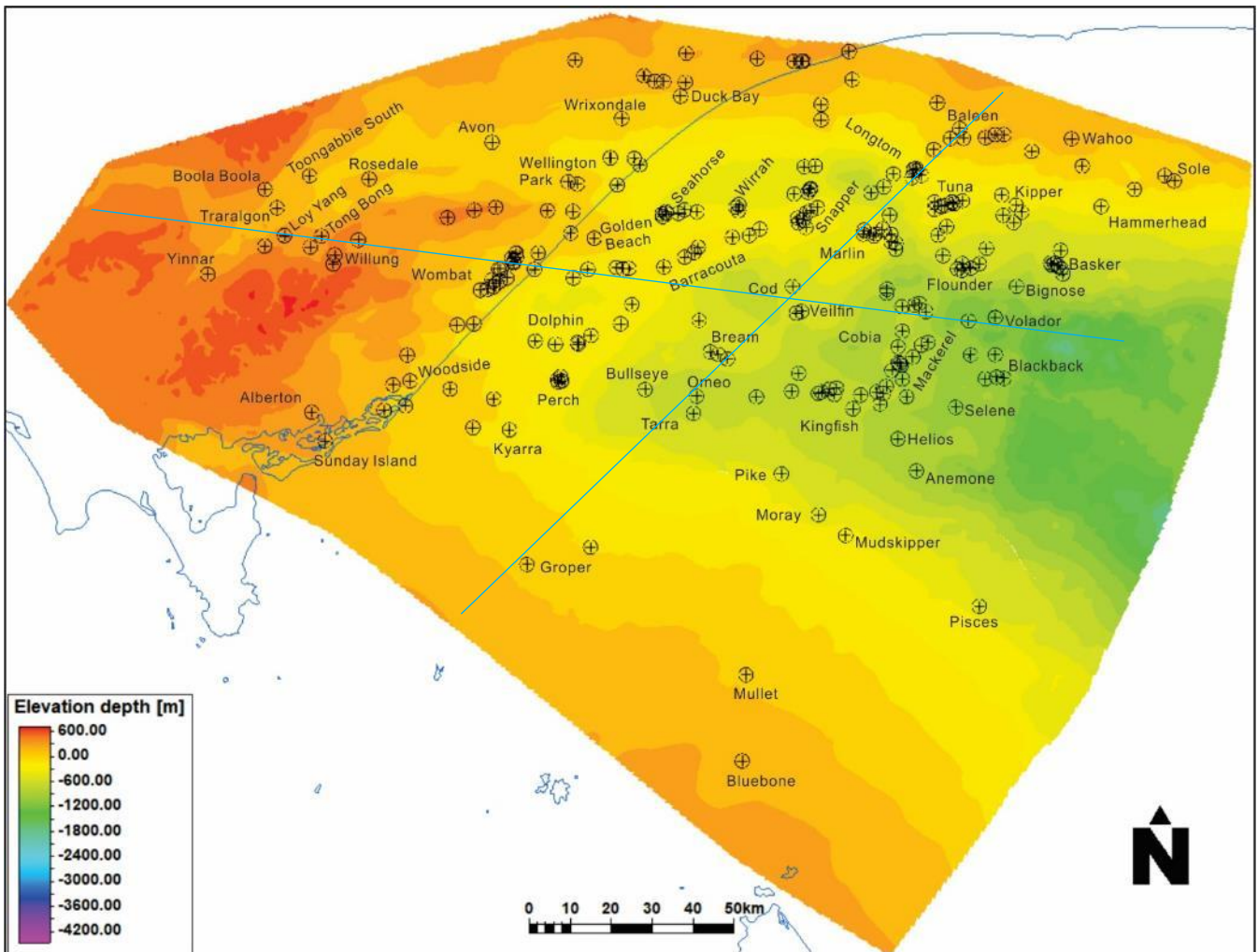


Figure 7-16 Wells with Temperature logs used to build the Temperature model. Background surface is top Traralgon Formation – top Latrobe group, dark blue line is coastline. Blue lines are the location of sections given in Figure 7-17.

The 3D temperature model implies that the formation temperature variation fits a localised linear function with depth and partly corresponds to the structure of the geological units (Figure 7-17). The model is based on actual data down to about 4-5 km and the good fit allows extrapolation of the temperatures to deeper depths. The onshore region has a deposition hiatus below the Latrobe Group passing into Strzelecki sediments in which the modelled temperature reaches 190 degC at the base of the Strzelecki. The North and South platforms in the Gippsland Basin, which mainly comprise thin late Eocene to present-day sediments, show a low-temperature range with a maximum modelled value of 160 degC. The Central Deep area contains over 10 km of sediment from the Early Cretaceous to the present. Hence, the modelled maximum temperature at the base up to 300 degC.

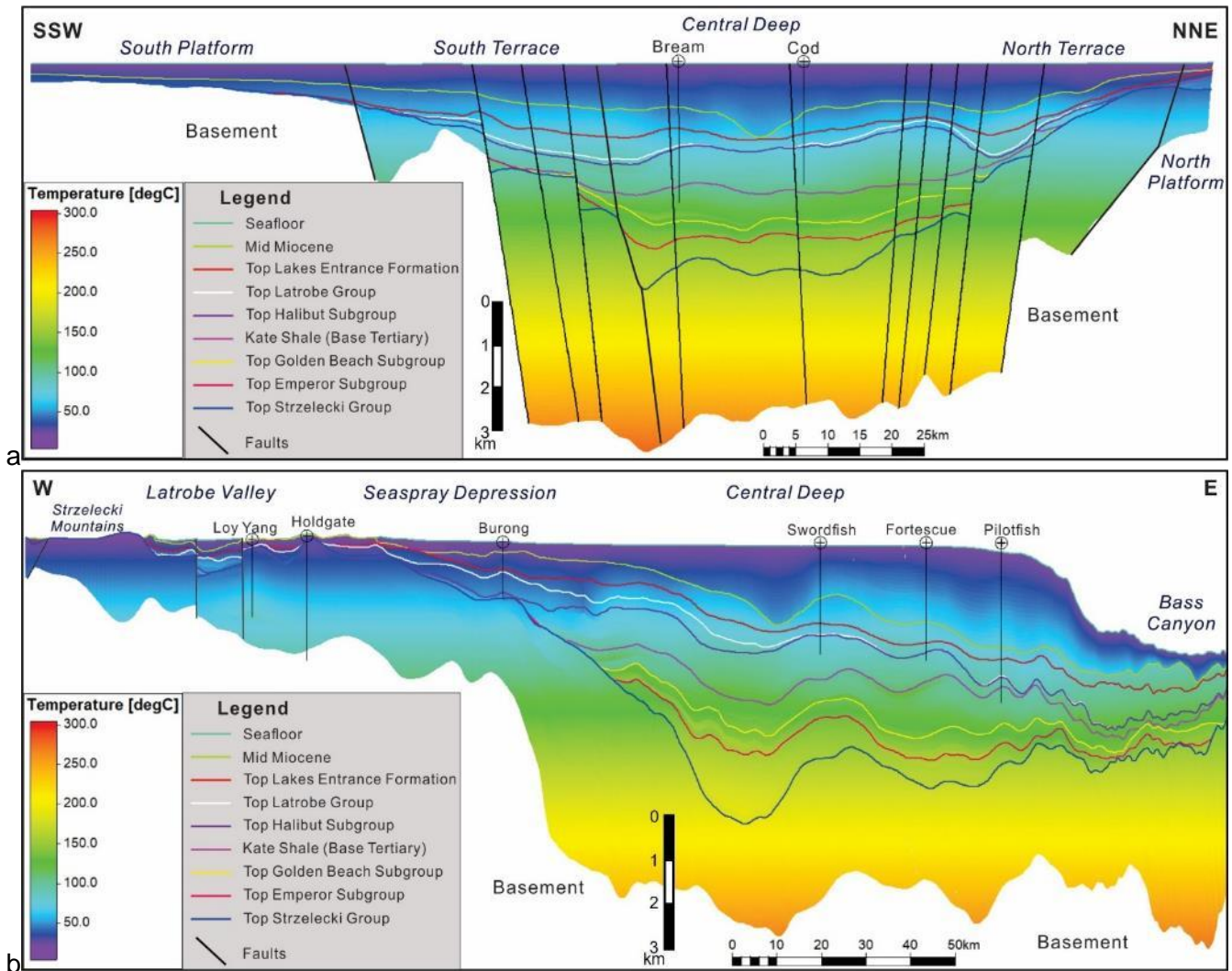
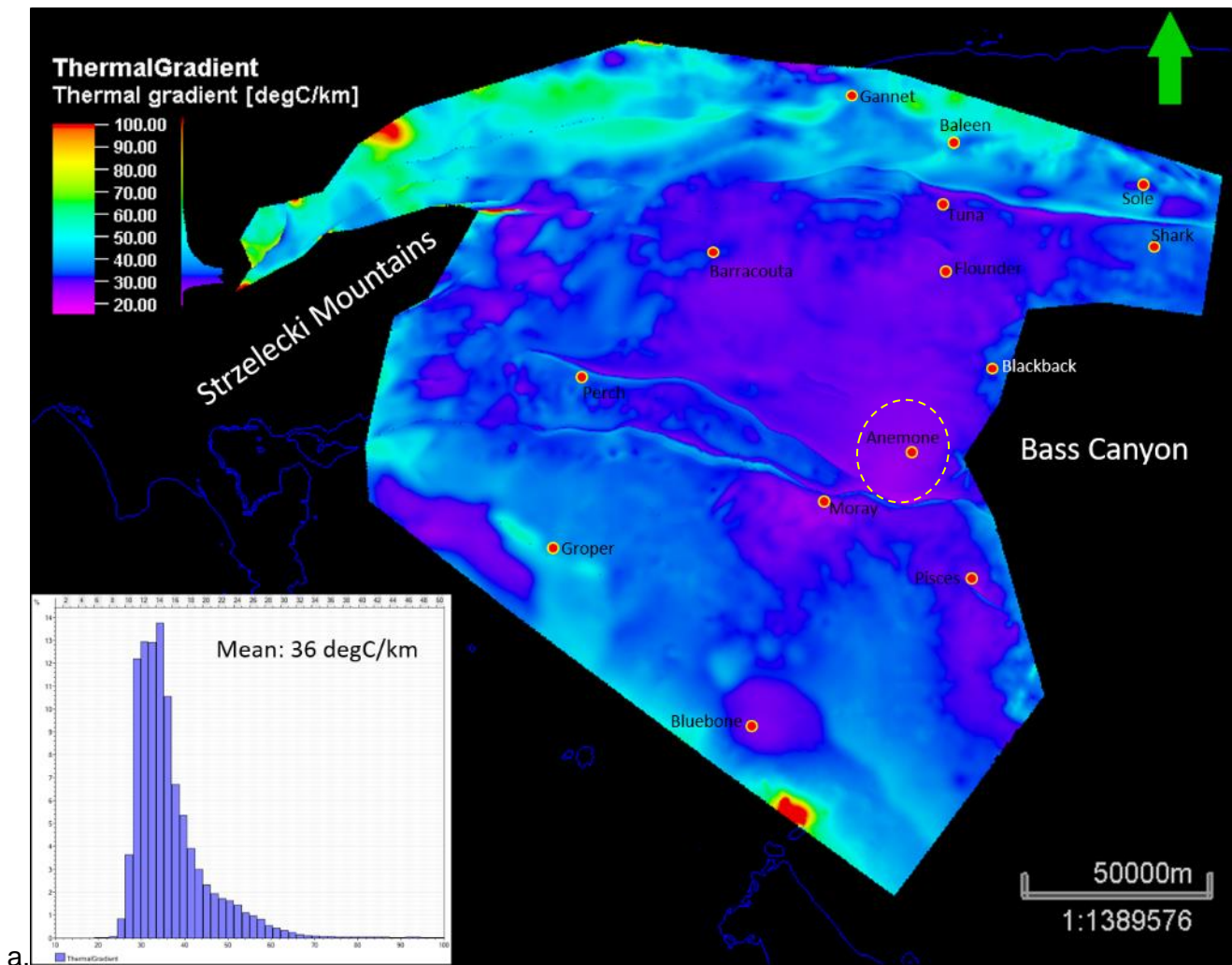


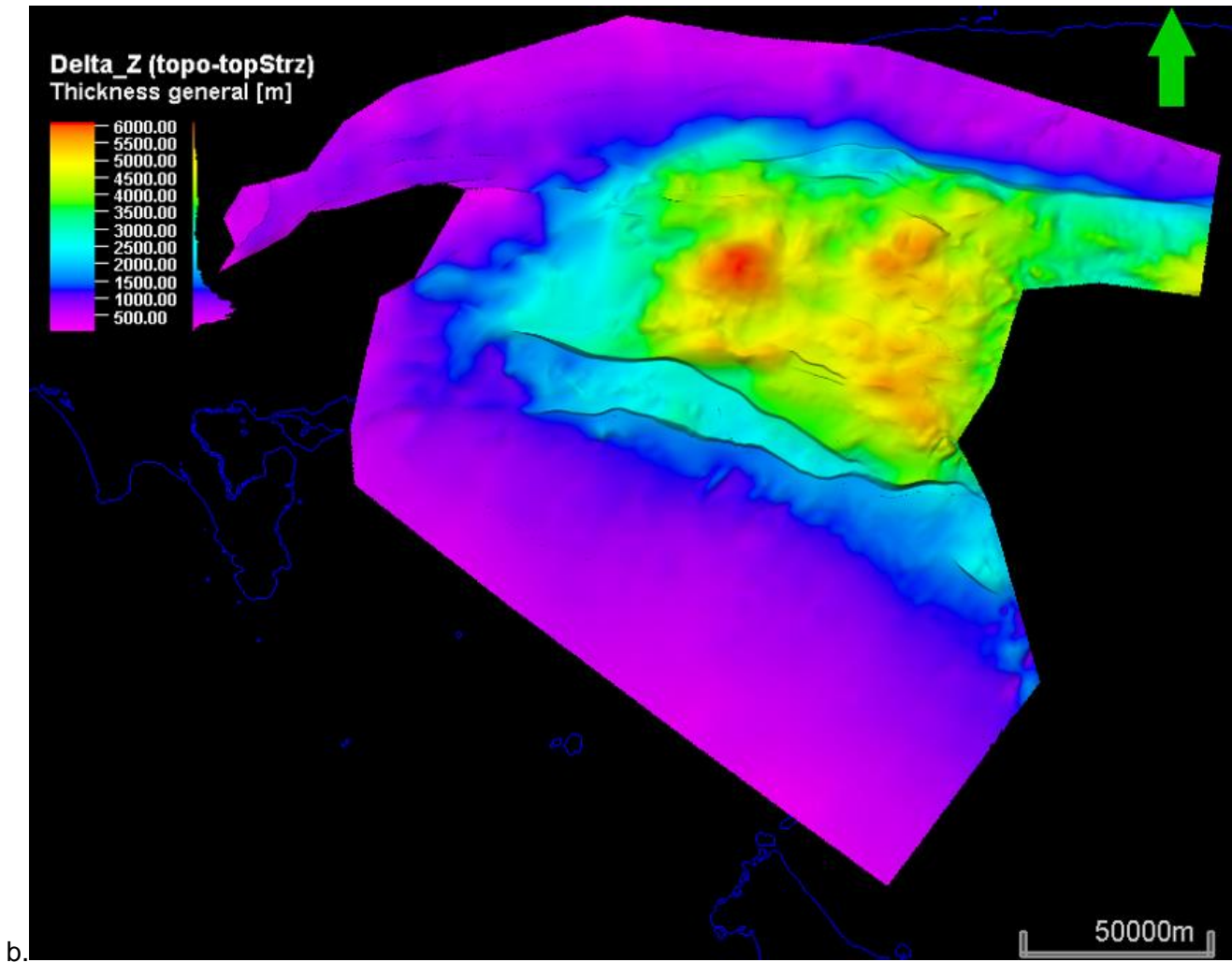
Figure 7-17 Two cross-sections of the Temperature property model. a: SSW-NNE geological cross-section through South Platform, South Terrace, Central Deep (Bream, Cod), North terrace to North Platform; b: west-east cross-section from the Latrobe Valley (Loy Yang), through the Seaspray Depression (Burong) to the Central Deep (Swordfish, Pilotfish) in the east. See Figure 7-16 for the location of section lines.

The thermal gradient map generated from the 3D temperature model shows significant variation in the thermal gradients across the basin from the onshore to offshore areas (Figure 7-18, a). Marked gradient changes are apparent across the major faults, with the gradients decreasing from the high side to the low side, with the difference being up to 12 degC/km across some of the major boundary faults. As expected, the Central Deep is significantly cooler per metres depth than other parts of the basin with thermal gradients of about 30 degC/km. The South Platform and the Seaspray Depression are also relatively cool with typical thermal gradients of about 30-40 degC/km but up to 50 degC/km. In contrast, the north and western parts of the Gippsland Basin including the Latrobe Valley, Lake Wellington depression, Lakes Entrance Platform, North Terrace and North Platform are the hottest regions with typical thermal gradients from 40-50 degC/km and up to 70 degC/km or more.

Clearly, the main control on the geothermal gradient in the Gippsland Basin is the sediment thickness and rate of burial as modelled in Chapter 5 (Figure 7-18, b). Notably, the average thermal gradient

around Anemone (yellow circle) is about 27 degC/km, which is lower than the average thermal gradient in the rest of Central Deep (Figure 7 16). However, the sediment thickness effect cannot fully explain the low thermal gradient in that area.





b.

Figure 7-18 a: Thermal Gradient map, calculated from topography-bathymetry to top Strzelecki group; b: Thickness map, calculated from topography-bathymetry to top Strzelecki group. The area without data control has been removed.

7.2.3 Vitrinite reflectance model (Ro)

Vitrinite reflectance (Ro) indicates the maturation level of the organic matter in a sample (e.g., potential source rock) and is also a good burial-thermal history indicator. A total of 112 petroleum wells and 20 bores have been utilised to build the Vitrinite reflectance model in the Gippsland Basin. The wells and bores provide a good coverage including over the main oil and gas fields (Figure 7-19). The vitrinite reflectance property model mainly uses vitrinite reflectance (Ro) data analysed from core data complemented with some vitrinite reflectance data from cuttings. A surface vitrinite reflectance value of 0.2% has been assigned to the wells to help guide the property model. The upscaled Ro logs are analysed and modelled using the Kriging method.

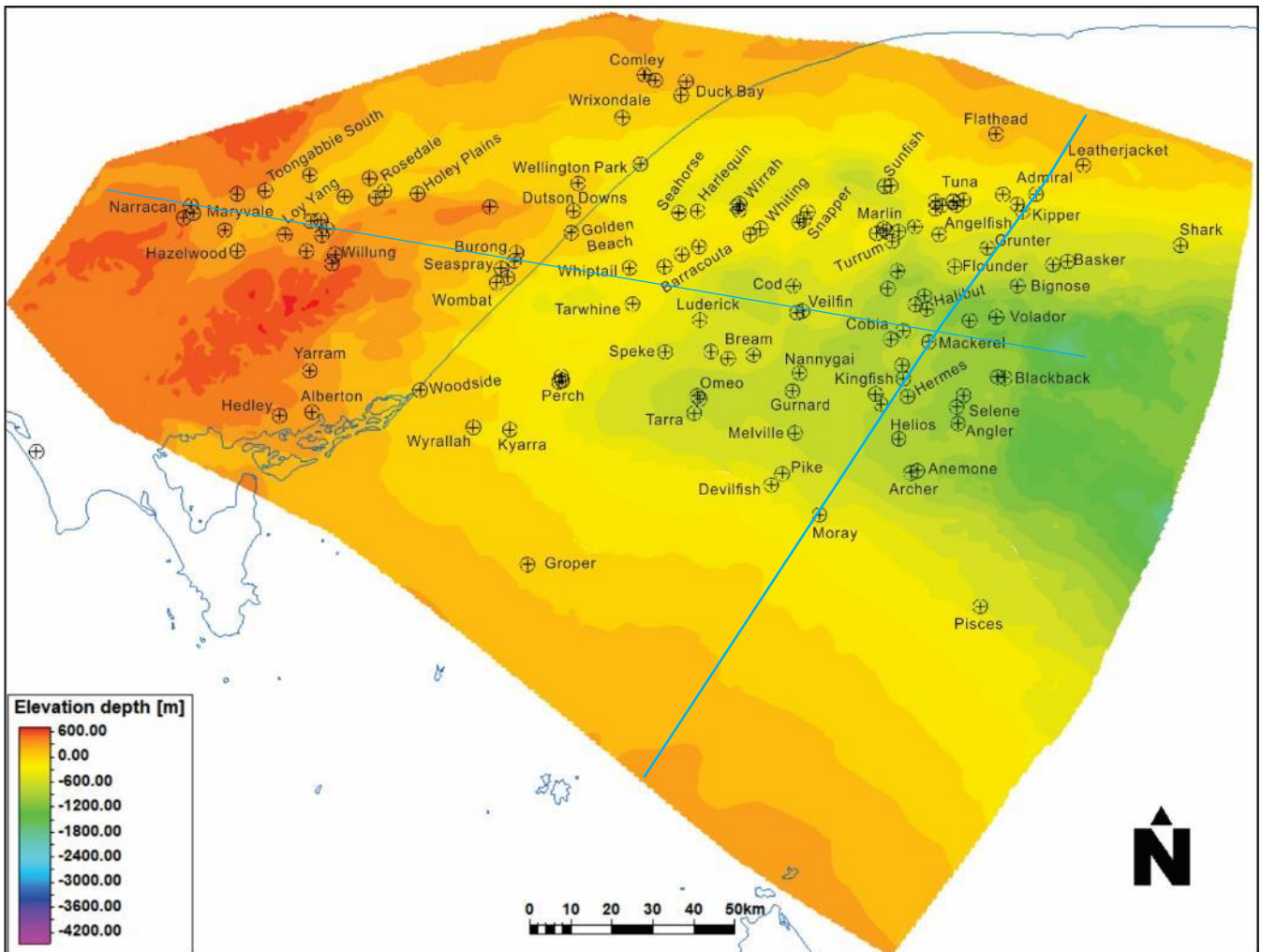


Figure 7-19 Wells with vitrinite reflectance data used to build the vitrinite reflectance model. Background surface is top Traralgon Formation – top Latrobe group, dark blue line is coastline. Light blue lines are the cross-section locations in Figure 7-20.

The property model demonstrates the Ro variation, with the primary control being the absolute depth of burial and temperature. The vitrinite reflectance values in general divide the basin into two regions: the onshore and inshore regions that have not been buried deeply with relatively low Ro values; and the Terraces and Central Deep that have undergone much greater burial where the Ro values are high.

The Onshore areas and the North and South platforms mainly have Holocene to Cobia Group sediments unconformably overlying the Strzelecki Group, with the older Latrobe Group sediments thin or absent. The Ro values in these zones mostly lie in the range from 0.2-0.45% (Table 7-1). The Strzelecki Group sediments jump to much higher Ro values below the unconformity up to 3.0% or in some fault blocks much higher (Holdgate et al., 2015).

The Central Deep and the North and South Terraces where burial has been greater have reached higher Ro values, with the Latrobe Group sediments ranging from Ro values of 0.4% up to about 2.0% in the deeply buried areas. The Strzelecki Group sediments in these areas are mostly beyond drilling

depths and the modelling estimates they typically range from 1.7% to 3.5% towards the base and they may be much higher.

The vitrinite reflectance property model was built based on an approximately linear relationship between R_o and the burial depth but this varies across the basin significantly, indicating different parts of the basin have experienced diverse burial histories and burial rates. Some deep wells show a non-linear trend at greater depths indicating that the rate of R_o increase itself changes with depth of burial (Figure 7-21).

A secondary control is the rate of burial and rate of temperature change. For example, for a given depth R_o is significantly lower on the downthrown side of major growth faults and in the synclines relative to the adjacent structural highs (e.g., upthrown blocks or anticlines) (Figure 7-20). The rate of R_o change with Depth (Z) or the Reflectance Gradient ($\nabla R_o/\nabla Z$) is shown in Figure 7-22 and is comparable to the geothermal gradient.

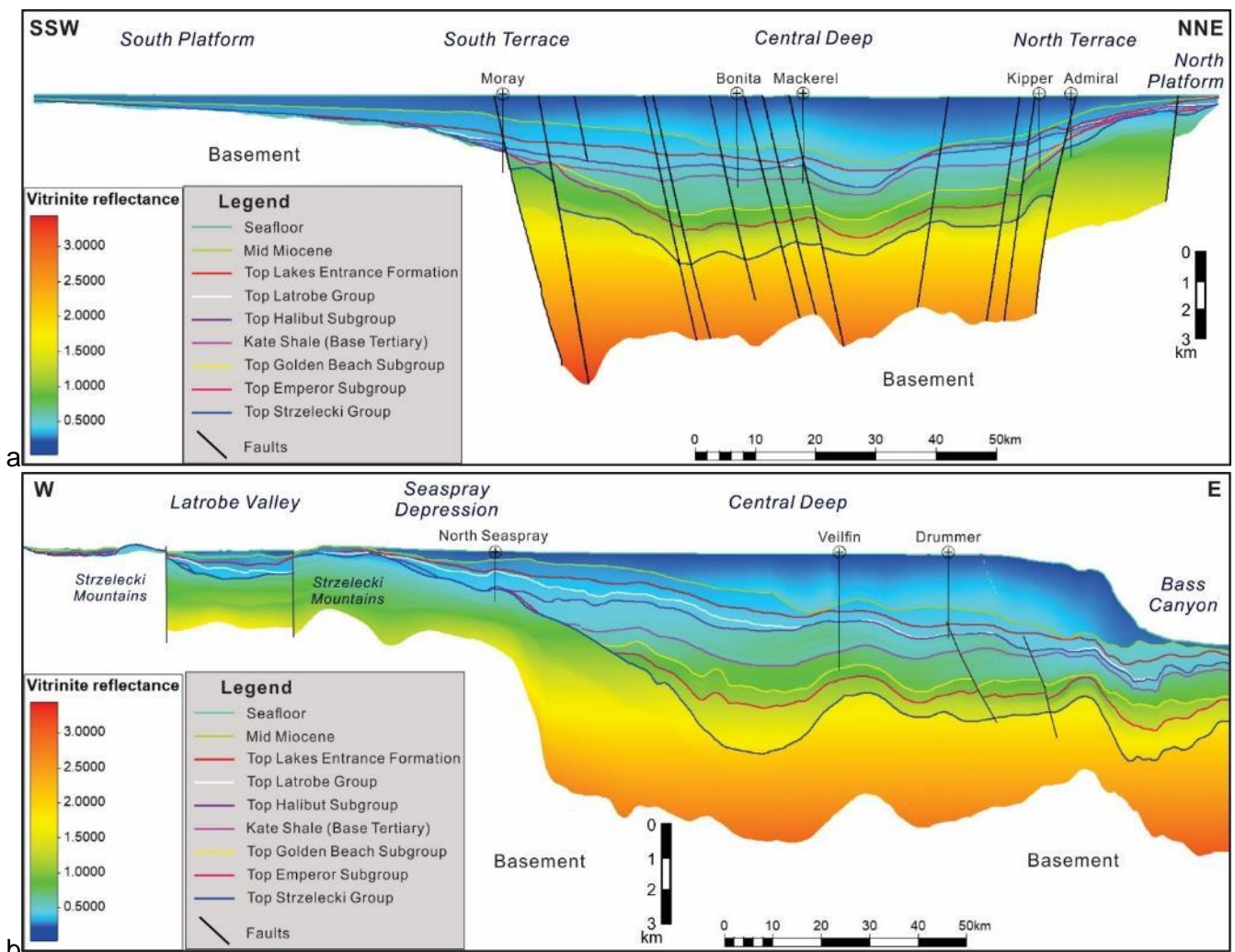


Figure 7-20 Two cross-sections show the Vitrinite reflectance (R_o) property model variation with depth. a: SSW-NNE geological cross-section through South Platform, South Terrace (Moray), Central Deep (Bonita, Mackerel), North Terrace

(Kipper, Admiral) to North Platform; b: west-east cross-section from the Latrobe Valley, through Seaspray Depression (North Seaspray) to the Central Deep (Veilfin, Drummer) in the east. See Figure 7-19 for the location of section lines.

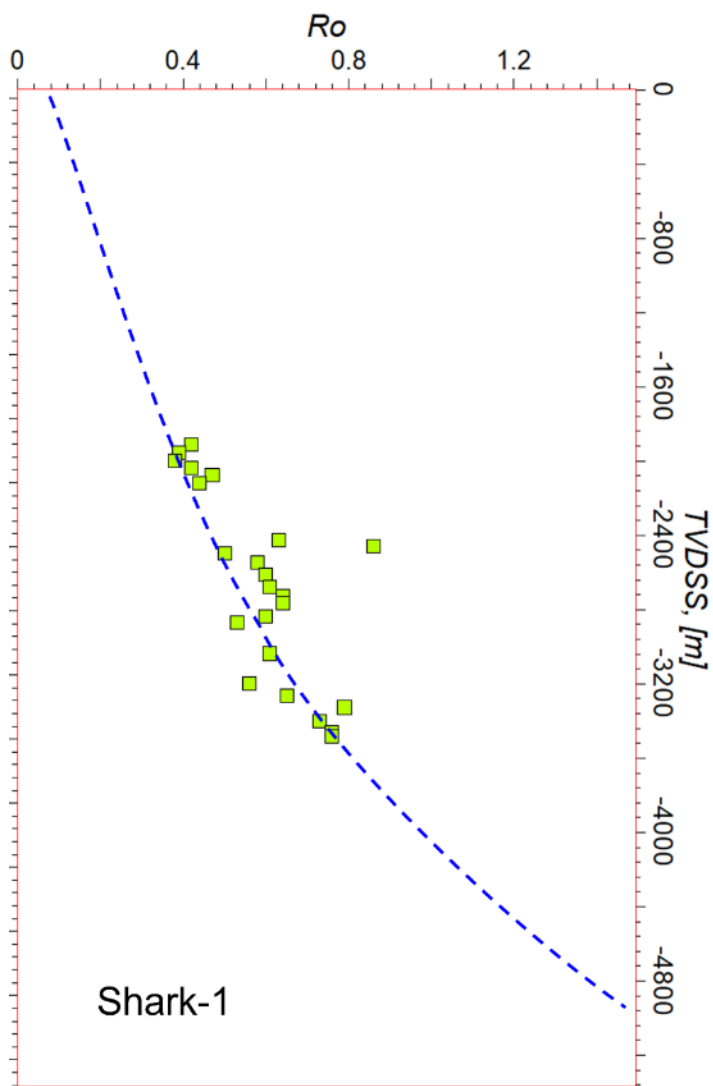


Figure 7-21 Shark-1 vitrinite reflectance values from core samples. Blue dashed line shows the R_o trend.

Table 7-1 Mean Vitrinite Reflectance (R_o) values calculated in different areas for stratigraphic zones.

	Onshore, North and South Platforms	Central Deep, North and South Terraces
Post Mid-Miocene	0.25	0.26
Early-Middle Miocene	0.30	0.36
Lakes Entrance Formation	0.34	0.41
Cobia Subgroup	0.36	0.41
Upper Halibut Subgroup	0.43	0.50
Lower Halibut Subgroup	0.45	0.65
Golden Beach Subgroup	0.54	0.86
Emperor Subgroup	0.69	1.09
Strzelecki Group	0.72	1.87

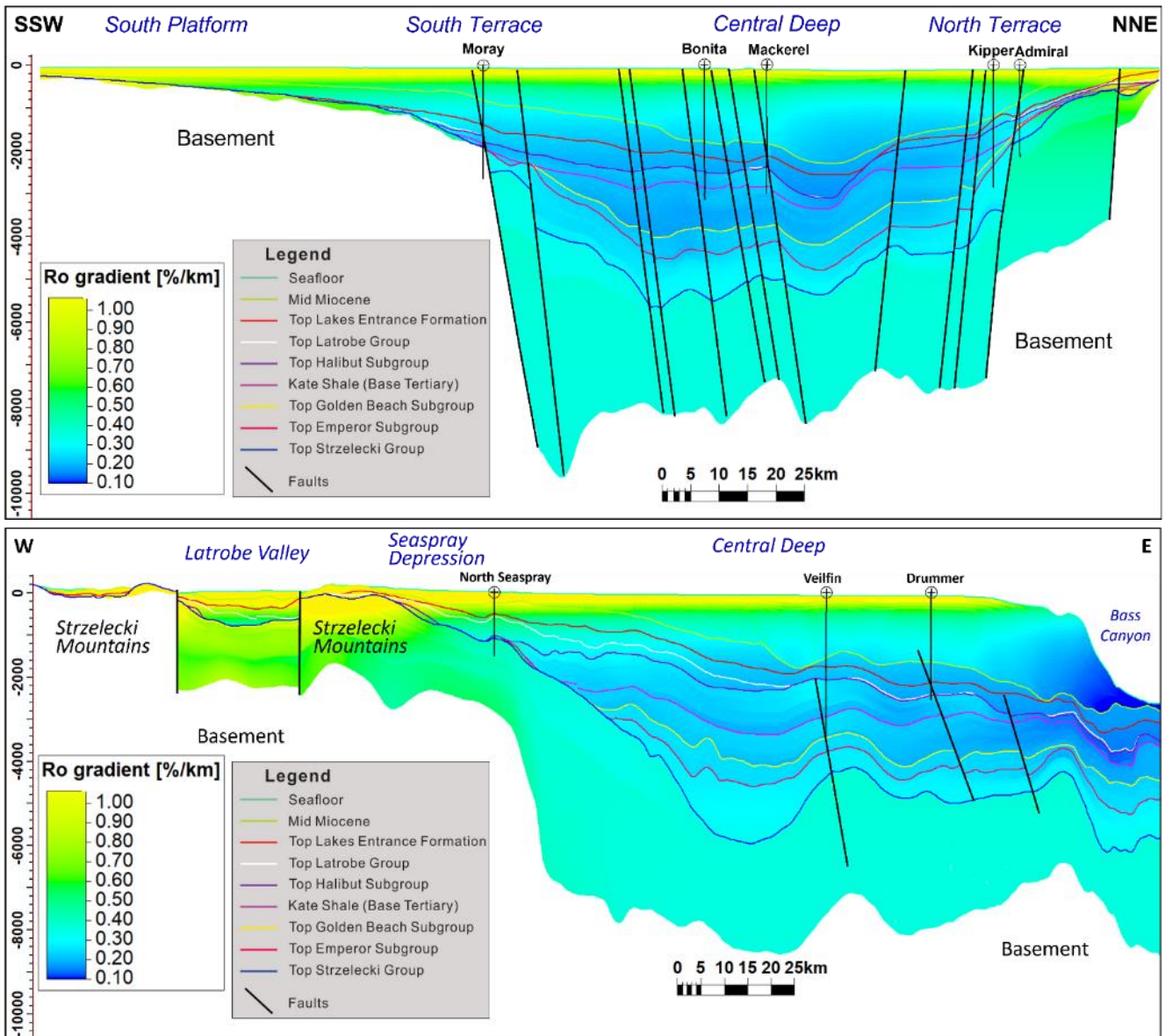


Figure 7-22 Two cross-sections showing Reflectance Gradient with Depth Ro/Z property model. a: SSW-NNE geological cross-section through South Platform, South Terrace (Moray), Central Deep (Bonita, Mackerel), North terrace (Kipper, Admiral) to North Platform; b: west-east cross-section from the Latrobe Valley, through Seaspray Depression (North Seaspray) to the Central Deep (Veilfin, Drummer) in the east. See Figure 7-19 for the location of section lines.

There is no strong control on the Ro values by the age of the strata, as shown in a map of Ro at top Halibut, which shows varying Ro values resulting from different depths of burial (Figure 7-23). This indicates that the age of a formation is not a prime control on Ro, if it was then the Ro values would be the same at the top Halibut Subgroup or for any other formation, instead they change substantially within an age zone (Table 7-1). The burial plot comparison of Bream-5 and Omeo-1 shows that Bream has thicker Latrobe Group sediment deposition with much faster and greater burial than the nearby syncline, whereas Omeo-1 has not undergone as much burial (Figure 7-24). Hence, the burial depth and burial history are critical factors for the vitrinite reflectance evolution in the basin.

Igneous intrusions only have a local effect on the vitrinite reflectance with the localised extra heat increasing the Ro value in addition to the burial process (Figure 7-25). The intrusion effect decreases

quickly away from a single intrusive layer. Hence, these anomalous high Ro values caused by intrusions are removed from the Ro log for the regional modelling.

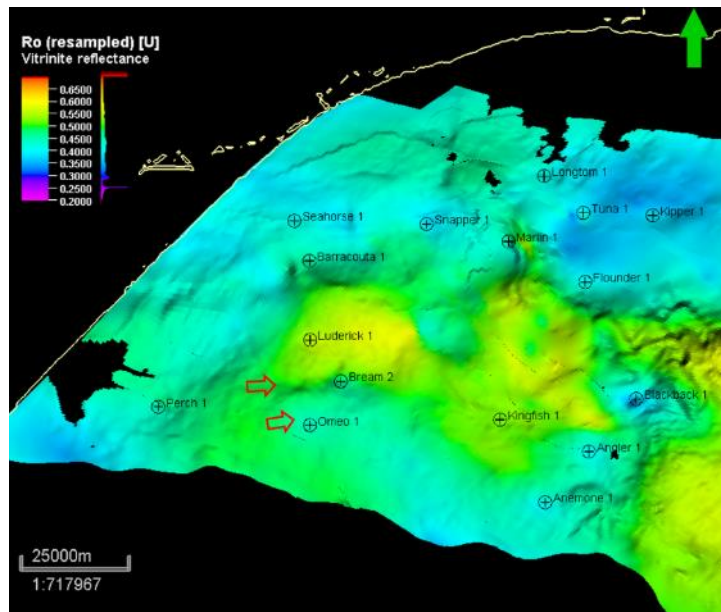


Figure 7-23 Vitrinite reflectance value extracted at top Halibut subgroup, central deep, north and south terraces showing that Ro is not related to the age of the sample (ie. Time).

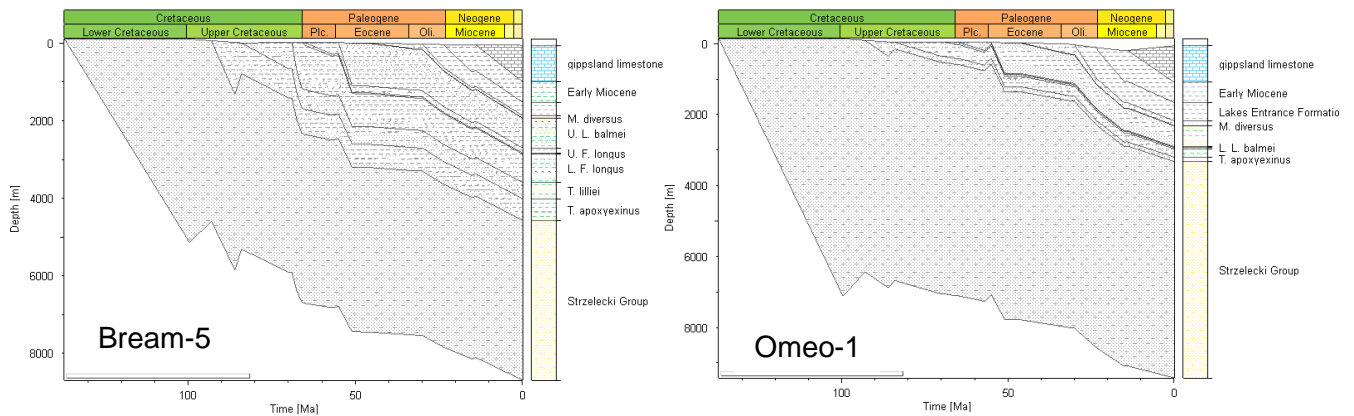


Figure 7-24 Burial plots of well Bream-5 and Omeo-1, extracted from 3D burial and thermal model (See Chapter 8).

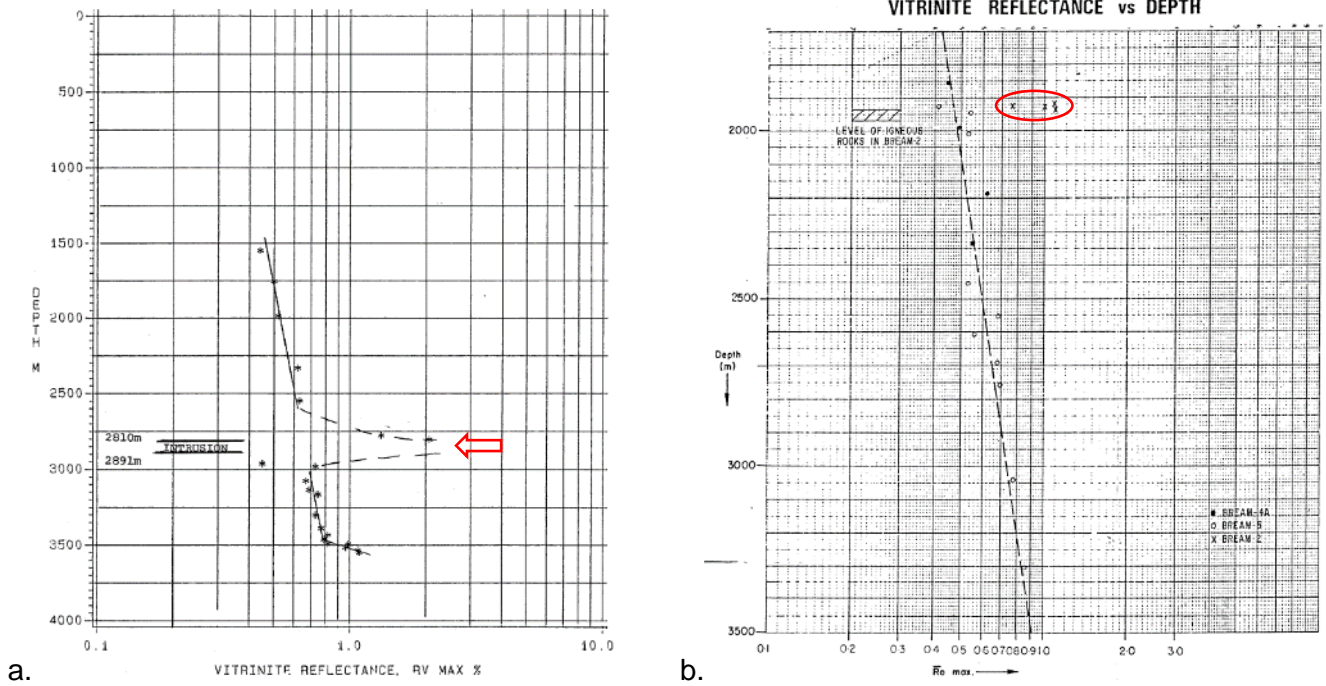


Figure 7-25 Vitrinite reflectance vs Depth chart: a. Whiting-2 (Bostwick, 1986); b. Bream field (Lindsay & Djacic, 1985). The red symbol highlights the outliers of R_o , which are produced by the intrusion.

7.2.4 Pressure model

The pressure property model uses hydrostatic pressure data, which include test results from the drill stem test (DST), formation interval test (FITP), and wireline formation test (WFT). The original pressure data contain outliers caused by gas/oil content within the formation, and the outliers have different gradients to the regional water pressure gradient. Thus, the hydrocarbon pressure data were removed before being input into the model. Over 160 petroleum wells have been utilised to build the hydrostatic pressure property model. The location of the wells is shown in Figure 7-26, which indicates a good coverage of the whole basin.

A surface pressure value has been added to the pressure log for each well. The surface pressure value is calculated using the seawater pressure gradient ($\nabla p = 0.465$ psi/ft, for a typical Gulf coast water gradient) and surface depth value $Pressure = \nabla p \times Depth$. Then, the new pressure log is resampled at a 0.5 metre interval. The resampled pressure logs have been upscaled, data analysed, and modelled using the Kriging method.

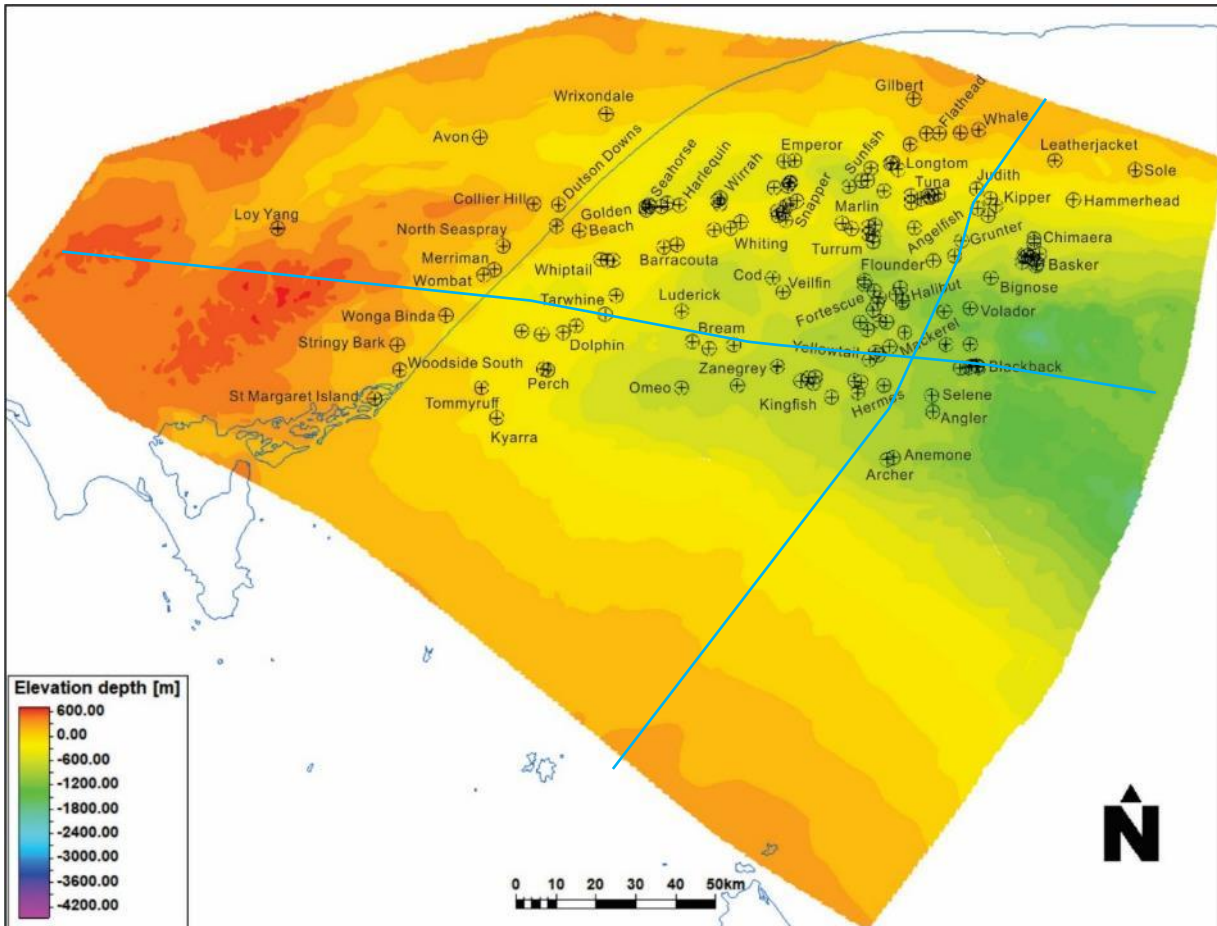


Figure 7-26 Wells with pressure log, which have been used to build the pressure model. Background surface is top Traralgon Formation – top Latrobe group, dark blue line is coastline. Light blue lines are the location of Figure 7-27.

The hydrostatic pressure property model indicates a linear function between the pressure and depth as expected. The pressure gradient across the entire basin is relatively even showing normal pressures. Regionally the structure has no significant effect which implies good pressure communication that has equilibrated with time (Figure 7-27). The model doesn't show obvious overpressure in the Gippsland Basin and this is consistent with known drilling conditions in most formations with only slight pressure buildup in the Seaspray Group before entering the Latrobe Group. Locally, exceptions can occur where entering a hydrocarbon trap or in isolated thin sands deep within the Latrobe Group. Pressure changes with burial over time are modelled in *PetroMod* (Chapter 8).

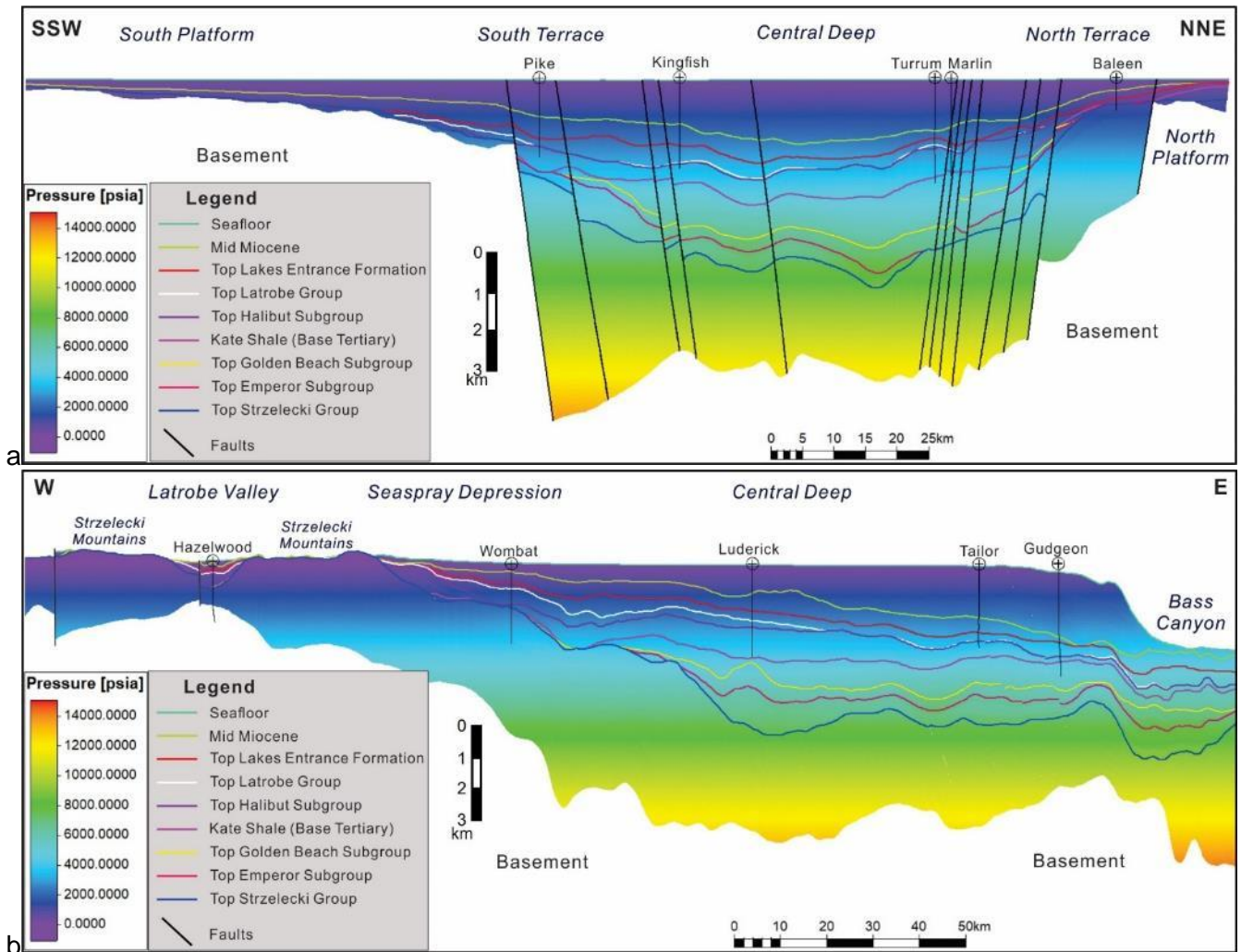


Figure 7-27 Two cross-sections showing the Pressure property model. a: SSW-NNE geological cross-section through South Platform, South Terrace (Pike), Central Deep (Kingfish, Marlin), North Terrace (Baleen) to North Platform; b: west-east cross-section from the Latrobe Valley (Hazelwood), through the Seaspray Depression (Wombat) to the Central Deep (Luderick, Gudgeon) in the east. See Figure 7-26 Figure 7-16 for the location of section lines.

7.3 Realistic model input data for Thermal Modelling

One of the key aims of this research is to utilise empirical data to constrain and guide the theoretical modelling. The property models built in *Petrel* allow generation of a simpler 3D model, properties and several maps that can be used as input data for the *PetroMod* theoretical modelling.

7.3.1 Simple 3D grid

Building a detailed 3D burial-thermal model in *PetroMod* requires a lot of information, including chronostratigraphic data, depth maps of each horizon, fault systems, time maps (palaeo-water depth maps), lithofacies definition, facies maps and source rock geochemical properties (e.g., TOC, HI etc.). The Schlumberger software *Petrel* and *PetroMod* can be linked and this allows porting of much of the required data directly from the *Petrel* models to *PetroMod*. However, *PetroMod* cannot handle complex

grids so the detailed 3D grid model in *Petrel* was converted into a simple 3D grid depth model in *Petrel* into which were inserted the required properties ready for the 3D burial-thermal modelling.

The simple grid model is built using depth maps in a 500*500 metres grid. Ten depth maps were used to build the simple grid: Topography - Bathymetry, Mid Miocene, top Lakes Entrance Formation, top Latrobe Group, top Halibut Subgroup, Kate Shale, top Golden Beach Subgroup, top Emperor Subgroup, top Strzelecki Group and top Basement. In the 'Make zones' process, the Halibut Subgroup is further divided into the Flounder Formation, Kingfish Formation and Barracouta-Mackerel Formation. The Volador Formation was added and refined the zone between the Kate shale and the top Golden Beach Subgroup. All these depth maps were generated from the entire Gippsland Structural-stratigraphic model and tied to the well tops. The layering process is consistent with the detail required by the burial-thermal modelling and produces 172 layers in total with about 80-100 metres vertical resolution producing a very large model.

The facies table for the petroleum system model requires a more detailed lithological definition for different lithofacies at each of the stratigraphic levels. The previous simple lithology template is refined based on formation units and selected kinetics information for the different types of potential source rocks. Overall, 46 different lithofacies were defined and represent the different sediment types in each formation. These lithofacies determine other parameters such as thermal conductivity, radiogenic elements, heat capacity and mechanical properties.

Once the simple grid populated with the property models is complete, the 'Exploration Geology' module in *Petrel* is used as the bridge to link *Petrel* and *PetroMod*. A 3D petroleum system model is made via the 'Make 3D petroleum systems model' process for export into *PetroMod*. The 3D simple grid model thereby provides the horizons and properties including the facies, TOC, HI in this process. The fault history table utilises all the faults from the pillar gridding structural-stratigraphic model. The palaeo-water depth maps and erosion maps are also assigned to the model. At this point, the 3D model is ready to export to *PetroMod* to simulate the heat flow and burial-thermal history. For more details, please see Chapter 8. Further details of the important facies and property models used by *PetroMod* are described below.

7.3.2 Facies model

The facies property model used a similar process as the previous facies model:

- Scale-up well log: use 'Most of' average method with facies weighted at individual zone level.
- Data analysis: use proportional weighting, analyze facies log for each zone, fit the proportion curves to the histogram.
- Facies modelling: use the same settings as for the full Gippsland facies model (see 7.2.1 Facies model).
- Change facies template: use property index filter and property calculator to change simpler lithology template to more detailed lithology template.

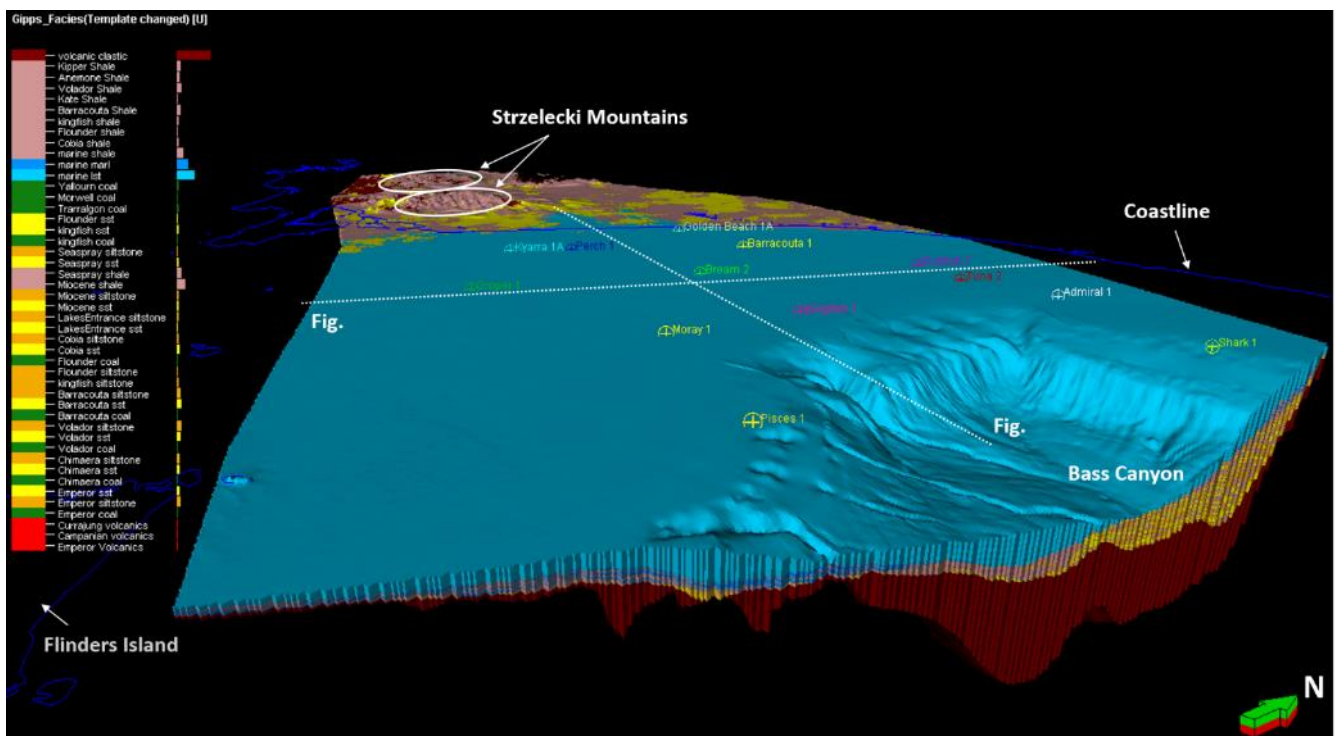


Figure 7-28. The refined lithofacies property model for the entire Gippsland Basin.

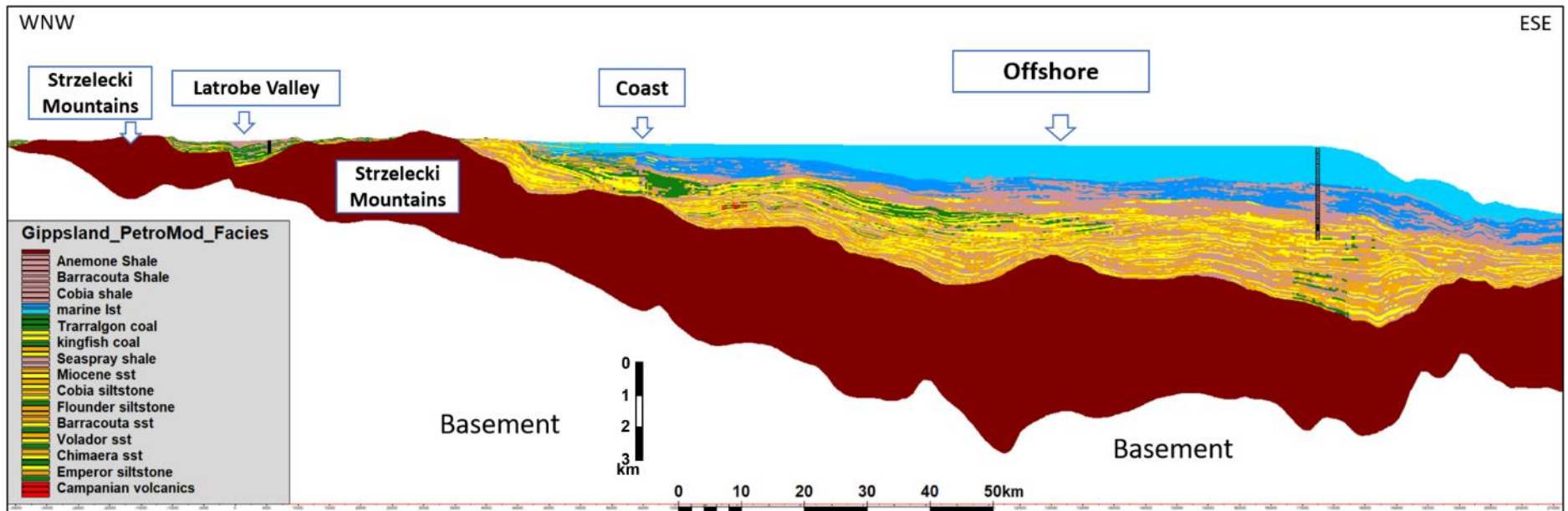


Figure 7-29 A cross-section reveals the facies property through the basin from WNW-ESE direction and crosses Strzelecki Mountains, Latrobe Valley, near shore, broad offshore and Bass Canyon. Location shows in Figure 7-28.

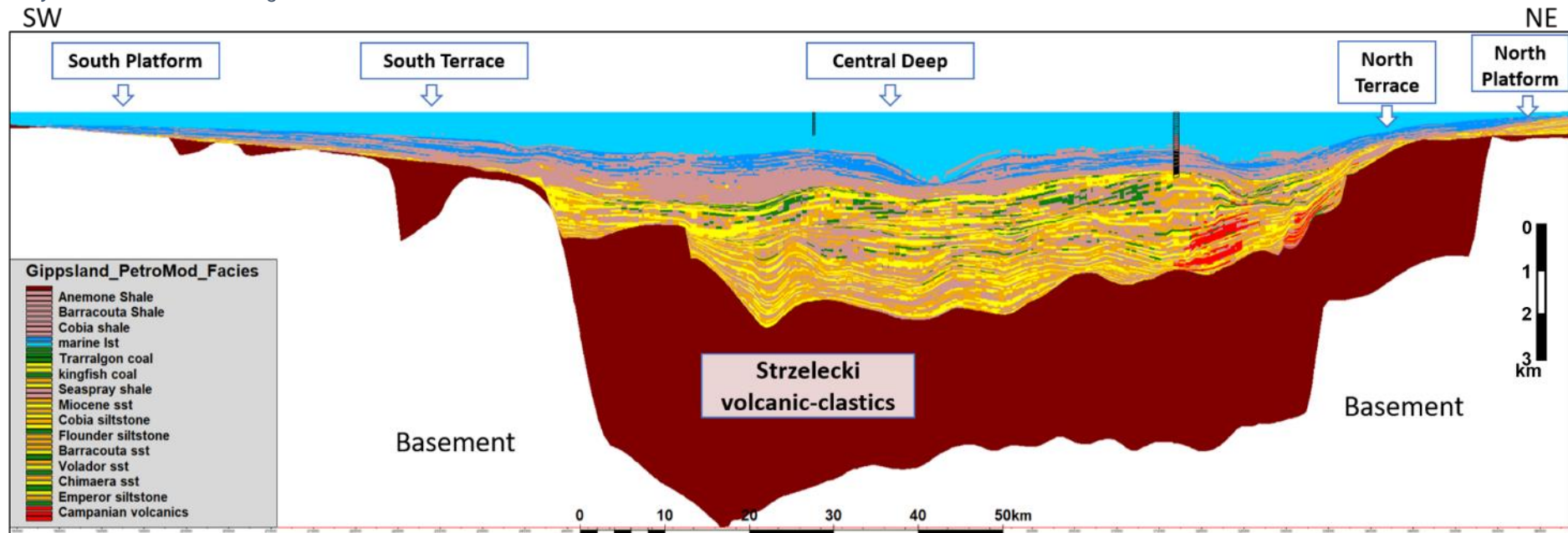


Figure 7-30 A cross-section reveals the facies property through the basin from SW-NE direction and crosses South Platform, South Terrace, Central Deep, North Terrace and North Platform. Location shows in Figure 7-28.

7.3.3 Total Organic Content (TOC)

The Total Organic Content (TOC) property helps to identify organic-rich intervals within each stratigraphic level and indicates units with source rock potential. The TOC values are mostly measured in samples from rocks thought to have potential for high organic contents, such as coal, shale, and organic-rich carbonates. In the Gippsland Basin, the Seaspray Group carbonate rocks are mainly cold-water carbonates, mostly lacking organics and primarily act as sealing packages in the petroleum system. The primary potential source rocks in the Gippsland Basin are fine-grained clastic rocks within the Latrobe Group and coaly sediments and consequently most of the TOC analyses are on these samples. The organic sediments in the Strzelecki Group are not considered here since they are too deep to be potential source rocks for the main oil and gas fields in the offshore Gippsland Basin though they may be relevant for onshore and inshore traps. Since lithofacies is the main control on the organic matter content in the sediments, the TOC property model is guided by the lithofacies property model.

The TOC property modelling processes consist of three steps:

- Scale-up TOC well logs: use 'Arithmetic' average method.
- Data analysis: use appropriate transformations (e.g., input truncation, normal score and Beta distribution) to analyse coal and shale for each zone to get the range and distribution. For other lithology types (e.g., sandstone, siltstone, limestone etc.), turn off zone separation and analyse based on individual lithology only.
- Petrophysical modelling: model each zone with facies control, using Gaussian random function simulation, variogram settings use those calculated for the full basin structure and facies models in the previous data analysis given in Chapter 4.

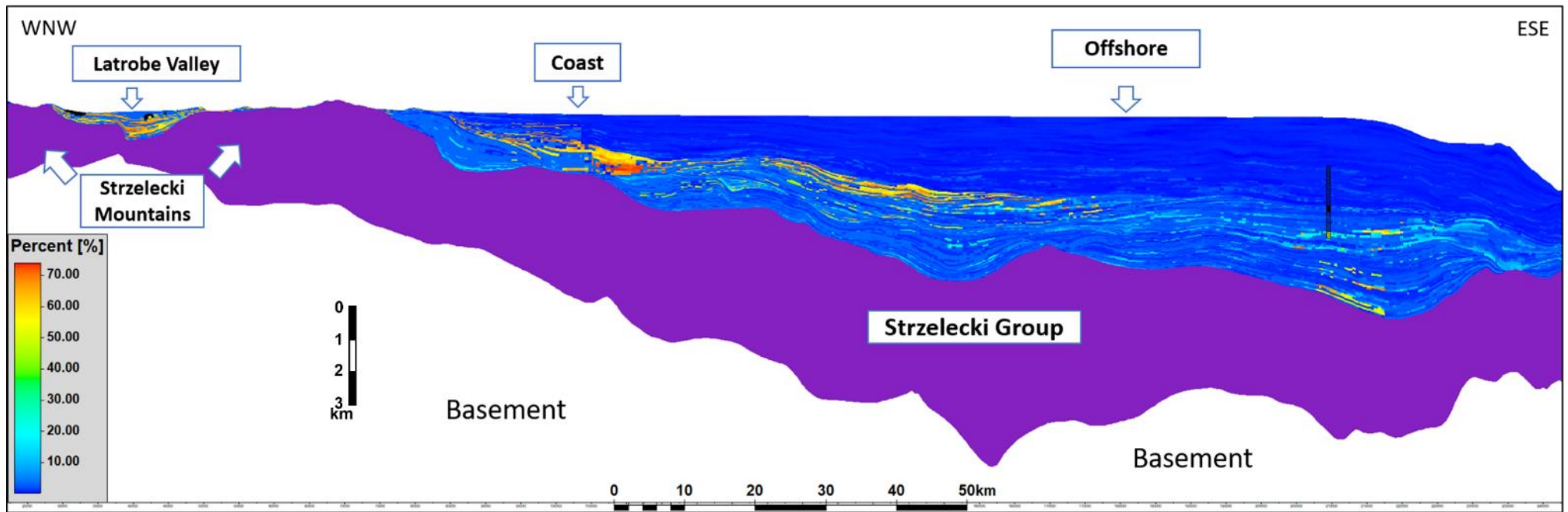


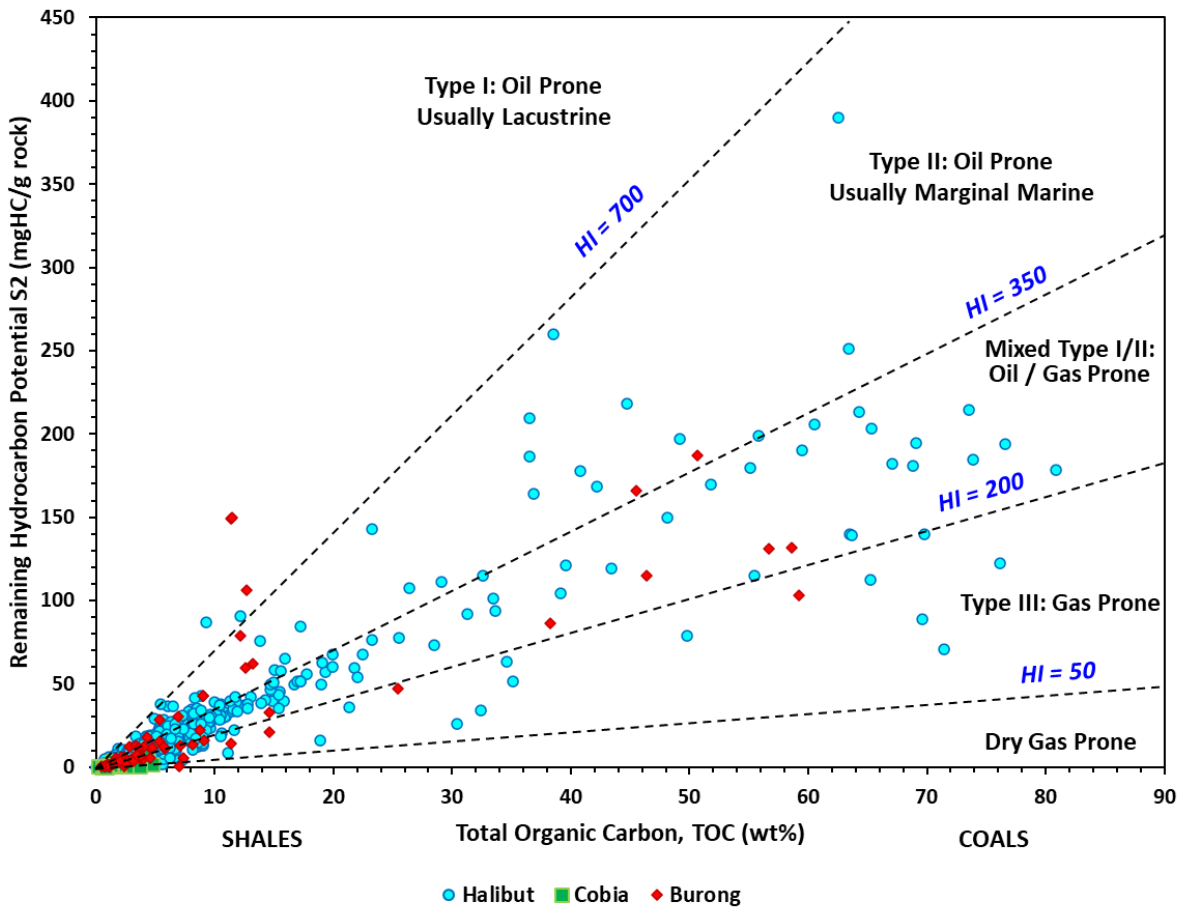
Figure 7-31 A cross-section showing the TOC value, same section as Figure 7-29. Location shows in Figure 7-28.

The highest TOC values occur in the coal seams in the Latrobe Valley and upper Latrobe Group (Cobia and Halibut subgroups) as shown in Figure 7-31 correspond to the coal seams in Figure 7-29. The Latrobe Valley thick coals are comprised of coal lithotypes that include dark and medium dark vitrains, medium light and light clarains and pale cannel coals. Typically, the dark lithotypes have low S₂ values (~70 mg/g) and Hydrogen Indices (~100 mg/g) which increase in the light and pale lithotypes to high S₂ values (~150-250 mg/g) and high Hydrogen Indices (~300-400 mg/g) (Verheyen et al., 1984). Although the Latrobe Valley coals have not been sufficiently buried to be mature, similar coal lithotypes occur in the Cobia and Halibut Sub-groups offshore where they are buried sufficiently to be in the oil window and have high potential for hydrocarbon generation (Figure 7-32). These formations also contain interbedded organic rich shales with TOC values much >2% varying from coaly shales to lower coastal plain liptinite rich oil shales including lamalginites (Figure 7-32). The TOC property model suggests localised high TOC values in the lower Latrobe Group (Golden Beach and Emperor subgroups), mainly shales around Tuna, Kipper, Grunter and Angelfish near the North Terrace, though this may result from more wells intersecting these units in those areas (Figure 7-32).

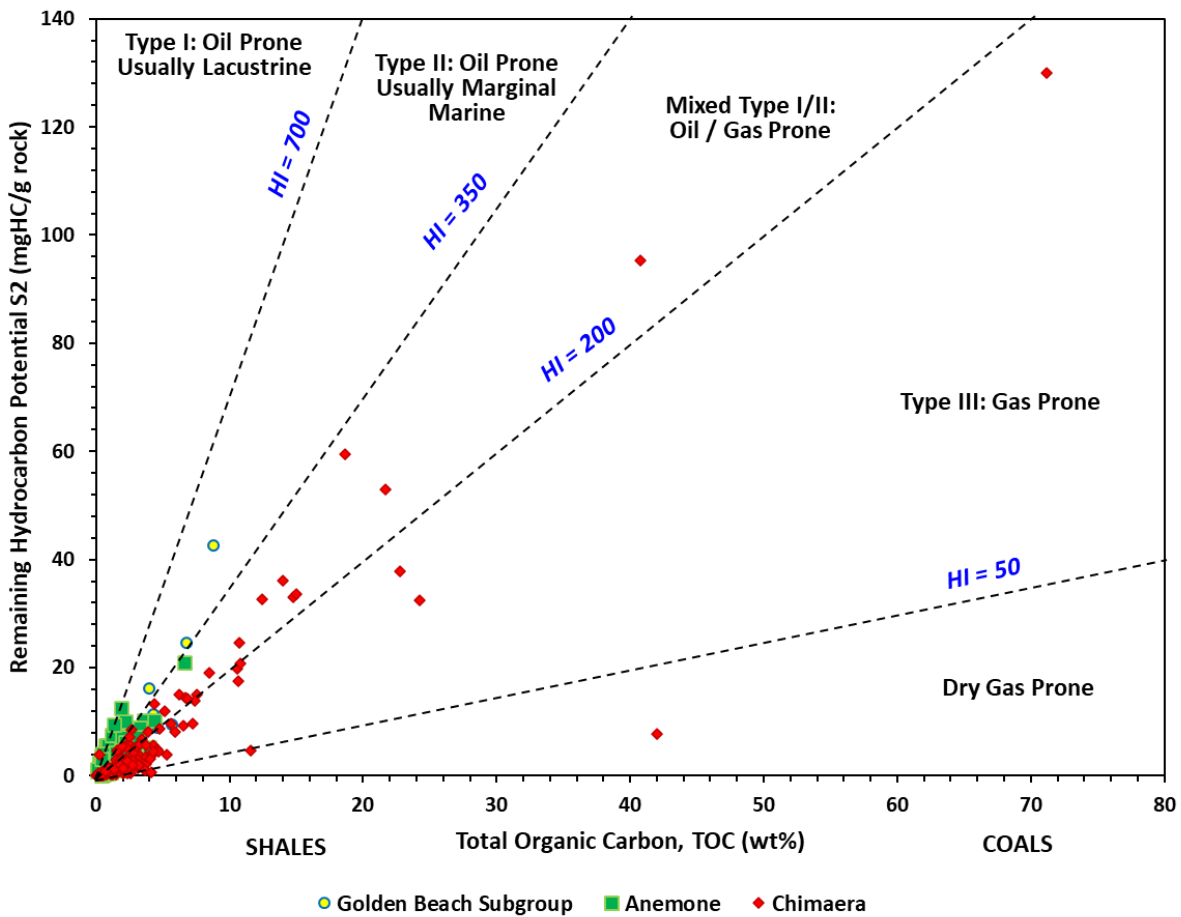
The Golden Beach Subgroup mainly contains organic rich shales in the non-marine to marginal marine Chimaera Formation. This includes some shales with high TOC and Type I/II, II and III organic matter with good potential for hydrocarbon generation (Figure 7-32). The marine Anemone Formation has less sample analyses and from the results it appears to have lower potential for hydrocarbon generation.

The Emperor Subgroup has very few samples, and only a few organic rich samples with high liptinite contents have been sampled, which are discussed further in the next section.

Kerogen Quality Cobia – Halibut Subgroups



Kerogen Quality Golden Beach Subgroup



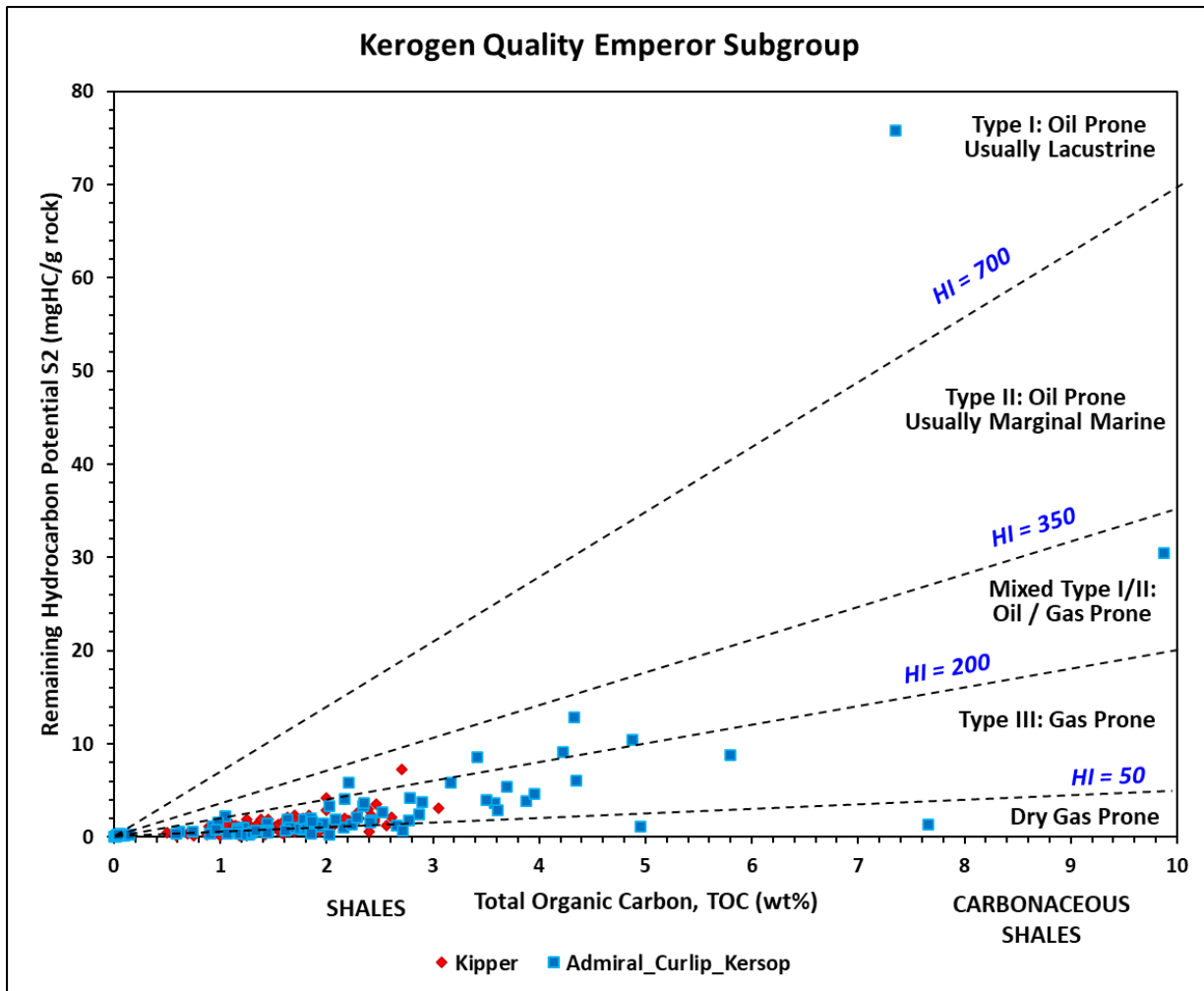


Figure 7-32 Hydrocarbon Potential plots of S2 versus Total Organic Carbon from RockEval analyses for the main stratigraphic zones. Note, the very different amounts of organic matter in the coals relative to the shales requires use of different scales for the three main stratigraphic sub-groups

7.3.4 Hydrogen Index (HI)

The Hydrogen Index (HI) is calculated from Rock-Eval data ($HI = S2/TOC \times 100$) and is used as an organic matter type indicator normalised to the amount of TOC. The HI value is available in a large number of organic rich samples for which there are Rock-Eval TOC measurements in the Gippsland Basin.

The HI property modelling process consists of three steps (scale-up logs, data analysis, petrophysical modelling) as described above in detail for the TOC property modelling. A long dip cross-section through the HI model shows that some high values occur mainly in the Cobia and Halibut Subgroups (Figure 7-33).

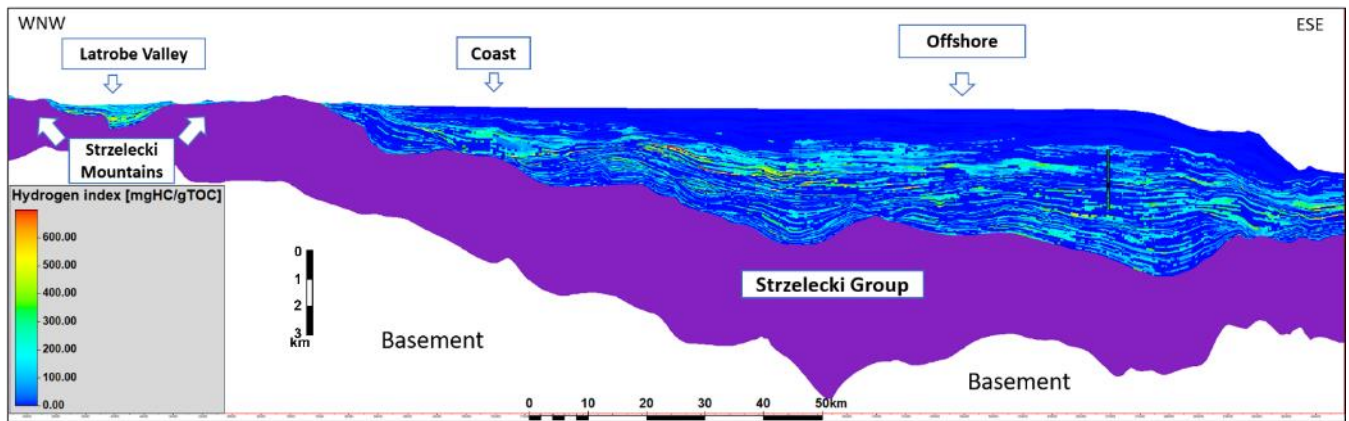


Figure 7-33 A cross-section shows the HI value, exact location as Figure 7-29. Location shows in Figure 7-28.

The plots of HI versus OI show how the organic matter type varies between the main stratigraphic groups (Figure 7-34). The spread of the HI values in each of the stratigraphic groups is shown in the histograms (Figure 7-35).

Most of the Seaspray Group comprises shelf marls and limestones and the organic content is very lean with TOC values <2% and HI values of <100 mgHC/gTOC. Also, RockEval data is not reliable at these low TOC values due to the dilution effect.

In contrast, the Latrobe Valley coals and associated lacustrine shales have high TOC of 60-70% or more, with HI values mostly from 100 to 300 mgHC/gTOC but up to 600mgHC/gTOC in some coal lithotypes.

The Cobia Subgroup sediments also contain perhydrous coals with HI values mostly ranging from 250 – 600 mgHC/gTOC and low Oxygen Index (OI) values (Figure 7-34 and Figure 7-35). This suggests a coastal plain depositional environment with swamps, marshes and back barrier lagoons which matches the paleo-environment history. The associated shales have a wide range of HI values, from very low TOC shales with HI values up to 200 mgHC/gTOC, to high TOC shales having HI values up to 450 mgHC/gTOC. The coals and shales in the Halibut Subgroup are in general not as organic rich and have lower HI values, consistent with their more upper delta plain environments of deposition.

The Golden Beach Subgroup mainly comprises shales with mixed Type II/III and Type I organic matter with TOC mostly <10%, but with some up to 25%, and HI values mostly in the 50-300 range but up to 600 mgHC/gTOC. Coals are not common but have similar values to the shales.

The wells that drilled into Emperor Subgroup and Kipper Shale are mainly located on the Terrace and Platform areas around the basin edge and there is a lack of information for the Emperor Subgroup in

the Central Deep area. Most of the samples have TOC values <10% and HI values in the range 50-300 mgHC/gTOC and represent Type II/III mixed facies. However, the petrographic analysis of side wall cores in the Shark-1 well demonstrates that common Botryococcus spp. related telalginite existed in the Emperor Subgroup and some RockEval samples also had very high HI (Table 7 2), both of which support the probable occurrence of Type 1 or Type II/III mixed facies organic matter (Figure 7-34 and Figure 7-35). That would indicate fresh water lacustrine environments, which is consistent with the *Badlands* simulations that model a shallow inland water system during its formation (Chapter 6).

Table 7-2 The Rock-Eval interpretation of the Emperor Subgroup Shale sample

Parameter	Sample Value	Interpretation (Tissot and Welte, 1978; Kaye, 2006)
TOC (Wgt%)	7.35	>5.0, Excellent
Tmax (degC)	431	430-442, Early Mature (oil window)
S1 (mg/g)	0.46	0-0.5, Poor free oil yield
S2 (mg/g)	75.81	>20, Excellent source rock potential
S1+S2 (mg/g)	76.27	>6, Good to Excellent genetic potential
HI (mgHC/gTOC)	1031	>600, Type I (oil), Stratified Lacustrine environment

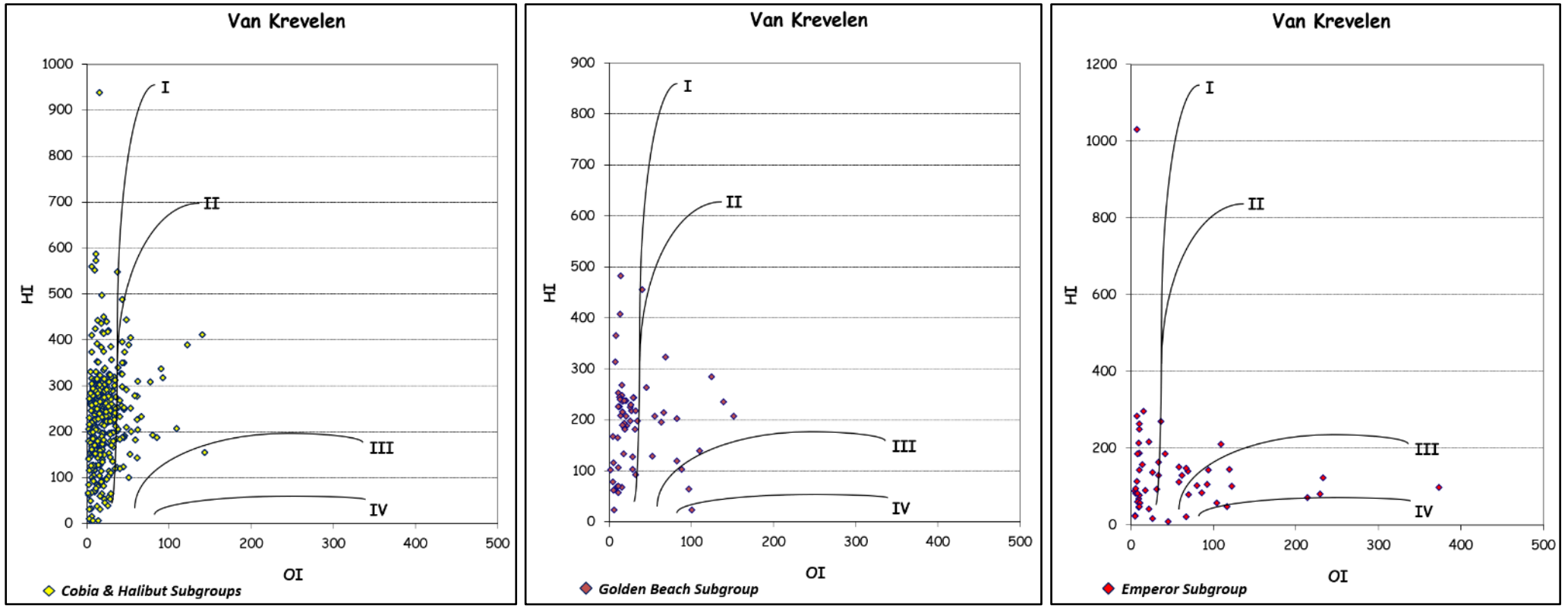
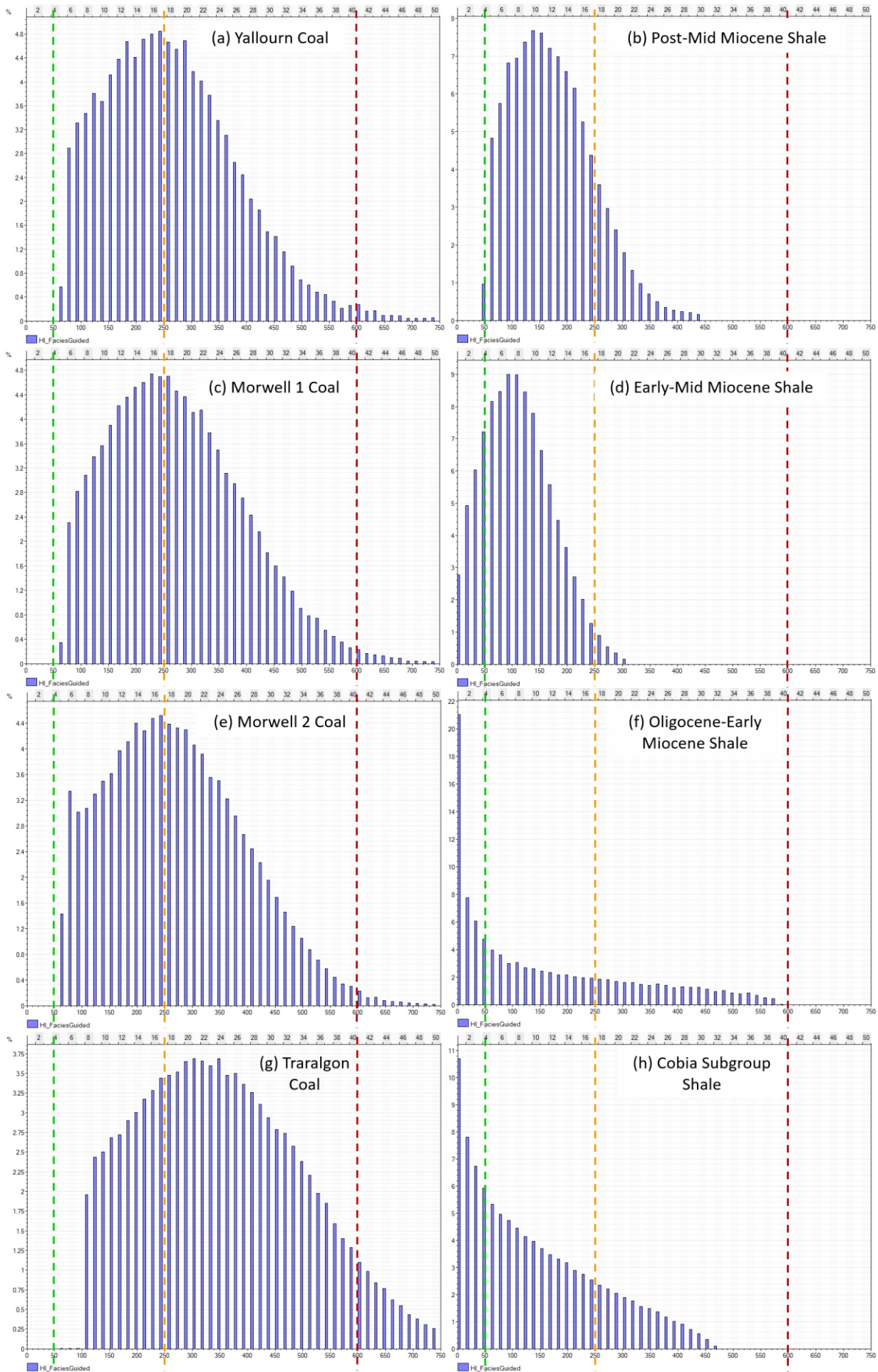


Figure 7-34 Plot of HI versus OI values for samples from the main geo-zones in the Gippsland Basin.



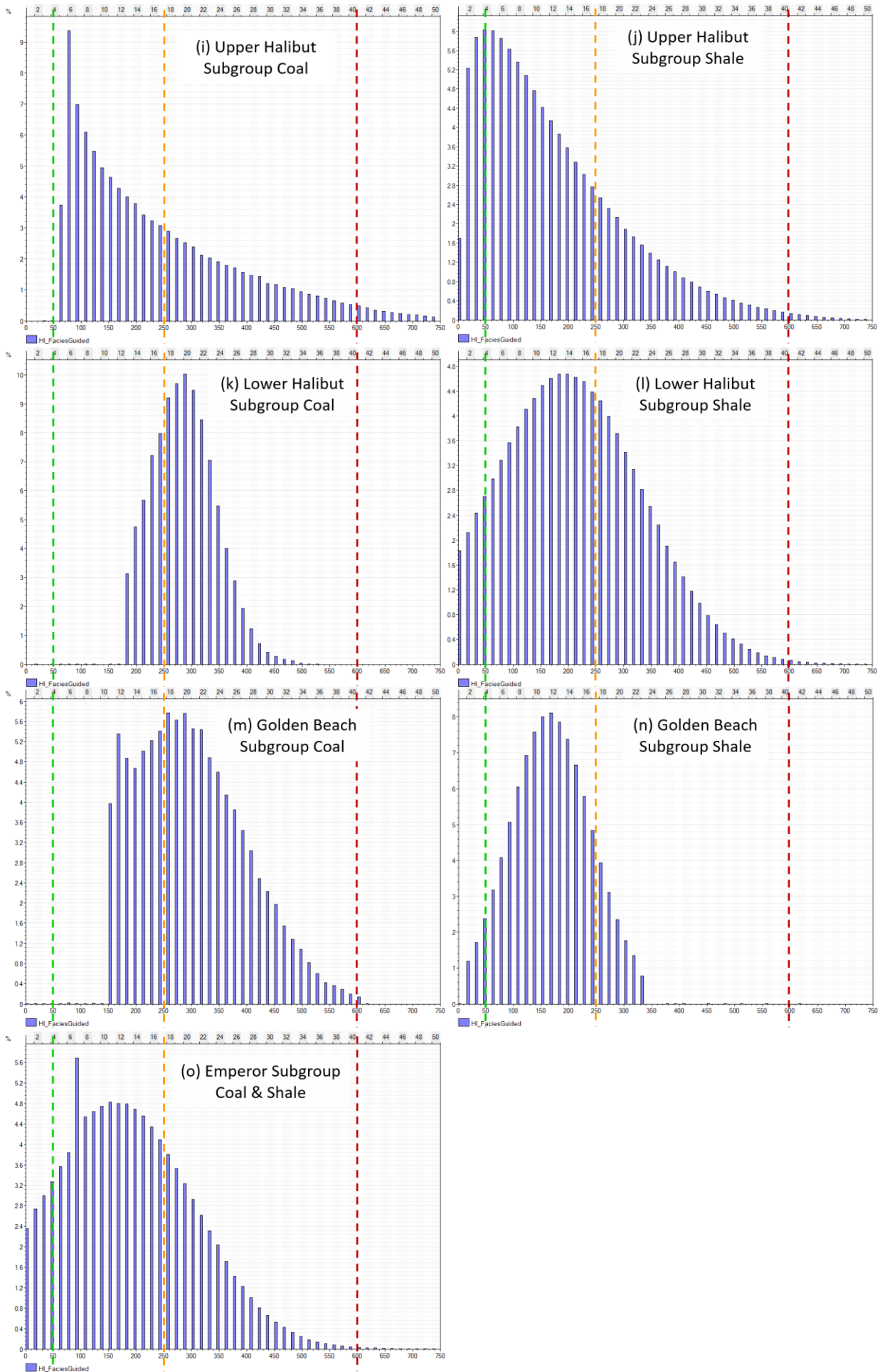


Figure 7-35 Histogram of HI for each lithofacies in the main geo-zones. The green, yellow, and red dashed lines represent the HI value of 50, 250 and 600 mgHC/gTOC.

Chapter 8. 3D Burial History Model

A series of 1D, 2D, and 3D burial history models of the onshore and offshore Gippsland Basin has been used to recreate the burial-thermal history from the Early Cretaceous to present using *PetroMod* (Schlumberger software). The models are calibrated to a corresponding full 3D realistic structural, stratigraphic and property model of the basin built in *Petrel* that is used to constrain the sedimentary, stratigraphic, burial and thermal histories. The burial and thermal models allow estimation and mapping of the burial, uplift, erosion and thermal histories, and testing of palaeo heat flow values. The analysis of the best fit models of heat flow in the Gippsland Basin allows testing of the extent to which models such as the McKenzie's uniform pure shear extension model fit the observations made in the basin. The results of the 3D burial history models are important for understanding hydrocarbon generation history and have highlighted potential mature source rocks, including previously unrecognised occurrences.

8.1 Workflow

Extensive geological datasets were used to build a realistic 3D structural and stratigraphic property model in *Petrel*, based on 2D and 3D seismic data, more than 200 onshore and offshore wells with logs, analytical and bio-stratigraphic data, and interpreted gravity data (open-source data from Geoscience Australia, NOPIMS and Victoria Earth Resources websites). There is a noticeable difference in the density of the data between the northern part of the basin where coverage is good and the southern part where data is more sparse. Key depth maps and fault frameworks were extracted from the realistic model and used to constrain the depth and age simulations of the burial history model in *PetroMod* (Chapter 4). Reconstruction of the depositional history is constrained and guided by the stratigraphic and property models detailed in Chapter 4 and Chapter 7, including the gridding, age assignment, layering, faults, and facies definition. The age assignment and the layer processes are guided by the structural-stratigraphic model and tied to the well tops.

The summary workflow is shown in Figure 8-1:

- a. Select wells based on basin structure and gravity map, build 1D and 2D burial models through selected wells in *PetroMod*. The 1D and 2D models help to understand better the burial and

thermal history of the basin, for example, amount of erosion, palaeo-water depth, base temperature.

- b. Prepare erosion maps, palaeo-water depth maps; build a 3D petroleum system model in *Petrel* using the 3D structural, stratigraphic, and property models. The 3D petroleum system model includes the key depth maps, fault framework, erosion maps, palaeo-water depth maps, lithofacies, and source rock properties such as maps for the total organic carbon (TOC) and hydrogen index (HI) properties (Chapter 7). These property maps ensure that measured well sedimentary and thermal data constrain the 3D burial history model at critical geological times.
- c. Set up heat flow related parameters (e.g., crust/mantle thickness, rift phase timing, base temperature, etc.) for the 3D burial-thermal model and simulate in *PetroMod*.

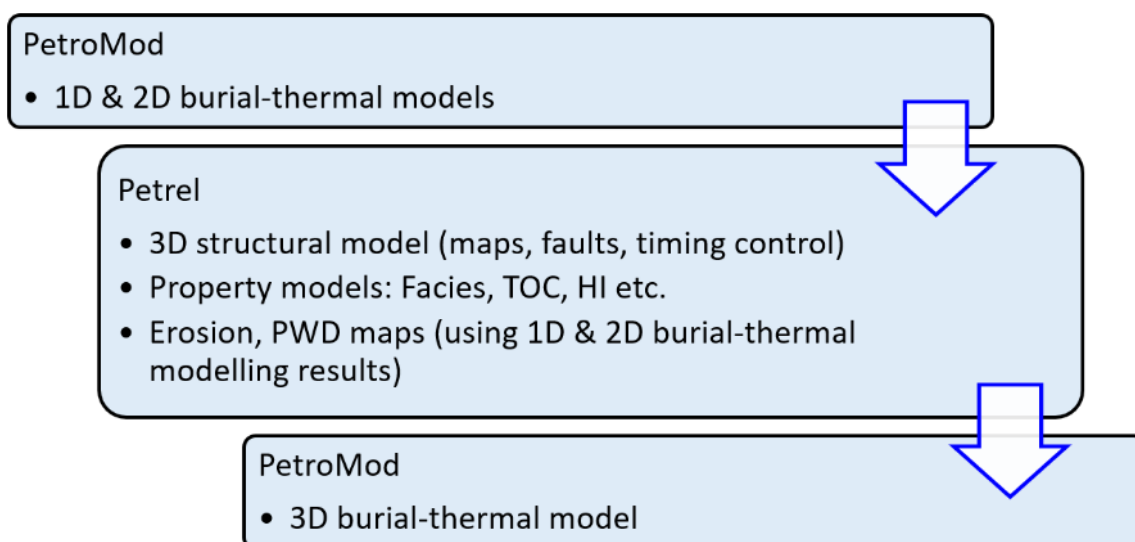


Figure 8-1 The summary process workflow for the *Petrel* to the *PetroMod* modelling.

8.2 Geological input settings

The *PetroMod* 3D burial-thermal simulation requires a variety of geological inputs to reconstruct the burial-thermal history, including the depositional history, timing and amount of erosion events, palaeo-water depth, rifting phases, pre-rift thicknesses and lithology of crust and mantle. The Gippsland Basin experienced two rift phases between the Early and Late Cretaceous, and there is a noticeable difference in the burial and depositional between the onshore and offshore parts of the Gippsland Basin (Chapter 4 and Figure 2-1). Hence, it is necessary to build 1D and 2D models to assess and prepare the required geological data for the 3D model that can properly model these lateral and vertical differences in the geological histories in time and space.

Initially, ten 1D burial and thermal models were built at selected wells across the basin (Figure 8-2). Six 2D burial-thermal models were built on regional cross-sections covering the Central Deep and the eastern edge of the basin (Figure 8-2). The structural interpretation for the 2D model includes 11 major stratigraphic units which are tied to the corresponding well tops and the major faults (Figure 8-3). These 1D and 2D models provide estimates of heat flow, timing and amount of the main erosion events, and palaeo-water depth, which were utilised to generate 3D inputs.

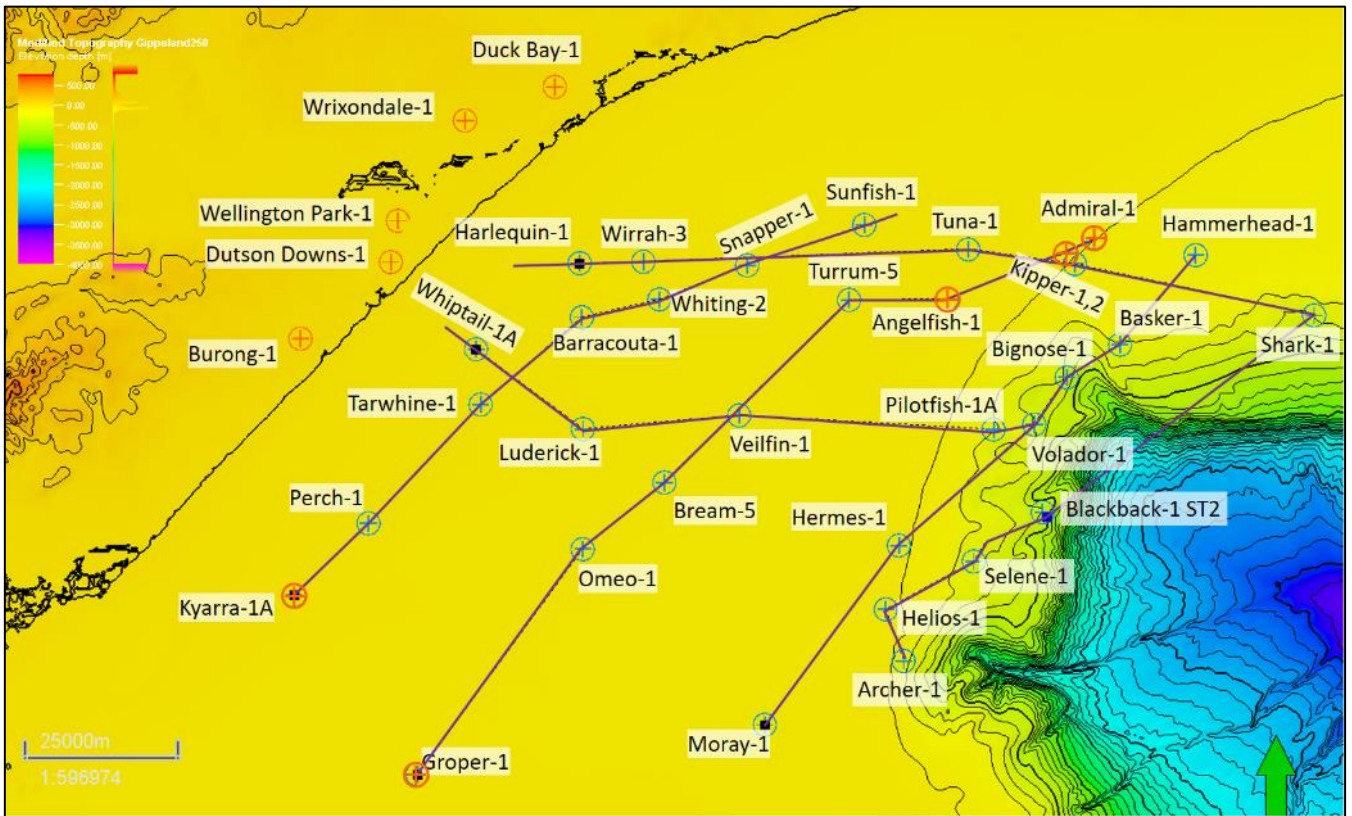


Figure 8-2 The locations of 1D and 2D burial-thermal models and related wells. The wells used to build the 1D models are coloured in orange, and the lines used to build the 2D model are coloured in purple.

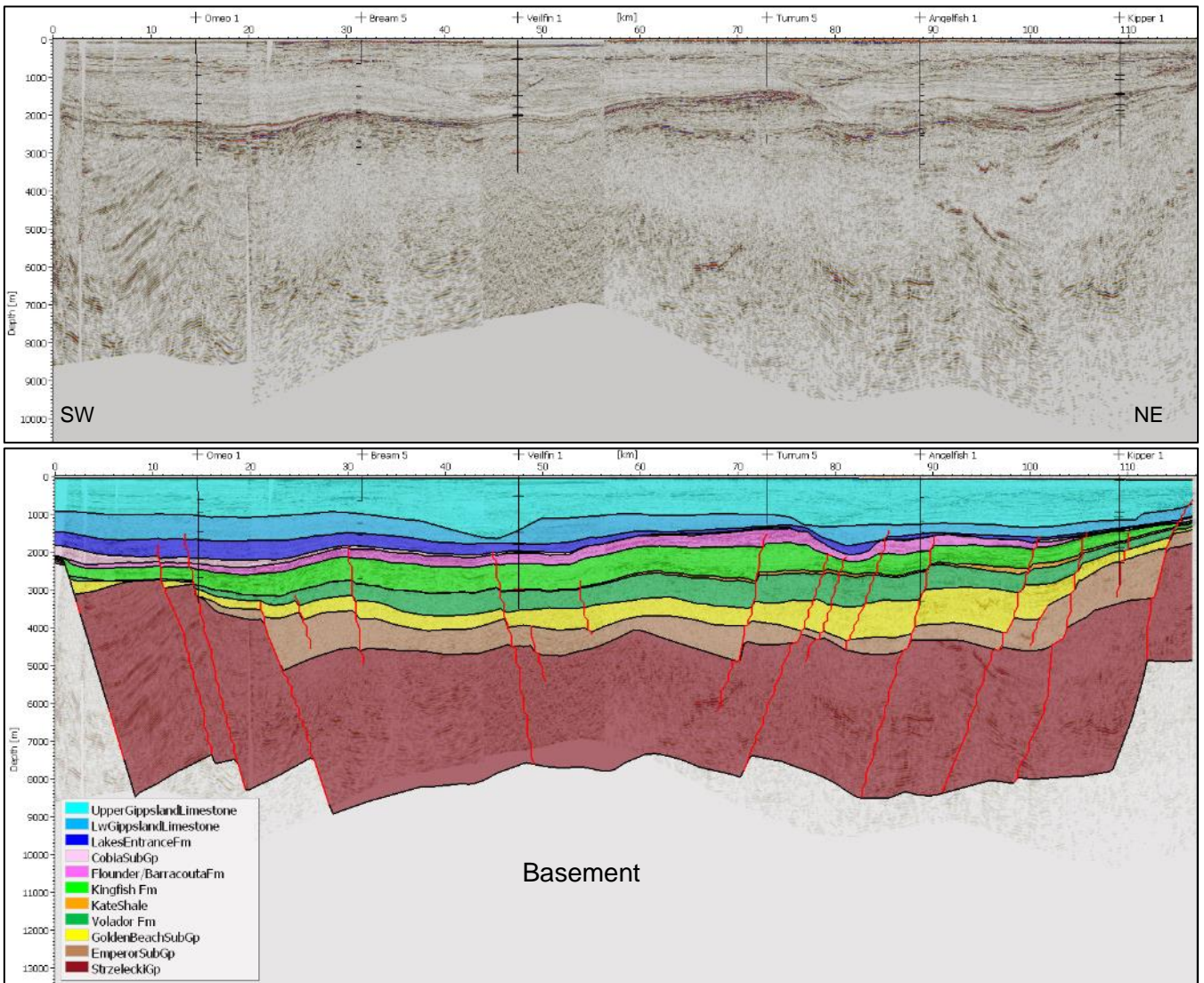


Figure 8-3 Uninterpreted (top) and Interpreted (bottom) southwest-northeast seismic profile in the Gippsland Basin showing the structure with formations and faults. See the location in Figure 8-2. The top Basement surface is modified from the OZSEEBASE Interpreted Gravity map.

The heat flow evolution can be simulated and generated based on the McKenzie heat flow model in *PetroMod*. The *PetroMod* 1D model only simulates a simple rift event with one rift phase, which does not match the tectonic history of the Gippsland Basin, and the modelled temperature trends of the 1D models are much lower than the measured well temperature data (Figure 8-4). This implies that a single rift model is not sufficient to generate the heat flow trends that are required to match observed temperatures. However, the *PetroMod* 2D and 3D simulations allow simulation of multiple rift phases by using advanced heat flow simulations (e.g., the 'McKenzie crustal model'), which result in much better temperature matches (Figure 8-5). The simulation of two rift phase provides good estimations of the heat flow and R_o in 2D models (Figure 8-6). Overall, the 1D and 2D burial models assess the approximate erosion amount, palaeo-water depth and heat flow settings by testing thermal calibrations that help to prepare the corresponding 3D input data.

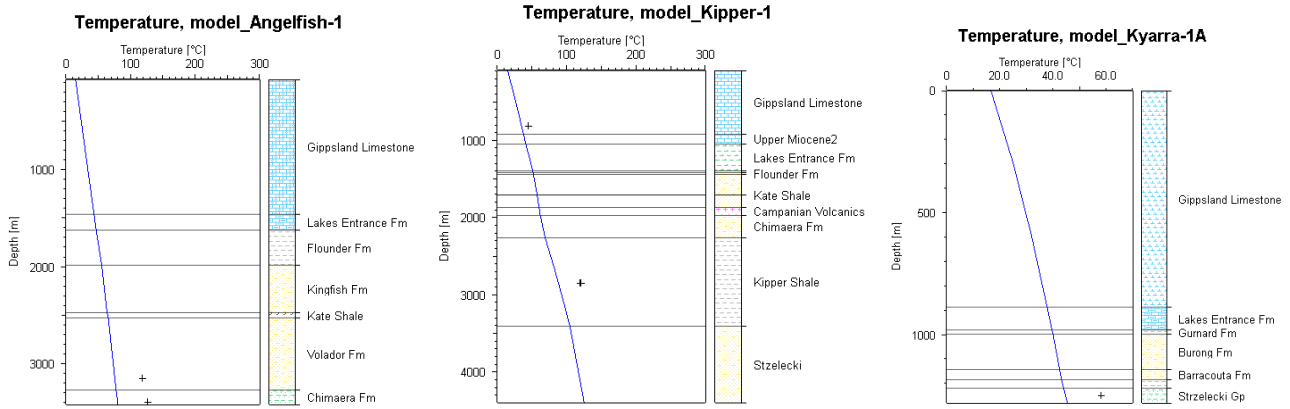


Figure 8-4 The temperature calibrations from the 1D models indicate that modelled temperature trends are much lower than the measured data.

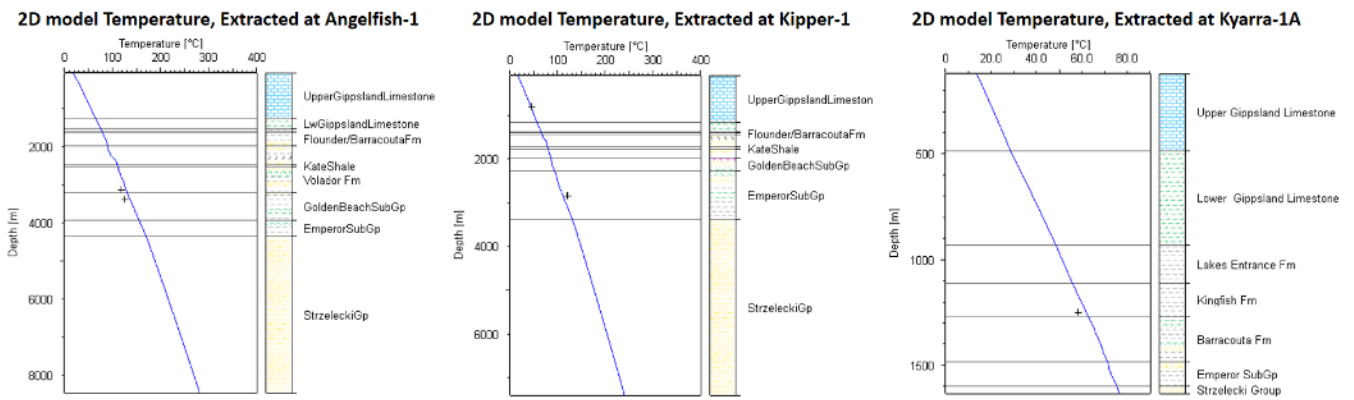


Figure 8-5 The temperature calibrations from 2D models indicate that modelled temperature trends start to provide better matches to the measured data.

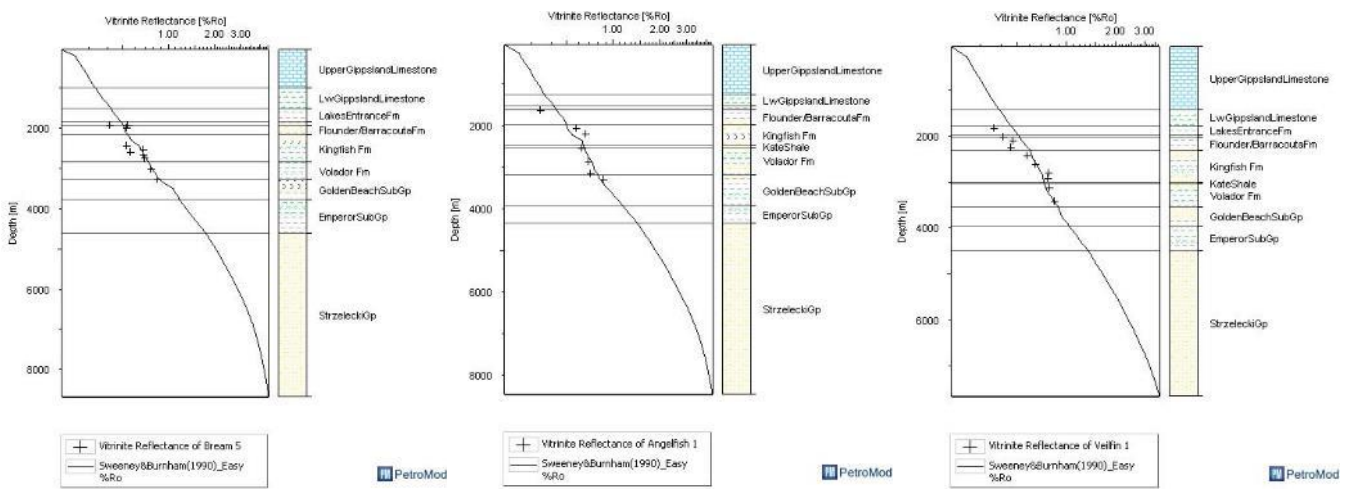
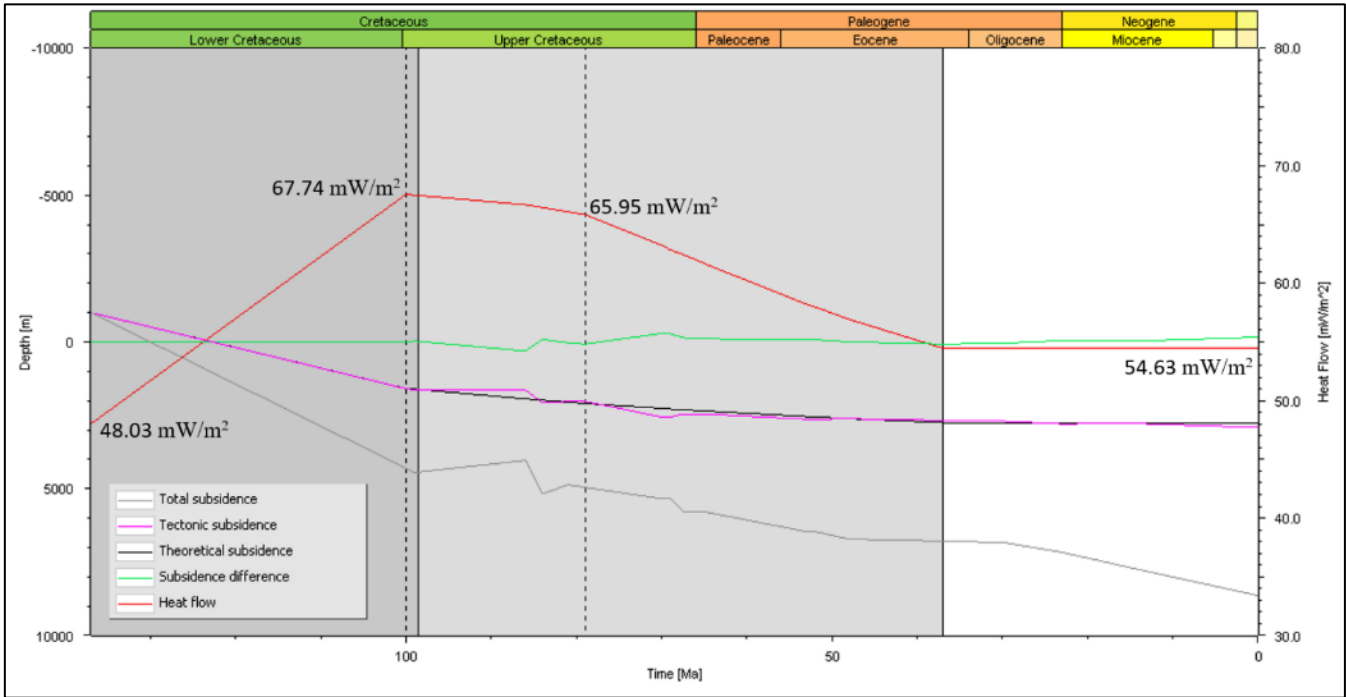


Figure 8-6 The 2D model results: the calculated heat flow trend at Bream-5 (top); the vitrinite reflectance calibrations at Bream-5, Angelfish-1 and Veilfin-1 (bottom).

8.2.1 Erosion events

Based on the tectonostratigraphic history of the Gippsland Basin, four main unconformable events were included (Figure 2-1): mid-Cretaceous Otway unconformity; ca. Coniacian Longtom unconformity; ca. end Campanian Seahorse unconformity; and Early-Middle Eocene Marlin unconformity. The mid-Cretaceous Otway unconformity is a regional uplift event, which created widespread removal of section typically between 1 and 3.5km, but more in some areas, with a high denudation rate of 250m/Ma (Smith, 1982; Moore et al., 1986; Weber et al., 2004; Aghaei et al., 2014, 2017; Holdgate et al., 2015). The younger unconformities are less extensive, mainly removing thinner sections in the offshore areas, with the Marlin unconformity related mostly to the development of incised valleys and submarine canyon systems (Johnstone et al., 2001). Parts of the onshore areas have been exposed and eroded

from about 70 Ma to the present day, though denudation rates are relatively slow down to about 50 m/Ma according to Weber et al. (2004). This slow continuous denudation removed another ca. 1-3 km of sediments across the onshore basin.

A three-step approach is used to generate the erosion maps:

1. Utilise measured vitrinite reflectance (Ro) data to estimate the amount of erosion for each unconformity at individual wells (~ 38 wells). The Ro data are assigned as well tops in *Petrel*, by measuring the difference in depth between observed Ro values and the depth predicted by a linear increase in Ro trend, as shown in Figure 8-7. First-pass erosion maps were then generated based on the estimated erosional thickness attribute. However, the available Ro data from selected 38 wells do not cover or intersect every unconformity, which is insufficient for the first pass maps to capture all the erosional details.
2. Multiple cross-sections were created to cover the basin and generate 2D burial-thermal models in *PetroMod*. In the 2D modelling processes, generated erosion lines were adjusted by fitting the modelled temperature and Ro to measured data. Secondly, the amounts of erosion at each unconformity are extracted for the specific well locations. The six cross-section locations are shown in Figure 8-2.
3. Import the amount of erosion at the wells from step two to the *Petrel* project, merge with step one data, and generate the erosion maps for each unconformity (Figure 8-8b).

Overall, seven erosion maps were created and imported back into the *PetroMod* for the 3D modelling: These are: the Otway unconformity (ca. 99 Ma), Longtom unconformity (ca. 84 Ma), Seahorse unconformity (ca. 70 Ma), *L. balmei* erosion (ca. 56.5 Ma), Marlin unconformity (ca. 48 Ma), Early Oligocene erosion (ca. 32 Ma), and Mid-Miocene erosion (ca. 15 Ma) (given in Appendix 13).

The erosion maps represent different amounts and types of erosion across the basin that result from several different causes. The Gippsland Onshore, Terraces and Platforms have experienced greater and relatively more continuous erosion related to the long-term exposure in depositional environments such as alluvial and floodplains surrounded by highlands. In contrast, the Central Deep has experienced frequent transgressive-regressive cycles from the Palaeocene to Early Oligocene associated with fluvial-deltaic-shallow marine deposition and incision that has removed thinner

amounts of section but over very wide areas (Figure 8-9). The offshore shelf environments have experienced more focussed cut and fill by large submarine canyon systems some of which have cut deep into the older strata (Figure 8-10). The erosion maps indicate how greater amounts of erosion occurred within the canyons and over some of the anticlines (Figure 8-11).

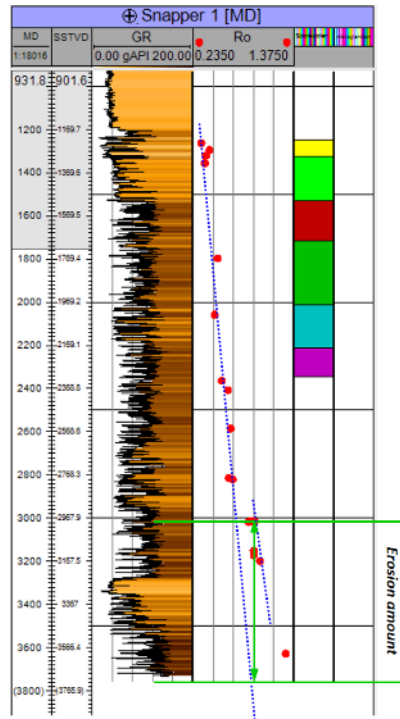


Figure 8-7 Composite diagram illustrating stratal erosion amount using vitrinite reflectance data in Petrel.

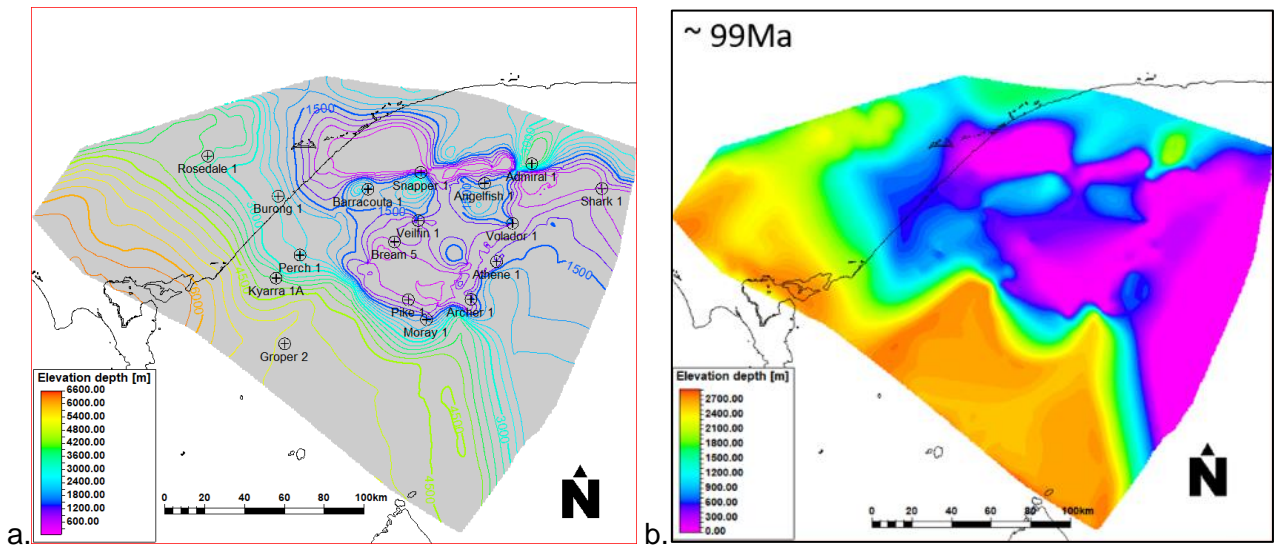


Figure 8-8 a: The total erosion amount of seven erosion events; b: Erosion map simulating the Otway Unconformity at ca. 99Ma. See Appendix 13 for the erosion maps at the other unconformities.



Figure 8-9 The simulated best fit palaeo-landscape of the Gippsland Basin, at 33, 32 and 31Ma.

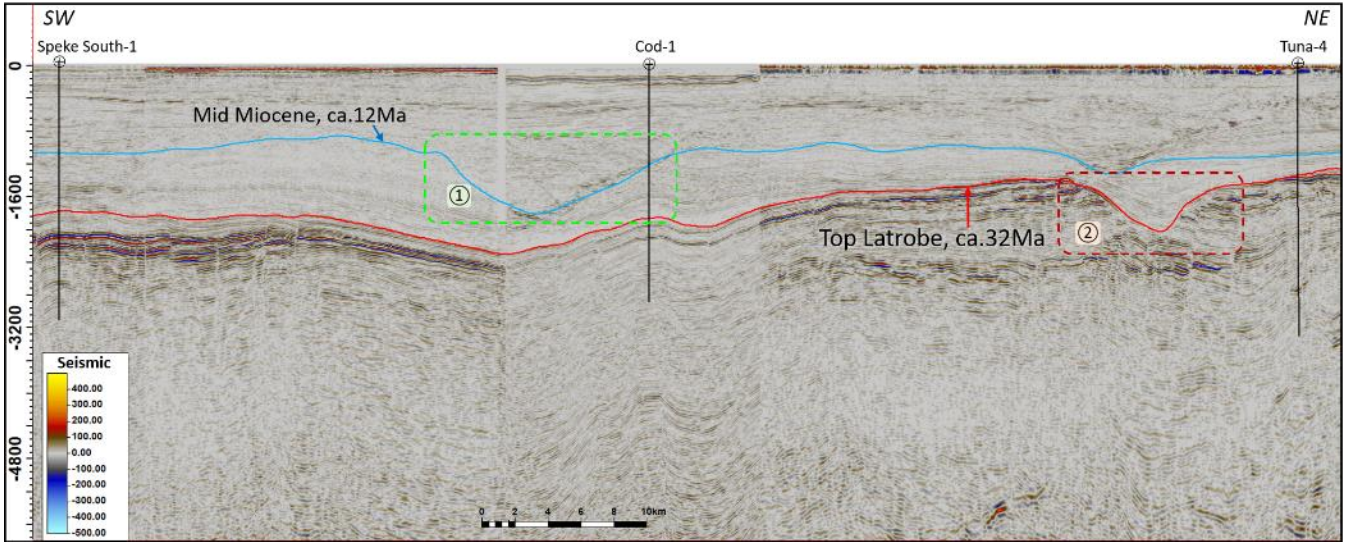


Figure 8-10 A seismic cross-section indicates the canyon systems formed at different ages: mid Miocene canyon (1) and Early Oligocene canyon (2). The mid Miocene surface is coloured in blue and top Latrobe surface is coloured in red.

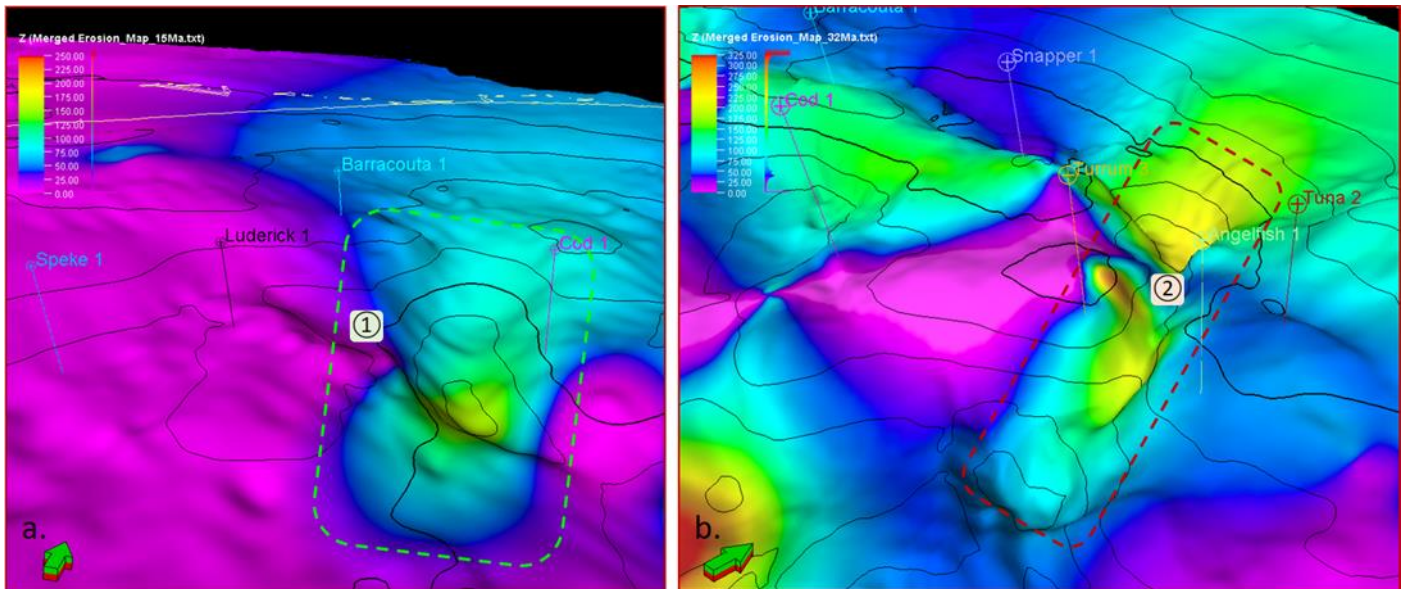


Figure 8-11 (a) Mid-Miocene and Early Oligocene structural maps coloured with the corresponding erosion amount. The green dashed-line highlights the mid-Miocene canyon system. (b) the Early Oligocene canyon system is marked with a red dash line.

8.2.2 Reconstruction of the basin geometry

The structural and stratigraphic construction of the *PetroMod* 3D burial model based on the *Petrel* model and the additional erosion surfaces produces 12 stratigraphic unit layers, excluding the basement layer, and covers a present-day sediment interval of up to 10km from surface to basement.

The model comprises an area of 38,714 km² with an overall grid cell size of 1 × 1 km (Figure 8-12). The combination of horizontal and vertical resolution and the study area means the model has a total number of ca. 11.5 million grid cells. The stratigraphic layers in the Latrobe Group are tied with palynological zones since most formations in the basin are diachronous (Figure 2-1). The 3D burial model includes 71 faults and uses 12 depth maps to define the stratigraphic units.

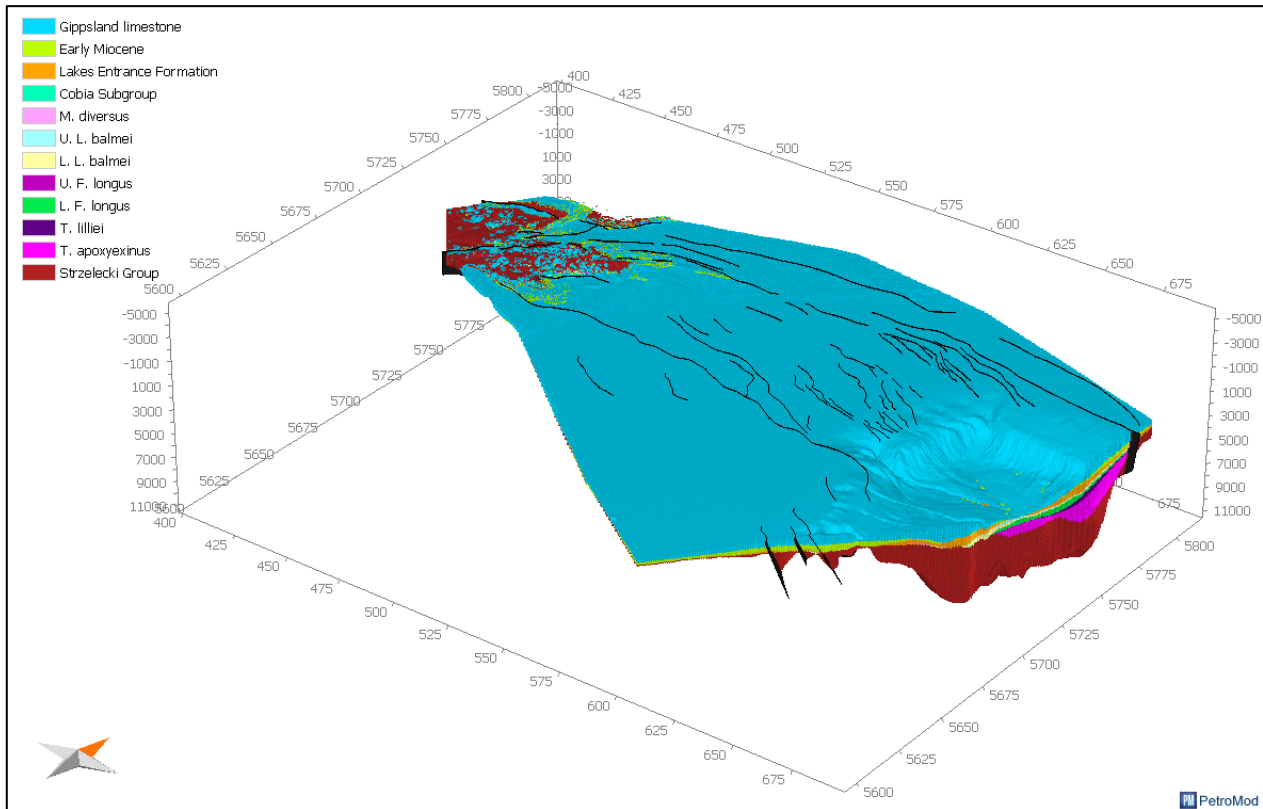


Figure 8-12 The 3D model illustrating the present-day geometry with faults in black, orange arrow points to the north, vertical scale in metres and horizontal scale in km.

8.2.3 Boundary Conditions: Paleo Water Depth, Interface temperature & Heat flow

The paleo water depth is generated based on biostratigraphic data from 30 key wells and previous palaeo-environment studies (Smith, 1982; Bodard et al., 1986; Rahmanian et al., 1990; Bernecker and Partridge, 2001; Johnstone et al., 2001; Riordan et al., 2004; Root et al., 2004). The boundary conditions input to the model consist of sediment-water interface temperature (SWIT) and Heat Flow.

The SWIT maps are generated using the automatic SWIT tool (based on Wygrala, 1989), which extracts the standard temperature at sea level over geological time based on the present-day geographic location and paleo latitude, which is set as 'Southern Australia' at a latitude of 38 degrees.

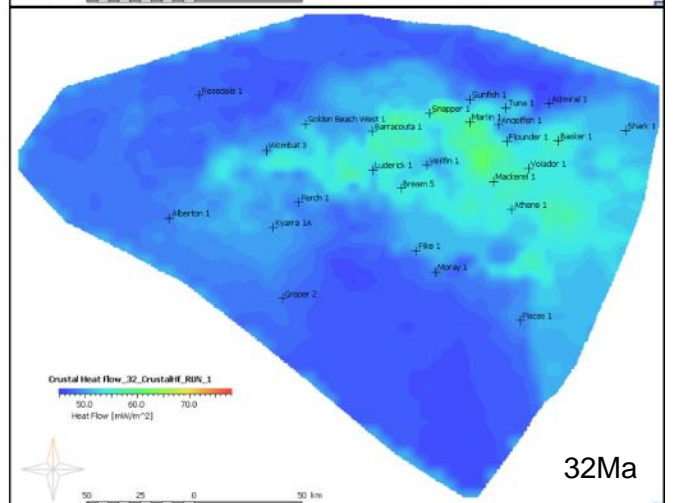
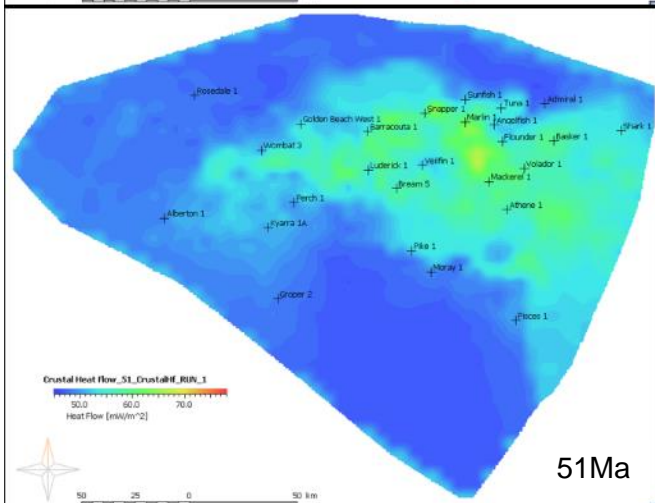
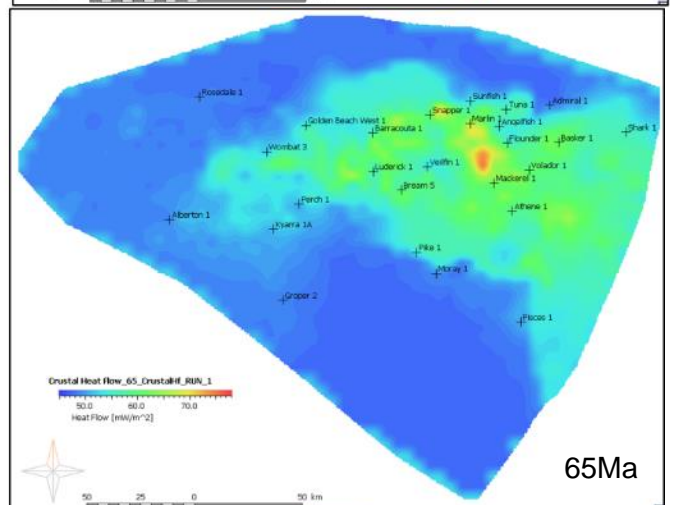
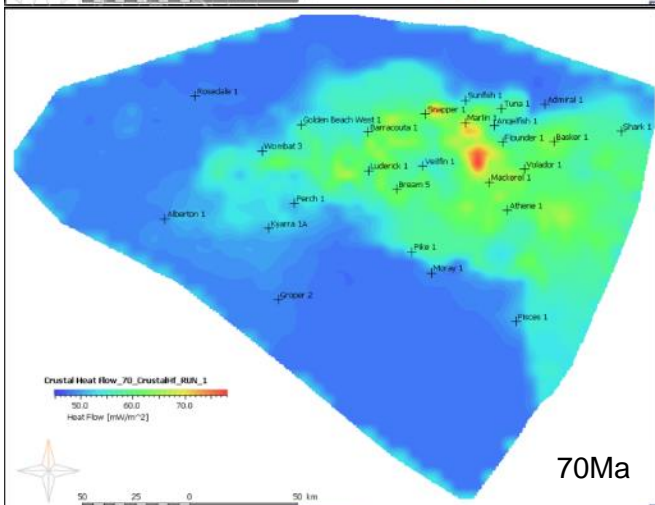
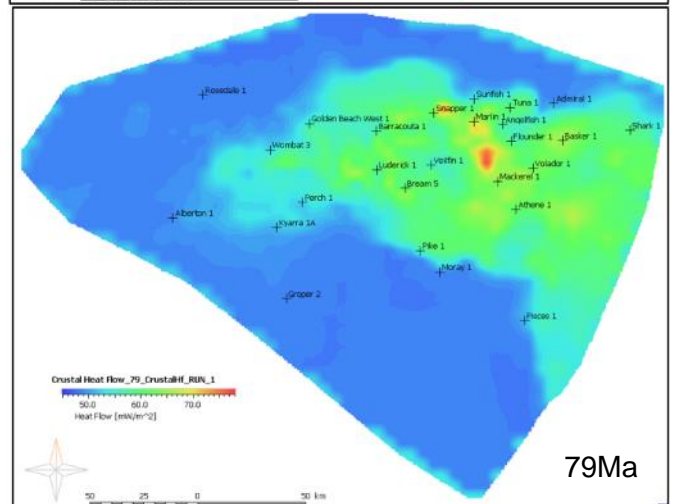
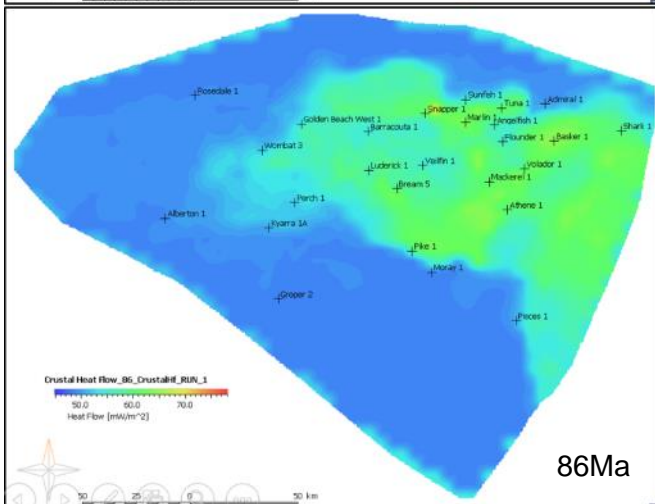
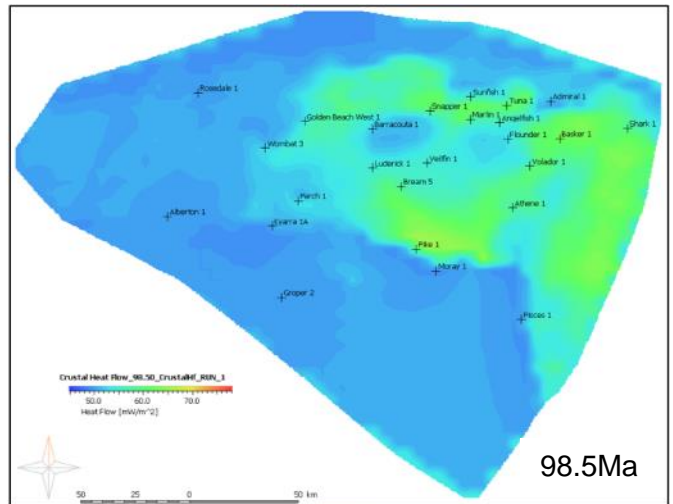
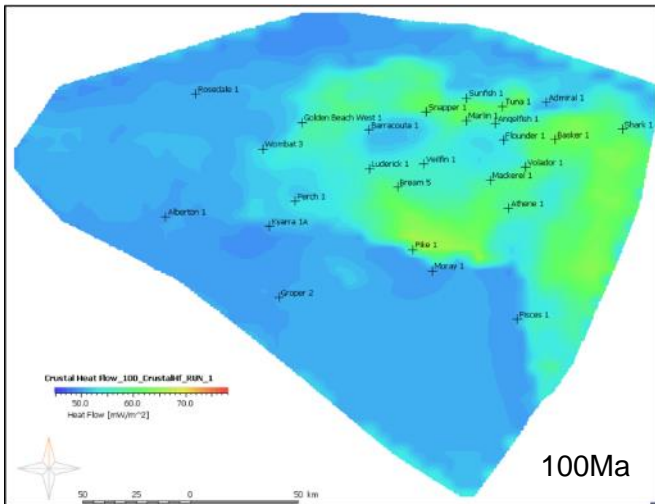
The Gippsland basin burial and tectonic history are complicated by two rift events with extension continuing for some time later followed by late-stage mild compression as discussed in Chapter 4. This means the heat flow trend created from the simple option McKenzie Model in *PetroMod* cannot readily

fit the Gippsland Basin. The present-day heat flow, which is generated by the simple option, is only about 30~40 mW/m², whereas actual data, including recent studies, indicate the present-day heat flow varies between 35-105 mW/m², with a mean of 65.5 mW/m² (Goutorbe et al., 2008; Harrison et al., 2012). Hence, this study uses the option that allows the insertion of multiple syn-rift phases, which provides a better fit to the tectonic evolution of the basin. The first syn-rift phase for the Strzelecki Group was set from 137 Ma to 100 Ma (note younger than in the Otway Basin), with a short uplift phase at the end of the Early Cretaceous. The second syn-rift phase for the Tasman Sea opening in Gippsland was set from 98.5 Ma to 79 Ma. This is followed by a normal fault controlled thermal subsidence phase until 37 Ma when the Gippsland basin changed from extensional to compressional tectonic conditions (Smith, 1988; Bernecker and Partridge, 2001; Johnstone et al., 2001; Power et al., 2001; Müller et al., 2019; Mahon and Wallace, 2020).

The crustal lithology is set as 'upper crust (continental, granite)', and the mantle lithology is set as 'upper mantle (lithosphere)'. The lithospheric studies suggest the crustal thickness in the Gippsland basin region is about 30-40 km, with an upper mantle thickness of ca. 75 km (Clitheroe et al., 2000; Kennett and Blewett, 2012; Müller et al., 2019). The *PetroMod* uses the McKenzie-type crust model, the crust thins and mantle thickening in the rift phase, to simulate the stretching and heatflow, and the second rift event happened right after the first rifting in the Gippsland Basin. Hence, the pre-rift crust and upper mantle thicknesses of two rift events are set as 35 km and 70 km, and 30 km and 75 km, respectively. The crustal stretching maps were calculated to conform to a stretching factor β of 1~1.5 with a maximum ~2 (Hegarty et al., 1985; Power et al., 2001; Weller, 2015; Müller et al., 2019) (Figure 8-42). The plate tectonic reconstruction, crustal thickness and stretching factors are derived using *GPlates* software (Chapter 4).

The temperature at the base of the lithosphere is set to 1400 °C to increase the heat flow trend slightly from the default of 1333 °C (the pyrolite melting temperature at the theoretical lower to upper Mantle boundary) that precluded attainment of a good match to the thermal history. The calculated heat flow maps at key time steps are shown in Figure 8-13. These demonstrate that the crustal heat flow evolution across the basin varies between different areas. The North, South, and Lakes Entrance Platforms, South Terrace, Latrobe Valley, Seaspray Depressions, and Strzelecki mountains (where fewer sediments are preserved) show similar heat flow evolution. In those areas the palaeo-heat flow

values vary between 45 and 55 mW/m², and the values are higher during the rifting phases then gradually cool in the post-rift phase. In contrast, the Central Deep, North Terrace and Lake Wellington Depression (where thicker sediments are preserved) follow a different evolution trend with higher heat flow values. The palaeo-heat flow reached 66 mW/m² at the southern boundary faults at the end of the first syn-rift phase (ca. 100 Ma) and reached 77.5 mW/m² at the Central Deep close to the North Terrace at the end of the second rift phase (ca. 79 Ma). The Central Deep, North Terrace and Lake Wellington Depression areas cool slowly in the post-rift phase and result in a range of crustal heat flow values between 50 and 61.3 mW/m² at the present-day.



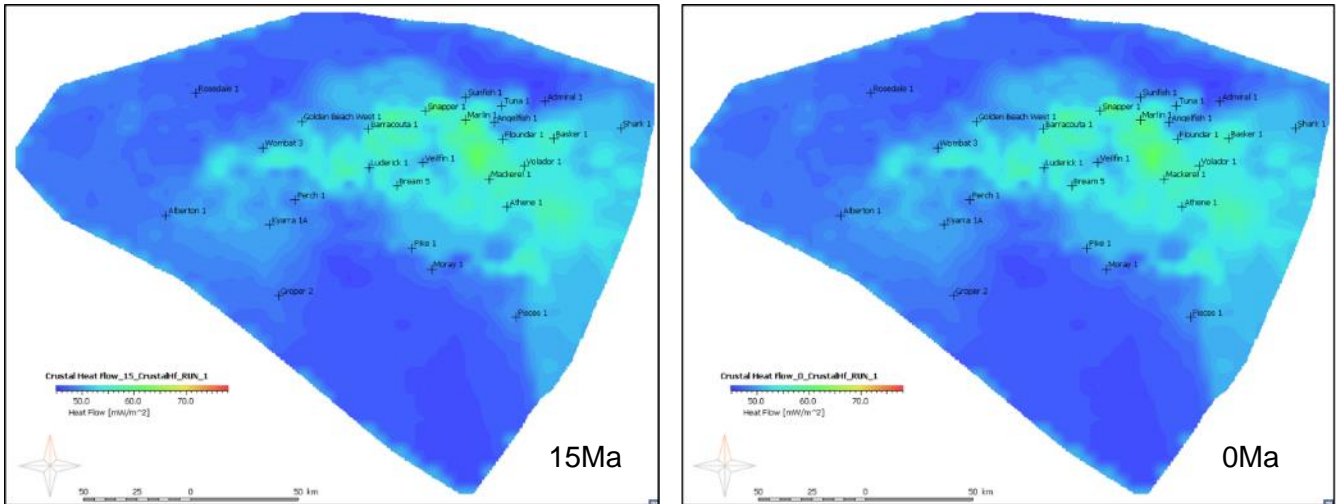


Figure 8-13 Calculated heat flow maps for the entire Gippsland Basin.

8.2.4 Lithology/Facies

The 3D burial modelling requires lithological information and lateral facies distribution for the different stratigraphic units. A lithofacies property model, based on onshore and offshore petroleum wells and coal bores, has been made in *Petrel* software with the same resolution as the 3D realistic model geometry (Chapter 7). Figure 8-14 shows the facies model which has been transferred into *PetroMod* software. The heat flow related physical parameters required by *PetroMod* for sedimentary lithologies used the *PetroMod* default parameters as given in Table 8-1 since these are reasonably fundamental properties and they were assigned to the corresponding lithofacies imported from *Petrel* to *PetroMod*.

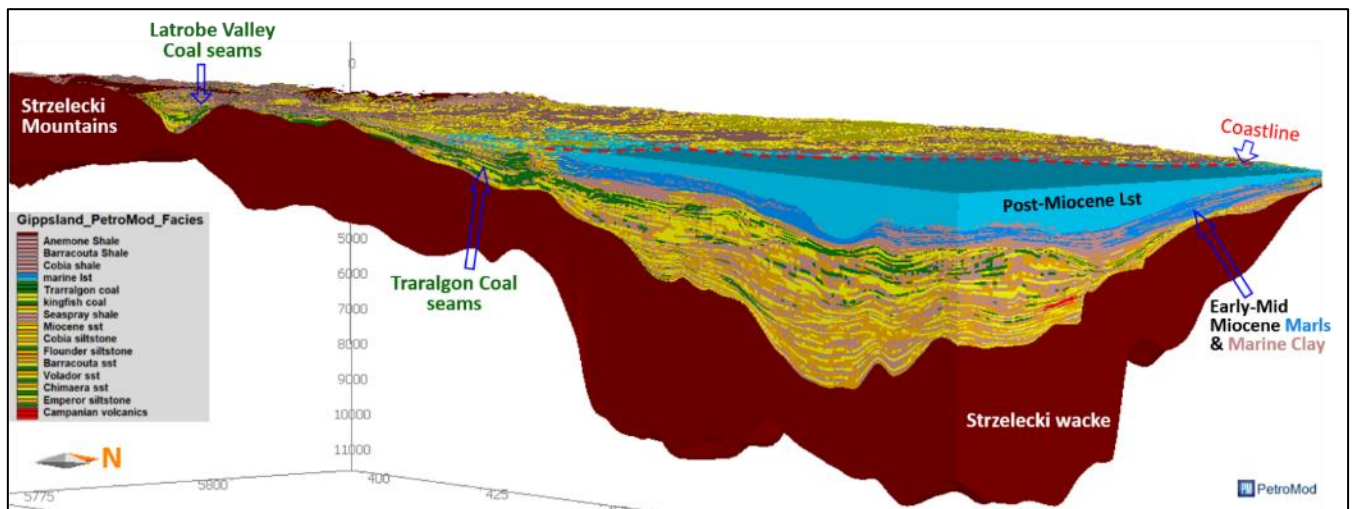


Figure 8-14 Clipped 3D facies model in *PetroMod*, exported from *Petrel* facies property model (see Chapter 7).

Table 8-1 Physical parameters of the sedimentary rocks used in the 3D model (PetroMod default parameters).

Lithology	Thermal conductivity (W/m/K)		Radiogenic elements			Heat capacity (kcal/kg/K)		Mechanical properties	
	20°	100°	U (ppm)	Th (ppm)	K (%)	20°	100°	Density (kg/m ³)	Initial porosity (%)
Limestone (organic rich - typical)	2	1.96	5	1.5	0.26	0.2	0.23	2680	51
Marl	2	1.96	2.5	5	2	0.2	0.23	2700	50
Coal (pure)	0.3	0.71	1.5	3	0.55	0.31	0.36	1600	76
Sandstone (quartzite, typical)	6.15	5	0.6	1.8	0.9	0.21	0.25	2640	42
Sandstone (typical)	3.95	3.38	1.3	3.5	1.3	0.2	0.24	2720	41
Shale (organic lean, silty)	1.77	1.79	3	11	2.6	0.21	0.24	2700	67
Shale (organic rich, 3% TOC)	1.45	1.55	5	12	2.8	0.21	0.24	2610	70
Shale (organic rich, 8% TOC)	1.2	1.37	10	11	2.9	0.21	0.25	2500	70
Shale (organic rich, typical)	1.25	1.41	5	12	2.8	0.21	0.25	2600	70
Shale (typical)	1.64	1.69	3.7	12	2.7	0.21	0.24	2700	70
Siltstone (organic lean)	2.05	1.99	2	5	1	0.22	0.25	2720	55
Basalt (normal)	1.8	1.81	9	2.7	0.8	0.19	0.22	2870	1
Sandstone (wacke)	2.6	2.4	2.5	8	2.5	0.2	0.23	2780	39

8.2.5 Source-rock properties and kinetics

The maturity and kerogen type for the main geo-zones are shown in the HI versus Tmax plot of the Rock-Eval data which shows that the majority of the source rocks are type II and III with some samples being type I as discussed in Chapter 7 and shown in Figure 8-15. The available kinetics data for source rocks in *PetroMod* are based on a four-fold classification (Pepper & Corvi, 1995) termed organofacies A (marine: high Sulphur Type 2S), B (marine: low sulphur, Type 2), C (lacustrine: freshwater algae, Type 1), D/E (deltaic-estuarine: waxy perhydrous higher plants, Type 3H), and F (fluvial: lignin rich higher plants, Type 3/4). In *PetroMod* these affect the allocated kinetics and therefore the timing and amount of generation from each organic matter type, though in this study the burial and thermal modelling is the main focus not the amount of generated petroleum. The organic facies were allocated as per the classifications shown in Table 8-2.

The Emperor shale is set as the organofacies type C based on the small number of type I algal samples and the interpreted intracratonic lacustrine environment (Chapter 6), notwithstanding that most of the shale samples from the Emperor Group that have been analysed are type II/III (Chapter 7).

The Chimaera Formation shales and coals were deposited in fluvial-deltaic environments and the analytical data indicates it contains mainly non-marine Type II/III organic matter, though some shales and coals are perhydrous with high HI indices. Hence, the organofacies type for the Chimaera shale is set as F though it may be D/E and the thin coal beds are set to C.

The main upper Latrobe Group source rock units, such as Kingfish shale, Kate shale and Volador shale, are allocated to type D/E, which corresponds to the analytical data (Figure 8-15). The coal seams and interbedded shales are upper and lower coastal plain sediments developed in swamps and marshes. They have perhydrous compositions consisting of both higher land plant tissue, liptinites (e.g., spores, cutinite and algae) with almost no inertinite. Hence, they are classified as C and in part as D/E organic matter types. The Flounder shale and equivalents are dominated by transgressive shallow marine and estuarine sediments, probably matching the organofacies type B, though this lithofacies is volumetrically minor.

Table 8-2 Kinetic data of source rock units

Facies	Lithology	Kinetic
Yallourn coal	Coal (pure)	Pepper&Corvi(1995)_TI(C)
Morwell coal	Coal (pure)	Pepper&Corvi(1995)_TI(C)
Traralgon coal	Coal (pure)	Pepper&Corvi(1995)_TI(C)
Flounder coal	Coal (pure)	Pepper&Corvi(1995)_TI(C)
Flounder shale	Shale (organic lean, silty)	Pepper&Corvi(1995)_TII(B)
kingfish coal	Coal (pure)	Pepper&Corvi(1995)_TI(C)
kingfish shale	Shale (organic rich, 3% TOC)	Pepper&Corvi(1995)_TIIH(DE)
L. L.balmei coal	Coal (pure)	Pepper&Corvi(1995)_TI(C)
L. L.balmei Shale	Shale (organic rich, 3% TOC)	Pepper&Corvi(1995)_TIIH(DE)
Kate Shale	Shale (organic rich, typical)	Pepper&Corvi(1995)_TIIH(DE)
Volador coal	Coal (pure)	Pepper&Corvi(1995)_TI(C)
Volador Shale	Shale (organic rich, 8% TOC)	Pepper&Corvi(1995)_TIIH(DE)
Chimaera Shale	Shale (organic rich, 3% TOC)	Pepper&Corvi(1995)_TIII-IV(F)
Chimaera coal	Coal (pure)	Pepper&Corvi(1995)_TI(C)
Emperor coal	Coal (pure)	Pepper&Corvi(1995)_TI(C)
Emperor Shale	Shale (organic rich, 3% TOC)	Pepper&Corvi(1995)_TI(C)

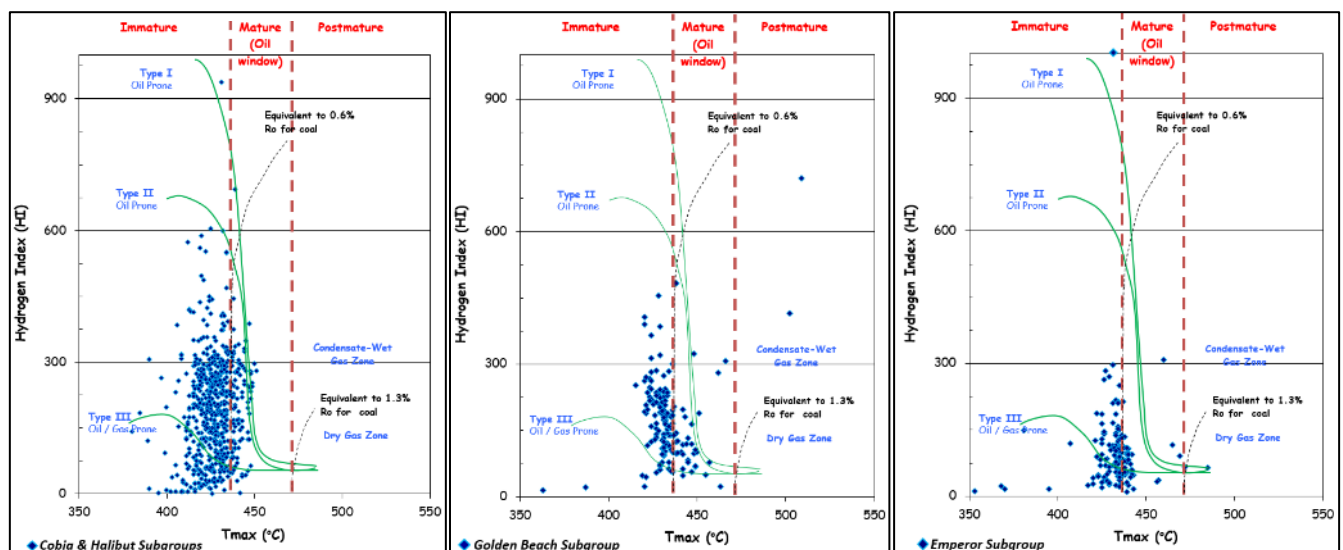


Figure 8-15 The maturity and kerogen type plot of source rock in different subgroups: Cobia & Halibut, Golden Beach, and Emperor Subgroups.

The source rock properties - total organic carbon (TOC) and hydrogen index (HI) are assigned in the 3D *PetroMod* model (Figure 8-16) by exporting the values directly from the corresponding property models which were generated in *Petrel* using the well data (Chapter 7). The TOC and HI property models that resulted in *PetroMod* in a dip cross-section are shown in (Figure 8-16). The Latrobe Valley and upper Latrobe Group coals and interbedded shales show as the high TOC units and the coals and shales show as the high HI units.

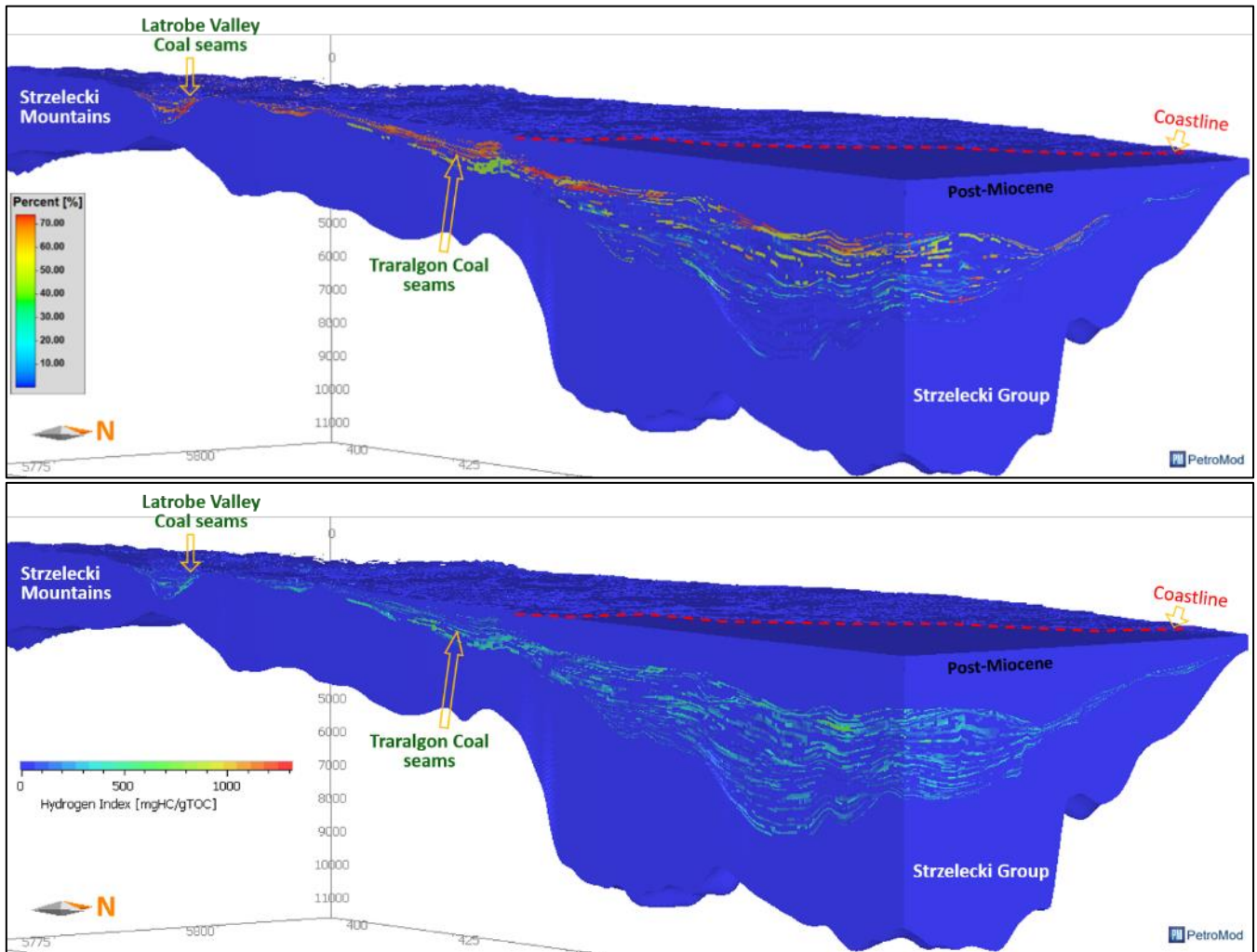


Figure 8-16 Total organic carbon (TOC) (top) and hydrogen index(HI) (bottom) for the source rock units assigned in the *PetroMod* 3D model.

8.3 Quality control & thermal calibration

The 3D *PetroMod* model is an excellent fit to the measured data in the *Petrel* model. This can be seen from twelve representative wells that are selected across the basin to compare the modelled temperature and vitrinite reflectance trends with the measured data (Figure 8-18 and Figure 8-18).

Additional wells are compared in Appendix 14.

The measured downhole temperature data is generally a good fit, especially in wells that have several data points. In some wells the measured data is slightly lower than the estimated thermal gradient mostly where there is only a single bottom hole temperature. This probably results from the bottom-hole temperature reading not attaining equilibrium and attempts to interpret a higher maximum temperature still being too low (eg Horner plot adjustment to higher values).

The calibration of modelled and measured vitrinite reflectance shows an excellent match and the wells used in this dataset all have many analysed samples. This is probably the first study where such good matches to the data have been obtained for a basin-wide 3D model.

The pressure model also provided a good match between the 3D modelled hydrostatic pressure data and the measured downhole pressure data (Figure 8-19).

The good calibration results of temperature, vitrinite reflectance and pressure suggest that the assigned geological settings used in the *PetroMod* 3D model as described earlier are good estimates (e.g., syn-rift, post-rift timings, crust and mantle facies and thicknesses, etc). Moreover, the excellent fit of the 3D basin-wide *PetroMod* model means it can be used to predict and analyse the Gippsland Basin's burial history.

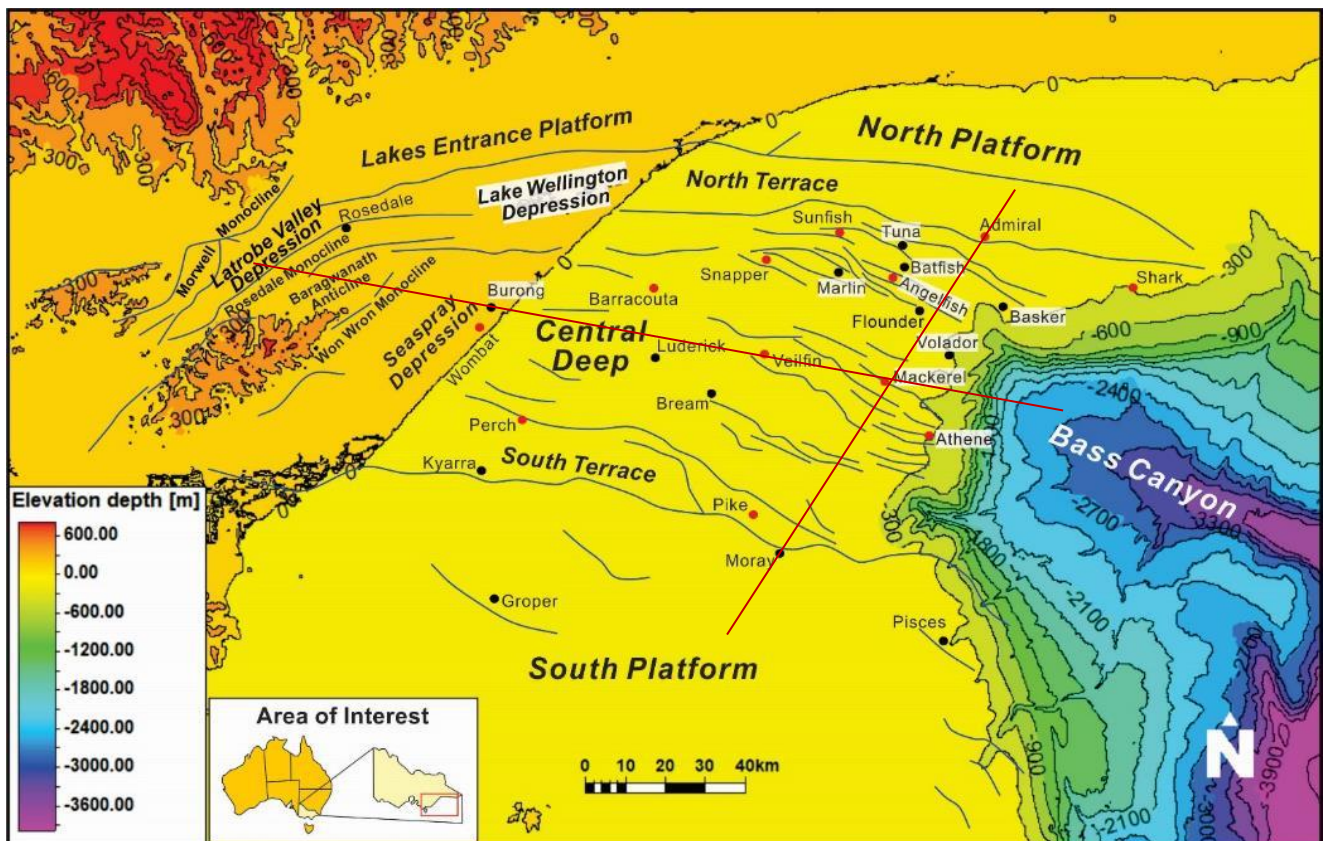
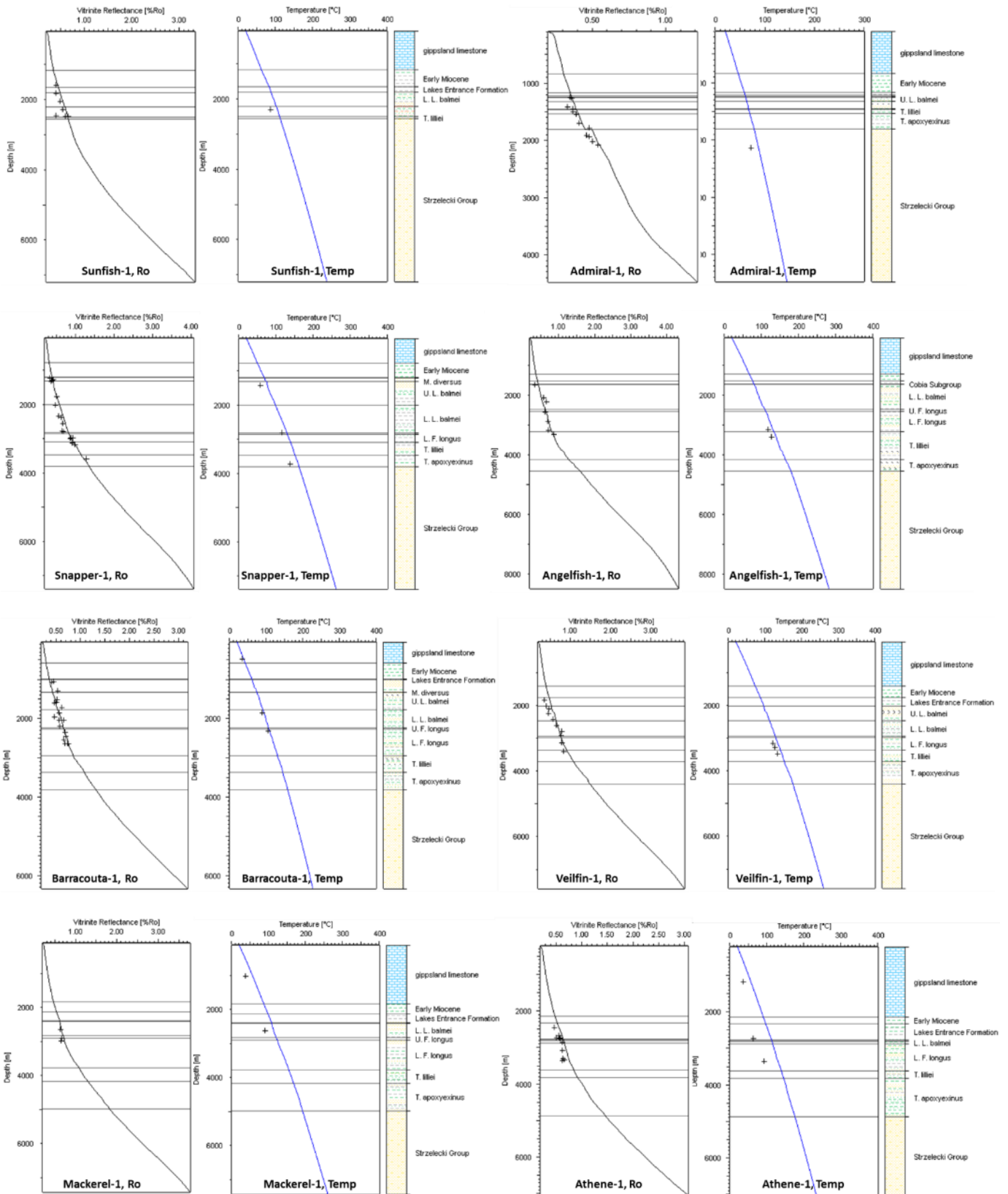


Figure 8-17 Map showing locations for wells used as examples of model fits in Figure 8-18. Red lines show locations of Figure 8-23, Figure 8-38.



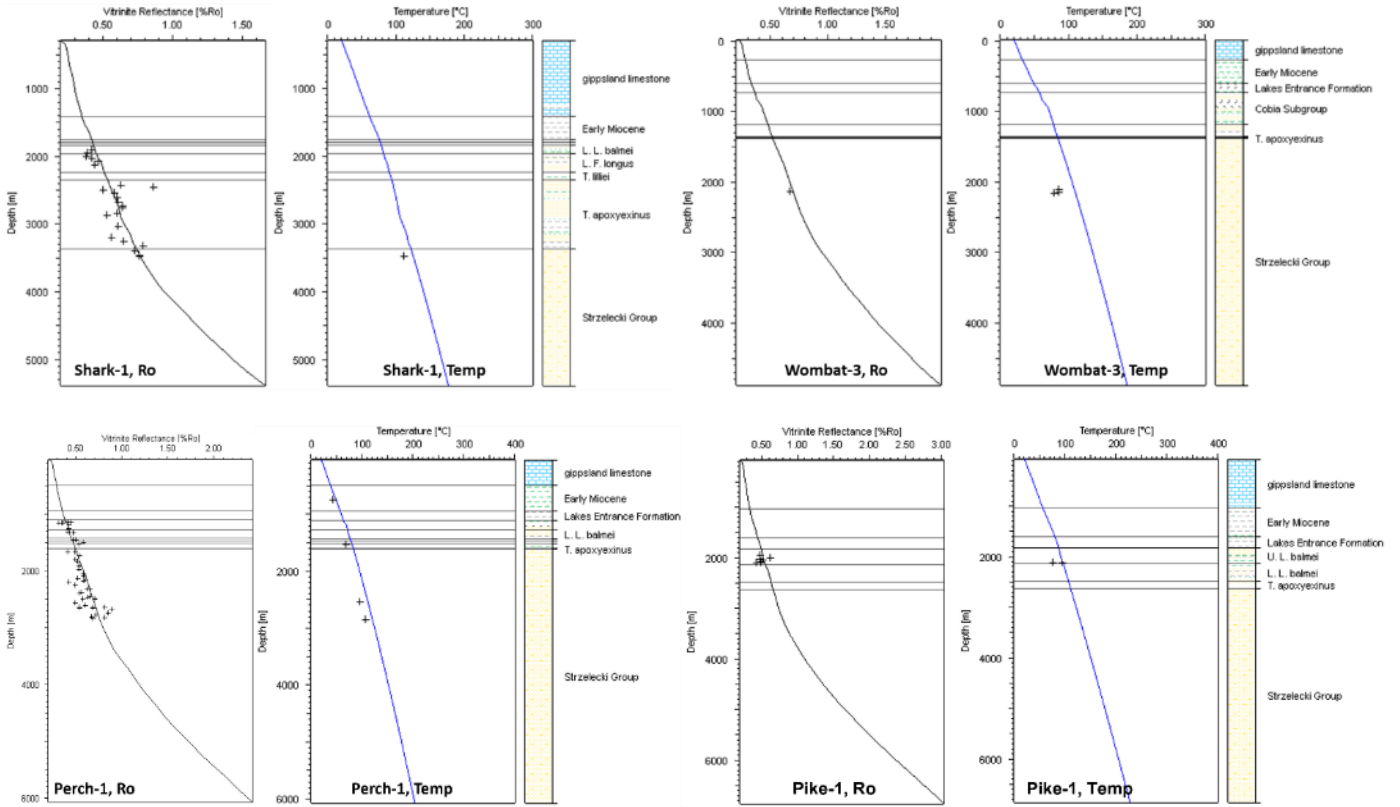


Figure 8-18 Comparison of modelled temperature and vitrinite reflectance trends (lines) and measured data (crosses). The trends are extracted at corresponding wells from the 3D burial-thermal model. The selected wells are highlighted in red in Figure 8-17, while the wells shown in black are given in Appendix 14

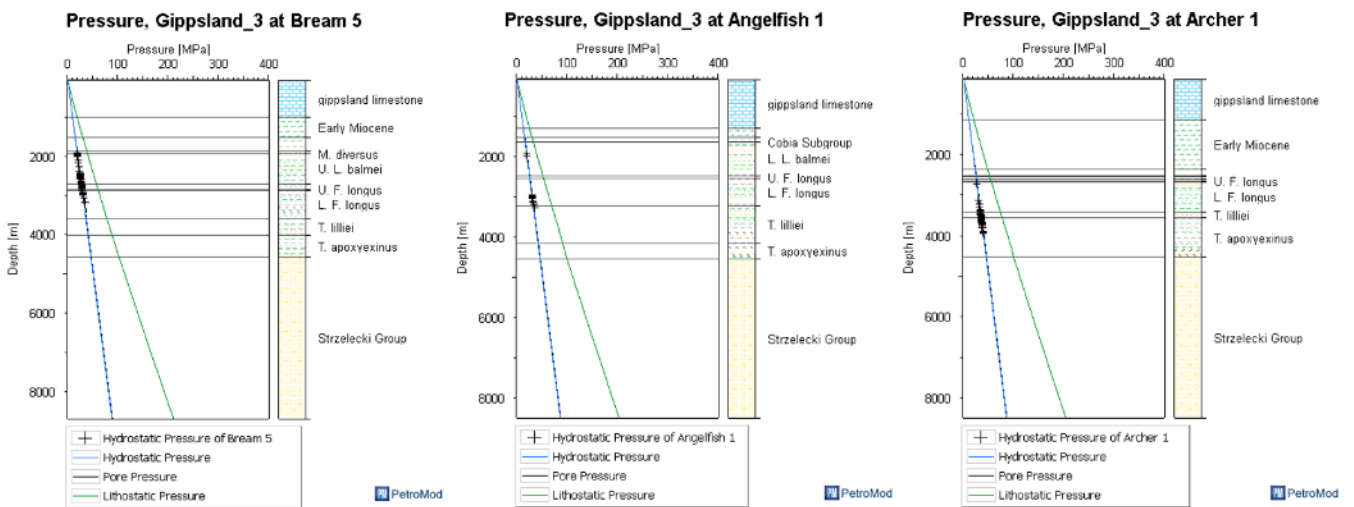


Figure 8-19 Pressure depth calibration between the 3D PetroMod model and measured well data; example wells are Bream-5, Angelfish-1 and Archer-1.

8.4 PetroMod Modelling Results

The *PetroMod* models for the burial, downhole temperatures, vitrinite reflectance and pressure data have statistically high matches to the actual well data (Yang and Smith, in prep) and are discussed separately in the sections below.

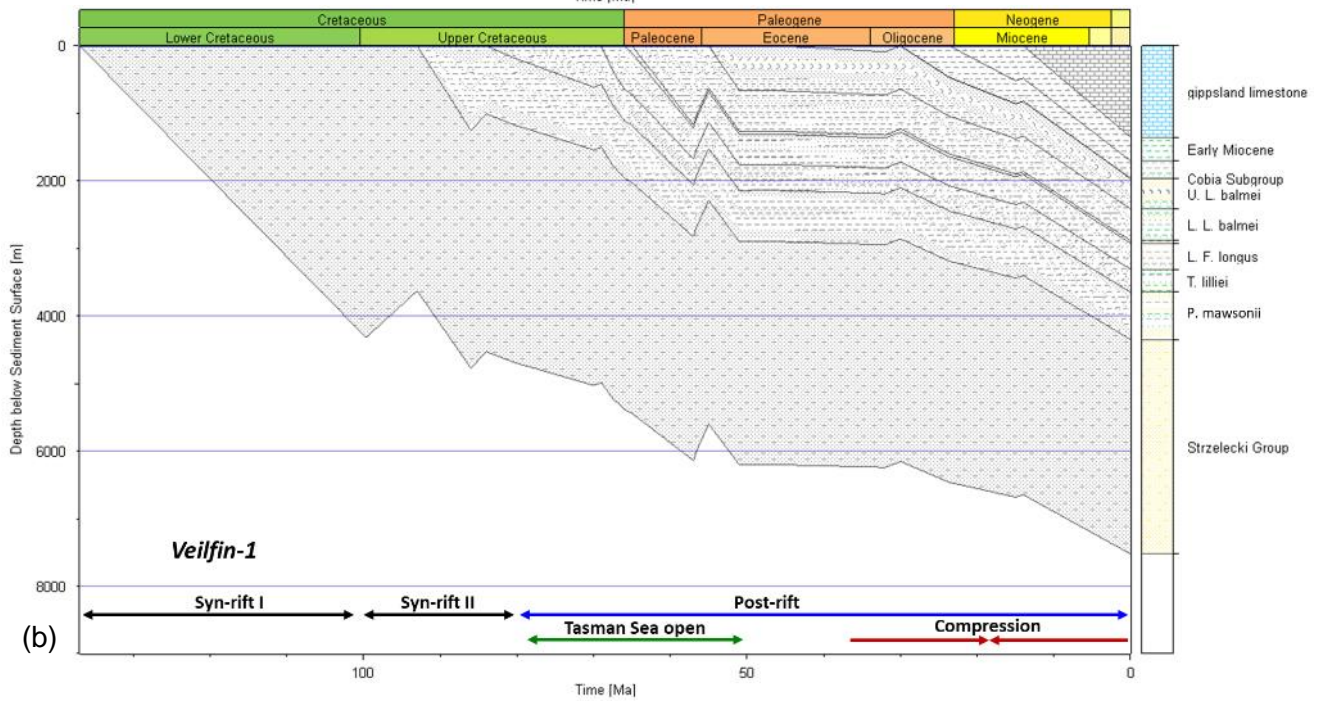
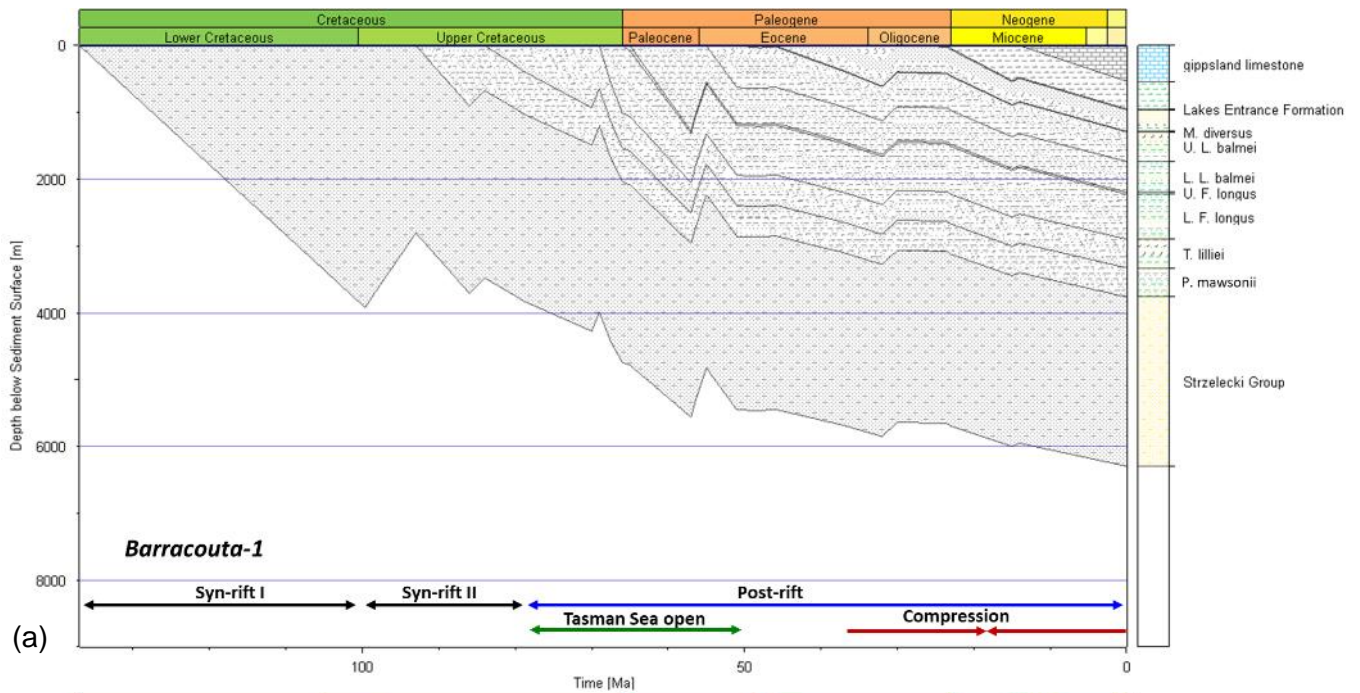
8.4.1 Burial Model

The burial history varies across the Gippsland Basin and can be divided into four groups: Inshore, Central Deep, Shelf edge and Terrace. Barracouta-1 represents wells located inshore or close to the edge of the Central Deep that records reasonably continuous thick sections, such as Golden Beach, Snapper, Seahorse and Wirrah. They have similar burial histories, characterised by substantial rapid burial histories in the Cretaceous rift phases and the Tasman Sea opening in Paleocene, which slowed afterwards (ca. 50 Ma). In Barracouta the total sediment thickness is about 6000m with thick Latrobe Group (~ 3000 m) and about 500 m post Mid-Miocene carbonates.

Veilfin-1 represents wells located within the main Central Deep that record thick sections, such as Luderick, Bream and Marlin. They underwent substantial rapid burial processes in the Cretaceous rift phases and the Tasman Sea opening in Paleocene, with a very slowed steady burial process during the Eocene to Early Oligocene ca. 50-30 Ma. In Veilfin-1, the base of the Strzelecki Group reached about 7500 m, with about 2200m thick Latrobe Group sediments. The burial rate slightly increased after 15 Ma and ended up with post Mid-Miocene carbonates about 1500 m thick.

Mackerel-1 represents wells located at the shelf edge that record thick sections with rapid late stage burial to about 2000 m, such as Halibut, Athene, Kingfish, Flounder and Selene. In addition to the substantial rapid burial process in the Cretaceous rift phases and Tasman Sea opening in Paleocene, they experienced a very slowed burial process during the Eocene to Mid-Oligocene ca. 50-28 Ma followed by continuous but much quicker burial, especially after Mid-Miocene. In Mackerel-1, nearly 2000 m sediments were deposited during the late stage (ca. 15-0 Ma). Notable Late Eocene- Early Oligocene erosion has been recorded in the burial history, matching seismic and well log data.

Omeo-1 represents wells located at the South and North Terraces that record thick Strzelecki Group with very thin Latrobe Group sediments, such as Pike, Kyarra, Admiral, Leatherjacket. They have similar burial history in the Cretaceous rift phases and the Tasman Sea opening in Paleocene to Early Eocene, with significant erosion in Paleocene and Mid-Late Eocene. After mid-Oligocene, a quicker burial process generated thick Seaspray Group sediments. In Omeo-1, the Strzelecki Group is over 5000 m thick, and only 1000 m Latrobe Group remained. Due to the quicker burial process since the Late Oligocene, the Seaspray Group thickness reaches over 2000 m.



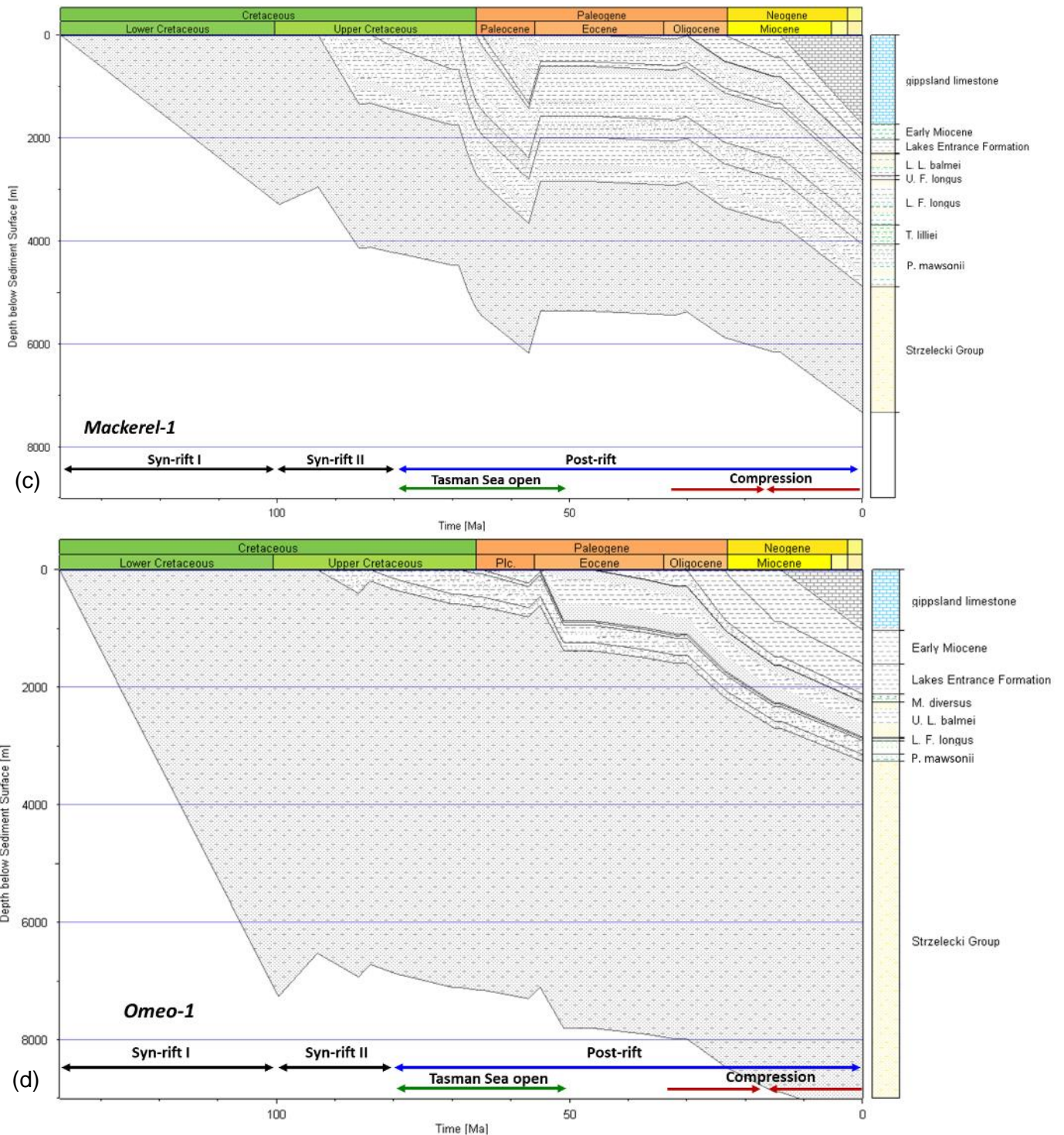


Figure 8-20 Burial history plots extracted from the 3D model at inshore area (Barracouta-1), Central Deep (Veilfin-1), shelf edge (Mackerel-1) and Terrace (Omeo-1).

8.4.2 Temperature Model

The modelled downhole temperature are good fits to the actual well data. The models suggest that, in the deeply buried parts of the Central Deep, the temperature at the base of the Strzelecki Group was about 55 °C at 130 Ma (after some ~7 Ma burial), reached 100 °C by 120 Ma, and 150 °C by 110 Ma.

The present-day rift I temperature at the base of the Strzelecki Group is estimated to be over 320 °C

(Figure 8-21). The temperature at the base of Emperor Subgroup sediments reached 100 °C by ca. 86

Ma, while that at the base Golden Beach Subgroup exceeded 100 °C by ca. 71 Ma. The lower part of the Halibut Subgroup reached 100 °C from ca. 66 Ma, and most of the lower Halibut Subgroup sediments passed 100 °C in the Early-Middle Miocene. Examples extracted from the model at the Angelfish-1, Veilfin-1 and Mackerel-1 location is shown in Figure 8-22.

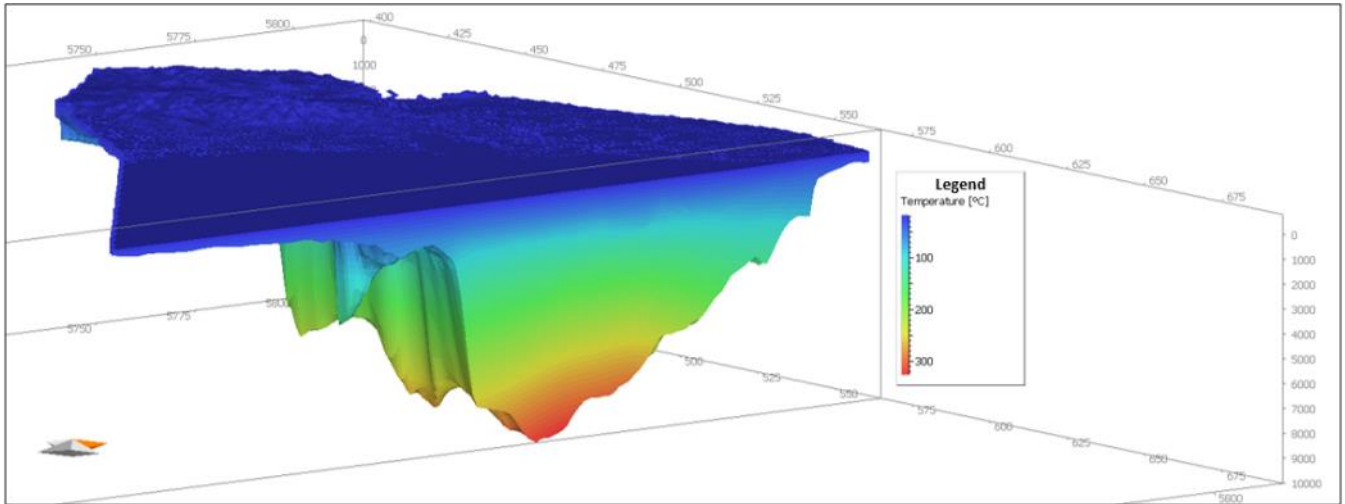


Figure 8-21 3D present-day temperature model clipped across the maximum temperature area.

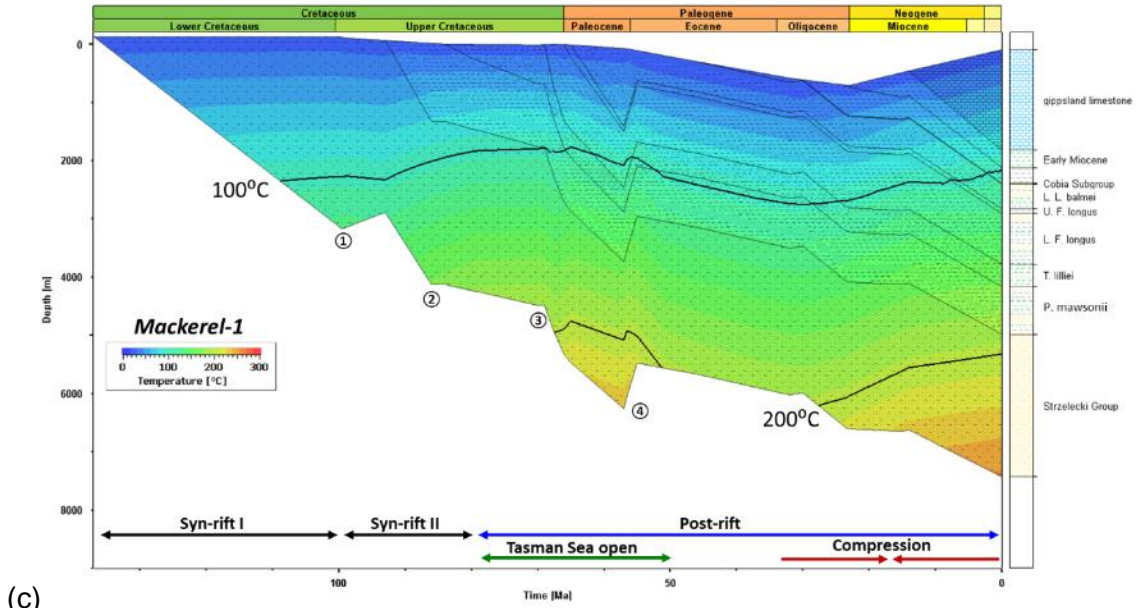
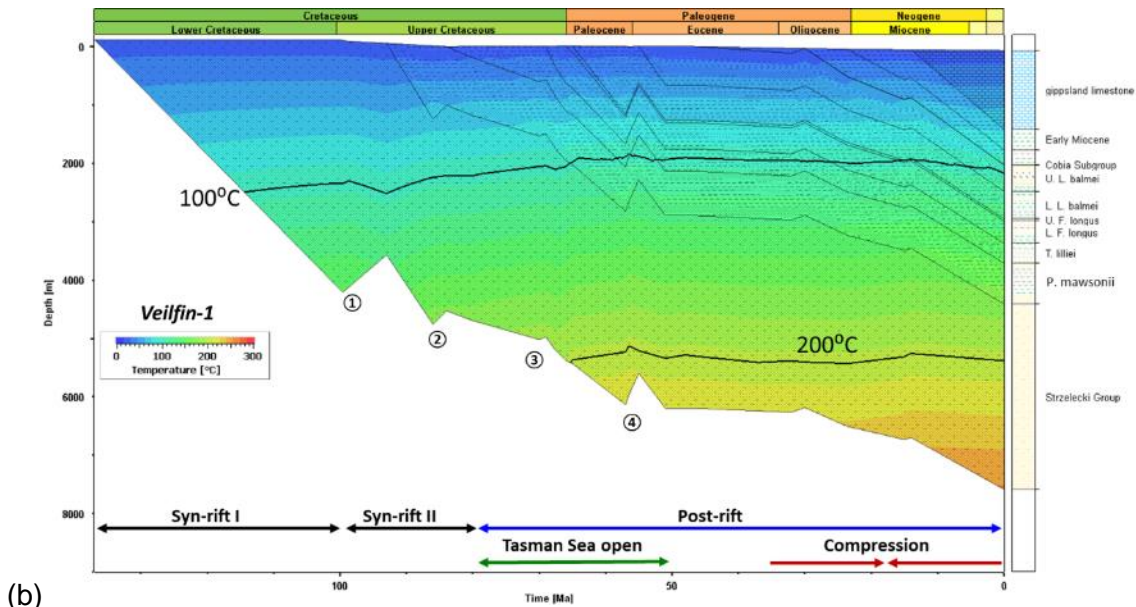
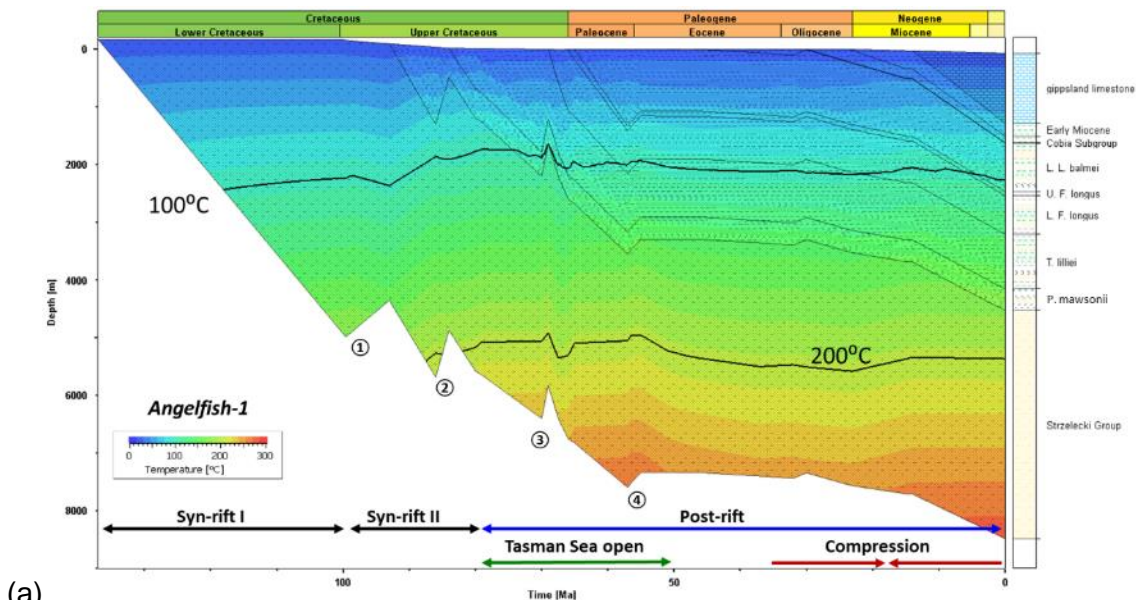


Figure 8-22 Burial-thermal history plots extracted from the 3D model at Angelfish-1, Veilfin-1 and Mackerel-1 showing the modelled temperature overlay. The circled numbers mark the regional unconformities: Otway, North Longtom, Seahorse and Marlin unconformities.

8.4.3 Reflectance Maturation Model

The modelled vitrinite reflectance (R_o) trends correspond to the R_o core analysis data from multiple wells across the basin in the 3D model as discussed above in Quality control & thermal calibration. The 2D strike and dip cross-sections through the centre of the model allow a good overall view of the results and are shown in Figure 8-23. They indicate that the Strzelecki Group in the Central Deep has attained estimated R_o over 2% putting it in the dry gas window (e.g., Sweeney & Burnham, 1990) though it progressively decreases on the basin margins and the North Terrace is currently in the oil window. The Emperor and Golden Beach Subgroups in the Central Deep have attained R_o mostly over 1.3% placing them in the wet gas window. In contrast, the Halibut and Cobia Subgroups in the Central Deep have estimated R_o values mostly over 0.7% but below 1.3% which puts them in the commonly accepted main to late oil window. All other formations and areas have $R_o < 0.7%$ indicating the organic matter is either immature or in the early oil window. The area of low maturity includes wells with the entire Latrobe Group immature, such as Perch-1, Kyarra-1A and Admiral-1, and wells where part of lower Latrobe Group has entered the early oil window between the Middle Eocene and Middle Miocene (e.g., Pike-1, Shark-1).

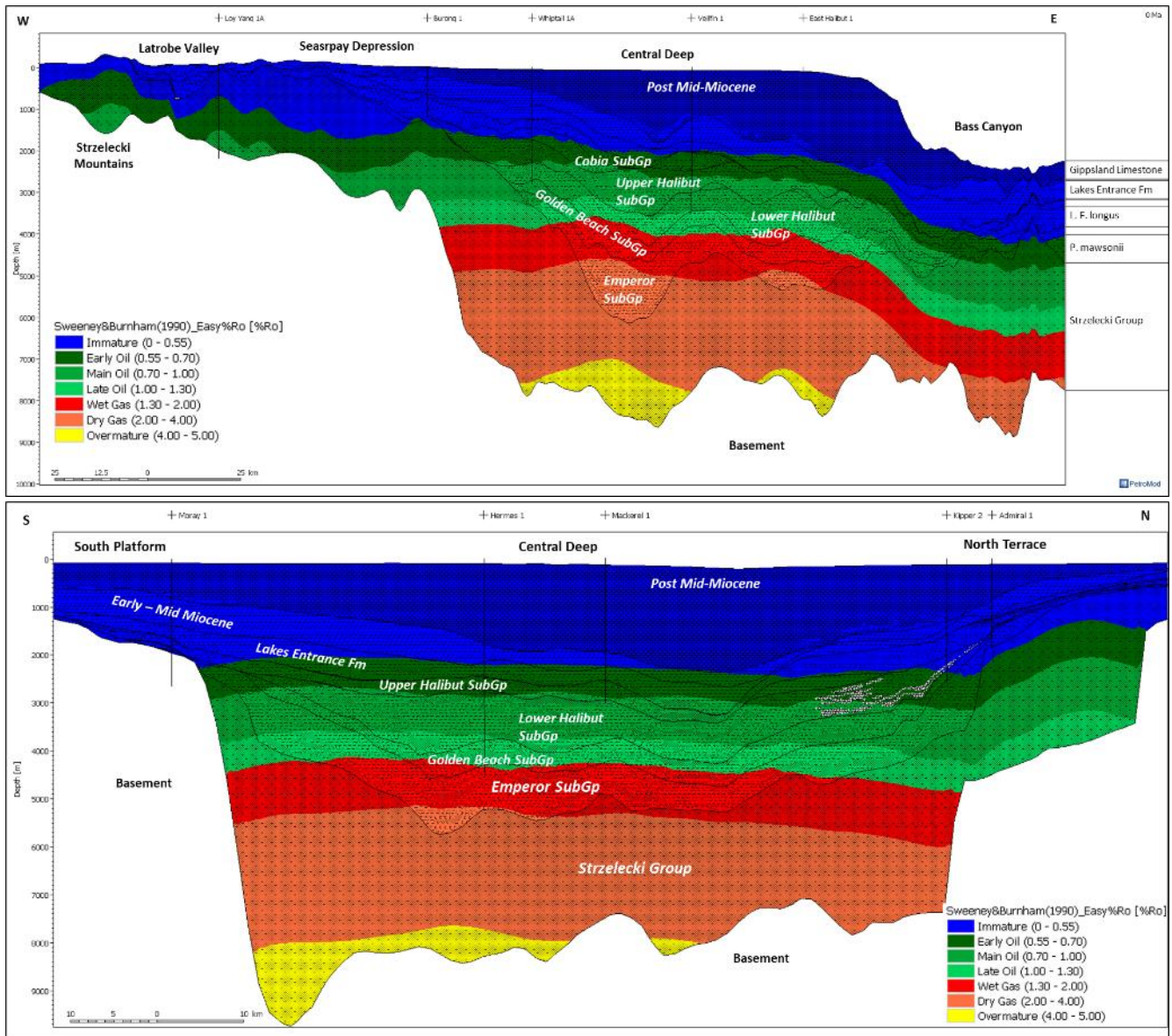


Figure 8-23 Cross-sections are showing the modelled thermomaturity at present-day. Locations are shown in Figure 8-17.

The burial versus Ro plots for 20 wells selected from across the basin indicate a variety of maturity histories, which can be divided into four main groups. An example well plot from each of the four groups (Mackerel-1, Marlin-1, Barracouta-1 and Perch-1) is shown in Figure 8-24. The rest of the plots are included in Appendix 16.

Wells out on the current shelf edge located on the eastern margin of the Central Deep have significantly different maturation histories to the inshore wells and those in the centre of the Central Deep. They include wells in the large oil fields at Kingfish, Mackerel, Blackback, Halibut-Fortescue, Flounder and nearby wells such as Athene-1. These wells underwent moderate burial and maturation in the rift phases, significant erosion of section at Top Latrobe, and substantial rapid burial in the Neogene-Holocene associated with the thermal subsidence, loading and flexural collapse of the shelf. In Mackerel-1 the Strzelecki Group just entered the oil window prior to substantial uplift in the mid-

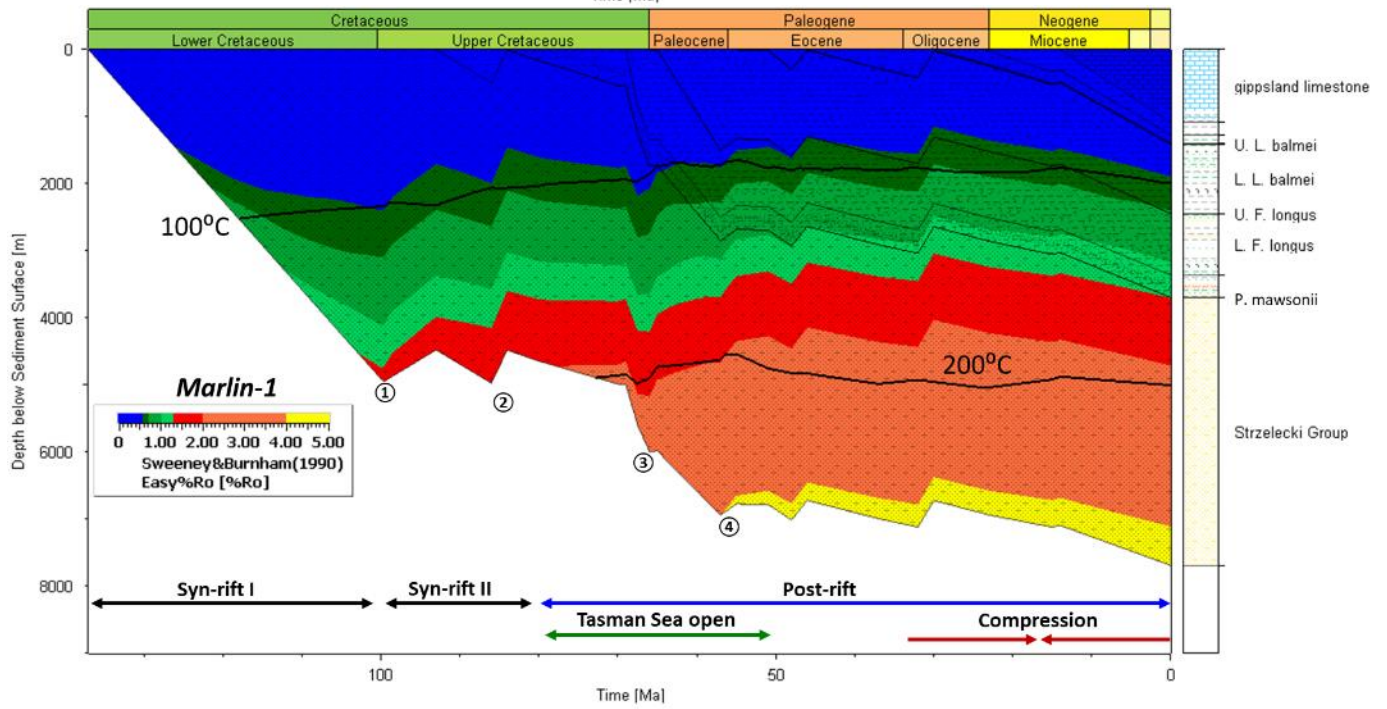
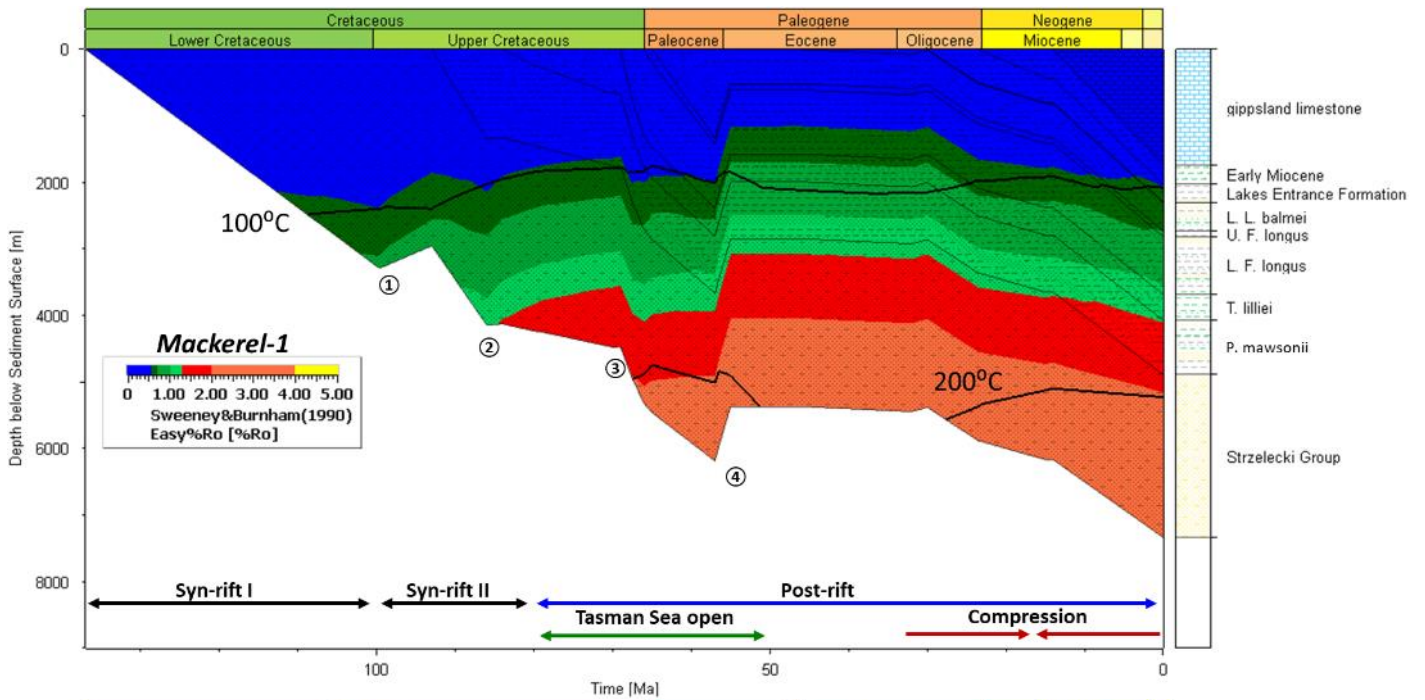
Cretaceous, then went through the oil window in the Late Cretaceous, reaching 4.1 km depth in the Paleocene that put it into the gas window. The Emperor Subgroup (including the Kipper Shale) reached the early and main oil window in Maastrichtian (ca. 68 Ma), the late oil window in the middle Palaeocene (ca. 62 Ma) and is reached the wet gas window in the Middle Miocene (ca. 13 Ma). The Golden Beach Subgroup (Chimaera/Anemone formations) entered the early oil window in the middle Palaeocene (ca. 65 Ma) and reached the late oil window in Late Miocene (ca. 10 Ma). The Early Palaeocene Kate Shale entered the early oil window in the Late Miocene (ca. 9 Ma), placing most Halibut Subgroup in the oil window during the Neogene (Figure 8-24).

Marlin-1 represents wells located within the main Central Deep that record reasonably continuous thick sections, such as Veilfin-1, Luderick-1, Bream-5 and Angelfish-1. They have similar maturation histories, characterised by substantial rapid early maturation histories in the rift phases, which slowed or almost stopped during the Cainozoic. In Marlin-1, the base of the Strzelecki Group reached $R_o \sim 2\%$ and 5km depth by the end of the Early Cretaceous (~ 100 Ma) and continued rapid burial in the Late Cretaceous to depths approaching 8km. Remarkably, the Emperor Subgroup (including the Kipper Shale) reached the early oil window in the Campanian (ca. 75 Ma), the main oil window in the Maastrichtian (ca. 67 Ma) and the wet gas window in the late Oligocene (ca. 23 Ma). The Golden Beach Subgroup (Chimaera/Anemone formations) entered the early oil window in the Maastrichtian (ca. 66 Ma), the main oil window in the Middle Palaeocene (ca. 61 Ma) and the late oil window in the Early Miocene (ca. 23 Ma). Since the Cretaceous, this area remained stable with only minor burial of about 1km since the Miocene so that the organic matter has stayed near its maximum burial temperatures for some 55Ma without further temperature increases. This also means the Early Palaeocene Kate Shale sat near the surface for a long period and did not enter the early oil window until the late Miocene (ca. 10 Ma) and most of the source rocks in the Halibut and Cobia Subgroups are only just entering the oil window or immature (Figure 8-24). In Angelfish-1, the modelled present-day R_o results match the Rock-Eval T_{max} values (~444 degC), measured within the Golden Beach Subgroup.

Barracouta-1 represents wells which are located inshore or close to the edge of the Central Deep, including large gas fields, that underwent slower more continuous early maturation histories, with moderately rapid burial in both rift phases, but which was followed by continuous but much slower

burial in the Cainozoic. In Barracouta-1, the Strzelecki Group just entered the oil window prior to a substantial uplift in the mid-Cretaceous, then went through the oil window in the Late Cretaceous, reaching 5km depth in the Paleocene that put it into the gas window. The Emperor Subgroup (including the Kipper Shale) reached the early oil window in Early Palaeocene (ca. 65 Ma) and has stayed in the oil window and is only just about to reach the wet gas window at the present day. The Golden Beach Subgroup (Chimaera/Anemone formations) entered the early oil window in the middle Palaeocene (ca. 62 Ma) and reached the late oil window in late Miocene (ca. 7 Ma). The Early Palaeocene Kate Shale entered the early oil window in the Early Miocene (ca. 23 Ma) placing most of the Halibut Subgroup in the oil window during the Neogene. The younger strata are continuous with little loss of section at the top Latrobe Group but this section is immature (Figure 8-24).

Wells such as Barracouta-1 grade into wells located further inshore or onshore in which the entire Latrobe Group has remained immature, such as Perch-1 (Figure 8-24), Kyarra-1A and Admiral-1 (Appendix 16).



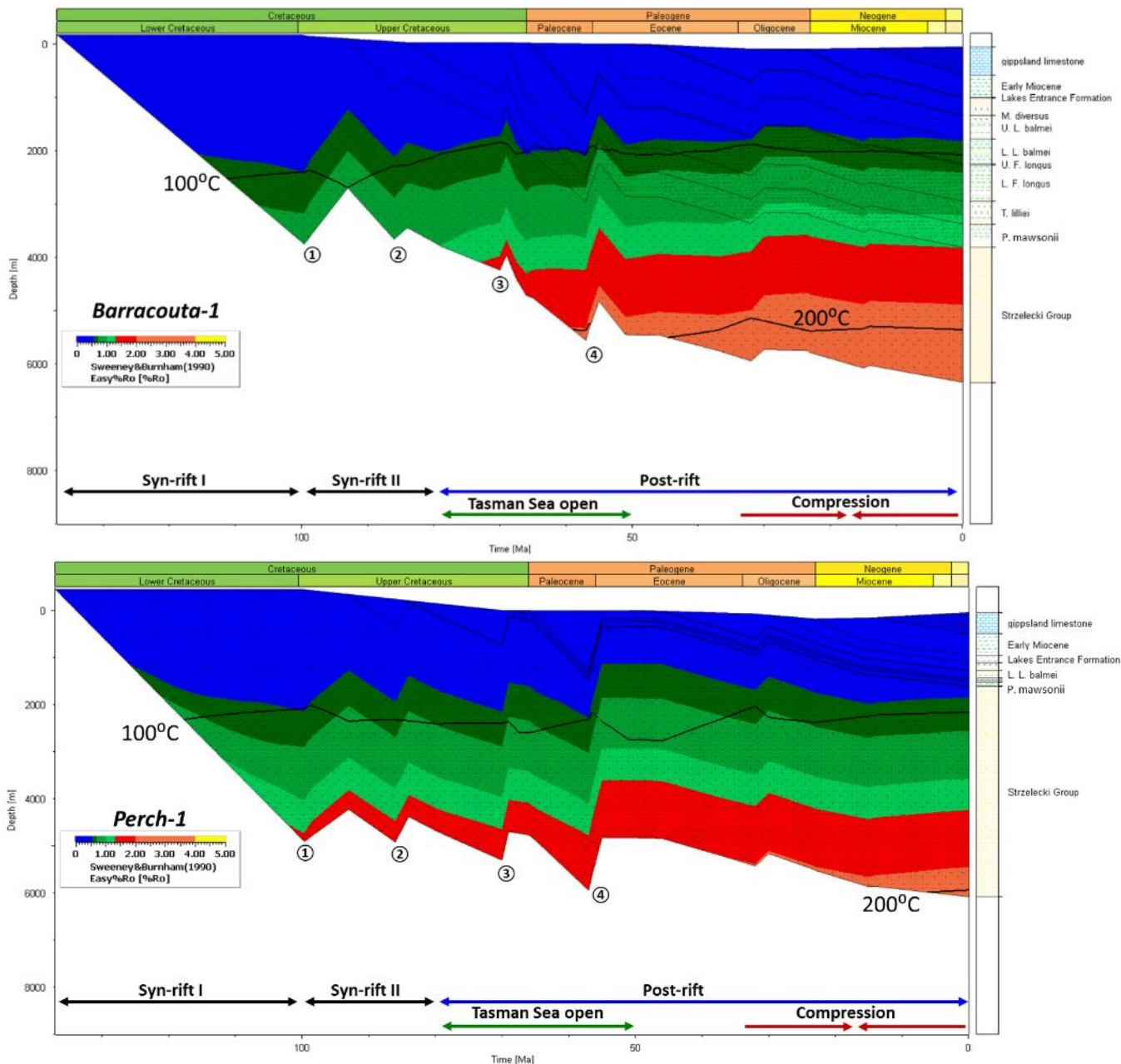


Figure 8-24 Burial-thermal history extracted from the 3D model at well Mackerel-1, Marlin-1, Barracouta-1 and Perch-1 (from top to bottom), overlay with Ro. The circled numbers marked the regional unconformities: Otway, North Longtom, Seahorse and Marlin unconformities.

8.4.4 Pressure Model

The pressure models show a general linear relationship between downhole pressures and depth. As expected, the present-day hydrostatic pressures are lower than the lithostatic pressure (Figure 8-25). Most of the well sections are essentially normally pressured given the general good lateral and vertical migration through most of the Latrobe Group. The modelled maximum hydrostatic pressure is 102.2 MPa, while that of lithostatic pressure in the Gippsland Basin model reaches 246.4 MPa.

Some minor areas of overpressure are estimated from the combination of facies, burial and maturation models that control the calculation of overpressure zones. The modelled present-day overpressure simulation indicates a number of overpressure zones in the deeper formations within the lower Latrobe

Group (Figure 8-26). They are mainly developed in or beneath coal, shale and volcanic lithologies. The overpressures associated with the shales and coal seams are minor. They include within the deeply buried coals and Kipper Shale within the Emperor Subgroup where the overpressures are between 1.8-5 MPa and in shales within the Golden Beach Subgroup where they are between 1.5-8 MPa. Higher overpressures occur in the Volador Formation where the overpressures associated with the shales and coals reach 11.2 MPa. Anomously higher overpressures occur in or below the volcanics, though these very high values probably result from erroneous petrophysical characteristics in *PetroMod* that allocates very low permeabilities for the volcanics (Figure 8-27).

Overall, the overpressure zones are sporadic, but tend to be mainly associated with the deeply buried shales in the Kipper, Golden Beach and Volador formations in the east and south-east of the Central Deep (Figure 8-26). A second group tend to occur more along the North Terrace where there are more numerous volcanics, though this may be partly spurious. There is a weak correlation with the large oil fields in the south-east and with the gas fields in the north-west, which might point to primary and secondary migration of oil and gas into the Gippsland petroleum traps, from the source rocks in the eastern parts of the Central Deep.

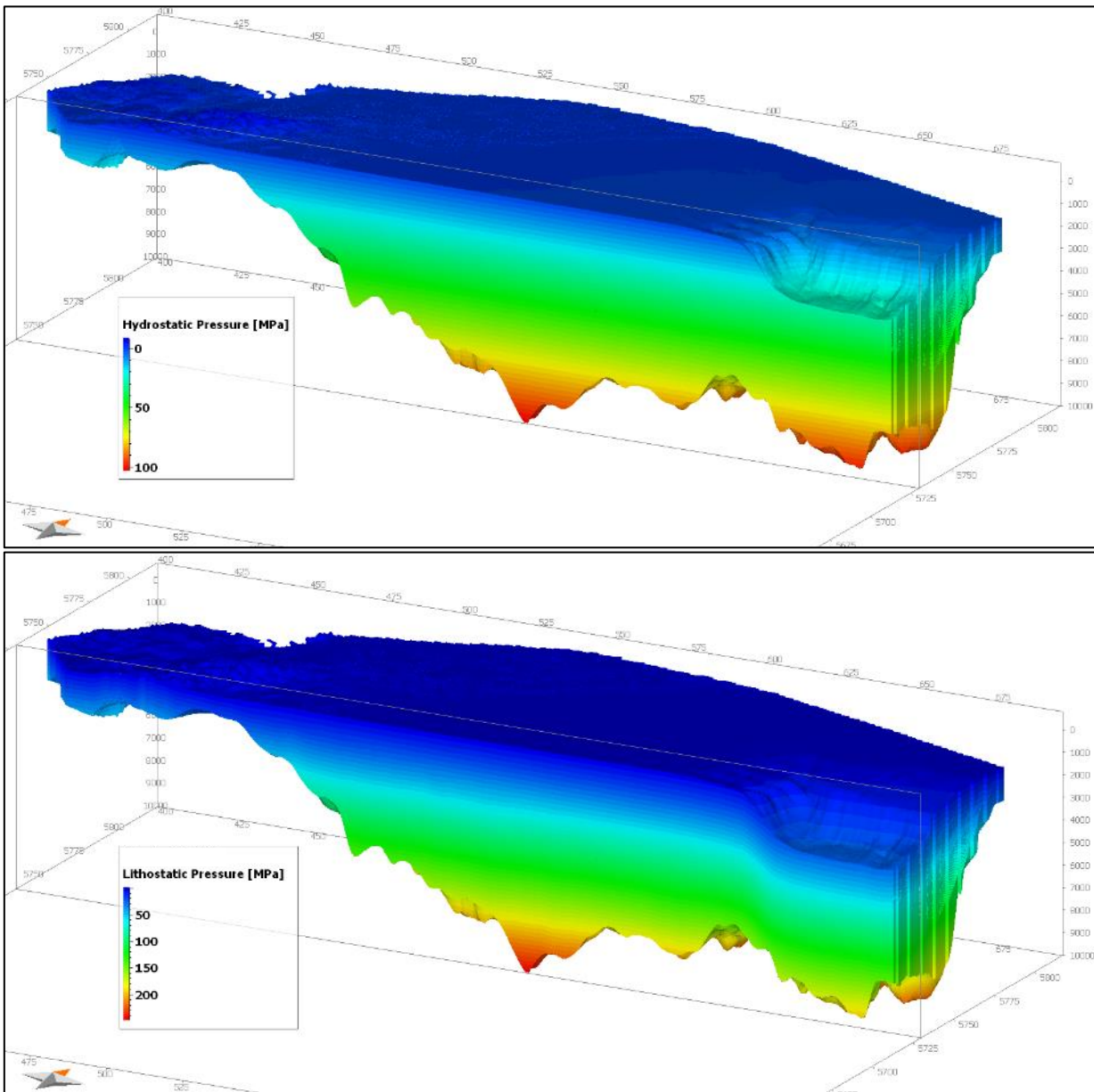


Figure 8-25 3D present-day pressure models: hydrostatic pressure (top) and lithostatic pressure (bottom), with the southern part of the 3D volume clipped to show an axial section through the maximum pressure area.

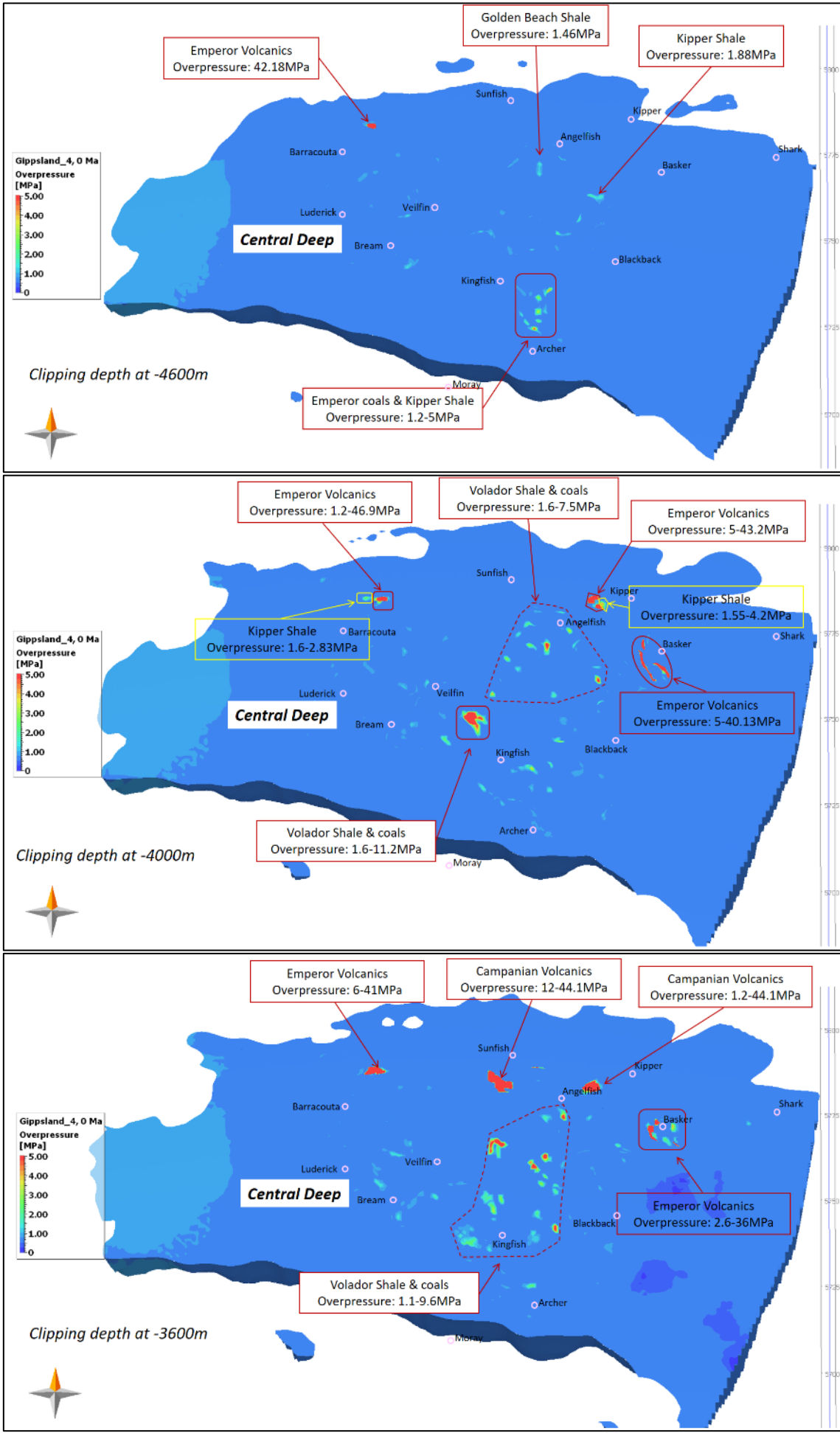


Figure 8-26 Simulated 3D overpressure model, shown on depth slices at -4600m, -4000m and 3600m.

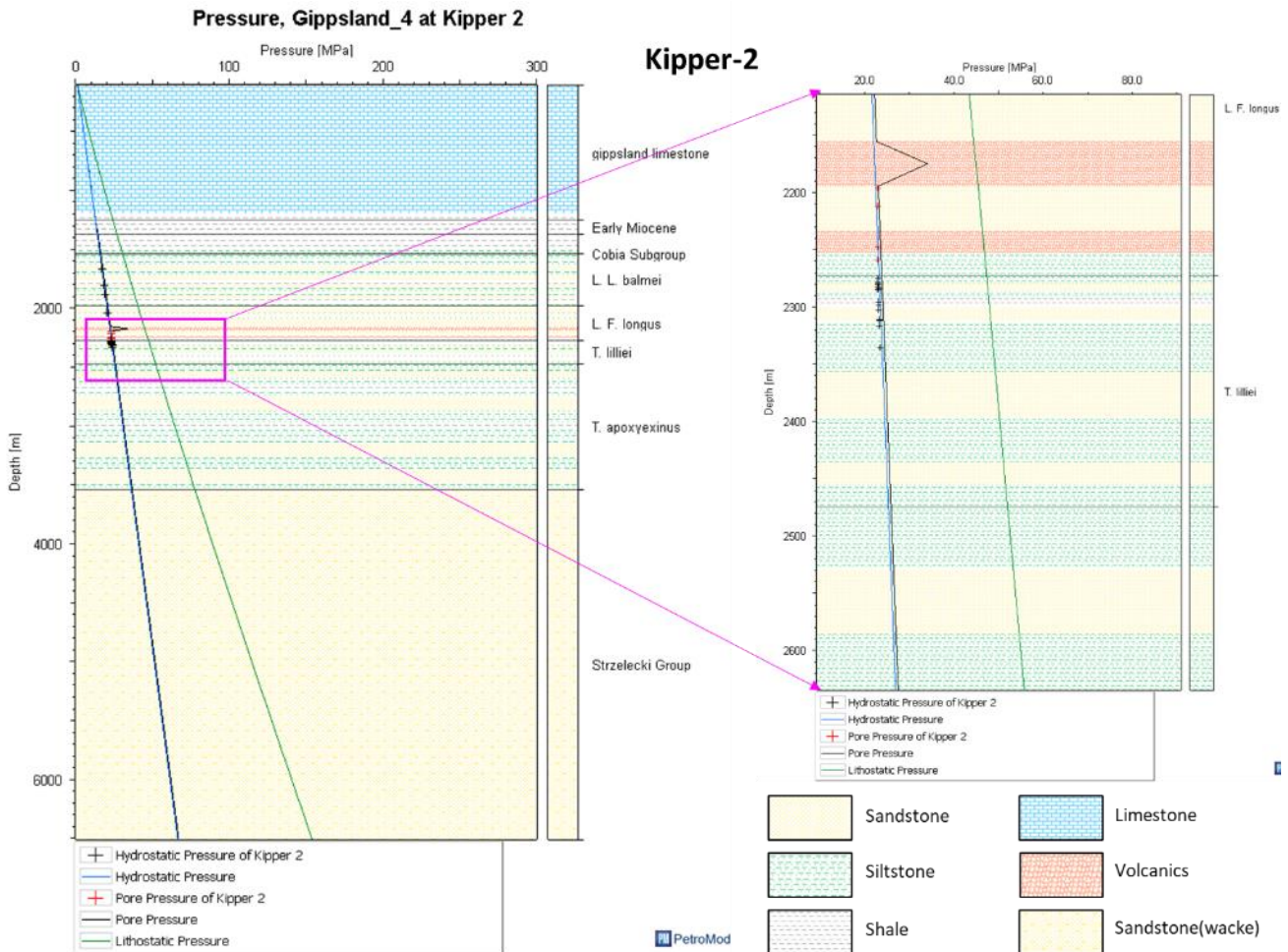


Figure 8-27 Pressure plot extracted from the 3D burial model for Kipper-2 showing the match to the measured pressure data. The overpressure is associated with volcanic intervals.

8.4.5 Validating Temperature, Ro and Pressure values in *PetroMod* using the *Petrel* Model

Temperature, pressure and time are important variables which affect the burial diagenesis and coalification processes. Vitrinite reflectance (Ro) is one of the more sensitive indicators that represent the geothermal rank and maturity of organic matter. The property models built in *Petrel* utilised a large amount of measured data from hundreds of petroleum wells, such as temperature, pressure, Ro, TOC, HI. The good coverage and considerable amount of measured data allow the property models to be used as realistic models and compared with the theoretical models built in *PetroMod*.

The temperature model comparison is very good throughout most of the basin with an overall difference of slightly over 5% (Figure 8-28). The *PetroMod* modelled temperature (maximum 321.6 degC) is slightly higher than the realistic temperature model (maximum 304.2 degC). The temperature difference between the theoretical and realistic models is more apparent in the deeply buried Central Deep area than onshore, on the Platforms or Terraces. The main area where the temperatures are different is in the southeast of the Central Deep area around Archer-1 (Figure 8-29) with a temperature variation of about 40 degC at lower Halibut Subgroup. The extracted 1D calibration of the wells along

the shelf edge in the south-east shows that the *PetroMod* theoretical model results in higher temperature values than the measured data (e.g., Athene-1, Figure 8-18; Archer-1, Figure 8-29c). The thermal gradient map calculated from the realistic model indicates that the southeast Central Deep area, where Archer-1, Anemone-1, Selene-1 and Helios-1 are located) has a relatively lower average thermal gradient than the rest of the Central Deep area (Figure 7-18).

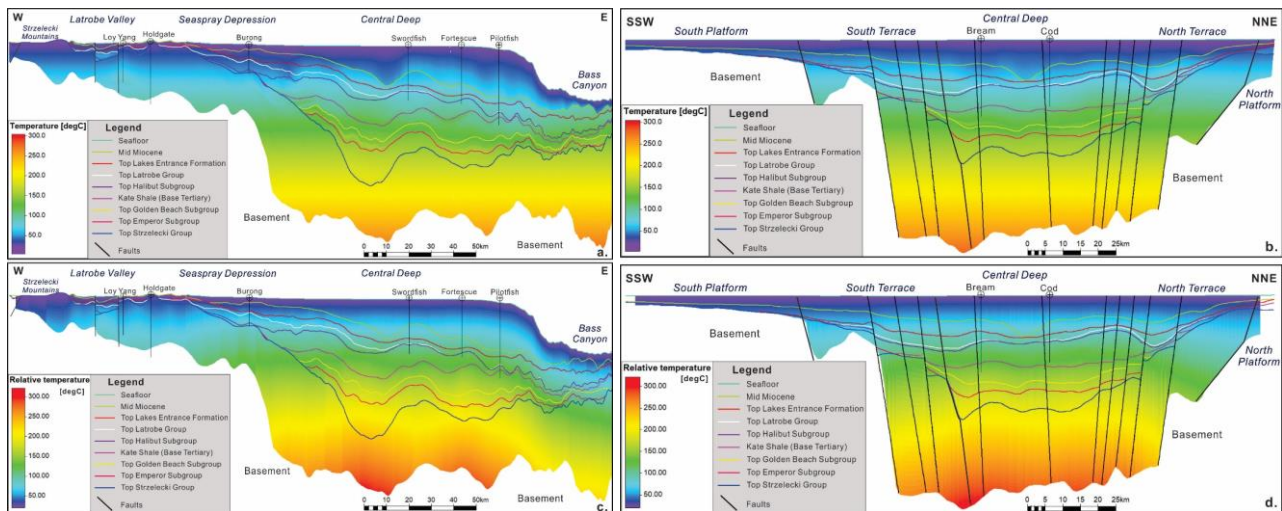


Figure 8-28 E-W and NNE-SSW sections comparing the *Petrel* temperature model (a top) and the *PetroMod* temperature model (b bottom).

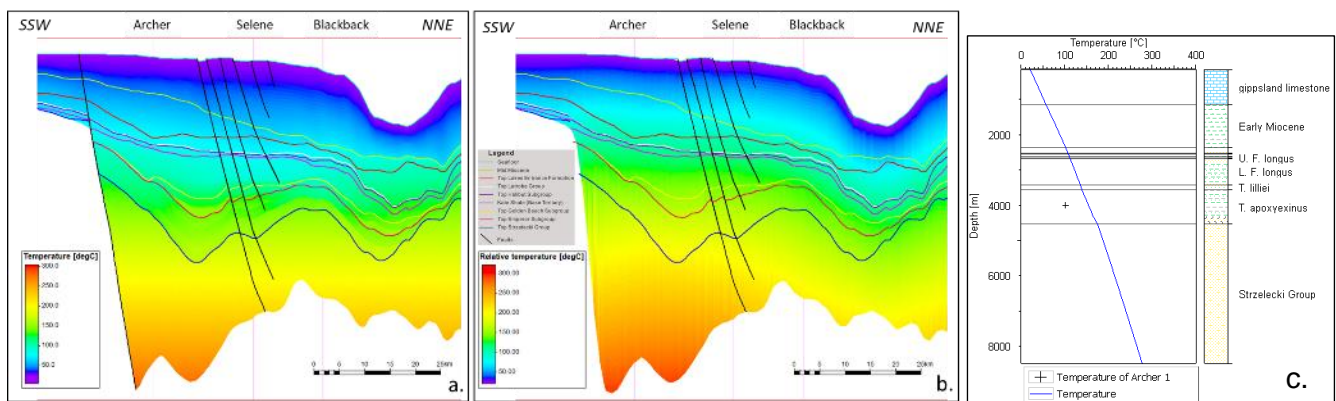


Figure 8-29 NNE-SSW sections through Archer-1, Selene-1 and Blackback-1 comparing the *Petrel* model (a) and the *PetroMod* model (b) at the shelf edge of the Central Deep. c: The temperature calibration extracted from the *PetroMod* theoretical 3D model at well Archer-1. The marked horizons are the same as in Figure 8-28.

The modelled vitrinite reflectance (R_o) results show good agreement over much of the basin where there is well control, such as in the Central Deep and down to the base Palaeocene, but differences increase where well control diminishes, such as great depth, on the flanks of the Central Deep and onshore in the Strzelecki Group (Figure 8-29 and Figure 8-30). The cross-sections show that the R_o values in the *Petrel* model tend to follow the structure with lower R_o values in the synclines and higher R_o values on the highs. This results from good honouring and fitting of the well data and is exacerbated by extrapolation of the well data within the stratigraphic zones. In contrast, the R_o values in the *PetroMod* model are mostly temperature-depth controlled, so while honouring the well data they

do not honour the structure when extrapolated between wells. The two different methods used to generate the *Petrel* and *PetroMod* models have essentially created two different scenario models, both are wrong but it is instructive to compare them to understand the cause of the differences and assess which is most likely to estimate the Ro in areas of sparse data.

The difference in Ro at the Top Latrobe Group -Top Traralgon Seam horizon is <0.1% Ro over most of the basin, with the Ro in the *Petrel* model being less than in the *PetroMod* model, and the difference increasing slightly in the synclines where the *Petrel* modelled Ro values are some 0.2% lower (Figure 8-30). The difference is reversed in the deep Bass Canyon where the *Petrel* Ro > the *PetroMod* Ro values because the *Petrel* model continues the well data trend in the stratigraphic zones beneath the water column whereas the *PetroMod* model uses the temperature-depth relationship below the seabed. The largest difference is in the Strzelecki Ranges where the *PetroMod* model grossly underestimates the Ro by relying on the temperature-depth relationship and does not predict the large increase in Ro, even though it has the missing section map, because the Ro calculation does not depend on time as shown best by the dip sections (Figure 8-29).

These differences are continued with depth, being similar at the Base Palaeocene horizon but becoming more extreme at the Top Emperor horizon and in the Strzelecki Group (Figure 8-29 and Figure 8-30). The above results in differences in the levels of maturation predicted by the two models, with the *PetroMod* theoretical Ro model indicating a higher maturation than the realistic *Petrel* model in the Central Deep area. The extreme difference is at the Strzelecki Group level in the deep basin centre, where the *PetroMod* burial model suggests the deepest part of the Strzelecki Group sediments has entered the over mature phase with Ro reaching a maximum of ~4.6%, while the realistic model implies the Strzelecki Group would still be in the dry gas window with a Ro of ~3.4%.

In contrast, the maturation level of the *PetroMod* theoretical model is lower than the *Petrel* realistic model in the North and South Terraces and onshore. The realistic Ro model indicates that the lower part of the Strzelecki group entered the wet gas window on the North Terrace (which is consistent with the oil and gas occurrences), whereas the theoretical model suggests it has only reached the late oil phase. The substantially lower Ro results onshore in the theoretical *PetroMod* model, especially the Strzelecki Group beneath the Latrobe Valley Tertiary sediments, have the largest impact on estimated maturation levels. The maturation level indicated by the *Petrel* model has the Strzelecki Group mostly

in the oil to wet gas phase, whereas the theoretical *PetroMod* model has it mainly immature or in the early oil window.

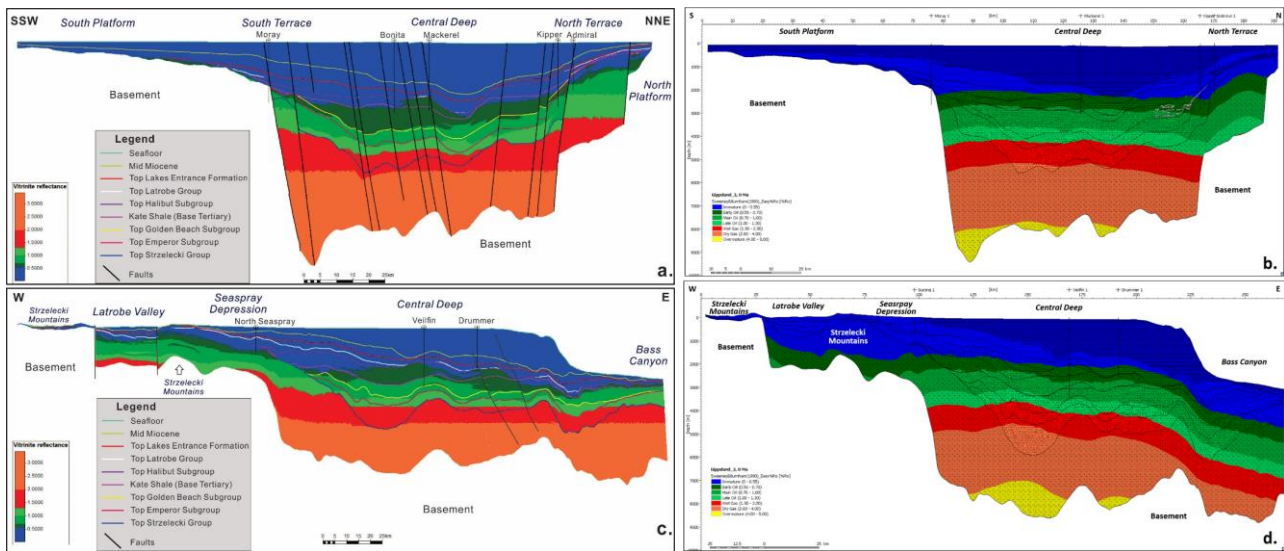


Figure 8-30 The comparison of modelled R_o results between *Petrel* realistic model (a & c) and *PetroMod* theoretical model (b & d). The results are extracted from the same cross-section locations, shows in Figure 8-17.

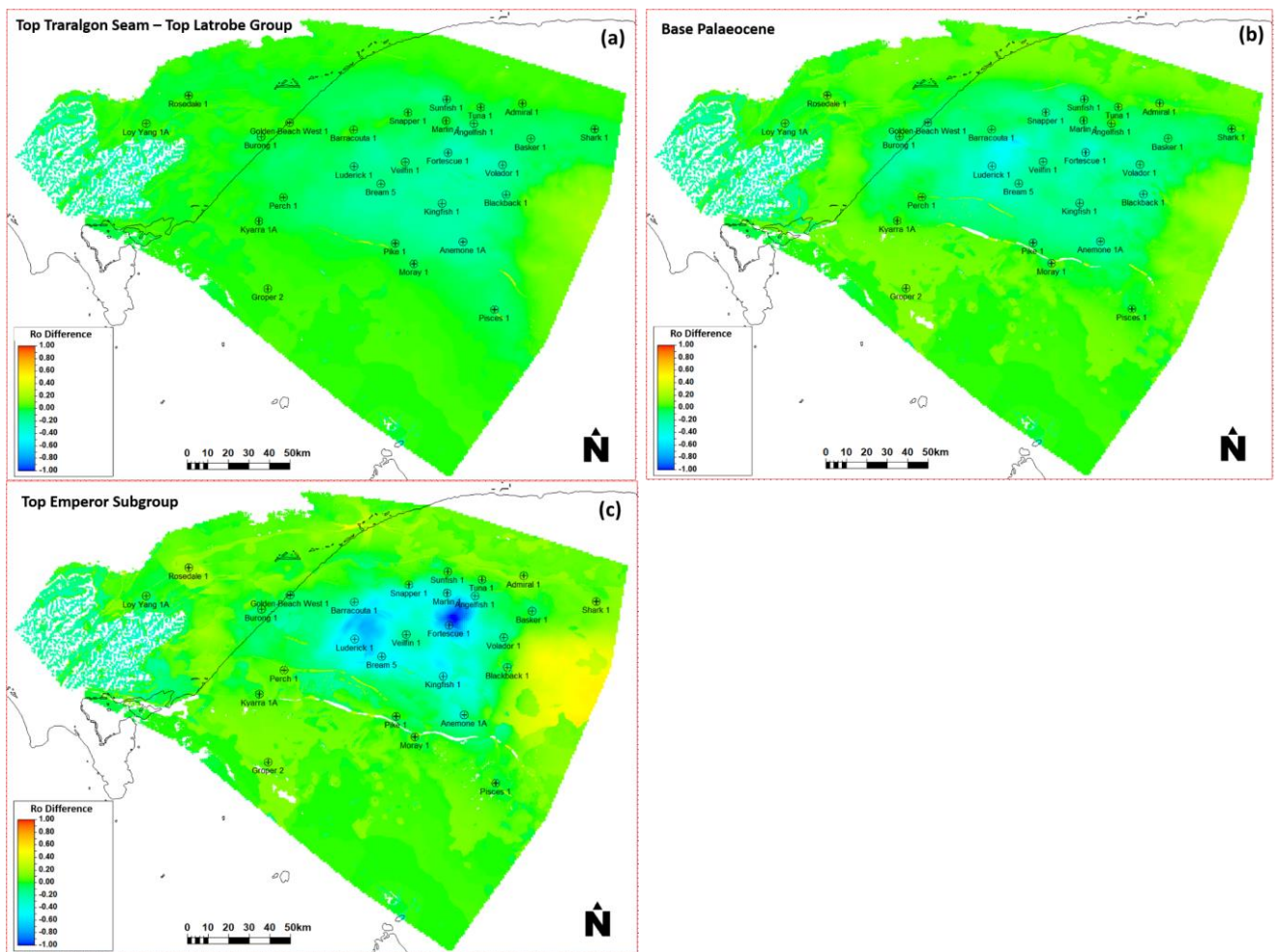


Figure 8-31 Maps showing difference between R_o in *Petrel* and *PetroMod* models at Top Traralgon Seam-Top Latrobe, Base Palaeocene, Top Emperor Subgroup

Again, the modelled R_o values at the southeast edge of the Central Deep indicates a significant difference between the *Petrel* realistic model and the *PetroMod* theoretical model (Figure 8-32). The

present-day maturation modelled from the measured well data suggests an early-late oil window for the lower Latrobe Group (Golden Beach and Emperor Subgroups), dry gas window at the base Strzelecki, and the overlying sections are mainly immature. However, the theoretical model implies more mature stages for the sediments deposited in that area, such as the Lakes Entrance sediments having entered the early oil window, and the base Strzelecki sediments reaching the over mature phase. Similar overfitting remained till the edge of the Bass Canyon, where the Blackback well is located.

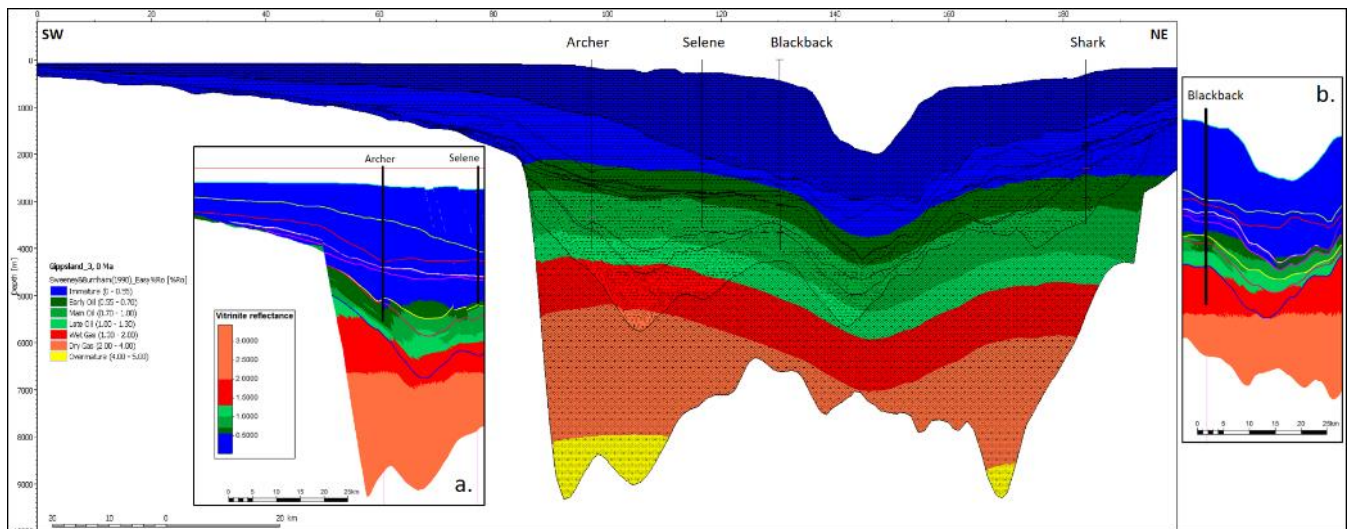


Figure 8-32 The maturation phase comparison between the 3D realistic Petrel model (a & b) and the PetroMod forward model.

Different settings were assigned to the same 2D cross-section across the southeast edge of the Central Deep to analyse the cause of overheating in that area. The erosion amount on the South Platform and the crust lithology are the two variables which has been tested. The palaeo-landscape model (Chapter 6) demonstrates long-term alluvial or fluvial-deltaic environments with continuous erosion, and Weber et al. (2004) suggest the Furneaux Islands had experienced 2-4 km burial depth at ~120 Ma. Hence, the erosion amount on the south platform can be relatively large as the Gippsland onshore denudation amount reaches 1-3.5 km. In the 3D model, the mid-Cretaceous erosion amount at that area is set as ~2.4 km, resulting in overheating compared to measured geothermic data. However, the temperature results of the testing model indicate minimal improvement, with a larger erosion amount of ~5 km (Figure 8-33). The test model using different crust lithology, continental average crust rather than continental granite crust, shows a better improvement of the temperature simulation at the southeast edge of the Central Deep area (Figure 8-34, left). The palaeo-heat flow simulated in test model decreased by about 9mW/m² at each time step. However, the continental average crust cannot provide enough heat; for example, the Ro calibration at well Shark-1 indicates an

unsatisfactory fitting (Figure 8-34, right). More examples are in Appendix 17. This shows that crust lithology has more significant effects on the heat flow simulation process in *PetroMod* modelling.

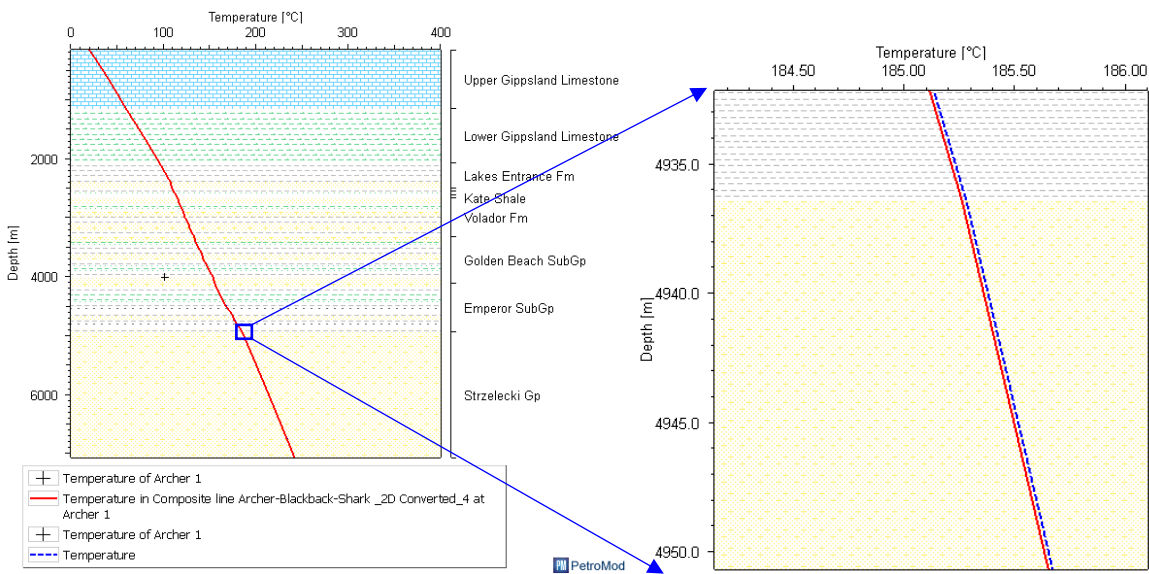


Figure 8-33 Temperature calibration plot extracted at well Archer-1. Blue dash line is the initial model using a 2.4 km erosion amount; the red is the modelled curve using a 5 km erosion amount.

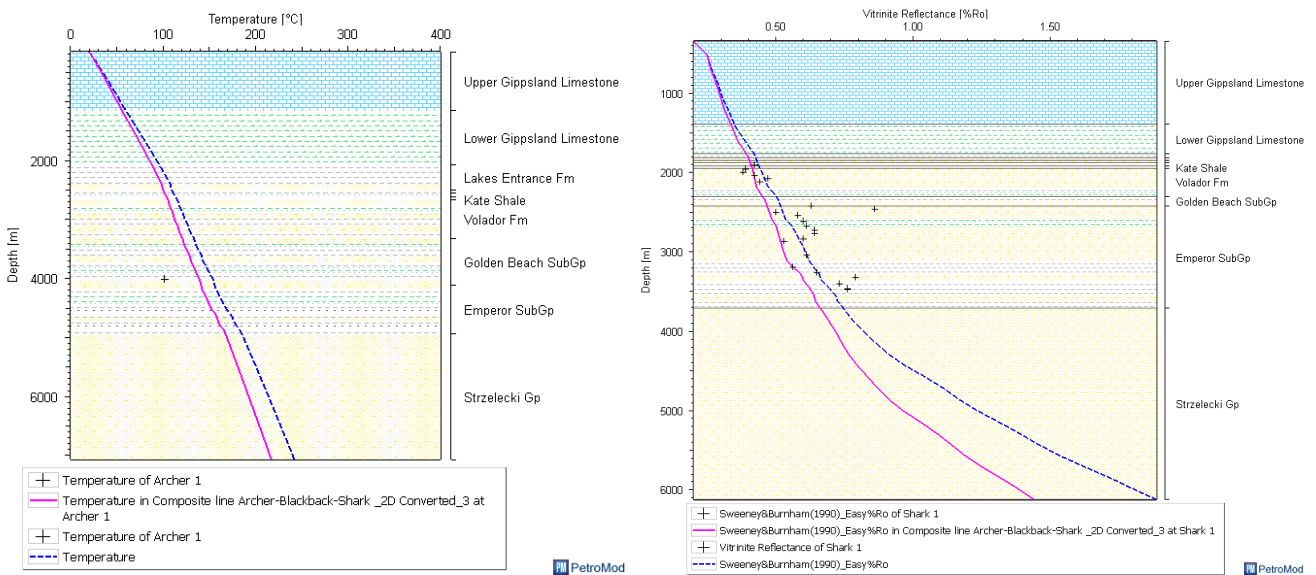


Figure 8-34 Left: the temperature calibration plot extracted at well Archer-1. Right: the vitrinite reflectance calibration plot extract at Shark-1. The blue dash-line is the initial model using continental granite crust, while the pink line is the modelled curve using continental average crust. Crosses denote the measured data.

The hydrostatic pressure model comparison is shown in Figure 8-35 indicates the *PetroMod* modelled pressure (maximum 14595 pisa) is very close to the *Petrel* realistic pressure model (maximum 15070 pisa). The results between the two models are very similar across different parts of the entire basin, as the hydrostatic pressure is mainly a linear function that responds to true vertical depth.

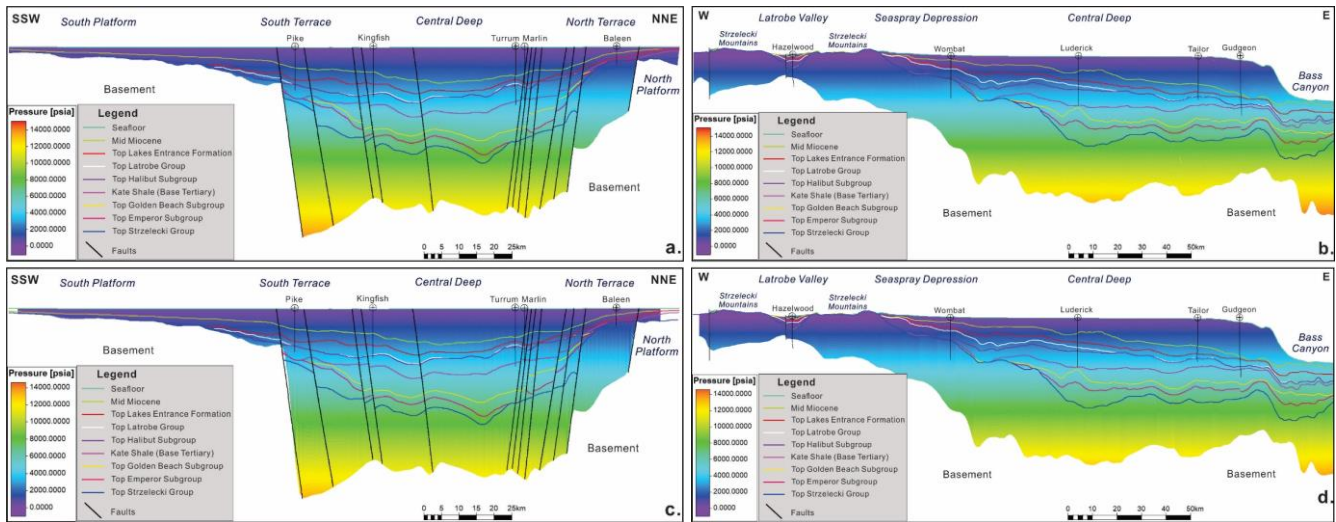


Figure 8-35 The pressure model compares the Petrel property model (a, b) and the PetroMod burial-thermal model (c, d) using SSW-NNE and west-east cross-sections.

8.5 Discussion

8.5.1 Potential Source Rocks

The forward 3D landscape modelling for the offshore Central Deep in the early Late Cretaceous (93 to 89 Ma) begins with an intracratonic syn-rift basin in which the Emperor Subgroup sediments were deposited in fluvial dominated paleo-environments with multiple lakes, that probably developed at some stage into a large shallow inland sea, with intracratonic deltas and coastal marshes developed around its shoreline (Chapter 6). This regional facies model should promote deposition of perhydrous organic-rich shales in a variety of lithofacies recognised as the *Kipper Shale*, and these potential source rocks coincidentally formed during the Cenomanian-Turonian ocean anoxic event, and now lie beneath the major petroleum fields, including Barracouta, Bream, Flounder, Kingfish, Kipper, Marlin and Perch (Figure 8-36).

Once the Tasman Sea spreading began between 86 Ma and 83 Ma, deposition of fluvio-lacustrine, deltaic and restricted marine sediments started, initially with more shallow seas, producing potential source rocks within the *Chimaera Formation* in the Golden Beach Subgroup. The *Badlands* simulation shown in Figure 8-36 is an example of how large amounts of clastic sediment were deposited in low energy clastic environments, with peatlands, lacustrine, lagoonal and newly developed restricted marine facies, that commonly produce good source rocks with high amounts of perhydrous organic matter, typically including liptinites and alginite, as found in the *Chimaera Formation*.

A well established and long-lived aggradational shoreline system established through the Late Cretaceous with extensive barrier systems building into the Palaeogene, behind which accumulated

thick successions of fluvio-deltaic and coastal depositional sediments characterised by perhydrous coals and organic rich lacustrine, interdistributary and lagoonal shales (*Halibut Subgroup*). Frequent transgressive-regressive cycles occurred, with the simulated Kate shale (ca. 65 Ma) representing one of the major incursions, that would have ponded the coastal and floodplains producing extensive source rock facies throughout the Latrobe Group (Figure 8-36). The *Cobia Subgroup* developed during the Eocene to early Oligocene when the fluvio-deltaic-coastal systems were pushed back over a hundred kilometres by successive marine transgressions creating extensive and continuous ponding and resulting in widespread and probably the best developed source rocks.

These Latrobe Group source rocks are together credited with generation of the giant oil and gas fields in the Gippsland Basin (it should be noted that the oils are very light API oils mostly retrograde condensates). The petroleum is typed primarily to the mixed non-marine and marginal marine source rocks in the Halibut and Cobia Subgroups (Burns et al., 1984, 1987; Moore et al., 1992; Abassi et al., 2016). Less is known about the deeper source rocks in the Golden Beach and Emperor Groups though these have also been typed to petroleum accumulations as more wells are drilled on the flanks of the Central Deep (Edwards et al., 2016).



Figure 8-36 Palaeo-landscape of the Gippsland Basin at 93 Ma, 84 Ma and 65 Ma (Appendix 7).

The modelled Organic Transformation ratios (TR) in Figure 8-37 and Figure 8-38 show that current TR values over 80 mainly occur in the Emperor Subgroup (Kipper shale), Golden Beach Subgroup and lower Halibut Subgroup (Volador formation) and that the source rocks surpass the critical TR > 50% more in some parts of the basin, such as near the southern and northern platforms.

The individual plots of estimated TR for wells, Snapper-1, Marlin-1, Barracouta-1, Luderick-1, Veilfin-1, Halibut-1, Mackerel-1, Kingfish-1 and Angelfish-1 (Figure 8-39) show that the Emperor Subgroup commences significant organic transformation in the Palaeocene (TR > 10%) and passes the TR > 50% threshold during the late Palaeocene to Early Eocene. The Golden Beach Subgroup commences

significant organic transformation during the late Eocene to Oligocene (TR > 10%) and passes the TR > 50% threshold in the Miocene. In most areas, the lower Halibut Subgroup source rocks start organic transformation (TR > 10%) in the late Miocene and areas with rapid late stage burial reach TR>50% by the Late Miocene (e.g., Halibut-1, Luderick-1). In Marlin-1, the thick lower Halibut Subgroup source rocks commence surpassed the significant organic transformation during the late Paleocene (TR > 10%) and passed the TR > 50% threshold in the Late Eocene.

Hence, the temperature and maturity simulations accompanying the burial history highlight multiple potential source rock intervals within the lower Latrobe Group spanning the Late Cretaceous to Early Palaeocene within the Gippsland Basin. They include the organic rich rocks in the Emperor, Golden Beach and Halibut Subgroups to form three source rock assemblages. The timing of the maturation of these source rock assemblages is different, with the early maturing source rocks in some areas occurring before trap formation, such as the source rocks near base Emperor Subgroup. Some younger Emperor Subgroup source rock intervals passed the TR > 50% threshold in the Late Oligocene and over 80% at Recent, such as Veilfin-1 and Mackerel-1. Although the late maturing source rocks in the lower Halibut Subgroup is not well spread across the basin, the timing of the maturation is occurring after trap formation, for instance, Halibut-1, Luderick-1.

The most structural traps in the Gippsland Basin are active from Miocene to Holocene. The organic transformation ratio (TR) maps of Golden Beach Subgroup and lower Halibut Subgroup source rocks at 30 Ma, 15 Ma and 0 Ma highlight the maturation process and location. At 30 Ma, the Golden Beach Subgroup source rocks with TR>30% are mainly located at Northwestern parts of the Central Deep, next to Marlin, Turrum, Barracouta, Whiting, Snapper and Bream. Close to the shelf edge, Kingfish, the source rocks reached TR values over 10%. At 15 Ma, the Golden Beach Subgroup source rock area passes the TR > 50% threshold expanded and occurs in the centre area next to Veilfin. At 0Ma, the Golden Beach Subgroup source rocks in the Central Deep reached 50%, and the TR value passes 80 close to some oil/gas fields, such as Barracouta, Kingfish, Turrum, Marlin, Fortescue/Halibut and Flounder. The lower Halibut Subgroup source rocks with TR>10% are located at similar places as the Golden Beach Subgroup at 30Ma, which mainly occurred northwest next to Marlin, Turrum, Barracouta, Whiting, Snapper and Bream, with few TR over 70%. At 15 Ma, the lower Halibut Subgroup source rocks with TR>10% expanded towards east and south, reaching Kingfish, Tarwhine

and Omeo. At 0 Ma, the lower Halibut Subgroup source rocks within the Central Deep commence significant organic transformation (TR>10%), with most areas passing 50%. The TR value reaches 80% near oil/gas fields, such as Tarwhine, Turrum, Marlin, Fortescue/Halibut and Flounder. The syncline next to Barracouta-Whiting folds shows the lower Halibut Subgroup source rocks TR value reaches 90% at Recent.

The organic transformation ratio maps of the Emperor Subgroup source rocks at 30 Ma, 15 Ma and 0 Ma, are attached in Appendix 18.

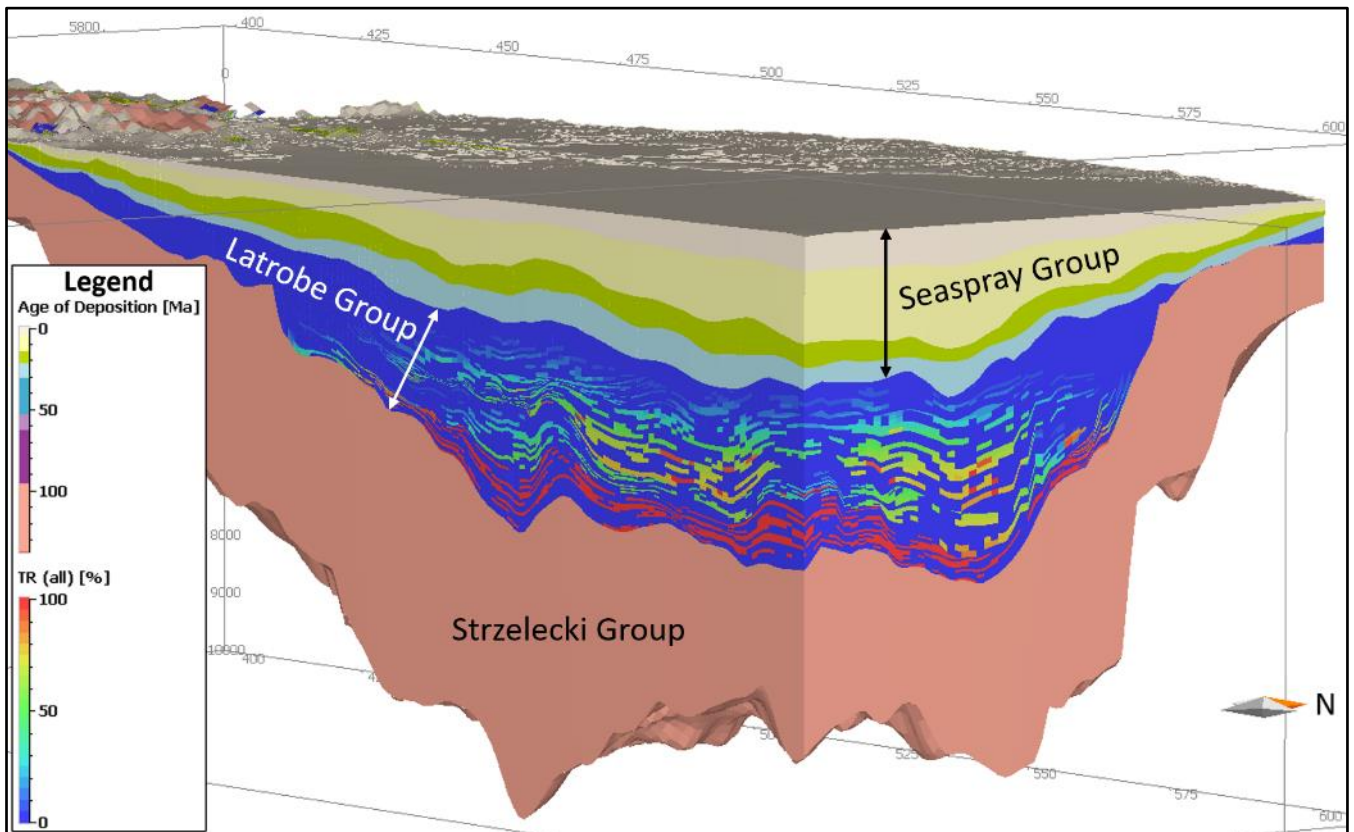
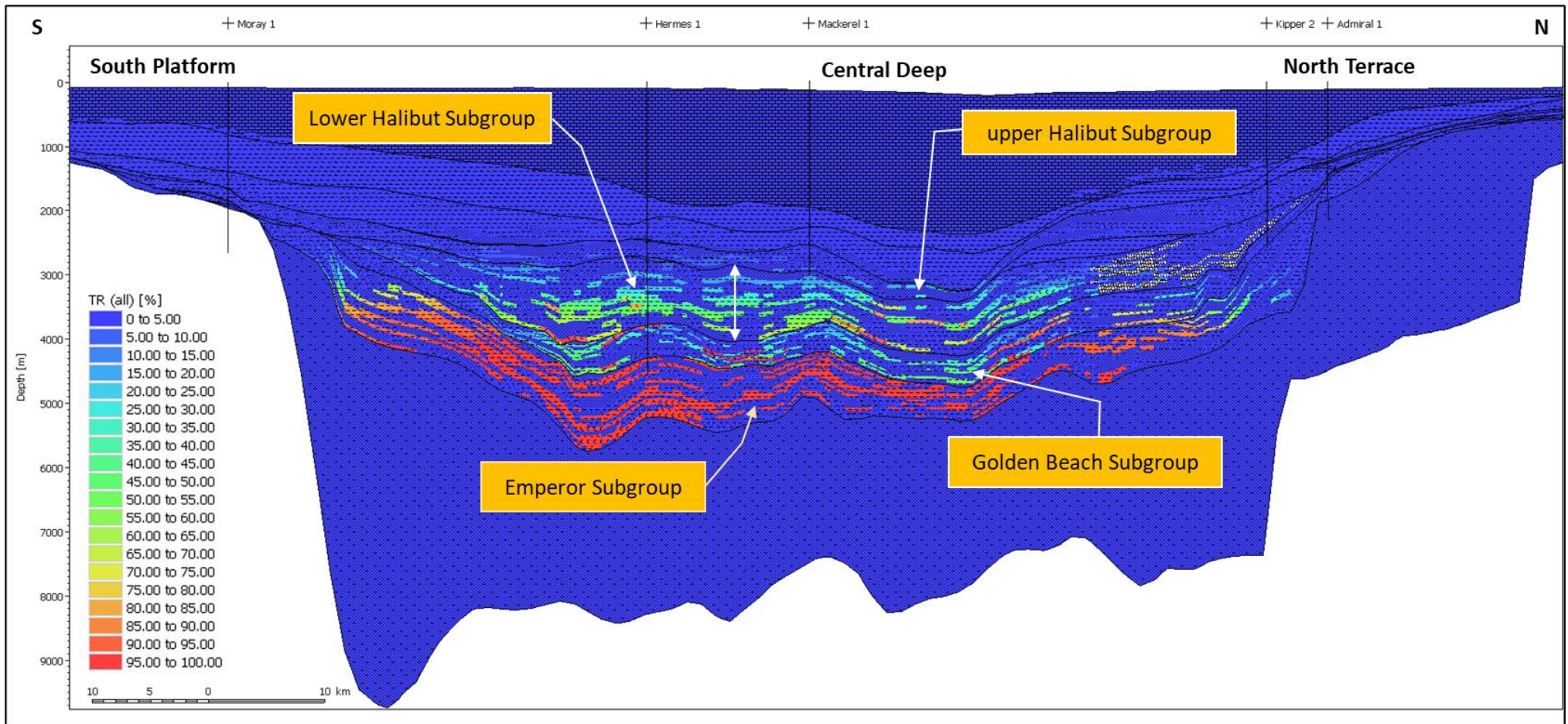


Figure 8-37 Clipped 3D model in PetroMod, the Latrobe Group, coloured by TR and the Seaspray and Strzelecki Groups are coloured by the age of deposition.



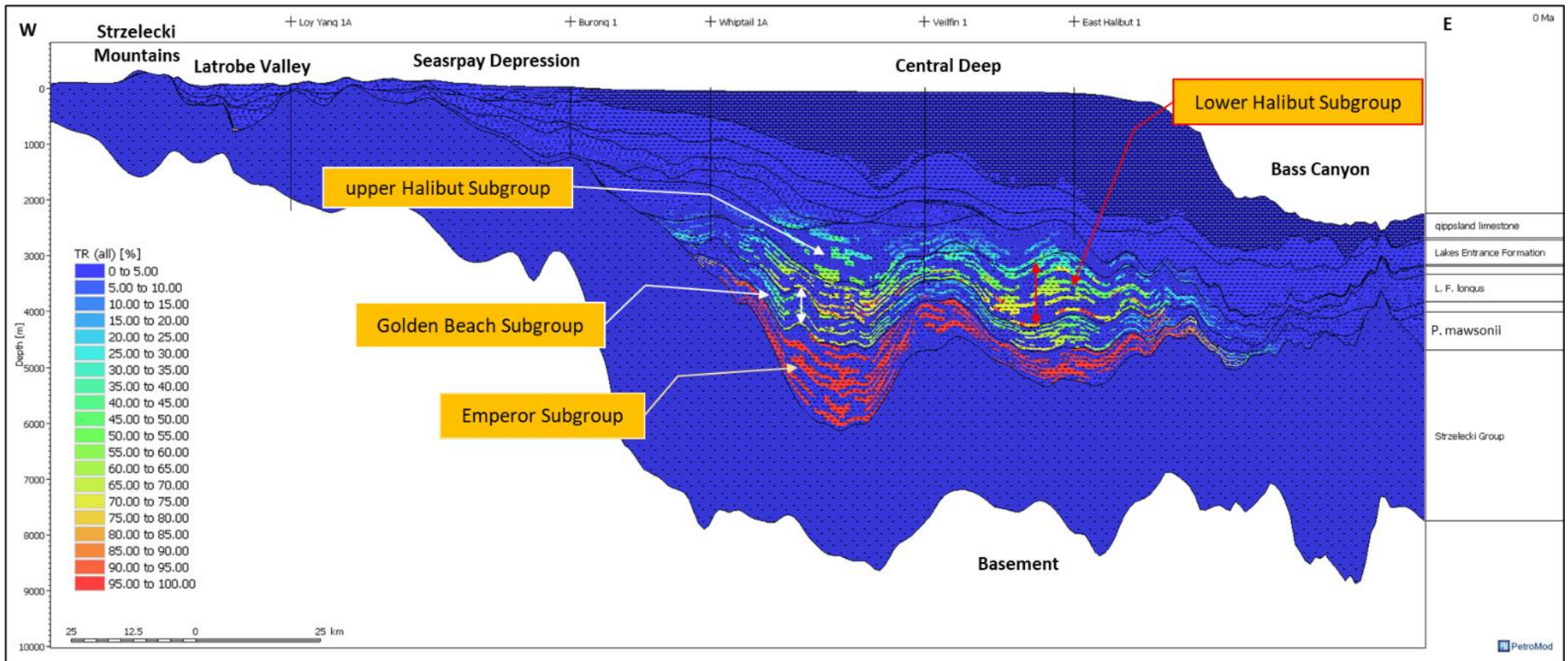
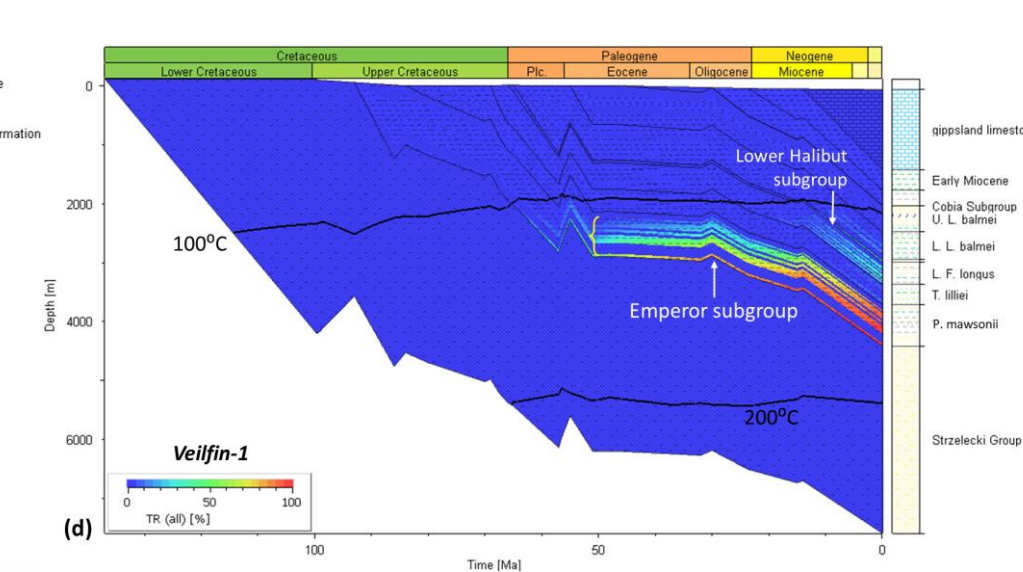
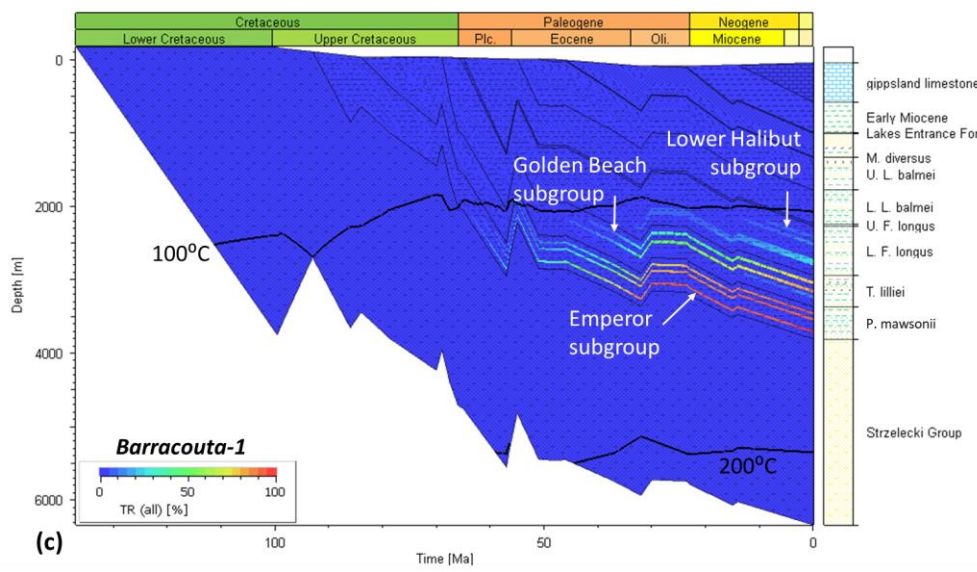
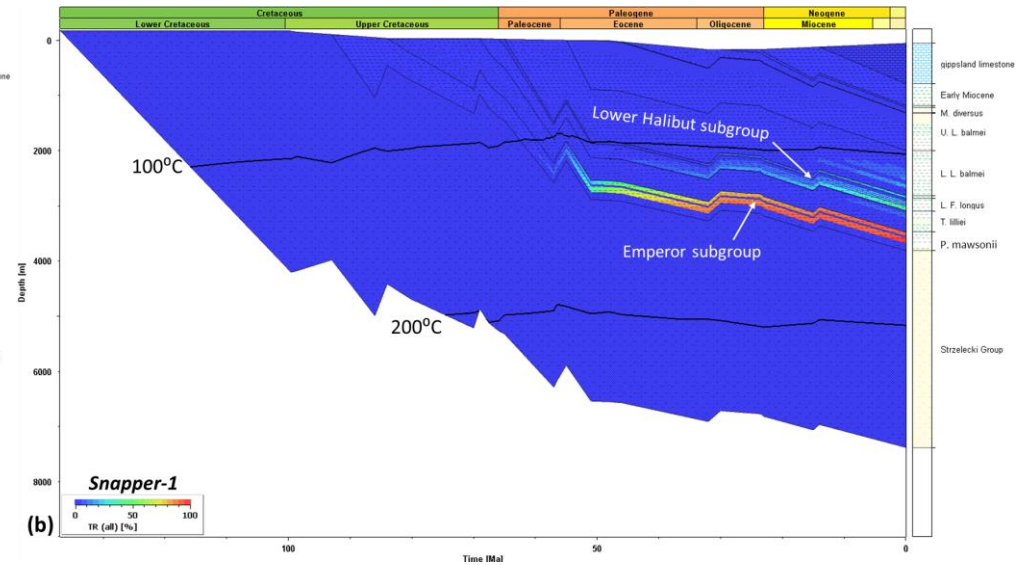
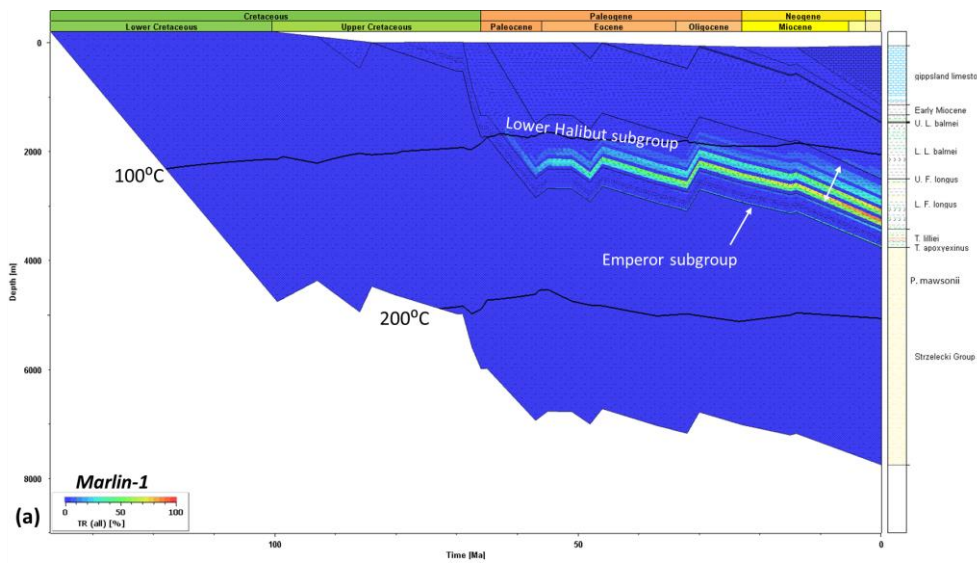
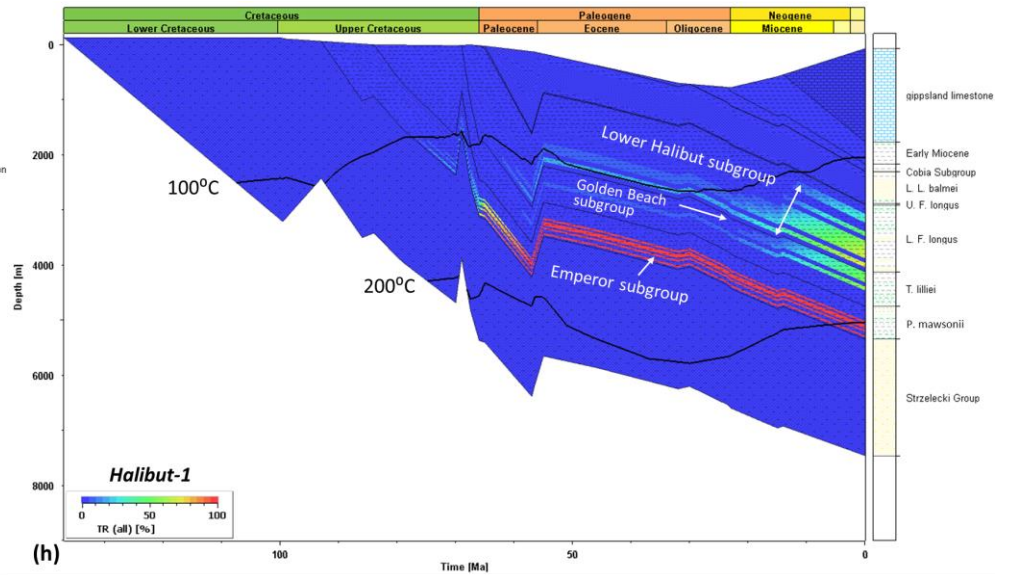
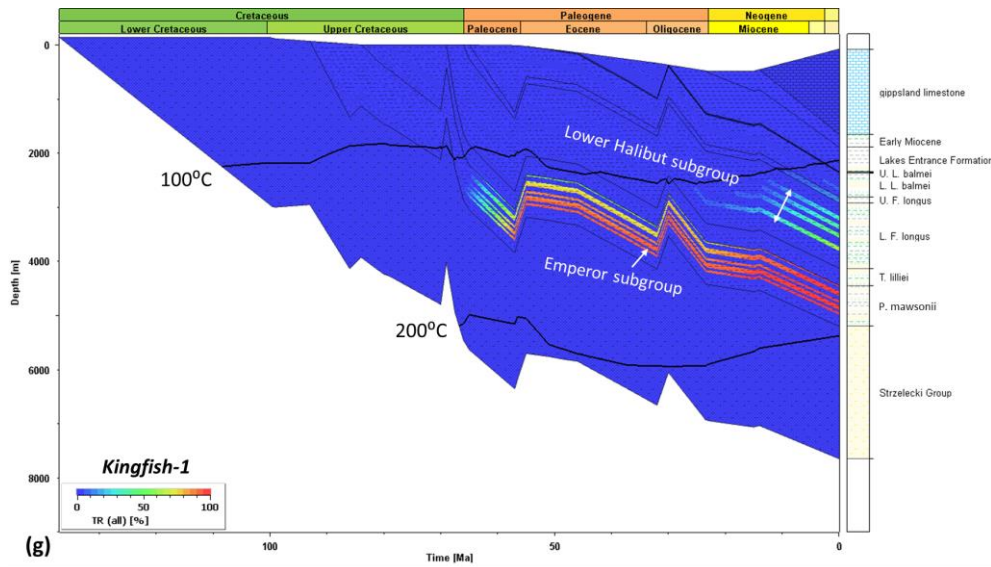
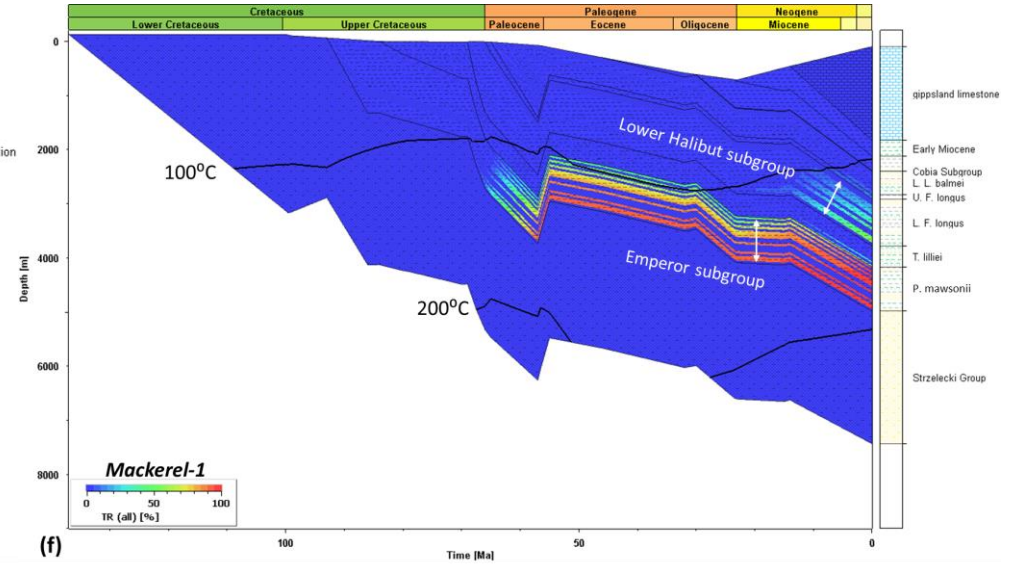
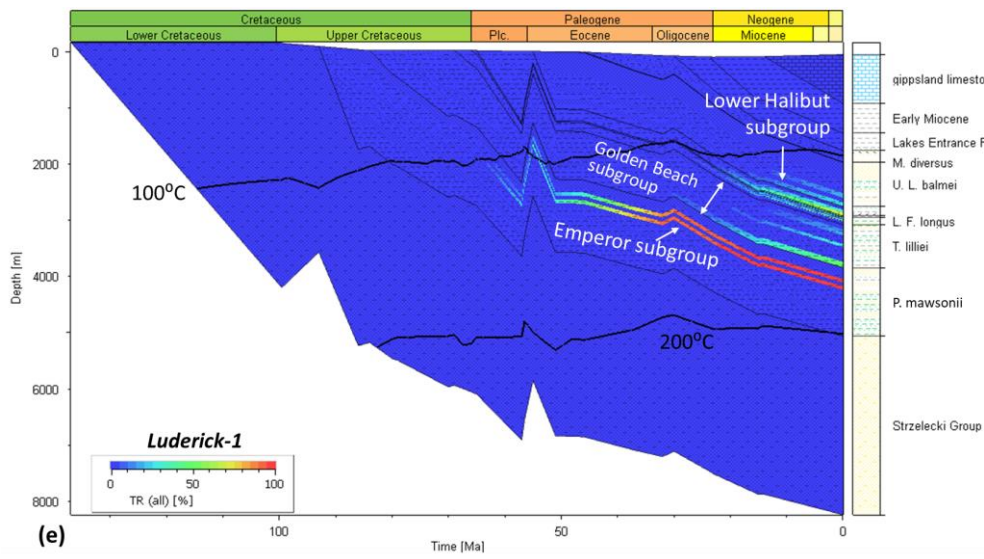


Figure 8-38 Cross-sections demonstrate the modelled organic transformation (TR) at present-day. Locations are shown in Figure 8-17.





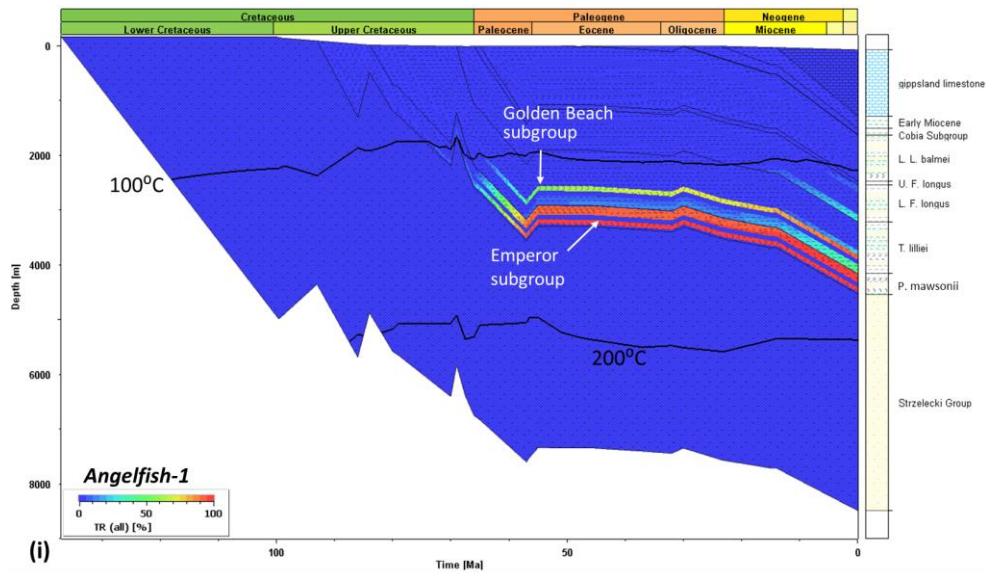
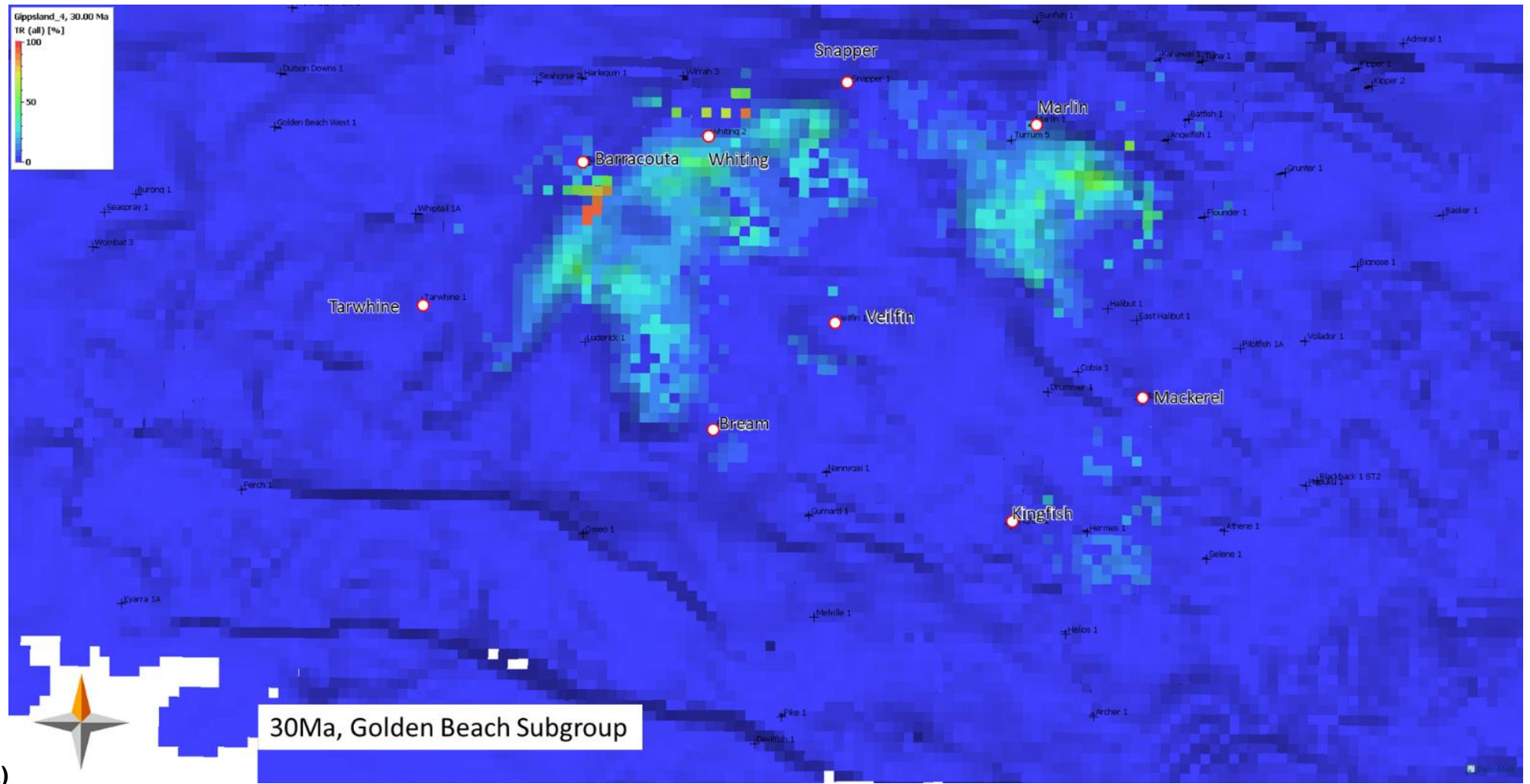
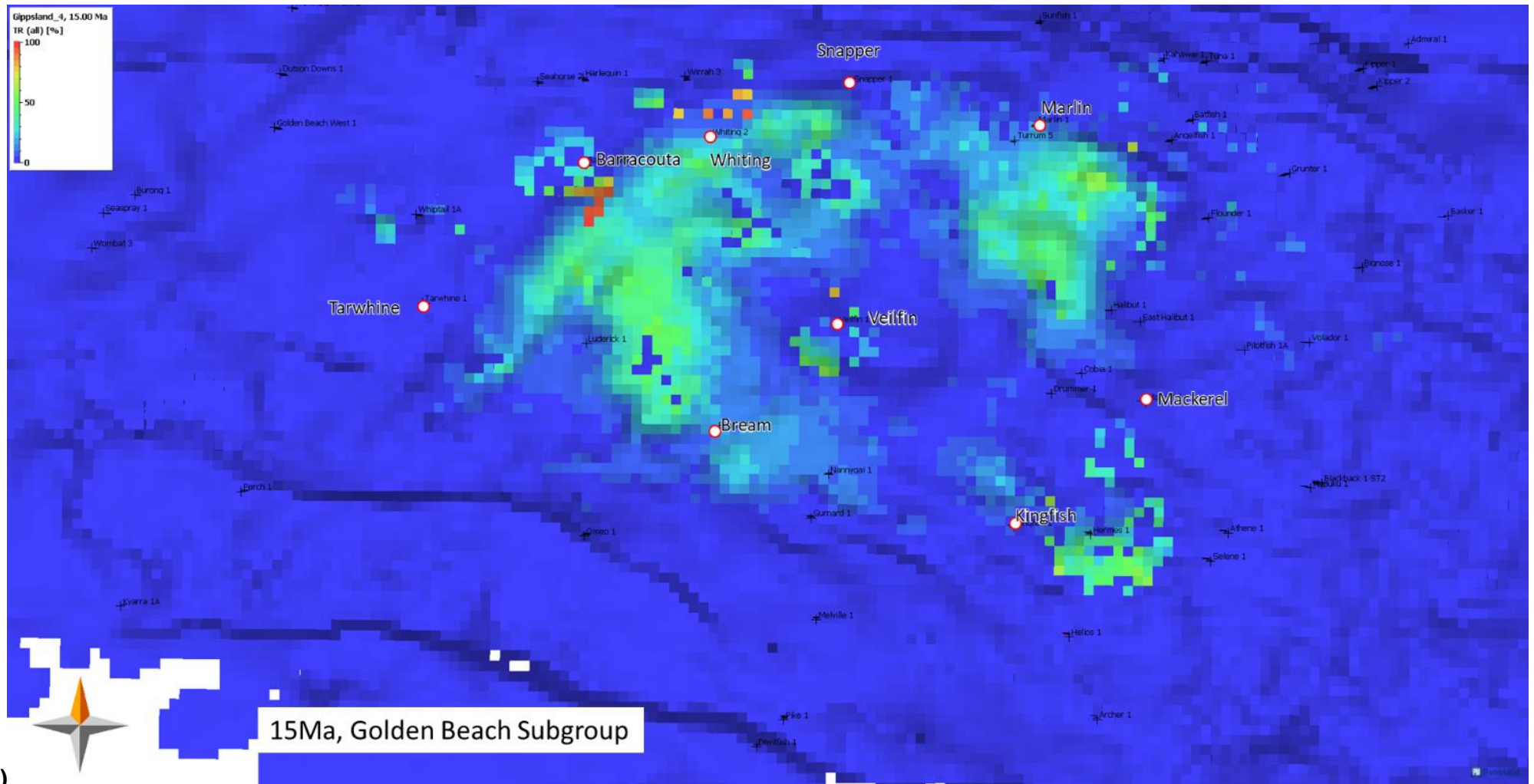
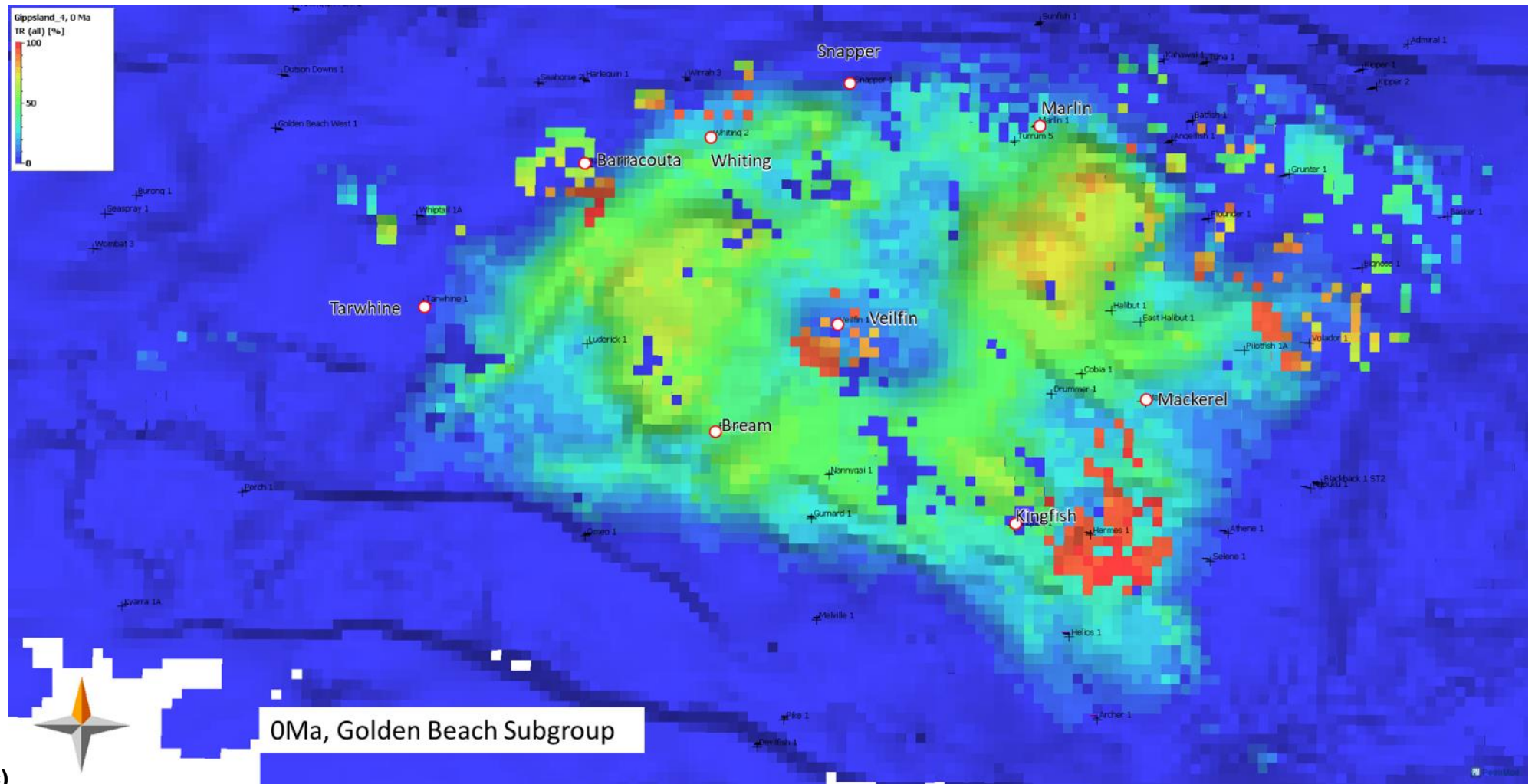


Figure 8-39 The Organic Transformation ratio (TR, %) plots extracted at Angelfish-1, Veilfin-1, Barracouta-1 and Luderick-1.

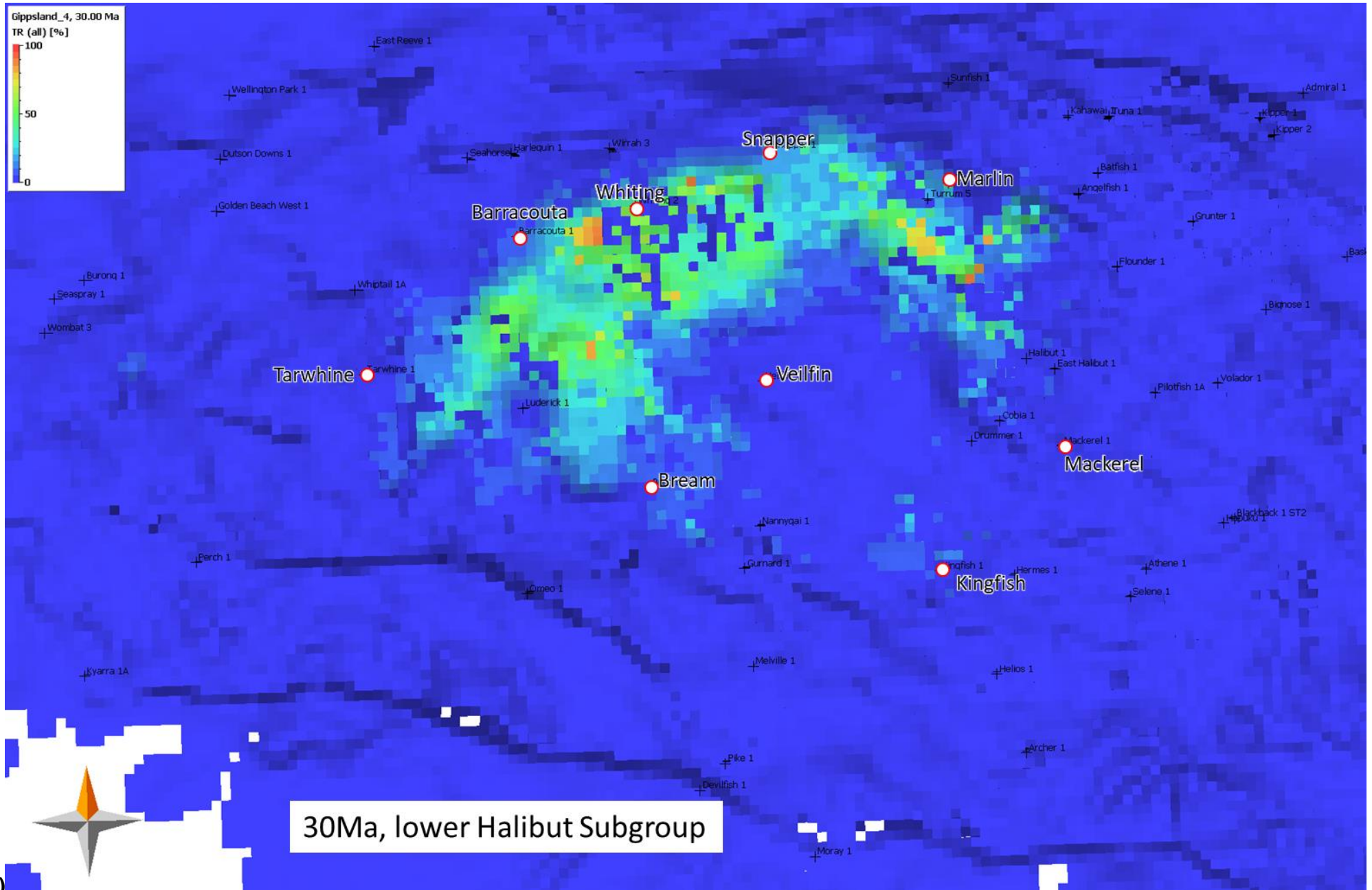




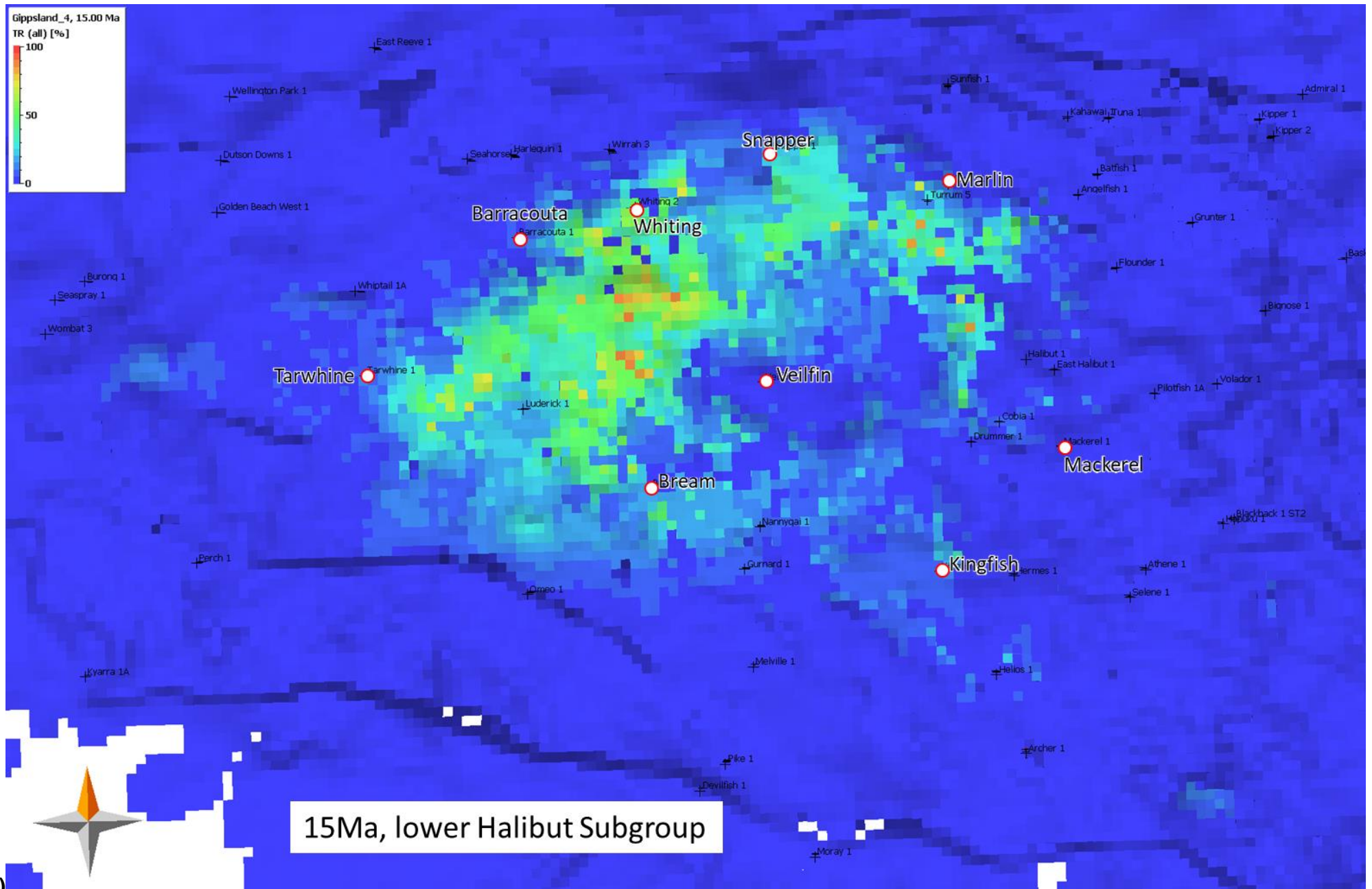
(b)



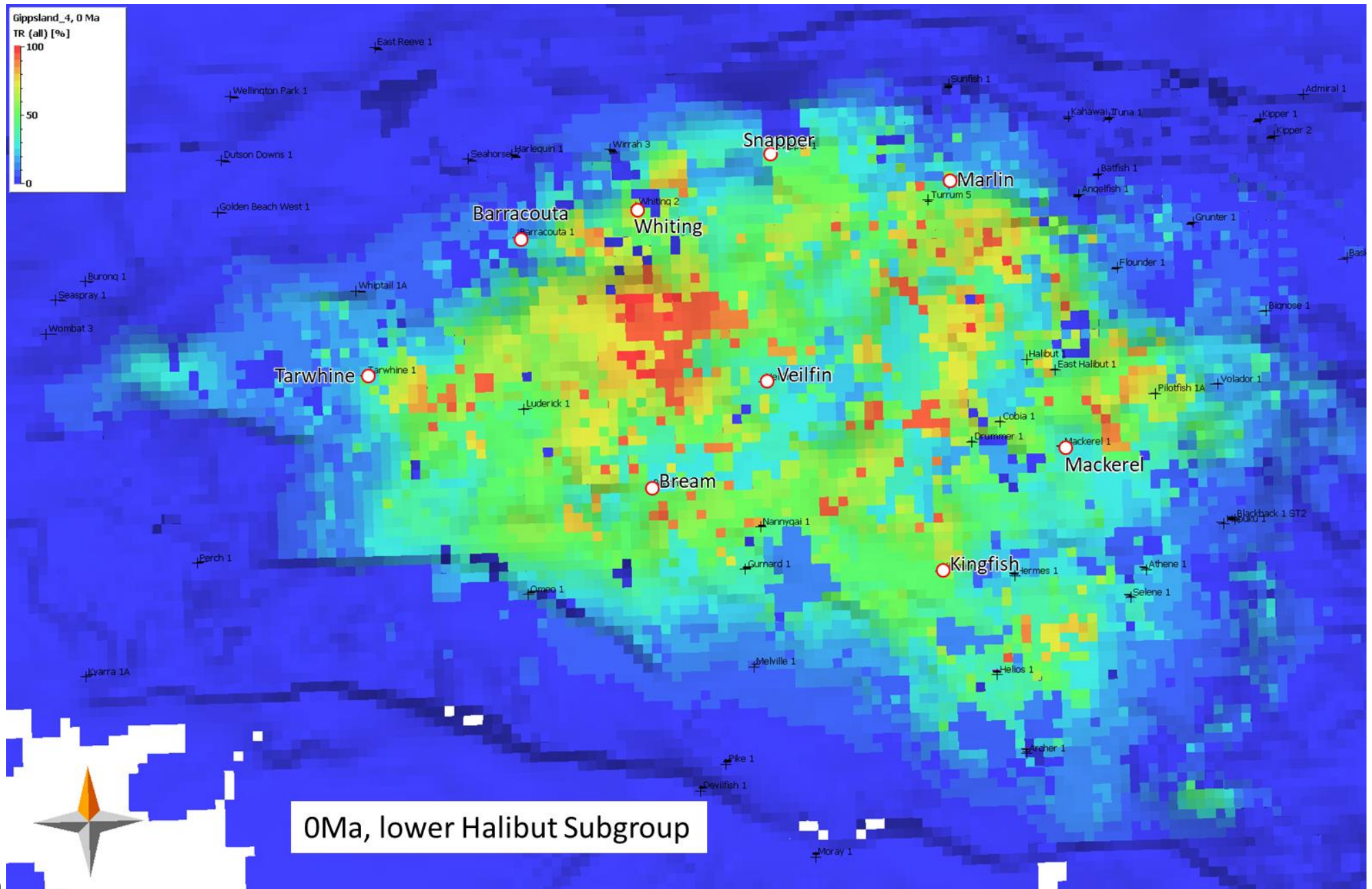
(c)



(d)



(e)



(f)

Figure 8-40 Organic transformation ratio (TR) maps of Golden Beach Subgroup and lower Halibut Subgroup source rocks at 30 Ma, 15 Ma and 0 Ma.

8.5.2 Tectonic evolution

The dual rift model for the Gippsland Basin provides sufficient heat to obtain good thermal calibration to the temperature and maturation models. This contrasts with previous simplified single rift models that have not been able to attain good matches, partly because a dual rift model is difficult to set-up in *PetroMod*. For example, Röth et al. (2021) tried to use a single rift model in just the offshore part of the basin by only including the Early Cretaceous Otway rifting for the Strzelecki Group history, and treating the Tasman Sea rifting as part of the post-rift thermal subsidence phase. This meant they were not able to obtain matches to the thermal or maturation history measured in the offshore wells and they did not attempt to model any part of the onshore basin.

In this study, the entire Gippsland Basin was modelled and the two rift phases were included for the basin heat flow simulation in a dual rift model. This meant not only were good matches obtained to most wells but surprisingly, for the first time, the modelled responses of the two rift events show there are significant differences between some regions within the basin as explained below.

The different heating histories for parts of the basin can be demonstrated using calculated heat flow trends extracted at Pike-1 on the South Terrace, Snapper-1 in the Central Deep, and Tuna-1 on the North Terrace are shown in Figure 8-41 (more examples in Appendix 15). These wells show how the two rift phases are active in different areas of the basin at different times and result in different amounts of stretching between the two rift phases (Figure 8-42). The first syn-rift phase was widespread and affected the entire basin, with the maximum stretching occurring along the boundary faults to the north and south. The example heat flow plots indicate a significant heat flow peak occurred at the end of the first syn-rift Strzelecki phase in all wells, with the maximum heating highest in the south and decreasing to the north. The impact of the second rift phase is greatest in the Central Deep area, with the Snapper-1 heat flow plot showing that in these wells a second heat flow peak occurred at the end of the Tasman rift. In the south the heating decayed without an additional Tasman rift heat pulse (e.g., Pike-1) while in the north the heating decayed with a small heat pulse during the Tasman rift (e.g., Tuna-1). The heat flow is much reduced in the post rift phase and stabilised in the post-rift compressional phase. The result of this dual rift thermal model is that the modelled thermal history

matches well with the burial subsidence (Figure 8-41). Also, the resulting simulated present-day heat flow varies across the basin from 45.51 to 61.27 mW/m², with a mean of 50.36 mW/m².

The crust and mantle stretching factor maps of two syn-rift events show the changes with time that control the tectonic evolution in the Gippsland Basin. The first syn-rift crust stretching factor varies from 1.05 to 1.69, with the largest stretching occurring at the south boundary fault. Moreover, almost the entire Gippsland Basin experienced significant crustal stretching in the first syn-rift phase, including the Strzelecki Ranges (which may be underestimated due to sparse data) and the South Platform. The map suggests the Strzelecki stretching links towards the Otway Basin to the west and possibly to the south towards the Bass Strait. This is expected since it corresponds to the Otway rifting associated with the separation of Antarctica from Australia (Figure 8-43). The successful rift arms bounded the southern margin of the Otway Basin and the western edge of Tasmania, while the Gippsland Basin acted as a failed third rift arm. The second rift crust stretching factor varies between 1 to 1.38, with the majority of extension limited to the Central Deep and part of the North Terrace, expanding to the northeastern edge of the basin. Again, the Gippsland Basin became the third failed rift arm in the second rift event, which is associated with the Tasman Sea opening in which the successful rift arms are bounded by the east coast of mainland Australia and the eastern margin of Tasmania. The crust stretching factor maps for the two rift events clearly show that the first rift event in the Early Cretaceous is well developed across the entire Gippsland Basin, while the second rift event in Mid-Late Cretaceous is more localised in the Central Deep of the basin and is not active over most of the South Terrace and South Platform (e.g., Pike-1, Melville-1, Groper-2, Moray-1, Pisces-1 and Admiral-1).

The 3D burial thermal model has captured this switch of the main rift areas between the two rift events, which also explains why the depocentres switched towards the north during the formation of the Emperor Subgroup (Norvick, 2005) as shown in Figure 8-44. The Late Cretaceous burial in the South Terrace and southern part of the Central Deep appears to result from rapid thermal subsidence after the first rift phase event. In contrast, the Late Cretaceous burial in the North Terrace results from the second rift phase and this is also the case in the Central Deep.

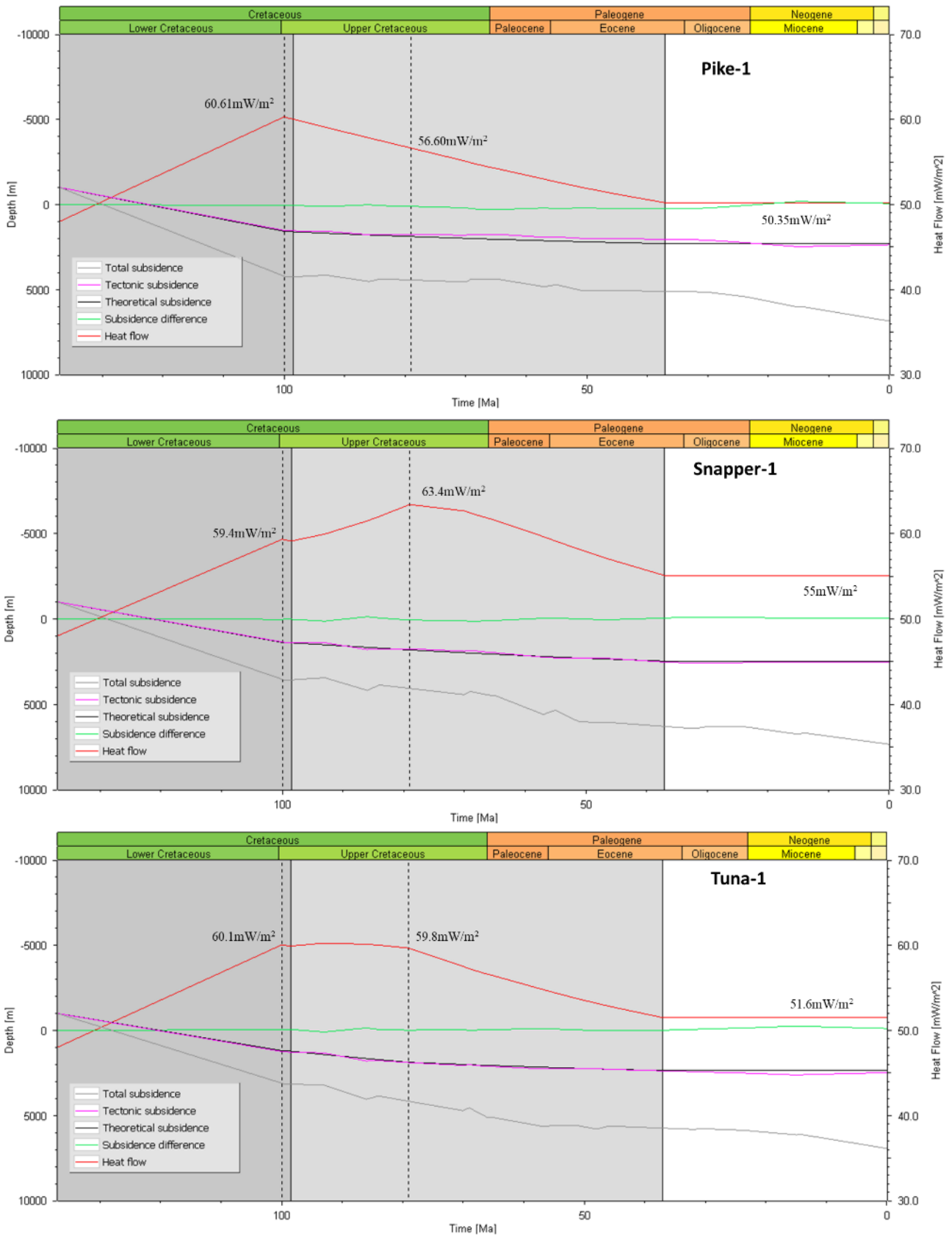


Figure 8-41 The calculated heat flow trends extracted at Pike-1, Snapper-1 and Tuna-1, the dashed lines mark the approximated end time for each of the two syn-rifts.

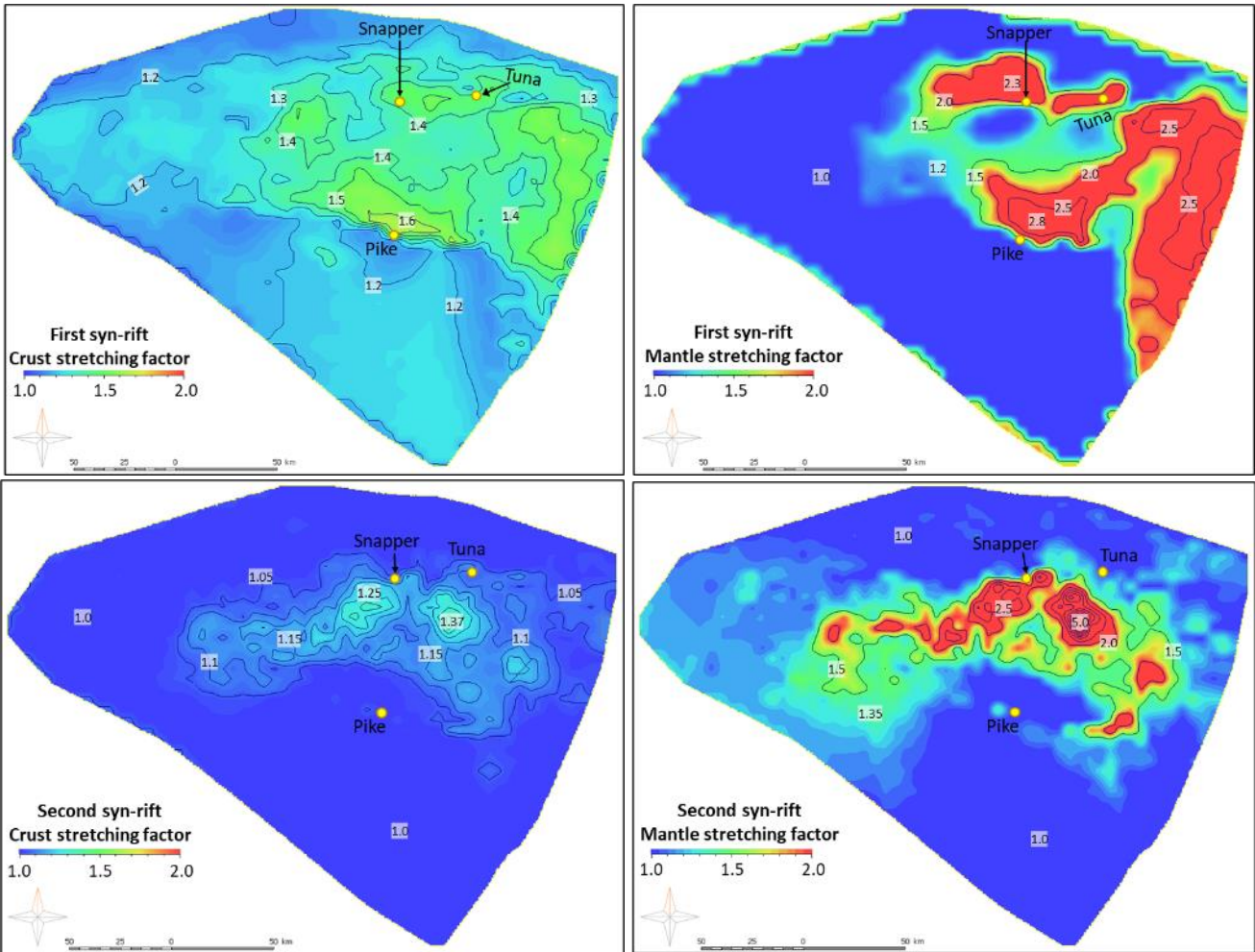


Figure 8-42 Maps of Crust and Mantle stretching factors for the two rift phases.

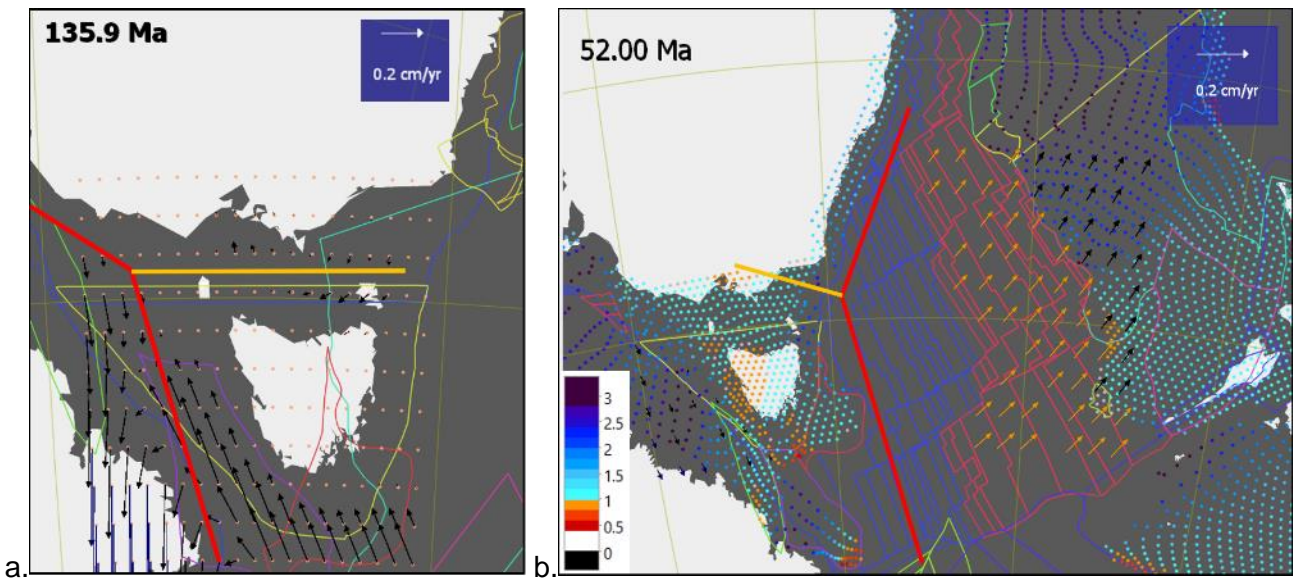


Figure 8-43 Reconstruction model from GPlates showing the three-arm rifting style of the first rift event (a) and the second rift event (b). The red lines indicate the two successful rift arms, and the orange line shows the failed rift arm.

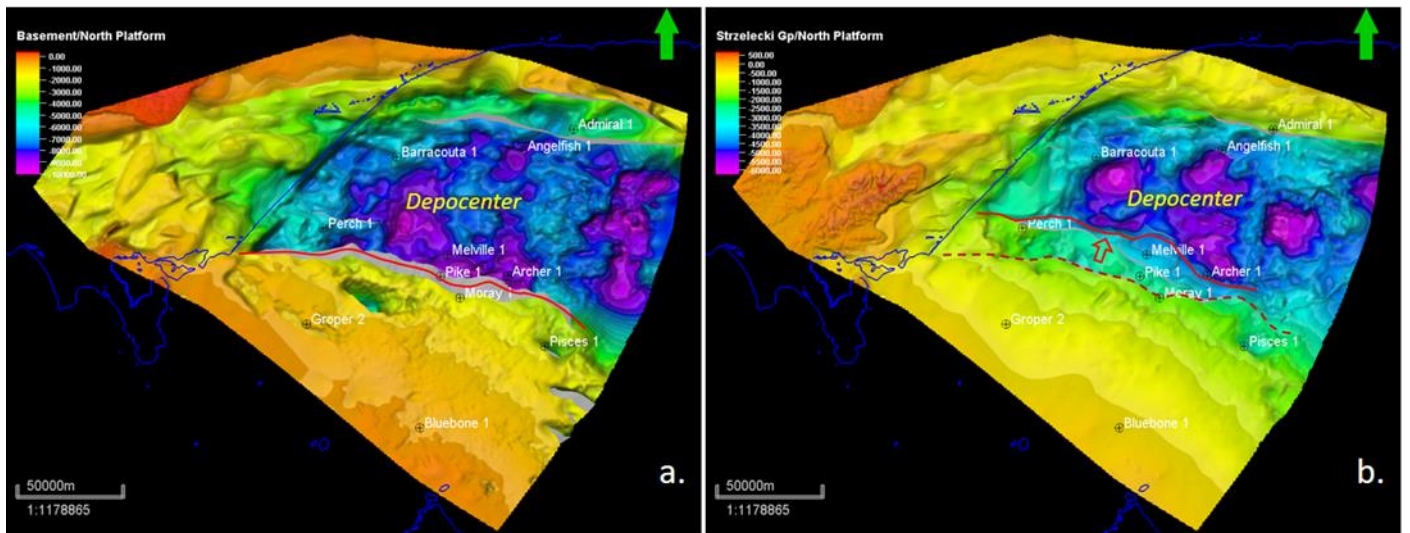


Figure 8-44 a: Top Basement structural map; b: Top Strzelecki Group structural map. The red line marks the southern boundary of the depocenter which shifts to the north from the Otway rift to the Tasman rift.

Chapter 9 Discussion

The previous Chapters have presented an integrated basin analysis of the entire onshore and offshore Gippsland Basin from the Early Cretaceous to the present. This study is the first to provide realistic 3D structural, stratigraphic, lithofacies and property models for the entire Gippsland Basin and use them to constrain and guide a range of theoretical sedimentary, burial and thermal simulation models. The 3D forward palaeo-landscape *Badlands* simulations, guided by an optimised experimental design analysis, have reconstructed the most likely basin evolution and identified the critical controlling variables for basinwide sedimentary evolution through deep time. The 3D burial, temperature, pressure and maturation history models, matched to the *GPlates* tectonic model and to the well data, provide the most likely evolution and give new insights into a number of aspects of the basin burial, thermal and tectonic history. The key individual conclusions and insights from this research are discussed and summarised below.

9.1 Tectono-Stratigraphic Model

The regional seismic maps and the large number of wells provide a sound basis for fitting and testing both the understanding of the regional stratigraphic and structural geology, and for testing forward modelling of the Gippsland Basin evolution, as shown in Chapter 4.1. Integration with the *GPlates* has allowed a clear understanding of the geology on a grander scale while the detail in the 3D models provides ground-truthing to the local scale and helped solve several long debated issues. Previously, doubts have been expressed as to the efficacy of the various plate reconstructions and how to balance the competing information from geology and geophysics (Brown et al., 2003; Williams et al., 2019).

GPlates, *Badlands* and *PetroMod* models can be used to test different scenarios, and by building and constraining them with a robust 3D geological model in *Petrel* based on the actual data, this research has identified the most likely geological history of the Gippsland Basin. The stratigraphic history can confidently be said now to result from two rifting events both of which “failed” in the sense that neither lead to separation along their axis. The first Strzelecki (Otway) rift essentially occurred between about 136 Ma and tailed off by 100 Ma to produce the intracratonic rift infill known as the Strzelecki Group. This was the more substantial rift but the Gippsland rift was by-passed by the main Australian-Antarctica rift axis which shifted to west of Tasmania to accommodate continued extension on the

Australian southern margin. Nevertheless this had a major sedimentary, structural and thermal imprint on the Gippsland Basin but it is not sufficient on its own.

A major period of regional thermal uplift followed in the Gippsland Basin during the mid-Cretaceous for several million years or more which initiated the top Strzelecki Group unconformity which was shown in the *Badlands* modelling to be a composite unconformity at least in the onshore part of the basin, with further subsequent erosion at later times. The second Tasman rift phase followed which is associated with separation of the south-east Australian margin with Zealandia. This rifting renewed subsidence and extension in the offshore part of the basin from about 98.5 Ma, but tailed off by 79 Ma after spreading began, which continued until about 51.5 Ma during which time subsidence and extension waned. This marks the real onset of post rift thermal subsidence and the increasing influence of sediment loading and flexural collapse of the developing shelf. The Tasman rift-drift tectonic history corresponds well to the *Badlands* modelling which showed how the depositional rate changed with time during the Late Cretaceous and to the *PetroMod* modelling which showed how these changes control the thermal models.

Finally, the initiation of compression in the Eocene about 45 Ma from the spreading changes at the South Tasman Rise and the plate boundary changes on the Australian eastern margin, together explain the long debated origin and timing of the reverse movements and folding in Gippsland, and why they built up with time into the Miocene. This demonstrates the utility of coupling the *GPlates* modelling with the *Badlands* models and the 3D realistic geological models in *Petrel*.

9.2 Regional Gippsland and Latrobe Valley Models

The regional Gippsland Basin model (Chapter 4.3.1) was built primarily to act as the control for the theoretical basin modelling and covers the onshore and offshore parts of the basin. This is probably the first full 3D basin model constructed successfully with sufficient detailed geology including structure, stratigraphy, facies and properties. The models are based on interpreted and depth converted seismic, tied to a very large number of wells and bores, and populated with the corresponding log and analytical data (Chapter 4.2). These models can be used in future research for a wide variety of studies and more detailed sub-models can be readily built in particular areas. The model can be easily updated with new seismic horizons, for example, using the new CGG seismic dataset that may become available soon.

The detailed Latrobe Valley 3D *Petrel* model given in Chapter 4.3.2 has been used to show how the coal seams change laterally under the influence of the Eocene to Miocene transgressions and vertically under the relatively shallow burial and the increasing influence of regional compression (mainly WNW-ESE trending; Tokarev et al., 1999). The maps of lateral extent of the seams show the seams retreating from the south-east where the Traralgon Seam was deposited, back into the Latrobe Valley when the Morwell Seams accumulated, with the final Yallourn Seam moving slightly back into the basin.

The physical rank clearly changes from the near surface down to the top of the Strzelecki Group but the chemical rank barely shows any change as is expected in low rank coals. The moisture property model is the best indicator of physical rank and shows that burial depth is the main factor influencing the coal moisture content. The moisture content, which is a measure of porosity or compaction, is inversely proportional to and varies rapidly with increasing burial depth from values over 65% near surface to 55% at about 400-500 m depth or down to 45% or lower in some deep bores by about 800 m. Overall, the most critical factor causing variation in coal seam moisture content in the Latrobe Valley is the burial depth. This has been shown by earlier workers though they have rarely had access to a detailed 3D model of the region and the model offers scope to measure these changes with depth at any location.

The moisture changes with lithotype have not been studied here. However, the tectonic effects are a secondary factor controlling the moisture, which are more localised and can be limited to an individual seam scale. The normal growth faults only produce a minor moisture variation directly across the fault between the down-thrown and up-thrown sides of the fault in the order of about 1 percentage points. The more significant effect on the moisture values occurs in some compressional structures where the moisture declines within the same seam, such as in the area adjacent to reverse faults (both sides) and strongly folded areas. This indicates that tectonic effects are a cause of moisture variation though it is not clear how much results from uplift of previously deeply buried coal or secondary compaction from the compressional stress. If the latter, then measurement of moisture content has potential to be an indicator of localised stress activity, which is similar to use of maximum vitrinite reflectance and anisotropy for measuring local stress fields in underground coal mines (Levine and Davis, 1989).

The carbon model is a measure of chemical change and shows that chemical coal rank in the Latrobe Valley is very low, and only shows a slight increase of carbon content occurs from shallow level coal seams (Yallourn seams) to the deep level coal seams (Traralgon seams). This demonstrates that at very low coal ranks the most significant changes are physical with a minor increase in chemical rank as expected (Holdgate, 1985; 2005).

This detailed but regional 3D model of the Latrobe Valley is currently under-utilised and could be used in future to study many aspects of coal formation, its relation to various sedimentary facies, structural controls on coal formation, and to detailed rank changes with increasing depth.

9.3 Controls on Basin Sedimentary Evolution

In Chapter 5 it was shown that basin-wide landscape studies over deep time can be carried out successfully using comprehensive forward simulations provided they are constrained by realistic 3D models. Meaningful and robust statistical analyses can be used to better understand the effect of the variables modelled in forward simulation software such as *Badlands*, if the simulations are guided by an Experimental Design. A good experimental design is more efficient in the long run than running countless sensitivities without a design. This study only required simulation of 22 scenarios to test and fit 12 identified variables, including possible interactions with each other. The most probable best-fit response functions derived in Chapter 5 are comparable to the result produced by running many thousands of simulations (e.g., via Bayesian analysis). The experimental design also provides a useful tool to explore the complex multi-dimensional space of the depositional controls through the geological history of the basin, and allowed logical assessment of the observed changes in palaeo-landscape through time. Several iterations of scenario analysis allow better focus on the critical variables and some variables that are not significant can be removed or replaced by other candidate variables.

The initial simulation runs had an immediate impact on the understanding of the geological history of the Gippsland Basin, by demonstrating that mountains in the north, south and east of the Early Cretaceous rift basin were required to provide enough sediment supply to balance the sediment budget and fill the accommodation space during the first syn-rift phase. This simple outcome had not been shown numerically before and has settled a debate on sediment source that has continued for many decades, showing that we should expect sediment from the Palaeozoic basement and granite intrusions as well as volcanics from the east, which is exactly what the geological data confirms.

Similarly, the analyses of the required uplift is a good fit to empirical estimates of several km, but shows that continuous or episodic uplift over time and over a large area can produce an enormous amount of erosion and sediment supply, sufficient to fill a young rift basin such as the Gippsland Basin. Hence, a large amount of erosion and removal of section does not require highly elevated topography at any particular time.

Basin evolution is a complex feedback process between all the controlling variables with both external and internal factors working together to produce an outcome. Simple concepts of sediment supply and accommodation space produced by sea level changes and subsidence or uplift are not sufficient. Neither are surface landscape studies looking at erosion and deposition processes on their own. Simulated basin evolution models can have very different histories through time but end up with similar landscapes and overall stratigraphy. This lack of unique solutions also highlights a trap: simulation models that show a good fit to the present day landscape may not be a good fit to a basin's history through all time steps.

In landscape evolution the most significant controlling variables on land include internal influences such as *Slope* and *Erodibility*, and external influences such as Climate (with its proxy here being *Rainfall*) and its combination with *Area* (modelled via the exponent m). In the marine depositional environment, the accommodation space is also important (mainly via the *maximum % Marine Deposition* parameter). The variables *Rainfall*, *Area*, *Slope* and *Erodibility* also have significant interactions with each other that can unexpectedly boost their effects. Alternatively, although variables such as *Erodibility* are highly significant, their effects can be countered by combinations and interactions with other variables that can greatly change the basin filling process.

Variables such as Grade or base level, *Critical Slope* (and its exponent n) and *Sea Level* are significant second order controls. Surprisingly, the rate of sea level change has a greater effect if it is out of step with the other variables such as sediment supply and subsidence (ie a negative interaction), with rapid sea level change being most effective in post-rift phases when subsidence and sediment supply have waned. Variables such as *Aerial Sediment Flux*, the rate of inshore marine dispersion of river deposits and marine gravity sediment flux mostly have small impacts on basin fill.

The phase of a basin's history is also important and the influence of the controlling variables can change markedly with time. The Initial Topography can be influential in the early phase of a basin's

history but has little effect with further time. Similarly, subsidence rate and continuity and hinterland uplift are most important in the rift phase and less so in the post-rift phases. The response equations for average basinwide Depositional Rates for the rift and post-rift phases clearly showed that deposition in the rift phase (mean about 50-60 m/Ma) was typically twice as fast as in the post-rift phase (mean of about 20-30 m/Ma). The numerical analysis (Chapter 5) shows quantitatively how the non-marine variables control the intracratonic phase (especially *Rainfall* and *Erodibility*) whereas the marine variables hold sway in the post-rift phase when the basin is inundated by marine incursions and sedimentation is dominated by marine shelf progradation much of which is not land derived but produced organically.

Scenarios that maintain balanced fill and good fits through time exist but other scenarios are possible especially over some phases of a basin's history. In contrast, some scenarios follow geological histories where subsidence outstrips sediment supply generating under-filled starved basins which is especially relevant during rapidly subsiding rift events. Conversely, simulations can be made where combinations of sediment supply via erosion, accommodation space and subsidence can create an over-filled basin, which although probably unrealistic over the long term, can help constrain the real inputs and lead to a better understanding of the basin.

9.4 Palaeo-landscape evolution

The realistic 3D *Petrel* model and statistical experimental design constrained and guided the *Badlands* theoretical modelling process to reconstruct the most likely evolution of the Gippsland Basin as documented in Chapter 6. The *Badlands* simulations of the palaeo-landscape and geological history have been able to capture and clarify the main features of this detailed geological history and identify other possible scenarios during each phase of the basin history. The results are summarised and discussed below:

- Early Cretaceous: the Gippsland Basin formed as an intracratonic rift basin, initially with non-marine deposition in a narrow east to west drainage basin, and the simulations showed it had to be surrounded on three sides by steep highlands that gradually eroded producing a lower relief and wider basin. An inland sea appeared at the western edge of the basin that was probably connected with the Otway Basin. Fluvio-deltaic sediments build into this shallow inland sea

during Albian-Cenomanian time with continued rifting, and the sea expands from west to east into western Gippsland.

- Mid-Cretaceous: The Strzelecki rift valley topography was rejuvenated by widespread uplift but overall remained considerably below the original palaeo-topography. The simulations show how the ongoing erosion was able to remove large thicknesses of Strzelecki Group sediments contemporaneously with the uplift in a dynamic process, so that the Strzelecki highlands did not attain a great height at any time. This highlights the power of 3D forward simulations to visually see and measure how this process works.

In the Early Cenomanian, the emerging landscape resulted in retreat of the inland Strzelecki sea, which was replaced by a large-scale east to west trending fluvial system again dominated by flood plain and braid plain deposition fed by widespread erosion of the uplands. In the Turonian, hinterland uplift continued in western Gippsland Basin but rift subsidence began in eastern Gippsland initiated by the Tasman Sea rifting, resulting in deposition of thick fluvial and widespread inland lacustrine sediments in the offshore basin area. This changing balance of tectonism led to the gradual capture of the individual river systems in the western highland valleys, and flipping of the fluvial drainage system from a westerly direction to an easterly direction in the eastern part of the basin. A very similar process of river capture is happening in the current East African Rift Valleys. By the Coniacian, a large amount of clastic sediments had been transported via these new fluvial systems filling up the inland lake systems.

Again, the forward simulation models were able to show how this complicated interplay of laterally changing uplift and subsidence with time switched the basin-wide landscapes. This also explained the origin of a major unconformity in the middle of a syn-rift succession, that previous workers had tried unsuccessfully to connect to some far-field plate tectonic event.

- Late Cretaceous: The rate of deposition and subsidence decreased from the Santonian to Maastrichtian and the simulations were able to match the erosion, deposition, subsidence and hinterland uplift. The Santonian to Campanian in the offshore basin saw deposition of fluvio-lacustrine sediments in the west (Chimaera Formation). The first, shallow marine, restricted sediments were deposited further to the east (Anemone Formation) resulting from flooding of the rifts after the onset of break-up further south of Gippsland Basin. This phase required some uplift on the basin margins around 80Ma to balance the sediment supply and matches the local

development of unconformities. However, it is not clear if the uplift should be credited to isostatic rebound accompanying the transition of rifting to spreading, or simply from erosional unloading during the preceding rifting, or some far-field plate boundary effect. The simulations from 79-75 Ma show the initial marine sediments in the east were succeeded by a regressive phase, leading to deposition of a widespread flat floodplain, with fluvial and deltaic sediments over much of the basin. The overlying sediments between about 74-65 Ma record aggradational coastal plain facies with episodic transgressive phases.

- Palaeocene to Eocene: The Palaeocene saw a change to major marine incursions with at least three cycles and waning of extensional fault movement. The Eocene records more frequent and shorter transgressive-regressive cycles, with the fluviodeltaic sediments being pushed back behind barrier systems, that progressively jumped the shorelines westwards to the onshore part of the basin by the early Oligocene. This produced a widespread unconformity across the offshore basin with sediment starvation further offshore from the barrier systems. Compression started to influence the basin in this phase producing inversion of the previous normal faults with structural control of the river channel belts and the submarine canyons, especially in the Kingfish, Halibut-Mackerel and Marlin areas. Together with the transgressions this results in an irregular embayed coastline. The *Badlands* simulations were able to mimic this complicated tectono-sedimentary evolution and closely match the palaeo-facies maps of Johnstone et al. (2001). However, the simulation fits could be greatly improved by running them at less than 1Ma time steps and with a finer grid size by restricting the area to the offshore basin.
- Oligocene to Recent: The offshore basin during this period required simulation of the cold water carbonate deposition using the *Badlands* carbonate module. This successfully added a carbonate rain to the clastic dispersion from the land. The episodic canyon cut and fill that accompanied the rapid subsidence of the shelf and the changes in sea level were simulated with the canyon module. Together these simulations showed how the canyons were linked to development of the incised valleys and in part structurally controlled by the anticlines that developed after the onset of regional compression. The most probable simulations resulted in a present-day coastline that is a good fit to the 1 Ma simulation which is remarkable after simulating 137 Ma of the basin history.

Another good feature of the tectono-stratigraphic simulations was their ability to highlight the potential reservoirs and source rocks of Cretaceous age in Gippsland Basin, many of which are beyond drilling depths, especially those in the Emperor and Golden Beach Subgroups. The simulations also modelled the facies development in the younger Halibut and Cobia Subgroups but as these are well known only the older potential reservoir and source rocks are mentioned below:

- **Early Cretaceous Strzelecki Reservoirs:** the Strzelecki Group sandstones have mostly been considered poor reservoirs because many units contain volcanolithic and feldspathic sandstones. However, the simulations show that rivers from northern and southern highlands and erosion of the basement produced coarse grained clastic sediments derived from Palaeozoic rocks, deposited into both the Tyers River and Wonthaggi sub-groups, and these form much better reservoirs. The simulations also demonstrate that these sediments formed a long-term essentially continuous sediment supply into the basal sequences, marginal fans and braided stream facies that continue up through the section.
- **Early Cretaceous Source Rocks:** The simulations predict the occurrence of widespread shallow marine lacustrine, marginal marine and coaly sediments in the Strzelecki that is confirmed by the known geology. This suggests that the sequences could have source rock potential though this has not been seriously considered by industry. Good quality source rocks have been recognised in a few wells, such as in the Locmany Member of the Tyers River Subgroup by Holdgate et al. (2015). The Rock-Eval data showed good TOC >5% and hydrogen indices >350, together suggesting oil prone potential. Many fault blocks in the Strzelecki Ranges have $R_o > 2\%$ but the vitrinite reflectance data further west places these source rocks in the oil window. Alginite macerals have not been reported by the organic petrologists though algae should be common in shallow marginal marine environments.
- **Potential Emperor Reservoirs:** The mid-Cretaceous uplift began to change the source provenance, with more mature clastics transported from the north, south-west and west with unroofing of both Palaeozoic and Strzelecki strata, and granites in the south along the Flinders Island-Wilsons Promontory trend. The supply of volcanio-clastics from the east started to be shut down with initiation of the Tasman Sea rifting and any intra-rift volcanics started to be overwhelmed by the volume of siliclastic sediment.

- Potential Emperor Source rocks: The simulations show that an area of pervasive lacustrine to shallow inland seaway lies beneath all of the major petroleum fields, including the large oilfields Kingfish, Halibut, Fortescue, Flounder and Mackerel and the large gas fields Barracouta, Snapper, Marlin, Bream and Tuna. These lacustrine to shallow sea facies were reasonably persistent and stabilised over a period of about 4-7 million years, long enough to deposit thick non-marine organic rich black shales and sapropelic coals. To date, very few wells have penetrated these shales and few organic geochemistry studies are available to understand the precise facies variability.
- Potential Golden Beach Source rocks: The simulations indicate further development of low energy peatlands, lacustrine facies, lagoonal and newly developed restricted marine facies that provide good potential source rocks. These source rock facies are known to be widespread around the margins of the Central Deep including the Barracouta and Snapper areas and are simulated to extend all the way to the Blackback field on the eastern margin but again have not been drilled in the Central Deep.

The *Badlands* simulations of the basin history provide the opportunity to demonstrate the theoretical models, test various assumptions and reproduce the main features of the most likely basin evolution process. Overall, the results closely match the tectono-stratigraphic style and evolution, notwithstanding that obviously the 1 Ma time step resolution used here cannot capture the precise details at time scales less than 1 Ma. In summary, an efficient and robust set of scenarios have been simulated, using an empirical 3D model to constrain the results, guided by a statistical experimental design to ensure optimised coverage of the possible ranges, that provide a reliable dataset on which to base the above conclusions.

9.5 3D Burial, Pressure and Thermal models

The 3D structural, facies and burial history reconstructions provide a better understanding of the Gippsland basin thermal history and hydrocarbon migration and entrapment than simple 1D or even 2D models. The fit of the heat flow model with the Gippsland thermal history suggests that a simple and single phase McKenzie model, with uniform pure shear extension, is not adequate for the Gippsland Basin. Simple models cannot provide enough heat for this basin. The second syn-rift event also needs to be modelled to allow a satisfactory rise in the paleo heat flow to reasonably high values so that good

matches are obtained for the simulated thermal trends and the measured empirical data. Surprisingly, although the entire basin was assigned two rift events, not all the areas responded to the second rifting and this is the prime reason previous modelling has not been successful – the devil is in the detail and one size does not fit all.

The erosion history in the Gippsland basin is complex and hard to reconstruct due to a lack of well penetrations through the deep sections. The available data and the simulations indicate that the onshore area, Northern Terrace, North Platform, Southern Terrace, and South Platform have experienced large amounts of erosion (over 1.5-3.5 km). Significant episodic erosion has occurred at the Otway unconformity (top Strzelecki, ca. Albian to Cenomanian time) but has continued since then, especially during the Late Cretaceous and middle Eocene over parts of the onshore area, Northern and Southern Terraces.

The temperature and burial plots indicate greatest burial in the east and Central Deep areas with rapid late stage burial on the eastern margin. The Ro model suggests a favourable maturation of the Gippsland Basin overall, with most source rocks now in the oil or gas window. The deeply buried sediments have reached the overmature zone, mainly the Strzelecki Group in the Central Deep. The Organic Transformation ratio model estimates that TR values over 80 mainly occur in the lower Latrobe Group within the Central Deep. The temperature, maturity and pressure simulations accompanying the burial history highlight three potential source rock intervals within the Latrobe Group should have produced hydrocarbons, namely: the Emperor, Golden Beach and Halibut subgroups, spanning the Late Cretaceous to early Palaeocene within the Gippsland Basin. The areas in the east and margins of the Central Deep were buried into the oil and gas zones early prior to trap formation and traps in these areas are largely gas prone. In contrast, areas to the east have undergone late stage burial and the younger Latrobe Group sediments, even including the Cobia, are now in the oil window and traps in these areas are oil prone.

The modelled present-day overpressure simulation shows a general linear relationship between downhole pressures and depth and most sections are normally pressured resulting from the good lateral and vertical migration in the Latrobe Group. Some minor overpressures occur within the regional seals in the Seaspray Group and within the Latrobe Group in the deeper formations, including beneath or associated with the volcanic, coals and some extensive thicker shales. The apparent more common

occurrence of volcanics along the North Terrace produces overpressure zones in the pressure model though this may in-part result from *PetroMod* assuming very low permeabilities in all volcanics which may not always be the case in Gippsland.

9.6 Insights and Suggestions

This study promotes further research and discussion on other relevant topics. Some insights and suggestions of potential applications and researches are listed below.

9.6.1 Theoretical modelling guided by empirical data

This study successfully used the 3D realistic model to constrain different 3D theoretical models of the Gippsland Basin for different research purposes: in particular, palaeo-landscape reconstruction and burial-thermal history analysis. This approach helps to efficiently assess a reasonable reconstruction of the basin history by not testing impossible scenarios and obviously produces a 3D burial and thermal models that better fit to the real geology. However, it has some limitations for different simulations. The reconstruction of palaeo-landscape in *Badlands* requires a good understanding of the basin being studied. Even although a wealth of empirical data have been used in the simulation of the Gippsland Basin this does not include some of the fundamental landscape simulation variables, such as erodibility, critical slope etc. Since they vary between different basins and can may also vary within a basin the results can be affected by the size/domain of the area being simulated. However, empirical data from other places can still be used as a starting point for sensitivity tests and to constrain the probable range for each variable. In addition, the results in this study suggest that a good fit to present-day landscape does not guarantee a good fit to the entire basin history. Hence, the reconstruction of the palaeo-landscape of a sedimentary basin needs different checkpoints with time in the basin evolution, and this could be difficult especially in a basin with few empirical data available.

Similarly, the burial and thermal modelling works much better with detailed realistic data control. However, the preparation to build a realistic model requires knowledge of erosion estimates and application of multi-disciplinary skills, including structural-stratigraphic modelling, facies, TOC and HI modelling, vitrinite reflectance and fission-track data analysis. This is a complex workflow and each step takes a considerable amount of time so it is no wonder this approach is not often pursued to completion. Nevertheless, a good understanding of the geology and production of the realistic model

within a reasonable time frame, as applied in this approach, is very important to produce good 3D burial and thermal models.

9.6.2 Petroleum Systems

The Gippsland Basin is one of the world's major petroleum bearing basins, with hydrocarbon production spanning over 50 years. The main petroleum system involves hydrocarbon generation from coal-measure source rocks (organic-rich coastal plain mudstones and coals), which migrate into deltaic or barrier sandstone reservoirs, trapped within large anticlines that developed post Eocene, that lie unconformably beneath marine shelf sequences that provide a regional seal developed in the Oligocene to Miocene. This Top Latrobe play or slight variations of it have proved very successful and the large anticlines have all been drilled whereas deeper targets and stratigraphic traps have been elusive. Significant uncertainties about some elements of the petroleum system remain which increase risk and have resulted in significantly slowed exploration for additional targets. The results of this study provide some insights and should help to reduce the remaining uncertainties.

One of the main uncertainties is the lateral and vertical distribution of the source rock units and their generative history both of which are not fully understood. This is primarily because only a few wells have penetrated the mature hydrocarbon intervals of the lower Halibut, Golden Beach and Emperor subgroups. The 3D tectonic, burial and thermal models show how the different parts of the Gippsland Basin have undergone very different amounts and timing of heating that can be related back to the rift-drift histories. The models also show how the main potential source rocks within the Latrobe Group are buried and mature over time, highlighting the lateral and vertical differences between the Emperor, Golden Beach, Halibut and Cobia subgroups, and how those differences probably control the gas and oil distribution across the Gippsland Basin.

The calculated heat flow trends show that greater heat flow occurred in the western and northern parts of the Central Deep and the stretching factors map explained how the heating difference is related to the rifting events, with these areas undergoing rapid early burial and heating. This maturation history needs to be carefully tied to timing of the traps since the large anticlines are post-Eocene. Together the rapid early maturation and the late structuring probably explain why these areas are gas prone with large top Latrobe gas fields. In contrast, intra-Latrobe oil/gas accumulations might be found in the east and south-east (e.g., near the Archer/Anemone and Angler region) where the maturation is very

different to deeper parts of the Central Deep. The realistic thermal models indicate that the thermal gradient around Archer/Anemone and Angler wells is notably lower than the average thermal gradient in the rest of the Central Deep. This matches the vitrinite reflectance data indicate a lower and later maturation process than other parts of the Central Deep.

Secondly, the location and extent of the early palaeo-coastline during deposition of the Golden Beach Subgroup is poorly known. The sedimentary facies evolution models in this study should provide a much better understanding of reservoirs, seals and source rocks in the eastern parts of the basin. Deep intra-Latrobe targets here would require drilling wells in deep water and possibly to over 4500m total depth and are viewed as high risk because to-date only small hydrocarbon accumulations have been found (e.g., Archer/Anemone and Angler wells). However, large oil accumulations have been found at top Latrobe in analogous younger marginal marine facies at the Blackback and Terakihi fields so the source and maturation is not the problem. The best fit 3D forward palaeo-landscape model shows the palaeo-coastline migration and palaeo-depositional environment changes from the Early Cretaceous to Holocene, which provides a chance to visualise the deposition of potential reservoirs and co-located source rocks in the lower Halibut, Emperor and Golden Beach subgroups.

Thirdly, economic intra-Latrobe traps are few, though some have been proven at depth when drilling the main anticlines. The pressure modelling here showed that more intra-Latrobe traps may occur beneath the reasonably extensive shales (e.g., in Tuna Deep) and beneath the volcanics (e.g., Kipper field). This play may work best to the west, north and centre of the Central Deep, where the pressure models suggest intra-Latrobe extensive shales, coals and volcanics occur the most. However, similar traps could be targeted anywhere in the basin including outside of the main anticlines (e.g., in tilted fault traps).

9.6.3 Geothermal Energy

A typical geothermal gradient in the normal continental crust is about 25 °C/km, within the first 3-5 km and decreases to about 16 °C/km at a depth of 40 km (DiPietro, 2013). The temperature model of the Gippsland Basin shows the average thermal gradient is 36 °C/km, calculated from topography-bathymetry to top Strzelecki Group (within 6 km). It is significantly higher than the value in normal continental crust and can be a good potential source of geothermal energy exploration. In addition, the direct use of geothermal energy accepts temperature ranges from 30 °C to 180 °C, and the electricity

can be generated using temperatures as low as 100 °C (Ayling et al., 2007). The subsurface temperature in onshore Gippsland can reach 100 °C at 2-3 km depth and at 3-4 km in the Central Deep, offshore Gippsland Basin. Currently, hot water is produced from observation water bores and has been used for workplace showers. Hence, the Gippsland Basin is a good basin for potential geothermal energy exploration.

In addition, borehole temperature data is one of the basic measurements made in petroleum wells, many coal and water bores and is freely available from Geoscience Australia and other industry databases. For example, Geoscience Australia has released the OZTemp Well Temperature database, containing 5,513 individual wells and 17,247 temperature and/or temperature gradient data records. Hence, thermal models can be built using data from the exploration and development of the Gippsland Basin to help identify suitable geothermal resources.

9.6.4 Basin Architecture

The seismic and well data help to build the basin architecture, which is the fundamental basis of this study. The Gippsland Basin is a relatively large basin with some regional maps available, and this study focused on basin modelling. Hence, the project doesn't include a detailed new seismic interpretation of the entire basin from top to bottom. The 3D seismic survey of the Gippsland Basin is an new merged survey based on several old 3D surveys, and retains some amplitude differences across the basin. For example, the seismic data deeper than -1600 ms (tw) are very low resolution towards the west, while in the eastern part of the basin the seismic data is barely traceable at a shallow level between -1260 to -1600 ms. This caused difficulty for the interpretation in the study. However, the Gippsland regeneration 3D re-processing and acquisition project has been carried out by CGG, and the re-processed data should be completed in Q4 2021. It will provide a great opportunity for detailed interpretation of the Gippsland Basin and better understanding of the numerous channel systems and deeper structures (e.g., the Emperor Subgroup, top Strzelecki Group, top basement). In addition, the offshore Gippsland Basin is considered to be highly prospective for CO₂ storage. This re-processed 3D seismic data will provide better imaging of faults and coal horizons, and together with Petrophysical property modelling (permeability model), may help to support future CO₂ storage activities.

The *Petrel* models made in this study can be easily updated with any new horizons and faults using the workflow manager. The updated models can then be used as input to rerun the *PetroMod* models though the *Badlands* modelling would need more manual input via the Python scripts.

Chapter 10 Conclusions

This research provides a best-practice case study how to make a realistic 3D geological model and use it to constrain theoretical models of sedimentation, burial, temperature, pressure and maturation (R_o).

The data-driven realistic 3D geological model was used to determine:

- structural controls on burial compaction using coal moisture that showed how it was most sensitive to burial depth but also to compression.

The main controls on landscape evolution have been quantified:

- The critical controls on sediment supply are Erodibility, Slope and Rainfall combined with basin Area;
- Rapid changes in sea level can outpace the other variables, whereas constant linear changes either slow or fast, are mostly accommodated by sediment supply and subsidence;
- Subsidence and uplift are secondary controls mainly operative in the rift phase;
- The rate of deposition is greatest in the rift phase and wanes in the post-rift phase, except on shelf margins where loading and flexure become dominant.

The 3D palaeo-landscape evolution model of the Gippsland rift Basin shows that:

- Quite different landscapes, facies and depositional rates were present in 2 rift and post-rift phases;
- Continuous uplift of large areas can fill rift basins without much mountain uplift;
- Different basin evolution histories can produce similar landscapes; a good fit to present day landscape doesn't guarantee a good fit to the entire basin history.

Burial and thermal history analysis of the Gippsland Basin shows that:

- Two rift and heating phases controlled basin development and they affected different areas of the basin over different times;
- There were three main source rock intervals and they underwent different maturation histories in different parts of the basin which controlled how oil and gas were generated.

References

- Abbassi, S., Edwards, D. S., George, S. C., Volk, H., Mahlstedt, N., di Primio, R., & Horsfield, B. (2016). Petroleum potential and kinetic models for hydrocarbon generation from the Upper Cretaceous to Paleogene Latrobe Group coals and shales in the Gippsland Basin, Australia. *Organic Geochemistry*, *91*, 54-67.
- Aghaei, H., Hall, M., & Wagstaff, B. (2020). How thermal maturity analysis supports stratigraphic restoration in heavily faulted fluvial outcrops: a case study on Strzelecki Group outcrops, West Gippsland, Victoria, Australia. *Australian Journal of Earth Sciences*, *67*(5), 749-757.
- Aghaei, H., Hall, M., Tait, A., & Wagstaff, B. (2014). Reconstruction of Upper Strzelecki Stratigraphy based on Vitrinite Reflectance and Palynology Analyses, and New Ideas on the Amount of Erosion and Present Day Thickness. *AAPG International Conference & Exhibition*. Istanbul, Turkey: AAPG.
- Aghaei, H., Hall, M., Wagstaff, B., & Tait, A. (2017). Stratigraphic reconstruction of the Strzelecki Group outcrops in west Gippsland: new data on the present-day thickness and amount of erosion. *Australian Journal of Earth Sciences*, *64*(2), 251-264.
- Aghaei, H., Valenta, C., Hall, M., & Tait, A. (2015). Detailed stratigraphic and structural analysis of the early cretaceous outcrops in West Gippsland, Victoria, Australia. *Eastern Australian Basins Symposium: Publication of Proceedings* (pp. 115-130). Petroleum Exploration Society of Australia (PESA).
- Alexander, R., Kralert, P. G., Marzi, R., Kagi, R. I., & Evans, E. J. (1991). A Geochemical Method for Assessment of the Thermal Histories of Sediments: A Two-Well Case Study from the Gippsland Basin, Australia. *APEA Journal*, *31*(1), 325-332.
- Allardice, D. J. (1991). The water in brown coal. In R. A. Durie (Ed.), *The science of Victorian brown coal* (pp. 103-150). Butterworth-Heinemann.

- Ayling, B. F., Budd, A. R., Holgate, F. L., & Gerner, E. (2007). *Direct-use of geothermal energy: opportunities for Australia*. Geoscience Australia, Educational Factsheet GA10660.
- Bernecker, T., & Partridge, A. D. (2001). Emperor and Golden Beach subgroups: the onset of Late Cretaceous sedimentation in the Gippsland Basin, S.E. Australia. *Eastern Australasian Basins Symposium* (pp. 391-401). Melbourne: Petroleum Exploration Society of Australia.
- Bernecker, T., Partridge, A. D., & Webb, J. A. (1997). Mid-late Tertiary deep-water temperate carbonate deposition, offshore Gippsland Basin, southeastern Australia. *Special Publications of Society for Sedimentary Geology*.
- Bialas, J., Frank, M., SARKAR, S., Basak, C., Berndt, C., Huuse, M., & Badhanis, S. (2019). Late Eocene onset of the Proto-Antarctic Circumpolar Current.
- Birch, G. F., & Lound, S. P. (2021). The Late Quaternary geological history of the lower Sydney estuary (Australia). *Regional Studies in Marine Science*, 47, 101915.
- Blake, R. (1986). Seismic-stratigraphic interpretation of coastal barrier systems of Late Eocene age, offshore Gippsland Basin. *Second South-Eastern Australia Oil Exploration Symposium* (pp. 159-169). Melbourne: Petroleum Exploration Society of Australia (PESA).
- Bodard, J. M., & Wall, V. J. (1985). Lithostratigraphic and depositional architecture of the Latrobe Group, offshore Gippsland Basin. In R. C. Glenie (Ed.), *Second South-Eastern Australia Oil Exploration Symposium* (pp. 137-153). Melbourne: Petroleum Exploration Society of Australia.
- Bodard, J. M., Wall, V. J., & Kanen, R. A. (1986). Lithostratigraphic and Depositional Architecture of the Latrobe Group, Offshore Gippsland Basin. *Second South-Eastern*

- Australia Oil Exploration Symposium* (pp. 113-136). Melbourne: Petroleum Exploration Society of Australia.
- Bostwick, T. R. (1986). *Geochemical Report, Well Completion Report Whiting-2 Interpretive Data Vol II*. Esso Australia Ltd.
- Braun, J., Guillocheau, F., Robin, C., Baby, G., & Jelsma, H. (2014). Rapid erosion of the Southern African Plateau as it climbs over a mantle superswell. *Journal of Geophysical Research: Solid Earth*, 119(7), 6093-6112.
- Brewer, C. J., Hampson, G. J., Whittaker, A. C., Roberts, G. G., & Watkins, S. E. (2020). Comparison of methods to estimate sediment flux in ancient sediment routing systems. *Earth-Science Reviews*, 103217.
- Brown, B. J., Müller, R. D., Gaina, C., Struckmeyer, H., Stagg, H., & Symonds, P. (2003). Formation and evolution of Australian passive margins: Implications for locating the boundary between continental and oceanic crust. *SPECIAL PAPERS-GEOLOGICAL SOCIETY OF AMERICA*, 223-244.
- Brown, B. R. (1985). Offshore Gippsland Silver Jubilee. In R. C. Glenie (Ed.), *Second South-Eastern Australia Oil Exploration Symposium* (pp. 29-56). Petroleum Exploration Society of Australia.
- Bryan, S., Constantine, A., Stephens, C., Ewart, A., Schön, R., & Parianos, J. (1997). Early Cretaceous volcano-sedimentary successions along the eastern Australian continental margin: Implications for the break-up of eastern Gondwana. *Earth and Planetary Science Letters*, 153(1-2), 85-102.
- Burns, B. J., & Emmett, J. K. (1984). Final Report GE 83B geochemical (sniffer) survey, offshore Gippsland Shelf. November 1983. *Report on work program undertaken under the Petroleum (Submerged Lands) Act (unpublished)*. Held by the Bureau of Resources Sciences, Reference(83/47).

- Burns, B. J., Bostwick, T. R., & Emmett, J. K. (1987). Gippsland terrestrial oils – recognition of compositional variations due to maturity and biodegradation. *The APEA Journal*, 27, 73-85.
- Burns, B. J., James, A. T., & Emmett, J. K. (1984). The use of gas isotopes in determining the source of some Gippsland Basin oils. *The APEA Journal*, 24, 217-221.
- Chen, A., Darbon, J., & Morel, J. M. (2014). Landscape evolution models: A review of their fundamental equations. *Geomorphology*, 219, 68-86.
- Clitheroe, G., Gudmundsson, O., & Kennett, B. L. (2000). The crustal thickness of Australia. *Journal of Geophysical Research: Solid Earth*, 105(B6), 13697-13713.
- Collinson, R., Gupta, R., Smith, G., & Van Elk, J. (2008). Scenario Analysis Tool for Probabilistic Analysis of Reserves. *SPE Asia Pacific Oil and Gas Conference and Exhibition* (p. 116378). Society of Petroleum Engineers.
- Constantine, A. E. (2001). Sedimentology, stratigraphy and paleo-environment of the Late Jurassic–Early Cretaceous Strzelecki Group. *Unpublished PhD thesis*. Victoria: School of Geosciences, Monash University.
- Corcoran, D. V., & Doré, A. G. (2005). A review of techniques for the estimation of magnitude and timing of exhumation in offshore basins. *Earth-Science Reviews*, 72(3-4), 129-168.
- Cull, J. P., & Beardsmore, G. R. (1992). Estimates of Heat Flow and Geothermal Gradients in the Gippsland Basin. *Gippsland Basin Symposium* (pp. 15-24). Melbourne: The Australasian Institute of Mining and Metallurgy.
- Czarnota, K., Roberts, G. G., White, N. J., & Fishwick, S. (2014). Spatial and temporal patterns of Australian dynamic topography from River Profile Modeling. *Journal of Geophysical Research: Solid Earth*, 119(2), 1384-1424.

- Dayal, V. (2015). *An introduction to R for quantitative economics*. SpringerBriefs in Economics.
- Debnath, K., Nikora, V., Aberle, J., Westrich, B., & Muste, M. (2007). Erosion of cohesive sediments: Resuspension, bed load, and erosion patterns from field experiments. *Journal of hydraulic engineering*, 133(5), 508-520.
- Dettmann, M., & Douglas, J. (1976). Mesozoic palaeontology. In *Geology of Victoria: Geological Society of Australia Special Publication* (Vol. 5, pp. 164-169).
- DiPietro, J. A. (2013). Keys to the interpretation of geological history. In J. A. DiPietro, *Landscape evolution in the United States* (pp. 3-95). Elsevier Waltham, MA.
- Duddy, I., & Green, P. (1992). Tectonic development of the Gippsland Basin and environs: identification of key episodes using apatite fission track analysis (AFTA). 'ENERGY, ECONOMICS AND ENVIRONMENT' GIPPSLAND BASIN SYMPOSIUM, (pp. 111-119).
- Dudley, P. (1959). *Oil possibilities of Petroleum Prospecting License Number 212 in the South Gippsland Highlands*. Report prepared for Victoria Oil Ltd (unpubl.).
- Edwards, A. B., & Baker, G. (1943). *Jurassic arkose in southern Victoria*. Royal Society of Victoria.
- Edwards, A. B., Baker, G., & Knight, J. L. (1944). The geology of the Wonthaggi coal field, Victoria. *Proceedings Australasian Institute Mining & Metallurgy*, 135, pp. 1-54.
- Edwards, D. S., Ahmed, M., Bernecker, T., Boreham, C. J., Chen, J., Gong, S., . . . Langford, R. P. (2015). A geochemical overview of Gippsland Basin hydrocarbon accumulations. *International Conference and Exhibition* (p. 281). Melbourne: Society of Exploration Geophysicists and American Association of Petroleum.
- Featherstone, P., Aigner, T., Brown, L., King, M., & Leu, W. (1991). Stratigraphic modelling of the Gippsland Basin. *The APPEA Journal*, 31(1), 10-115.

- Ferrier, K. L., Huppert, K. L., & Perron, J. T. (2013). Climatic control of bedrock river incision. *Nature*, 496(7444), 206-209.
- Flemings, P. B., & Jordan, T. E. (1989). A Synthetic Stratigraphic Model of Foreland Basin Development. *Journal of Geophysical Research*, 94(B4), 3851-3866.
- Gaina, C., Müller, R. D., Roest, W. R., & Symonds, P. (1998). The opening of the Tasman Sea: a gravity anomaly animation. *Earth interactions*, 2(4), 1-23.
- Gallagher, S. J., Smith, A. J., Jonasson, K., Wallace, M. W., Holdgate, G. R., Daniels, J., & Taylor, D. (2001). The Miocene palaeoenvironmental and palaeoceanographic evolution of the Gippsland Basin, Southeast Australia: a record of Southern Ocean change. *Palaeogeography, Palaeoclimatology, Palaeoecology*, 172(1-2), 53-80.
- George, A. M., & Mackay, G. H. (1991). Petrology. In R. A. Durie (Ed.), *The Science of Victorian Brown Coal* (pp. 45-102). Butterworth-Heinemann.
- Gippsland Basin*. (2021). Retrieved from Geoscience Australia:
<https://www.ga.gov.au/scientific-topics/energy/province-sedimentary-basin-geology/petroleum/offshore-southern-australia/gippsland>
- Gleadow, A. J., & Duddy, I. R. (1981). A natural long-term track annealing experiment for apatite. *Nuclear Tracks*, 5(1-2), 169-174.
- Goutorbe, B., Lucazeau, F., & Bonneville, A. (2008). Surface heat flow and the mantle contribution on the margins of Australia. *Geochemistry, Geophysics, Geosystems*, 9(5).
- Granjeon, D., Have, P., Coatleven, J., Pegaz-Fiornet, S., & Chauveau, B. (2018). High performance stratigraphic modeling of shelf to deep-water plays. *In AAPG 2018 Annual Convention and Exhibition*.

- Green, P. F., Japsen, P., Chalmers, J. A., Bonow, J. M., & Duddy, I. R. (2018). Post-breakup burial and exhumation of passive continental margins: Seven propositions to inform geodynamic models. *Gondwana Research*, 53, 58-81.
- Griffiths, C. M., Dyt, C., Paraschivoiu, E., & Liu, K. (2001). Sediment in hydrocarbon exploration. *In Geologic modeling and simulation* (pp. 71-97). Boston, MA: Springer.
- Grosser, M. (2005). *Megascolides-1 well completion report, Karoon Gas, PEP162/EL 4537*. Open File Petroleum Data Base, Department of Sustainability, Development, Business and Innovation. Victorian Government, Report No. PE911464.
- Hallet, B., Hunter, L., & Bogen, J. (1996). Rates of erosion and sediment evacuation by glaciers: A review of field data and their implications. *Global and Planetary Change*, 12(1-4), 213-235.
- Haq, B. U., Hardenbol, J. A., & Vail, P. R. (1987). Chronology of fluctuating sea levels since the Triassic. *Science*, 235(4793), 1156-1167.
- Harrison, B., Taylor, D., Tingate, P., & Sandiford, M. (2012). Heat flow modelling and thermal history of the onshore Gippsland Basin: upside potential for unconventional gas and geothermal resources. *Eastern Australasian Basins Symposium IV* (pp. 49-63). Brisbane: Petroleum Exploration Society of Australia.
- Hegarty, K. A., Duddy, I. R., Green, P. F., Gleadow, A. J., Fraser, I., & Weissel, J. K. (1985). Regional evaluation of the tectonic and thermal history of the Gippsland Basin. *Petroleum Exploration Society of Australia (PESA)*, 65-74.
- Hobley, D. E., Sinclair, H. D., Mudd, S. M., & Cowie, P. A. (2011). Field calibration of sediment flux dependent river incision. *Journal of Geophysical Research: Earth Surface*, 116(F4).
- Holdgate, G. R. (1985). Latrobe Valley brown coals—their geometry and facies equivalents as a guide to depositional environment. *Australian Coal Geology*, 5, 53-68.

- Holdgate, G. R. (2003). Coal. In W. D. Birch (Ed.), *Geology of Victoria* (pp. 489–516). Geological Society of Australia.
- Holdgate, G. R. (2005). Geological processes that control lateral and vertical variability in coal seam moisture contents—Latrobe Valley (Gippsland Basin) Australia. *International Journal of Coal Geology*, 63, 130-155.
- Holdgate, G. R., & Gallagher, S. J. (2003). Tertiary, Gippsland Basin. In W. D. Birch (Ed.), *Geology of Victoria* (pp. 324-335). Geological Society of Australia Special Publication No. 23.
- Holdgate, G. R., Geurin, B., Wallace, M. W., & Gallagher, S. J. (2001). Marine geology of Port Phillip, Victoria. *Australian Journal of Earth Sciences*, 48(3), 439-455.
- Holdgate, G. R., Sluiter, I. R., Clowes, C. D., & Hannah, M. J. (2021). The spatial and temporal occurrence and significance of dinoflagellates and other marine fossils within onshore coal measures, Gippsland Basin, Australia. *Australian Journal of Earth Sciences*, 1-20.
- Holdgate, G. R., Wallace, M. W., & Forbes, S. (2015). Pre-Cenozoic geology of the Latrobe Valley Area—onshore Gippsland Basin, S.E. Australia. *Australian Journal of Earth Sciences*, 62(6), 695-716.
- Holdgate, G. R., Wallace, M. W., Gallagher, J., Daniels, S. J., Keene, J. B., & Smith, A. J. (2000). Controls on Seaspray Group sonic velocities in the Gippsland Basin—a multidisciplinary approach to the canyon ‘seismic velocity problem’. *The APPEA Journal*, 40(1), 293-313.
- Holdgate, G., & Clarke, J. (2000). A review of Tertiary brown coal deposits in Australia: their depositional factors and eustatic correlations. *AAPG bulletin*, 84(8), 1129-1151.

- Holdgate, G., Wallace, M., Gallagher, S., & Taylor, D. (2000). A review of the Traralgon Formation in the Gippsland Basin—a world class brown coal resource. *International Journal of Coal Geology*, 45(1), 55-84.
- Howard, A. D., & Kerby, G. (1983). Channel changes in badl. *Geological Society of America Bulletin*, 94(6), 739-752.
- James, B., & Emmett, J. (1984). The use of gas isotopes in determining the source of some Gippsland Basin oils. *The APPEA Journal*, 24(1), 217-221.
- Jarvis, I., Lignum, J. S., Gröcke, D. R., Jenkyns, H. C., & Pearce, M. A. (2011). Black shale deposition, atmospheric CO₂ drawdown, and cooling during the Cenomanian-Turonian Oceanic Anoxic Event. *Paleoceanography*, 26(3).
- Johnstone, E. M., Jenkins, C. C., & Moore, M. A. (2001). An integrated structural and palaeogeographic investigation of Eocene erosional events and related hydrocarbon potential in the Gippsland Basin. *Eastern Australasian Basins Symposium*, 403-412.
- Jones, J., & Veevers, J. (1982). A Cainozoic history of Australia's southeast highlands. *Journal of the Geological Society of Australia*, 29(1-2), 1-12.
- Kear, B. P. (2006). Plesiosaur remains from Cretaceous high-latitude non-marine deposits in southeastern Australia. *Journal of Vertebrate Paleontology*, 26(1), 196-199.
- Kennett, B. L., & Blewett, R. S. (2012). Lithospheric framework of Australia. *Episodes*, 35(1), 9-22.
- Levine, J., & Davis, A. (1989). The relationship of coal optical fabrics to Alleghanian tectonic deformation in the central Appalachian fold-and-thrust belt, Pennsylvania. *Geological Society of America Bulletin*, 101(10), 1333-1347.
- Lindsay, G. A., & Djakic, A. (1985). *Bream Field Study, Vol. 1*. Esso Exploration and Production Australia Inc.

- Liu, K., Paterson, L., & Jian, F. (1994). Depositional modelling of the Gippsland Basin and the Barrow–Exmouth Sub-basins. *The APPEA Journal*, 34, 350-365.
- Lowry, D. C., & Longley, I. M. (1991). A new model for the mid-Cretaceous structural history of the northern Gippsland Basin. *The APPEA Journal*, 31(1), 143-153.
- Mahon, E. M., & Wallace, M. W. (2020). Cenozoic structural history of the Gippsland Basin: Early Oligocene onset for compressional tectonics in SE Australia. *Marine and Petroleum Geology*, 114, 104243.
- McLean, M. A., & Blackburn, G. J. (2013). *A new regional velocity model for the Gippsland Basin*. Melbourne: Department of Primary Industries, Energy & Earth Resources Group.
- Mitchell, J. K., Holdgate, G. R., & Wallace, M. W. (2007). Pliocene – Pleistocene history of the Gippsland Basin outer shelf and canyon heads, southeast Australia. *Australian Journal of Earth Sciences*, 54, 49-64.
- Montgomery, D. C. (2017). *Design and Analysis of Experiments*. New York, NJ, 734pp.: John Wiley & Sons.
- Moore, D. H., & Wong, D. (2001). Down and out in Gippsland: using potential fields to look deeper and wider for new hydrocarbons. *Eastern Australasian Basins Symposium* (pp. 363-371). Melbourne: Petroleum Exploration Society of Australia (PESA).
- Moore, D. H., Burns, B. J., Emmett, J. K., & Guthrie, D. A. (1992). Integrated source, maturation and migration analysis, Gippsland Basin, Australia. *The APEA Journal*, 32(1), 313-324.
- Moore, M. E., Gleadow, A. J., & Lovering, J. F. (1986). Thermal evolution of rifted continental margins: new evidence from fission tracks in basement apatites from southeastern Australia. *Earth and Planetary Science Letters*, 78(2-3), 255-270.

- Müller, R. D., Cannon, J., Qin, X., Watson, R. J., Gurnis, M., Williams, S., . . . Zahirovic, S. (2018). GPlates: building a virtual Earth through deep time. *Geochemistry, Geophysics, Geosystems*, 19(7), 2243-2261.
- Müller, R. D., Zahirovic, S., Williams, S. E., Cannon, J., Seton, M., Bower, D. J., . . . Gurnis, M. (2019). A global plate model including lithospheric deformation along major rifts and orogens since the Triassic. *Tectonics*, 38(6), 1884-1907.
- Murphy, B. P., Johnson, J. P., Gasparini, N. M., & Sklar, L. S. (2016). Chemical weathering as a mechanism for the climatic control of bedrock river incision. *Nature*, 532(7598), 223-227.
- Murray, A., He, Z., & Edwards, C. (2021). Oil by exception: Where and why oil occurs in the gassy petroleum systems of the NW Shelf of Australia. *AAPG GTW Perth March 2021 keynote talk with speaker notes. Advanced Petroleum Systems Analysis in the Asia Pacific Region: New Technology and Applications*.
- Norvick, M. (2005). Plate tectonic reconstructions of Australia's southern margins. *Geoscience Australia Record*, 7.
- Norvick, M. S., & Smith, M. A. (2001). Mapping the plate tectonic reconstruction of southern and southeastern Australia and implications for petroleum systems. *The APPEA Journal*, 41(1), 15-35.
- Norvick, M. S., Smith, M. A., & Power, M. R. (2001). The Plate Tectonic Evolution of Eastern Australasia Guided by the Stratigraphy of the Gippsland Basin. *PESA Eastern Australasian Basins Symposium* (pp. 15-23). Melbourne: The Australasian Institute of Mining and Metallurgy.
- O'Halloran, G. J., & Johnstone, E. M. (2001). Late Cretaceous Rift Volcanics of the Gippsland Basin, SE Australia-New Insights from 3D Seismic. *Eastern Australasian*

- Basins Symposium* (pp. 353-361). Melbourne: Petroleum Exploration Society of Australia (PESA).
- O'Sullivan, P. B., Mitchell, M. M., O'Sullivan, A. J., Kohn, B. P., & Gleadow, A. J. (2000). Thermotectonic history of the Bassian Rise, Australia: implications for the breakup of eastern Gondwana along Australia's southeastern margins. *Earth and Planetary Science Letters*, 182(1), 31-47.
- Partridge, A. (2006). Late Cretaceous–Cenozoic palynology zonations, Gippsland Basin. In E. Monteil (Ed.), *Australian Mesozoic and Cenozoic palynology zonations—updated to the 2004 geologic time scale*. Geoscience Australia Record 2006/23.
- Partridge, A. D. (1999). *Late Cretaceous to Tertiary geological evolution of the Gippsland Basin, Victoria*. PhD thesis, Bundoora, Victoria, La Trobe University.
- Partridge, A. D. (2006). Jurassic-Early Cretaceous dinocyst zonations NWS Australia: 1st update of HMP 2004. In E. Monteil (Ed.), *Australian Mesozoic and Cenozoic Palynology Zonations –*. Geoscience Australia, Record 2006/23.
- Perron, J. T., Kirchner, J. W., & Dietrich, W. E. (2009). Formation of evenly spaced ridges and valleys. *Nature*, 460(7254), 502-505.
- Planchon, O., & Darboux, F. (2002). A fast, simple and versatile algorithm to fill the depressions of digital elevation models. *Catena*, 46(2-3), 159-176.
- Powell, W. D., Nourollah, M. H., Tait, A. M., Saitta, A. J., Kirk, R., Woollard, K., & Bubrzycki, M. (2020). *Regional 3D geological framework model Gippsland Basin, Victoria*. The Geological Survey of Victoria (GSV).
- Power, M. R. (2003). *Structural evolution and hydrocarbon play fairways of the Gippsland Basin*. University of Melbourne, School of Earth Sciences.

- Power, M. R., Hill, K. C., Hoffman, N., Bernecker, T., & Norvick, M. (2001). The Structural and Tectonic Evolution of the Gippsland Basin: Results From 20 Section Balancing and 30 Structural Modelling. *Eastern Australasian Basins Symposium*, 373-384.
- R Core Team. (2021). *The R Project for Statistical Computing*. Retrieved from The R Foundation: <https://www.r-project.org/>
- Rahmanian, V. D., Moore, P. S., Mudge, W. J., & Spring, D. E. (1990). Sequence stratigraphy and the habitat of hydrocarbons, Gippsland Basin, Australia. *Classic Petroleum Provinces, Geological Society Special Publication*, 50(1), 525-541.
- Riordan, S. J., Lang, S. C., & Payenberg, T. H. (2004). Sequence stratigraphy of the intra-Latrobe Group, Flounder Field, Gippsland Basin. Implications for the building and upscaling of 3D geological models. *PESA Eastern Australasian Basins Symposium II* (pp. 523-536). Adelaide: Petroleum Exploration Society of Australia.
- Root, R. S., Gibson-Poole, C. M., Lang, S. C., Streit, J. E., Unterschultz, J., & Ennis-King, J. (2004). Opportunities for geological storage of carbon dioxide in the offshore Gippsland Basin, SE Australia: an example from the upper Latrobe Group. *PESA Eastern Australasian Basins Symposium II* (pp. 367-388). Adelaide: Petroleum Exploration Society of Australia.
- Rosendahl, B. R. (1987). Architecture of continental rifts with special reference to East Africa. *Annual Review of Earth and Planetary Science*, 15, 445-503.
- Röth, J., Parent, A., Warren, C., Hall, L. S., Palmowski, D., & Koronful, N. (2021). Lithospheric evolution, thermo-tectonic history and source-rock maturation in the Gippsland Basin, Victoria, southeastern Australia. *Australian Journal of Earth Sciences*, 1-30.

- Salles, T. B., Griffiths, C. M., Dyt, C. P., & Li, F. (2011). Australian shelf sediment transport responses to climate change-driven ocean perturbations. *Marine Geology*, 282(3-4), 268-274.
- Salles, T., & Duclaux, G. (2015). Combined hillslope diffusion and sediment transport simulation applied to landscape dynamics modelling. *Earth Surface Processes and Landforms*, 40(6), 823-839.
- Salles, T., & Hardiman, L. (2016). Badlands: An open-source, flexible and parallel framework to study landscape dynamics. *Computers & Geosciences*, 91, 77-89.
- Salles, T., Ding, X., & Brocard, G. (2018). pyBadlands: A framework to simulate sediment transport, landscape dynamics and basin stratigraphic evolution through space and time. *PloS one*, 13(4), e0195557.
- Salles, T., Ding, X., & Brocard, G. (2019). *Getting started with badlands*. Retrieved from Badlands: <https://badlands.readthedocs.io/en/latest/>
- Scher, H. D., Whittaker, J. M., Williams, S. E., Latimer, J. C., Kordesch, W. E., & Delaney, M. L. (2015). Onset of Antarctic Circumpolar Current 30 million years ago as Tasmanian Gateway aligned with westerlies. *Nature*, 523(7562), 580-583.
- Seidl, M. A., Dietrich, W. E., & Kirchner, J. W. (1994). Longitudinal profile development into bedrock: An analysis of Hawaiian channels. *The Journal of Geology*, 102(4), 457-474.
- Seidl, M. A., Dietrich, W. E., Schmidt, K. H., & de Ploey, J. (1992). The problem of channel erosion into bedrock. *Functional geomorphology*, 101-124.
- Shobe, C. M., Hancock, G. S., Eppes, M. C., & Small, E. E. (2017). Field evidence for the influence of weathering on rock erodibility and channel form in bedrock rivers. *Earth Surface Processes and Landforms*, 42(13), 1997-2012.

- Smith, G. C. (1982). A review of the Tertiary–Cretaceous tectonic history of the Gippsland Basin and its control on coal measure sedimentation. *Australian Coal Geology*, 4(1), 1-38.
- Smith, G. C. (1988). Oil and Gas, Gippsland Basin. In J. a. Douglas (Ed.), *Geology of Victoria* (pp. 514-531). Geological Society of Australia Victorian Division.
- Smith, G. C., & Cook, A. C. (1984). Petroleum Occurrence in the Gippsland Basin and its Relationship to Rank and Organic Matter Type. *APEA Journal*, 24(1), 196-216.
- Smith, G., Rayfield, M., DePledge, D., & Gupta, R. (2004). The Chinguetti deepwater turbidite field, Mauritania: reserve estimation and field development using uncertainty management and experimental designs for multiple scenario 3D models. *The APPEA Journal*, 44(1), 521-542.
- Stock, J. D., & Montgomery, D. R. (1999). Geologic constraints on bedrock river incision using the stream power law. *Journal of Geophysical Research: Solid Earth*, 104(B3), 4983-4993.
- Sustainable Energy Authority. (2004). *Wave and tidal power assessment for the Victorian coastline*. Water Technology Technical Report J, 121.
- Sweeney, J., & Burnham, A. (1990). Evaluation of a simple model of vitrinite reflectance based on chemical kinetics. *AAPG bulletin*, 74(10), 1559-1570.
- Tarlo, L. B. (1959). *Stretosaurus* gen. nov., a giant pliosaur from the Kimmeridge Clay. *Palaeontology*, 2(1), 39-55.
- Tokarev, V., Sandiford, M., & Gostin, V. (1999). Landscape evolution in the Mount Lofty Ranges: implications for regolith development. *New approaches to an old continent, 3rd Australian Regolith Conference Proceedings, Regolith*, 98, pp. 127-134.

- Tosolini, A. P., McLoughlin, S., & Drinnan, A. N. (1999). Stratigraphy and fluvial sedimentary facies of the Neocomian lower Strzelecki Group, Gippsland Basin, Victoria. *Australian Journal of Earth Sciences*, 46(6), 951-970.
- Tucker, G. E., & Hancock, G. R. (2010). Modelling landscape evolution. *Earth Surface Processes and Landforms*, 35(1), 28-50.
- Tucker, G. E., & Slingerland, R. L. (1994). Erosional dynamics, flexural isostasy, and long-lived escarpments: A numerical modeling study. *Journal of Geophysical Research: Solid Earth*, 99(B6), 12229-12243.
- Tuite, M. L., Flannery, D. T., & Williford, K. H. (2016). Organic geochemistry of a high-latitude Lower Cretaceous lacustrine sediment sample from the Koonwarra Fossil Beds, South Gippsland, Victoria, Australia. *Memoirs of Museum Victoria*, 74, 73-79.
- Veevers, J. J., Jones, J. G., & Powell, C. M. (1982). Tectonic framework of Australia's sedimentary basins. *The APPEA Journal*, 22(1), 283-300.
- Verheyen, T. V., Johns, R. B., & Espitalié, J. (1984). An evaluation of Rock-Eval pyrolysis for the study of Australian coals including their kerogen and humic acid fractions. *Geochimica et Cosmochimica Acta*, 48(1), 63-70.
- Weber, U. D., Hill, K. C., Brown, R. W., Gallagher, K., Kohn, B. P., Gleadow, A. J., & Foster, D. A. (2004). Sediment supply to the Gippsland Basin from thermal history analysis: constraints on Emperor-Golden Beach reservoir composition. *The APPEA Journal*, 44(1), 397-416.
- Whipple, K. X., & Tucker, G. E. (1999). Dynamics of the stream-power river incision model: Implications for height limits of mountain ranges, landscape response timescales, and research needs. *Journal of Geophysical Research: Solid Earth*, 104(B8), 17661-17674.

- Willcox, J., Colwell, J., & Constantine, A. (1992). New ideas on Gippsland Basin regional tectonics. *'ENERGY, ECONOMICS AND ENVIRONMENT' GIPPSLAND BASIN SYMPOSIUM* (pp. 93-109). Petroleum Exploration Society of Australia (PESA).
- Willcox, J., Sayers, J., Stagg, H., & Van De Beuque, S. (2001). Geological framework of the Lord Howe Rise and adjacent ocean basins. *Eastern Australasian Basins Symposium*, 211-225.
- Yang, X., & Smith, G. (2019). Gippsland Basin 3D forward modelling in Badlands. *ASEG Extended Abstracts, 2019*, pp. 1-5.
- Young, R., & McDougall, I. (1993). Long-term landscape evolution: Early Miocene and modern rivers in southern New South Wales, Australia. *The Journal of Geology*, *101*(1), 35-49.

Appendix

Appendix 1 Log cut-offs and the calculator functions.....	261
Appendix 2 Complete well correlation section, using Bignose-1 and Barracouta-1 as examples.	261
Appendix 3 Settings of advanced velocity model in the Petrel Software.	264
Appendix 4 Average velocity model, well report.....	265
Appendix 5 The four main steps of the pillar gridding method.	271
Appendix 6 GPlates reconstruction animation.....	273
Appendix 7 Badlands Animation (Best fit case).....	273
Appendix 8 Badlands Python script, Reference Case.....	274
Appendix 9 Sea Level Curve, used in Badlands modelling.....	278
Appendix 10 Badlands input Uplift maps.....	279
Appendix 11 Data analysis of Latrobe Valley Moisture.....	280
Appendix 12 Weighted settings of scale up facies log for entire Gippsland Basin	281
Appendix 13 Erosion maps used in PetroMod 3D modelling.....	282
Appendix 14 Comparison of modelled Temperature and Vitrinite Reflectance vs measured data	283
Appendix 15 The calculated heat flow trends extracted at individual wells from 3D model	289
Appendix 16 Burial Plot overlay with Vitrinite Reflectance	295
Appendix 17 Comparison of Vitrinite Reflectance calibration between different crust lithology.	301
Appendix 18 Organic transformation ratio (TR) maps at ca. 30Ma, 15Ma, and 0Ma.....	303

Appendix 1 Log cut-offs and the calculator functions

$$V_{\text{shale}} = \frac{\text{GR} - \text{GR.min}}{\text{GR.max} - \text{GR.min}}$$

$$\text{GRnorm} = \frac{\text{GR} - \text{GR.min}}{\text{GR.max} - \text{GR.min}}$$

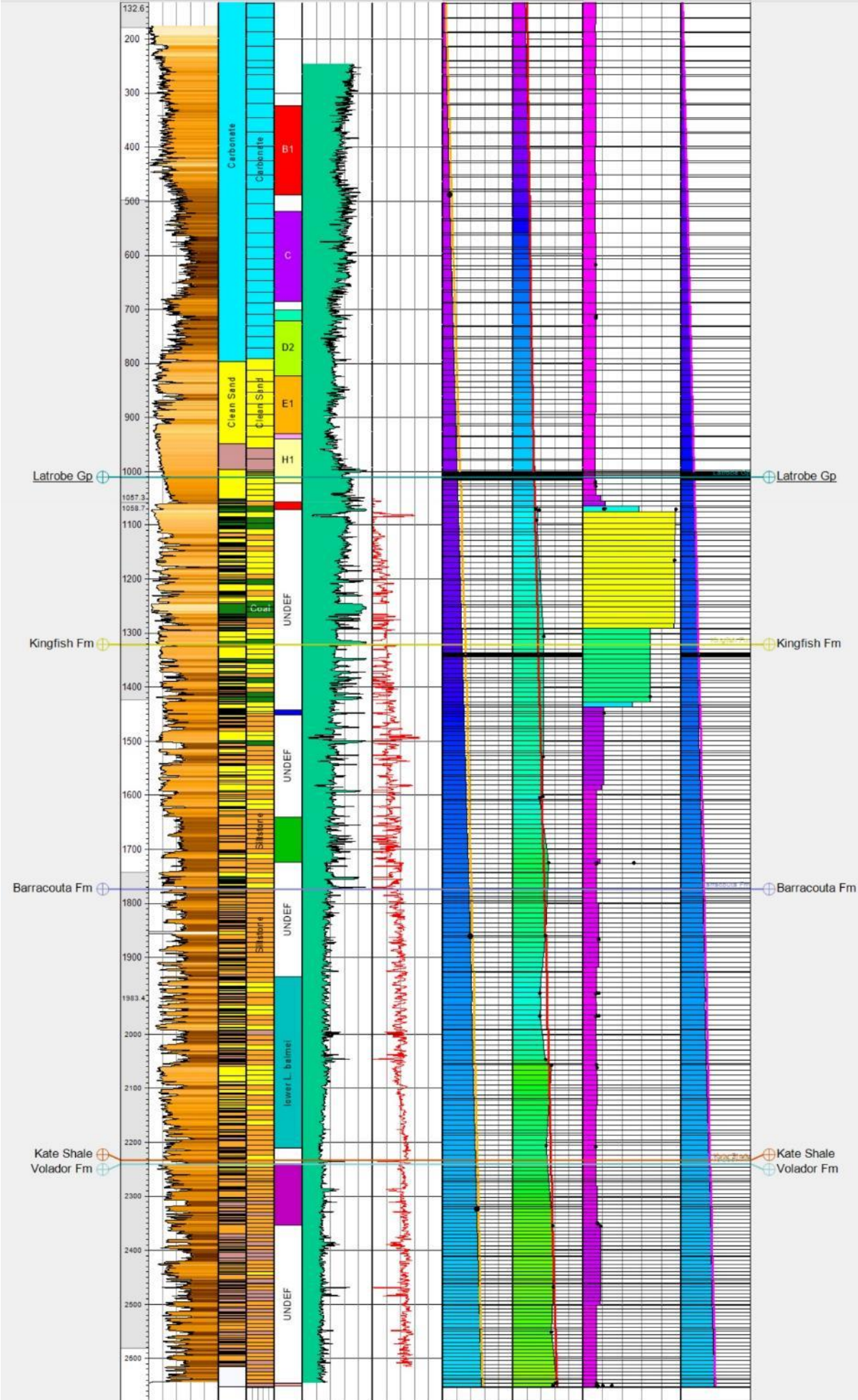
$$\text{RHOB_NPHI} = \left(\frac{\text{RHOB} - \text{RHOB.min}}{\text{RHOB.max} - \text{RHOB.min}} \right) - \left(\frac{\text{NPHI.max} - \text{NPHI}}{\text{NPHI.max} - \text{NPHI.min}} \right)$$

$$\text{DT} = \text{DT} * 3.28084 \text{ (uniform the sonic unit to us/ft)}$$

Appendix 2 Complete well correlation section, using Bignose-1 and Barracouta-1 as examples.

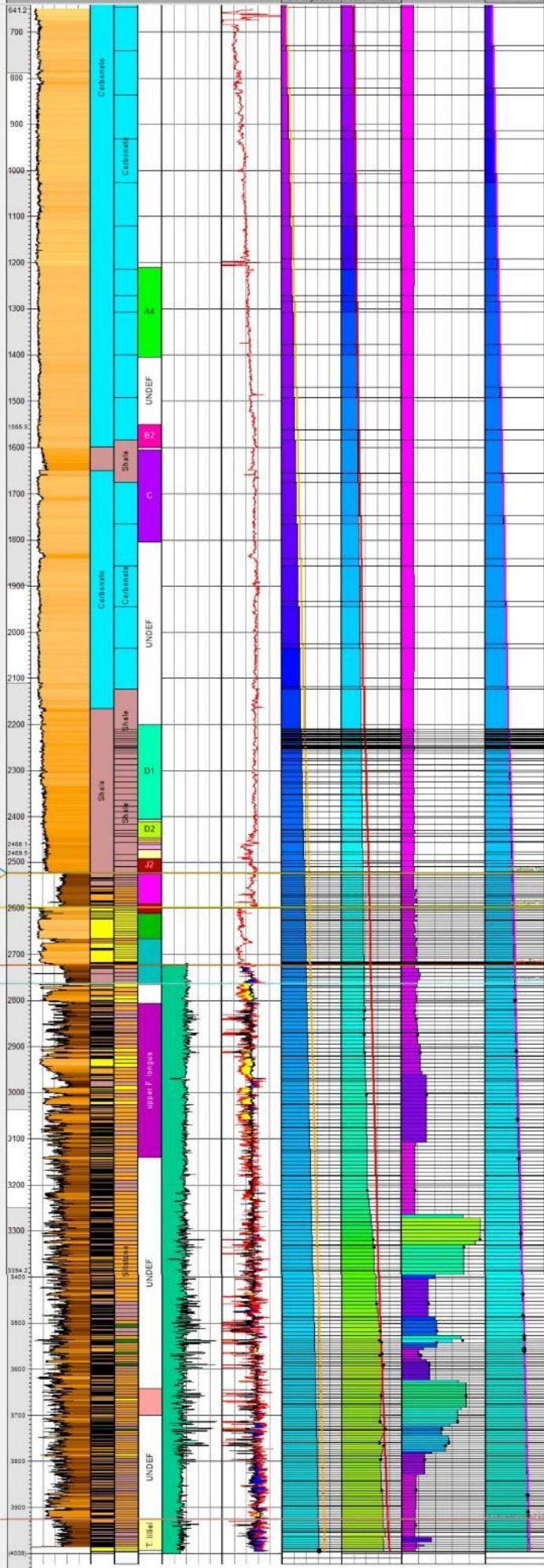
From left to right: GR, Facies log, Facies property, Palynology, DT, NPHI & RHOB, Temperature (property shown as filled blocks, Temperature log shown as black dots), Vitrinite reflectance (property shown as filled blocks, core measured Ro shown as black dots), TOC (property shown as filled blocks, TOC log shown as black dots), Pressure (property shown as filled blocks, Wireline Formation Test Pressure shown as black dots).

⊕ Barracouta 1 [MD]									
MD	GR	DT	RHOB	BHT	Ro	TOC	Hydratatic Pressure		
15000	0.00 API 200.00	134.39 us/m 544.40	1.9500 g/cm3 2.9000	15.0 degC 200.0	0.0000 1.2000	70.00	0.0000 psi 0.000000	0.0000 psi 0.000000	0.0000 psi 0.000000
	Color fill	Color fill		Temperature	TOC_guided by Facies [U]	Hydratatic Pressure [U]			
				15.00 degC 200.00	0.0000 1.2000	70.00			
				Temperature (log) [U]	Ro (resampled) [U]	Color fill	Pressure		
				15.0 degC 200.0	0.0000 1.2000				



♣ Bignose 1 [MD]

MD	GR	DT	NPVI	EHT	Ro	TOC	WFT_Pressure
15200	0.09 gAPI 200.00	64.71 uAPI 240.40	0.5525 por 0.15000	13.0 degC 200.00	0.0000 1.2000	10.00	60.00
	Color fill	Color fill	RHOBS	Temperature	TOC_guided by Facies (U)	Hydrostatic Pressure	
			1.9800 g/cm3 2.9000	14.00 degC 200.00	0.0000 1.2000	60.00	15200 psi 0.200000
			Colr	Temperature (U)	Ro (resampled) (U)	Color fill	Hydrostatic Pressure (U)
				15.0 degC 200.00	0.0000 1.2000		15200 psi 0.200000



Golden Beach Subgroup

Golden Beach Subgroup

Advanced velocity model

Make velocity model Hints

Create new: Gippsland Average Velocity Tied Model 6_Expand20

Edit existing: **Gippsland Average Velocity Tied Model 6_Expand20 (TWT to Z or back)**

Convert from: TWT to: Z or back. Make bi-directional model (at no additional cost)

Datum

Time: SRD Z=0.

Other:

Apply filter: With Checkshots Hide settings

	Base	Correction	Model	
Surface	Seafloor TWT Calc from Topo Gippsland250 using Vel 1515m/s	None	V=V0=VInt	1515
Surface	Top Latrobe tied with well tops	Well tops Latrobe Gp	V=V0+K*Z	K: Well TDR - Constant
Surface	Strzelecki_300	Well tops Strzelecki Gp	V=V0+K*Z	K: Well TDR - Constant
Surface	Update basement300	None	Same as above	

Correction and output Well TDR estimation Uncertainty

Thickness

Depth tolerance: 4 Time tolerance: 4

Surfaces

X inc: 500 Interpolation method: Convergent

Y inc: 500 Point weighting: Inverse distance quadr

Correction

None

Adjust

Use influence radius: 800

Use zone logs:

MD inc: 10 Threshold: 25

Use radius: 400 Tolerance: 5

Output

Well points

Time logs Velocity logs MD inc: 10

Time-depth Velocity Number of samples: 100

Interval velocity maps

Add residual attribute to well tops

Replace dip and azimuth on well tops

Make well report

Reset sheet first

Appendix 4 Average velocity model, well report

Velocity model:	Gippsland Average Velocity Tied Model 6_Expand20						
From:	TWT [ms]						
To:	Z [m]						
XY:	[m]						
Top Latrobe	Well	X-value	Y-value	Z-value	Horizon after	Diff after	Corrected?
	Fortescue 2	610647.7	5745634.5	-2405.08	-2405.14	0.06	Yes
	Snapper 3	586513	5770385.4	-1256.8	-1256.8	0.01	Yes
	Anemone 1A	615638.7	5708695.8	-2554.47	-2554.03	-0.43	Yes
	Turrum 2	609405.3	5766511.3	-1536.74	-1536.15	-0.6	Yes
	Ayu 1	611913.5	5725918.5	-2462	-2462.36	0.36	Yes
	West Seahorse 2	553580.8	5771347.9	-1395.04	-1395.03	-0.01	Yes
	Angler 1	625520.5	5720157.1	-2737.91	-2738.17	0.26	Yes
	West Fortescue 1	608416.3	5753076.9	-2399.61	-2399.46	-0.15	Yes
	Basker 1	648583.5	5758902.8	-2095.47	-2095.24	-0.23	Yes
	Bream 2	569510.8	5736048.3	-1797.01	-1796.48	-0.53	Yes
	Archer 1	613943.9	5708237.3	-2530.87	-2530.47	-0.41	Yes
	Conger 1	592958.4	5754141.2	-1791.58	-1791.26	-0.33	Yes
	Bream B 17	570224	5736383.9	-1761.16	-1783	21.85	No
	Smiler 1	621144.9	5740018.5	-2480.76	-2479.74	-1.02	Yes
	Seahorse 1	559031.7	5772363.4	-1362.52	-1362.29	-0.23	Yes
	Tarwhine 1	546223.7	5749306.3	-1324.14	-1324.14	0	Yes
	Flounder A 3A	628860.6	5759043.3	-1956.47	-1977.14	20.67	No
	Barracouta 3	554073.4	5758479	-1084.78	-1084.77	-0.01	Yes
	Mackerel 1	618460.3	5740057.2	-2357.17	-2358.74	1.57	Yes
	Admiral 1	644458.6	5776060.2	-1213.84	-1213.83	-0.01	Yes
	Grunter 1	632675.3	5763045.3	-1831.8	-1831.99	0.18	Yes
	Fortescue 1	608315.6	5752097.1	-2388.01	-2387.95	-0.07	Yes
	Grayling 1A	613277.6	5775513.7	-1483.27	-1535.59	52.32	No
	Kingfish 4	595627.7	5727357.4	-2227.35	-2242.22	14.86	No
	Whaleshark 1	665217.4	5748715.2	-2698.63	-2698.62	-0.01	Yes
	Marlin 1	607397	5767689.3	-1371.85	-1371.72	-0.12	Yes
	Bream 3	567322.1	5737128.9	-1725.69	-1726.02	0.33	Yes
	Whiting 2	574838.8	5766135.2	-1241.69	-1241.76	0.06	Yes
	Devilfish 1	579967.3	5705251.4	-1618.19	-1618.23	0.04	Yes
	Shark 1	679653	5763584.1	-1786.71	-1786.72	0.01	Yes
	Wasabi 1	522991.8	5739959.1	-1205.52	-1205.74	0.22	Yes
	Barracouta 1	562431.9	5763274.8	-1000.77	-1001.42	0.65	Yes
	Speke 1	554163.5	5737650.7	-1797.74	-1797.81	0.07	Yes
	Barracouta 5	558032	5761160.4	-1022.23	-1022.43	0.2	Yes
	Whiptail 1A	545506.7	5758165.4	-1104.35	-1104.41	0.06	Yes
	Blackback 1 ST1	636279	5731938.7	-2735.92	-2793.77	57.85	No
	Barracouta 4	561414.8	5762040.6	-1015.64	-1015.28	-0.36	Yes
	Leatherjacket 1	656061.3	5783095.9	-724	-724.02	0.02	Yes
	Remora 1	604501.7	5776607.5	-2062	-2061.79	-0.21	Yes
	Kingfish 7	594452.7	5728698.4	-2232.74	-2233.58	0.84	Yes
	Tailor 1	611119.3	5738989	-2393.94	-2393.64	-0.29	Yes
	Snapper 6	588649.6	5768110.7	-1309.67	-1309.78	0.11	Yes
	Marlin 2	603273.7	5764156.5	-1431.84	-1431.86	0.02	Yes

	Fortescue 3	610829.1	5750447.7	-2388.99	-2389.65	0.66	Yes
	Kahawai 1	620022.8	5774346.8	-1368.94	-1362.49	-6.45	No
	Sole 2	676171.8	5780785.6	-744.97	-740.69	-4.28	No
	Bonita 1A	612166.1	5731150.5	-2468.09	-2468.05	-0.05	Yes
	Opah 1	611549.7	5734908.1	-2392.15	-2393.77	1.62	Yes
	Maclean 1	635826.3	5787931.6	-561.05	-577.39	16.34	No
	Pilotfish 1A	628328.7	5745333.5	-2895.59	-2895.89	0.31	Yes
	Kingfish 5	608257.7	5729354.3	-2316.75	-2317.19	0.44	Yes
	Wyrallah 1	507479.8	5719250	-852.98	-852.98	0	Yes
	Manta 1	650752.7	5762543.5	-1930.98	-1979.5	48.51	No
	Orange Roughy 1	590874.8	5729205.3	-2249.92	-2250.09	0.17	Yes
	Nannygai 1	586903.4	5732529.1	-2178.08	-2178.09	0.02	Yes
	Snapper 2	591525.6	5772981.2	-1190.48	-1190.47	-0.01	Yes
	Coelacanth 1	613186.7	5714183.4	-2556.26	-2555.91	-0.36	Yes
	Helios 1	611090.7	5716544.2	-2556.41	-2556.67	0.27	Yes
	Scallop 1	639318.3	5769310.7	-1696.62	-1728.45	31.82	No
	Omeo 1 ST1	562561.9	5726169.4	-2158.11	-2159.41	1.3	Yes
	Longtom 3 ST1	614995.9	5783070.1	-1193.62	-1197.32	3.71	No
	Palmer 1	528834.9	5731758	-1165	-1165.02	0.02	Yes
	Snapper A 21	589785.2	5772203.4	-1185.76	-1186.34	0.59	Yes
	Billfish 1	635288.9	5718859.3	-2855.68	-2856.01	0.33	Yes
	Trevally 1	622084.7	5761234.5	-1921.86	-1921.75	-0.11	Yes
	Barracouta A 3	559267.6	5761034.7	-1010.61	-1048.51	37.89	No
	Flathead 1	634797.4	5790752.7	-437.45	-437.44	-0.01	Yes
	Perch 1	528278.7	5730293.7	-1096.52	-1096.67	0.15	Yes
	Terakihi 1	634830.5	5737068.3	-2815.15	-2815.21	0.06	Yes
	Flounder 3	628889.7	5758254	-1966.24	-1966.23	-0.01	Yes
	Marlin 3	602591.3	5766474.1	-1441.55	-1441.38	-0.16	Yes
	Gummy 1	652196.4	5759678	-2040.56	-2040.22	-0.34	Yes
	Turrum 5	605212.3	5766064.3	-1361.08	-1361.31	0.24	Yes
	Moby 1	632428.7	5790068.1	-533.99	-534	0	Yes
	Flounder 6	625636.6	5758024.3	-1907.44	-1908.76	1.32	Yes
	Kipper 2	641320.1	5771837.2	-1516.72	-1551.54	34.83	No
	Great White 1	641952.2	5742782.9	-3189.63	-3190.17	0.54	Yes
	Turrum 1	609101.8	5771129.1	-1911.48	-1939.72	28.24	No
	South East Longtom 1	621489.7	5779922.2	-1263.48	-1263.88	0.4	Yes
	Veilfin 1	587613.3	5747596.4	-1964.7	-1963.04	-1.65	Yes
	Patricia 1	627057.7	5789890.8	-659.99	-659.93	-0.07	Yes
	Blenny 1	536265.5	5741763.4	-1207	-1207	0	Yes
	Halibut 1	615064.3	5749215	-2291.18	-2291.16	-0.02	Yes
	Moonfish 1 ST1	588850.8	5777086.3	-1484.04	-1480.36	-3.68	Yes
	Albacore 1	616131.1	5730665.4	-2547.03	-2546.97	-0.06	Yes
	Melville 1	585816.9	5717962.6	-2188.4	-2188.43	0.02	Yes
	Basker 3	650336	5758614.3	-2117.86	-2118.3	0.44	Yes
	Tuna 2	621602.9	5773331.1	-1319.18	-1273.23	-45.95	No
	Yellowtail 2	611842.6	5734421.2	-2392.47	-2393.26	0.79	Yes
	Anemone 1	615638.5	5708693.9	-2553.38	-2554.07	0.7	Yes
	East Kingfish 1	605903.4	5728084.8	-2283.03	-2363.7	80.67	No
	Cod 1	585364	5753742.4	-1872.93	-1872.93	0	Yes
	Mackerel 2	616815.6	5739440.7	-2299.96	-2299.69	-0.28	Yes

	Athene 1	626869.7	5727048.5	-2736.81	-2736.86	0.05	Yes
	Groper 1	536132.1	5690092.6	-920.97	-920.97	0	Yes
	Fortescue A 29A	612375.6	5750039.7	-2339.96	-2331.7	-8.26	No
	Turrum 4	610519	5762812.4	-1895.89	-1853.22	-42.67	No
	Dolphin 2	532921.7	5740042.3	-1179.66	-1202.41	22.75	No
	Bignose 1	640044.7	5753693.9	-2497.03	-2496.95	-0.09	Yes
	Bream 4A	565283.6	5737776.4	-1814.89	-1814.2	-0.69	Yes
	East Pilchard 1	636767.2	5771025.1	-1618.77	-1618.74	-0.03	Yes
	Tuna 4	619988.4	5772503.5	-1348.73	-1352.67	3.95	No
	Dolphin 1	533130	5739671.6	-1160.95	-1209.37	48.43	No
	East Halibut 1	617944.3	5748093.3	-2369.63	-2369.83	0.2	Yes
	West Moonfish 1	585688.5	5777081.4	-1523.17	-1523.14	-0.02	Yes
	Roundhead 1	606701.9	5725041.9	-2356.94	-2357.33	0.39	Yes
	Flying Fish 1	531963.4	5755774.7	-1096.73	-1096.49	-0.24	No
	Bullseye 1	549453.4	5728580.3	-2033.55	-2033.53	-0.02	Yes
	Kyarra 1A	516355.7	5718754.3	-982.47	-982.47	0	Yes
	West Seahorse 1	554631.7	5771471.8	-1370.39	-1370.38	-0.01	Yes
	Dart 1	668768.8	5777446.3	-912.37	-912.38	0.01	Yes
	Barracouta A 1	559115.2	5761148.4	-1002.13	-1043.45	41.32	No
	Snapper A 21A	589560.3	5772413.7	-1190.34	-1190.2	-0.13	Yes
	Marlin 4	611022.5	5766964.2	-1813.46	-1813.99	0.54	Yes
	Edina 1	576588.6	5726753.3	-2220.31	-2220.38	0.07	Yes
	Sunfish 1	607643.7	5778060.6	-1672.18	-1673.55	1.38	Yes
	Kipper 1	639931.9	5773559.6	-1398.97	-1405.69	6.72	No
	Wirrah 1	571559.7	5773028.2	-1443.88	-1443.85	-0.03	Yes
	Blackback 1	636352.5	5731915	-2795.31	-2791.2	-4.11	Yes
	Kingfish 6	607538.7	5727674.3	-2310.72	-2309.36	-1.36	Yes
	Longtom 2	615472.1	5781904.5	-1263.28	-1265.4	2.12	Yes
	Bream 5	575643.7	5736876.7	-1841.69	-1841.79	0.1	Yes
	Barracouta 2	559037.5	5760914.3	-1031.19	-1046.89	15.7	No
	Chimaera 1	650757.6	5763491.6	-1897.87	-1963.37	65.51	No
	Kingfish 8	592472.6	5727998.1	-2247.97	-2247.97	0	Yes
	Tuna 1	624274.9	5774157.7	-1301.49	-1301.38	-0.11	Yes
	Longtom 1	615419.4	5782472.8	-1219.54	-1216.14	-3.4	Yes
	Whale 1	636996.7	5790831.2	-429.74	-429.88	0.14	Yes
	South East Remora 1	606557.3	5775575.9	-2058.92	-2058.56	-0.36	Yes
	Mudskipper 1	598334.8	5692928.7	-1447.73	-1447.72	0	Yes
	Madfish 1	632560.3	5720208.4	-2801.91	-2801.33	-0.59	Yes
	Speke South 1	553887.9	5736655.1	-1789.19	-1789.09	-0.1	Yes
	Yellowtail 1	611172.9	5735235.1	-2383.41	-2380.86	-2.56	Yes
	North Wirrah 1	573483.6	5773597.3	-1496.51	-1496.02	-0.49	Yes
	Blackback A 1 ST1	635155.1	5736096.6	-2809.47	-2878.07	68.6	No
	Gurnard 1	585145.9	5728136.7	-2170.93	-2170.7	-0.23	Yes
	Stonefish 1	636583.7	5765398.4	-1793.2	-1793.22	0.02	Yes
	Moonfish 1	588968.3	5777338.4	-1475.35	-1482.05	6.7	Yes
	Harlequin 1	562086.6	5771928.9	-1386.96	-1387.13	0.17	Yes
	Kingfish 2	602020.3	5727246.6	-2232.27	-2231.83	-0.45	Yes
	Sole 1	678467.9	5779480.8	-798.06	-798.05	0	Yes
	Longtom 1 ST1	615418.2	5782463.2	-1219.56	-1216.97	-2.59	Yes
	Broadbill 1	501873.4	5728682.1	-818.39	-818.41	0.01	Yes

	Hapuku 1	635083.9	5731591.4	-2797.12	-2796	-1.11	Yes
	Fur Seal 1	600986.4	5779139.6	-2175.71	-2175.77	0.06	Yes
	Kingfish 3	596094.2	5728939.7	-2234.12	-2233.4	-0.73	Yes
	Luderick 1	562605.6	5745422.1	-1756.03	-1756.04	0.02	Yes
	Cobia 1	612114	5742824.2	-2371.9	-2371.72	-0.19	Yes
	Blackback 3	632391.2	5731195.9	-2795.77	-2795.93	0.16	Yes
	Perch 2	529091.5	5730718.3	-1096.99	-1096.2	-0.79	Yes
	Amberjack 1	527611.2	5739647.6	-1237.99	-1237.84	-0.15	Yes
	Snook 1	535506.7	5757873	-1105.94	-1105.98	0.05	Yes
	Pike 1	582656.4	5707977.2	-1819.2	-1819.19	-0.01	Yes
	Groper 2	520634.8	5685853.7	-750.07	-750.07	0	Yes
	Flounder 1	624666.9	5758505.1	-1900.22	-1899.35	-0.87	Yes
	Baleen 1	626146.6	5792258.5	-628.47	-628.52	0.05	Yes
	Threadfin 1	609590.1	5733267.1	-2372.41	-2373.73	1.32	Yes
	Halibut 2	616273.9	5749597.6	-2306.45	-2306.17	-0.28	Yes
	Omeo 2A	561990	5726914.4	-2157.67	-2156.74	-0.93	Yes
	Blackback 1 ST2	636312	5731903.3	-2793.38	-2797.22	3.84	Yes
	Sweep 1	643724.7	5786729	-730.89	-730.87	-0.02	Yes
	Whiting 1	577440.8	5767746.8	-1260.91	-1260.67	-0.24	Yes
	Snapper 4	587994.7	5770023.1	-1238.56	-1237.9	-0.67	Yes
	Volador 1	634848.9	5746159.4	-2912.82	-2912.63	-0.19	Yes
	Turram 3	609439.1	5764631	-1549.87	-1550.13	0.26	Yes
	Wahoo 1	653418	5789776.6	-419.88	-419.87	-0.01	Yes
	Drummer 1	609108.1	5740809.3	-2410.89	-2411.22	0.33	Yes
	Salmon 1	586304.4	5747184.2	-1957.98	-1958.15	0.17	Yes
	Hermes 1	613173.7	5726780.3	-2481.07	-2481.07	0	Yes
	Mackerel 3	618945.7	5740900.3	-2363.07	-2364.42	1.35	Yes
	Perch 4	529223	5730733.3	-1097.04	-1108.83	11.79	No
	Culverin 1	644466.8	5748312.2	-2882.96	-2882.98	0.02	Yes
	Kingfish 1	605463.5	5727396.5	-2367.51	-2367.39	-0.12	Yes
	Golden Beach 1A	537055.2	5765532.4	-622.53	-622.57	0.03	Yes
	Flounder 5	626795.7	5759304.4	-1899.2	-1898.81	-0.39	Yes
	Wirrah 3	572286.8	5772175.5	-1467.98	-1467.86	-0.12	Yes
	Dory 1	634790.1	5727712	-2744.13	-2743.85	-0.28	Yes
	Swordfish 1	588022.7	5750259.4	-1974.21	-1973.67	-0.54	Yes
	Snapper 5	586733.7	5769311.5	-1270.96	-1270.95	-0.01	Yes
	Hammerhead 1	660689.3	5773222.6	-1269.4	-1269.43	0.03	Yes
	Sperm Whale 1	619808.6	5787148.2	-740.07	-740.08	0	Yes
	Tommyruff 1	512535.9	5726313.2	-870.99	-870.99	0	Yes
	West Halibut 1	612091.6	5748807	-2351.55	-2351.38	-0.17	Yes
	Emperor 1	588277.9	5782964.4	-1506.97	-1506.9	-0.07	Yes
	Torsk 1	543493.9	5744644.2	-1309.91	-1309.89	-0.02	Yes
	Moray 1	591696.5	5698014.3	-1647.23	-1647.22	-0.01	Yes
	Mulloway 1	542410.4	5758356.9	-1105.92	-1105.9	-0.02	Yes
	Longtom 3P	614998.6	5783054.8	-1197.76	-1197.61	-0.16	Yes
	Selene 1	625160.3	5724208.9	-2798.79	-2798.57	-0.22	Yes
	Omeo 1	562561.9	5726169.4	-2158.11	-2159.41	1.3	Yes
	Seahorse 2	557515.1	5771564	-1372.44	-1372.44	0.01	Yes
	Longtom 4P	616887	5781544.4	-1214	-1123.05	-90.96	No
	Tarra 1	561228.7	5722750.7	-2108.43	-2108.44	0	Yes

	Blackback 2	634557.8	5731331.9	-2755.96	-2757.56	1.59	Yes
	Garfish 1	610000	5781176.9	-1584.55	-1550.84	-33.71	No
	Tuna 3	626857.9	5774580.9	-1330.89	-1330.89	0	Yes
	Sunfish 2	609166.6	5778117.2	-1588.89	-1588.25	-0.64	Yes
	Cobia 2	613930.7	5742662.3	-2364.79	-2365.1	0.31	Yes
	Judith 1	636402.6	5776006.5	-1429.93	-1423.63	-6.3	No
	Perch 3	528099.5	5730966.3	-1053.15	-1135.54	82.38	No
	Fortescue 4	611554.2	5747416.7	-2389.49	-2389.54	0.05	Yes
	Turrum 7	610650.4	5764231.2	-1738.57	-1736.91	-1.66	No
	Basker South 1	647789.8	5757592.6	-2182.95	-2182.95	0	Yes
	Turrum 6	602830	5767473.3	-1435.03	-1439.26	4.23	No
	Batfish 1	622967.4	5768348	-1444.39	-1444.5	0.11	Yes
	Gudgeon 1	628558.1	5736692.7	-2831.34	-2832.11	0.77	Yes
	Wirrah 2	572282.6	5773682.1	-1466.86	-1467.34	0.48	Yes
	Kingfish 9	600107.7	5723919.7	-2281.41	-2281.79	0.38	Yes
	Sweetlips 1	590924.8	5783162.7	-1483.83	-1484.06	0.23	Yes
	Teraglin 1	617310.1	5751266.7	-2395.57	-2396.46	0.89	Yes
	Wrasse 1	610803.6	5757396.3	-2541.97	-2542.01	0.04	Yes
	Flounder 2	626690.9	5757687.5	-1938.81	-1938.45	-0.36	Yes
	Snapper 1	588884.9	5771600.4	-1182.68	-1182.71	0.04	Yes
	Morwong 1	614998.7	5768186.3	-1643.2	-1643.39	0.19	Yes
	Cobia F 35	614593.7	5746495	-2362.07	-2355.95	-6.12	No
	Sawbelly 1	590489.2	5752252.2	-1962.57	-1963.66	1.09	Yes
	Rockling 1	607353.8	5742607.1	-2459.74	-2459.62	-0.11	Yes
	Pisces 1	630915	5675672.4	-1773.81	-1773.82	0.02	Yes
	Trumpeter 1	617910.6	5747614.5	-2427	-2427.7	0.7	Yes
	Flounder 4	630942.7	5759273.4	-1942.75	-1942.55	-0.2	Yes
	Mackerel 4	614746.7	5736518.4	-2355.09	-2355.46	0.36	Yes
	Angelfish 1	620890.9	5766246.7	-1626.98	-1626.94	-0.04	Yes
	Bazzard 1	592933.5	5747530	-2068.87	-1918.87	-150	No
Strzelecki	Well	X-value	Y-value	Z-value	Horizon after	Diff after	Corrected?
	Anemone 1A	615593.1	5708706.7	-4744.57	-4744.57	0	Yes
	Basker 1	648583.5	5758958.9	-3964.83	-3964.83	0	Yes
	Admiral 1	644492.1	5776081.2	-2094.56	-2094.56	0	Yes
	Fake_BassStrait4	664782.3	5700304.9	-3934.33	-4673.95	739.62	No
	Fake_BassStrait5	653289.2	5738510.8	-5193.76	-6156.6	962.84	No
	Leatherjacket 1	656061.3	5783097.2	-827.99	-827.99	0	Yes
	Omeo 1 ST1	562560.9	5726199.2	-3163.15	-3163.15	0	Yes
	Barracouta A 3	559339.3	5761017.4	-3563.16	-3563.16	0	Yes
	Flathead 1	634797.4	5790753.3	-467.16	-467.16	0	Yes
	Perch 1	528281.1	5730301	-1528.3	-1528.3	0	Yes
	Fake_BassStrait3	646487.6	5711123.2	-4060	-4872.13	812.13	No
	Moby 1	632428.3	5790068.1	-567.99	-567.99	0	Yes
	South East Longtom 1	621489.8	5779922.1	-2713.48	-2713.48	0	Yes
	Patricia 1	627057.7	5789892.5	-777.31	-777.31	0	Yes
	Fake_BassStrait8	680566.7	5743603.4	-4383	-5286.93	903.93	No
	Kyarra 1A	516355.7	5718757.4	-1220.44	-1220.44	0	Yes
	Fake_BassStrait2	676599.8	5717299.8	-4562.47	-4562.47	0	Yes
	Dart 1	668768.3	5777447.6	-1113.7	-1113.7	0	Yes

Sunfish 1	607652	5778049.6	-2405.87	-2405.87	0	Yes
Tuna 1	624274.9	5774228.2	-3630.09	-3630.1	0	Yes
Fake_BassStrait1	660470.3	5724249.7	-4991.78	-4991.78	0	Yes
Longtom 1	615419.4	5782522	-1907.66	-1907.66	0	Yes
Whale 1	636996.7	5790831.7	-472.02	-472.02	0	Yes
Mudskipper 1	598334.8	5692935.3	-1584.57	-1568.97	-15.6	No
Madfish 1	632572.8	5720883.5	-4556.41	-4556.41	0	Yes
Sole 1	678467.9	5779485.6	-1096.06	-1096.06	0	Yes
Longtom 1 ST1	615343.5	5782223.7	-1856.94	-1998.96	142.01	No
Broadbill 1	501886.9	5728694.6	-1308	-1275.67	-32.34	No
Fur Seal 1	600992.3	5779140.3	-2544.34	-2544.34	0	Yes
Baleen 1	626146.6	5792259.2	-697.64	-697.64	0	Yes
Omeo 2A	561990	5727063.7	-4385.71	-4233.42	-152.29	No
Sweep 1	643724.7	5786729.6	-816.89	-816.89	0	Yes
Volador 1	634848.9	5746189.3	-4585.39	-4585.39	0	Yes
Wahoo 1	653420.7	5789779.2	-568.86	-568.86	0	Yes
Salmon 1	586346.1	5747242.1	-4398.99	-4398.99	0	Yes
Golden Beach 1A	537055.2	5765556.1	-2394.77	-2394.77	0	Yes
Hammerhead 1	660689.5	5773235.4	-1925.66	-1925.66	0	Yes
Sperm Whale 1	619808.6	5787152.1	-886.23	-886.23	0	Yes
Tommyruff 1	512535.9	5726314.2	-1468.99	-1468.99	0	Yes
Emperor 1	588275.1	5782968.5	-1886.53	-1886.53	0	Yes
Moray 1	591690.8	5698010.1	-1913.95	-1913.95	0	Yes
Omeo 1	562561.9	5726206.8	-3163.33	-3171.98	8.65	Yes
Tarra 1	561228.7	5722768.5	-2551.22	-2551.22	0	Yes
Judith 1	636418.8	5776029	-2936.51	-2936.51	0	Yes
Fake_BassStrait7	670461.3	5741567.2	-4602.65	-5614.24	1011.59	No
Pisces 1	630915	5675683.3	-2557.72	-2557.72	0	Yes

Using the entire Gippsland model as an example:

1. Pillar gridding:

- Set up 500*500 increment for the entire model;
- Use boundary which constrains the model under empirical data coverage;
- 74 faults and 30 trends are used to divide the model into different segments and balance the grids (Figure 1);
- The dash lines are trends, and the solid lines are faults;
- The colour of lines indicates the direction between the faults/trends and grids: Green lines are along I-direction, Red lines are along J-direction, and White lines are arbitrary to the grids.

2. Make horizons:

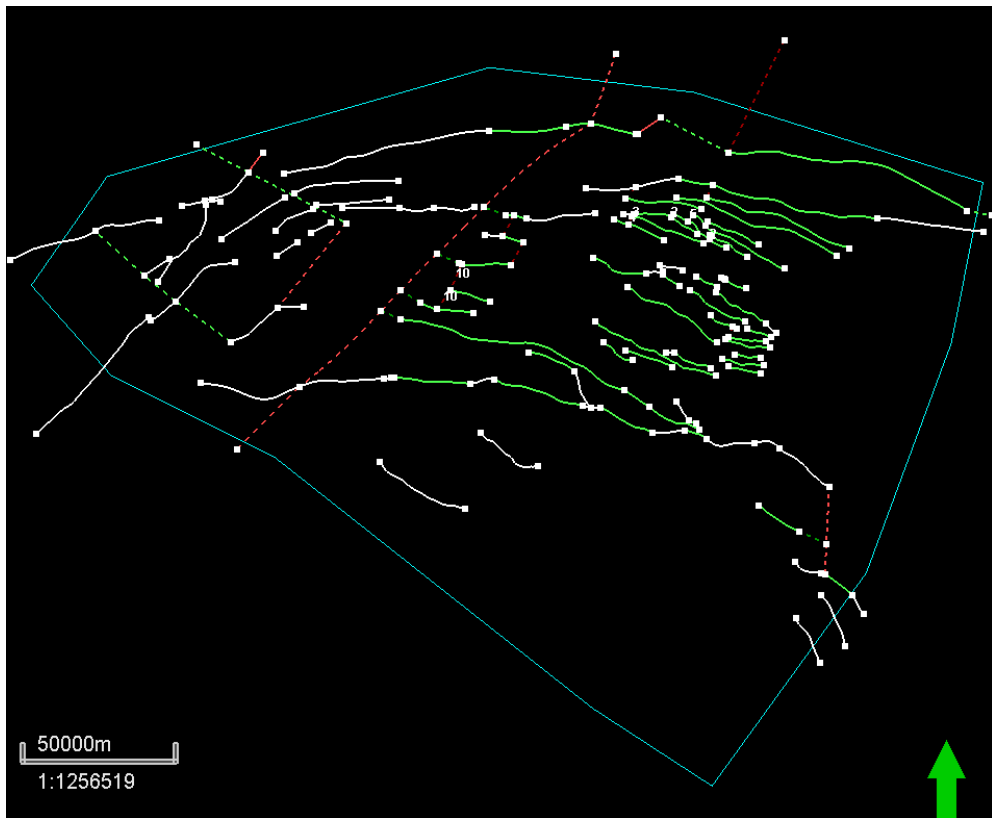
- Settings for Horizon: select input main horizons and applied segments, define horizon type, tie to the correspondent well tops;
- Settings for Faults: define fault activity, horizon back-off from fault plane distance, displacement settings of each fault at every horizon level.
- Settings for Well adjustment: using across segments method, with a residual surface by moving average, inverse distance squared point weighting.

3. Make zones

- Use isochore maps and well tops to divide the stratigraphic interval, build along with the stratigraphic thickness.
- Zone 'Latrobe Group - Kate Shale' is split into the Cobia subgroup and Upper Halibut subgroup.
- Zone 'Golden Beach subgroup – Strzelecki Group' is split into the Golden Beach and Emperor subgroups.

4. Layering

- Make layers using proportion, 540 layers in total.
- Seaspray Group zones use coarser layer thickness;
- Latrobe Group zones use finer layer thickness at an average of 10 metres.
- Strzelecki Group zone uses coarser layer thickness.
- Detailed zone division shows in Figure 3.



• Figure 1 Structural modelling (pillar gridding), boundary, faults and trends are shown in a 2D window view.

Index	Horizon name	Color	Calculate	Horizon type	Conform to another horizon	Status	Smooth iterations	Use horizon-fault lines	Well tops	Input #1	Input #2
1	Modified Topography G		<input checked="" type="checkbox"/> Yes	Conformable	No	1	Done	0	<input type="checkbox"/> Yes		Modified Topography
2	Updated Mid_Miocene		<input checked="" type="checkbox"/> Yes	Conformable	No	1	Done	0	<input type="checkbox"/> Yes		Updated Mid_Miocene
3	Lakes Entrance Fm		<input checked="" type="checkbox"/> Yes	Conformable	No	1	Done	0	<input checked="" type="checkbox"/> Yes	Lakes Entrance	Lakes Entrance (Depth)
4	Latrobe Gp		<input checked="" type="checkbox"/> Yes	Conformable	No	1	Done	0	<input checked="" type="checkbox"/> Yes	Latrobe Gp (Well)	Top Latrobe (Depth 1)
5	Kate Shale		<input checked="" type="checkbox"/> Yes	Conformable	No	1	Done	0	<input checked="" type="checkbox"/> Yes	Kate Shale (Well)	Updated kt_unc300 (Depth)
6	Golden Beach SubGp		<input checked="" type="checkbox"/> Yes	Conformable	No	1	Done	0	<input checked="" type="checkbox"/> Yes		Expand Golden Beach SubGp
7	Strzelecki Gp		<input checked="" type="checkbox"/> Yes	Base	No	1	Done	0	<input checked="" type="checkbox"/> Yes	Strzelecki Gp (Well)	Strzelecki_300 (Depth)
8	Basement		<input checked="" type="checkbox"/> Yes	Conformable	No	1	Done	0	<input checked="" type="checkbox"/> Yes	Basement (Well)	Basement300 (Depth)

• Figure 2 Settings for Horizon in 'Make horizon' process, entire Gippsland model.

Name	Color	Calculate	Zone division
Topo - Mid_Miocene		<input checked="" type="checkbox"/> Yes	Proportional Number of layers: 20
Mid_Miocene - Lakes Entrance		<input checked="" type="checkbox"/> Yes	Proportional Number of layers: 20
Lakes Entrance - Latrobe Gp		<input checked="" type="checkbox"/> Yes	Proportional Number of layers: 20
Cobia		<input checked="" type="checkbox"/> Yes	Proportional Number of layers: 30
Upper Halibut		<input checked="" type="checkbox"/> Yes	Proportional Number of layers: 100
Kate Shale - Golden Beach top		<input checked="" type="checkbox"/> Yes	Proportional Number of layers: 100
Golden Beach SubGp		<input checked="" type="checkbox"/> Yes	Proportional Number of layers: 100
Emperor SubGp		<input checked="" type="checkbox"/> Yes	Proportional Number of layers: 100
Strzelecki Gp - Basement		<input checked="" type="checkbox"/> Yes	Proportional Number of layers: 50

• Figure 3 Zone division of each zone, entire Gippsland model.

The critical step is the fault settings adjustment in the 'Make horizons' process. The horizon-fault lines at each horizon level are used to guide the horizon-fault plane contact gridding. Most faults use different distance values for horizons to back off from the fault plane to adjust better.

Appendix 6 GPlates reconstruction animation

See supplement 1.

Appendix 7 Badlands Animation (Best fit case)

See supplement 2.

Appendix 8 Badlands Python script, Reference Case

```

<?xml version="1.0" encoding="UTF 8"?>
- <badlands xmlns:xsi="http://www.w3.org/2001/XMLSchema-instance">
  <!-- Regular grid structure -->
  - <grid>
    <!-- Digital elevation model file path -->
    <demfile>data/Mid/initial_map17.csv</demfile>
    <!-- Boundary type: flat, slope, fixed or wall -->
    <boundary>fixed</boundary>
    <!-- Optional parameter (integer) used to decrease TIN resolution. The default value is set to 1. Increasing the factor value will multiply the digital elevation model resolution accordingly. -->
    <resfactor>1</resfactor>
    <nopit>1</nopit>
  </grid>
  <!-- Simulation time structure -->
  - <time>
    <!-- Simulation start time [a] -->
    <start>-137000000.</start>
    <!-- Simulation end time [a] -->
    <end>-0.</end>
    <!-- Display Interval [a] -->
    <display>1000000.</display>
  </time>
  <!-- Simulation stratigraphic structure -->
  - <strata>
    <!-- Stratal grid resolution [m] -->
    <stratdx>1000.</stratdx>
    <!-- Stratal layer interval [a] -->
    <laytime>1000000.</laytime>
  </strata>
  <!-- Sea-level structure -->
  - <sea>
    <!-- Relative sea-level position [m] -->
    <position>0.</position>
    <curve>data/Mid/sea.csv</curve>
  </sea>
  <!-- Tectonic structure -->
  - <tectonic>
    <!-- Is 3D displacements on ? (1:on - 0:off). Default is 0.-->
    <disp3d>0</disp3d>
    <!-- Only relevant when 3D displacements is on. Closest distance [m] between nodes before merging happens. This is optional if not given the merging distance is set to half the resolution of the digital elevation input file. -->
    <merge3d>1000.</merge3d>
    <!-- Only relevant when 3D displacements is required. This is useful if the horizontal displacements provided in each maps are larger than the TIN resolution. In this case, it is recommended to split each displacement periods in evenly spaced intervals of given time duration [a]. -->
    <time3d>1000000.</time3d>
    <!-- Number of tectonic events -->
    <events>9</events>
    <!-- Displacement definition -->
    - <disp>
      <!-- Displacement start time [a] -->
      <dstart>-137000000.</dstart>
      <!-- Displacement end time [a] -->
      <dend>-113000000.</dend>
      <!-- Displacement map [m] -->
      <dfile>data/LowED2/Basement-Strz.csv</dfile>
    </disp>
    - <disp>
      <!-- Displacement start time [a] -->
      <dstart>-113000000.</dstart>
      <!-- Displacement end time [a] -->
      <dend>-98000000.</dend>
      <!-- Displacement map [m] -->
      <dfile>data/LowED2/Strz-Sag1.csv</dfile>
    </disp>
    - <disp>
      <!-- Displacement start time [a] -->
      <dstart>-98000000.</dstart>
      <!-- Displacement end time [a] -->
      <dend>-95000000.</dend>
      <!-- Displacement map [m] -->
      <dfile>data/LowED1/Uplift100-90_3.csv</dfile>
    </disp>
    - <disp>
      <!-- Displacement start time [a] -->
      <dstart>-95000000.</dstart>
      <!-- Displacement end time [a] -->
      <dend>-92000000.</dend>
      <!-- Displacement map [m] -->
      <dfile>data/StrzeleckiSag3.csv</dfile>
    </disp>
    - <disp>
      <!-- Displacement start time [a] -->
      <dstart>-92000000.</dstart>
      <!-- Displacement end time [a] -->
      <dend>-84000000.</dend>
      <!-- Displacement map [m] -->
      <dfile>data/LowED2/Strz-80.csv</dfile>
    </disp>
    - <disp>
      <!-- Displacement start time [a] -->
      <dstart>-84000000.</dstart>
      <!-- Displacement end time [a] -->
      <dend>-65000000.</dend>
      <!-- Displacement map [m] -->
      <dfile>data/80-70event+Sag13.csv</dfile>
    </disp>
    - <disp>
      <!-- Displacement start time [a] -->
      <dstart>-65000000.</dstart>
      <!-- Displacement end time [a] -->
      <dend>-32000000.</dend>
      <!-- Displacement map [m] -->
      <dfile>data/LowED2/80-Latrobe.csv</dfile>
    </disp>
    - <disp>
      <!-- Displacement start time [a] -->
      <dstart>-32000000.</dstart>
      <!-- Displacement end time [a] -->
      <dend>-23000000.</dend>
      <!-- Displacement map [m] -->
      <dfile>data/LowED2/Latrobe-Lakes.csv</dfile>
    </disp>
    - <disp>
      <!-- Displacement start time [a] -->
      <dstart>-23000000.</dstart>
      <!-- Displacement end time [a] -->
      <dend>-0.</dend>
      <!-- Displacement map [m] -->
      <dfile>data/LowED2/Lakes-Topo.csv</dfile>
    </disp>
  </tectonic>

```

```

<!-- Precipitation structure -->
- <precipitation>
  <!-- Number of precipitation events -->
  <climates>3</climates>
  <!-- Precipitation definition -->
  <!--rain-->
  <!-- Rain start time [a] -->
  <!--rstart>14500000.</rstart-->
  <!-- Rain end time [a] -->
  <!--rend>0.</rend-->
  <!-- Precipitation value [m/a] - (optional) -->
  <!--rval>0.2</rval-->
  <!--/rain-->
  <!-- Linear orographic precipitation model definition -->
- <rain>
  <!-- Rain start time [a] -->
  <rstart>-14500000.</rstart>
  <!-- Rain end time [a] -->
  <rend>-5000000.</rend>
  <!-- Rain computation time step [a] -->
  <ortime>100000.</ortime>
  <!-- Minimal precipitation value [m/a] -->
  <rmin>0.2</rmin>
  <!-- Maximal precipitation value [m/a] -->
  <rmax>5</rmax>
  <!-- Maximal elevation for computing linear trend [m] -->
  <rzmax>3000.</rzmax>
</rain>
- <rain>
  <!-- Rain start time [a] -->
  <rstart>-5000000.</rstart>
  <!-- Rain end time [a] -->
  <rend>-4500000.</rend>
  <!-- Rain computation time step [a] -->
  <ortime>100000.</ortime>
  <!-- Minimal precipitation value [m/a] -->
  <rmin>0.2</rmin>
  <!-- Maximal precipitation value [m/a] -->
  <rmax>1.5</rmax>
  <!-- Maximal elevation for computing linear trend [m] -->
  <rzmax>3000.</rzmax>
</rain>
- <rain>
  <!-- Rain start time [a] -->
  <rstart>-4500000.</rstart>
  <!-- Rain end time [a] -->
  <rend>-0.</rend>
  <!-- Rain computation time step [a] -->
  <ortime>100000.</ortime>
  <!-- Minimal precipitation value [m/a] -->
  <rmin>0.2</rmin>
  <!-- Maximal precipitation value [m/a] -->
  <rmax>1</rmax>
  <!-- Maximal elevation for computing linear trend [m] -->
  <rzmax>3000.</rzmax>
</rain>
</precipitation>
<!-- Stream power law parameters: The stream power law is a simplified form of the usual expression of sediment transport by water flow, in which the transport rate is assumed to be equal to the local carrying capacity, which is itself a function of boundary shear stress. -->
- <sp_law>
  <!-- Make the distinction between purely erosive models (0) and erosion / deposition ones (1). Default value is 1 -->
  <dep>1</dep>
  <!-- Critical slope used to force aerial deposition for alluvial plain, in [m/m] (optional). -->
  <slp_cr>0.001</slp_cr>
  <!-- Maximum percentage of deposition at any given time interval from rivers sedimentary load in alluvial plain. Value ranges between [0,1] (optional). -->
  <perc_dep>0.95</perc_dep>
  <!-- Planchon & Darboux filling thickness limit [m]. This parameter is used to defined maximum accumulation thickness in depression area per time step. Default value is set to 1. -->
  <fillmax>8000</fillmax>
  <!-- Values of m and n indicate how the incision rate scales with bed shear stress for constant value of sediment flux and sediment transport capacity. Generally, m and n are both positive, and their ratio (m/n) is considered to be close to 0.5 -->
  <m>0.5</m>
  <n>1.1</n>
  <!-- The erodibility coefficient is scale-dependent and its value depend on lithology and mean precipitation rate, channel width, flood frequency, channel hydraulics. In case where the erodibility structure is turned on, this coefficient is applied to the reworked sediments. -->
  <erodibility>2.e-7</erodibility>
  <!-- Number of steps used to distribute marine deposit. Default value is 5 (integer). (optional) -->
  <diffnb>10</diffnb>
  <!-- Proportion of marine sediment deposited on downstream nodes. It needs to be set between ]0,1[. Default value is 0.9 (optional). -->
  <diffprop>0.6</diffprop>
  <!-- Critical density of water+sediment flux to trigger hyperpycnal curve off shore - (optional) -->
  <dens_cr>1015.</dens_cr>
  <!-- Deep basin depth under which hyperpycnal flow are forced to deposit [m] - (optional) -->
  <deepbasin>-1400.</deepbasin>
</sp_law>
<!-- Linear slope diffusion parameters: Parameterisation of the sediment transport includes the simple creep transport law which states that transport rate depends linearly on topographic gradient. -->
- <creep>

```

```

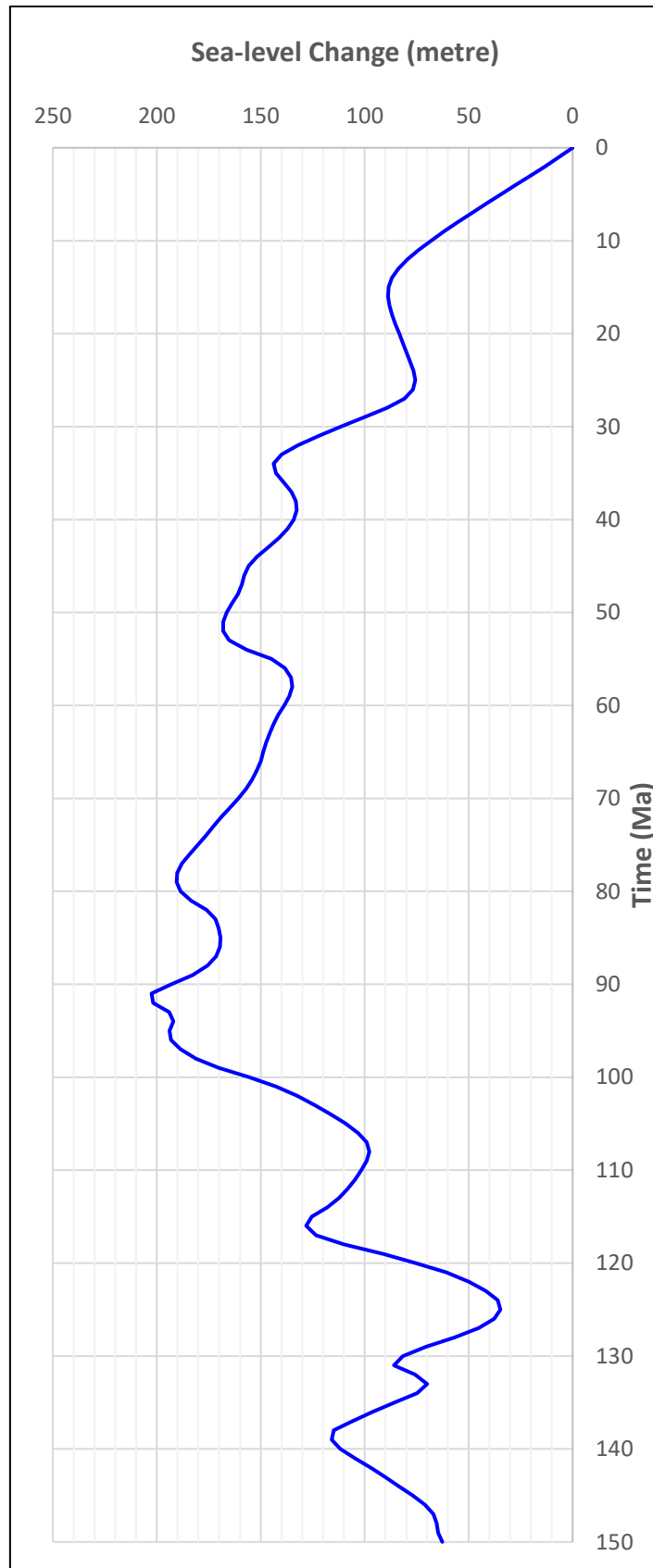
<!-- Surface diffusion coefficient [m2/a] -->
<caerial>0.001</caerial>
<!-- Marine diffusion coefficient [m2/a] -->
<marine>0.005</marine>
<!-- River transported sediment diffusion coefficient in marine realm [m2/a] -->
<river>10.</river>
</creep>
<!-- Wave global parameters structure -->
- <waveglobal>
  <!-- Wave model to consider either SWAN or WaveSed. Default is WaveSed (wmodel = 0). -->
  <wmodel>0</wmodel>
  <!-- Wave interval [a] -->
  <twave>1000000.</twave>
  <!-- Wave grid resolution [m] -->
  <wres>2000.</wres>
  <!-- Maximum depth for wave influence [m] -->
  <wbase>20</wbase>
  <!-- Number of wave climate temporal events. -->
  <events>1</events>
  <!-- Mean grain size diameter [m] -->
  <d50>0.0001</d50>
  <!-- Wave sediment diffusion coefficient. Default is 50. -->
  <wCd>50.</wCd>
  <!-- Wave sediment entrainment coefficient. Value needs to be set between ]0,1], Default is 0.5 -->
  <wCe>0.5</wCe>
  <!-- Maximum wave-induced erosion [m] -->
  <wEro>0.5</wEro>
  <!-- Maximum depth for wave influence [m] -->
  <wbase>10</wbase>
  <!-- Steps used to perform sediment transport. Default is 1000. -->
  <lsteps>500</lsteps>
  <!-- Steps used to perform sediment diffusion. Default is 1000. -->
  <dsteps>500</dsteps>
</waveglobal>
<!-- Wave definition based on wave global structure. The wave field needs to be ordered by increasing start time. The time needs to be continuous between each field without overlaps. -->
- <wave>
  <!-- Wave start time [a] -->
  <start>-32000000.</start>
  <!-- Wave end time [a] -->
  <end>0</end>
  <!-- Wave climates number -->
  <climNb>1</climNb>
  <!-- Climatic wave definition for WaveSed model. -->
  - <climate>
    <!-- Climatic wave definition for WaveSed model. -->
    - <climate>
      <!-- Percentage of time this event is active during the time interval. -->
      <perc>0.3</perc>
      <!-- Significant wave height (in m) -->
      <hs>2.</hs>
      <!-- Wave direction in degrees (between 0 and 360) from the X-axis (horizontal) anti-clock wise. It specifies where the waves are actually coming from. The wave directions are reduced to 8 possible ones: East (dir = 0) - North (dir = 90) - West (dir = 180) - South (dir = 270) - NE (0<dir<90) - NW (90<dir<180) - SW (180<dir<270) - SE (dir>270). -->
      <dir>315</dir>
    </climate>
  </climate>
</wave>
<!-- Carbonate growth definition based on carbonate global structure. The events need to be ordered by increasing start time. The time needs to be continuous between each event without overlaps. -->
- <carb>
  <!-- Specify initial basement structure (0) for hard rock and (1) for loose sediment. -->
  <baseMap>data/High2km/gbrbase1.csv</baseMap>
  <!-- Carbonate growth time interval [a] -->
  <tcarb>100000.</tcarb>
  <!-- Specify the number of reef growth events -->
  <growth_events>4</growth_events>
  <!-- Specify Species 1 and 2 growth rates for specific reef growth events-->
  - <event>
    <!-- Reef growth event start time [a] -->
    <gstart>-32000000.</gstart>
    <!-- Reef growth event end time [a] -->
    <gend>-20000000.</gend>
    <!-- Species 1 growth rate during event [m/yr]. -->
    <growth_sp1>0.000025</growth_sp1>
    <!-- Species 2 growth rate during event [m/yr]. -->
    <growth_sp2>0</growth_sp2>
  </event>
  - <event>
    <!-- Reef growth event start time [a] -->
    <gstart>-20000000.</gstart>
    <!-- Reef growth event end time [a] -->
    <gend>-11000000.</gend>
    <!-- Species 1 growth rate during event [m/yr]. -->
    <growth_sp1>0</growth_sp1>
    <!-- Species 2 growth rate during event [m/yr]. -->
    <growth_sp2>0.000075</growth_sp2>
  </event>
  - <event>
    <!-- Reef growth event start time [a] -->
    <gstart>-11000000.</gstart>
    <!-- Reef growth event end time [a] -->

```

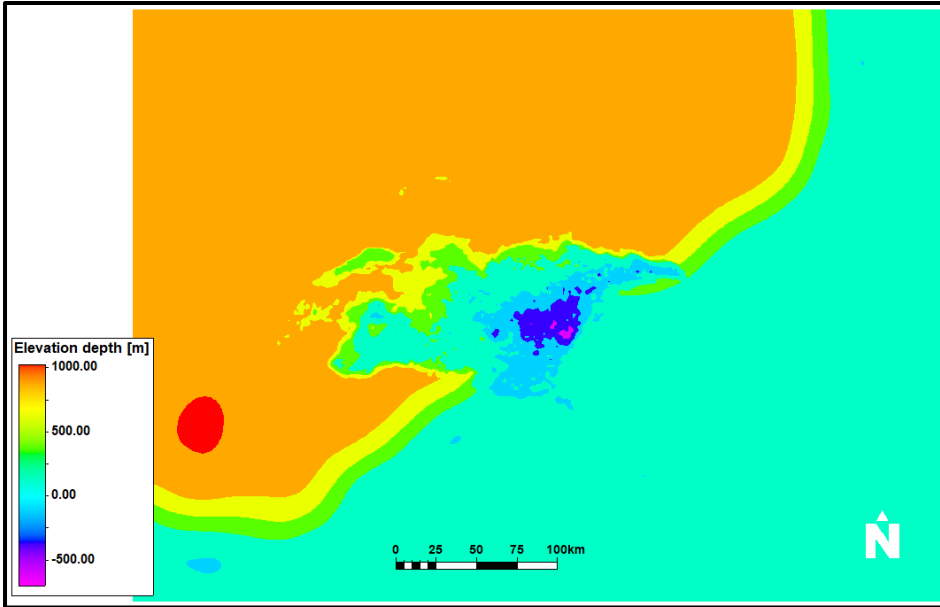
```

<gend>-100000.</gend>
  <!-- Species 1 growth rate during event [m/yr]. -->
  <growth_sp1>0</growth_sp1>
  <!-- Species 2 growth rate during event [m/yr]. -->
  <growth_sp2>0.00006</growth_sp2>
</event>
- <event>
  <!-- Reef growth event start time [a] -->
  <gstart>-100000.</gstart>
  <!-- Reef growth event end time [a] -->
  <gend>0.</gend>
  <!-- Species 1 growth rate during event [m/yr]. -->
  <growth_sp1>0</growth_sp1>
  <!-- Species 2 growth rate during event [m/yr]. -->
  <growth_sp2>0.00009</growth_sp2>
</event>
</carb>
<!-- Specify species 1 growth functions based on 3 main controlling forces: depth, sedimentation rate and ocean wave height. These functions are defined as csv files produced using pre-processing IPython notebook. -->
- <species1>
  <!-- Depth control on species 1 evolution. -->
  <depthControl>data/Ref/pelagiccontrol_gipps11.csv</depthControl>
  <!-- Ocean wave height control on species 1 evolution. -->
  <waveControl>data/fakecarbWave.csv</waveControl>
  <!-- Sedimentation control on species 1 evolution. -->
  <sedControl>data/fakecarbSed.csv</sedControl>
</species1>
<!-- Specify species 2 growth functions based on 3 main controlling forces: depth, sedimentation rate and ocean wave height. These functions are defined as csv files produced using pre-processing IPython notebook. -->
- <species2>
  <!-- Species 2 growth rate [m/yr]. -->
  <!-- Depth control on species 2 evolution. -->
  <depthControl>data/Ref/pelagiccontrol_gipps14.csv</depthControl>
  <!-- Ocean wave height control on species 2 evolution. -->
  <waveControl>data/fakecarbWave.csv</waveControl>
  <!-- Sedimentation control on species 2 evolution. -->
  <sedControl>data/fakecarbSed.csv</sedControl>
</species2>
<!-- Specify pelagic deposition functions based on depth control. The function is defined as csv file produced using pre-processing IPython notebook. -->
<!-- Output folder path -->
<outfolder>ReferenceCase_5</outfolder>
</badlands>

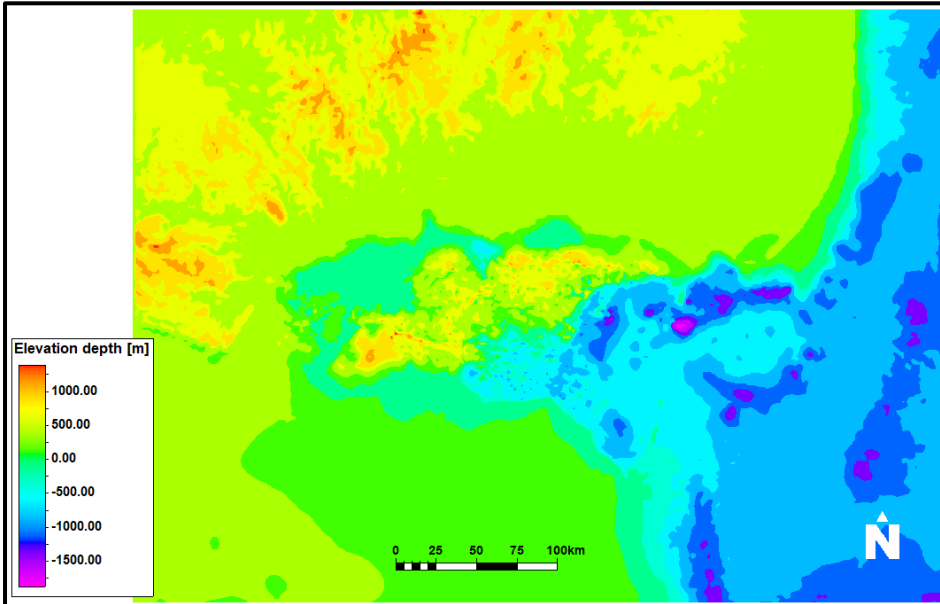
```



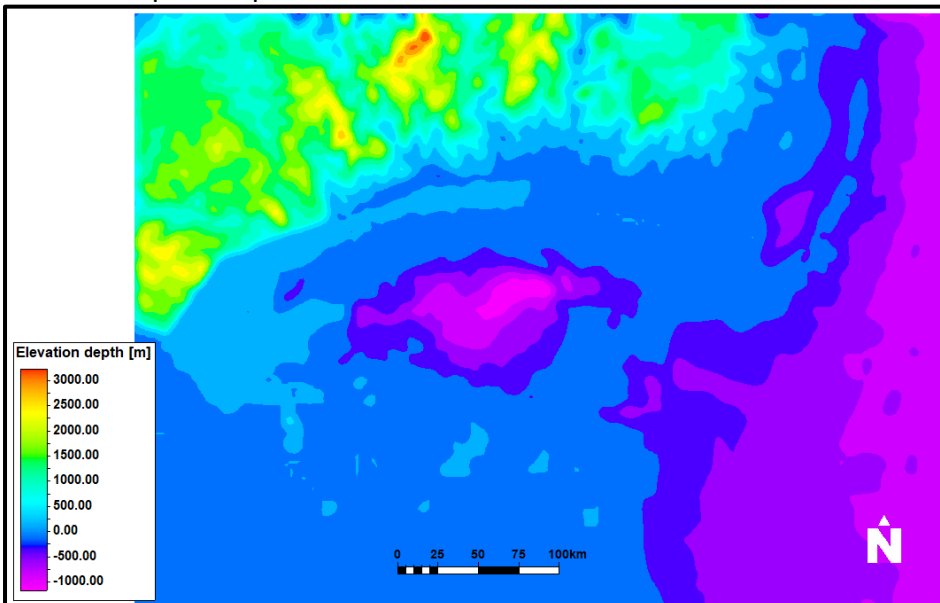
Mid Cretaceous Uplift maps (98-95 Ma)



Late Cretaceous Uplift map (84-65 Ma)



65-32 Ma uplift map



Data analysis with 'Full Depth model (faults&property)March20/Part of Latrobe_valley_3D grid_20Mar20'

Property: Coal_Moisture1 [U]

Decimation Decimated number of data: 10000

Zones: All zones modeled together (Toggle 'Together' in Petrophysical modeling)

Facies: Lith [U] 7: Coal

Transformations Variograms

Experimental variogram computation Search only inside zone

Direction	Azimuth	Dip	Number lags	Lag distance	Search radius	Band width	Tolerance angle	Lag tolerance	Thickness
Vertical	NA	90	8	25	200	50	45	50	NA
Major	20	0	20	350	7000	1500	45	50	10
Minor	290	0	20	350	7000	1500	45	50	10

Variogram model fitting

Nugget: 0.1199 Total sill: 0.5507

Structure 1

Type	Spherical
Sill	0.4308
Major range	4543.967
Minor range	3125.289
Vertical range	10

Vertical direction Major direction Minor direction

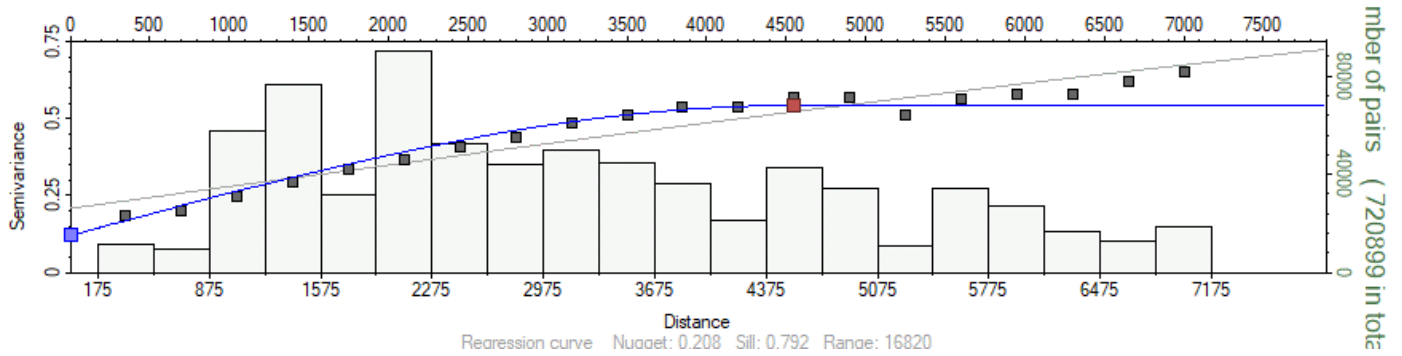
Search zone:

Regression curve Nugget: 0.208 Sill: 0.792 Range: 16820

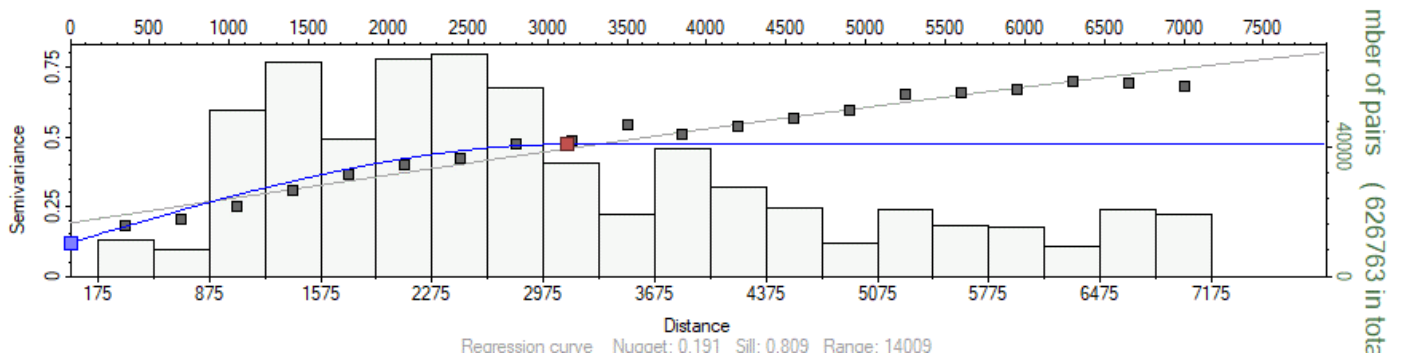
number of pairs (720899 in total)

Apply OK Cancel

Major direction




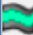







Minor direction

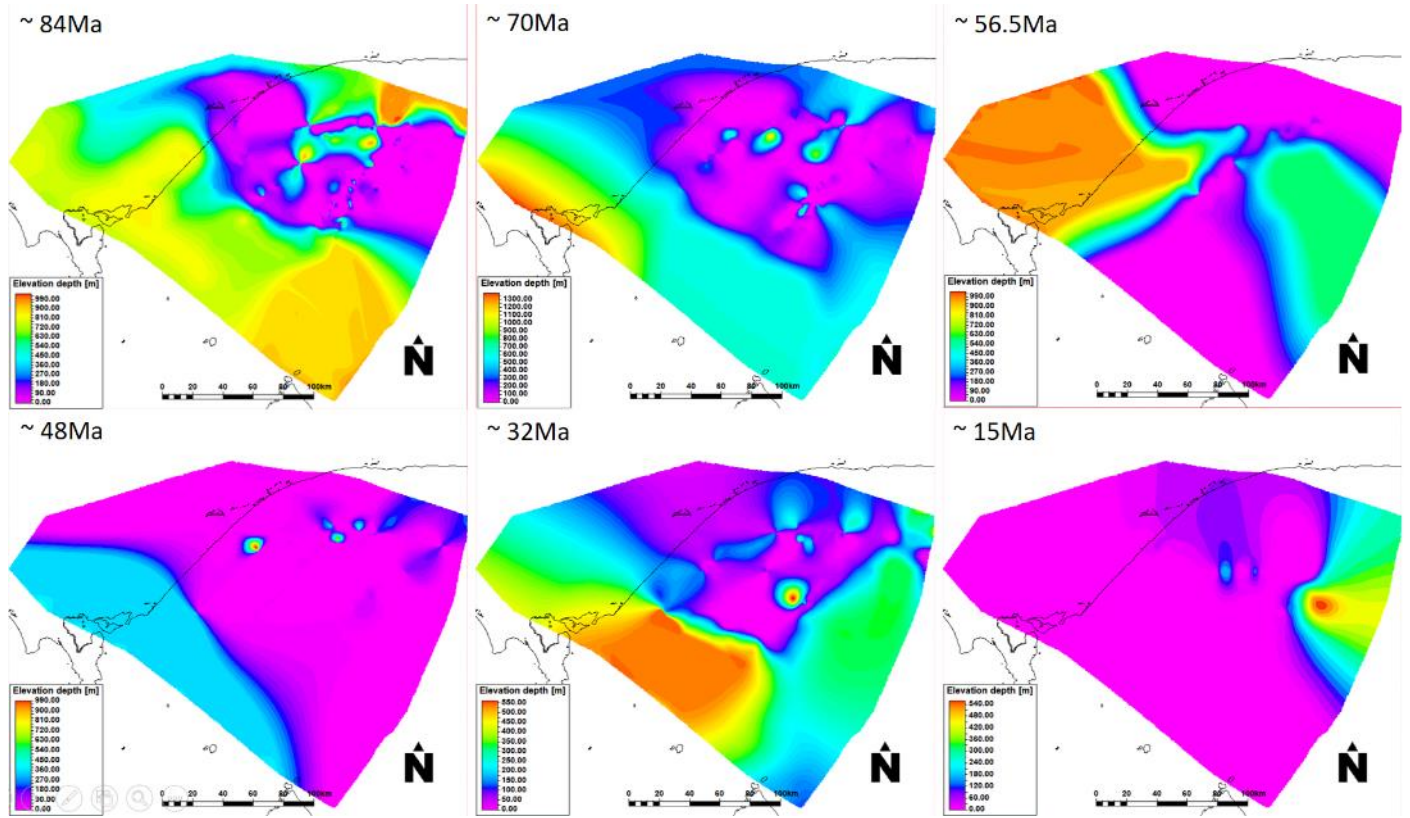


Appendix 12 Weighted settings of scale up facies log for entire Gippsland Basin

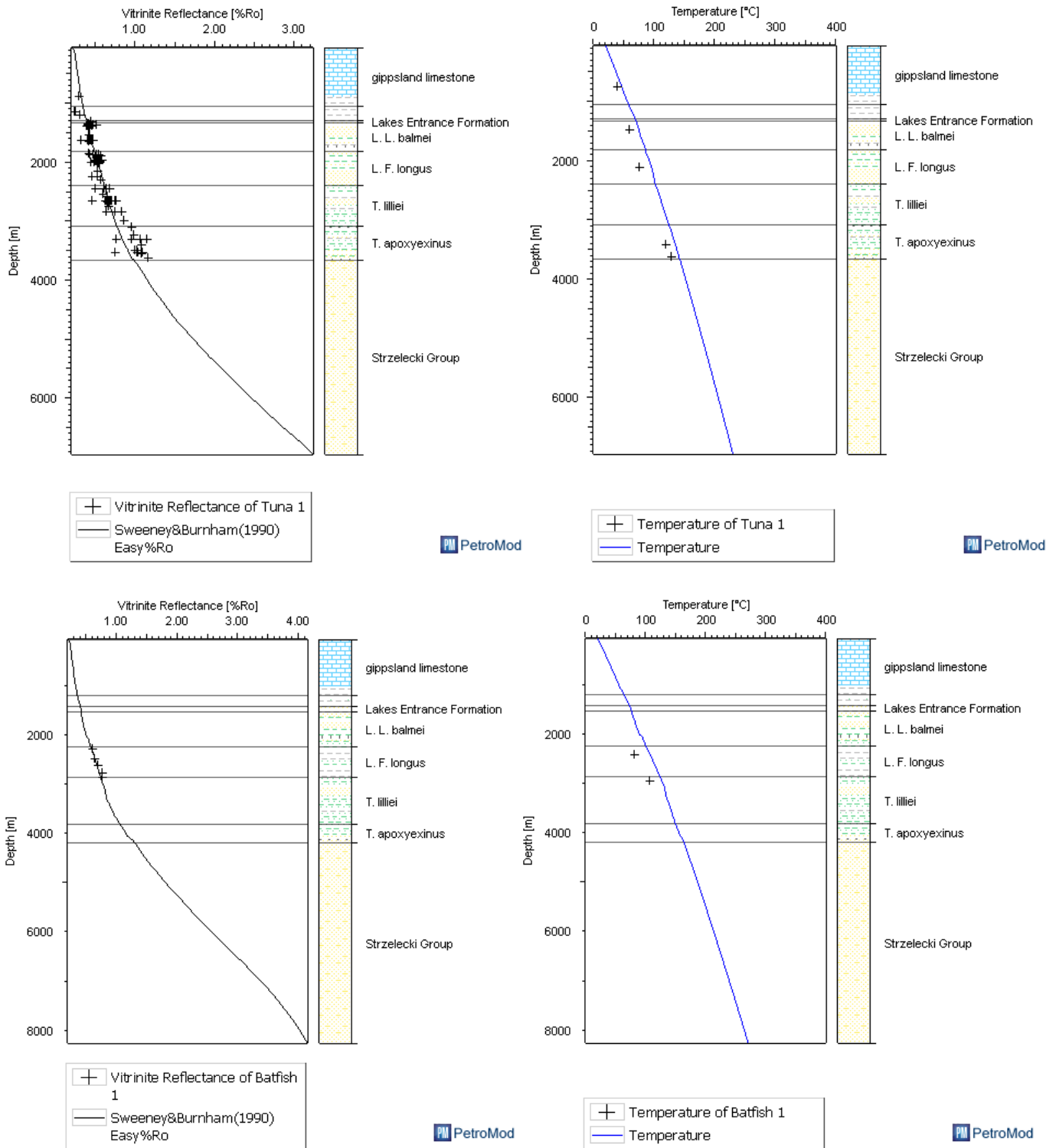
Settings Zones Weighted Seed Horizon mapping

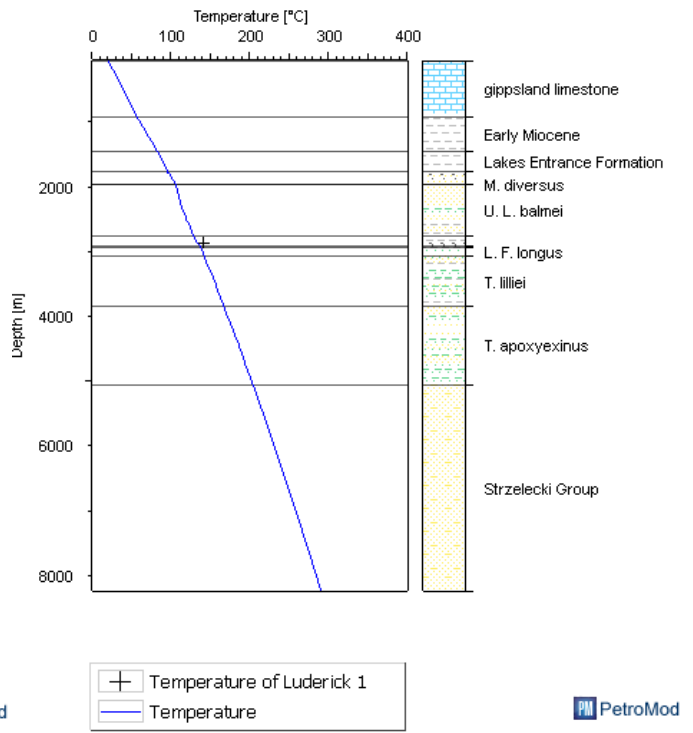
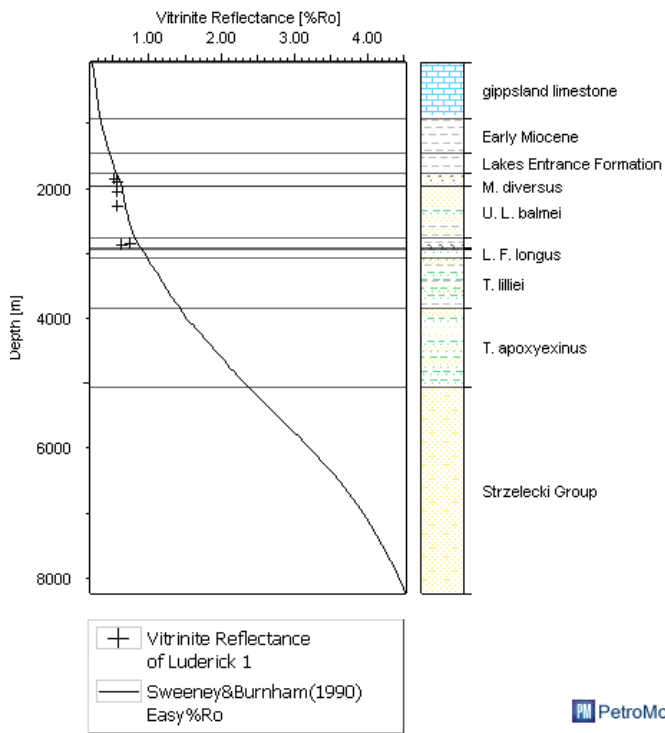
Equal for all zones

	Zone	Clean Sand	Siltstone	Carbonate	Shale	Coal	Igneous
	Topo - Mid_Miocene	1.00	1.00	1.00	1.00	1.00	1.00
	Mid_Miocene - Lakes Entrance	1.00	1.00	1.00	1.00	1.00	1.00
	Lakes Entrance - Latrobe Gp	1.00	1.00	1.00	1.00	1.00	1.00
	Cobia	0.95	1.50	1.00	1.20	1.10	1.00
	Upper Halibut	1.00	1.20	1.00	1.00	1.75	1.00
	Kate Shale - Golden Beach top	1.00	1.05	1.00	0.95	2.10	1.00
	Golden Beach SubGp	1.00	1.05	1.00	1.00	1.65	0.85
	Emperor SubGp	1.00	1.05	1.00	1.00	1.45	1.00
	Strzelecki Gp - Basement	1.00	1.00	1.00	1.00	1.00	1.00



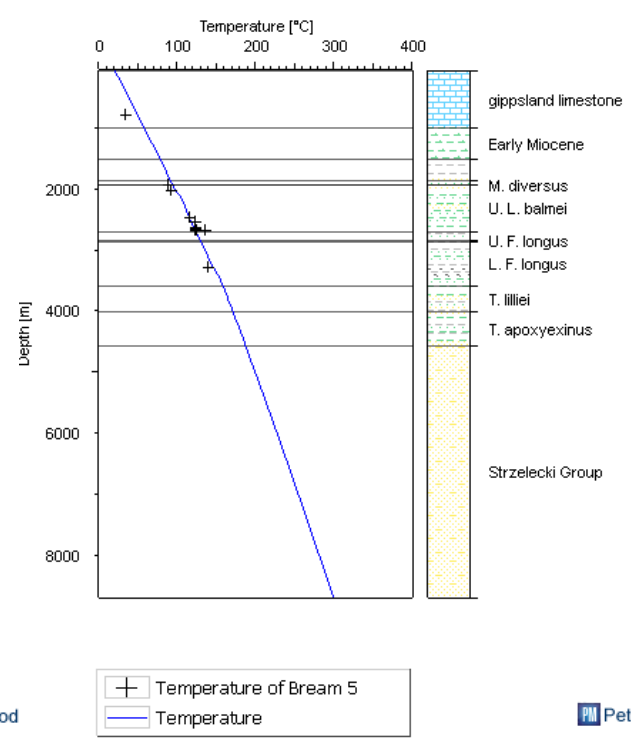
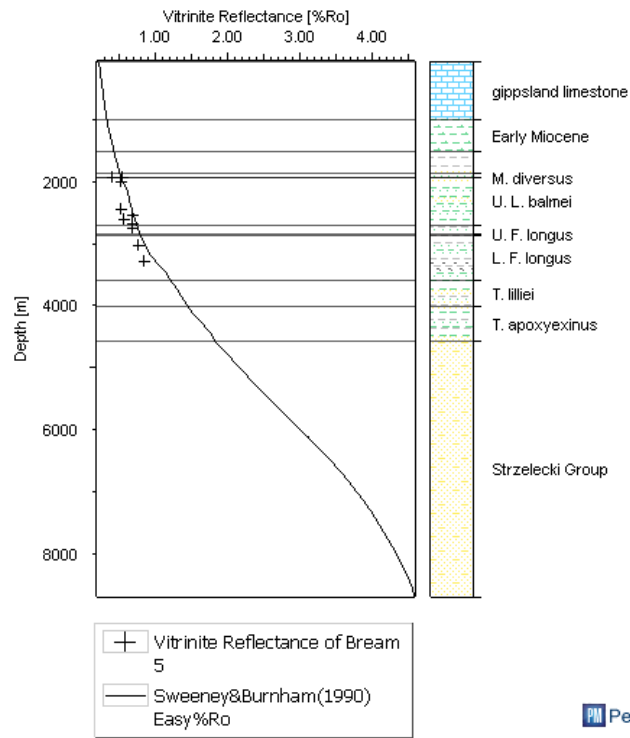
Appendix 14 Comparison of modelled Temperature and Vitrinite Reflectance vs measured data





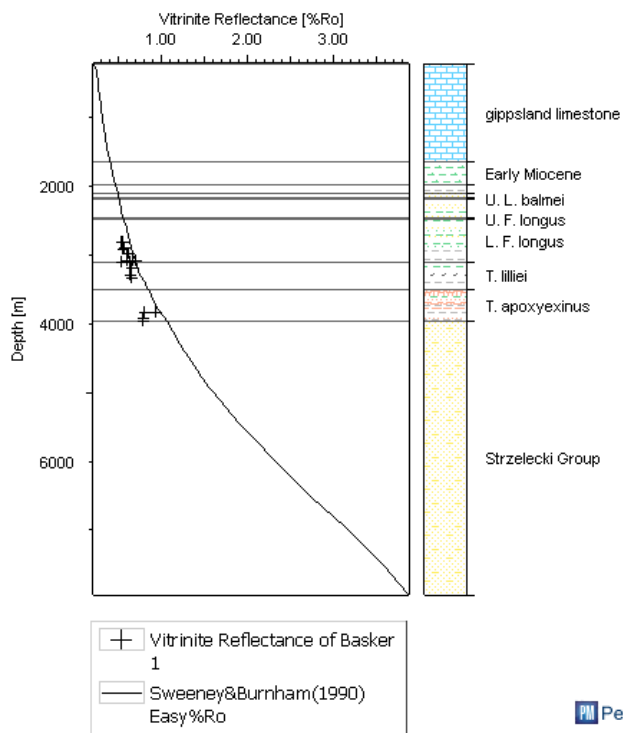
PM PetroMod

PM PetroMod

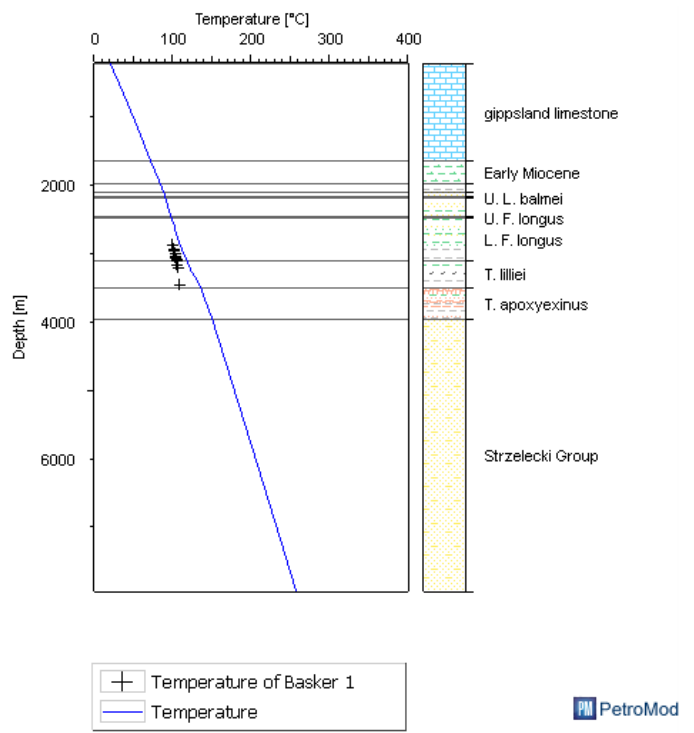


PM PetroMod

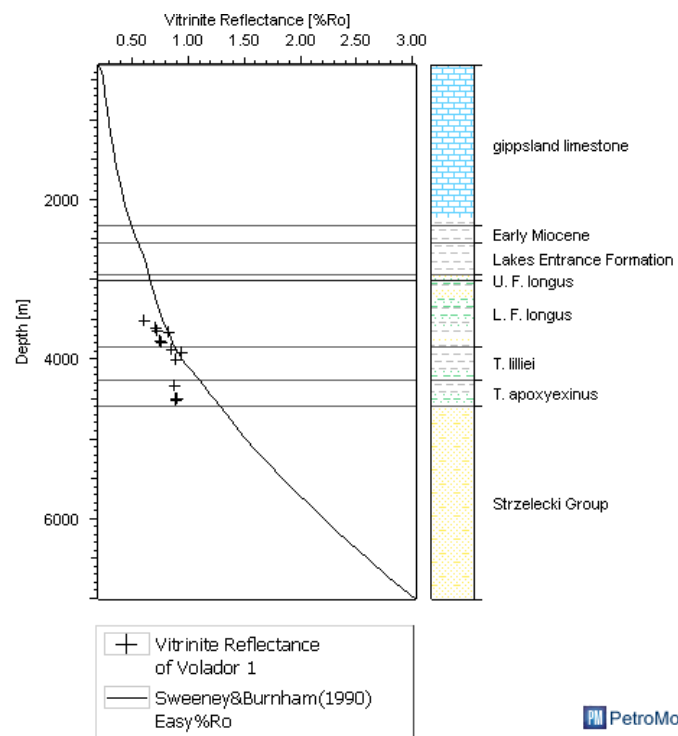
PM PetroMod



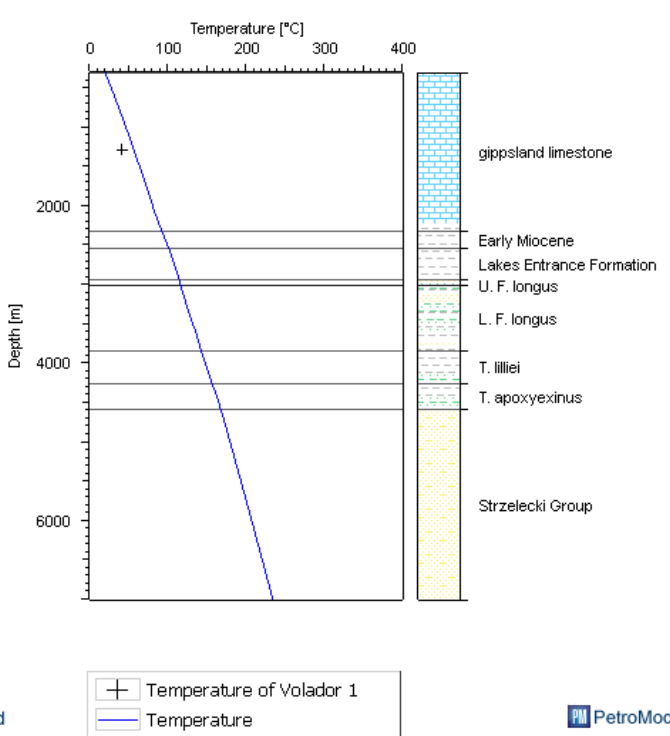
PM PetroMod



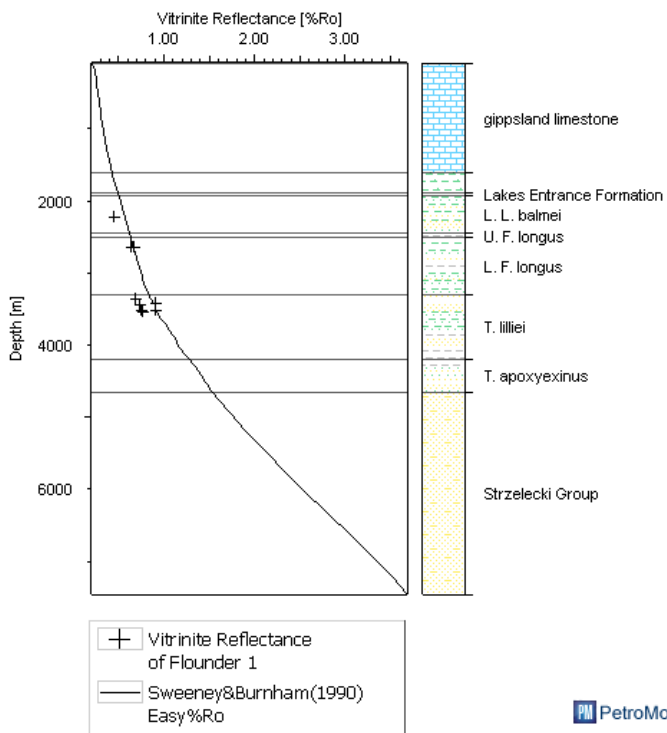
PM PetroMod



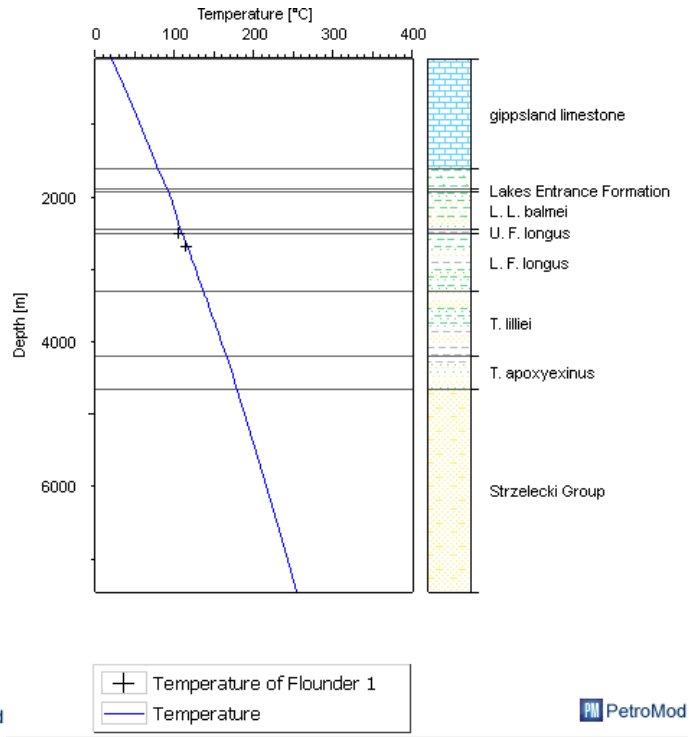
PM PetroMod



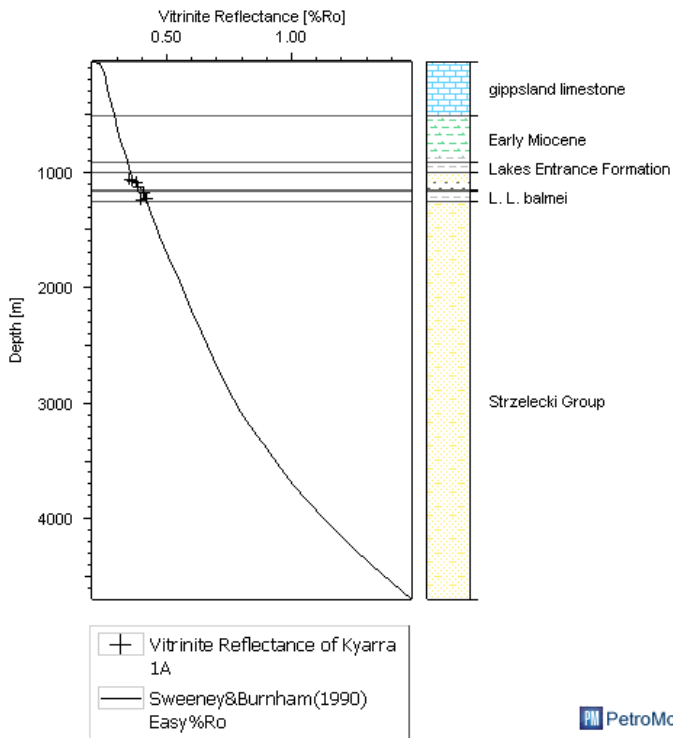
PM PetroMod



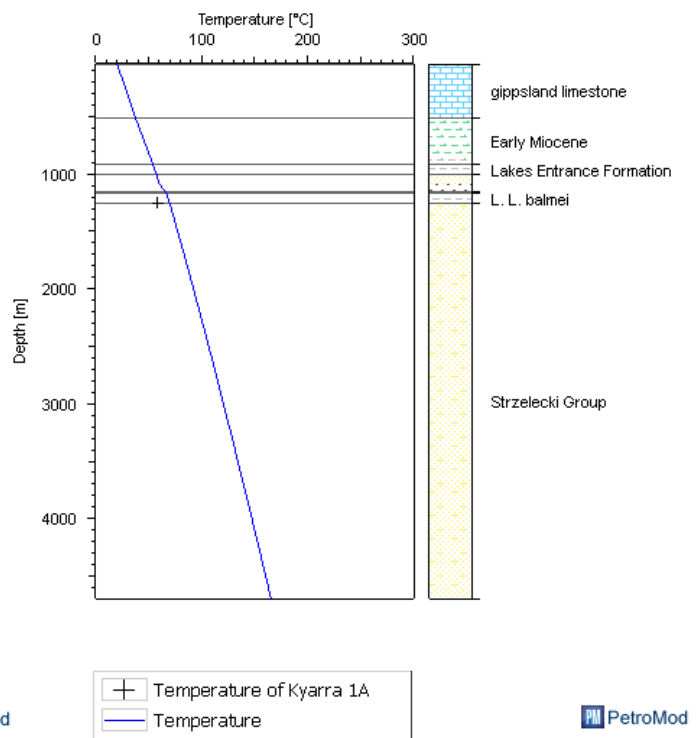
PetroMod



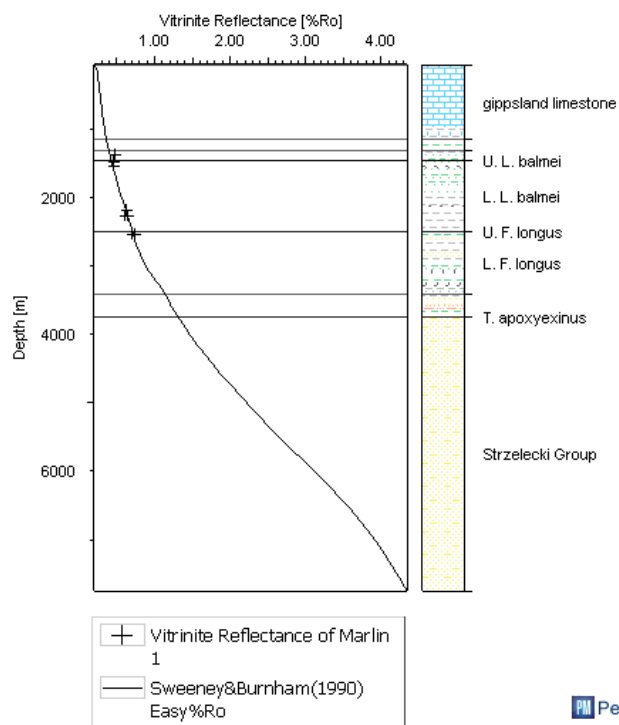
PetroMod



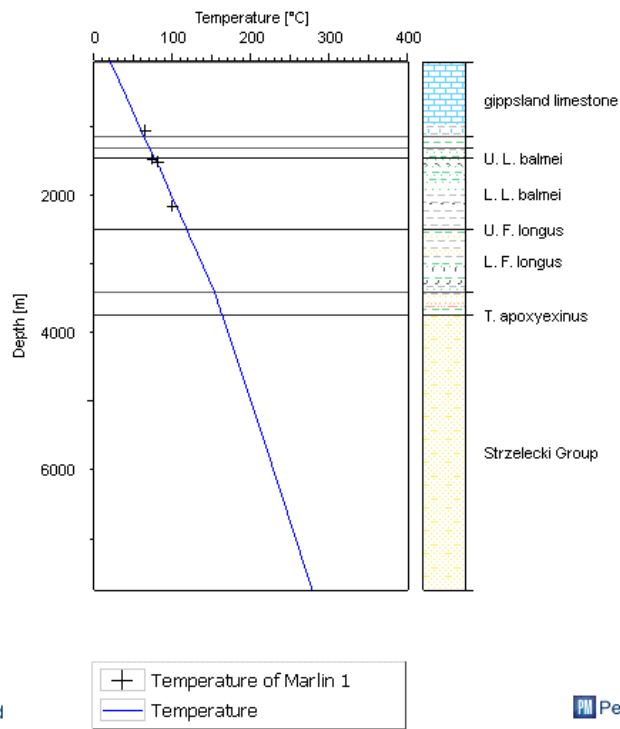
PetroMod



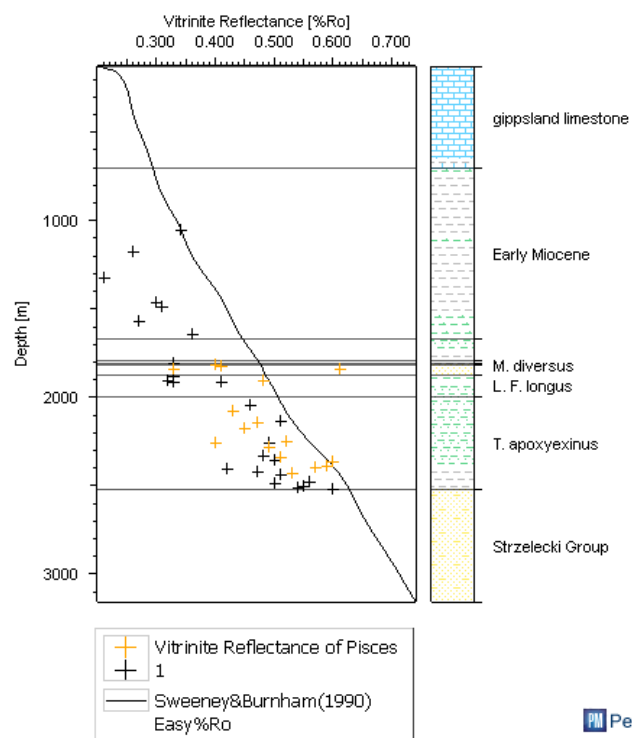
PetroMod



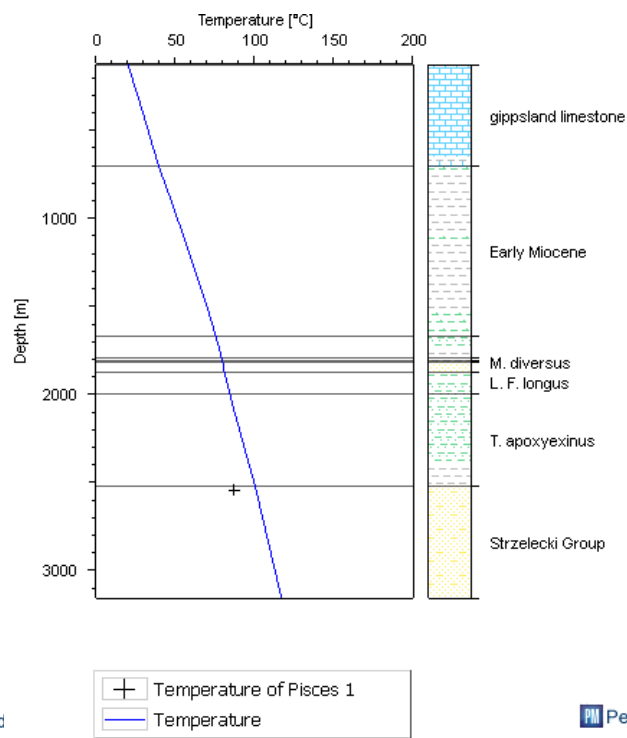
PM PetroMod



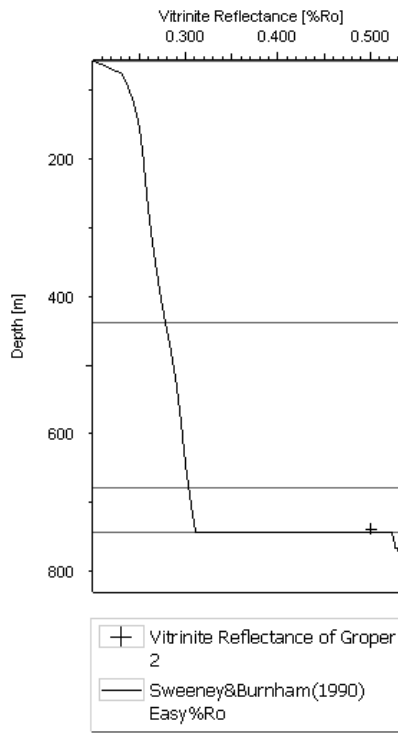
PM PetroMod



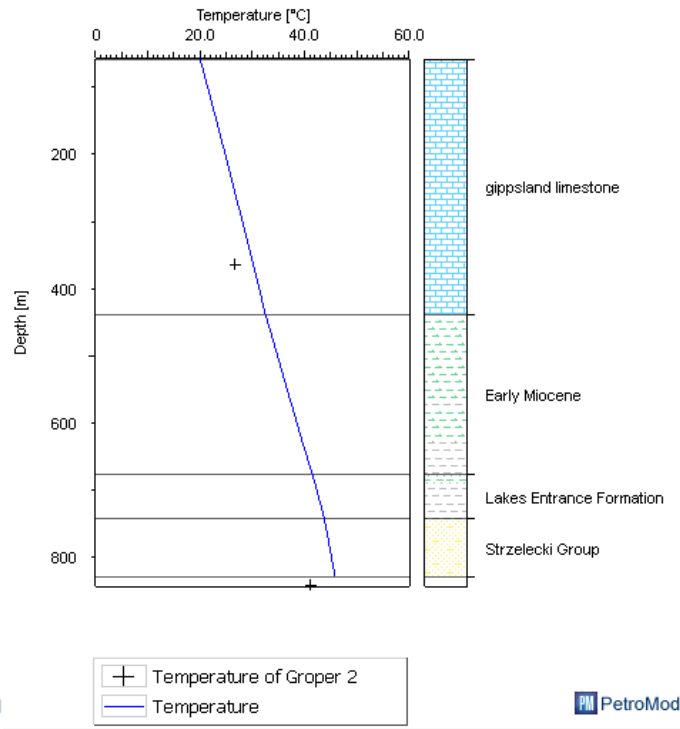
PM PetroMod



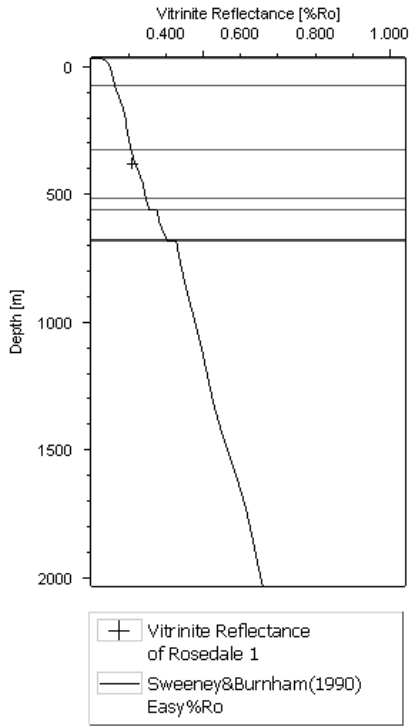
PM PetroMod



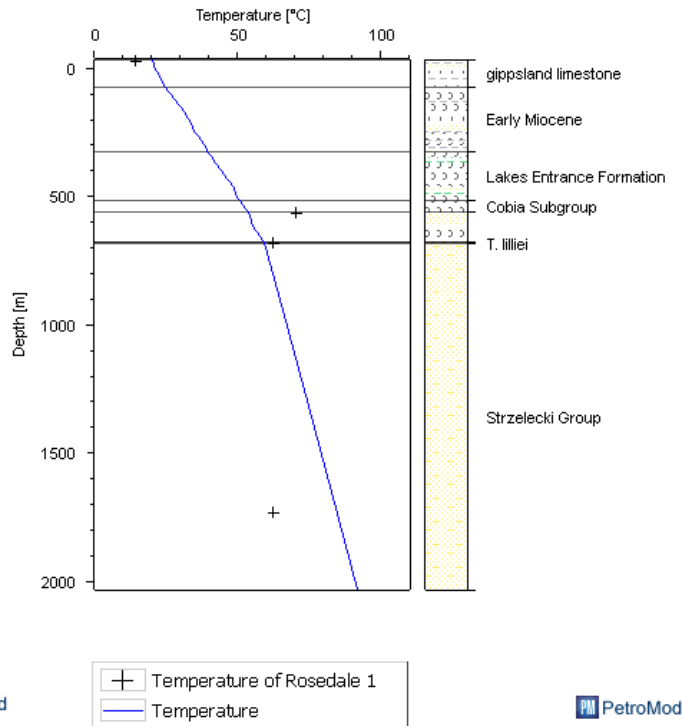
PM PetroMod



PM PetroMod

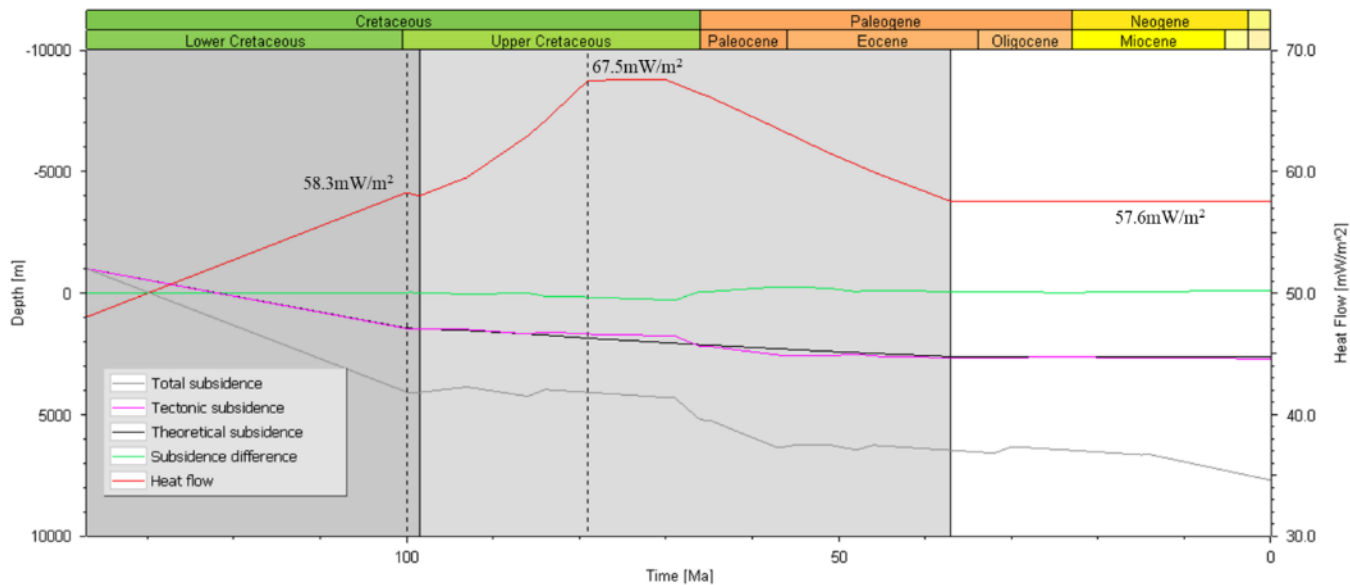


PM PetroMod

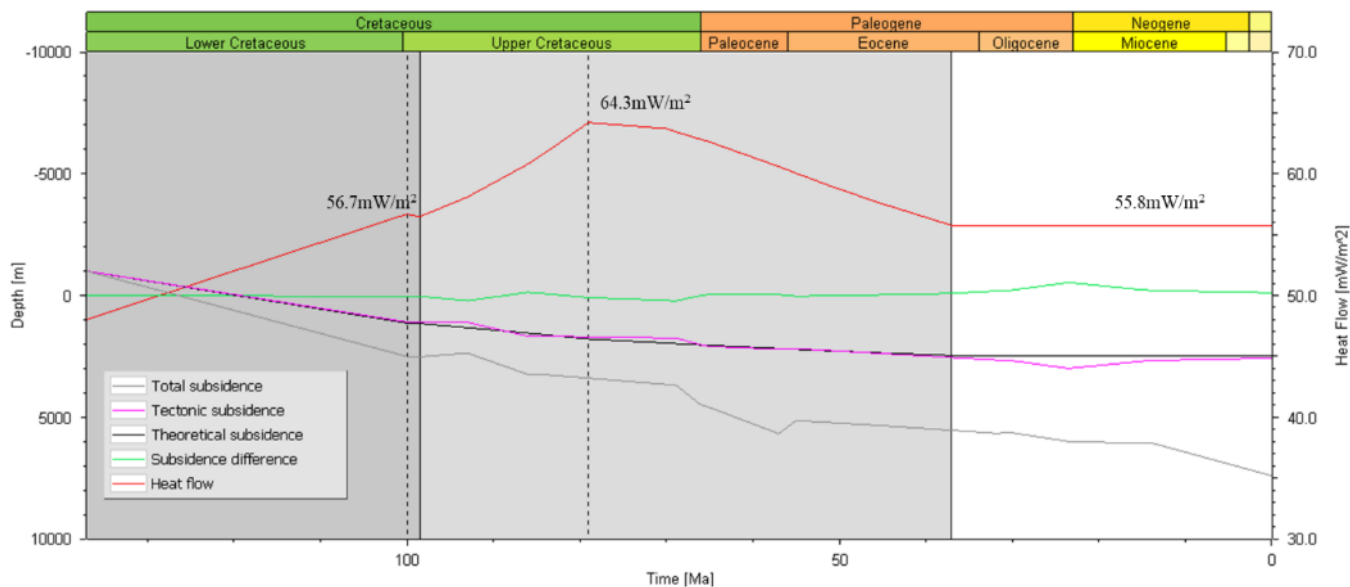


PM PetroMod

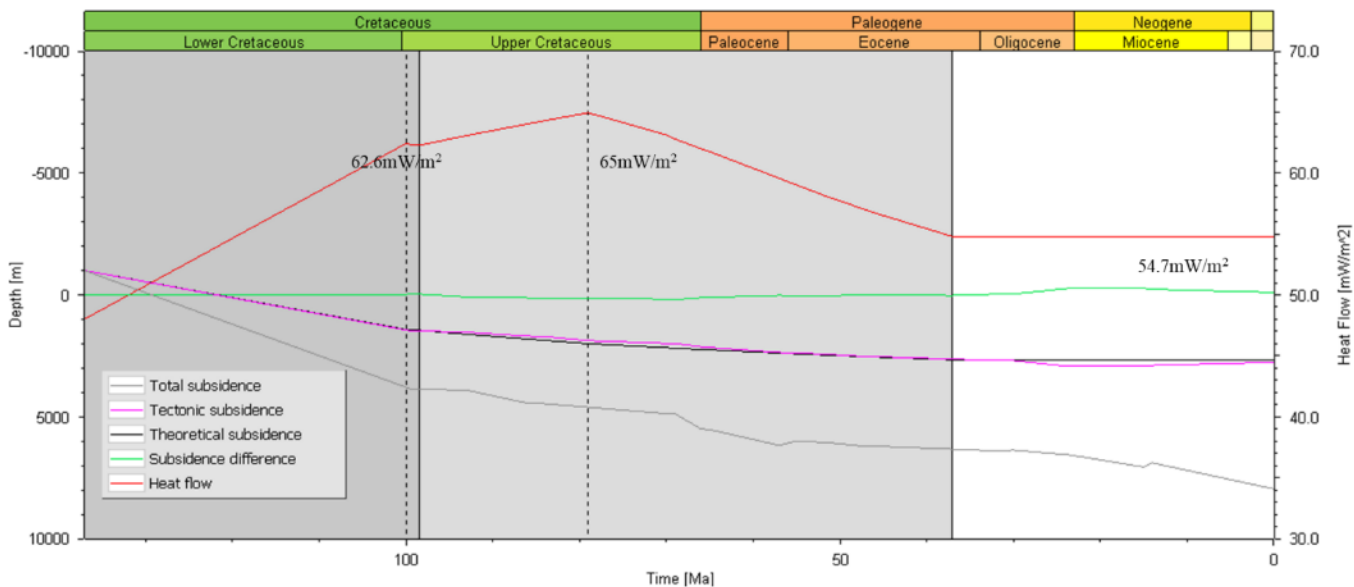
Marlin-1



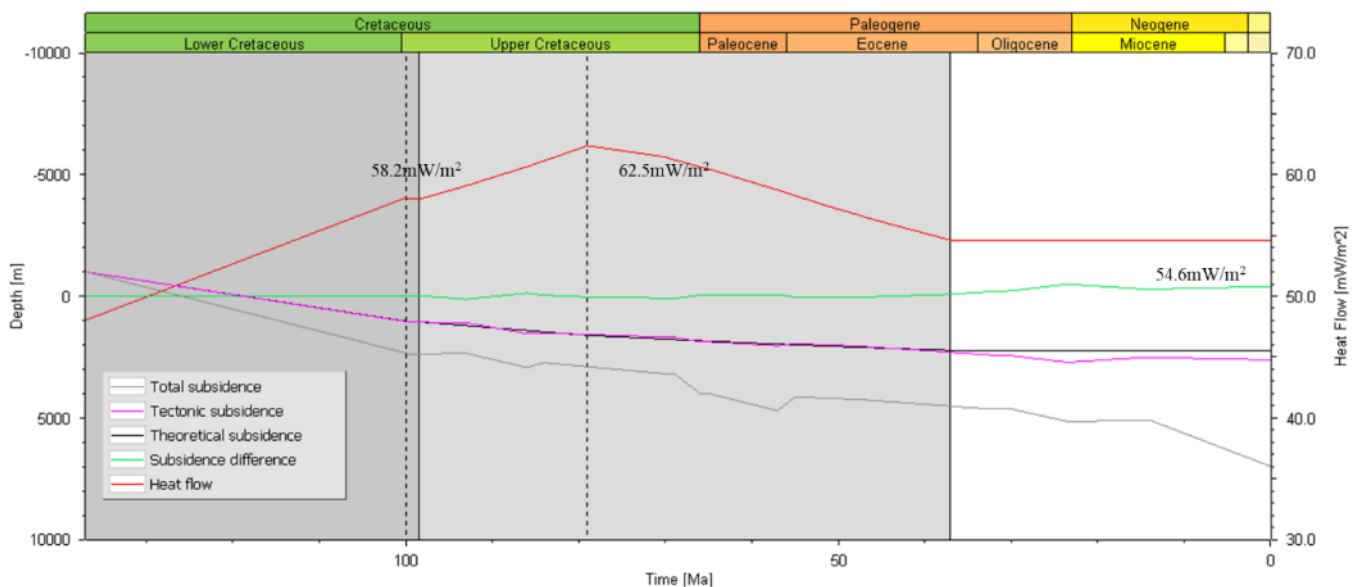
Mackerel-1



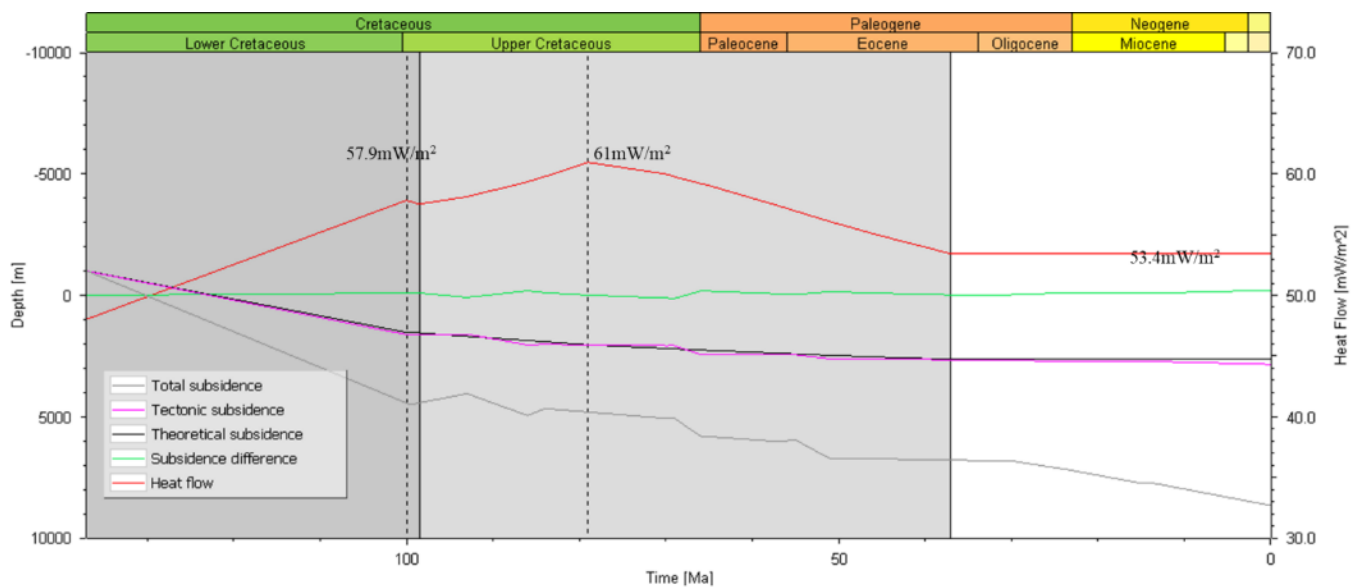
Basker-1



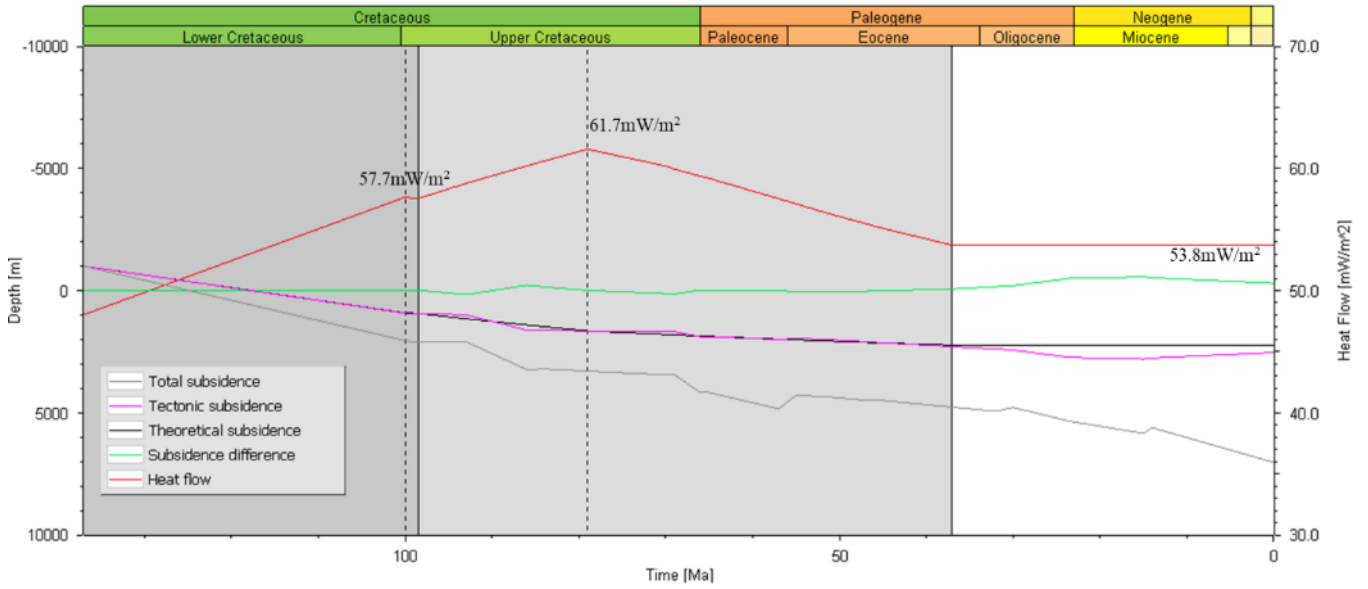
Volador-1



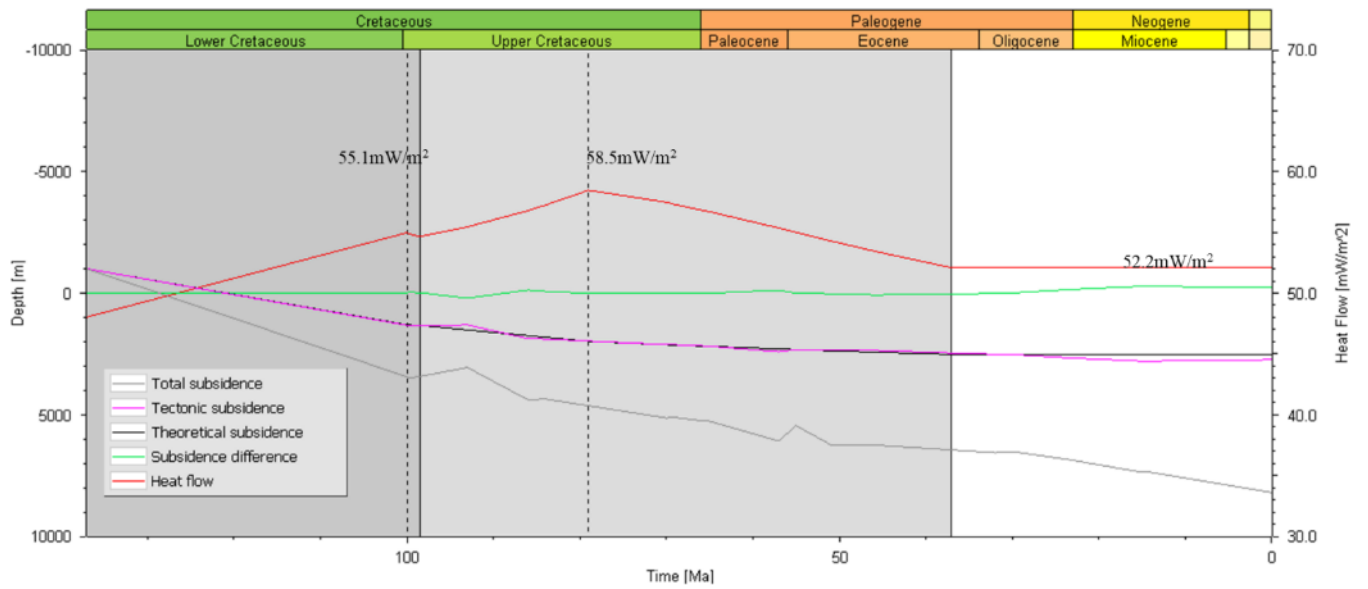
Bream-5



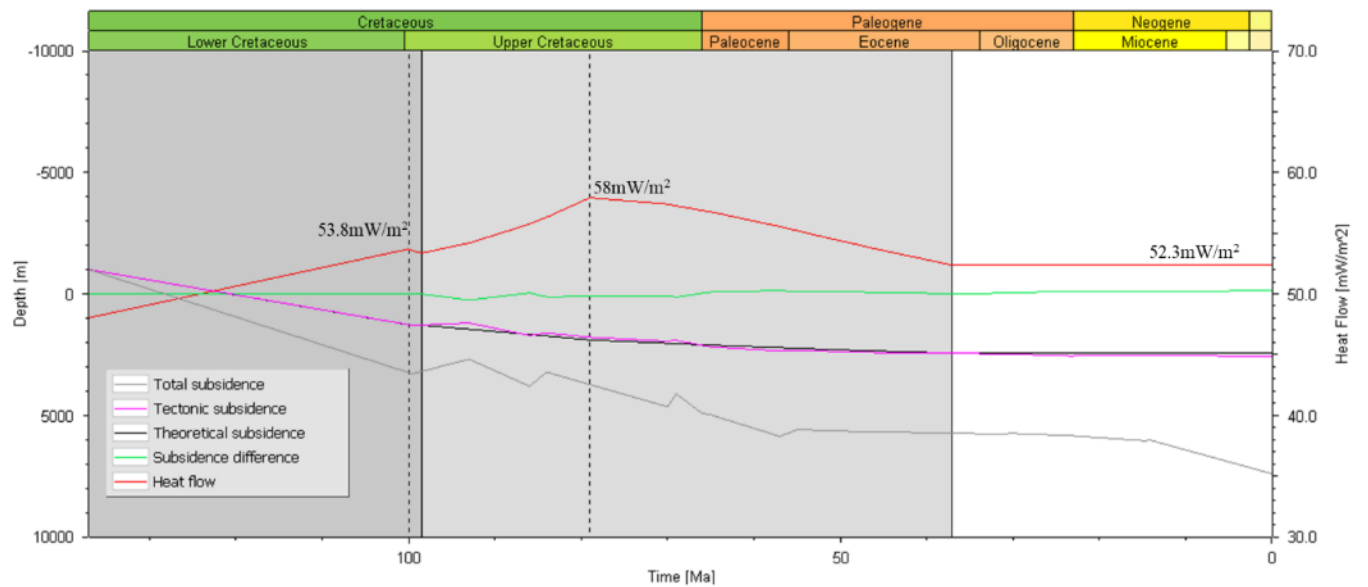
Athene-1



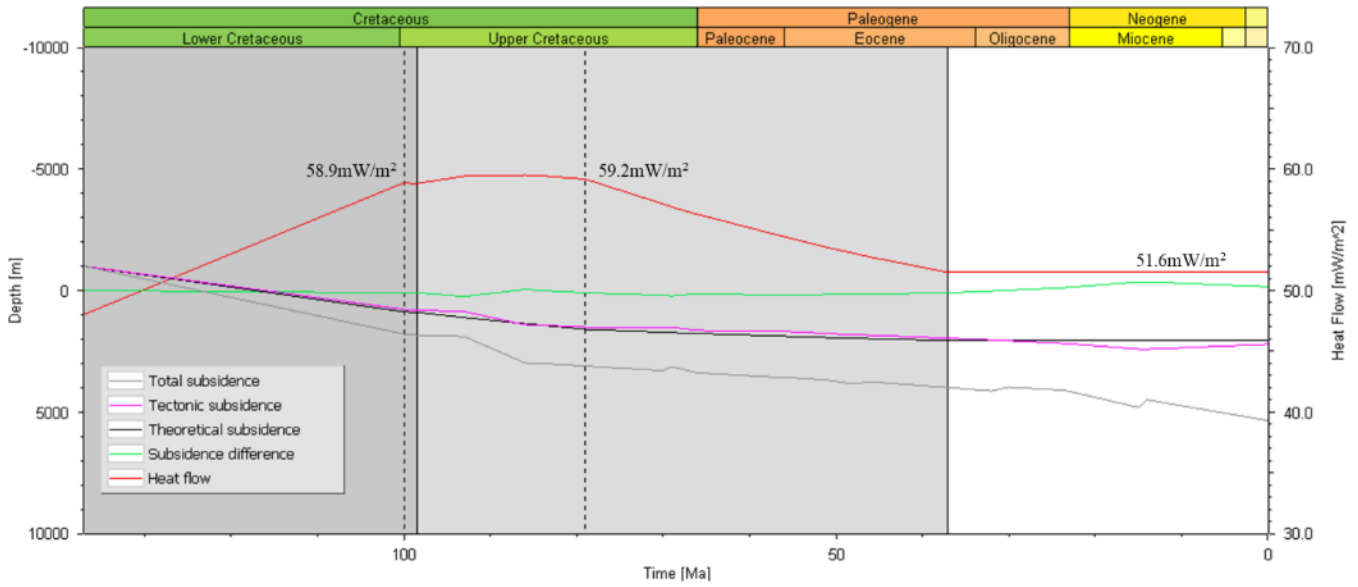
Luderick-1



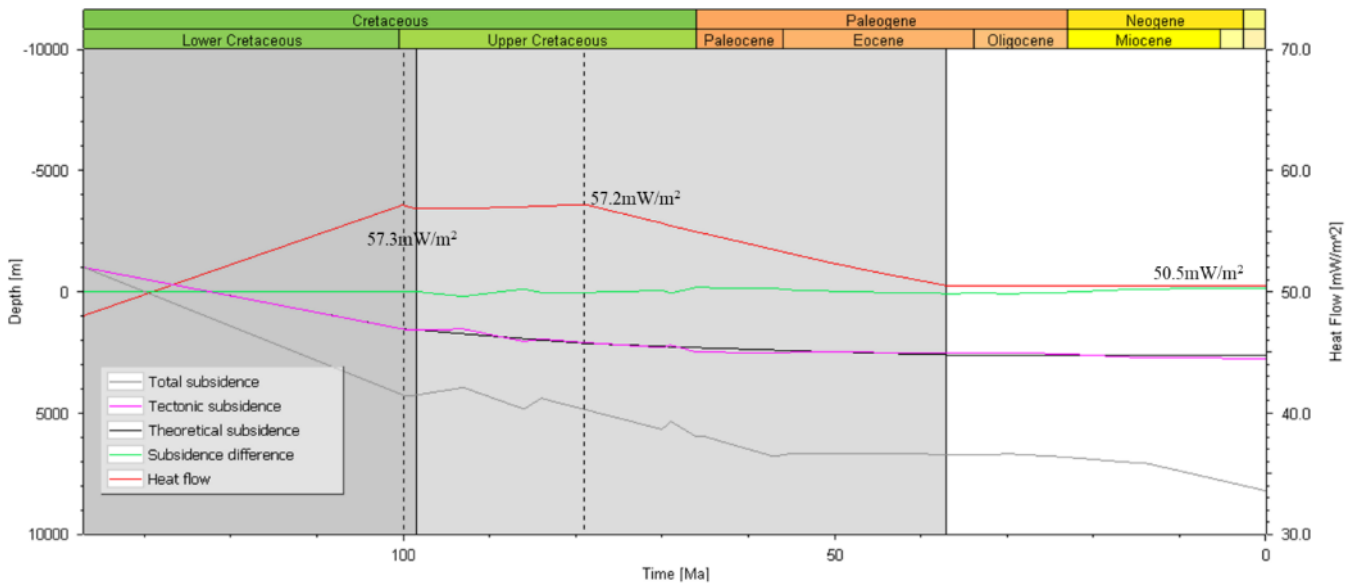
Flounder-1



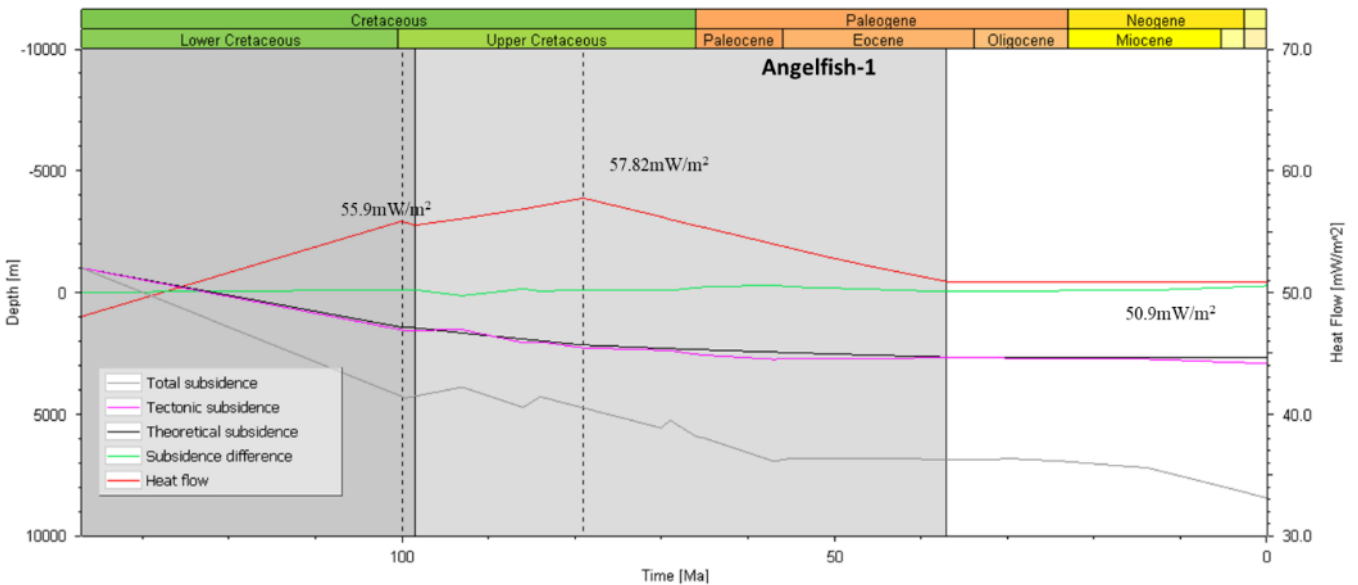
Shark-1



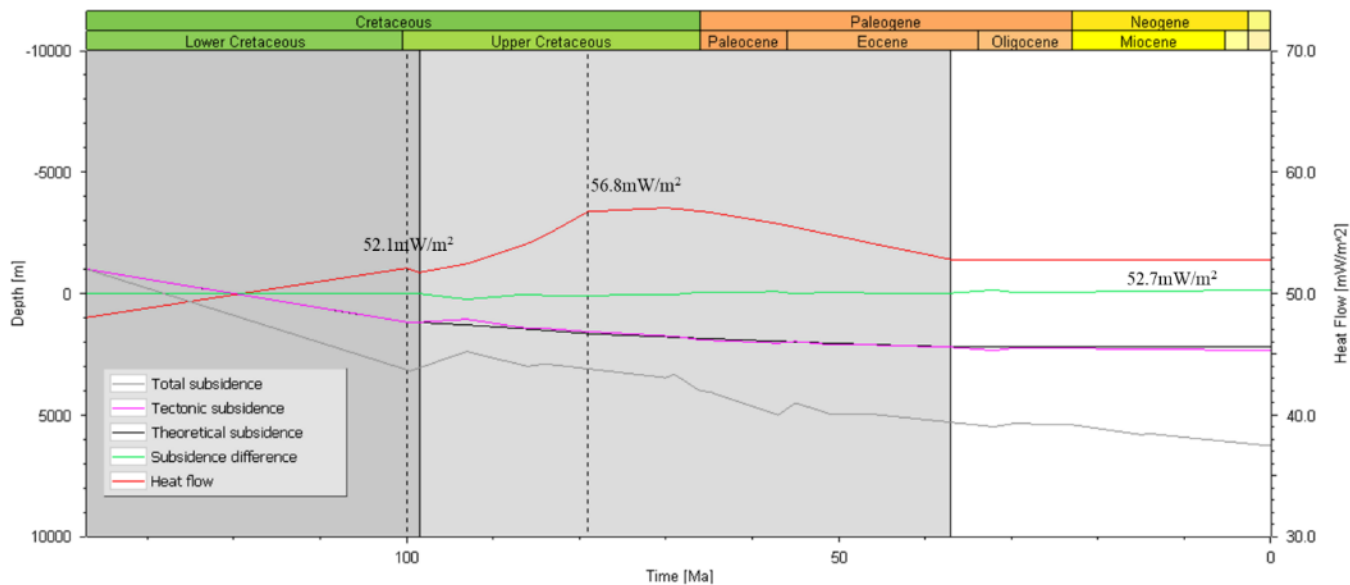
Batfish-1



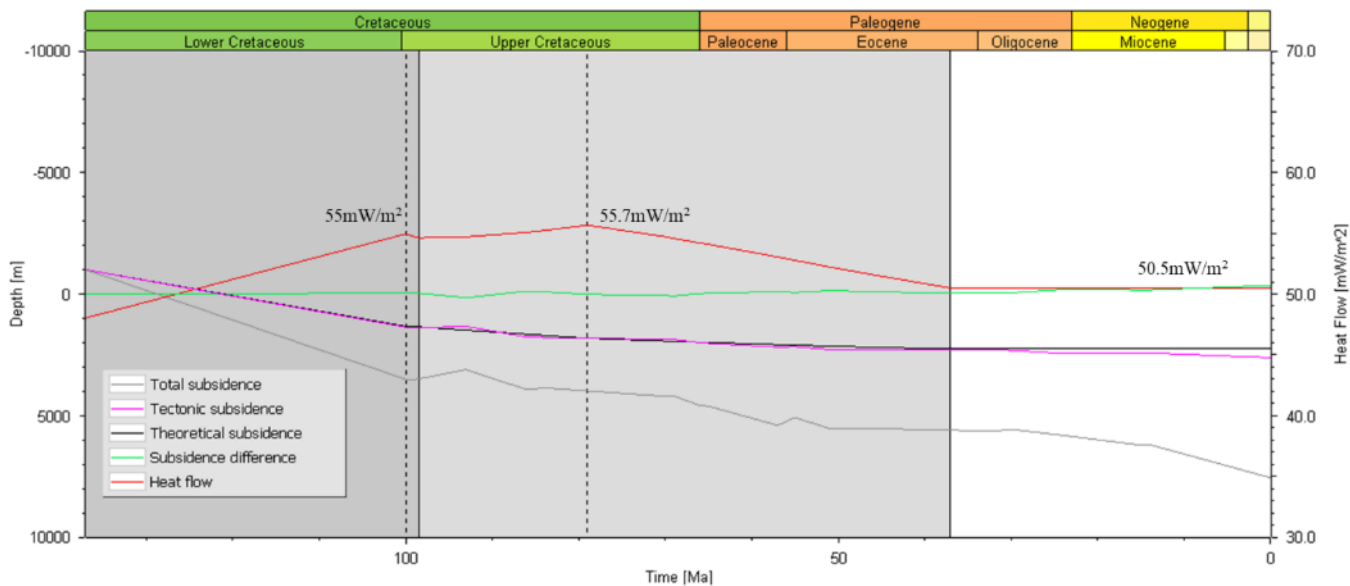
Angelfish-1



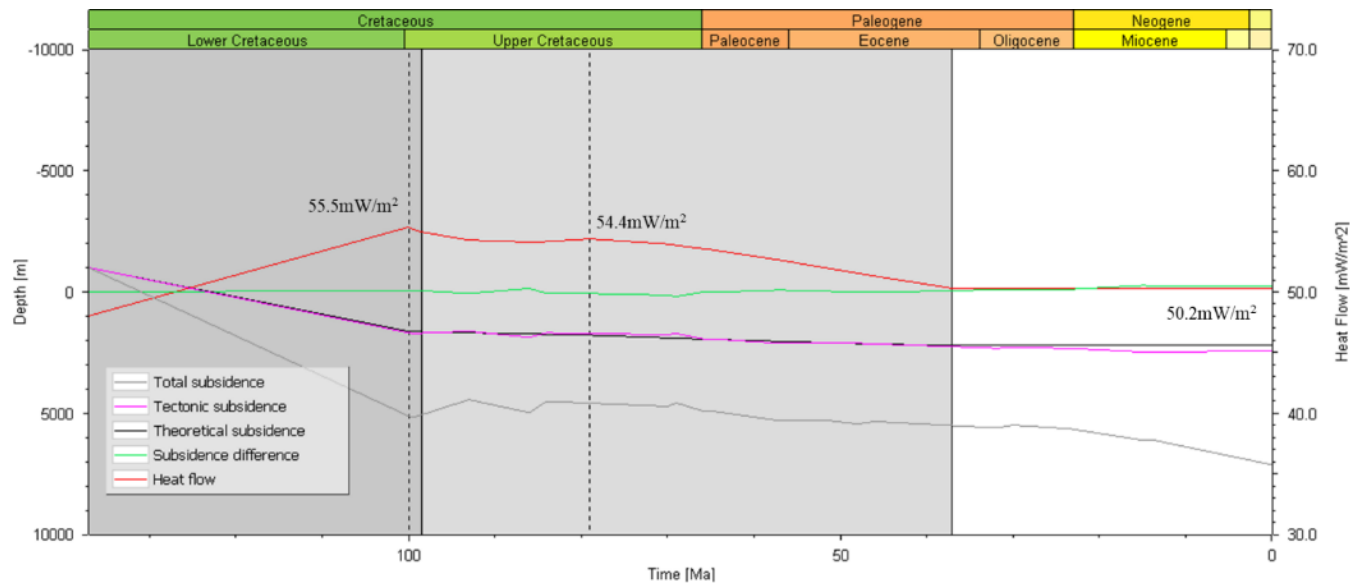
Barracouta-1



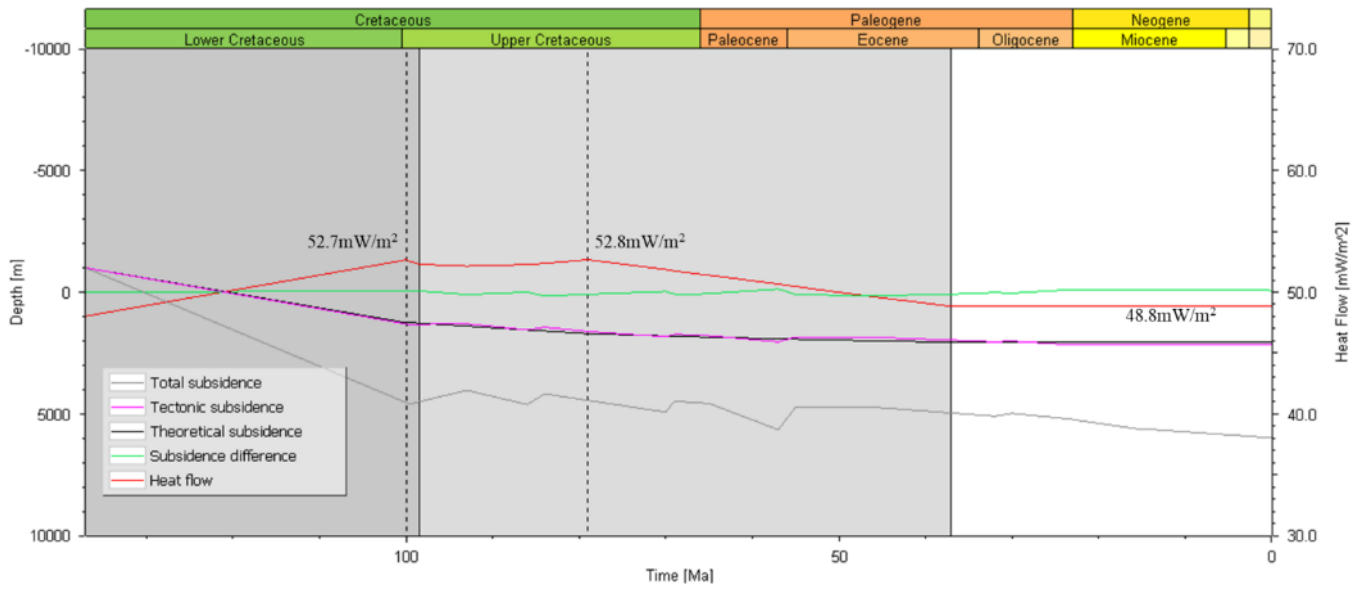
Veilfin-1



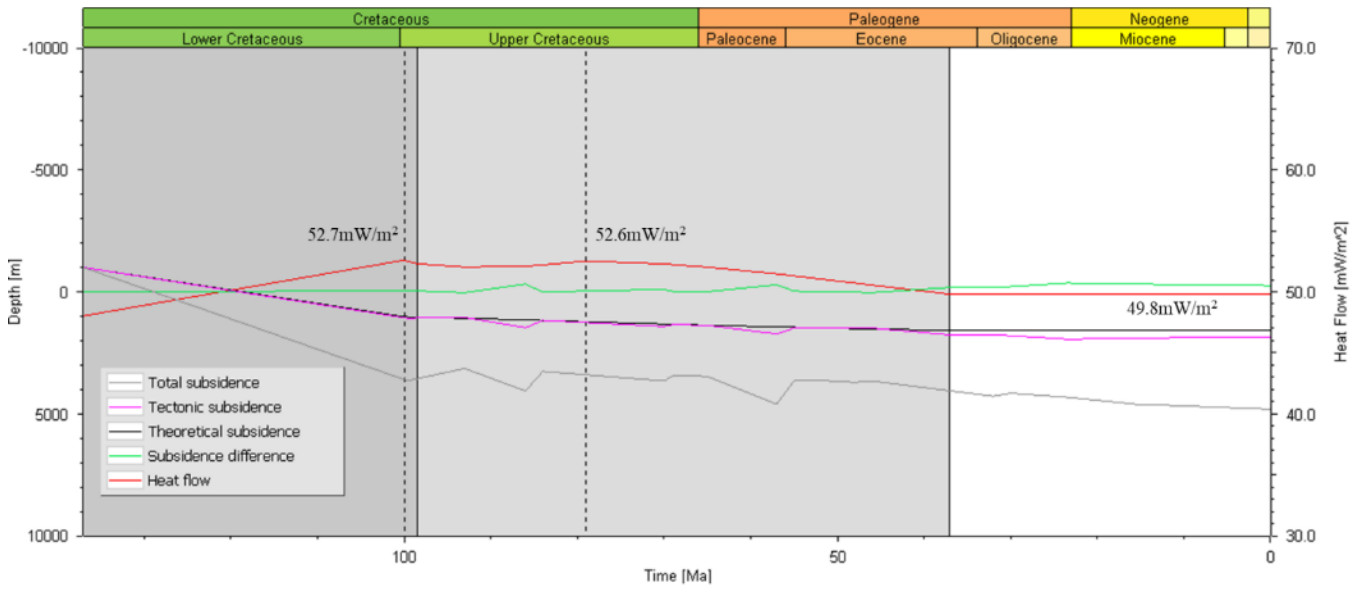
Sunfish-1



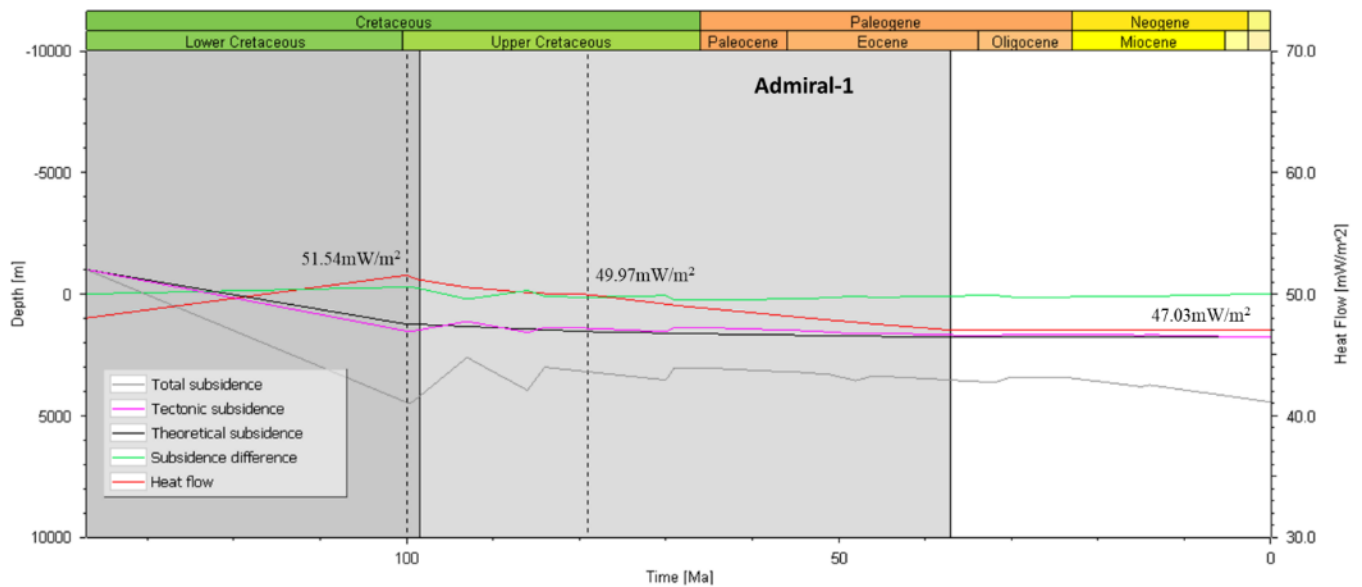
Perch-1



Wombat-3

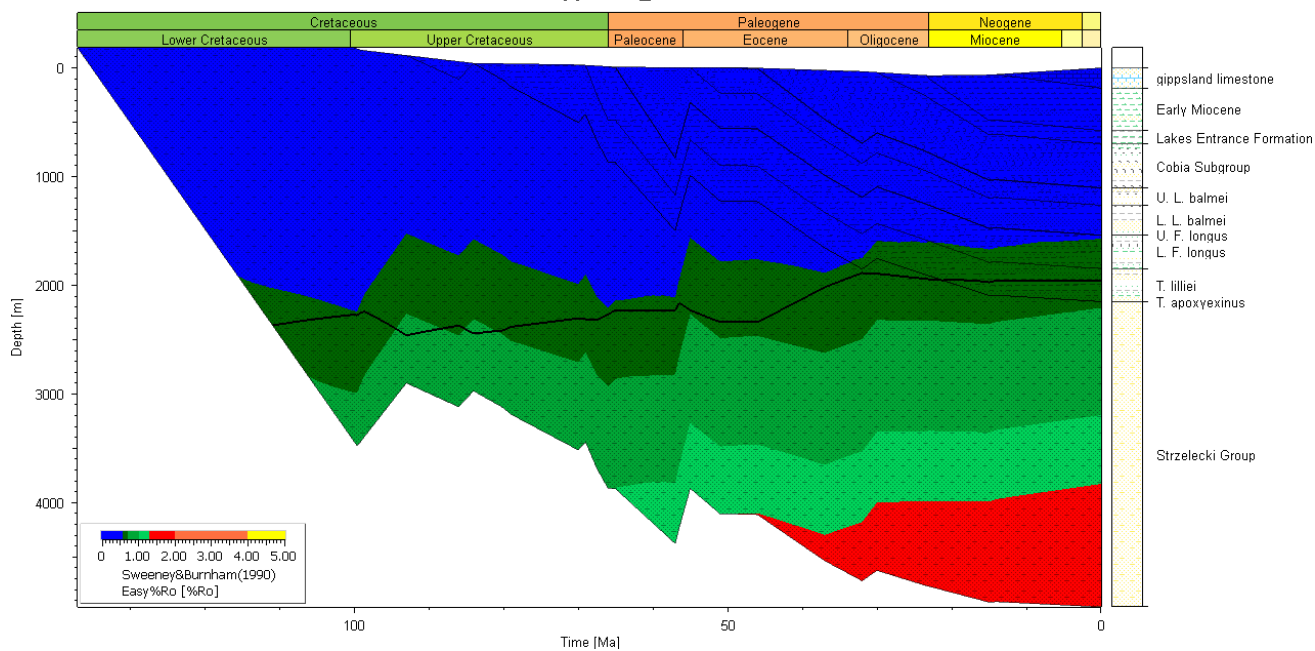


Admiral-1

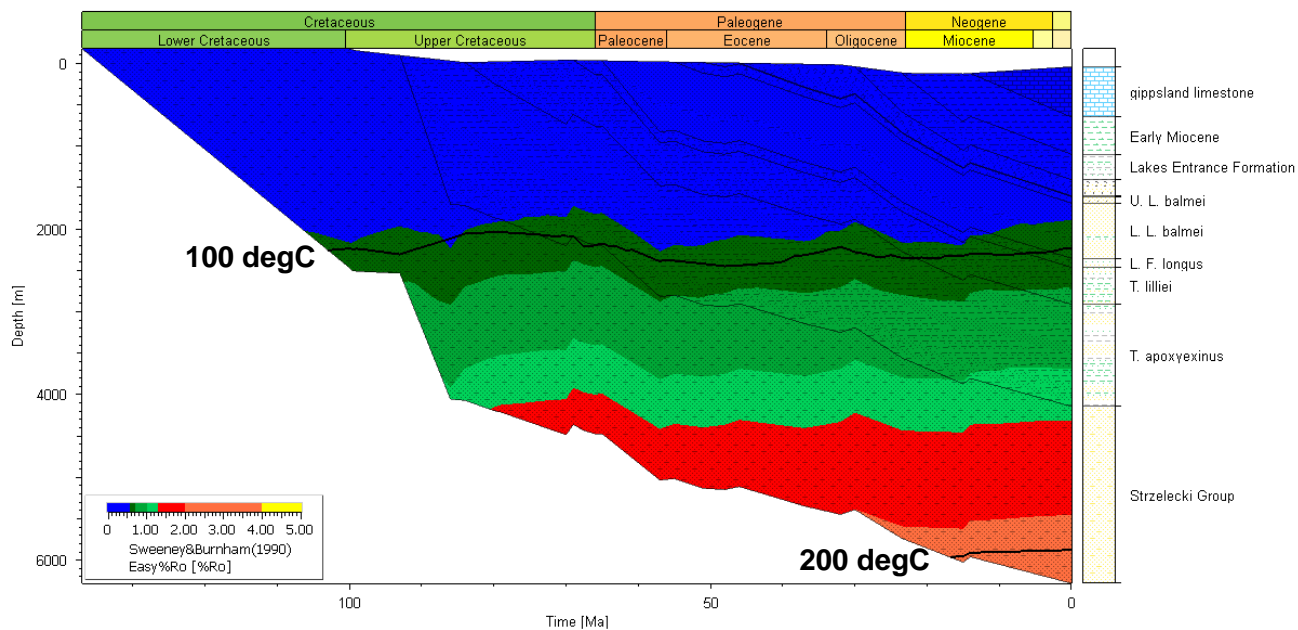


Thick black lines are temperatures at 100degC and 200degC, respectively.

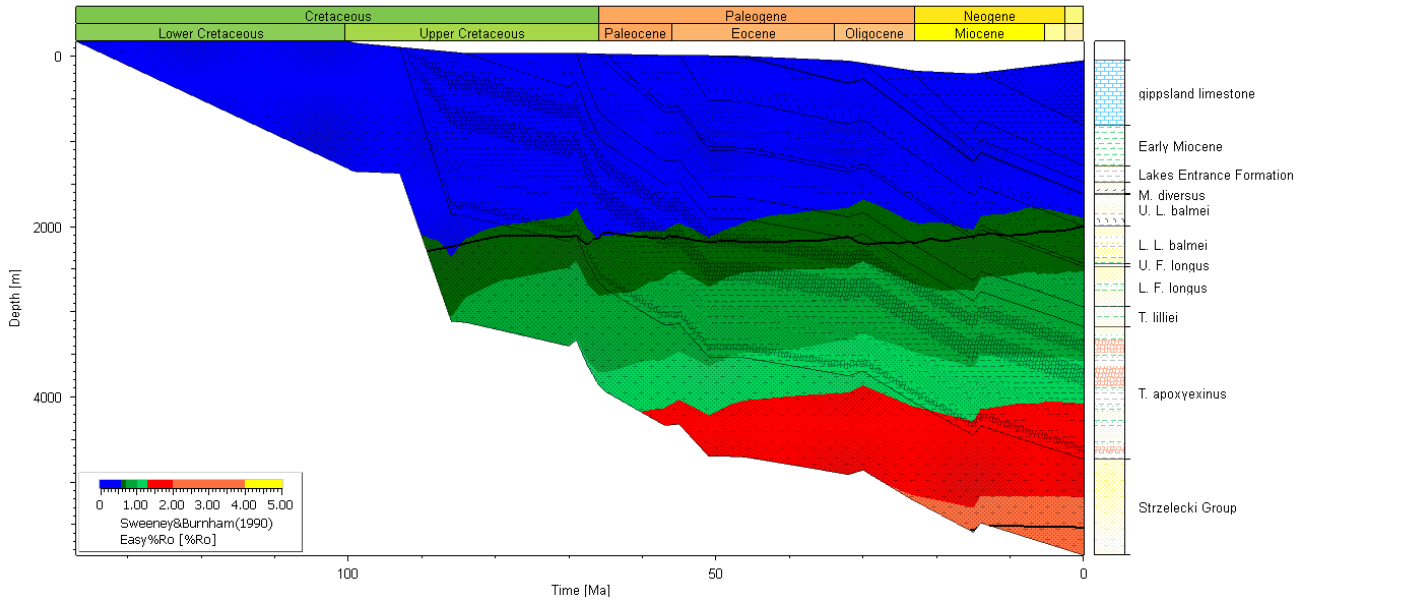
Default Burial Plot, Gippsland_4 at Golden Beach West 1



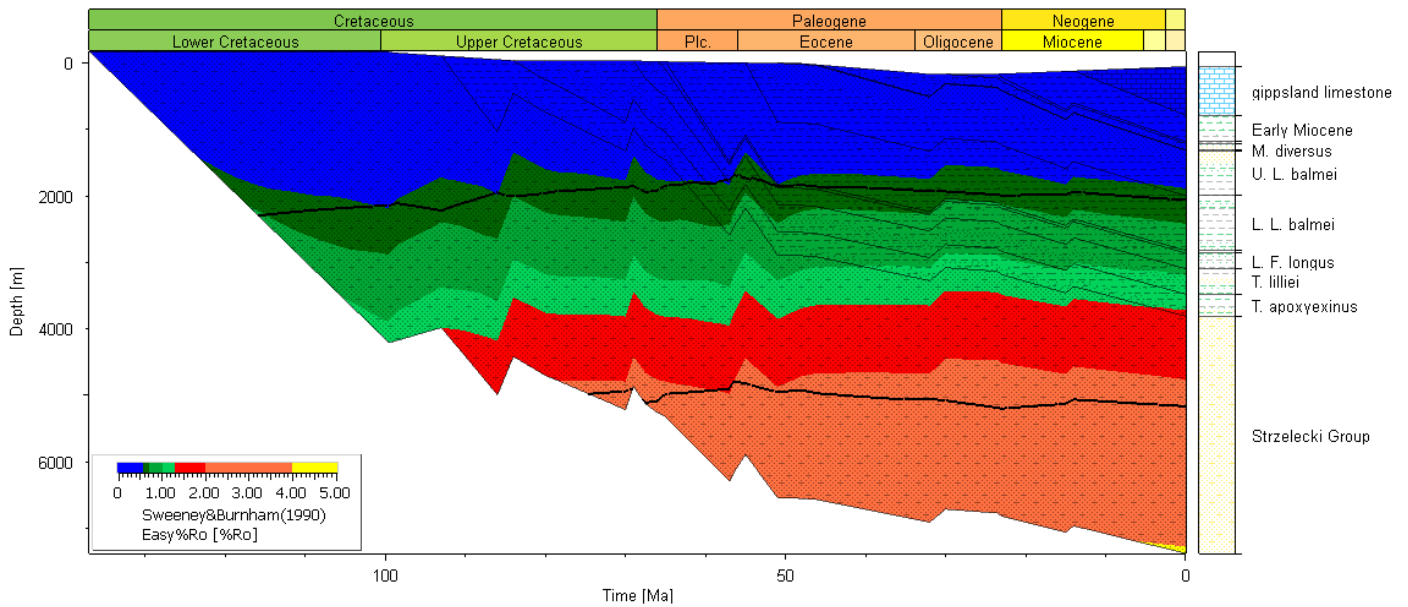
Default Burial Plot, Gippsland_4 at Seahorse 2



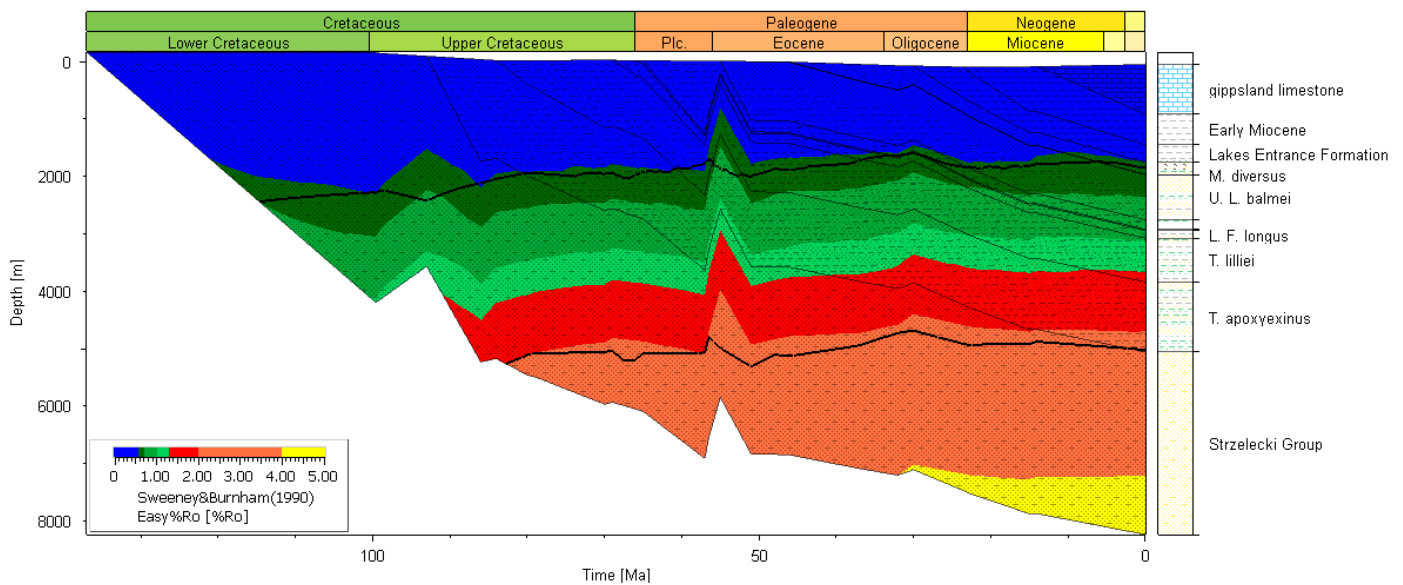
Default Burial Plot, Gippsland_4 at Wirrah 3



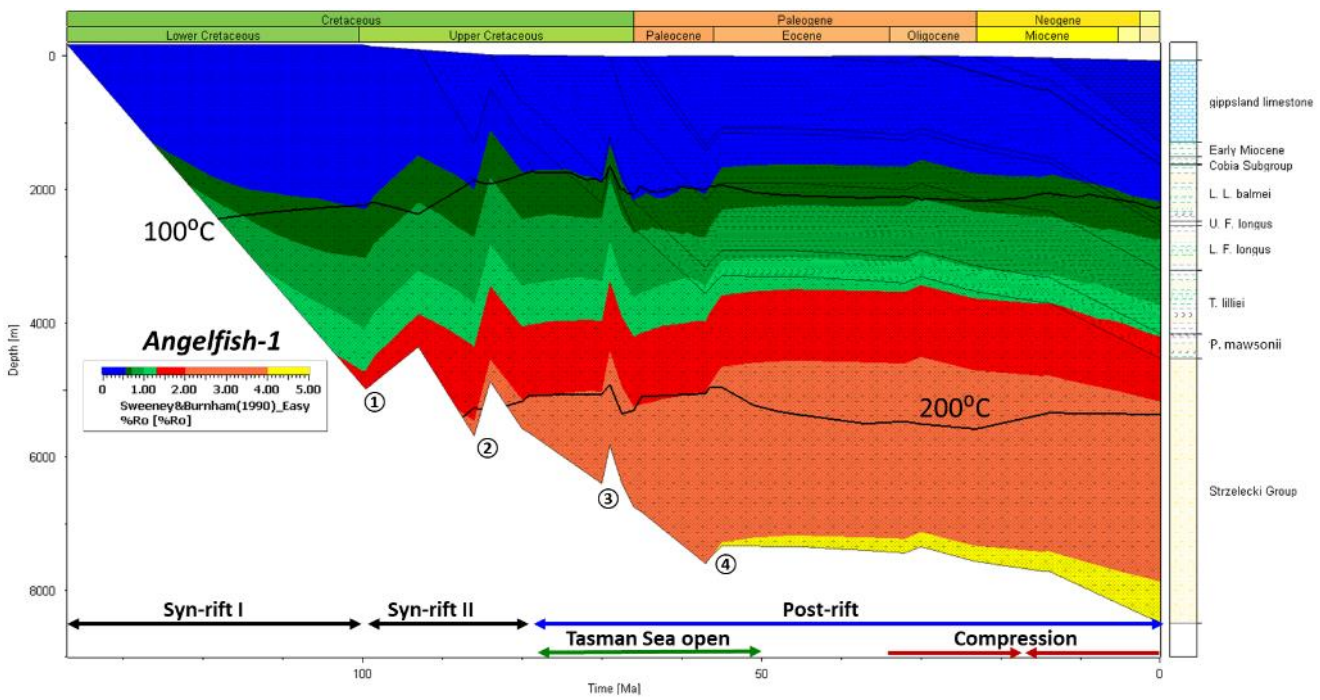
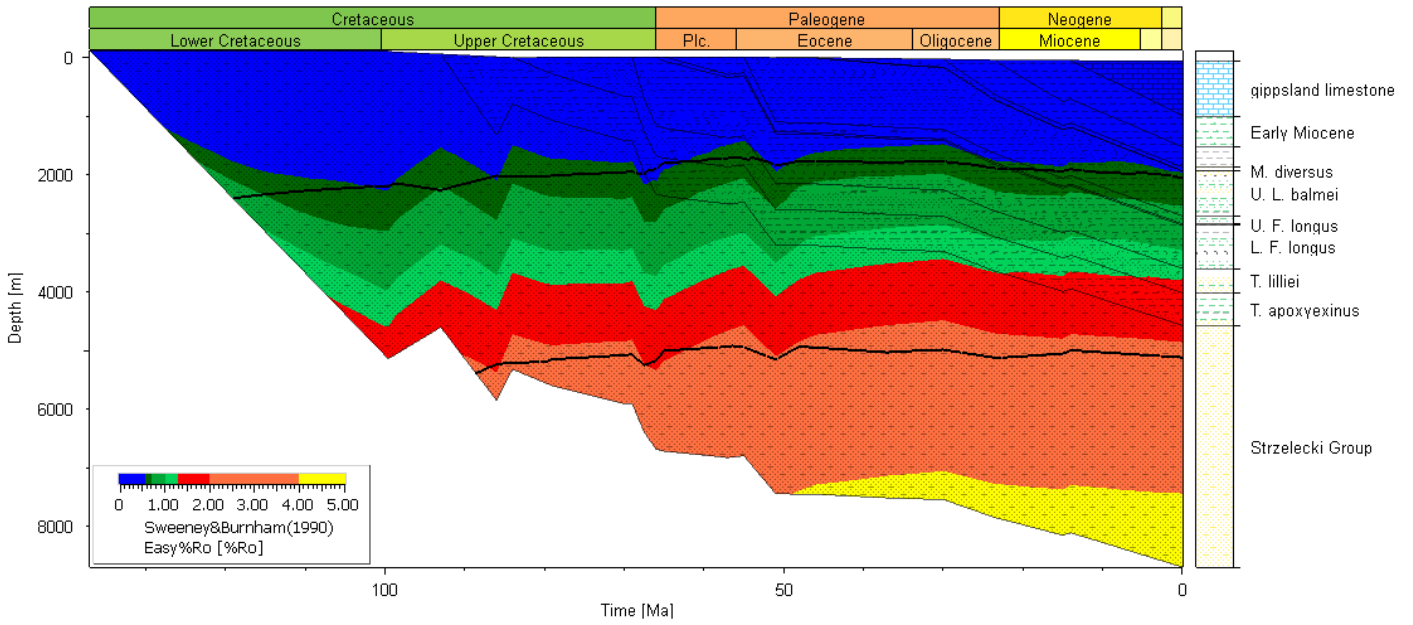
Default Burial Plot, Gippsland_4 at Snapper 1



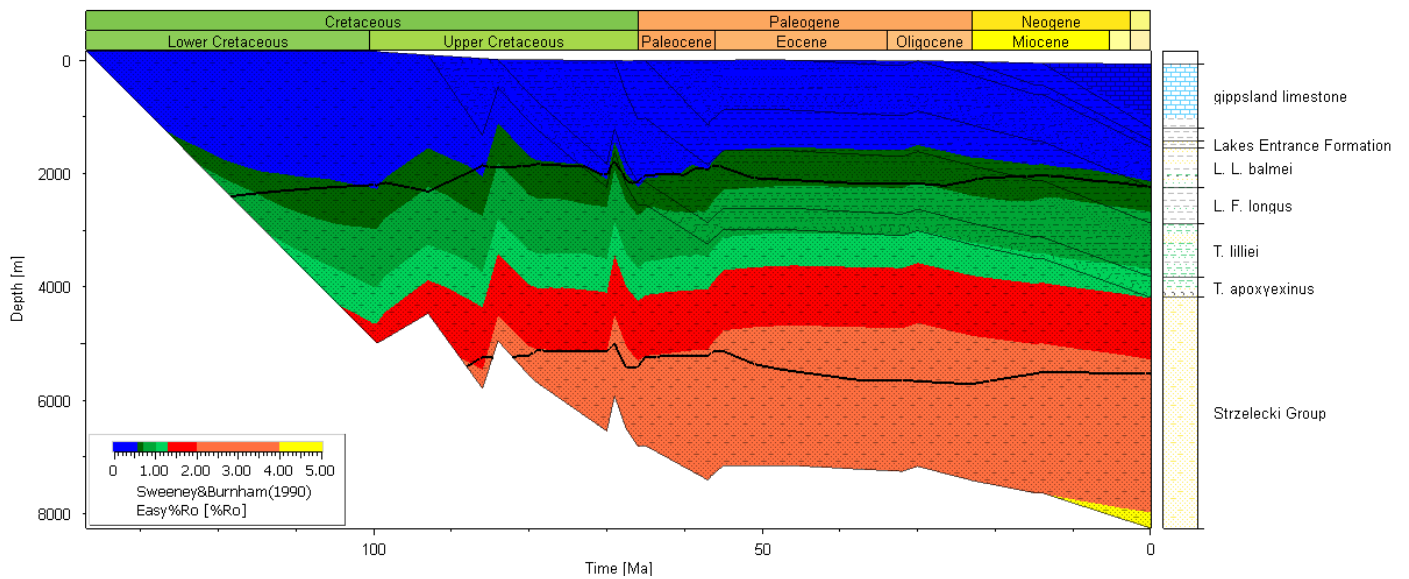
Default Burial Plot, Gippsland_4 at Luderick 1



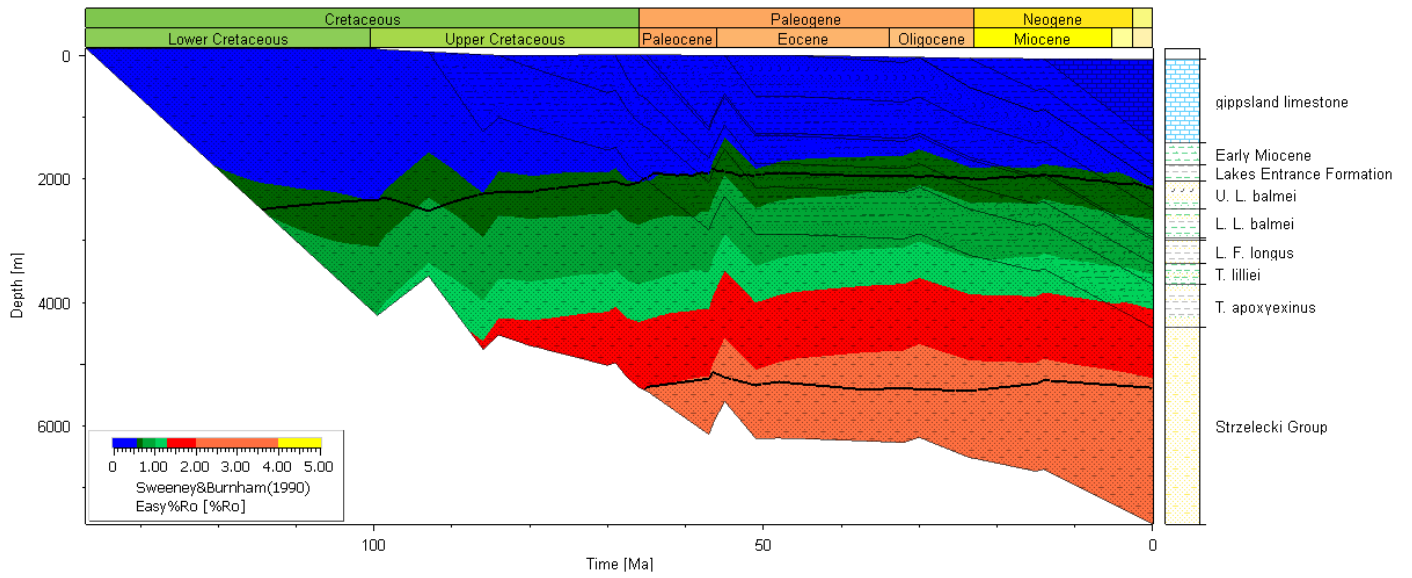
Default Burial Plot, Gippsland_4 at Bream 5



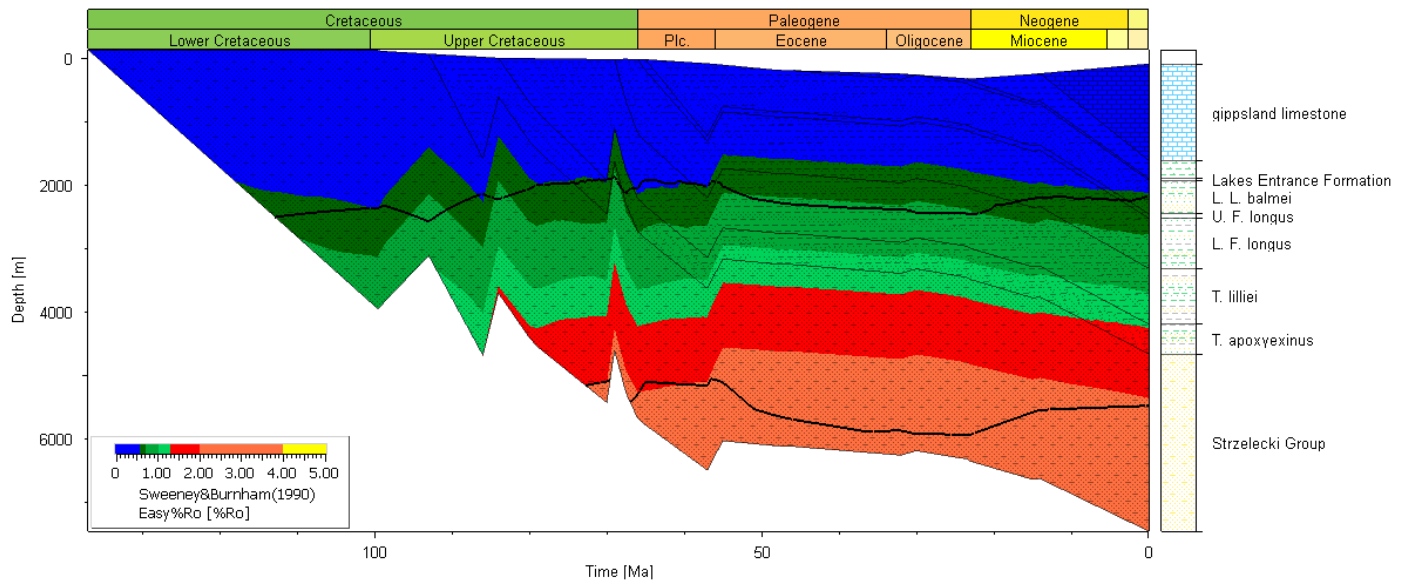
Default Burial Plot, Gippsland_4 at Batfish 1



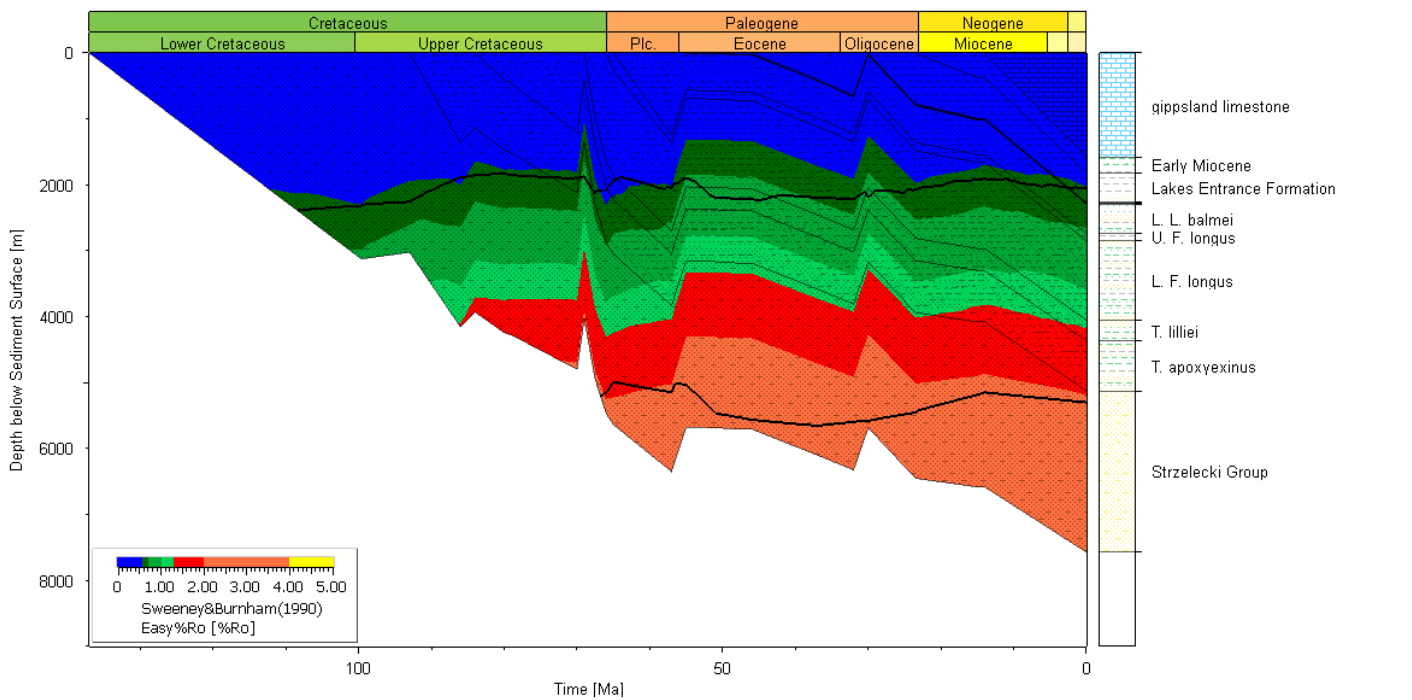
Default Burial Plot, Gippsland_4 at Veilfin 1



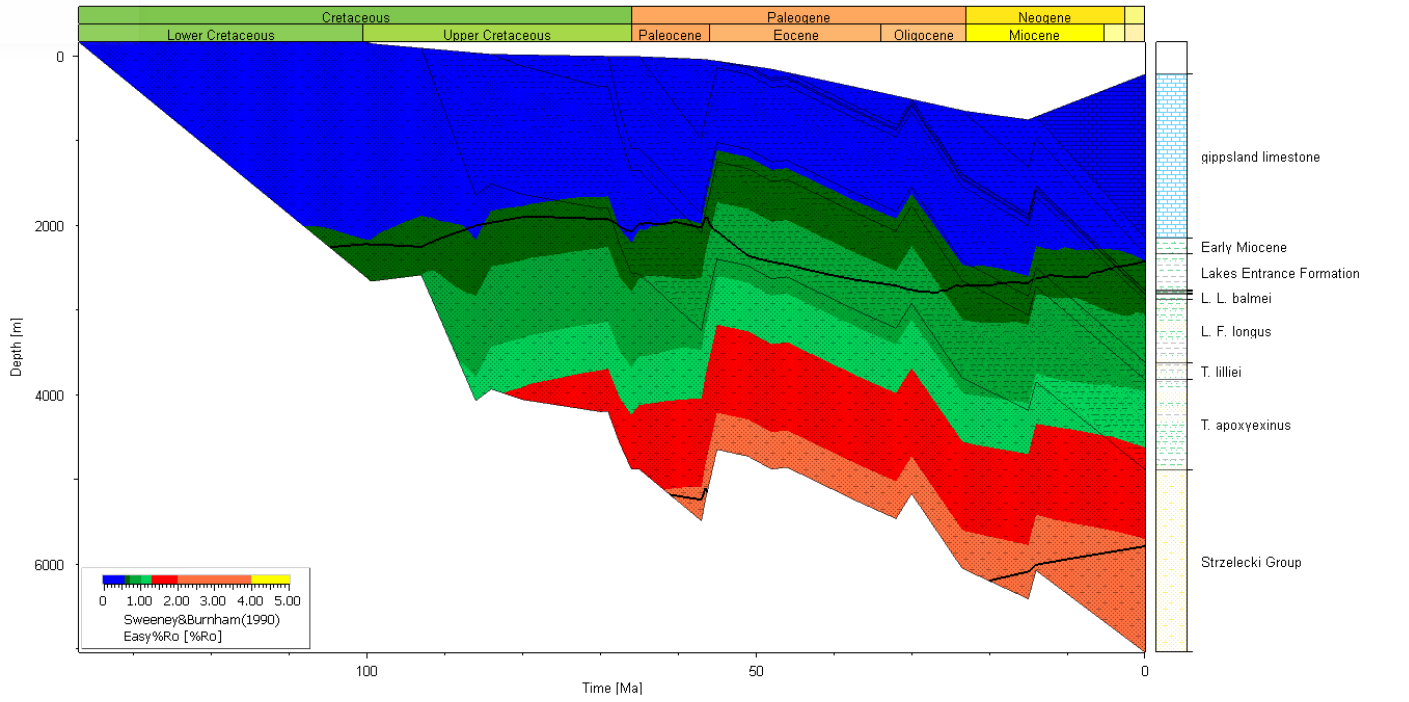
Default Burial Plot, Gippsland_4 at Flounder 1



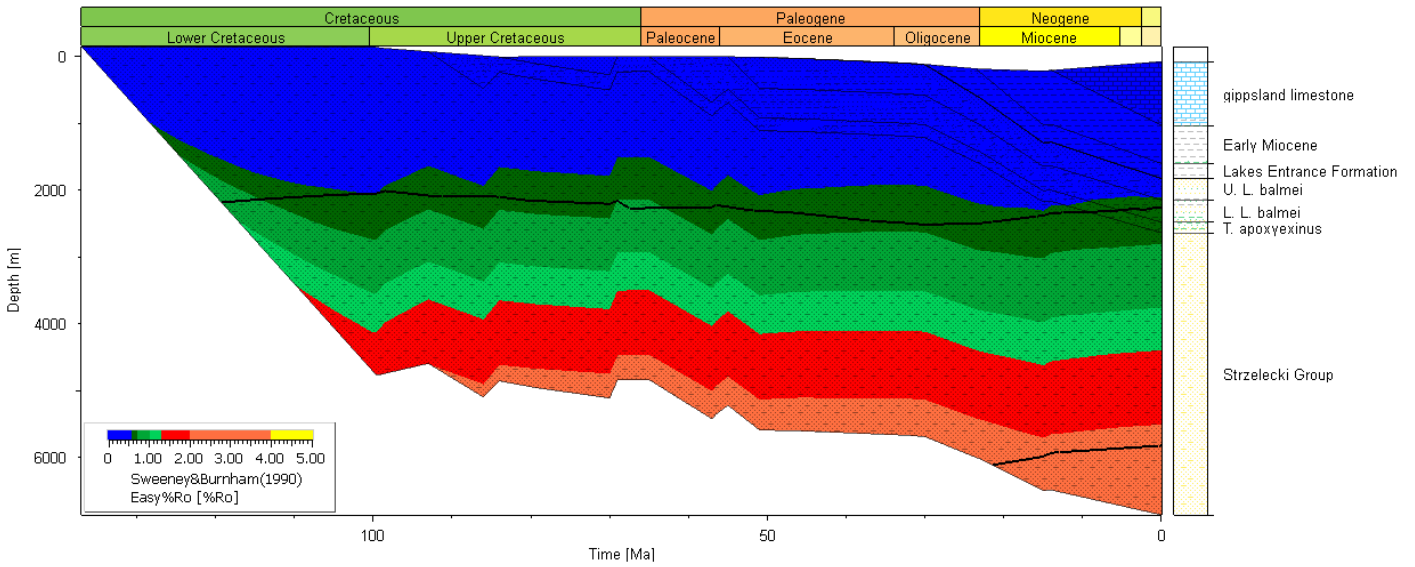
Default Burial Plot, Gippsland_4 at Kingfish 1



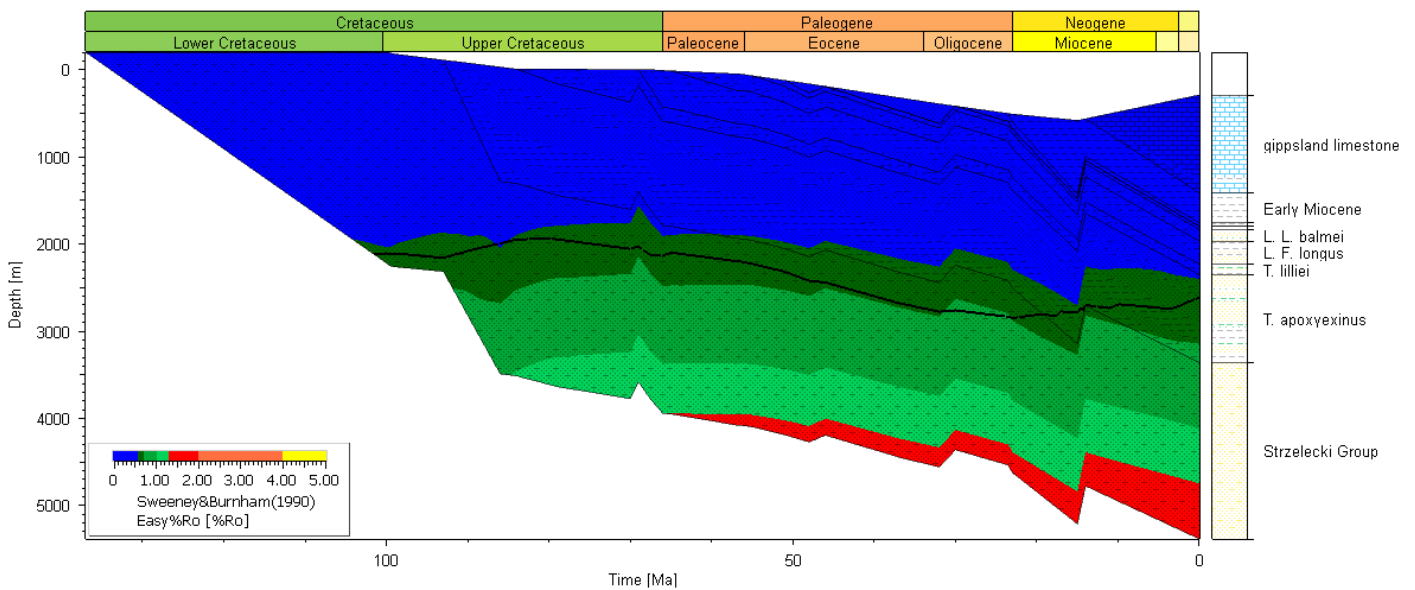
Default Burial Plot, Gippsland_4 at Athene 1



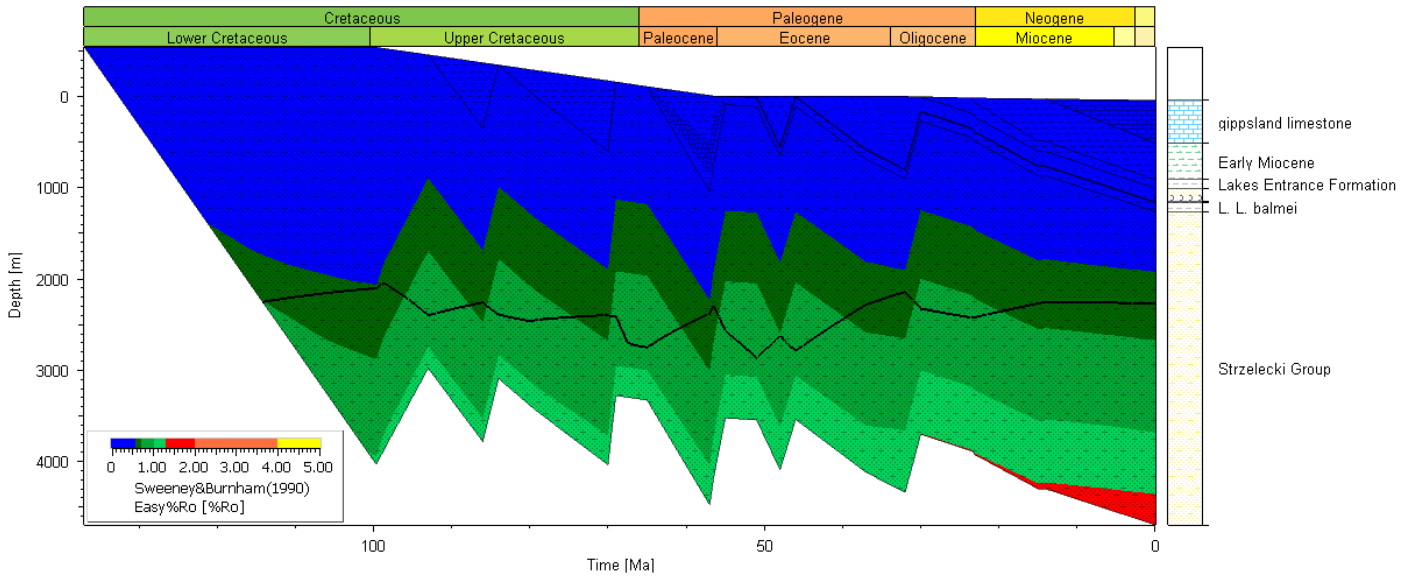
Default Burial Plot, Gippsland_4 at Pike 1



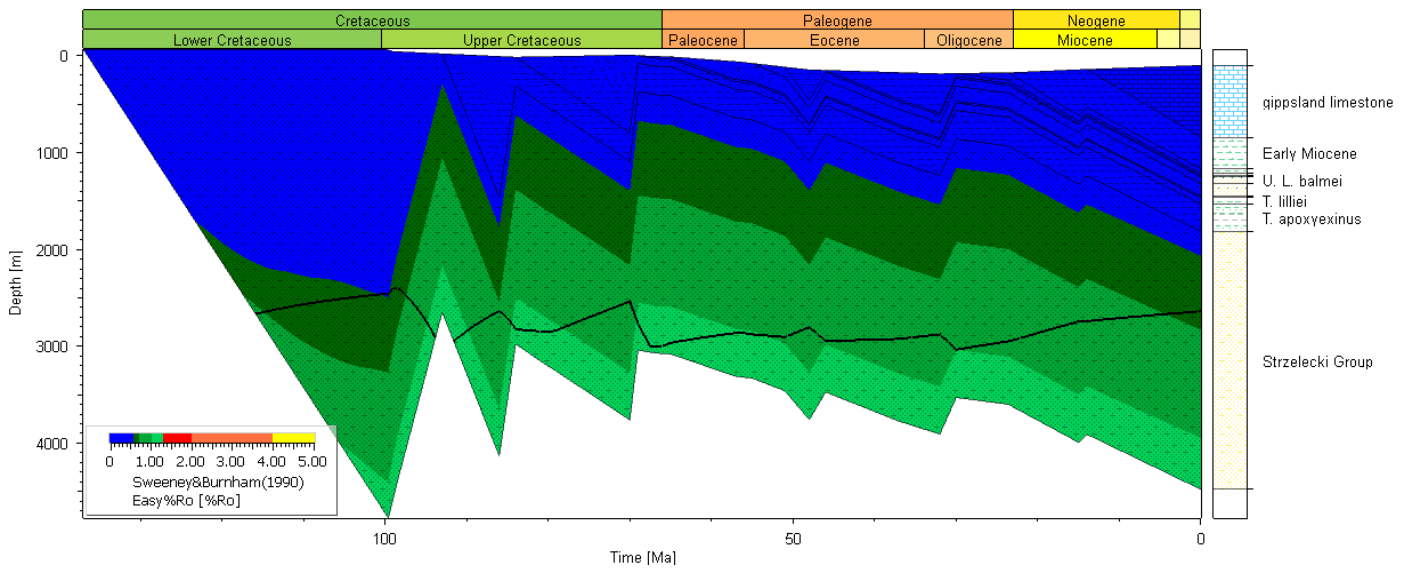
Default Burial Plot, Gippsland_4 at Shark 1



Default Burial Plot, Gippsland_4 at Kyarra 1A



Default Burial Plot, Gippsland_4 at Admiral 1



The blue dash-line is the initial model using continental granite crust, while the pink line is the test model using continental average crust. Crosses are the measured data.

